Contribution to the Study of Fourier Methods for Quasi–Periodic Functions and the Vicinity of the Collinear Libration Points

José María Mondelo

Departament de Matemàtica Aplicada i Anàlisi
Universitat de Barcelona

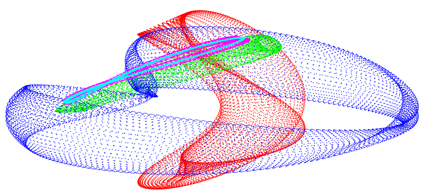

Programa de doctorat de Matemàtica Aplicada i Anàlisi.
Bienni 1996–98.

Memòria presentada per a aspirar al grau de Doctor en Matemàtiques per la Universitat de Barcelona

Certifico que la present memòria ha estat realitzada per José María Mondelo González i dirigida per mi.

Barcelona, 23 de maig de 2001

Gerard Gómez i Muntané

A mi familia.

Acknowledgements

I would like to thank my thesis advisor, G. Gómez, for the many hours we have spent together, and for his support and advice, which has never been just academic. I am also indebted with C. Simó, who has always been aware of this work and has given many hints and ideas that have been critical for its developement. I would like to thank also À. Jorba, for several suggestions and for introducing me in the world of parallel computing. J. Masdemont has provided me software to acces the JPL ephemeris and to evaluate the c_i functions of Appendix A. I would like to mention also J. Font and J. Timoneda, who have always provided me one of the most powerful computing enviornments of the Department. They have also shared with me their expertise in hardware and system management, which has allowed me to get my current job. All my colleages of the Department of Applied Mathematics and Analysis of the University of Barcelona have contributed to provide a very friendly environment to work in. I would like to especially mention A. González, F. Naselli and J. Puig, for their friendship and support during my last year there. And finally, I would like to thank my family. Whithout their support, this work would never have been done.

Preface

This work has been organized in three parts. The first two ones contain the main results, and the last one, which has been divided in several appendices, has complementary results.

The first part of the work (Chapters 1 to 5) is dedicated to the development and study of a procedure for the accurate computation of frequencies, as well as the related Fourier coefficients, of a quasi–periodic function, using as only input input a equally–spaced sampling of the function to be analyzed over a finite time interval.

The first technique for the accurate determination of frequencies has been introduced by J. Laskar ([18], [20], [19]). It is based on the maximization of the formula that gives the Fourier coefficients of a function with respect to the harmonic index, but taking it as a real number. This procedure has been applied to the study of the long–term dynamics of the Solar System ([18]), as well as to the study of chemistry and particle accelerator models through the computation of *frequency maps* ([19]). Some methodology for frequency determination has also been introduced in [12],[13],[10],[11]. In these works, the determination of frequencies has been applied to development of semi–analytical models for the motion in the Solar System.

Our procedure takes the methodology developed in [12],[13],[10][11] as a starting point. It is based in asking for equality between the Discrete Fourier Transform (DFT) of the analyzed function and its quasi–periodic approximation. Error estimates are obtained and illustrated with numerical examples. Also, in the line of the previously–mentioned works, we apply our procedure to the development of simplified models for the motion in the Solar System.

The second part of the work (Chapters 6 to 7) is devoted to the study to the dynamics in the vicinity of the collinear equilibrium points of the three–dimensional Restricted Three–Body Problem (RTBP) for the Earth–Moon mass parameter.

The first systematic study of this vicinity has been done in [10] and [16], using as a tool the reduction to the central manifold of the collinear equilibrium points. This is a semi–analytical technique, which limits the region that can be explored by the convergence of the expansions computed. The same methodology has also been applied to the study of the collinear equilibrium points of a model for the Earth–Moon system, called the Quasi–Bicircular Problem ([3]). In this last study, the convergence constraints are still more severe.

In this work, we follow the families of periodic orbits and invariant 2D tori of the center manifolds of the three collinear libration points using purely numerical procedures. With this approach, we can extend the analysis of the phase space done in [10] and [16] to a wider range of energy values, that now include several bifurcations, and also to the L_3 libration point. The methodology used for the continuation of invariant tori is based in [7], with some modifications in order to account for variable excitations and some additional parameters needed for our exploration. We have followed parallel strategies in order to cope with the large amount of computations required. They have been carried out on HIDRA, one of the Beowulf clusters of the Barcelona Dynamical Systems Group.

The third and last part of this report consists in several appendices, which give some additional results that have been taken apart from the main text in order to improve its readability.

Contents

Part I

Numerical Fourier analysis of quasi–periodic functions

This part is devoted to the development and study of a procedure to compute the frequencies and the related amplitudes of a quasi–periodic function. In Chapter 1 we introduce some notation and methodology related to the Discrete Fourier Transform (DFT), which is the main tool in which our procedure is based. In Chapter 2 we describe the procedure, as well as some aspects of its computer implementation. Chapter 3 is devoted to the obtention of error estimates, which are collected in Theorem 3.4.1 and illustrated with a numerical example in Chapter 4. In Chapter 5, we apply the methodology to the development of simplified models for the motion in the Solar System.

Chapter 1

The Discrete Fourier Transform (DFT)

This chapter gives the basic notation and definitions needed to develop our Fourier analysis procedure in Chapter 2. It is started with the introduction of the DFT and some related notation. After that, we discuss the concept known in the literature as *leakage*, which leads to the introduction of filtering through the use of Hanning functions. We end the Chapter with some comments about how the concept known as *aliasing* arises in our setting.

1.1 Preliminaries and notation

Let D be the space of real valued functions defined on a discrete set of N equally spaced points $t_0, ..., t_{N-1}$ over the interval $[0, T]$, i.e. $t_l = l \cdot \Delta t$, with $\Delta t = T/N$. The equality of the spacing is only a technical requirement, since the DFT could be adapted to a non equally spaced set of samples. Nevertheless, all what follows has been written assuming Δt constant. From now on N is assumed to be even. If $f,\ g\ \in D$, we define their discrete scalar product as

$$\langle f, g\rangle = \sum_{l=0}^{N-1} f(t_l)g(t_l).$$

The set of functions $\{\{\varphi_j\}_{j=0}^{N/2}, \{\psi_j\}_{j=1}^{N/2-1}\} \subset D$, being

$$\varphi_j(t) = \cos(\frac{2\pi jt}{T}), \quad \psi_j(t) = \sin(\frac{2\pi jt}{T}),$$

form an orthogonal basis of D. Therefore, every function $f \in D$ can be written as

$$f(t_l) = P_{f,T,N}(t_l) \qquad l = 0, \dots, N-1,$$

where

$$\begin{aligned} P_{f,T,N}(t) &= \frac{1}{2}\Big(c_{f,T,N}(0) + c_{f,T,N}(\frac{N}{2})\cos(\frac{2\pi\frac{N}{2}t}{T})\Big) \\ &\quad + \sum_{j=1}^{N/2-1}\Big(c_{f,T,N}(j)\cos(\frac{2\pi jt}{T}) + s_{f,T,N}(j)\sin(\frac{2\pi jt}{T})\Big). \end{aligned} \tag{1.1}$$

with

$$c_{f,T,N}(j)=\delta_j\frac{\langle f,\varphi_j\rangle}{\langle\varphi_j,\varphi_j\rangle},\quad j=0,\dots,\frac{N}{2},\qquad s_{f,T,N}(j)=\frac{\langle f,\psi_j\rangle}{\langle\psi_j,\psi_j\rangle},\quad j=1,\dots,\frac{N}{2}-1,$$

with

$$\delta_j=\begin{cases}2, & j=0,\\ 1, & j=1,...,N/2-1,\\ 2, & j=N/2,\end{cases}$$

Equation (1.1) defines the *Discrete Fourier Transform in sines and cosines* (DFT) of $f\in D$ as a function of the discrete set of frequencies j/T, $j=0,\dots,N/2$. The values $c_{f,T,N}(j)$ and $s_{f,T,N}(j)$ are the coefficients related to the j/T frequency of the trigonometric interpolating polynomial $P_{f,T,N}(t)$ of the function f at the nodes $\{t_l\}_{l=0}^{N-1}$. All the frequencies of $P_{f,T,N}(t)$ are multiples of $1/T$. The DFT coefficients can be explicitly written as

$$\begin{aligned}c_{f,T,N}(j) &= \frac{2}{N}\sum_{l=0}^{N-1}f(t_l)\cos(2\pi\frac{j}{N}l),\quad j=0,...,N/2,\\ s_{f,T,N}(j) &= \frac{2}{N}\sum_{l=0}^{N-1}f(t_l)\sin(2\pi\frac{j}{N}l),\quad j=1,...,N/2-1.\end{aligned}$$

For a general complex–valued function f, using the discrete scalar product $\langle f,g\rangle=\sum_{l=0}^{N-1}f(t_l)\overline{g(t_l)}$ and the orthogonal basis $\{e^{2\pi i\frac{j}{T}t}\}_{j=0}^{N-1}$, we can define the DFT as

$$F_{f,T,N}(j)=\frac{1}{N}\sum_{l=0}^{N-1}f(t_l)e^{-2\pi i\frac{j}{T}t_l},\quad j=0,...,N-1. \tag{1.2}$$

If f takes real values, $F_{N-j}(f)=\overline{F_j(f)}$, the $F_{f,T,N}(j)$, $c_{f,T,N}(j)$, $s_{f,T,N}(j)$ coefficients are related by

$$F_{f,T,N}(j)=\frac{1}{2}(c_{f,T,N}(j)-is_{f,T,N}(j))\quad j=0,\dots,\frac{N}{2},$$

where we assume $s_{f,T,N}(0)=s_{f,T,N}(N/2)=0$. This allows to compute efficiently the $c_{f,T,N}(j)$, $s_{f,T,N}(j)$ coefficients using a standard Fast Fourier Transform (FFT) algorithm (see, for instance, [6], [5] or [21]).

The complex–valued function

$$\phi_{f,T}(\alpha)=\frac{1}{T}\int_0^T f(t)e^{-i2\pi\alpha t}dt$$

will be called *Truncated Continuous Fourier Transform* (TCFT) of f. Note that $\phi_{f,T,N}(\frac{j}{T})$, $j\in\mathbb{Z}$, are the coefficients of the Fourier series of f on the interval $[0,T]$. Note also that the DFT can be seen as a Riemann sum of the TCFT, more concretely

$$\phi_{f,T}\Big(\frac{k}{T}\Big)=\frac{1}{T}\int_0^T f(t)e^{-2\pi i\frac{k}{T}t}dt\approx\frac{1}{T}\sum_{l=0}^{N-1}f(t_l)e^{-2\pi i\frac{k}{T}t_l}\frac{T}{N}=F_{f,T,N}(k). \tag{1.3}$$

Consequently, we can obtain the TCFT as the limit when $N\to\infty$ of the DFT. In section 3, Lemma 3.2.4, we will give an explicit bound of the difference between the DFT and the TCFT of a complex exponential term $e^{i2\pi\omega t}$.

1.2 Leakage effect and filtering

For periodic functions, when the length T of the time interval spanned by the samples is not an integer multiple of the period of the function (or equivalently, when the frequency of the function is not an integer multiple of the "basic frequency" $1/T$ associated to the sample interval $[0, T]$), there appear in the DFT spurious frequencies, that is, the DFT is different from zero at frequencies not being multiple of the frequency of the function. This is a phenomenon known as *leakage*, for which we give a graphical example in figure 1.1. Leakage also affects the TCFT.

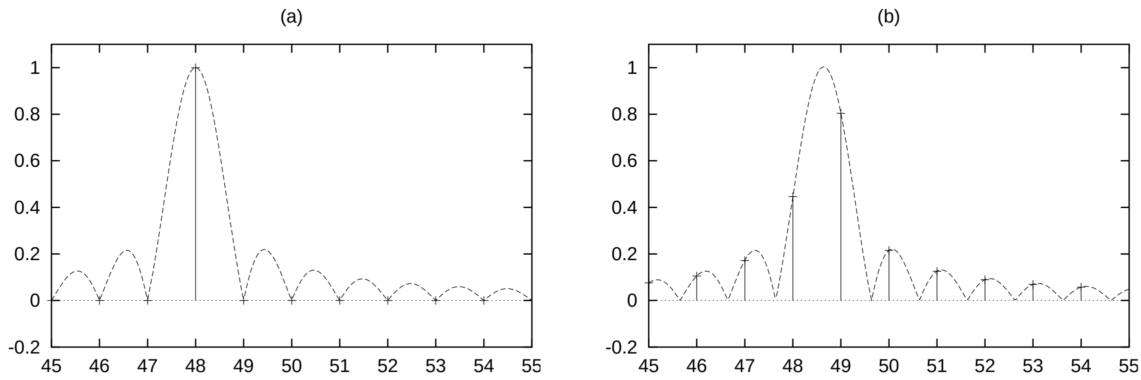

Figure 1.1: Plot of $[(c_{f,T,N}(j))^2 + (s_{f,T,N}(j))^2]^{1/2}$ as a function of j (dashed line) and for $j = 45, \dots, 55$ (solid vertical lines), with $f(t) = \cos(2\pi\omega t)$, $T = 64$ and $N = 256$. In (a) $\omega = 0.75$, so $48 \cdot (0.75)^{-1} = 64 = T$ and there is no leakage. This is not the case for (b), where $\omega = 0.76$.

For the procedures that will be described later, we are interested in reducing leakage for functions of the form $e^{2\pi i\omega t}$. The way to do this is to use a filter or window function.

Definition 1.2.1 *$H(t)$ is said to be a* filter function of degree $r \geq 0$ for the interval $[0, T]$ *if it is a positive function of class C^{r-1} with $H^{(j)}(0) = H^{(j)}(T) = 0$ for $j = 0, \dots, r-1$, such that $H^{(r)}$ is continuous except for a finite set of jump discontinuities, and has bounded variation. We also assume that*

$$\frac{1}{T}\int_0^T H(t)dt = 1. \tag{1.4}$$

It is enough to focus on the TCFT, since it is the limit of the DFT when $N \to \infty$ (equation (1.3)). The reduction of leakage for the TCFT of $H(t)e^{2\pi i\omega t}$, which depends directly on the regularity of the filter function, is given by corollary 1.2.1.

Proposition 1.2.1 If g is a filter function of degree r for the interval $[0, 2\pi]$, then

$$\Big|\int_0^{2\pi} g(t)e^{i\alpha t}dt\Big| \leq \frac{2B(g^{(r)}) + V(g^{(r)})}{|\alpha|^{r+1}},$$

where $B(g^{(r)})$ is a bound for $g^{(r)}$ in $[0, 2\pi]$ and $V(g^{(r)})$ is the variation of $g^{(r)}$ in the same interval. Moreover, if we assume $g^{(r)}(0) = g^{(r)}(2\pi) = 0$, then

$$\Big|\int_0^{2\pi} g(t)e^{i\alpha t}dt\Big| \leq \frac{V(g^{(r)})}{|\alpha|^{r+1}}.$$

Proof: Let $t_1, \dots t_{m-1}$ be the jump discontinuities of $g^{(r)}$ in $(0, 2\pi)$, and let $t_0 = 0$, $t_m = 2\pi$ (which may be jump discontinuities or not). Successive integrations by parts yield

$$\begin{aligned}
\int_0^{2\pi} g(t)e^{i\alpha t}dt &= \Big[g(t)\frac{e^{i\alpha t}}{i\alpha}\Big]_{t=0}^{t=2\pi} - \frac{1}{i\alpha}\int_0^{2\pi} g'(t)e^{i\alpha t}dt \\
&= \dots = \Big(\frac{-1}{i\alpha}\Big)^{r-1}\sum_{j=0}^{m-1}\int_{t_j}^{t_{j+1}} g^{(r-1)}(t)e^{i\alpha t}dt \\
&= \Big(\frac{-1}{i\alpha}\Big)^{r-1}\Big(\sum_{j=0}^{m-1}\Big[g^{(r-1)}(t)\frac{e^{i\alpha t}}{i\alpha}\Big]_{t=t_j}^{t=t_{j+1}} + \frac{-1}{i\alpha}\sum_{j=0}^{m-1}\int_{t_j}^{t_{j+1}} g^{(r)}(t)e^{i\alpha t}dt\Big).
\end{aligned}$$

The first sum vanishes because it is a telescopic sum and $g^{(r-1)}(0) = g^{(r-1)}(2\pi) = 0$.

Given $\varepsilon > 0$, let δ_j be such that, for $t^*, t^{**} \in [t_j, t_{j+1}]$, if $|t^* - t^{**}| < \delta_j$ then $|g^{(r)}(t^*) - g^{(r)}(t^{**})| < \varepsilon$ ($j = 0 \div m-1$). These δ_j exist because $g^{(r)}$ is uniformly continuous in each interval $[t_j, t_{j+1}]$. Reducing δ_j if necessary, we can assume $t_{j+1} - t_j = n_j\delta_j$ for $n_j \in \mathbb{N}$. Define $M = n_0 + \dots + n_{m-1}$ and

$$\begin{aligned}
&s_0 = t_0,\ s_1 = t_0 + \delta_0,\ \dots,\ s_{n_0-1} = t_0 + (n_0 - 1)\delta_0,\ s_{n_0} = t_0 + n_0\delta_0 = t_1, \\
&s_{n_0+1} = t_1 + \delta_1,\ \dots,\ s_{n_0+\dots+n_{m-1}-1} = t_{m-1} + (n_{m-1} - 1)\delta_{m-1},\ s_M = t_m.
\end{aligned}$$

Denoting by $\xi_j = \frac{1}{2}(s_j + s_{j+1})$,

$$\begin{aligned}
\int_0^{2\pi} g(t)e^{i\alpha t}dt &= \Big(\frac{-1}{i\alpha}\Big)^r\sum_{j=0}^{M-1}\int_{s_j}^{s_{j+1}}(g^{(r)}(\xi_j) + g^{(r)}(t) - g^{(r)}(\xi_j))e^{i\alpha t}dt \\
&= \Big(\frac{-1}{i\alpha}\Big)^r\sum_{j=0}^{M-1}\Big(g^{(r)}(\xi_j)\frac{e^{i\alpha s_{j+1}} - e^{i\alpha s_j}}{i\alpha} + \int_{s_j}^{s_{j+1}}(g^{(r)}(t) - g^{(r)}(\xi_j))e^{i\alpha t}dt\Big) \\
&= \Big(\frac{-1}{i\alpha}\Big)^r\Big[\frac{1}{i\alpha}\Big(-g^{(r)}(\xi_0)e^{i\alpha s_0} + g^{(r)}(\xi_{M-1})e^{i\alpha s_M} \\
&\qquad + \sum_{j=1}^{M-1}(g^{(r)}(\xi_{j-1}) - g^{(r)}(\xi_j))e^{i\alpha s_j}\Big) \\
&\qquad + \sum_{j=0}^{M-1}\int_{s_j}^{s_{j+1}}(g^{(r)}(t) - g^{(r)}(\xi_j))e^{i\alpha t}dt\Big],
\end{aligned}$$

and hence

$$\Big|\int_0^{2\pi} g(t)e^{i\alpha t}dt\Big| \leq \frac{1}{|\alpha|^r}\Big[\frac{1}{|\alpha|}(2B(g^{(r)}) + V(g^{(r)})) + 2\pi\varepsilon\Big].$$

Since $\varepsilon > 0$ is arbitrary, doing $\varepsilon \to 0$ we get the first equality of the proposition. The second bound follows immediately from the above computations. $\square$

For $\alpha = j/T$, the above Proposition is a standard result about the decaying of the Fourier coefficients (see, e.g., [5] and references therein). The above proof covers the case $\alpha \neq j/T$.

Corollary 1.2.1 If H is a filter function of degree r for $[0, T]$, then

$$\phi_{H(t)e^{2\pi i\nu t/T},T}(\alpha/T) = O\Big(\frac{1}{|\nu - \alpha|^{r+1}}\Big).$$

Proof: We have

$$\phi_{H(t)e^{2\pi i\nu t/T},T}(\alpha/T) = \frac{1}{T}\int_0^T H(t)e^{2\pi i(\nu-\alpha)t/T}dt = \frac{1}{2\pi}\int_0^{2\pi} H(\frac{T}{2\pi}s)e^{i(\nu-\alpha)s}ds,$$

and hence

$$|\phi_{H(t)e^{2\pi i\nu t/T},T}(\alpha/T)| \leq \frac{2B(H^{(r)}) + V(H^{(r)})}{2\pi|\nu - \alpha|^{r+1}}.$$

$\square$

We will use as a filter function the *Hanning window function*, which is defined as

$$H_T(t) = 1 - \cos\left(2\pi\frac{1}{T}t\right).$$

and has degree 2. To increase the degree of the filter, the Hanning function can be iterated and we can consider *Hanning functions of order* $n_h \in \mathbb{N}$, defined as

$$H_T^{n_h}(t) = q_{n_h}\left(1 - \cos\left(2\pi\frac{1}{T}t\right)\right)^{n_h},$$

where the constants q_{n_h} are computed in order to fulfill (1.4), so

$$q_{n_h} = \left[\frac{1}{T}\int_0^T \left(1 - \cos\left(2\pi\frac{1}{T}t\right)\right)^{n_h} dt\right]^{-1} = \frac{n_h!}{(2n_h - 1)!!}.$$

The advantage of the Hanning function with respect to other well-known window functions (see [21]) is its degree of differentiability. For instance, $H^{n_h}(t)$ has degree $2n_h$, whereas a general "triangle window function" $T^{n_t}(t)$ defined as

$$T^{n_t}(t) = \frac{n_t + 1}{n_t}\Big(1 - \Big|\frac{2}{T}t - 1\Big|^{n_t}\Big).$$

has degree just n_t. The *Parzen window* and the *Welch window* are the particular cases $n_t = 1$ and $n_t = 2$ of $T^{n_t}(t)$ respectively. The Hanning function has its simplicity as an additional advantage. The properties of trigonometric functions allow to obtain relations like Lemma 1.2.1.

The DFT coefficients with Hanning order n_h of $f(t)$ are defined as the DFT coefficients of $H_T^{n_h}(t)f(t)$, and will be denoted by

$$\begin{aligned} F^{n_h}_{f,T,N}(j) &= F_{H^{n_h}f,T,N}(j), \\ c^{n_h}_{f,T,N}(j) &= c_{H^{n_h}f,T,N}(j), \\ s^{n_h}_{f,T,N}(j) &= s_{H^{n_h}f,T,N}(j). \end{aligned}$$

Analogously, for the TCFT we will have

$$\phi^{n_h}_{f,T,N}(\alpha) = \frac{1}{T}\int_0^T H^{n_h}(t)f(t)e^{-2\pi i\alpha t}dt.$$

The following lemma relates the coefficients of filtered and non–filtered transforms of a function $f(t)$:

Lemma 1.2.1 The following relations hold:

(a) $$F^{n_h}_{f,T,N}(j) = \frac{q_{n_h}}{2^{n_h}}\sum_{l=-n_h}^{n_h}(-1)^l\binom{2n_h}{n_h+l}F_{f,T,N}(j+l) = \sum_{l=-n_h}^{n_h}\frac{(-1)^l(n_h!)^2F_{f,T,N}(j+l)}{(n_h+l)!(n_h-l)!}.$$

(b) $$\phi^{n_h}_{f,T,N}(\alpha) = \frac{q_{n_h}}{2^{n_h}}\sum_{l=-n_h}^{n_h}(-1)^l\binom{2n_h}{n_h+l}\phi_{f,T,N}(\alpha+\frac{l}{T}) = \sum_{l=-n_h}^{n_h}\frac{(-1)^l(n_h!)^2\phi_{f,T,N}(\alpha+l/T)}{(n_h+l)!(n_h-l)!}.$$

Proof: We only prove (a). Similar calculations are valid for (b). Using that $1-\cos x = 2\sin^2\frac{x}{2}$, we have

$$\begin{aligned} F^{n_h}_{f,T,N}(j) &= \sum_{l=0}^{N-1} q_{n_h}\Big(1-\cos(2\pi\frac{1}{T}t_l)\Big)^{n_h} f(t_l)e^{-2\pi i\frac{j}{T}t_l} \\ &= \sum_{l=0}^{N-1} q_{n_h}2^{n_h}\sin^{2n_h}(\pi\frac{1}{T}t_l)f(t_l)e^{-2\pi i\frac{j}{T}t_l} \\ &= \sum_{l=0}^{N-1} q_{n_h}2^{n_h}\frac{(e^{\pi i\frac{1}{T}t_l}-e^{-\pi i\frac{1}{T}t_l})^{2n_h}}{(2i)^{2n_h}}f(t_l)e^{-2\pi i\frac{j}{T}t_l} \\ &= \sum_{l=0}^{N-1}\frac{q_{n_h}}{(-2)^{n_h}}\sum_{l=0}^{2n_h}\binom{2n_h}{l}e^{\pi i\frac{2n_h-l}{T}t_l}(-1)^l e^{-\pi i\frac{l}{T}t_l}f(t_l)e^{-2\pi i\frac{j}{T}t_l} \\ &= \frac{q_{n_h}}{2^{n_h}}\sum_{l=0}^{2n_h}(-1)^{l-n_h}\binom{2n_h}{l}\sum_{l=0}^{N-1}f(t_l)e^{-2\pi i\frac{j+(l-n_h)}{T}t_l}. \end{aligned}$$

Shifting the index by n_h units, and using that

$$\frac{q_{n_h}}{2^{n_h}}\binom{2n_h}{n_h+l} = \frac{(n_h!)(n_h!)(2n_h)!}{(n_h!)2^{n_h}(2n_h-1)!!(n_h+l)!(n_h-l)!} = \frac{(n_h!)^2(2n_h)!}{(2n_h)!(n_h+l)!(n_h-l)!},$$

we get (a). □

For $c^{n_h}_{f,T,N}(j)$ and $s^{n_h}_{f,T,N}(j)$ relations similar to those of Lemma 1.2.1(a) hold. For instance, for $n_h = 1, 2$ we get

$$\begin{aligned}
F^1_{f,T,N}(j) &= -\frac{1}{2}F_{f,T,N}(j-1)+F_{f,T,N}(j)-\frac{1}{2}F_{f,T,N}(j+1),\\
F^2_{f,T,N}(j) &= \frac{1}{6}F_{f,T,N}(j-2)-\frac{2}{3}F_{f,T,N}(j-1)+F_{f,T,N}(j)-\frac{2}{3}F_{f,T,N}(j+1)+\frac{1}{6}F_{f,T,N}(j+2).
\end{aligned}$$

As H^{n_h} is a filter function of degree $2n_h$, according to Corollary 1.2.1 we have

$$\phi^{n_h}_{e^{2\pi i\nu t/T},T}(\alpha/T) = O\Big(\frac{1}{(|\nu-\alpha|)^{2n_h+1}}\Big).$$

In fact, it can be explicitly calculated that

$$\phi^{n_h}_{e^{2\pi i\nu t/T},T}(\alpha/T) = \frac{(-1)^{n_h}(n_h!)^2(e^{2\pi i(\nu-\alpha)}-1)}{2\pi i\psi_{n_h}(\nu-\alpha)} \tag{1.5}$$

being

$$\psi_{n_h}(x) = \prod_{l=-n_h}^{n_h}(x+l). \tag{1.6}$$

1.3 Aliasing effect

Apart from leakage, another common effect when performing DFT is *aliasing*. It consists in the fact that any frequency greater than half the frequency associated to the sampling width, i.e. any frequency greater than $\omega_c := \frac{N}{2T}$, is *aliased* in a frequency less than ω_c. This is due to the following fact. Denoting $p^{n_h}_{f,T,N}(j) = ((c^{n_h}_{f,T,N}(j))^2 + (s_{f,T,N})^2(j))^{1/2}$, we have that

$$\begin{aligned}
p^{n_h}_{\mathrm{cs}(2\pi(\omega+\frac{N}{T})t,T,N}(j) &= p^{n_h}_{\mathrm{cs}(2\pi\omega t),T,N}(j),\\
p^{n_h}_{\mathrm{cs}(2\pi(-\omega)t),T,N}(j) &= p^{n_h}_{\mathrm{cs}(2\pi\omega t)}(j),
\end{aligned}$$

where cs stands for any of the functions cos or sin. If $\omega > \frac{N}{2T}$ and $m \in \mathbb{Z}$ is such that $\widetilde{\omega} := \omega - m\frac{N}{T} \in [-\frac{N}{2T}, \frac{N}{2T}]$, then the frequencies ω and $|\widetilde{\omega}|$ are undistinguisheable from a DFT point of view when using the p function. The frequency ω_c is called the *Nyquist critical frequency* in the literature.

Indeed, when all the frequency components are confined to the interval $[-\omega_c, \omega_c]$, the function is called *band-width limited*. More concretely, in terms of the continuous Fourier Transform, this means

$$\int_{-\infty}^{\infty} f(t)e^{-2\pi i\omega t}dt = 0, \qquad \text{for} \qquad |\omega| > \omega_c.$$

In this case, assuming that we have a sampling of infinite size $\{j \cdot \Delta t\}_{j\in\mathbb{Z}}$, the *Shannon sampling theorem* (see [5], [21]) allows to reconstruct the function $f(t)$ from its samples, namely

$$f(t) = \Delta t \sum_{j=-\infty}^{\infty} f(t_j) \frac{\sin(2\pi\omega_c(t-t_j))}{\pi(t-t_j)},$$

where $\omega_c = \frac{1}{2\Delta t}$. Note that quasi–periodic functions are not band–width limited.

Chapter 2

Procedures for the refined Fourier analysis

This chapter is devoted to the description of our Fourier analysis procedure. It starts with the detailed description of the three steps in which it is carried out, namely: first approximation of frequencies, computation of the related amplitudes and iterative improvement of both frequencies and amplitudes. After that, we discuss some aspects regarding to its practical implementation: the algorithm to follow, the use of trigonometric recurrences and the accurate evaluation of the DFT of sines and cosines.

2.1 Introduction

Given N values, $\{f(t_l)\}_{l=0}^{N-1}$, $t_l \in [0, T]$ of a certain function $f(t)$, which is assumed to be quasi–periodic, we want to find a polynomical trigonometric approximation with a fixed number of frequencies N_f,

$$Q_f(t) = A_0^c + \sum_{l=1}^{N_f} (A_l^c \cos(\frac{2\pi\nu_l t}{T}) + A_l^s \sin(\frac{2\pi\nu_l t}{T})). \tag{2.1}$$

A standard approach to detect the frequencies of a given signal is to look for "peaks" of the modulus of the DFT, $p_{f,T,N}^{n_h}(j)$, which is also known as *power spectral density* in the literature. J. Laskar ([18], [20], [19]) introduced a refinement of this procedure, which consists in looking for maxima of $|\phi_{f,T,N}^{n_h}(j/T)|$, assuming that j takes real values. Additional methodology for frequency determination has been introduced in [13],[11]. It is the starting point for the methodology that will be developed here.

Our procedure is based entirely on the DFT for reasons that will be given below. The basic idea is to ask for the equality between the DFT of the sampled initial function and the DFT of its quasi–periodic approximation. It has three main steps: to get first approximations of the frequencies (either following the standard approach or using the method of Laskar), to compute the related approximated amplitudes and, finally, to perform a simultaneous improvement of frequencies and amplitudes.

2.2 First approximation of frequencies

If f has only one complex exponential term $f(t) = ae^{2\pi i \frac{\nu}{T} t}$, it follows from (1.5) that the modulus of its TCFT is

$$|\phi^{n_h}_{f,T}(\alpha/T)| = \frac{(n_h!)^2 |a| |1 - e^{i2\pi(\nu-\alpha)}|}{2\pi |\psi_{n_h}(\nu - \alpha)|}.$$

This function has a maximum at $\alpha = \nu$ (see Fig. 2.1). So, the problem of finding ν can be reduced to maximize the previous function with respect to α.

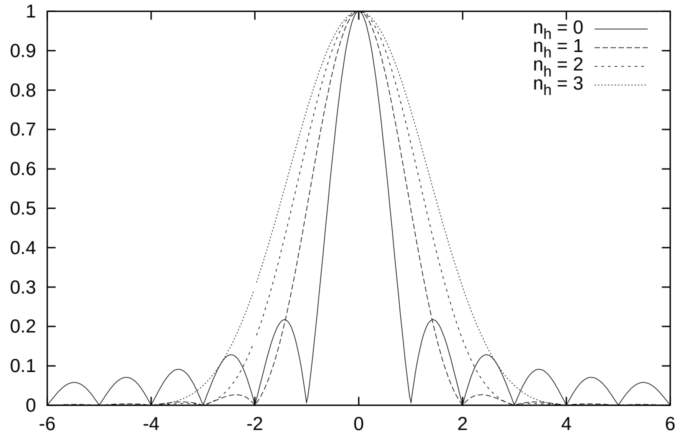

Figure 2.1: Plot of $|\phi^{n_h}_{e^{2\pi i\nu t/T},T}(\alpha/T)|$ as a function of $(\nu - \alpha)$ for $n_h = 0, 1, 2, 3$.

In a more general case, if $f(t)$ has m different frequencies,

$$f(t) = \sum_{l=1}^{m} a_l e^{2\pi i \frac{\nu_l}{T} t},$$

then $|\phi^{n_h}_{f,T}(\alpha/T)|$ does not have its maxima exactly at $\nu_1, \ldots, \nu_m$, but we can write

$$|\phi^{n_h}_{f,T}(\alpha/T) - \phi^{n_h}_{a_j e^{i2\pi\nu_j t/T},T}(\alpha/T)| \leq \sum_{\substack{l=1 \\ l\neq j}}^{m} |\phi^{n_h}_{a_l e^{i2\pi\nu_l t/T},T}(\alpha/T)|.$$

If α is close to ν_j, then $\sum_{l\neq j} |\phi^{n_h}_{a_l e^{i2\pi\nu_l t/T},T}(\alpha/T)|$ (that is, leakage from the other frequencies) will be small, so $|\phi^{n_h}_{f,T}(\alpha/T)|$ will be close to $|\phi^{n_h}_{a_j e^{i2\pi\nu_j t/T},T}(\alpha/T)|$, and therefore will have a maximum near ν_j. In this way, looking to the local maxima of the function $|\phi^{n_h}_{f,T}(\alpha/T)|^2$, we get a first procedure for computing an estimate of the frequencies. This is the method used by Laskar ([18], [20], [19]). In his procedure, used for the computation and analysis of *frequency maps* related to dynamical systems defined by the function $f(t)$, he looks for the local maxima of the function $|\phi^{n_h}_{f,T}(\alpha/T)|^2$ using some numerical quadrature formula for the evaluation of the TCFT at a discrete set of values of the argument α.

Once some values of α near the maxima have been computed, the values of the maxima are refined by interpolation.

Since leakage is responsible for the maxima of $|\phi_{f,T}^{n_h}(\alpha/T)|$ not being the true frequencies, the use of filtering improves this procedure, since it reduces leakage. However, it is not advisable to take n_h too large, since as we increase n_h the "peaks" of the TCFT become wider and may shade nearby frequencies (see Fig. 2.1).

In our procedure, we maximize the modulus of the filtered DFT of the initial function, $|F_{f,T,N}^{n_h}(j)|$ (where j may take real values), instead of approximating the TCFT using a numerical quadrature formula and maximizing this approximation. The reasons for this are:

- Although the DFT suffers from aliasing, whereas the TCFT does not, numerical quadrature formulae suffer aliasing at least as much as the DFT does. For instance, using a Newton-Côtes formula with all the sampling points as nodes, which is assumed to be written as $\int_0^T f(t)dt \approx \sum_{l=0}^{N-1} A_l f(lT/N)$, we have

$$\begin{aligned}
\phi_{f,T}^{n_h}\Big(\frac{\alpha+N}{T}\Big) &= \frac{1}{T}\int_0^T H_T^{n_h}(t)f(t)e^{\frac{-i2\pi(\alpha+N)t}{T}}dt \\
&\approx \frac{1}{T}\sum_{l=0}^{M} A_l H_T^{n_h}(l\tfrac{T}{N})f(l\tfrac{T}{N})e^{\frac{-i2\pi(\alpha+N)}{T}l\frac{T}{N}} \\
&= \frac{1}{T}\sum_{l=0}^{M} A_l H_T^{n_h}(l\tfrac{T}{N})f(l\tfrac{T}{N})e^{\frac{-i2\pi\alpha}{T}l\frac{T}{N}} \approx \phi_{f,T}^{n_h}(\frac{\alpha}{T})
\end{aligned}$$

- The use of a numerical quadrature formula does not guarantee the accuracy of the theoretical TCFT, since the error formulas include a power of the integration step, which in our case is the sampling width, and it does not need to be small. However, the DFT is close to the TCFT when there is no aliasing, as it will be shown in Lemma 3.2.4.

We use Newton's method to maximize $|F_{f,T,N}^{n_h}(j)|$. For that, we need to evaluate $\frac{\partial}{\partial j}|F_{f,T,N}^{n_h}(j)|$, and $\frac{\partial^2}{\partial j^2}|F_{f,T,N}^{n_h}(j/T)|$. Expressions for these functions can be obtained from (1.2). We take the "peaks" of the DFT as initial approximations for Newton's method. That is, given j_0 such that $p_{j_0-1} < p_{j_0} > p_{j_0+1}$, we use $\alpha = j_0$ as initial approximation.

2.3 Computation of the amplitudes assuming known frequencies

Once we know the frequencies $\{\nu_l\}_{l=1}^{N_f}$ in (2.1), we can compute the related amplitudes $\{A_l^c\}_{l=0}^{N_f}$, $\{A_l^s\}_{l=1}^{N_f}$ by asking the DFT of the current quasi–periodic approximation Q_f of f to be equal to the DFT of the sampled data $\{f(t_l)\}_{l=0}^{N-1}$. That is,

$$F_{Q_f,T,N}^{n_h}(j) = F_{f,T,N}^{n_h}(j), \tag{2.2}$$

for suitable values of j. Since we are interested in real functions, we will use the sines–cosines form of the DFT instead of the complex one. In order to get a square system for the $1+2N_f$ unknowns, we select values of j in (2.2) in such a manner that we get

$$\begin{array}{rcl} A_0^c + \sum_{l=1}^{N_f} \left(A_l^c \overline{c}_{\nu_l,N}^{n_h}(0) + A_l^s \widetilde{c}_{\nu_l,N}^{n_h}(0) \right) &=& c_{f,T,N}^{n_h}(0), \\ A_0^c c_1^{n_h}(j_i) + \sum_{l=1}^{N_f} \left(A_l^c \overline{c}_{\nu_l,N}^{n_h}(j_i) + A_l^s \widetilde{c}_{\nu_l,N}^{n_h}(j_i) \right) &=& c_{f,T,N}^{n_h}(j_i), \\ \sum_{l=1}^{N_f} \left(A_l^c \overline{s}_{\nu_l,N}^{n_h}(j_i) + A_l^s \widetilde{s}_{\nu_l,N}^{n_h}(j_i) \right) &=& s_{f,T,N}^{n_h}(j_i), \end{array} \tag{2.3}$$

where

$$\begin{array}{rclrcl} c_1^{n_h}(j) &=& c_{1,T,N}^{n_h}(j), && & \\ \overline{c}_{\nu,N}^{n_h}(j) &=& c_{\cos(\frac{2\pi\nu}{T}),T,N}^{n_h}(j), & \overline{s}_{\nu,N}^{n_h}(j) &=& s_{\cos(\frac{2\pi\nu}{T}),T,N}^{n_h}(j), \\ \widetilde{c}_{\nu,N}^{n_h}(j) &=& c_{\sin(\frac{2\pi\nu}{T}),T,N}^{n_h}(j), & \widetilde{s}_{\nu,N}^{n_h}(j) &=& s_{\sin(\frac{2\pi\nu}{T}),T,N}^{n_h}(j), \end{array} \tag{2.4}$$

and the j_i are chosen as the closest integers to ν_i, that is, such that $|j_i - \nu_i| \le 1/2$ for $i = 1 \div N_f$. Note that $c_1^{n_h}(j)$ is independent of T and N. The fact that $\overline{c}_{\nu,N}^{n_h}(j)$, $\overline{s}_{\nu,N}^{n_h}(j)$, $\widetilde{c}_{\nu,N}^{n_h}(j)$ and $\widetilde{s}_{\nu,N}^{n_h}(j)$ do not depend on T will be shown in Section 2.5.3.

In this way we get a $(1+2N_f) \times (1+2N_f)$ linear system, which, assuming that $j_i \ge 1 + n_h$ for $i = 1 \div N_f$, can be written in compact block form as

$$\begin{pmatrix} 2 & u_1 & \dots & u_{N_f} \\ 0 & B_1^1 & \dots & B_{N_f}^1 \\ \vdots & \vdots & \ddots & \vdots \\ 0 & B_1^{N_f} & \dots & B_{N_f}^{N_f} \end{pmatrix} \begin{pmatrix} A_0^c \\ v_1 \\ \vdots \\ v_{N_f} \end{pmatrix} = \begin{pmatrix} c_{f,T,N}^{n_h}(0) \\ w_1 \\ \vdots \\ w_{N_f} \end{pmatrix}, \tag{2.5}$$

where

$$\begin{array}{rclrcl} u_l &=& \left(\overline{c}_{\nu_l,N}^{n_h}(0) \quad \widetilde{c}_{\nu_l,N}^{n_h}(0) \right), & B_{i,l} &=& \begin{pmatrix} \overline{c}_{\nu_l,N}^{n_h}(j_i) & \widetilde{c}_{\nu_l,N}^{n_h}(j_i) \\ \overline{s}_{\nu_l,N}^{n_h}(j_i) & \widetilde{s}_{\nu_l,N}^{n_h}(j_i) \end{pmatrix}, \\ v_i &=& \begin{pmatrix} A_i^c \\ A_i^s \end{pmatrix}, & w_i &=& \begin{pmatrix} c_{f,T,N}^{n_h}(j_i) \\ s_{f,T,N}^{n_h}(j_i) \end{pmatrix}. \end{array} \tag{2.6}$$

Since the DFT decreases as $|\nu - j|$ goes away from zero, this system is near to block–diagonal and therefore is well conditioned. In theorem 3.4.1 we give a bound of the inverse of its coefficient matrix. Moreover, because of its structure, it is very well suited for a 2×2 block Jacobi method, which can be written, if we remove the first equation of (2.5), as

$$v_i^{(n+1)} = B_{i,i}^{-1} \Big(- \sum_{\substack{j=1 \\ j \ne i}}^{N_f} B_{i,j} v_j^{(n)} + w_i \Big), \qquad i = 1 \div N_f. \tag{2.7}$$

Once we have values for $\{A_l^c, A_l^s\}_{l=1}^{N_f}$, we can compute A_0^c from the first equation of (2.5). In corollary 3.4.1 we give a result about the convergence of this Jacobi procedure. In practice, the results have shown that the convergence is very fast when starting from the values given directly by the DFT. Usually 3 or 4 iterates of the block Jacobi method are enough for Hanning level $n_h = 2$ and a tolerance of 10^{-15} for the maximum difference between two consecutive iterates (these values correspond to the analysis of a trigonometric polynomial with three frequencies).

2.4 Simultaneous improvement of frequencies and amplitudes

Given approximations of frequencies and amplitudes, we can improve them simultaneously by solving a system of equations similar to the one used in the previous section. With respect to that system, we need now an additional equation for each frequency, since frequencies are now unknown. We therefore solve iteratively the system

$$\begin{array}{rcclclcl}
A_0^c & + & \displaystyle\sum_{l=1}^{N_f} & (& A_l^c \overline{c}_{\nu_l,N}^{n_h}(0) & + & A_l^s \widetilde{c}_{\nu_l,N}^{n_h}(0) &) = c_{f,T,N}^{n_h}(0), \\
A_0^c c_1^{n_h}(j_i) & + & \displaystyle\sum_{l=1}^{N_f} & (& A_l^c \overline{c}_{\nu_l,N}^{n_h}(j_i) & + & A_l^s \widetilde{c}_{\nu_l,N}^{n_h}(j_i) &) = c_{f,T,N}^{n_h}(j_i), \\
 & & \displaystyle\sum_{l=1}^{N_f} & (& A_l^c \overline{s}_{\nu_l,N}^{n_h}(j_i) & + & A_l^s \widetilde{s}_{\nu_l,N}^{n_h}(j_i) &) = s_{f,T,N}^{n_h}(j_i), \\
A_0^c cs_1^{n_h}(j_i^+) & + & \displaystyle\sum_{l=1}^{N_f} & (& A_l^c \overline{cs}_{\nu_l,N}^{n_h}(j_i^+) & + & A_l^s \widetilde{cs}_{\nu_l,N}^{n_h}(j_i^+) &) = cs_{f,T,N}^{n_h}(j_i^+),
\end{array} \tag{2.8}$$

for $\{\nu_l\}_{l=1}^{N_f}$, $\{A_l^c\}_{l=0}^{N_f}$, $\{A_l^s\}_{l=1}^{N_f}$, where j_i and j_i^+ are defined as

$$\begin{array}{ll}
j_i = [\nu_i],\ j_i^+ = [\nu_i] + 1 & \text{if } \nu_i - [\nu_i] \le 1/2, \\
j_i = [\nu_i] + 1,\ j_i^+ = [\nu_i] & \text{otherwise,}
\end{array}$$

for $i = 1 \div N_f$. In the last equation of (2.8), cs denotes either c or s; the criterium to choose one or the other is given bellow.

If $j_i \ge 1 + n_h$ for $i = 1 \div N_f$, the differential of (2.8) with respect to the unknowns

$$\left(A_0^c \quad \nu_1 \quad A_1^c \quad A_1^s \quad \dots \quad \nu_{N_f} \quad A_{N_f}^c \quad A_{N_f}^s \right),$$

which is needed in order to apply Newton's method, can be written as

$$M = \begin{pmatrix} 2 & v_1 & \dots & v_{N_f} \\ 0 & B_1^1 & \dots & B_{N_f}^1 \\ \vdots & \vdots & \ddots & \vdots \\ 0 & B_1^{N_f} & \dots & B_{N_f}^{N_f} \end{pmatrix},$$

being

$$\begin{aligned} v_l &= \begin{pmatrix} A_l^c \partial \overline{c}_{\nu_l,N}^{n_h}(0) + A_l^s \partial \widetilde{c}_{\nu_l,N}^{n_h}(0) & \overline{c}_{\nu_l,N}^{n_h}(0) & \widetilde{c}_{\nu_l,N}^{n_h}(0) \end{pmatrix}, \\ B_{i,l} &= \begin{pmatrix} A_l^c \partial \overline{c}_{\nu_l,N}^{n_h}(j_i) + A_l^s \partial \widetilde{c}_{\nu_l,N}^{n_h}(j_i) & \overline{c}_{\nu_l,N}^{n_h}(j_i) & \widetilde{c}_{\nu_l,N}^{n_h}(j_i) \\ A_l^c \partial \overline{s}_{\nu_l,N}^{n_h}(j_i) + A_l^s \partial \widetilde{s}_{\nu_l,N}^{n_h}(j_i) & \overline{s}_{\nu_l,N}^{n_h}(j_i) & \widetilde{s}_{\nu_l,N}^{n_h}(j_i) \\ A_l^c \partial \overline{cs}_{\nu_l,N}^{n_h}(j_i^+) + A_l^s \partial \widetilde{cs}_{\nu_l,N}^{n_h}(j_i^+) & \overline{cs}_{\nu_l,N}^{n_h}(j_i^+) & \widetilde{cs}_{\nu_l,N}^{n_h}(j_i^+) \end{pmatrix}, \end{aligned} \tag{2.9}$$

where ∂ denotes derivative with respect to ν. As in the preceding section, this matrix is close to block–diagonal and, therefore, the system to be solved at each Newton iteration is well conditioned.

For each block $B_{i,l}$, the criterium to choose cs from c and s is to set it equal to the one that minimizes $\|B_{i,i}^{-1}\|_\infty$. This further improves the well–conditioning of the system, and is theoretically justified in Section 3 (Lemma 3.2.9).

With the exception of rounding errors, the only source of error in this procedure is the leakage from frequencies that we are skipping, as will be shown in Section 3. In particular, this method is exact for trigonometric polynomials (the combination of the procedures of Sections 2.2 and 2.3 is not).

As a final remark note that, because of the use of the DFT, both this procedure and the one of the previous section suffer from the aliasing effect introduced in Section 1.3.

2.5 Implementation details

In this section we give some details for the implementation of the procedures described in the previous section.

2.5.1 Algorithm for the procedure

Starting from the sampling $\{f(t_l)\}_{l=0}^{N-1}$ of a function which is known to have a quasi–periodic behavior, we carry out its Fourier analysis by finding initial approximations for the frequencies using the procedure of Section 2.2, obtaining the related amplitudes using Section 2.3 and iteratively refining the approximations of frequencies and amplitudes through Section 2.4.

In order to prevent some frequencies to "hide" nearby frequencies of lower amplitude, it is advisable to proceed iteratively, in such a way that at each iteration we only consider those frequencies whose amplitude is greater than a given tolerance.

Concretely, the algorithm used for the numerical examples of the last section is the following.

Algorithm 2.5.1 *Provided a minimum amplitude b_{min} for the frequencies to be computed, and a number of iterations n for the procedure, first define*

$$p_{max} = \max_{j=1\div\frac{N}{2}} p_{f,T,N}^{n_h}(j), \qquad db = (b_{min}/p_{max})^{1/n},$$

where $p_{f,T,N}^{n_h}(j) = ((c_{f,T,N}^{n_h}(j))^2 + (s_{f,T,N}^{n_h}(j))^2)^{1/2}$, and set

$$Q_f(t) = 0, \qquad b = p_{max}, \qquad N_f = 0.$$

$Q_f(t)$ will be the current quasi–periodic approximation of f, b the minimum amplitude of the frequencies to be detected in the current iteration, and N_f the number of frequencies computed. Then, while $b > b_{min}$, proceed as:

1. *Set $b \leftarrow b{\cdot}db$. Let $k_{N_f+1}, \ldots, k_{N_f+m}$ be the peaks of the modulus of the DFT of $f - Q_f$ with minimum amplitude b, that is, $\{k_{N_f+1}, \ldots k_{N_f+m}\} = \{j \in \mathbb{Z} : n_h + 2 \le j \le \frac{N}{2} - n_h - 2,\ p^{n_h}_{f-Q_f,T,N}(j) \ge b,\ p^{n_h}_{f-Q_f,T,N}(j-1) \le p^{n_h}_{f-Q_f,T,N}(j) \ge p^{n_h}_{f-Q_f,T,N}(j+1)\}$. For each k_l, apply the procedure of Section 2.2 to obtain ν_l.*

2. *Solve (2.3), according to Section 2.3, to get $\{A^c_l\}_{l=0}^{N_f+m}$ and $\{A^s_l\}_{l=1}^{N_f+m}$ from $\{\nu_l\}_{l=1}^{N_f+m}$.*

3. *Solve (2.8), according to Section* 2.4 *to iteratively refine $\{\nu_l\}_{l=1}^{N_f+m}$, $\{A^c_l\}_{l=0}^{N_f+m}$ and $\{A^s_l\}_{l=1}^{N_f+m}$.*

4. *Update the number of frequencies and the current quasi–periodic approximation,*

$$N_f \leftarrow N_f + m, \qquad Q_f(t) \leftarrow A^c_0 + \sum_{l=1}^{N_f} (A^c_l \cos(\frac{2\pi\nu_l t}{T}) + A^s_l \sin(\frac{2\pi\nu_l t}{T}))$$

   and go to step 1.

We stop the algorithm if

- *N_f reaches a given maximum number of frequencies, or if*
- $\max_{l=0\div N-1} |f(t_l) - Q_f(t_l)|$ *is under a given tolerance, or if*
- $\max_{j=0\div j/2} p^{n_h}_{f-Q_f,T,N}(j)$ *is under a given tolerance, or if*
- *there appear two frequencies too close. We usually consider ν_{l_1}, ν_{l_2} to be too close if $|\nu_{l_1} - \nu_{l_2}| < 2 + n_h$.*

In practice, the DFT approximation is good enough for Newton's method of Section 2.4 to converge. That is, we can skip the preliminary determination of the frequencies of Section 2.2 by setting $\nu_l = k_l$ in step 1, and then compute the amplitudes related to these frequencies following step 2. It may be useful to use the procedure of Section 2.2 anyway when N_f is very large and we want to save some Newton iterates in step 3, since we have to solve a $(1 + 3N_f) \times (1 + 3N_f)$ linear system at each Newton iterate.

2.5.2 Use of trigonometric recurrences

Large amounts of computing time can be saved if we avoid the evaluation of the sin and cos functions when we have to evaluate the DFT using its definition in the procedure of Section 2.2, or when we have to compute $\{f(t_l) - Q_f(t_l)\}_{l=0}^{N-1}$ in step 1 of the algorithm given above. This can be accomplished through the use of trigonometric recurrences for the evaluation of $\cos(lx)$ and $\sin(lx)$ for $l \in \mathbb{N}$ and $x \in \mathbb{R}$. One has to be careful in choosing such recurrences, in order to avoid numerical instability (see [29] for a discussion). The recurrence we have used is given in [29], p. 24: first set

$$dc_1 := -2\sin^2\frac{x}{2}, \quad t := 2dc_1, \quad ds_1 := \sqrt{-dc_1(2+dc_1)}, \quad s_0 := 0, \quad c_0 := 1,$$

and then compute, for $m := 1, 2, \ldots$,

$$\begin{array}{rcll} c_m & := & c_{m-1} + dc_m, & dc_{m+1} := t \cdot c_m + dc_m, \\ s_m & := & s_{m-1} + ds_m, & ds_{m+1} := t \cdot s_m + ds_m. \end{array}$$

Just for illustrating purposes, we compare in Fig. 2.2 the errors produced by the trigonometric recurrence previously given with the following one: first set

$$cc_0 = 1, \quad cc_1 = \cos x, \quad ss_0 = 0, \quad ss_1 = \sin x,$$

and then compute, for $m := 2, 3, \ldots$,

$$\begin{array}{rcl} cc_{m+1} & = & (2\cos x)cc_m - cc_{m-1}, \\ ss_{m+1} & = & (2\cos x)ss_m - ss_{m-1}. \end{array}$$

2.5.3 Evaluation of the DFT of sines and cosines

Special care must be taken in the evaluation of the DFT of sines and cosines, in order to avoid cancellations and singularities. In this section we describe some of the strategies followed in our implementation, especially those related to small values of $\nu - j$.

The DFT of sines and cosines can be evaluated from the complex DFT of a complex exponential term through the following formulae:

$$\begin{array}{rcl} \overline{c}^{n_h}_{\nu,N}(j) & = & \operatorname{Re} F^{n_h}_{e^{i2\pi\nu t/T},T,N}(j) + \operatorname{Re} F^{n_h}_{e^{i2\pi(-\nu)t/T},T,N}(j), \\ \overline{s}^{n_h}_{\nu,N}(j) & = & -\operatorname{Im} F^{n_h}_{e^{i2\pi\nu t/T},T,N}(j) - \operatorname{Im} F^{n_h}_{e^{i2\pi(-\nu)t/T},T,N}(j), \\ \widetilde{c}^{n_h}_{\nu,N}(j) & = & \operatorname{Im} F^{n_h}_{e^{i2\pi\nu t/T},T,N}(j) - \operatorname{Im} F^{n_h}_{e^{i2\pi(-\nu)t/T},T,N}(j), \\ \widetilde{s}^{n_h}_{\nu,N}(j) & = & \operatorname{Re} F^{n_h}_{e^{i2\pi\nu t/T},T,N}(j) - \operatorname{Re} F^{n_h}_{e^{i2\pi(-\nu)t/T},T,N}(j). \end{array}$$

Derivating with respect to ν, we get similar relations that allow to obtain $\partial\overline{c}^{n_h}_{\nu,T,N}(j)$, $\partial\widetilde{c}^{n_h}_{\nu,T,N}(j)$, $\partial\overline{s}^{n_h}_{\nu,T,N}(j)$, $\partial\widetilde{s}^{n_h}_{\nu,T,N}(j)$ from $\partial F^{n_h}_{e^{i2\pi(-\nu)t/T},T,N}(j)$. As before, ∂ denotes derivative with respect to ν.

The non-filtered complex DFT of a complex exponential term is a geometric progression,

$$F_{e^{i2\pi\nu t/T},T,N}(j) = \frac{1}{N}\sum_{l=0}^{N-1} e^{i2\pi(\nu-j)l/N} = \frac{1-e^{i2\pi(\nu-j)}}{N(1-e^{i2\pi(\nu-j)/N})},$$

and its derivative with respect to ν is

$$\partial F^{n_h}_{e^{i2\pi\nu t/T},T,N}(j) = \frac{i2\pi}{N} \cdot \frac{\frac{1}{N}e^{i2\pi(\nu-j)} - e^{i2\pi(\nu-j)} + \frac{N-1}{N}e^{i2\pi(N+1)(\nu-j)/N}}{(1-e^{i2\pi(\nu-j)/N})^2}.$$

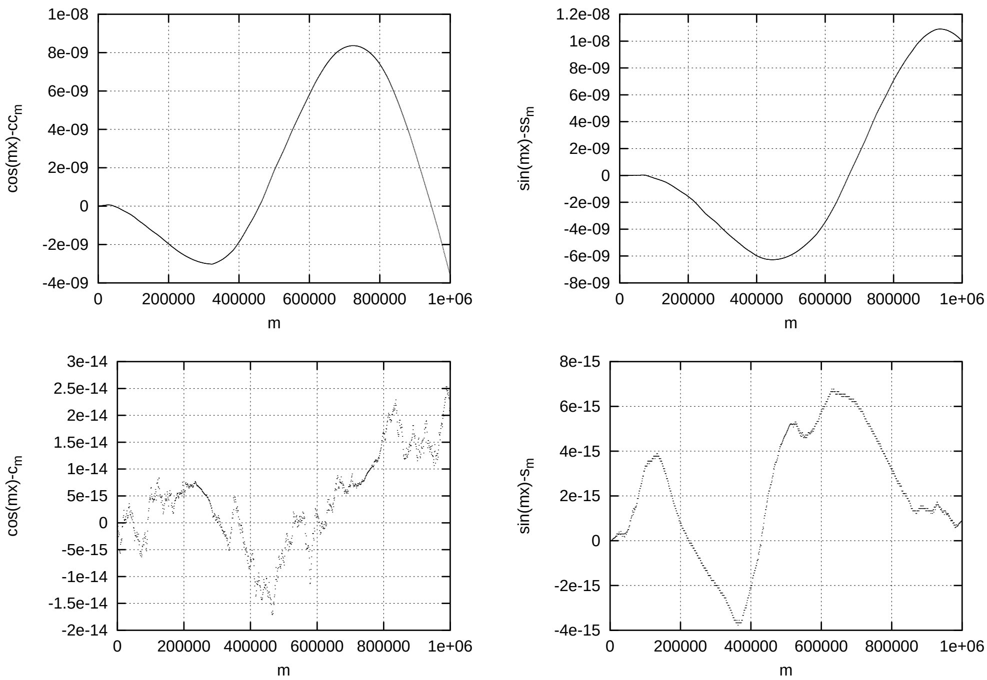

Figure 2.2: Illustration of the numerical instability of trigonometric recurrences. For $x = 2\pi \times 10^{-6}$ and $n = 10^6$, we have evaluated $\{\cos(mx), \sin(mx)\}_{m=0}^{n}$ and the values $\{c_m, s_m\}_{m=0}^{n}$ and $\{cc_m, ss_m\}_{m=0}^{n}$ using the recurrences detailed in the text. In the left–hand plots we show the differences $\cos(mx) - cc_m$ (top) and $\cos(mx) - c_m$ (bottom). In the right–hand ones, we show the differences $\sin(mx) - ss_m$ (top) and $\sin(mx) - s_m$. These values are machine and compiler–dependent. The program that has computed these plots has been compiled with GNU gcc 2.95.2 with the optimization option '–O3' on an Intel Pentium II processor.

Using the relations of Lemma 1.2.1 and its derivatives, we can get the filtered complex DFT of $e^{i2\pi\nu t/T}$, as well as its derivatives with respect to ν, from the non–filtered values.

The computation of $F_{e^{i2\pi\nu t/T},T,N}(j)$ is organized as follows:

$$F_{e^{i2\pi\nu t/T},T,N}(j) = \frac{1}{N}\Big(\frac{ac+bd}{c^2+d^2} + i\frac{bc-ad}{c^2+d^2}\Big),$$

being

$$\begin{aligned} a &= 1-\cos(2\pi(\nu-j)) = 2\sin^2(\pi(\nu-j)), & b &= -\sin(2\pi(\nu-j)), \\ c &= 1-\cos(2\pi(\nu-j)/N) = 2\sin^2(\pi(\nu-j)/N), & d &= -\sin(2\pi(\nu-j)/N). \end{aligned}$$

For a and c, we use the second expressions in order to avoid cancellations.

Concerning to $\partial F_{e^{i2\pi\nu t/T},T,N}(j)$, we compute it as

$$\partial F_{e^{i2\pi\nu t/T},T,N}(j) = \frac{2\pi}{N}\Big(\frac{ad-bc}{c^2+d^2} + i\frac{ac+bd}{c^2+d^2}\Big),$$

being

$$\begin{aligned} a &= \frac{1}{N}\cos\Big(\frac{2\pi(\nu-j)}{N}\Big) - \cos(2\pi(\nu-j)) + \frac{N-1}{N}\cos\Big(\frac{2\pi(N+1)(\nu-j)}{N}\Big) \\ &= \frac{2}{N}\sin\Big(\frac{\pi(2+N)(\nu-j)}{N}\Big)\sin(\pi(\nu-j)) - 2\sin\Big(\frac{\pi(2N+1)(\nu-j)}{N}\Big)\sin\Big(\frac{\pi(\nu-j)}{N}\Big), \\ b &= \frac{1}{N}\sin\Big(\frac{2\pi(\nu-j)}{N}\Big) - \sin(2\pi(\nu-j)) - 2\sin\Big(\frac{\pi(2N+1)(\nu-j)}{N}\Big)\sin\Big(\frac{\pi(\nu-j)}{N}\Big) \\ &= -\frac{2}{N}\cos\Big(\frac{\pi(2+N)(\nu-j)}{N}\Big)\sin(\pi(\nu-j)) + 2\cos\Big(\frac{2\pi(N+1)(\nu-j)}{N}\Big)\sin\Big(\frac{\pi(\nu-j)}{N}\Big), \\ e &= 1-\cos\Big(\frac{2\pi(\nu-j)}{N}\Big) = 2\sin^2\Big(\frac{\pi(\nu-j)}{N}\Big), \\ f &= -\sin\Big(\frac{2\pi(\nu-j)}{N}\Big), \\ c &= e^2-f^2, \\ d &= 2ef. \end{aligned}$$

As before, for a, b, and e we use the second form in order to avoid cancellations, although the second expression of b does not remove cancellations completely.

Since $F_{e^{i2\pi\nu t/T},T,N}(j) = h(\nu-j)$, being

$$h(\alpha) = \frac{1}{N}\sum_{l=0}^{N-1} e^{i2\pi\alpha l/N} = \frac{1-e^{i2\pi\alpha}}{N(1-e^{i2\pi\alpha/N})},$$

we can use the Taylor expansion of h to evaluate $F_{e^{i2\pi\nu t/T},T,N}(j)$ and $\partial F_{e^{i2\pi\nu t/T},T,N}(j)$ for $|\nu-j|$ small. Indeed, we could use this Taylor expansion for any $|\nu-j|$, because h is an entire function (it is a finite sum of exponentials), but the convergence of the expansion is slow for large $|\nu-j|$. We have set a threshold δ in such a way that for $|\nu-j|\geq\delta$ we use the previous formulation and for $|\nu-j|<\delta$ we use the Taylor expansion. The value of δ is chosen in order to have fast convergence of the Taylor expansion and a small error due to the cancellation in the second expression of b. We have taken $\delta = 0.1$, since

$$\lim_{N\to\infty} \frac{-\beta+\gamma}{\beta} = 0.1563,$$

being

$$\beta = \frac{2}{N}\cos\Big(\frac{\pi(2+N)\delta}{N}\Big)\sin(\pi\delta), \qquad \gamma = 2\cos\Big(\frac{2\pi(N+1)\delta}{N}\Big)\sin\Big(\frac{\pi\delta}{N}\Big),$$

and, in this way, the maximum loss of precision due to the cancellation of the second expression of b is one order of magnitude. Moreover, since

$$\Big|\frac{h^{(k)}(0)}{k!}\delta^k\Big| \leq \frac{(2\pi)^k}{(k+1)!}|\delta|^k,$$

the convergence of the Taylor expansion is fast for $|\nu - j| < \delta$.

For the evaluation of the Taylor expansion of h, we have used that

$$h^{(k)}(0) = \frac{(i2\pi)^k}{N^{k+1}} \sum_{l=0}^{N-1} l^k,$$

and, for $k \geq 1$,

$$\sum_{l=1}^{N-1} l^k = \frac{(N-1)^{k+1}}{k+1} + \frac{(N-1)^k}{2} + \frac{1}{2}\binom{k}{1}B_2(N-1)^{k-1} + \frac{1}{4}\binom{k}{3}B_4(N-1)^{k-3} + \dots,$$

where the sum ends at either $N-1$ or $(N-1)^2$, and B_i are the Bernoulli numbers.

Chapter 3

Error estimates

In this Chapter we develop error estimates for the numerical procedure described in the previous Chapter. We cover both the case of computation of the amplitudes from known frequencies and the iterative improvement of frequencies and amplitudes. The Chapter is ended with Theorem 3.4.1, which gives bounds for the error of our Fourier analysis procedure in terms of the parameters used for the analysis and the properties of the analyzed function.

3.1 Introduction and notation

In order to derive error bounds, we will assume through this section that the function f to be analyzed is real analytic and quasi–periodic, that is

$$f(t) = \sum_{k\in\mathbb{Z}^m} a_k e^{i2\pi k\omega t} = A_0^c + \sum_{\substack{k\in\mathbb{Z}^m\\ k\omega>0}} \left(A_k^c \cos(2\pi k\omega t) + A_k^s \sin(2\pi k\omega t)\right) \tag{3.1}$$

where $k\omega = k_1\omega_1 + \ldots + k_m\omega_m$, $A_k = 2\operatorname{Re} a_k$, $B_k = -2\operatorname{Im} a_k$, the frequency vector $\omega = (\omega_1, \ldots, \omega_m)$ is assumed to satisfy a Diophantine condition of the form

$$|k\omega| \geq \frac{D}{|k|^\tau}, \tag{3.2}$$

with $D, \tau > 0$, and the Fourier coefficients of f satisfy the *Cauchy estimates*,

$$|a_k| \leq Ce^{-\delta|k|}, \quad \forall k \in \mathbb{Z}^m. \tag{3.3}$$

We will also assume that we want to compute the frequencies of f up to order $|k| \leq r_0 - 1$ as well as its related amplitudes. That is, we want to approximate f by a trigonometric polynomial

$$p(t) = A_0^c + \sum_{l=1}^{N_f}(A_l^c \cos(\frac{2\pi\nu_l}{T}t) + A_l^s \sin(\frac{2\pi\nu_l}{T}t)),$$

being

$$\{\nu_1, \ldots, \nu_{N_f}\} = \{Tk\omega : k \in \mathbb{Z}^m, 1 \leq |k| \leq r_0 - 1, Tk\omega > 0\}. \tag{3.4}$$

We will give error bounds for two cases: the case in which we want to compute the amplitudes from known frequencies (Section 2.3) and the case in which both frequencies and amplitudes are unknown (Section 2.4). In order to perform error analysis for the second case, we split the right–hand side of (2.8) and rewrite it as

$$\begin{aligned}
A_0^c + \sum_{l=1}^{N_f} (A_l^c \overline{c}_{\nu_l,N}^{n_h}(0) + A_l^s \widetilde{c}_{\nu_l,N}^{n_h}(0)) &= c_{p,T,N}^{n_h}(0) + c_{f-p,T,N}^{n_h}(0) \\
A_0^c c_1^{n_h}(j_i) + \sum_{l=1}^{N_f} (A_l^c \overline{c}_{\nu_l,N}^{n_h}(j_i) + A_l^s \widetilde{c}_{\nu_l,N}^{n_h}(j_i)) &= c_{p,T,N}^{n_h}(j_i) + c_{f-p,T,N}^{n_h}(j_i) \\
\sum_{l=1}^{N_f} (A_l^c \overline{s}_{\nu_l,N}^{n_h}(j_i) + A_l^s \widetilde{s}_{\nu_l,N}^{n_h}(j_i)) &= s_{p,T,N}^{n_h}(j_i) + s_{f-p,T,N}^{n_h}(j_i) \\
\underbrace{A_0^c cs_1^{n_h}(j_i^+) + \sum_{l=1}^{N_f} (A_l^c \overline{cs}_{\nu_l,N}^{n_h}(j_i^+) + A_l^s \widetilde{cs}_{\nu_l,N}^{n_h}(j_i^+))}_{g(y+\Delta y)} &= \underbrace{cs_{p,T,N}^{n_h}(j_i^+)}_{b} + \underbrace{cs_{f-p,T,N}^{n_h}(j_i^+)}_{\Delta b} .
\end{aligned} \tag{3.5}$$

We would get the exact frequencies and amplitudes, which we denote as y for short, if we solved $g(y) = b$. But the system to be solved is $g(y+\Delta y) = b+\Delta b$, and therefore the error we have (assuming no rounding errors) can be bounded (in the first order approximation) by

$$\|\Delta y\|_\infty \lesssim \|Dg(y)^{-1}\|_\infty \|\Delta b\|_\infty$$

A similar argument is applied to the case in which the frequencies are known and we want to compute the amplitudes. In this case, g, y, Δy, b and Δb are defined as

$$\begin{aligned}
A_0^c + \sum_{l=1}^{N_f} (A_l^c \overline{c}_{\nu_l,N}^{n_h}(0) + A_l^s \widetilde{c}_{\nu_l,N}^{n_h}(0)) &= c_{p,T,N}^{n_h}(0) + c_{f-p,T,N}^{n_h}(0) \\
A_0^c c_1^{n_h}(j_i) + \sum_{l=1}^{N_f} (A_l^c \overline{c}_{\nu_l,N}^{n_h}(j_i) + A_l^s \widetilde{c}_{\nu_l,N}^{n_h}(j_i)) &= c_{p,T,N}^{n_h}(j_i) + c_{f-p,T,N}^{n_h}(j_i) \\
\underbrace{\sum_{l=1}^{N_f} (A_l^c \overline{s}_{\nu_l,N}^{n_h}(j_i) + A_l^s \widetilde{s}_{\nu_l,N}^{n_h}(j_i))}_{g(y+\Delta y)} &= \underbrace{s_{p,T,N}^{n_h}(j_i)}_{b} + \underbrace{s_{f-p,T,N}^{n_h}(j_i)}_{\Delta b} .
\end{aligned} \tag{3.6}$$

This section is devoted to the computation of bounds for $\|Dg(y)^{-1}\|_\infty$ and $\|\Delta b\|_\infty$ in terms of T, N, n_h and the properties of the analyzed function f. From now on, and unless otherwise stated, we will use the supremum norm.

3.2 Error bounds for $\|Dg(y)^{-1}\|_\infty$

In order to simplify the expressions to be manipulated, we will bound the TCFT instead of the DFT. That is, we will use $\mathcal{C}_{f,T}^{n_h}$ and $\mathcal{S}_{f,T}^{n_h}$ defined by

$$\phi_{f,T}^{n_h}(\frac{j}{T}) = \frac{1}{2}(\mathcal{C}_{f,T}^{n_h}(j) - i\mathcal{S}_{f,T}^{n_h}(j)), \tag{3.7}$$

(here $i = \sqrt{-1}$). As in the discrete case (2.4), we will note

$$
\begin{array}{rclrcl}
\mathcal{C}_1^{n_h}(j) & = & \mathcal{C}_{1,T,N}^{n_h}(j), & & & \\
\overline{\mathcal{C}}_\nu^{n_h}(j) & = & \mathcal{C}^{n_h}_{\cos(\frac{2\pi\nu t}{T}),T}(j), & \overline{\mathcal{S}}_\nu^{n_h}(j) & = & \mathcal{S}^{n_h}_{\cos(\frac{2\pi\nu t}{T}),T}(j), \\
\widetilde{\mathcal{C}}_\nu^{n_h}(j) & = & \mathcal{C}^{n_h}_{\sin(\frac{2\pi\nu t}{T}),T}(j), & \widetilde{\mathcal{S}}_\nu^{n_h}(j) & = & \mathcal{S}^{n_h}_{\sin(\frac{2\pi\nu t}{T}),T}(j),
\end{array}
$$

and the derivatives of $\overline{\mathcal{C}}_\nu^{n_h}(j)$, $\overline{\mathcal{S}}_\nu^{n_h}(j)$, $\widetilde{\mathcal{C}}_\nu^{n_h}(j)$ and $\widetilde{\mathcal{S}}_\nu^{n_h}(j)$ with respect to ν will be denoted as $\partial\overline{\mathcal{C}}_\nu^{n_h}(j)$, $\partial\overline{\mathcal{S}}_\nu^{n_h}(j)$, $\partial\widetilde{\mathcal{C}}_\nu^{n_h}(j)$ and $\partial\widetilde{\mathcal{S}}_\nu^{n_h}(j)$, respectively. We give expressions for these transforms in the following

Lemma 3.2.1 *Denote* $\psi_{n_h}(x) = \prod_{l=-n_h}^{n_h}(x+l)$. *We have*

$$
\begin{aligned}
\overline{\mathcal{C}}_\nu^{n_h}(j) &= \frac{(-1)^{n_h}(n_h!)^2}{2\pi}\Big(\frac{\sin(2\pi(\nu-j))}{\psi_{n_h}(\nu-j)} + \frac{\sin(2\pi(-\nu-j))}{\psi_{n_h}(-\nu-j)}\Big), \\
\widetilde{\mathcal{C}}_\nu^{n_h}(j) &= \frac{(-1)^{n_h}(n_h!)^2}{2\pi}\Big(\frac{1-\cos(2\pi(\nu-j))}{\psi_{n_h}(\nu-j)} - \frac{1-\cos(2\pi(-\nu-j))}{\psi_{n_h}(-\nu-j)}\Big), \\
\overline{\mathcal{S}}_\nu^{n_h}(j) &= \frac{(-1)^{n_h}(n_h!)^2}{2\pi}\Big(-\frac{1-\cos(2\pi(\nu-j))}{\psi_{n_h}(\nu-j)} - \frac{1-\cos(2\pi(-\nu-j))}{\psi_{n_h}(-\nu-j)}\Big), \\
\widetilde{\mathcal{S}}_\nu^{n_h}(j) &= \frac{(-1)^{n_h}(n_h!)^2}{2\pi}\Big(\frac{\sin(2\pi(\nu-j))}{\psi_{n_h}(\nu-j)} - \frac{\sin(2\pi(-\nu-j))}{\psi_{n_h}(-\nu-j)}\Big), \\
\partial\overline{\mathcal{C}}_\nu^{n_h}(j) &= \frac{(-1)^{n_h}(n_h!)^2}{2\pi}\Big(\frac{h_r(\nu-j)}{\psi_{n_h}(\nu-j)} - \frac{h_r(-\nu-j)}{\psi_{n_h}(-\nu-j)}\Big), \\
\partial\widetilde{\mathcal{C}}_\nu^{n_h}(j) &= \frac{(-1)^{n_h}(n_h!)^2}{2\pi}\Big(\frac{h_i(\nu-j)}{\psi_{n_h}(\nu-j)} + \frac{h_i(-\nu-j)}{\psi_{n_h}(-\nu-j)}\Big), \\
\partial\overline{\mathcal{S}}_\nu^{n_h}(j) &= \frac{(-1)^{n_h}(n_h!)^2}{2\pi}\Big(-\frac{h_i(\nu-j)}{\psi_{n_h}(\nu-j)} + \frac{h_i(-\nu-j)}{\psi_{n_h}(-\nu-j)}\Big), \\
\partial\widetilde{\mathcal{S}}_\nu^{n_h}(j) &= \frac{(-1)^{n_h}(n_h!)^2}{2\pi}\Big(\frac{h_r(\nu-j)}{\psi_{n_h}(\nu-j)} + \frac{h_r(-\nu-j)}{\psi_{n_h}(-\nu-j)}\Big),
\end{aligned}
$$

where

$$
\begin{aligned}
h_r(x) &= 2\pi\cos(2\pi x) - r_{n_h}(x)\sin(2\pi x), \\
h_i(x) &= 2\pi\sin(2\pi x) - r_{n_h}(x)(1-\cos(2\pi x)), \\
r_{n_h}(x) &= \sum_{l=-n_h}^{n_h}\frac{1}{x+l} = \frac{\psi'_{n_h}(x)}{\psi_{n_h}(x)}.
\end{aligned}
$$

Proof: We have

$$
\begin{aligned}
\overline{\mathcal{C}}_\nu^{n_h}(j) &= \mathcal{C}^{n_h}_{\cos(2\pi\nu t/T),T}(j) \overset{(3.7)}{=} 2\,\mathrm{Re}\,\phi^{n_h}_{\cos(2\pi\nu t/T),T}(j/T) \\
&= 2\,\mathrm{Re}\,\phi^{n_h}_{(e^{i2\pi\nu t/T}+e^{i2\pi(-\nu)t/T})/2,T}(j/T) \\
&= \mathrm{Re}\,\phi^{n_h}_{e^{i2\pi\nu t/T},T}(j/T) + \mathrm{Re}\,\phi^{n_h}_{e^{i2\pi(-\nu)t/T},T}(j/T),
\end{aligned}
$$

$$\begin{aligned}
\widetilde{\mathcal{C}}_\nu^{n_h}(j) &= \quad \operatorname{Im}\phi^{n_h}_{e^{i2\pi\nu t/T},T}(j/T) - \operatorname{Im}\phi^{n_h}_{e^{i2\pi(-\nu)t/T},T}(j/T),\\
\overline{\mathcal{S}}_\nu^{n_h}(j) &= -\operatorname{Im}\phi^{n_h}_{e^{i2\pi\nu t/T},T}(j/T) - \operatorname{Im}\phi^{n_h}_{e^{i2\pi(-\nu)t/T},T}(j/T),\\
\widetilde{\mathcal{S}}_\nu^{n_h}(j) &= \quad \operatorname{Re}\phi^{n_h}_{e^{i2\pi\nu t/T},T}(j/T) - \operatorname{Re}\phi^{n_h}_{e^{i2\pi(-\nu)t/T},T}(j/T).
\end{aligned}$$

Then, the lemma follows from (1.5) and

$$\frac{d}{d\nu}\phi^{n_h}_{e^{i2\pi\nu t/T},T}(j/T) = \frac{(-1)^{n_h}(n_h!)^2}{2\pi\psi_{n_h}(\nu-j)}\Big(2\pi e^{i2\pi(\nu-j)} - i(1-e^{i2\pi(\nu-j)})\sum_{l=-n_h}^{n_h}\frac{1}{\nu-j+l}\Big).$$

$\square$

In order to bound the error due to the approximation of the DFT by the TCFT, we need the following lemmas.

Lemma 3.2.2 *(Discrete Poisson summation formula) If $n_h \geq 1$, we have*

$$F^{n_h}_{f,T,N}(j) = \sum_{l=-\infty}^{\infty}\phi^{n_h}_{f,T}\Big(\frac{j+lN}{T}\Big).$$

In particular, $\overline{c}^{n_h}_{\nu,N}(j) = \sum_{l=-\infty}^{\infty}\overline{c}^{n_h}_{\nu}(j+lN)$, and analogous identities hold for $\widetilde{c}^{n_h}_{\nu,N}(j)$, $\overline{s}^{n_h}_{\nu,N}(j)$, $\widetilde{s}^{n_h}_{\nu,N}(j)$, and their derivatives with respect to ν.

Proof: This is a known result (see, for instance, [5]). We give a proof here for completeness, and also to clarify the need for the hypothesis $n_h \geq 1$.

We first note that, by definition of the TCFT, the Fourier expansion of $H^{n_h}_T(t)f(t)$ with respect to the interval $[0,T]$ is

$$\sum_{k=-\infty}^{\infty}\phi^{n_h}_{f,T}(\frac{k}{T})e^{\frac{i2\pi kt}{T}}.$$

The function $H^{n_h}_T(t)f(t)$ coincides with its Fourier expansion for all $t \in [0,T]$ because, since $n_h \geq 1$, we have $H^{n_h}_T(0)f(0) = H^{n_h}_T(T)f(T) = 0$.

Then, using the definition (1.2) of the complex DFT and the above Fourier expansion,

$$\begin{aligned}
F^{n_h}_{f,T,N}(j) &= \frac{1}{N}\sum_{l=0}^{N-1}\Big(\sum_{k=-\infty}^{\infty}\phi^{n_h}_{f,T}(\frac{k}{T})e^{\frac{i2\pi k}{T}l\frac{T}{N}}\Big)e^{-\frac{i2\pi j}{T}l\frac{T}{N}}\\
&= \frac{1}{N}\sum_{k=-\infty}^{\infty}\phi^{n_h}_{f,T}(\frac{k}{T})\sum_{l=0}^{N-1}e^{\frac{i2\pi(k-j)l}{N}},
\end{aligned}$$

and the lemma follows from the fact that the inner sum above is equal to N if $k-j$ is an integer multiple of N and zero otherwise. $\square$

Lemma 3.2.3 *For $|x| \geq n_h + 2$ we have*

$$\begin{aligned} |r_{n_h}(x)| &\leq \ln(|x|+n_h) - \ln(|x|-n_h-1), \\ |h_r(x)|, |h_i(x)| &\leq 2\pi + 2(\ln(|x|+n_h) - \ln(|x|-n_h-1)). \end{aligned}$$

Proof: For the first inequality, we have

$$|r_{n_h}(x)| = \sum_{l=-n_h}^{n_h} \frac{1}{|x|+l} \leq \int_{|x|-n_h}^{|x|+n_h+1} \frac{1}{z-1} dz = \ln(|x|+n_h) - \ln(|x|-n_h-1).$$

The bounds for $|h_r(x)|, |h_i(x)|$ follow from this one. □

Lemma 3.2.4 *For $j \geq 0$, $N-j-|\nu|-n_h > 0$, we have*

$$|F^{n_h}_{e^{i2\pi\nu t/T},T,N}(j) - \phi^{n_h}_{e^{i2\pi\nu t/T},T,N}(\frac{j}{T})| \leq \frac{2(n_h!)^2(1+\frac{1}{2n_h})}{\pi(N-j-|\nu|-n_h)^{1+2n_h}},$$

for $j, \nu \geq 0$, $N-j-\nu-n_h > 0$,

$$|\widetilde{\overline{cs}}^{n_h}_{\nu,N}(j) - \widetilde{\overline{\mathcal{CS}}}^{n_h}_{\nu}(j)| \leq \frac{4(n_h!)^2(1+\frac{1}{2n_h})}{\pi(N-j-\nu-n_h)^{1+2n_h}},$$

and for $j, \nu \geq 0$, $N-j-\nu-n_h \geq 2$,

$$|\partial\widetilde{\overline{cs}}^{n_h}_{\nu,N}(j) - \partial\widetilde{\overline{\mathcal{CS}}}^{n_h}_{\nu}(j)| \leq \frac{4(n_h!)^2(1+\frac{1}{2n_h})(\pi+\ln(N-j-\nu+n_h) - \ln(N-j-\nu-n_h-1))}{\pi(N-j-\nu-n_h)^{1+2n_h}}.$$

In the previous expressions, $\widetilde{\overline{cs}}$ denotes one of $\overline{c}$, $\widetilde{c}$, $\overline{s}$, $\widetilde{s}$, and $\widetilde{\overline{\mathcal{CS}}}$ denotes one of $\overline{\mathcal{C}}$, $\widetilde{\mathcal{C}}$, $\overline{\mathcal{S}}$, $\widetilde{\mathcal{S}}$.

Proof: For the first inequality, using the Discrete Poisson summation formula (Lemma 3.2.2),

$$\begin{aligned} |F^{n_h}_{e^{i2\pi\nu t/T},T,N}(j) - \phi^{n_h}_{e^{i2\pi\frac{\nu}{T}t},T}(\frac{j}{T})| &\leq \sum_{l=1}^{\infty}\Big(|\phi^{n_h}_{e^{i2\pi\frac{\nu}{T}t},T}(\frac{j+lN}{T})| + |\phi^{n_h}_{e^{i2\pi\frac{\nu}{T}t},T}(\frac{j-lN}{T})|\Big) \\ &\overset{(1.5)}{\leq} \sum_{l=1}^{\infty}\Big(\frac{(n_h!)^2}{\pi\psi_{n_h}(|\nu-j-lN|)} + \frac{(n_h!)^2}{\pi\psi_{n_h}(|\nu-j+lN|)}\Big). \end{aligned}$$

Now, if $N-j-|\nu| > n_h$, we have $|\nu-j\pm lN| \geq |j\pm lN| - |\nu| \geq lN-j-|\nu|$, and we can bound the previous series by

$$\begin{aligned} &\sum_{l=1}^{\infty} \frac{2(n_h!)^2}{\pi(lN-j-|\nu|-n_h)^{1+2n_h}} \\ &\leq \frac{2(n_h)^2}{N\pi}\Big(\frac{N}{(N-j-|\nu|-n_h)^{1+2n_h}} + \int_{2N-j-|\nu|-n_h}^{\infty} \frac{1}{(y-N)^{1+2n_h}} dy\Big) \\ &\leq \frac{2(n_h)^2}{N\pi}\Big(\frac{N}{(N-j-|\nu|-n_h)^{1+2n_h}} + \frac{1/(2n_h)}{(N-j-|\nu|-n_h)^{2n_h}}\Big) \\ &\leq \frac{2(n_h!)^2(1+\frac{1}{2n_h})}{(N-j-|\nu|-n_h)^{1+2n_h}}. \end{aligned}$$

Regarding to the other two inequalities, if we take into account that

$$\begin{aligned}
|\widetilde{\mathcal{CS}}_\nu^{n_h}(j)| &\leq \frac{2(n_h!)^2}{\pi\psi_{n_h}(|\nu-j|)}, \\
|\partial\widetilde{\mathcal{CS}}_\nu^{n_h}(j)| &\leq \frac{2(n_h!)^2(\pi+\ln(|\nu-j|+n_h)-\ln(|\nu-j|-n_h-1))}{\pi\psi_{n_h}(|\nu-j|)},
\end{aligned}$$

we can easily adapt the previous sequence of inequalities to both cases. Note that, for the second inequality above, we need the hypothesis $N-j-\nu-n_h \geq 2$ in order to apply Lemma 3.2.3. □

In order to bound $\|Dg(y)^{-1}\|$, we will further simplify $\overline{\mathcal{C}}_\nu^{n_h}(j)$, $\widetilde{\mathcal{C}}_\nu^{n_h}(j)$, etc., by eliminating the second term in the sums given by Lemma 3.2.1. For this we introduce $\bar{\mathfrak{c}}$, $\tilde{\mathfrak{c}}$, ..., according to the following

Definition 3.2.1 *We define*

$$\begin{aligned}
\bar{\mathfrak{c}}_\nu^{n_h}(j) &= \frac{(-1)^{n_h}(n_h!)^2}{2\pi}\cdot\frac{\sin(2\pi(\nu-j))}{\psi_{n_h}(\nu-j)}, & \bar{\mathfrak{s}}_\nu^{n_h}(j) &= -\tilde{\mathfrak{c}}_\nu^{n_h}(j), \\
\tilde{\mathfrak{c}}_\nu^{n_h}(j) &= \frac{(-1)^{n_h}(n_h!)^2}{2\pi}\cdot\frac{1-\cos(2\pi(\nu-j))}{\psi_{n_h}(\nu-j)}, & \tilde{\mathfrak{s}}_\nu^{n_h}(j) &= \bar{\mathfrak{c}}_\nu^{n_h}(j), \\
\partial\bar{\mathfrak{c}}_\nu^{n_h}(j) &= \frac{(-1)^{n_h}(n_h!)^2}{2\pi}\cdot\frac{h_r(\nu-j)}{\psi_{n_h}(\nu-j)}, & \partial\bar{\mathfrak{s}}_\nu^{n_h}(j) &= -\partial\tilde{\mathfrak{c}}_\nu^{n_h}(j), \\
\partial\tilde{\mathfrak{c}}_\nu^{n_h}(j) &= \frac{(-1)^{n_h}(n_h!)^2}{2\pi}\cdot\frac{h_i(\nu-j)}{\psi_{n_h}(\nu-j)}, & \partial\tilde{\mathfrak{s}}_\nu^{n_h}(j) &= \partial\bar{\mathfrak{c}}_\nu^{n_h}(j).
\end{aligned}$$

In the following lemma, we bound the error after this simplification.

Lemma 3.2.5 *If $|\nu+j| > n_h+2$, we have*

$$|\partial\bar{\mathfrak{c}}_\nu^{n_h}(j) - \partial\overline{\mathcal{C}}_\nu^{n_h}(j)| \leq \frac{(n_h!)^2(\pi+\ln(|-\nu-j|+n_h)-\ln(|-\nu-j|-n_h-1))}{\pi(|-\nu-j|-n_h)^{1+2n_h}},$$

and the same bound holds for $|\partial\tilde{\mathfrak{c}}_\nu^{n_h}(j)-\partial\widetilde{\mathcal{C}}_\nu^{n_h}(j)|$, $|\partial\bar{\mathfrak{s}}_\nu^{n_h}(j)-\partial\overline{\mathcal{S}}_\nu^{n_h}(j)|$, $|\partial\tilde{\mathfrak{s}}_\nu^{n_h}(j)-\partial\widetilde{\mathcal{S}}_\nu^{n_h}(j)|$. We also have

$$|\bar{\mathfrak{c}}_\nu^{n_h}(j) - \overline{\mathcal{C}}_\nu^{n_h}(j)| \leq \frac{(n_h!)^2}{\pi(|-\nu-j|-n_h)^{1+2n_h}},$$

and the same bound holds for $|\tilde{\mathfrak{c}}_\nu^{n_h}(j)-\widetilde{\mathcal{C}}_\nu^{n_h}(j)|$, $|\bar{\mathfrak{s}}_\nu^{n_h}(j)-\overline{\mathcal{S}}_\nu^{n_h}(j)|$, $|\tilde{\mathfrak{s}}_\nu^{n_h}(j)-\widetilde{\mathcal{S}}_\nu^{n_h}(j)|$.

Proof: It is a direct application of Definition 3.2.1 and Lemma 3.2.3. □

3.2.1 Error estimation for known frequencies

If we assume in (3.6) that $j_i \geq n_h + 1$ for $i = 1 \div N_f$, then $c_1^{n_h}(j_i) = 0$ for $i = 1 \div N_f$ and the first equation of system (3.6) is uncoupled with the other ones. Therefore, we can write $Dg(y)$ as

$$M = \begin{pmatrix} 2 & B_{0,1} & \dots & B_{0,N_f} \\ 0 & B_{1,1} & \dots & B_{1,N_f} \\ \vdots & \vdots & \ddots & \vdots \\ 0 & B_{N_f,1} & \dots & B_{N_f,N_f} \end{pmatrix},$$

where $B_{0,l} = u_l$ are 1×2 blocks, being v_l as defined in (2.6), and $B_{i,l}$, $i, l = 1 \div N_f$, are 2×2 blocks defined as in (2.6). Let us split M in its block–diagonal and block–off–diagonal parts, that is $M = M_D + M_O$, being

$$M_D = \begin{pmatrix} 2 & 0 & \dots & 0 \\ 0 & B_{1,1} & \dots & 0 \\ \vdots & \vdots & \ddots & \vdots \\ 0 & 0 & \dots & B_{N_f,N_f} \end{pmatrix}, \quad M_O = \begin{pmatrix} 0 & B_{0,1} & \dots & B_{0,N_f} \\ 0 & 0 & \dots & B_{1,N_f} \\ 0 & \vdots & \ddots & \vdots \\ 0 & B_{N_f,1} & \dots & 0 \end{pmatrix}.$$

From Definition 3.2.1 and lemmas 3.2.5 and 3.2.4, under suitable hypothesis, $\overline{cs}^{n_h}_{\nu,N}(j)$ and $\widetilde{cs}^{n_h}_{\nu,N}(j)$ decrease as ν goes away from j, and therefore M is close to its diagonal part. What we will do is to obtain bounds for $\|M_D^{-1}\|$ and $\|M_O\|$ and then use them to bound $\|M^{-1}\|$ using the following

Lemma 3.2.6 *If M and ΔM are $n \times n$ matrices satisfying that M is invertible and $\|M^{-1}\|\|\Delta M\| < 1$, then $M + \Delta M$ is inversible and satisfies*

$$\|(M + \Delta M)^{-1}\| \leq \frac{\|M^{-1}\|}{1 - \|M^{-1}\|\|\Delta M\|}$$

Proof: See [29], p. 188. □

To simplify notation, we introduce the following

Definition 3.2.2 *We will denote by $\mathcal{M}$, $\mathcal{M}_D$, $\mathcal{M}_O$ and $\mathcal{B}_{i,l}$ the equivalents of M, M_D, M_O and $B_{i,l}$, respectively, but replacing $\overline{c}^{n_h}_\nu$, $\widetilde{c}^{n_h}_\nu$, etc. by $\overline{\mathcal{C}}^{n_h}_\nu$, $\widetilde{\mathcal{C}}^{n_h}_\nu$, etc. That is, by replacing the DFT by the TCFT. We will also denote by $\mathfrak{M}$, $\mathfrak{M}_D$, $\mathfrak{M}_O$ and $\mathfrak{B}_{i,l}$ the equivalents of M, M_D, M_O and $B_{i,l}$, respectively, but replacing $\overline{c}^{n_h}_\nu$, $\widetilde{c}^{n_h}_\nu$, etc. by $\overline{\mathfrak{c}}^{n_h}_\nu$, $\widetilde{\mathfrak{c}}^{n_h}_\nu$, etc. In this way, for instance,*

$$\mathfrak{B}_{i,l} = \begin{pmatrix} \overline{\mathfrak{c}}^{n_h}_{\nu_l}(j_i) & \widetilde{\mathfrak{c}}^{n_h}_{\nu_l}(j_i) \\ \overline{\mathfrak{s}}^{n_h}_{\nu_l}(j_i) & \widetilde{\mathfrak{s}}^{n_h}_{\nu_l}(j_i) \end{pmatrix}$$

In the following proposition, we give bounds for $\|\mathfrak{M}_D^{-1}\|$ and $\|\mathfrak{M}_O\|$.

Proposition 3.2.1 *If* $\frac{TD}{(2r_0-2)^\tau} > \frac{1}{2} + n_h$*, where* D, τ *are given by (3.2) and* r_0 *is given by (3.4), then*

$$\|\mathfrak{M}_D^{-1}\| \le \frac{5}{3}, \qquad \|\mathfrak{M}_O\| \le \frac{\sqrt{2} N_f (n_h!)^2}{\pi\big(\frac{TD}{(2r_0-1)^\tau} - \frac{1}{2} - n_h\big)^{1+2n_h}}.$$

Proof: From the definitions of $\mathfrak{M}_D$ and $\mathfrak{M}_O$, we have

$$\|\mathfrak{M}_D^{-1}\| \le \max\Big(\max_{i=1,\dots,N_f} \|(\mathfrak{B}_{i,i})^{-1}\|, \frac{1}{2}\Big), \qquad \|\mathfrak{M}_O\| \le \max_{i=0,\dots,N_f} \sum_{l=1}^{N_f} \|\mathfrak{B}_{i,l}\| \tag{3.8}$$

For the second bound, we have used the fact that the bounds that will be found for $\|\mathfrak{M}_{i,l}\|$ are valid for $\|v_l\|$. So, in order to take into account the first row of $\|\mathfrak{M}_O\|$, we have allowed the sum to run for $l = i$.

Denoting $\rho_{i,l} = \nu_l - j_i$ and using the trigonometric identities $\sin(2\varepsilon)/2 = \sin(\varepsilon)\cos(\varepsilon)$, $(1-\cos(2\varepsilon))/2 = \sin^2(\varepsilon)$, we can write

$$\mathfrak{B}_{i,l} = \frac{(-1)^{n_h}(n_h!)^2 \sin(\pi\rho_{i,l})}{\pi\psi_{n_h}(\rho_{i,l})} \begin{pmatrix} \cos(\pi\rho_{i,l}) & \sin(\pi\rho_{i,l}) \\ -\sin(\pi\rho_{i,l}) & \cos(\pi\rho_{i,l}) \end{pmatrix}.$$

Therefore

$$(\mathfrak{B}_{i,l})^{-1} = \frac{\pi\psi_{n_h}(\rho_{i,l})}{(-1)^{n_h}(n_h!)^2 \sin(\pi\rho_{i,l})} \begin{pmatrix} \cos(\pi\rho_{i,l}) & -\sin(\pi\rho_{i,l}) \\ \sin(\pi\rho_{i,l}) & \cos(\pi\rho_{i,l}) \end{pmatrix}$$

and

$$\begin{aligned} \|\mathfrak{B}_{i,l}\| &= \Big|\frac{(n_h!)^2 \sin(\pi\rho_{i,l})}{\pi\psi_{n_h}(\rho_{i,l})}\Big| (|\cos(\pi\rho_{i,l})| + |\sin(\pi\rho_{i,l})|), \\ \|(\mathfrak{B}_{i,i})^{-1}\| &= \Big|\frac{\pi\psi_{n_h}(\rho_{i,i})}{(n_h!)^2 \sin(\pi\rho_{i,i})}\Big| (|\cos(\pi\rho_{i,i})| + |\sin(\pi\rho_{i,i})|). \end{aligned} \tag{3.9}$$

Let us define

$$F_1(\rho_{i,i}) = \Big|\frac{\pi\psi_{n_h}(\rho_{i,i})}{(n_h!)^2 \sin(\pi\rho_{i,i})}\Big|$$

Recalling that the j_i, $i = 1 \div N_f$, were chosen such that $|\nu_i - j_i| < 0.5$, we only have to bound (3.9) for $-0.5 \le \rho_{i,i} \le 0.5$. From the definition (1.6) of ψ_{n_h}, we can write $F_1(\rho_{i,i})$ as

$$F_1(\rho_{i,i}) = \Big|\frac{\pi\rho_{i,i}}{\sin(\pi\rho_{i,i})}\Big| \prod_{l=1}^{n_h} \frac{l^2 - \rho_{i,i}^2}{l^2},$$

and it is readily checked that if $-0.5 \le \rho_{i,i} \le 0.5$ then $F_1(\rho_{i,i})$ decreases as $n_h \to \infty$. The limit is a positive value because of the Weierstrass factorization formula for the sine (see, for instance, [31]):

$$\sin(\pi z) = \pi z \prod_{n=1}^{\infty}\Big(1 - \frac{z^2}{n^2}\Big) \qquad \text{for } z \in \mathbb{C}. \tag{3.10}$$

Therefore, $\mathfrak{B}_{i,i}$ is invertible and we can bound $\|(\mathfrak{B}_{i,i})^{-1}\|$ for $n_h \in \mathbb{N}$ by the bound for $n_h = 0$, which is

$$\|(\mathfrak{B}_{i,i})^{-1}\| \leq \left|\frac{\pi\rho_{i,i}}{\sin(\pi\rho_{i,i})}\right|(|\cos(\pi\rho_{i,i})| + |\sin(\pi\rho_{i,i})|) \leq \frac{5}{3} \qquad \text{for } -0.5 \leq \rho_{i,i} \leq 0.5. \quad (3.11)$$

For the actual behavior of $\|\mathfrak{B}_{i,i}^{-1}\|$ in terms of $\rho_{i,i}$, see Fig. 3.1.

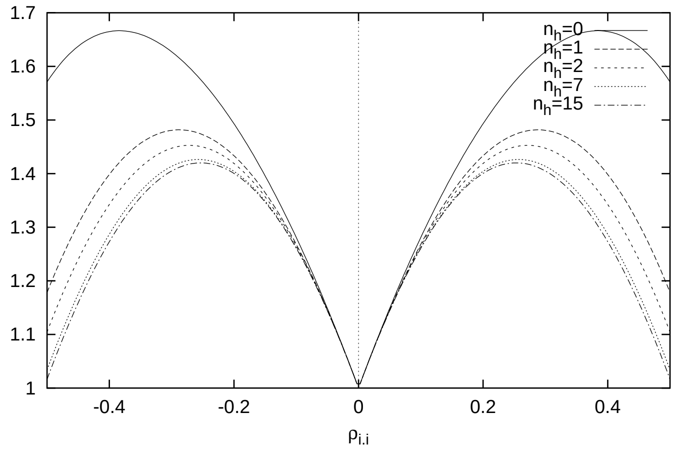

Figure 3.1: Graph of $\|\mathfrak{B}_{i,i}^{-1}\|_\infty$ for $-0.5 \leq \rho_{i,i} \leq 0.5$ and $n_h = 0, 1, 3, 5, 15$.

Concerning $\|\mathfrak{B}_{i,l}\|$, for $\rho_{i,l} \in \mathbb{R}$ and $n_h \in \mathbb{N}$, we have

$$\|\mathfrak{B}_{i,l}\| \leq \frac{(n_h!)^2}{\pi|\psi_{n_h}(\rho_{i,l})|} \max_{x\in\mathbb{R}}(|\cos(\pi x)| + |\sin(\pi x)|) = \frac{\sqrt{2}(n_h!)^2}{\pi|\psi_{n_h}(\rho_{i,l})|}. \qquad (3.12)$$

If we define $j_0 = 0$, the previous bound is also valid for $\|\mathfrak{B}_{0,l}\|$. For the actual behavior of $\|\mathfrak{B}_{i,l}\|$ in terms of $\rho_{i,l}$, see Fig. 3.2.

Now from (3.8), (3.11) and (3.12),

$$\|\mathfrak{M}_D^{-1}\| \leq 5/3, \qquad \|\mathfrak{M}_O\| \leq \max_{i=0\div N_f} \sum_{l=1}^{N_f} \frac{\sqrt{2}(n_h!)^2}{\pi|\psi_{n_h}(\nu_l - j_i)|}.$$

Since by definition $|\nu_i - j_i| \leq 1/2$, we have $|\nu_l - j_i| \geq |\nu_l - \nu_i| - 1/2 = T|(k_l - k_i)\omega| - 1/2$. Using the Diophantine condition (3.2),

$$T|(k_l - k_i)\omega| - \frac{1}{2} \geq \frac{TD}{|k_l - k_i|^\tau} - \frac{1}{2} \geq \frac{TD}{(2r_0 - 2)^\tau} - \frac{1}{2}.$$

Now since by hypothesis $\frac{TD}{(2r_0-2)^\tau} > \frac{1}{2} + n_h$, we get

$$\|\mathfrak{M}_O\| \leq \frac{\sqrt{2}N_f(n_h!)^2}{\pi\left(\frac{TD}{(2r_0-2)^\tau} - \frac{1}{2} - n_h\right)^{1+2n_h}},$$

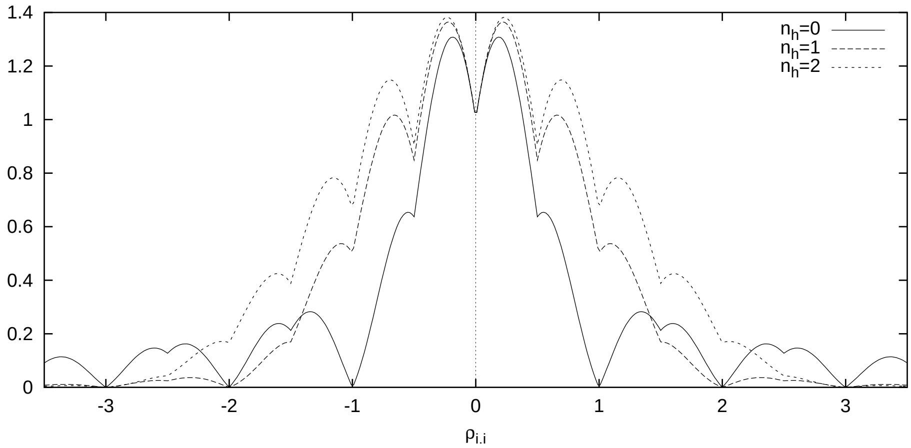

Figure 3.2: Graph of $\|\mathfrak{B}_{i,l}(\rho_{i,l})\|_\infty$ for $n_h = 0, 1, 2$.

and this ends the proposition. $\square$

From the bounds of $\|\mathfrak{M}_D^{-1}\|$ and $\|\mathfrak{M}_O\|$ and Lemma 3.2.6, we can get a bound for $\|M^{-1}\|$. For that, we need bounds of $\|\mathcal{M}_D - \mathfrak{M}_D\|$, $\|M_D - \mathcal{M}_D\|$, $\|\mathcal{M}_O - \mathfrak{M}_O\|$ and $\|M_O - \mathcal{M}_O\|$, which are given in the following lemmas.

Lemma 3.2.7 *If $[\nu_{min}] > n_h$, where $\nu_{min} = \min\{\nu_1, \dots, \nu_{N_f}\}$ and $[\ ]$ denotes integer part, we have*

$$\|\mathcal{M}_D - \mathfrak{M}_D\| \le \frac{2(n_h!)^2}{\pi(2[\nu_{min}] - n_h)^{1+2n_h}}, \qquad \|\mathcal{M}_O - \mathfrak{M}_O\| \le \frac{2N_f(n_h!)^2}{\pi([\nu_{min}] - n_h)^{1+2n_h}}$$

Proof: We have

$$\begin{aligned} \|\mathcal{M}_D - \mathfrak{M}_D\| &\le \max_{i=1\div N_f} \|\mathcal{B}_{i,i} - \mathfrak{B}_{i,i}\| \\ &= \max_{i=1\div N_f} (|\overline{\mathcal{CS}}^{n_h}_{\nu_i}(j_i) - \overline{\mathfrak{cs}}^{n_h}_{\nu_i}(j_i)| + |\widetilde{\mathcal{CS}}^{n_h}_{\nu_i}(j_i) - \widetilde{\mathfrak{cs}}^{n_h}_{\nu_i}(j_i)|), \end{aligned}$$

where either $\mathcal{CS} = \mathcal{C}$ and $\mathfrak{cs} = \mathfrak{c}$ or $\mathcal{CS} = \mathcal{S}$ and $\mathfrak{cs} = \mathfrak{s}$. Now, using Lemma 3.2.5 and the hypothesis, we get the first inequality:

$$\|\mathcal{M}_D - \mathfrak{M}_D\| \le \max_{i=1\div N_f} \frac{2(n_h!)^2}{\pi\psi_{n_h}(-\nu_i - j_i)} \le \frac{2(n_h!)^2}{\pi(2[\nu_{min}] - n_h)^{1+2n_h}}.$$

As for the second inequality,

$$\|\mathcal{M}_O - \mathfrak{M}_O\| \le \max_{i=0\div N_f} \sum_{\substack{l=1 \\ l\neq i}}^{N_f} (|\overline{\mathcal{CS}}^{n_h}_{\nu_l}(j_i) - \overline{\mathfrak{cs}}^{n_h}_{\nu_l}(j_i)| + |\widetilde{\mathcal{CS}}^{n_h}_{\nu_l}(j_i) + \widetilde{\mathfrak{cs}}^{n_h}_{\nu_l}(j_i)|),$$

where we denote $j_0 = 0$. Using Lemma 3.2.5 again,

$$\|\mathcal{M}_O - \mathfrak{M}_O\| \leq \max_{i=0\div N_f} \sum_{l=1}^{N_f} \frac{2(n_h!)^2}{\pi\psi_{n_h}(-\nu_l - j_i)} \leq \frac{2N_f(n_h!)^2}{\pi([\nu_{min}] - n_h)^{1+2n_h}}.$$

We lose the factor 2 in front of $[\nu_{min}]$ with respect to the bound of $\|\mathcal{M}_D - \mathfrak{M}_D\|$ because we have to consider the first row ($i = 0$). □

Lemma 3.2.8 *Assume that $N - T(2r_0 - 2)\|\omega\|_\infty - \frac{1}{2} - n_h > 0$, where r_0 is given by (3.4). Then*

$$\begin{aligned} \|M_D - \mathcal{M}_D\| &\leq \frac{8(n_h!)^2(1 + \frac{1}{2n_h})}{\pi\left(N - T(2r_0 - 2)\|\omega\|_\infty - \frac{1}{2} - n_h\right)^{1+2n_h}}, \\ \|M_O - \mathcal{M}_O\| &\leq \frac{8(n_h!)^2 N_f(1 + \frac{1}{2n_h})}{\pi\left(N - T(2r_0 - 2)\|\omega\|_\infty - \frac{1}{2} - n_h\right)^{1+2n_h}}. \end{aligned}$$

Proof: Using Lemma 3.2.4,

$$\|M_D - \mathcal{M}_D\| \leq \max_{i=1\div N_f} \|B_{i,i} - \mathcal{B}_{i,i}\| \leq \max_{i=1\div N_f} \frac{8(n_h!)^2(1 + \frac{1}{2n_h})}{\pi\left(N - j_i - \nu_i - n_h\right)^{1+2n_h}},$$

and, since by definition $|j_i - \nu_i| < 1/2$ and as $\nu_i = Tk_i\omega$ with $|k_i| \leq r_0 - 1$, we have that $j_i + \nu_i \leq 2\nu_i + 1/2 \leq T(2r_0 - 2)\|\omega\|_\infty + 1/2$, and the first inequality follows immediately. A similar argument proves the second inequality. □

The bound for $\|M^{-1}\|$ that follows from the previous results will be given in Theorem 3.4.1.

3.2.2 General case

As in the case of known frequencies, we assume in (3.5) that $j_i > n_h$ for $i = 1 \div N_f$ so the first equation of system (3.5) is uncoupled with the other ones and $M = Dg(y)$ can be written as

$$M = \begin{pmatrix} 2 & B_{0,1} & \dots & B_{0,N_f} \\ 0 & B_{1,1} & \dots & B_{1,N_f} \\ \vdots & \vdots & \ddots & \vdots \\ 0 & B_{N_f,1} & \dots & B_{N_f,N_f} \end{pmatrix}$$

where $B_{0,l} = v_l$ are 1×3 blocks, being v_l as defined in (2.9), and $B_{i,l}$, $i, l = 1 \div N_f$, are 3×3 blocks defined as in (2.9). We split M in its block–diagonal and block–off–diagonal parts,

$$M_D = \begin{pmatrix} 1 & 0 & \dots & 0 \\ 0 & B_{1,1} & \dots & 0 \\ \vdots & \vdots & \ddots & \vdots \\ 0 & 0 & \dots & B_{N_f,N_f} \end{pmatrix}, \quad M_O = \begin{pmatrix} 0 & B_{0,1} & \dots & B_{0,N_f} \\ 0 & 0 & \dots & B_{1,N_f} \\ 0 & \vdots & \ddots & \vdots \\ 0 & B_{N_f,1} & \dots & 0 \end{pmatrix}.$$

As before, we will obtain bounds for $\|M_D^{-1}\|$ and $\|M_O\|$ and then use them to bound $\|M\|$ through Lemma 3.2.6.

In order to obtain bounds for $\|M_D\|$, we first state the following

Definition 3.2.3 *We will denote by $\mathcal{M}$, $\mathcal{M}_D$, $\mathcal{M}_O$ and $\mathcal{B}_{i,l}$ the equivalents of M, M_D, M_O and $B_{i,l}$, respectively, but replacing $\overline{c}_\nu^{n_h}$, $\widetilde{c}_\nu^{n_h}$, etc. by $\overline{\mathcal{C}}_\nu^{n_h}$, $\widetilde{\mathcal{C}}_\nu^{n_h}$, etc. That is, by replacing the DFT by the TCFT. We will also denote by $\mathfrak{M}$, $\mathfrak{M}_D$, $\mathfrak{M}_O$ and $\mathfrak{B}_{i,l}$ the equivalents of M, M_D, M_O and $B_{i,l}$, respectively, but replacing $\overline{c}_\nu^{n_h}$, $\widetilde{c}_\nu^{n_h}$, etc. by $\overline{\mathfrak{c}}_\nu^{n_h}$, $\widetilde{\mathfrak{c}}_\nu^{n_h}$, etc. For instance,*

$$\mathfrak{B}_{i,i} = \begin{pmatrix} A_i^c \partial\overline{\mathfrak{c}}_{\nu_i,N}^{n_h}(j_i) + A_i^s \partial\widetilde{\mathfrak{c}}_{\nu_i,N}^{n_h}(j_i) & \overline{\mathfrak{c}}_{\nu_i,N}^{n_h}(j_i) & \widetilde{\mathfrak{c}}_{\nu_i,N}^{n_h}(j_i) \\ A_i^c \partial\overline{\mathfrak{s}}_{\nu_i,N}^{n_h}(j_i) + A_i^s \partial\widetilde{\mathfrak{s}}_{\nu_i,N}^{n_h}(j_i) & \overline{\mathfrak{s}}_{\nu_i,N}^{n_h}(j_i) & \widetilde{\mathfrak{s}}_{\nu_i,N}^{n_h}(j_i) \\ A_i^c \partial\overline{\mathfrak{cs}}_{\nu_i,N}^{n_h}(j_i^+) + A_i^s \partial\widetilde{\mathfrak{cs}}_{\nu_i,N}^{n_h}(j_i^+) & \overline{\mathfrak{cs}}_{\nu_i,N}^{n_h}(j_i^+) & \widetilde{\mathfrak{cs}}_{\nu_i,N}^{n_h}(j_i^+) \end{pmatrix},$$

where $\mathfrak{cs}$ denotes either $\mathfrak{c}$ or $\mathfrak{s}$.

In order to invert $\mathfrak{M}_D$, we only have to invert a block $\mathfrak{B}_{i,i}$. The possibility to do that is established by the following

Lemma 3.2.9 *If $(A_i^s, A_i^c) \neq (0,0)$, $\mathfrak{B}_{i,i}$ is invertible either setting $\mathfrak{cs} = \mathfrak{c}$ or $\mathfrak{cs} = \mathfrak{s}$.*

Proof: Consider the matrix

$$\mathfrak{A} = \begin{pmatrix} \partial\overline{\mathfrak{c}}_{\nu_i}^{n_h}(j_i) & \partial\widetilde{\mathfrak{c}}_{\nu_i}^{n_h}(j_i) & \overline{\mathfrak{c}}_{\nu_i}^{n_h}(j_i) & \widetilde{\mathfrak{c}}_{\nu_i}^{n_h}(j_i) \\ \partial\overline{\mathfrak{s}}_{\nu_i}^{n_h}(j_i) & \partial\widetilde{\mathfrak{s}}_{\nu_i}^{n_h}(j_i) & \overline{\mathfrak{s}}_{\nu_i}^{n_h}(j_i) & \widetilde{\mathfrak{s}}_{\nu_i}^{n_h}(j_i) \\ \partial\overline{\mathfrak{c}}_{\nu_i}^{n_h}(j_i^+) & \partial\widetilde{\mathfrak{c}}_{\nu_i}^{n_h}(j_i^+) & \overline{\mathfrak{c}}_{\nu_i}^{n_h}(j_i^+) & \widetilde{\mathfrak{c}}_{\nu_i}^{n_h}(j_i^+) \\ \partial\overline{\mathfrak{s}}_{\nu_i}^{n_h}(j_i^+) & \partial\widetilde{\mathfrak{s}}_{\nu_i}^{n_h}(j_i^+) & \overline{\mathfrak{s}}_{\nu_i}^{n_h}(j_i^+) & \widetilde{\mathfrak{s}}_{\nu_i}^{n_h}(j_i^+) \end{pmatrix},$$

and denote by $\mathfrak{A}_{l_1,l_2,l_3}^{i_1,i_2,i_3}$ the submatrix of $\mathfrak{A}$ obtained by selecting the rows i_1, i_2, i_3 and the columns l_1, l_2, l_3. Then, the determinant of a block $\mathfrak{B}_{i,i}$ is

$$\det \mathfrak{B}_{i,i} = \begin{cases} A_i^c \det \mathfrak{A}_{1,3,4}^{1,2,3} + A_i^s \det \mathfrak{A}_{2,3,4}^{1,2,3} & \text{if we set } \mathfrak{cs} = \mathfrak{c}, \\ A_i^c \det \mathfrak{A}_{1,3,4}^{1,2,4} + A_i^s \det \mathfrak{A}_{2,3,4}^{1,2,4} & \text{if we set } \mathfrak{cs} = \mathfrak{s}. \end{cases}$$

To see that there exists a choice of $\mathfrak{cs}$ that makes $\det \mathfrak{B}_{i,i} \neq 0$ is equivalent to see that the system

$$\begin{cases} A_i^c \det \mathfrak{A}_{1,3,4}^{1,2,3} + A_i^s \det \mathfrak{A}_{2,3,4}^{1,2,3} &= 0 \\ A_i^c \det \mathfrak{A}_{1,3,4}^{1,2,4} + A_i^s \det \mathfrak{A}_{2,3,4}^{1,2,4} &= 0 \end{cases},$$

with unknowns A_i^c, A_i^s, has unique solution. That is, that the determinant

$$\det \mathfrak{D} = \begin{vmatrix} \det \mathfrak{A}_{1,3,4}^{1,2,3} & \det \mathfrak{A}_{2,3,4}^{1,2,3} \\ \det \mathfrak{A}_{1,3,4}^{1,2,4} & \det \mathfrak{A}_{2,3,4}^{1,2,4} \end{vmatrix} \tag{3.13}$$

is different from zero. From Definition 3.2.1, and since $\nu_i - j_i^+ = \nu_i - j_i - \mathrm{sign}(\nu_i - j_i)$, this determinant only depends on the difference $\varepsilon = \nu_i - j_i$ which, by definition, ranges from $-1/2$ to $1/2$. In order to prove the lemma, we only need to see that the previous determinant is different from zero in this range (see Fig. 3.3 for the numerical evidence).

In order to simplify the notation, we denote

$$\mathfrak{A} = \begin{pmatrix} a_1 & a_2 & a_3 & a_4 \\ -a_2 & a_1 & -a_4 & a_3 \\ a_5 & a_6 & a_7 & a_8 \\ -a_6 & a_5 & -a_8 & a_7 \end{pmatrix}$$

and

$$A = \mathfrak{A}^{1,2,3}_{1,3,4}, \quad B = \mathfrak{A}^{1,2,4}_{1,3,4}, \quad C = \mathfrak{A}^{1,2,3}_{2,3,4}, \quad D = \mathfrak{A}^{1,2,4}_{2,3,4},$$

so that $\det \mathfrak{D} = \det A \det D - \det B \det C$.

First note that, using $-(\varepsilon - \text{sign}(\varepsilon)) = -\varepsilon - \text{sign}(-\varepsilon)$ and the fact that $\overline{\mathfrak{c}}^{n_h}_\nu(j)$ and $\widetilde{\mathfrak{c}}^{n_h}_\nu(j)$ are even and odd in ε respectively, we can check that $\det \mathfrak{D}$ is even in ε and therefore we can restrict to $[0, 1/2]$ the range of ε to be considered.

Let $0 < \varepsilon < 1/2$ and assume $\det \mathfrak{D} = 0$. We note that $\det A = \det D$ and $\det B = -\det C$, so that $\det \mathfrak{D} = (\det A)^2 + (\det B)^2$ and we have $\det A = \det B = 0$. Expanding through the first column, we get

$$\begin{aligned} \det A &= -a_1(a_3a_7 + a_4a_8) + a_2(a_3a_8 - a_4a_7) + a_5(a_3^2 + a_4^2) \\ \det B &= a_2(a_3a_7 + a_4a_8) + a_1(a_3a_8 - a_4a_7) - a_6(a_3^2 + a_4^2) \end{aligned}$$

The $a_3a_8 - a_4a_7$ term is readily checked to be zero. We denote $\psi = \psi_{n_h}(\varepsilon)$ and $\psi_m = \psi_{n_h}(\varepsilon - 1)$. We check that $a_3a_7 + a_4a_8$ has the same numerator as $a_3^2 + a_4^2$, due to the 1–periodicity in ε of the numerators of $a_1, \ldots, a_8$. The denominators are different: $\psi\psi_m$ for $a_3a_7 + a_4a_8$ and ψ^2 for $a_3^2 + a_4^2$. Setting $\det A = \det B = 0$ and simplifying numerators, we get

$$a_1\psi = a_5\psi_m, \qquad a_2\psi = a_6\psi_m.$$

Now, using the expressions for a_1 and a_5 from Definition 3.2.1, as well as $a_1\psi = a_5\psi_m$, we obtain $r_{n_h}(\varepsilon) = r_{n_h}(\varepsilon - 1)$, that is $\psi'/\psi = \psi'_m\psi_m$ (here $'$ denotes derivative), and therefore

$$\frac{d}{d\varepsilon}\frac{\psi_m}{\psi} = \frac{\psi'_m\psi - \psi_m\psi'}{\psi_m^2} = 0. \tag{3.14}$$

The condition $a_2\psi = a_6\psi_m$ leads to the same conclusion.

But

$$\frac{\psi_m}{\psi} = \frac{\varepsilon - n_h - 1}{\varepsilon + n_h} = 1 - \frac{2n_h + 1}{\varepsilon + n_h},$$

and its derivative with respect to ε is different from zero for $0 < \varepsilon \le \frac{1}{2}$, which is in contradiction with (3.14).

For $\varepsilon = 0$, $\det \mathfrak{D}$ is checked to be different from zero using the expressions of Definition 3.2.1 (it is necessary to compute the limits when $\varepsilon \to 0$). $\square$

Now that we know that a block $\mathfrak{B}_{i,i}$ is invertible, in order to actually invert it we state the following

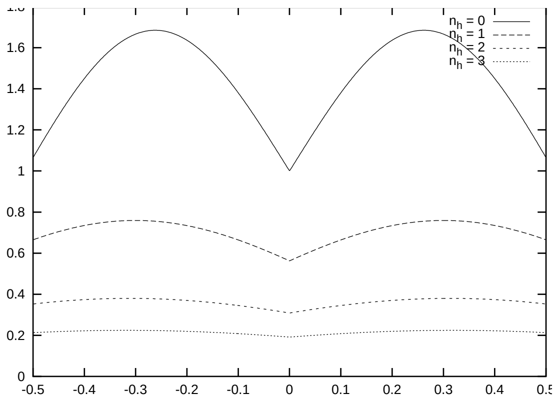

Figure 3.3: Plot of the determinant (3.13) for $-1/2 \le \nu_i - j_i \le 1/2$ and $n_h = 0, 1, 2, 3$.

n_h	0	1	2	3
G_{n_h}	4.84	8.83	13.3	17.7

Table 3.1: Some values of the G_{n_h} constants.

Definition 3.2.4 *For $n_h \in \mathbb{N}$, we define G_{n_h} to be an upper bound of*

$$\max_{\substack{\theta\in[0,2\pi]\\ |\nu-j|\le\frac{1}{2}}} \min_{\mathfrak{cs}\in\{\mathfrak{c},\mathfrak{s}\}} \left\| \begin{pmatrix} (\cos\theta)\partial\overline{\mathfrak{c}}^{n_h}_{\nu,N}(j) + (\sin\theta)\partial\widetilde{\mathfrak{c}}^{n_h}_{\nu,N}(j) & \overline{\mathfrak{c}}^{n_h}_{\nu,N}(j) & \widetilde{\mathfrak{c}}^{n_h}_{\nu,N}(j) \\ (\cos\theta)\partial\overline{\mathfrak{s}}^{n_h}_{\nu,N}(j) + (\sin\theta)\partial\widetilde{\mathfrak{s}}^{n_h}_{\nu,N}(j) & \overline{\mathfrak{s}}^{n_h}_{\nu,N}(j) & \widetilde{\mathfrak{s}}^{n_h}_{\nu,N}(j) \\ (\cos\theta)\partial\overline{\mathfrak{cs}}^{n_h}_{\nu,N}(j^+) + (\sin\theta)\partial\widetilde{\mathfrak{cs}}^{n_h}_{\nu,N}(j^+) & \overline{\mathfrak{cs}}^{n_h}_{\nu,N}(j^+) & \widetilde{\mathfrak{cs}}^{n_h}_{\nu,N}(j^+) \end{pmatrix}^{-1} \right\|.$$

In table 3.1 we give some values of the G_{n_h} constants found numerically. Just for illustration purposes, in figure 3.4 we display the behavior of

$$\min_{\mathfrak{cs}\in\{\mathfrak{c},\mathfrak{s}\}} \left\| \begin{pmatrix} (\cos\theta)\partial\overline{\mathfrak{c}}^{n_h}_{\nu,N}(j) + (\sin\theta)\partial\widetilde{\mathfrak{c}}^{n_h}_{\nu,N}(j) & \overline{\mathfrak{c}}^{n_h}_{\nu,N}(j) & \widetilde{\mathfrak{c}}^{n_h}_{\nu,N}(j) \\ (\cos\theta)\partial\overline{\mathfrak{s}}^{n_h}_{\nu,N}(j) + (\sin\theta)\partial\widetilde{\mathfrak{s}}^{n_h}_{\nu,N}(j) & \overline{\mathfrak{s}}^{n_h}_{\nu,N}(j) & \widetilde{\mathfrak{s}}^{n_h}_{\nu,N}(j) \\ (\cos\theta)\partial\overline{\mathfrak{cs}}^{n_h}_{\nu,N}(j^+) + (\sin\theta)\partial\widetilde{\mathfrak{cs}}^{n_h}_{\nu,N}(j^+) & \overline{\mathfrak{cs}}^{n_h}_{\nu,N}(j^+) & \widetilde{\mathfrak{cs}}^{n_h}_{\nu,N}(j^+) \end{pmatrix}^{-1} \right\| \tag{3.15}$$

in terms of θ and $\nu - j$.

In order to relate the bound of the previous definition to the bound of an actual block $\mathfrak{B}_{i,i}$, we will use the following

Lemma 3.2.10 *Let $\lambda \neq 0$ be a real number and v_1, v_2, v_3 3–dimensional row vectors. Then*

$$\left\| \begin{pmatrix} \lambda v_1 & v_2 & v_3 \end{pmatrix}^{-1} \right\|_\infty \le \max(\frac{1}{\lambda}, 1) \left\| \begin{pmatrix} v_1 & v_2 & v_3 \end{pmatrix}^{-1} \right\|_\infty .$$

Proof: Define w_1, w_2, w_3 according to

$$\begin{pmatrix} v_1 & v_2 & v_3 \end{pmatrix}^{-1} = \frac{1}{\det(v_1, v_2, v_3)} \begin{pmatrix} w_1^\top \\ w_2^\top \\ w_3^\top \end{pmatrix}.$$

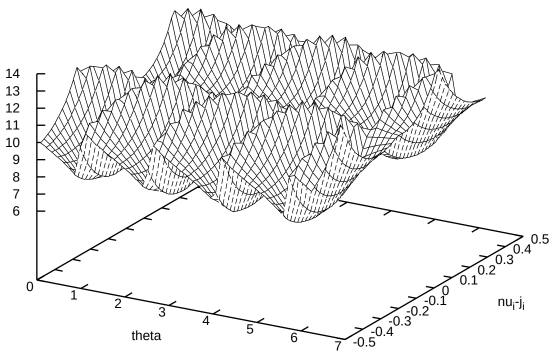

Figure 3.4: Plot of (3.15) for $0 \le \theta \le 2\pi$ and $-1/2 \le \nu_i - j_i \le 1/2$.

Then,

$$\begin{pmatrix} \lambda v_1 & v_2 & v_3 \end{pmatrix}^{-1} = \frac{1}{\det(\lambda v_1, v_2, v_3)} \begin{pmatrix} w_1^\top \\ \lambda w_2^\top \\ \lambda w_3^\top \end{pmatrix} = \frac{1}{\det(v_1, v_2, v_3)} \begin{pmatrix} w_1^\top/\lambda \\ w_2^\top \\ w_3^\top \end{pmatrix},$$

and therefore,

$$\begin{aligned} \left\| \begin{pmatrix} \lambda v_1 & v_2 & v_3 \end{pmatrix}^{-1} \right\|_\infty &= \frac{1}{|\det(v_1, v_2, v_3)|} \left\| \begin{pmatrix} w_1^\top/\lambda \\ w_2^\top \\ w_3^\top \end{pmatrix} \right\|_\infty \\ &= \frac{\max(\frac{1}{\lambda}\|w_1\|_1, \|w_2\|_1, \|w_3\|_1)}{|\det(v_1, v_2, v_3)|} \\ &\le \max(\frac{1}{\lambda}, 1) \frac{\max(\|w_1\|_1, \|w_2\|_1, \|w_3\|_1)}{|\det(v_1, v_2, v_3)|} \\ &= \max(\frac{1}{\lambda}, 1) \left\| \begin{pmatrix} v_1 & v_2 & v_3 \end{pmatrix}^{-1} \right\|_\infty. \end{aligned}$$

□

Let us denote $A_i = ((A_i^c)^2 + (A_i^s)^2)^{1/2}$. Using Definition 3.2.4 and Lemma 3.2.10 we have

$$\|(\mathfrak{B}_{i,i})^{-1}\| \le \max(A_i^{-1}, 1) G_{n_h},$$

and therefore,

$$\|\mathfrak{M}_D^{-1}\| \le \max(A_{min}^{-1}, 1) G_{n_h},$$

where $A_{min} = \min\{A_1, \ldots, A_{N_f}\}$.

Now we bound the simplified off–diagonal part of M.

Lemma 3.2.11 *Assume* $\frac{TD}{(2r_0-2)^\tau} > 3+n_h$. *Then,*

$$\|\mathfrak{M}_O\| \leq \frac{(n_h!)^2\Big[\sqrt{2}(\sum_{l=1}^{N_f}A_l)\Big(\pi+\ln\big(\frac{TD}{(2r_0-2)^\tau}-1+n_h\big)-\ln\big(\frac{TD}{(2r_0-2)^\tau}-2-n_h\big)\Big)+2N_f\Big]}{\pi\big(\frac{TD}{(2r_0-2)^\tau}-1-n_h\big)^{1+2n_h}}$$

Proof: We first note that, from Lemma 3.2.3 and Definition 3.2.1,

$$\begin{aligned}
|\bar{\mathfrak{c}}^{n_h}_\nu(j)|,|\widetilde{\mathfrak{c}}^{n_h}_\nu(j)|,|\bar{\mathfrak{s}}^{n_h}_\nu(j)|,|\widetilde{\mathfrak{s}}^{n_h}_\nu(j)| &\leq \frac{(n_h!)^2}{\pi(|\nu-j|-n_h)^{1+2n_h}},\\
|\partial\bar{\mathfrak{c}}^{n_h}_\nu(j)|,|\partial\widetilde{\mathfrak{c}}^{n_h}_\nu(j)|,|\partial\bar{\mathfrak{s}}^{n_h}_\nu(j)|,|\partial\widetilde{\mathfrak{s}}^{n_h}_\nu(j)| &\leq \\
&\frac{(n_h!)^2(\pi+\ln(|\nu-j|+n_h)-\ln(|\nu-j|-n_h-1))}{\pi(|\nu-j|-n_h)^{1+2n_h}}.
\end{aligned}$$

Therefore, using $|A^c_l|+|A^s_l|\leq\sqrt{2}((A^c_l)^2+(A^s_l)^2)^{1/2}=\sqrt{2}A_l$,

$$\begin{aligned}
\|\mathfrak{B}_{i,l}(j)\| &\leq \max_{\substack{j=j_i,j_i^+\\ \mathfrak{cs}=\mathfrak{c},\mathfrak{s}}}\Big(|A^c_i||\partial\widetilde{\mathfrak{cs}}^{n_h}_{\nu_i}(j)|+|A^s_i||\partial\widetilde{\mathfrak{cs}}^{n_h}_{\nu_i}(j)|+|\widetilde{\mathfrak{cs}}^{n_h}_{\nu_i}(j)|+|\widetilde{\mathfrak{cs}}^{n_h}_{\nu_i}(j)|\Big)\\
&\leq \max_{j=j_i,j_i^+}\frac{(n_h!)^2(\sqrt{2}A_l(\pi+\ln(|\nu_l-j|+n_h)-\ln(|\nu_l-j|-n_h-1))+2)}{\pi(|\nu_l-j|-n_h)^{1+2n_h}}.
\end{aligned}$$

Now, for $i,l=1\div N_f$ and $j=j_i,j_i^+$ there exists i_j such that $j\in\{[\nu_{i_j}],[\nu_{i_j}]+1\}$, so $|\nu_{i_j}-j|\leq 1$. As stated at the beginning of this section, we also have that there exists k_{i_j}, with $|k_{i_j}|\leq r_0-1$, such that $\nu_{i_j}=Tk_{i_j}\omega$. Then, using the Diophantine condition (3.2), we obtain

$$\begin{aligned}
|\nu_l-j| &\geq |\nu_l-\nu_{i_j}|-|j-\nu_{i_j}|\geq T|(k_l-k_{i_j})\omega|-1\geq\frac{TD}{|k_l-k_{i_j}|^\tau}-1\\
&\geq \frac{TD}{(2r_0-2)^\tau}-1,
\end{aligned}$$

and the lemma follows from

$$\|\mathfrak{M}_O\|\leq\max_{i=0\div N_f}\sum_{l=1}^{N_f}\|\mathfrak{B}_{i,l}\|,$$

where we denote $j_0=0$. □

In order to bound $\|M^{-1}\|$ from $\|M_D^{-1}\|$ and $\|M_O^{-1}\|$ by applying Lemma 3.2.6, we need the bounds of $\|\mathcal{M}_D-\mathfrak{M}_D\|$, $\|M_D-\mathcal{M}_D\|$, $\|\mathcal{M}_O-\mathfrak{M}_O\|$ and $\|M_O-\mathcal{M}_O\|$. We calculate them in the following lemmas.

Lemma 3.2.12 *Denote* $\nu_{min}=\min\{\nu_1,\dots,\nu_{N_f}\}$, $A_{max}=\max\{A_0,\dots,A_{N_f}\}$. *If* $[\nu_{min}]\geq 2+n_h$, *we have*

$$\|\mathfrak{M}_D-\mathcal{M}_D\| \leq \frac{(n_h!)^2\Big(\sqrt{2}A_{max}[\pi+\ln(2[\nu_{min}]+n_h)-\ln(2[\nu_{min}]-n_h-1)]+2\Big)}{\pi(2[\nu_{min}]-n_h)^{1+2n_h}},$$

$$\|\mathfrak{M}_O - \mathcal{M}_O\| \;\leq\; \frac{(n_h!)^2\Big(\sqrt{2}(\sum_{l=1}^{N_f} A_l)(\pi + \ln([\nu_{min}]+n_h) - \ln([\nu_{min}]-n_h-1)) + 2N_f\Big)}{\pi([\nu_{min}] - n_h)^{1+2n_h}},$$

Proof: From Definition 3.2.3 and Lemma 3.2.5,

$$\begin{aligned}\|\mathfrak{B}_{i,l} - \mathcal{B}_{i,l}\| &\leq \max_{j=j_i,j_i^+}\left(\begin{array}{c}|A_l^c||\partial\overline{\mathfrak{cs}}^{n_h}_{\nu_l}(j) - \partial\overline{\mathcal{CS}}^{n_h}_{\nu_l}(j)| + |A_l^s||\partial\widetilde{\mathfrak{cs}}^{n_h}_{\nu_l}(j) - \partial\widetilde{\mathcal{CS}}^{n_h}_{\nu_l}(j)| + \\ |\overline{\mathfrak{cs}}^{n_h}_{\nu_l}(j) - \overline{\mathcal{CS}}^{n_h}_{\nu_l}(j)| + |\widetilde{\mathfrak{cs}}^{n_h}_{\nu_l}(j) - \widetilde{\mathcal{CS}}^{n_h}_{\nu_l}(j)|\end{array}\right) \\ &\leq \frac{(n_h!)^2\Big(\sqrt{2}A_l(\ln(|-\nu_l - j| + n_h) - \ln(|-\nu_l - j| - n_h - 1)) + 2\Big)}{\pi(|-\nu_l - j| - n_h)^{1+2n_h}},\end{aligned}$$

where either $\mathfrak{cs} = \mathfrak{c}$ and $\mathcal{CS} = \mathcal{C}$ or $\mathfrak{cs} = \mathfrak{s}$ and $\mathcal{CS} = \mathcal{S}$. For the second inequality we have used that

$$|A_l^c| + |A_l^s| \leq \sqrt{2}((A_l^c)^2 + (A_l^s)^2)^{1/2} = \sqrt{2}A_l.$$

Now, the first inequality of the lemma follows from

$$\|\mathfrak{M}_D - \mathcal{M}_D\| \leq \max_{i=1\div N_f} \|\mathfrak{B}_{i,i} - \mathcal{B}_{i,i}\|$$

and the fact that $|-\nu_i - j_i|, |-\nu_i - j_i^+| \geq 2[\nu_{min}]$ for $i = 1 \div N_f$. The second inequality follows from

$$\|\mathfrak{M}_O - \mathcal{M}_O\| \leq \max_{i=0\div N_f} \sum_{\substack{l=1\\ l\neq i}}^{N_f} \|\mathfrak{B}_{i,l} - \mathcal{B}_{i,l}\|$$

and the fact that $|-\nu_l - j_i|, |-\nu_l - j_i^+| \geq [\nu_{min}]$ for $i = 0 \div N_f, l = 1 \div N_f$ (we denote $j_0 = j_0^+ = 0$). $\square$

Lemma 3.2.13 *Assume $N - T(2r_0 - 2)\|\omega\|_\infty > 3 + n_h$. Then,*

$$\begin{aligned}&\|\mathcal{M}_D - M_D\| \\ &\quad\leq \frac{4(n_h!)^2\Big(\sqrt{2}A_{max}(\pi + \ln(N-\Omega+n_h) - \ln(N-\Omega-1-n_h)) + 2\Big)(1 + \frac{1}{2n_h})}{\pi(N - \Omega - n_h)^{1+2n_h}},\\ &\|\mathcal{M}_O - M_O\| \\ &\quad\leq \frac{4(n_h!)^2\Big(\sqrt{2}(\sum_{l=1}^{N_f} A_l)(\pi + \ln(N-\Omega+n_h) - \ln(N-\Omega-1-n_h)) + 2N_f\Big)(1 + \frac{1}{2n_h})}{\pi(N - \Omega - n_h)^{1+2n_h}}.\end{aligned}$$

being $\Omega = T(2r_0 - 2)\|\omega\|_\infty + 1$.

Proof: For a 3×3 block, we apply Lemma 3.2.4 and obtain

$$\begin{aligned}
&\|\mathfrak{B}_{i,l} - \mathcal{B}_{i,l}\| \\
&\le \max_{j=j_i,j_i^+} \begin{pmatrix} |A_i^c||\partial\overline{\mathcal{CS}}^{n_h}_{\nu_l}(j) - \partial\overline{\mathfrak{cs}}^{n_h}_{\nu_l}(j)| + |A_i^s||\partial\widetilde{\mathcal{CS}}^{n_h}_{\nu_l}(j) - \partial\widetilde{\mathfrak{cs}}^{n_h}_{\nu_l}(j)| + \\ |\overline{\mathcal{CS}}^{n_h}_{\nu_l}(j) - \overline{\mathfrak{cs}}^{n_h}_{\nu_l}(j)| + |\widetilde{\mathcal{CS}}^{n_h}_{\nu_l}(j) - \widetilde{\mathfrak{cs}}^{n_h}_{\nu_l}(j)|, \end{pmatrix} \\
&\le \frac{4(n_h!)^2\Big(\sqrt{2}A_i(\pi + \ln(N-j-\nu_l+n_h) - \ln(N-j-\nu_l-n_h-1)) + 2\Big)(1+\frac{1}{2n_h})}{\pi(N-j-\nu_l-n_h)^{1+2n_h}},
\end{aligned}$$

where either $\mathfrak{cs} = \mathfrak{c}$ and $\mathcal{CS} = \mathcal{C}$ or $\mathfrak{cs} = \mathfrak{s}$ and $\mathcal{CS} = \mathcal{S}$. As $j \in \{j_i, j_i^+\}$ and $\nu_l = Tk_l\omega$ with $1 \le |k_l| \le r_0 - 1$, we have that $j + \nu_l \le Tk_i\omega + 1 + Tk_l\omega \le T(2r_0-2)\|\omega\|_\infty + 1 = \Omega$ for some $|k_i| \le r_0 - 1$. Using this, the lemma follows from

$$\begin{aligned}
\|M_D - \mathcal{M}_D\| &\le \max_{i=1\div N_f} \|B_{i,i} - \mathcal{B}_{i,i}\|, \\
\|M_O - \mathcal{M}_O\| &\le \max_{i=0\div N_f} \sum_{l=1}^{N_f} \|B_{i,l} - \mathcal{B}_{i,l}\|,
\end{aligned}$$

where we denote $j_0 = j_0^+ = 0$. $\square$

From these lemmas follows a bound for $\|Dg(y)^{-1}\|$, as will be stated in theorem 3.4.1.

3.3 Error bounds for $\|\Delta b\|_\infty$

We give first three definitions and one lemma in order to be able to bound finite sums of the type $\sum_{j=r_0}^{r_1} j^\alpha e^{-\delta j}$, with r_1 either finite or infinite.

Definition 3.3.1 *Given $z \in \mathbb{R}$, we define*

$$\forall x \in \mathbb{R}, \quad [x]_z = \max\{z + n : n \in \mathbb{Z}, z + n \le x\} = z + [x - z],$$

where [ ] denotes integer part.

Note that, for all $m \in \mathbb{Z}$, we have $[x]_z = [x]_{z+m}$.

In what follows, we will use the incomplete Gamma functions $\gamma(\alpha, x)$ and $\Gamma(\alpha, x)$, which are defined as (see, for instance, [1])

$$\gamma(\alpha, x) = \int_0^x e^{-t}t^{\alpha-1}dt, \qquad \Gamma(\alpha, x) = \int_x^\infty e^{-t}t^{\alpha-1}dt.$$

In order to be able to bound sums by integrals taking into account the intervals of monotonicity is convenient to introduce the following

Definition 3.3.2 *For $j_1, j_2, \alpha, \delta > 0$ we define the functions*

$$\begin{aligned} G_f(j_1, j_2, \alpha, \delta) &= \frac{1}{\delta^{\alpha+1}} \chi_{\{j_1 \le \frac{\alpha}{\delta}-1\}} \Big(\gamma(\alpha+1, \delta \min([\frac{\alpha}{\delta}]_{j_1}, j_2+1)) - \gamma(\alpha+1, \delta j_1) \Big) + \\ & \quad \chi_{\{j_1 \le \frac{\alpha}{\delta}, j_2 > \frac{\alpha}{\delta}-1\}} ([\frac{\alpha}{\delta}]_{j_1})^\alpha e^{-\delta[\frac{\alpha}{\delta}]_{j_1}} + \\ & \quad \chi_{\{j_1 < \frac{\alpha}{\delta}+1, j_2 > \frac{\alpha}{\delta}\}} ([\frac{\alpha}{\delta}]_{j_1}+1)^\alpha e^{-\delta([\frac{\alpha}{\delta}]_{j_1}+1)} + \\ & \quad \frac{1}{\delta^{\alpha+1}} \chi_{\{j_2 > \frac{\alpha}{\delta}+1\}} \Big(\gamma(\alpha+1, \delta j_2) - \gamma(\alpha+1, \max([\frac{\alpha}{\delta}]_{j_1}+1, j_1-1)) \Big), \end{aligned}$$

and

$$\begin{aligned} G_\infty(j_1, \alpha, \delta) &= \frac{1}{\delta^{\alpha+1}} \chi_{\{j_1 \le \frac{\alpha}{\delta}-1\}} \Big(\gamma(\alpha+1, \delta[\frac{\alpha}{\delta}]_{j_1}) - \gamma(\alpha+1, \delta j_1) \Big) + \\ & \quad \chi_{\{j_1 \le \frac{\alpha}{\delta}\}} ([\frac{\alpha}{\delta}]_{j_1})^\alpha e^{-\delta[\frac{\alpha}{\delta}]_{j_1}} + \\ & \quad \chi_{\{j_1 < \frac{\alpha}{\delta}+1\}} ([\frac{\alpha}{\delta}]_{j_1}+1)^\alpha e^{-\delta([\frac{\alpha}{\delta}]_{j_1}+1)} + \\ & \quad \frac{1}{\delta^{\alpha+1}} \Gamma(\alpha+1, \delta \max([\frac{\alpha}{\delta}]_{j_1}+1, j_1-1)). \end{aligned}$$

In the above formulas, $\chi_{\{\text{condition}\}}$ equals 1 if condition is true and 0 otherwise.

Lemma 3.3.1 *The functions G_f and G_∞ satisfy*

$$\sum_{j=j_1}^{j_2} j^\alpha e^{-\delta j} \le G_f(j_1, j_2, \alpha, \delta), \qquad \sum_{j=j_1}^{\infty} j^\alpha e^{-\delta j} \le G_\infty(j_1, \alpha, \delta).$$

Proof: To obtain the expressions for G_f, G_∞ in Definition 3.3.2 we have bounded the previous sums by integrals. This can be done easily for the subintervals of j of length 1, starting at j_0, for which the function $j^\alpha e^{-\delta j}$ is monotone. Some care must be taken for the intervals around the maximum of the function, which is attained at $j = \frac{\alpha}{\delta}$. This is the reason for the definition 3.3.1. Both inequalities follow after a careful examination of all the possibilities for the relative position between $[j_1, j_2]$ and the maximum $\frac{\alpha}{\delta}$. □

We recall from (3.5) that Δb is defined as,

$$\Delta b = \begin{pmatrix} c^{n_h}_{f-p,T,N}(0) \\ c^{n_h}_{f-p,T,N}(j_i) \\ s^{n_h}_{f-p,T,N}(j_i) \\ cs^{n_h}_{f-p,T,N}(j_i^+) \end{pmatrix},$$

where i ranges from 1 to N_f and cs denotes either c or s. We want to determine the trigonometric approximation $p(t)$ of $f(t)$ using frequencies up to order $r_0 - 1$, that is, $\{k\omega : |k| \le r_0 - 1\}$, so

$$f(t) - p(t) = \sum_{|k|=r_0}^{\infty} a_k e^{i2\pi k\omega t}.$$

Therefore, denoting by J the set of indices $\{0, j_i, j_i^+ : i = 1 \div N_f\}$, we have

$$\begin{aligned}
\|\Delta b\| &\leq 2\max_{j\in J} |F^{n_h}_{f-p,T,N}(j)| \\
&\leq 2\max_{j\in J} \sum_{|k|\geq r_0} |a_k||F^{n_h}_{e^{i2\pi k\omega t},T,N}(j)| \qquad (3.16)\\
&\leq 2\max_{j\in J} \sum_{|k|=r_0}^{r_*} |a_k||F^{n_h}_{e^{i2\pi k\omega t},T,N}(j)| + 2\sum_{|k|=r_*+1}^{\infty} |a_k|.
\end{aligned}$$

We will keep r_* as an unknown quantity for the moment, and bound the first term of the above sum but replacing the DFT by the TCFT.

Lemma 3.3.2 *The following inequality is fulfilled:*

$$\#\{k : |k| = j\} \leq \frac{2^m}{(m-1)!}\Big(j + \frac{m}{2}\Big)^{m-1}.$$

Proof: See [17], p. 114. □

Lemma 3.3.3 *If* $\frac{TD}{(r_*+r_0-2)^\tau} > 1 + n_h$, *we have*

$$\sum_{|k|=r_0}^{r_*-1} |a_k||\phi^{n_h}_{e^{i2\pi k\omega t},T}(\frac{j}{T})| \leq$$
$$\frac{2^m C(n_h!)^2 e^{\delta(r_0-1)} \sum\limits_{l=0}^{m-1} \binom{m-1}{l}\big(\frac{m}{2}-r_0+1\big)^{m-1-l} G_f(2r_0-1, r_*+r_0-2, l+\tau(1+2n_h), \delta)}{E_*(m-1)!\pi(TD)^{1+2n_h}}$$

where

$$E_* = \frac{(z_*-1-n_h)^{1+2n_h}}{z_*^{1+2n_h}}, \quad z_* = \frac{TD}{(r_*+r_0-1)^\tau}.$$

Proof: Using the Cauchy estimates and (1.5),

$$\begin{aligned}
\sum_{|k|=r_0}^{r_*-1} |a_k||\phi^{n_h}_{e^{i2\pi k\omega t},T}(\frac{j}{T})| &\leq C\sum_{|k|=r_0}^{r_*-1} e^{-\delta|k|}\frac{(n_h!)^2}{\pi\psi_{n_h}(|Tk\omega - j|)} \\
&\leq \frac{C(n_h!)^2}{\pi}\sum_{|k|=r_0}^{r_*-1}\frac{e^{-\delta|k|}}{(|Tk\omega-j|-n_h)^{1+2n_h}} \qquad (3.17)\\
&\leq \frac{C(n_h!)^2}{\pi}\sum_{|k|=r_0}^{r_*-1}\frac{e^{-\delta|k|}}{\big(\frac{TD}{(|k|+r_0-1)^\tau}-1-n_h\big)^{1+2n_h}} \qquad (3.18)
\end{aligned}$$

For the last step we have used that, since $j \in \{j_i, j_i^+\}$ for some $i = 1 \div N_f$, there exists $k_j \in \mathbb{Z}^m$ such that $|j - Tk_j\omega| \leq 1$, so

$$\begin{aligned} |Tk\omega - j| &\geq |Tk\omega - Tk_j\omega| - |j - Tk_j\omega| \geq T|(k-k_j)\omega| - 1 \geq \frac{TD}{|k-k_j|^\tau} - 1 \\ &\geq \frac{TD}{(|k| + r_0 - 1)^\tau} - 1. \end{aligned}$$

In order to be able to sum the above series with the aid of the incomplete Gamma functions, we choose E_* such that $(x - 1 - n_h)^{1+2n_h} \geq E_* x^{1+2n_h}$ for $x \in \{\frac{TD}{(|k|+r_0-1)^\tau}\}_{|k|=1}^{r_*-1}$. This is accomplished setting $E_* = \frac{(z_*-1-n_h)^{1+2n_h}}{z_*^{1+2n_h}}$ with $z_* = \frac{TD}{(r_*+r_0-2)^\tau}$. Therefore,

$$\begin{aligned} \Phi := \sum_{|k|=r_0}^{r_*-1} |a_k||\phi^{n_h}_{e^{i2\pi k\omega t},T}(\frac{j}{T})| &\leq \frac{C(n_h!)^2}{E_*\pi} \sum_{|k|=r_0}^{r_*-1} \frac{e^{-\delta|k|}}{(\frac{TD}{(|k|+r_0-1)^\tau})^{1+2n_h}} \\ &= \frac{C(n_h!)^2}{E_*\pi(TD)^{1+2n_h}} \sum_{|k|=r_0}^{r_*-1} e^{-\delta|k|}(|k| + r_0 - 1)^{\tau(1+2n_h)}. \end{aligned}$$

Now we apply Lemma 3.3.2,

$$\Phi \leq \frac{C(n_h!)^2}{E_*\pi(TD)^{1+2n_h}} \sum_{j=r_0}^{r_*-1} \frac{2^m}{(m-1)!}(j + \frac{m}{2})^{m-1} e^{-\delta j}(j + r_0 - 1)^{\tau(1+2n_h)},$$

shift the index j,

$$\Phi \leq \frac{2^m C(n_h!)^2}{E_*(m-1)!\pi(TD)^{1+2n_h}} \sum_{j=2r_0-1}^{r_*+r_0-2} (j + \frac{m}{2} - r_0 + 1)^{m-1} e^{-\delta(j-r_0+1)} j^{\tau(1+2n_h)},$$

and expand by Netwon's binomial,

$$\begin{aligned} \Phi &\leq \frac{2^m C(n_h!)^2}{E_*(m-1)!\pi(TD)^{1+2n_h}} \sum_{l=0}^{m-1} \binom{m-1}{l} (\frac{m}{2} - r_0 + 1)^{m-1-l} \sum_{j=2r_0-1}^{r_*+r_0-2} j^{l+\tau(1+2n_h)} e^{-\delta(j-r_0+1)} \\ &= \frac{2^m C(n_h!)^2 e^{\delta(r_0-1)}}{E_*(m-1)!\pi(TD)^{1+2n_h}} \sum_{l=0}^{m-1} \binom{m-1}{l} (\frac{m}{2} - r_0 + 1)^{m-1-l} \sum_{j=2r_0-1}^{r_*+r_0-2} j^{l+\tau(1+2n_h)} e^{-\delta j}. \end{aligned}$$

Now, to show the lemma, we only have to apply Lemma 3.3.1. □

In the proof of the previous lemma, we bounded the continuous Fourier transform of a complex exponential term as

$$|\phi^{n_h}_{e^{i2\pi k\omega t},T}(\frac{j}{T})| \leq \frac{(n_h!)^2}{\pi(\frac{TD}{(|k|+r_0-2)^\tau} - 1 - n_h)^{1+2n_h}}.$$

Therefore, an intrinsic way to choose r_* is to take it equal to the last value of $|k|$ for which the previous bound is < 1. In addition to that, and in order to avoid an excessive amplification of the bound due to the introduction of the E_* constant in the proof of the previous lemma, we will restrict r_* so that $z_* \geq 2(1+n_h)$ and

$$E_* \geq \frac{1}{2^{1+2n_h}}. \tag{3.19}$$

Therefore,

$$r_* = \Big[\Big(\frac{TD}{\max((\frac{(n_h!)^2}{\pi})^{\frac{1}{1+2n_h}}+1+n_h, 2(1+n_h))}\Big)^{\frac{1}{\tau}} - r_0 + 2\Big].$$

Now that we have chosen r_*, we need to bound the error due to the approximation of the discrete Fourier transform by the continuous one. This is done in the two following lemmas.

Lemma 3.3.4 *If* $N - T(r_* + r_0 - 2)\|\omega\|_\infty > 1 + n_h$, *then*

$$\Big|\sum_{|k|=r_0}^{r_*-1} a_k F^{n_h}_{e^{i2\pi k\omega t},T,N}(\frac{j}{T}) - \sum_{|k|=r_0}^{r_*-1} a_k \phi^{n_h}_{e^{i2\pi k\omega t},T}(\frac{j}{T})\Big| \leq$$
$$\frac{2^{m+1}C(n_h!)^2(1+\frac{1}{2n_h})e^{\delta\frac{m}{2}}G_f(r_0+\frac{m}{2}, r_*-1+\frac{m}{2}, m-1, \delta)}{\pi(m-1)!(N-T(r_*+r_0-2)\|\omega\|_\infty - 1 - n_h)^{1+2n_h}}$$

Proof: Using Lemma 3.2.4 and the Cauchy estimates (3.3),

$$\begin{aligned}\Big|\sum_{|k|=r_0}^{r_*-1} a_k F^{n_h}_{e^{i2\pi\frac{Tk\omega}{T}t},T,N}(\frac{j}{T}) - \sum_{|k|=r_0}^{r_*-1} a_k \phi^{n_h}_{e^{i2\pi\frac{Tk\omega}{T}t},T}(\frac{j}{T})\Big| \leq \\ \leq C\sum_{|k|=r_0}^{r_*-1} e^{-\delta|k|}\frac{2(n_h!)^2(1+\frac{1}{2n_h})}{\pi(N-T(r_*+r_0-2)\|\omega\|_\infty - 1 - n_h)^{1+2n_h}},\end{aligned}$$

since, for $|k| = r_0 \div r_* - 1$ and $j \in \{0, j_i, j_i^+ : i = 1 \div N_f\}$ there exists k_j with $|k_j| \leq r_0 - 1$ and $|Tk_j\omega - j| \leq 1$, and therefore

$$j + |Tk\omega| \leq T|k_j\omega| + 1 + T|k\omega| \leq T(|k_j| + |k|)\|\omega\|_\infty + 1 \leq T(r_0 + r_* - 2)\|\omega\|_\infty + 1.$$

Using Lemmas 3.3.2 and 3.3.1 and shifting the summation index by $\frac{m}{2}$ units, we get

$$\begin{aligned}\sum_{|k|=r_0}^{r_*-1} e^{-\delta|k|} &\leq \frac{2^m e^{\delta\frac{m}{2}}}{(m-1)!}\sum_{j=r_0+\frac{m}{2}}^{r_*-1+\frac{m}{2}} j^{m-1}e^{-\delta j} \\ &\leq \frac{2^m e^{\delta\frac{m}{2}}G_f(r_0+\frac{m}{2}, r_*-1+\frac{m}{2}, m-1, \delta)}{(m-1)!},\end{aligned}$$

from which the lemma follows. □

Note that the hypothesis of the previous lemma gives a new constraint for r_*, which is fulfilled if we take

$$r_* = \min\Bigg(\Big[\Big(\frac{TD}{\max((\frac{(n_h!)^2}{\pi})^{\frac{1}{1+2n_h}}+1+n_h, 2(1+n_h))}\Big)^{\frac{1}{\tau}} - r_0 + 2\Big], \Big[\frac{N-1-n_h}{T\|\omega\|_\infty} - r_0 + 1\Big]\Bigg)$$

Now, in order to complete the bound for $\|\Delta b\|$ we only have to bound the remainder.

Lemma 3.3.5 *The following inequality holds:*

$$\sum_{|k|=r_*}^{\infty} |a_k| \leq \frac{2^m C e^{\delta \frac{m}{2}} G_\infty(r_* + \frac{m}{2}, m-1, \delta)}{(m-1)!}$$

Proof: It follows from the Cauchy estimates (3.3), Lemma 3.3.2 and Definition 3.3.2. □

From lemmas 3.3.3, 3.3.4 and 3.3.5 follows a bound for $\|\Delta b\|_\infty$ that is stated in Theorem 3.4.1.

A more explicit description of the behavior of $\sum_{|k|=r_*+1}^{\infty} |a_k|$ is given in proposition 3.3.1. First we need two lemmas.

Lemma 3.3.6 *Define $P_l(j) = \#\{k \in \mathbb{Z}^l : |k| = j\}$. Then, for $j \geq 1$ the following recurrence is satisfied:*

$$P_l(j) = 2 + 2\sum_{s=1}^{j-1} P_{l-1}(s) + P_{l-1}(j), \tag{3.20}$$

with $P_1(j) = 2$. Moreover, $P_l(j)$ is a polynomial in j of degree $l-1$.

Proof: It is obvious that $P_1(j) = 2$. Assume $l \geq 2$. Then every $k \in \mathbb{Z}^l$ can be splitted as $k = (k_1, k_2)$ with $k_1 \in \mathbb{Z}^{l-1}$ and $k_2 \in \mathbb{Z}$. In this way

$$\{k \in \mathbb{Z}^l : |k| = j\} = \{(0, \pm j)\} \cup \left(\bigcup_{s=1}^{j-1} \{(k_1, \pm(j-s)) : |k_1| = s\} \right) \cup \{(k_1, 0) : |k_1| = j\},$$

and (3.20) follows from the fact that $\#\{(0, \pm j)\} = 2$, $\#\{(k_1, \pm(j-s)) : |k_1| = s\} = 2P_{l-1}(s)$ and $\#\{(k_1, 0) : |k_1| = j\} = P_{l-1}(j)$.

We see that $P_l(j)$ has degree $l-1$ in j by induction on l. For $l = 0$ it is true by definition. Assume it true for $l-1$, that is

$$P_{l-1}(j) = \sum_{r=0}^{l-2} c_r j^r.$$

Then

$$P_l(j) = 2 + 2\sum_{s=1}^{j-1} \sum_{r=0}^{l-2} c_r s^r + P_{l-1}(j) = 2 + 2\sum_{r=0}^{l-2} c_r \sum_{s=1}^{j-1} s^r + P_{l-1}(j),$$

and the property follows from the fact that

$$\sum_{s=1}^{j-1} s^r = \frac{1}{r+1} \sum_{s=0}^{r} \binom{r+1}{s} B_s j^{r-s+1}$$

(B_s are the Bernoulli numbers, see e.g. [22]) is a polynomial in j of degree $r+1$. □

Lemma 3.3.7 *(a) For $l, r \in \mathbb{N}$, $x \in \mathbb{C}$, $|x| < 1$ we have*

$$\sum_{j \geq r} j^l x^j = \frac{Q_l(x)}{(1-x)^{l+1}}, \tag{3.21}$$

where $Q_0(x) = x^r$ and $Q_l(x) = (x - x^2)Q'_{l-1}(x) + lxQ_{l-1}(x)$ for $l \geq 1$.

(b) $Q_l(x)$ is a polynomial in x with minimum degree r and maximum degree $r + l$. Moreover, every coefficient in x is a polynomial in r with maximum degree l.

Proof: For $l = 0$, (3.21) is the sum of a geometric series. Assume (3.21) true for $l - 1$. Then

$$\sum_{j \geq r} j^l x^j = x \sum_{j \geq r} j^l x^{j-1} = x \frac{d}{dx} \sum_{j \geq r} j^{l-1} x^j,$$

and using the induction hypothesis,

$$\begin{aligned} x \frac{d}{dx} \sum_{j \geq r} j^{l-1} x^j &= x \frac{d}{dx} \frac{Q_{l-1}(x)}{(1-x)^l} \\ &= \frac{(x - x^2)Q'_{l-1}(x) + lxQ_{l-1}(x)}{(1-x)^{l+1}}. \end{aligned}$$

As for (b), $Q_0(x)$ verifies (b) trivially and, assuming that (b) is true for $Q_{l-1}(x)$, it is readily checked that $Q_l(x) = (x - x^2)Q'_{l-1}(x) + lxQ_{l-1}(x)$ also verifies (b). □

Proposition 3.3.1 *We have*

$$\sum_{|k|=r}^{\infty} |a_k| = O(r^{m-1} e^{-r\delta}) \qquad \text{as } r \to +\infty.$$

Proof: Using the Cauchy estimates (3.3) and Lemma 3.3.6,

$$\sum_{|k|=r}^{\infty} |a_k| \leq C \sum_{|k|=r}^{\infty} e^{-\delta|k|} \leq C \sum_{j=r}^{\infty} P_m(j) e^{-\delta j}, \tag{3.22}$$

where $P_m(j)$ has degree $m - 1$ in j. Assume $P_m(j) = \sum_{s=0}^{m-1} c_{m,s} j^s$ and define $x = e^{-\delta}$. Then

$$\begin{aligned} C \sum_{j=r}^{\infty} P_m(j) e^{-\delta j} &= C \sum_{s=0}^{m-1} c_{m,s} \sum_{j=r}^{\infty} j^s x^j = C \sum_{s=0}^{m-1} c_{m,s} \frac{Q_s(x)}{(1-x)^{s+1}} \\ &= C \sum_{s=0}^{m-1} \Big(\frac{c_{m,s}}{(1-x)^{s+1}} \sum_{l=0}^{s} p_{s,l}(r) x^{r+l} \Big), \end{aligned}$$

where, following Lemma 3.3.7(b), we have expanded $Q_s(x)$ as $\sum_{l=0}^{s} p_{s,l}(r)x^{r+l}$, with $p_{s,l}(r)$ of maximum degree s in r.

To show that this expression is $O(r^{m-1}x^r)$ when $r \to \infty$, it is enough to see that

$$\lim_{r\to\infty} \frac{1}{r^{m-1}x^r} C \sum_{s=0}^{m-1} \Big(\frac{c_{m,s}}{(1-x)^{s+1}} \sum_{l=0}^{s} p_{s,l}(r)x^{r+l} \Big) = C \sum_{s=0}^{m-1} \Big(\frac{c_{m,s}}{(1-x)^{s+1}} \sum_{l=0}^{s} \Big(\lim_{r\to\infty} \frac{p_{s,l}(r)}{r^{m-1}} \Big) x^l \Big)$$

does not depend on r. This is true, since from Lemma 3.3.7(b) the $p_{s,l}$ polynomials are of degree $\le s \le m-1$ and therefore the limit in the right-hand side of the above equation does not depend on r. □

Lemmas 3.3.6 and 3.3.7 also allow to improve the bound of Lemma 3.3.5 for concrete values of m. For instance, if $m = 2$ we have

$$\sum_{\substack{|k|\ge r \\ |k|\in\mathbb{Z}^2}} |a_k| \le 4C \frac{re^{-\delta r} + (1-r)e^{-\delta(r+1)}}{(1-e^{-\delta})^2}.$$

3.4 Final results

We end this section by gathering all the previous results in a single theorem that gives the bound for the error in frequencies and amplitudes. We consider both the case of known and the case of unknown frequencies in a single theorem.

Theorem 3.4.1 *Assume that we perform Fourier analysis of an analytic quasi–periodic function*

$$f(t) = \sum_{k\in\mathbb{Z}^m} a_k e^{i2\pi\omega t},$$

that satisfies the Cauchy estimates with constants $C, \delta > 0$,

$$|a_k| \le Ce^{-\delta|k|},$$

and whose frequency vector $\omega = (\omega_1, \dots, \omega_m)$ satisfies a Diophantine condition of the form

$$|k\omega| > \frac{D}{|k|^\tau},$$

with $D, \tau > 0$. Assume we sample f in N points equally spaced over the interval $[0, T]$, and that we want to determine the frequencies $Tk\omega$ with $1 \le |k| \le r_0 - 1$, $Tk\omega > 0$, and the related amplitudes, from which we have approximations close enough to the actual ones. Assume that we carry out the procedure of section 2.4 with $n_h \ge 1$ and get an approximation of f of the form

$$p(t) = A_0^c + \sum_{l=1}^{N_f} \Big(A_l^c \cos(\frac{2\pi\nu_l t}{T}) + A_l^s \sin(\frac{2\pi\nu_l t}{T}) \Big).$$

Assume also that N is such that $N - T(2r_0-2)\|\omega\|_\infty > 3+n_h$, and T is such that $\frac{TD}{(2r_0-2)^\tau} > 3+n_h$ and $[\nu_{min}] > 2+n_h$. Then, the error in frequencies and amplitudes, which we denote as Δy, can be bounded, in the first order approximation, as

$$\|\Delta y\| \lesssim \|M^{-1}\|\|\Delta b\|, \tag{3.23}$$

where

$$\|M^{-1}\| \leq \frac{\|M_D^{-1}\|}{1-\|M_D^{-1}\|\|M_O\|}$$

and

$$\begin{aligned}\|M_O\| \;\leq\; & \frac{(n_h!)^2}{\pi}\Bigg(\frac{\sqrt{2}(\sum_{l=1}^{N_f} A_l)(\pi+\ln(\frac{TD}{(2r_0-2)^\tau}-1+n_h)-\ln(\frac{TD}{(2r_0-2)^\tau}-2-n_h))+2N_f}{(\frac{TD}{(2r_0-2)^\tau}-1-n_h)^{1+2n_h}}\\ & +\frac{\sqrt{2}(\sum_{l=1}^{N_f} A_l)(\pi+\ln([\nu_{min}]+n_h)-\ln([\nu_{min}]-1-n_h))+2N_f}{([\nu_{min}]-n_h)^{1+2n_h}}\\ & +\frac{4\Big(\sqrt{2}(\sum_{l=1}^{N_f} A_l)(\pi+\ln(N-\Omega_0+n_h)-\ln(N-\Omega_0-1-n_h))+2N_f\Big)(1+\frac{1}{2n_h})}{(N-\Omega_0-n_h)^{1+2n_h}}\Bigg)\end{aligned}$$

and

$$\|M_D^{-1}\| \leq \frac{\|\mathcal{M}_D^{-1}\|}{1-\|\mathcal{M}_D^{-1}\|\varepsilon_1}, \qquad \|\mathcal{M}_D^{-1}\| \leq \frac{\|\mathfrak{M}_D^{-1}\|}{1-\|\mathfrak{M}_D^{-1}\|\varepsilon_2}, \qquad \|\mathfrak{M}_D^{-1}\| \leq \frac{G_{n_h}}{\min(1,A_{min})},$$

with G_{n_h} as in Definition 3.2.4, being

$$\begin{aligned}\varepsilon_1 &= \frac{4(n_h!)^2\Big(\sqrt{2}A_{max}(\pi+\ln(N-\Omega_0+n_h)-\ln(N-\Omega_0-1-n_h))+2\Big)(1+\frac{1}{2n_h})}{\pi(N-\Omega_0-n_h)^{1+2n_h}},\\ \varepsilon_2 &= \frac{(n_h!)^2\Big(\sqrt{2}A_{max}(\pi+\ln(2[\nu_{min}]+n_h)-\ln(2[\nu_{min}]-n_h-1))+2\Big)}{\pi(2[\nu_{min}]-n_h)^{1+2n_h}},\\ \Omega_0 &= T(2r_0-2)\|\omega\|_\infty+1,\end{aligned}$$

As for $\|\Delta b\|$,

$$\begin{aligned}\|\Delta b\| \;\leq\; & \frac{2^{m+1}C}{(m-1)!}\Bigg(\\ & \chi_{\{r_*>r_0\}}\frac{(n_h!)^2 e^{\delta(r_0-1)}\sum_{l=0}^{m-1}\binom{m-1}{l}(\frac{m}{2}-r_0+1)^{m-1-l}G_f(2r_0-1,r_0+r_*-2,l+\tau(1+2n_h),\delta)}{E_*\pi(TD)^{1+2n_h}}\\ & +\chi_{\{r_*>r_0\}}\frac{2(n_h!)^2 e^{\delta\frac{m}{2}}(1+\frac{1}{2n_h})G_f(r_0+\frac{m}{2},r_*-1+\frac{m}{2},m-1,\delta)}{\pi(N-\Omega-n_h)^{1+2n_h}}\\ & +e^{\delta\frac{m}{2}}G_\infty(r_*+\frac{m}{2},m-1,\delta)\Bigg),\end{aligned} \tag{3.24}$$

where

$$
\begin{aligned}
\Omega &= T(r_*+r_0-2)\|\omega\|_\infty+1\\
r_* &= \max\Big(r_0, \min\Big(\Big[\Big(\frac{TD}{\max\big((\frac{(n_h!)^2}{\pi})^{\frac{1}{1+2n_h}}+1+n_h, 2(1+n_h)\big)}\Big)^{\frac{1}{\tau}}-r_0+2\Big],\\
&\qquad \Big[\frac{N-1-n_h}{T\|\omega\|_\infty}-r_0+1\Big]\Big)\Big) \qquad (3.25)\\
E_* &= \frac{(z_*-1-n_h)^{1+2n_h}}{z_*^{1+2n_h}},\\
z_* &= \frac{TD}{(r_*+r_0-2)^\tau},
\end{aligned}
$$

and the G_f, G_∞ functions are those of Definition 3.3.2.

If we assume that the frequencies $\{Tk\omega\}_{|k|\le r_0-1}$ are known and want to compute the amplitudes using the procedure described in Section 2.3, formula (3.23) is still valid, where the bounds for $\|\Delta b\|$ are the same as before and the bounds for $\|M^{-1}\|$ are given by

$$\|M^{-1}\| \le \frac{\|M_D^{-1}\|}{1-\|M_D^{-1}\|\|M_O\|}$$

being

$$
\begin{aligned}
\|M_O\| \;\le\; \frac{N_f(n_h!)^2}{\pi}\Big(&\frac{\sqrt{2}}{\pi(\frac{TD}{(2r_0-1)^\tau}-\frac{1}{2}-n_h)^{1+2n_h}}+\frac{2}{\pi([\nu_{min}]-n_h)^{1+2n_h}}\\
&+\frac{8(1+\frac{1}{2n_h})}{\pi(N-T(2r_0-2)\|\omega\|_\infty-\frac{1}{2}-n_h)^{1+2n_h}}\Big)
\end{aligned}
$$

and

$$\|M_D^{-1}\| \le \frac{\|\mathcal{M}_D^{-1}\|}{1-\|\mathcal{M}_D^{-1}\|\varepsilon_1}, \qquad \|\mathcal{M}_D^{-1}\| \le \frac{\|\mathfrak{M}_D^{-1}\|}{1-\|\mathfrak{M}_D^{-1}\|\varepsilon_2}, \qquad \|\mathfrak{M}_D^{-1}\| \le \frac{5}{3},$$

being

$$\varepsilon_1 = \frac{8(n_h!)^2(1+\frac{1}{2n_h})}{\pi(N-T(2r_0-2)\|\omega\|_\infty-\frac{1}{2}-n_h)^{1+2n_h}}, \qquad \varepsilon_2 = \frac{2(n_h!)^2}{\pi(2[\nu_{min}]-n_h)^{1+2n_h}}.$$

Remark 3.4.1 *The bound for $\|\Delta y\|$ given by the previous theorem can be improved by replacing the first term in the bound for $\|\Delta b\|$ by any of the intermediate inequalities of the proof of Lemma 3.3.3. In this case, it may be necessary to modify the definition of r_*. We will give examples in the following section.*

Corollary 3.4.1 *The block Jacobi method as stated in (2.7), used to obtain the amplitudes from known frequencies, is convergent provided that*

$$\|M_D^{-1}\|\|M_O\| < 1,$$

where for $\|M_D^{-1}\|$ and $\|M_O\|$ we use the bounds given in the previous theorem in the case of known frequencies, but replacing N_f by N_f-1.

Proof: The norm of the iteration matrix of the block Jacobi method (2.7) is

$$\max_{i=1\div N_f}\left(\|B_{i,i}^{-1}\|\sum_{\substack{l=1\\l\neq i}}^{N_f}\|B_{i,l}\|\right) < \|M_D^{-1}\|\|M_O\|.$$

The reason for replacing N_f by N_f-1 in the bounds of the previous theorem is that we apply the block Jacobi method to system (2.3) without its first equation. $\square$

Chapter 4

A numerical example

In this Chapter we apply the procedure developed in Chapter 2 to a family of quasi–periodic functions for which explicit expressions for its frequencies and amplitudes can be computed. These expressions are used to test the error estimates developed in Chapter 3.

4.1 The family of functions analyzed

In order to illustrate the procedures described and to test the error bounds obtained, we have analyzed a family of quasiperiodic functions from which the Fourier coefficients can be explicitly calculated. The functions are

$$f_\mu(t) = \frac{\sin(2\pi\omega_1 t + \varphi_1)}{1-\mu\cos(2\pi\omega_1 t+\varphi_1)} \cdot \frac{\sin(2\pi\omega_2 t + \varphi_2)}{1-\mu\cos(2\pi\omega_2 t+\varphi_2)}, \qquad \mu \in [0,1).$$

They verify $f_\mu(t) = \sum_{k\in\mathbb{Z}^2} a_k^{\mu,\varphi} e^{2\pi i(\omega,k)t}$ with

$$a_k^{\mu,\varphi} = \begin{cases} \frac{-\operatorname{sign}(k_1k_2)}{\mu^2} c_2^{|k|} e^{i(k,\varphi)} & \text{if } k_1, k_2 \neq 0 \\ 0 & \text{if } k_1 = 0 \text{ or } k_2 = 0 \end{cases} \tag{4.1}$$

being

$$\omega = (\omega_1,\omega_2), \quad \varphi = (\varphi_1,\varphi_2) \quad \text{and} \quad c = \frac{1-\sqrt{1-\mu^2}}{\mu}$$

The parameter μ is directly related to the parameter δ in the Cauchy estimates (3.3), namely

$$\delta = \operatorname{Im}\arccos\frac{1}{\mu} = -\log c.$$

4.2 Numerical results

In this section we will show the results corresponding to apply the algorithm described in 2.5.1 to the f_μ functions for $\omega = (1,\sqrt{2})$, $\varphi = (\sqrt{0.2},\sqrt{0.3})$, $n_h = 2$ and several values of μ, T and N. For the chosen value of ω, the parameters D and τ of the Diophantine condition (3.2) are 0.85355 and 1, respectively. We have stopped the procedure when all the frequencies (with nonzero amplitudes) of order $|k| \leq 5$ have been refined. The error of the Fourier approximation as well as the corresponding bound, as given by theorem 3.4.1, are shown in Fig. 4.1.

It must be noted that the error in frequencies and amplitudes is much smaller than the difference between the analyzed function f and its computed quasi–periodic approximation Q_f. For instance, in the case of $\mu = 0.9$, from (4.1) the maximum amplitude of the frequencies not determined is ${c_2}^6/\mu^2 = 0.6268$, whereas we reach errors as small as 10^{-14} for some values of T and N. This is due to the fact that the truncation error of our procedure is not introduced by the difference $f - Q_f$ but by its DFT, as is seen in Section 3.

We observe that, for every value of T, as N increases the error decreases and becomes constant after a value of N. We also note that the minimum error for each value of T decreases as we increase T. This behavior of the error in terms of the parameters T, N, can be explained in terms of the bound (3.16).

Let r_1 be such that $2C \sum_{|k|=r_1}^{\infty} e^{-\delta|k|} |F^{n_h}_{e^{i2\pi k\omega t},T,N}(Tk\omega - j)|$ is small (this might be different from the order r_* of Section 3, which is "the order up to which the TCFT helps"). Then the frequencies of order greater than r_1 can be considered irrelevant and we can focus in frequencies of orders from r_0 to $r_1 - 1$. If N is large enough, we can replace the DFT by the TCFT in (3.16), that is

$$\|\Delta b\| \lesssim \max_{j \in \{0, j_i, j_i^+\}_{i=1}^{N_f}} 2C \sum_{|k|=r_0}^{r_1-1} e^{-\delta|k|} |\phi^{n_h}_{e^{i2\pi k\omega t},T}(\frac{Tk\omega - j}{T})|.$$

In order to normalize, we note that $|\phi^{n_h}_{e^{i2\pi k\omega t},T}(\frac{Tk\omega-j}{T})| \leq |g^{n_h}(Tk\omega - j)| = |\widetilde{g}^{n_h}(Tk\omega - j)|$, being

$$g^{n_h}(\alpha) = \frac{(-1)^{n_h}(n_h!)^2(e^{i2\pi\alpha} - 1)}{2\pi i \psi_{n_h}(\alpha)}, \qquad \widetilde{g}^{n_h}(\alpha) = \frac{(-1)^{n_h}(n_h!)^2}{\pi i \psi_{n_h}(\alpha)}.$$

The moduli of these functions are plotted in Fig. 4.2. As T increases, the differences $|Tk\omega - j|$ become larger and, since $|\widetilde{g}^{n_h}(\alpha)|$ decreases with $|\alpha|$, this explains why, for sufficiently large N, the error decreases as T increases.

In order to consider the case in which N is not large, we note $|F^{n_h}_{e^{i2\pi k\omega t,T,N},T,N}(j)| = |h^{n_h}_N(Tk\omega - j)| \leq |\widetilde{h}^{n_h}_N(Tk\omega - j)|$, being

$$\begin{aligned} h^0_N(\alpha) &= \frac{1 - e^{i2\pi\alpha}}{N(1 - e^{i2\pi\alpha/N})}, & h^{n_h}_N(\alpha) &= \frac{q_{n_h}}{2^{n_h}} \sum_{l=-n_h}^{n_h} (-1)^l \binom{2n_h}{n_h + l} h^0_N(\alpha + l), \\ \widetilde{h}^0_N(\alpha) &= \frac{2}{N(1 - e^{i2\pi\alpha/N})}, & \widetilde{h}^{n_h}_N(\alpha) &= \frac{q_{n_h}}{2^{n_h}} \sum_{l=-n_h}^{n_h} (-1)^l \binom{2n_h}{n_h + l} \widetilde{h}^0_N(\alpha + l). \end{aligned}$$

The moduli of these functions are plotted in Fig. 4.2. Now, if N is not large enough, it may happen that one of the $|Tk\omega - j|$ approaches N and raises the bound (3.16). This explains the fact that, for a fixed value of T, as we decrease N the error ends up increasing.

The qualitative behaviour of the bound given by theorem 3.4.1 is not the same as the one of the real error. For each value of T, as N increases, the bound given by theorem

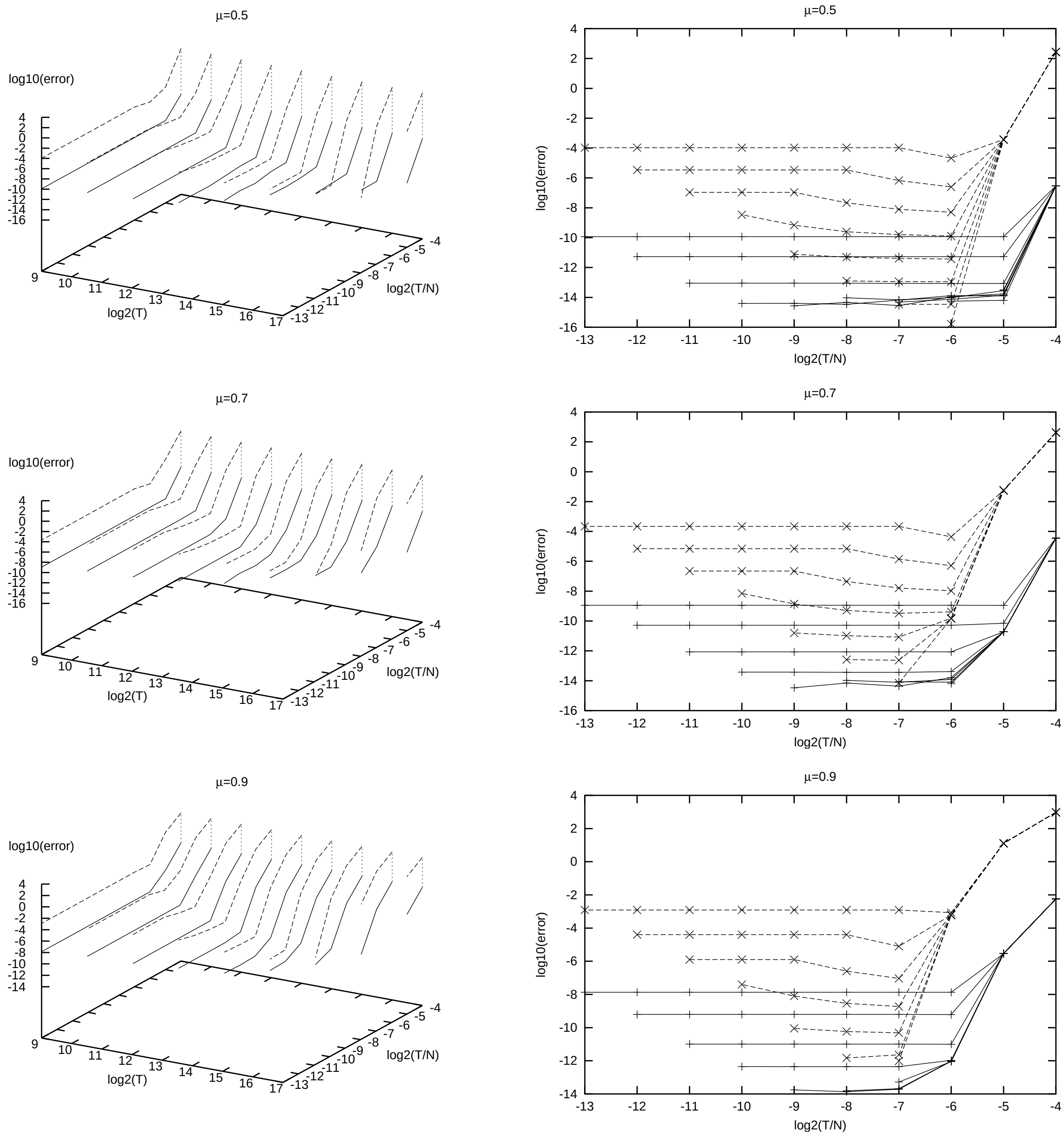

Figure 4.1: Fourier analysis of the f_μ functions for $\mu = 0.5, 0.7, 0.9$ and several values of T and N. Points corresponding to analysis with the same value of T have been joined by lines. The solid lines represent the error in frequencies and amplitudes of the corresponding Fourier analysis. This means that we have represented the maximum value between the error in the frequencies in the error in the amplitudes. The points joined by dashed lines correspond to the bound given by theorem 3.4.1. The right–hand figures are the (y, z) projection of the left–hand side ones.

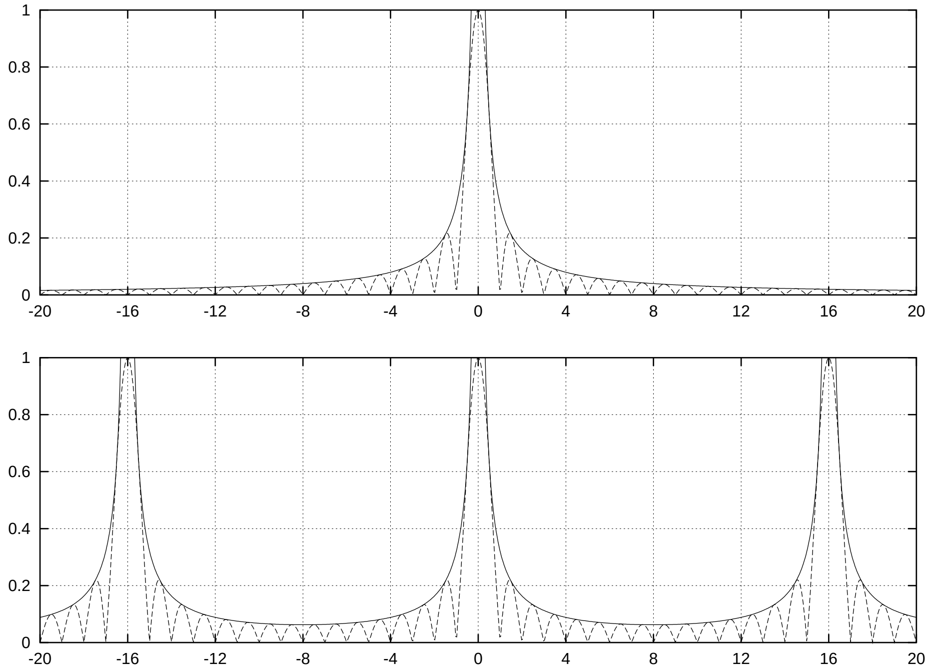

Figure 4.2: Top: graph of the functions $|g^{n_h}(\alpha)|$ (dashed line) and $|\widetilde{g}^{n_h}(\alpha)|$ (solid line) for $n_h = 0$. Bottom: graph of the functions $|h_N^{n_h}(\alpha)|$ (dashed line) and $|\widetilde{h}_N^{n_h}(\alpha)|$ (solid line) for $n_h = 0$ and $N = 16$.

3.4.1 decreases up to a minimum value, then increases slightly and becomes constant. This increasing is due to the introduction of the E_* constant in the proof of the Lemma 3.3.3, which can enlarge the bound by a factor $1/E_*$ (at most 32 for $n_h = 2$, see (3.19)). In Fig. 4.3, we evaluate the bound for $\|\Delta y\|$ replacing the first term in (3.24) by (3.18), which is the last bound in the proof of 3.3.3 before the introduction of E_*. We see how the increasing of the bound after the minimum of Fig 4.1 disappears.

The drawback of this approach is that the sum in (3.18) runs over multiindices $|k| = r_0 \div r_* - 1$ instead of their orders $j = r_0 \div r_* - 1$, and its evaluation can be prohibitive in terms of computing time, especially if the number of basic frequencies m is large. An alternative could be to lower r_* in (3.25) in order to raise the minimum value of E_*. For instance, if we set r_* equal to

$$r_* = \max\Big(r_0, \min\Big(\Big[\big(\frac{TD}{\max\big(\big(\frac{(n_h!)^2}{\pi}\big)^{\frac{1}{1+2n_h}} + 1 + n_h, \frac{1+n_h}{1-(1/2)^{1/(1+2n_h)}}\big)}\big)^{1/\tau} - r_0 + 2\Big], \Big[\frac{N-1-n_h}{T\|\omega\|_\infty} - r_0 + 1\Big]\Big)\Big),$$

then the minimum allowed value of E_* is $1/2$. But this can lead to a worse global bound if the Fourier coefficients $|a_k|$ decrease slowly, as we illustrate in table 4.1. A different alternative is to take as value of r_* the one that minimizes the bound given by theorem 3.4.1. The results in this case are given in Fig. 4.5. Of course, they are worse that the ones of Fig. 4.3.

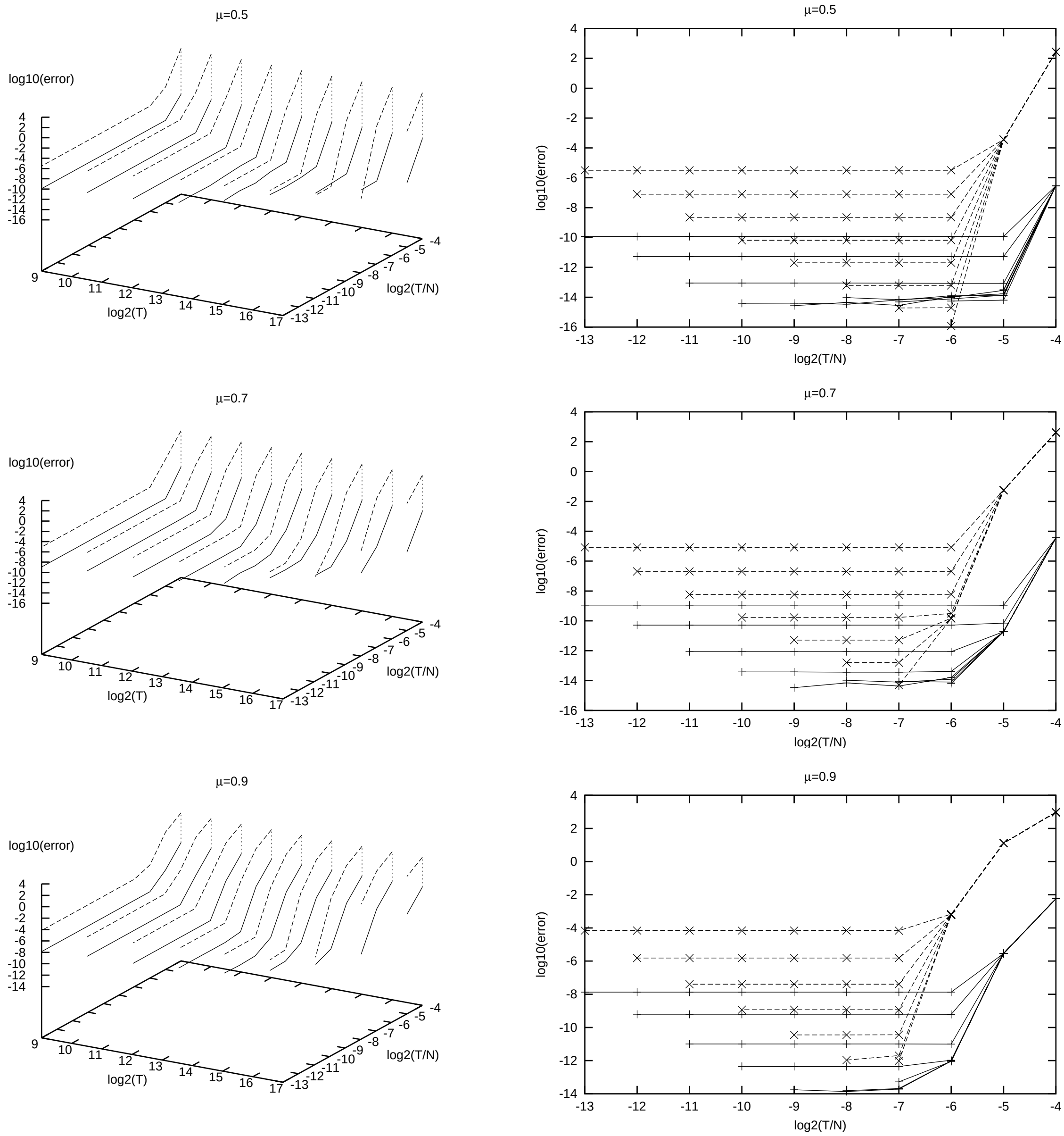

Figure 4.3: This is the same exploration as the one of Fig. 4.1, except that the dashed lines represent the bound obtained replacing the first term in (3.24) by (3.18).

$\max 1/E_*$	μ	T	N	r_*	actual $1/E_*$	bound
32	0.9	1024	262144	61	3.53332	4.53023E–06
32	0.9	1024	524288	121	16.4812	2.08997E–05
32	0.9	1024	1048576	141	31.2714	3.96552E–05
2	0.9	1024	262144	33	1.97207	1.32447E–02
2	0.9	1024	524288	33	1.97207	1.32447E–02
2	0.9	1024	1048576	33	1.97207	1.32447E–02

Table 4.1: Computation of the bound given by theorem 3.4.1 using two different maximum allowed values for $1/E_*$. We see how, by lowering the maximum value of $1/E_*$, the bound can increase drastically.

In Fig. 4.3, the bound is still several orders of magnitude larger than the actual error. This is due to the Diophantine condition, which give only a lower bound for the difference between frequencies. This difference reaches the Diophantine condition in very few cases, as shown in Fig. 4.4. In Fig. 4.6 we evaluate the bound of theorem 3.4.1 by replacing the first term of the bound of $\|\Delta b\|$ by (3.17). We see that in this case there is a very good agreement between the error predicted and the actual error.

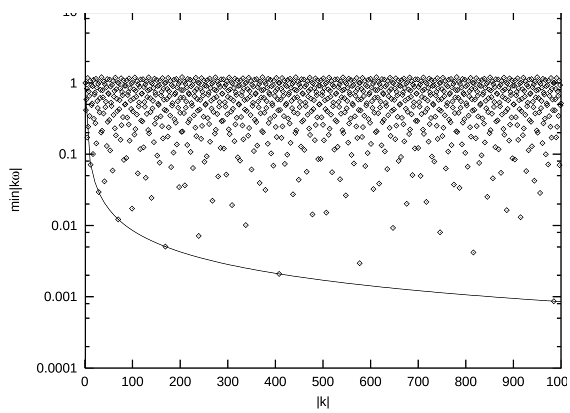

Figure 4.4: Illustration of the non–optimality of the Diophantine condition. The points represent the values of $\min_{|k|=\text{const.}} |k\omega|$ for $|k| = 1 \div 1000$. The curve represents the values of the Diophantine condition $0.85355/|k|$. The only points that are approximately on the curve $0.85355/|k|$ correspond to the values $|k|$=1, 2, 5, 12, 29, 70, 169, 408, 985.

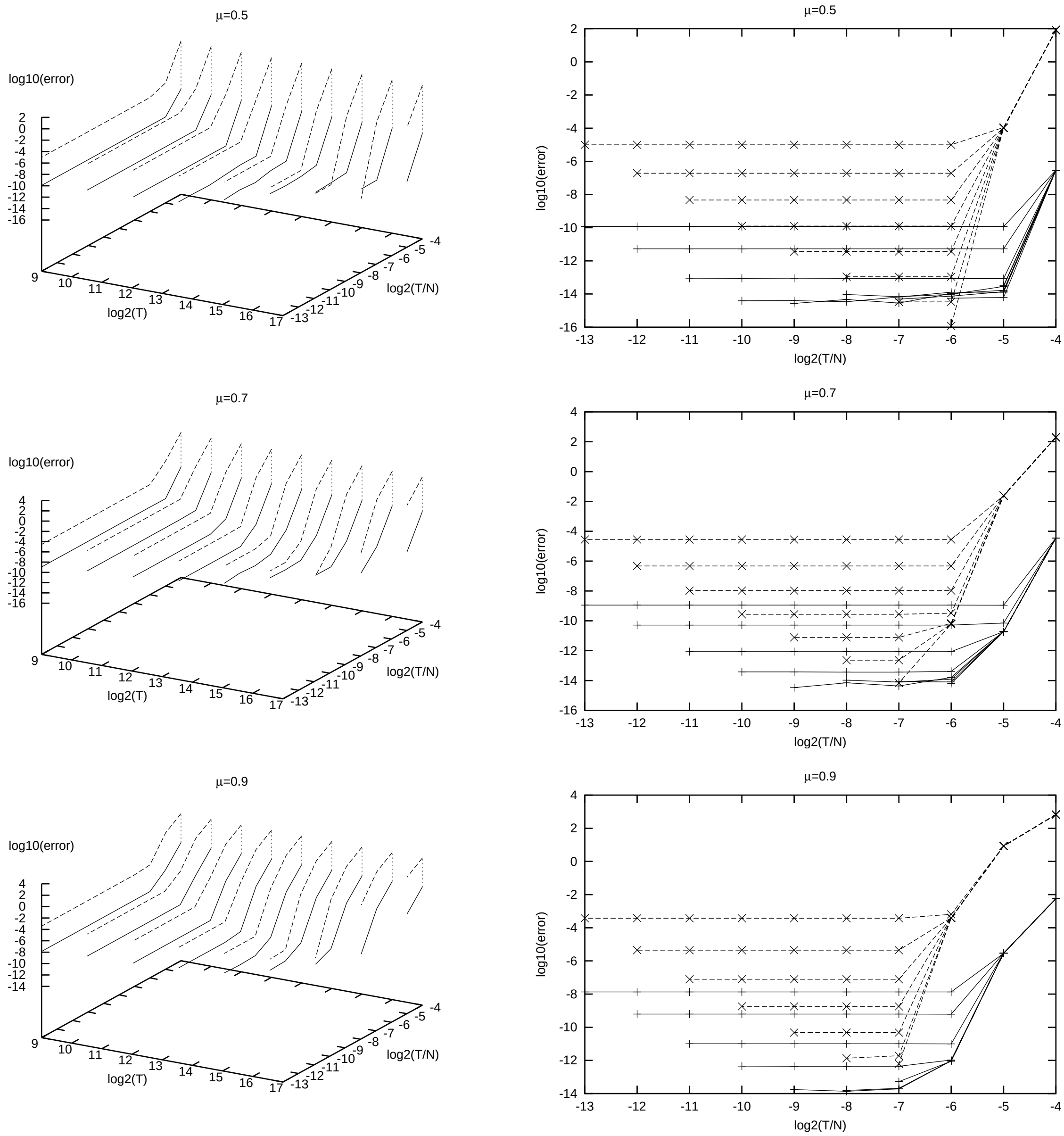

Figure 4.5: This is the same exploration as the one of Fig. 4.1, except that the error bound represented by the dashed lines is obtained by minimizing $\|\Delta b\|$ with respect to r_* in theorem 3.4.1, instead of using (3.25).

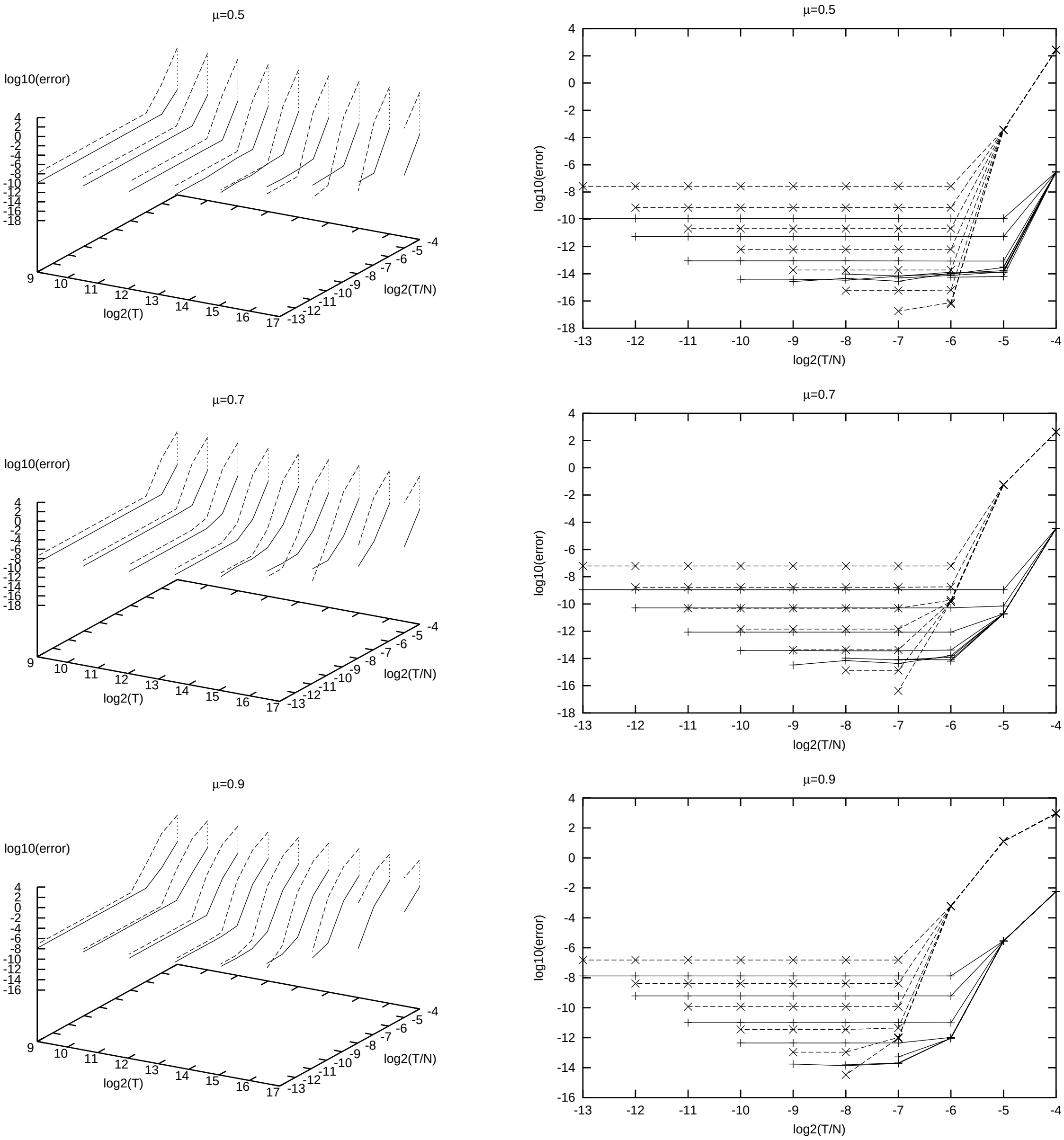

Figure 4.6: This is the same exploration as the one of Fig. 4.1, except that the error bound represented by the dashed lines is obtained by replacing the first term of (3.24) by (3.17).

Chapter 5

Application to the development of Solar System models

In this chapter we apply the procedures of Chapter 2 to the development of simplified models for the motion in the Solar System. They are based on Fourier analysis of the time–dependent part of the real Solar System equations of motion written as a perturbation of the RTBP (see Appendix A). We develop models for the Earth–Moon and Sun–Earth+Moon systems by selecting frequencies from the computed Fourier expansions in a suitable manner. These models are tested against other well–known models through the computation of residual accelerations along selected orbits.

5.1 Introduction

Through this chapter, we will denote the bodies of the Solar System as

$$\mathcal{S} = \{P_1, \ldots, P_9, P_{10}, P_{11}\} \tag{5.1}$$

where $P_1,\ldots,P_{11}$ denote Mercury, Venus, Earth, Mars, Jupiter, Saturn, Uranus, Neptune, Pluto, the Moon and the Sun, respectively. We will also denote the Earth, the Moon and the Sun as E, M and S, respectively. The mass of $P_I \in \mathcal{S}$ will be denoted as m_{P_I}.

Sometimes we will be interested in considering the Earth and the Moon as a single body, located at the Earth–Moon barycentre. We will denote this "virtual" body as P_{12}. In this case, we will consider a modified Solar System

$$\mathcal{S} = \{P_1, P_2, P_4, \ldots, P_9, P_{11}, P_{12}\}, \tag{5.2}$$

which is denoted as before in order to reduce notation.

Let us consider two bodies $I, J \in \mathcal{S}$ (either the "true" Solar System or the modified one) with $m_I > m_J$, which we will call *primaries*. We can choose coordinates $(x, y, z)^\top$ and time units t such that

- the bodies I, J remain fixed at the positions $(\mu_{I,J}, 0, 0)^\top$ and $(\mu_{I,J} - 1, 0, 0)^\top$, respectively, being
$$\mu_{I,J} = \frac{m_J}{m_I + m_J},$$

- the body J completes a revolution around I in 2π time units.

Such coordinates will be called *adimensional* and are introduced in Appendix A (Section A.4). In these coordinates, the equations of motion of a particle under the Newtonian attraction of the bodies of the Solar System can be written as

$$\left\{\begin{array}{rcl}\ddot{x} & = & c_1 + c_4\dot{x} + c_5\dot{y} + c_7 x + c_8 y + c_9 z + c_{13}\dfrac{\partial\Omega}{\partial x},\\ \ddot{y} & = & c_2 - c_5\dot{x} + c_4\dot{y} + c_6\dot{z} - c_8 x + c_{10} y + c_{11} z + c_{13}\dfrac{\partial\Omega}{\partial y},\\ \ddot{z} & = & c_3 - c_6\dot{y} + c_4\dot{z} + c_9 x - c_{11} y + c_{12} z + c_{13}\dfrac{\partial\Omega}{\partial z},\end{array}\right. \tag{5.3}$$

being

$$\begin{aligned}\Omega &= \frac{1-\mu_{I,J}}{\sqrt{(x-\mu_{I,J})^2+y^2+z^2}} + \frac{\mu_{I,J}}{\sqrt{(x-\mu_{I,J}+1)^2+y^2+z^2}}\\ &\quad + \sum_{\substack{j\in\mathcal{S}\\ j\neq I,J}} \frac{\mu_{I,J,j}}{\sqrt{(x-x_j)^2+(y-y_j)^2+(z-z_j)^2}}\end{aligned} \tag{5.4}$$

where

$$\mu_{I,J,j} = \frac{m_j}{m_I + m_J},$$

and $(x_j, y_j, z_j)^\top$ are the adimensional coordinates of the body $j \in \mathcal{S}$. In system (5.3), $\{c_i\}_{i=1\div 13}$ are time–dependent functions which can be computed in terms of the positions, velocities, accelerations and over–accelerations of the two primaries I, J. The actual formulae are given in Appendix A. If we set $c_5 = 2$, $c_7 = c_{10} = c_{13} = 1$ and the remaining c_i equal to zero, and we skip the sum in (5.4), then (5.3) become the RTBP equations (A.1) with mass parameter $\mu_{I,J}$. Therefore, we can see (5.3) as a perturbation of the RTBP equations. We can get an idea of the order of this perturbation by looking at the coefficient A_1 of the Fourier expansions of the c_i functions in Appendix A, tables C.1 to C.13 and C.41 to C.53.

In order to evaluate the previous system of equations, we need the positions of the bodies of the Solar System, as well as its derivatives with respect to time up to order three. They can be computed from any analytical or numerical planetary ephemeris. In the computations we have used the JPL ephemeris DE406, because of its high precision over a 6000–year time span. It has the drawback of introducing discontinuities in accelerations and over–accelerations, which are discussed in Appendix B. Higher precision can be obtained by using DE405, but the time span is reduced to 600 years in this case.

In the following sections, we will develop intermediate models between the RTBP and the "real" Solar System (5.3). The strategy followed is to "add basic frequencies" to the RTBP, these frequencies being computed by applying the techniques described in Chapter 2 to the $\{c_i\}_{i=1\div 13}$ and $\{(x_j, y_j, z_j)^\top\}_{j\in\mathcal{S}}$ functions. The models will be developed for

- the Earth–Moon case, which means to consider $I = P_3$ and $J = P_{10}$, being $\mathcal{S}$ as in (5.1), and

- the Sun–Earth+Moon case, which means to consider $I = P_{11}$ and $J = P_{12}$, being $\mathcal{S}$ as in (5.2).

Although we will only cover these two cases, the methodology used can be applied to any pair of primaries.

5.2 Fourier analysis of the time-dependent part of the real Solar System in adimensional coordinates

We give in this section the results of the Fourier analysis of the time–dependent part of system (5.3).

5.2.1 Fourier analysis of the c_i functions

Applying the algorithm described in section 2.5.1, we have performed Fourier analysis of the $\{c_i\}_{i=1\div 13}$ functions, both for the Earth–Moon case and the Sun–Earth+Moon case. The parameters used have been: number of total iterates in the Fourier procedure $n = 10$, minimum value of the frequency threshold $b_{min} = 1\text{E–}10$, Hanning level $n_h = 2$ and several values of the length of the time interval T and the number of points N whose choice will be discussed bellow. The frequency threshold b of the algorithm of 2.5.1 has never reached the value b_{min}, because all the analysis have finished due to the detection of close frequencies. In each analysis, we have computed the maximum difference between the analyzed c_i function and its quasi–periodic approximation, that is,

$$d_{max} = \max_{l=0\div N-1} |c_i(l\tfrac{T}{N}) - Q_{c_i}(l\tfrac{T}{N})|, \tag{5.5}$$

where c_i is the analyzed function and Q_{c_i} its quasi–periodic approximation. In figures 5.1 (Earth–Moon case) and 5.2 (Sun–Earth+Moon case), we have represented the minimum of d_{max} with respect to N for each value of T.

Since we have no a priori information of the behavior of the c_i functions, we have based our choice of the T, N parameters according to the following criteria:

- We have chosen time intervals starting at Jan 1st 2001 and of length at least 95 years.
- We have followed strategies to avoid aliasing.
- We have considered that a set of frequencies is “better” than another if the value of d_{max} related to the first set is smaller than the one related to the second one.

Due to our implementation of the Fourier analysis procedures, the N parameter must range over powers of two. For consistency, the T parameter has also been chosen to range over a geometric progression. The time interval of all analysis starts in January 1st, 2001. The smallest time interval length, T_{min}, has been taken of 95 years (34698.75

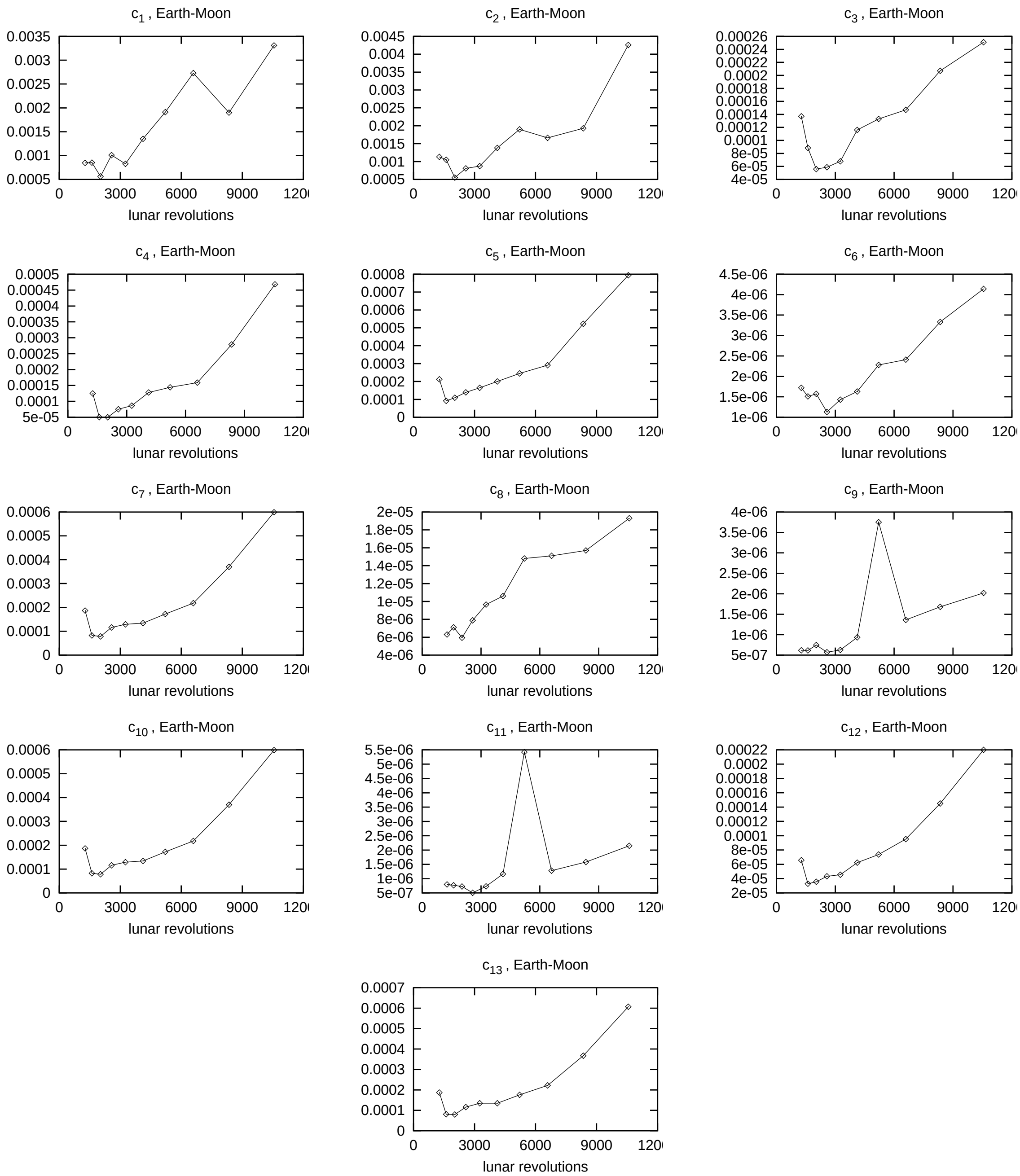

Figure 5.1: Error results of the Fourier analysis of the c_i functions in the Earth–Moon case. For each value of T explored, we have represented the minimum value of d_{max} with respect to N.

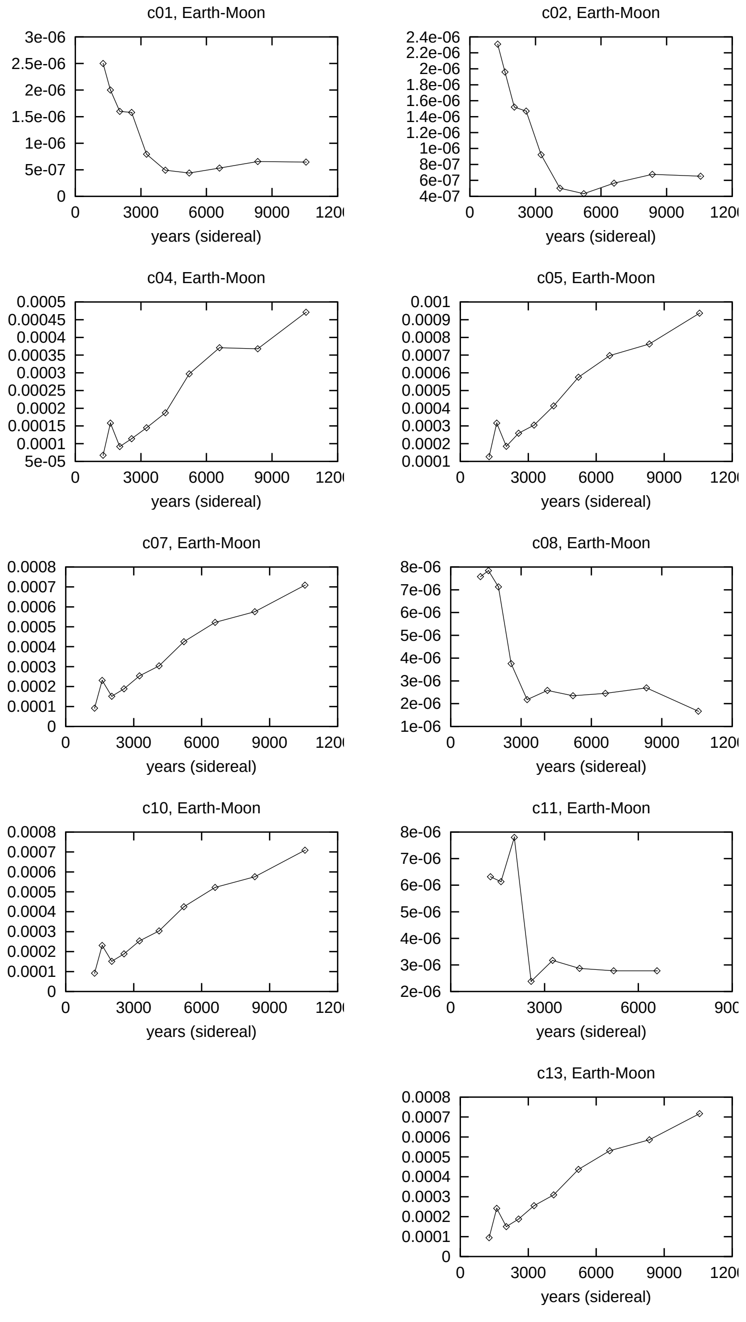

Figure 5.2: Same as Fig. 5.1 but for the Sun–Earth+Moon case.

Julian days). The greatest time-interval length, T_{max}, has been chosen as the maximum time interval given by the JPL DE406 ephemerides after Jan 1st 2001, which is 364938 Julian days (999.15 years). Therefore, we have let T range over the set $\{\delta^n T_{min}\}_{n=0}^{10}$ where $\delta = (T_{max}/T_{min})^{1/10}$. The time units used for these Fourier analysis are revolutions of the secondary (J) around the primary (I), or equivalently, adimensional time divided by 2π. The reason for this is that, in this way, the frequency 1.0 corresponds to one revolution of J around I, which has a more intuitive meaning (one lunar month in the Earth–Moon case, one sidereal year in the Sun–Earth+Moon case). Moreover, in order to evaluate the trigonometric approximations of the c_i functions, we only have to multiply the frequencies found by adimensional time, without the need of an additional 2π factor. For instance, T_{min} is equal to 7979.72 in the Earth–Moon case, which means that during this time span the Moon has given 7979.72 revolutions around the Earth. For the Sun–Earth+Moon case, $T_{min} = 596.891$ (see Appendix A.4 for the details).

The maximum number of samples N_{max} has been chosen to be 2^{20}, in order to allow for "comfortable" runs on machines with 64MB of memory (or, equivalently, bi–processor machines with 128MB). For each value of T, the minimum number of samples has been chosen such that $\frac{T}{2N} \geq 1.5$, in order to make the maximum detectable frequency to be at least 1.5.

In order to control aliasing, two different strategies have been followed. The first one is based on time–domain, and consists in computing the difference between the initial function and its quasi-periodic approximation over a refinement of the grid used for the Fourier analysis. This difference will be denoted as α_1. If it increases significantly with respect to the difference over the Fourier samples, then aliasing is very likely to occur. We usually take $16N$ points equally spaced on $[0, T]$ for this test.

The second anti–aliasing strategy is based on frequency–domain. It consists in computing the number of rightmost consecutive harmonics of the residual DFT that have modulus less than a fraction of the maximum modulus of the residual DFT. Then, we divide this number by $N/2$, the total number of harmonics. That is, we compute

$$\alpha_2 = \frac{\max\{j : p^{n_h}_{c_i-q,T,N}(i) \leq p_{max}/25 \text{ for } i = j \div N/2\}}{N/2}$$

being $p_{max} := \max_{j=0\div N/2} p^{n_h}_{c_i-q,T,N}(j)$, where $p^{n_h}_{c_i-q,T,N}(j)$ is defined as in Section 1.3, c_i is the analyzed function and q its quasi–periodic approximation. Then, for instance, a value of 0.2 for α_1 means that there are no frequencies greater than $0.8\omega_{max}$, being $\omega_{max} = \frac{N}{2T}$, with amplitude greater than 1/25 times the modulus of the residual DFT, so we do not expect aliasing in the corresponding Fourier analysis. We are assuming here that amplitudes decrease as frequencies increase, which is ensured by the Cauchy estimates (3.3) for an analytic quasi–periodic function.

As an example of aliasing and how the two previously–described strategies detect it, we have represented in Fig. 5.3 the residual DFT of some of the Fourier analysis of the c_1 function in the Earth-Moon case. We give some details about these analysis in Table 5.1. In the left plot, we see that for $N = 16384$ there are frequencies of high amplitude near $\omega_{max} = \frac{T}{2N} = \frac{16384}{2\times 2033.24} = 4.02903$. As we increase N, the amplitude of the frequencies near ω_{max} decrease and the values of d_{max} and the first anti–aliasing strategy of Table 5.1 become closer.

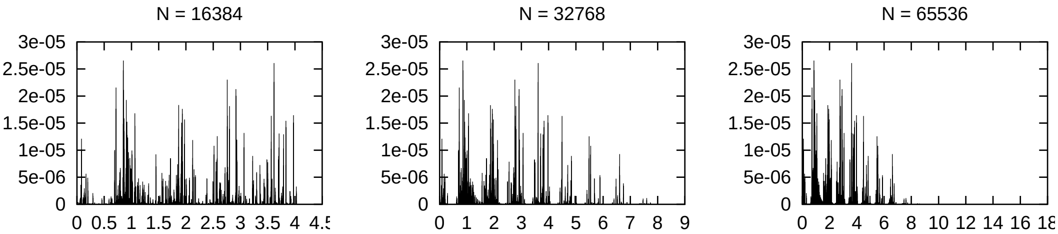

Figure 5.3: Modulus of the residual DFT some of the Fourier analysis of the c_1 function in the Earth–Moon case. From left to right, the values ω_{max} of the right–end of the DFT window are: 4.02903, 8.05806 and 16.1161.

day_0	day_f	T	N	p_{max}	d_{max}	α_1	α_2
366	55917.4	2033.24	16384	2.66E–05	4.90E–04	2.29E–03	0.0007
366	55917.4	2033.24	32768	2.66E–05	5.30E–04	5.67E–04	0.1633
366	55917.4	2033.24	65536	2.66E–05	5.63E–04	5.67E–04	0.5816

Table 5.1: Parameters associated to the Fourier analysis of Fig. 5.3. From left to right: day_0 and day_f are the starting and ending Julian days of the time interval used for each Fourier analysis, taking Jan 1st, 2001 as origin, T is the length of the Fourier interval, in J–revolutions, N is the number of points used, p_{max} is the maximum modulus of the residual DFT, d_{max} is the maximum difference between c_1 and its quasi–periodic approximation over the Fourier analysis samples, and α_1, α_2 are the values of the two anti–aliasing strategies described in the text.

According to this, for the results displayed in figures 5.1 and 5.2 only those analysis with $\alpha \geq 0.2$ have been taken into account.

For the generation of simplified models for the Solar System, among all the analysis performed we have selected the best ones in terms of minimum p_{max}. They are given in tables 5.2 (Earth–Moon) and 5.3 (Sun–Earth+Moon).

5.2.2 Fourier analysis of the positions of the planets

In order to complete the quasi–periodic approximation of all the time-dependent part in the vector–field (5.3), we give in this section the results of the Fourier analysis of the positions of the Solar System bodies in adimensional coordinates. For each coordinate x_{P_i}, y_{P_i}, z_{P_i}, we have performed Fourier analysis using the same parameters as for the analysis of the c_i functions. The minimum value of p_{max} with respect to N for fixed values of T is plotted in figures 5.4 (Earth–Moon) and 5.6 (Sun–Earth+Moon). The best analysis are given in tables 5.4 and 5.5.

function	T (days)	T (years)	T (J–rev.)	N	p_{max}	d_{max}
c_1	55551.4	152.091	2033.24	65536	2.66E–05	5.63E–04
c_2	55551.4	152.091	2033.24	65536	2.67E–05	5.49E–04
c_3	55551.4	152.091	2033.24	32768	3.30E–06	5.58E–05
c_4	55551.4	152.091	2033.24	65536	2.31E–06	5.01E–05
c_5	43904.0	120.203	1606.94	32768	4.85E–06	9.16E–05
c_6	70288.7	192.440	2572.64	32768	3.92E–08	1.13E–06
c_7	55551.4	152.091	2033.24	65536	3.51E–06	7.81E–05
c_8	55551.4	152.091	2033.24	524288	1.96E–07	5.94E–06
c_9	70288.7	192.440	2572.64	65536	1.97E–08	5.69E–07
c_{10}	55551.4	152.091	2033.24	65536	3.51E–06	7.83E–05
c_{11}	70288.7	192.440	2572.64	65536	1.67E–08	5.05E–07
c_{12}	43904.0	120.203	1606.94	32768	1.58E–06	3.29E–05
c_{13}	55551.4	152.091	2033.24	65536	3.51E–06	7.99E–05

Table 5.2: Values of the parameters for the best Fourier analyses of the c_i functions for the Earth–Moon case.

function	T (days)	T (J–rev)	N	p_{max}	d_{max}
c_1	142382.6	389.815	65536	4.95E–08	4.40E–07
c_2	142382.6	389.815	65536	4.95E–08	4.33E–07
c_3	112529.5	308.083	131072	2.28E–09	2.68E–08
c_4	34698.8	94.998	4096	8.34E–06	6.74E–05
c_5	34698.8	94.998	4096	1.75E–05	1.26E–04
c_6	88935.7	243.488	262144	1.76E–08	5.71E–07
c_7	34698.8	94.998	4096	1.36E–05	9.17E–05
c_8	288422.1	789.642	524288	9.65E–08	1.67E–06
c_9	88935.7	243.488	131072	9.71E–09	3.19E–07
c_{10}	34698.8	94.998	4096	1.36E–05	9.17E–05
c_{11}	70288.7	192.436	524288	2.35E–08	2.38E–06
c_{12}	34698.8	94.998	4096	3.92E–06	4.06E–05
c_{13}	34698.8	94.998	4096	1.34E–05	9.47E–05

Table 5.3: Values of the parameters for the best Fourier analyses of the c_i functions for the Sun–Earth+Moon case. Note that, in this case, J–revolutions are sidereal years.

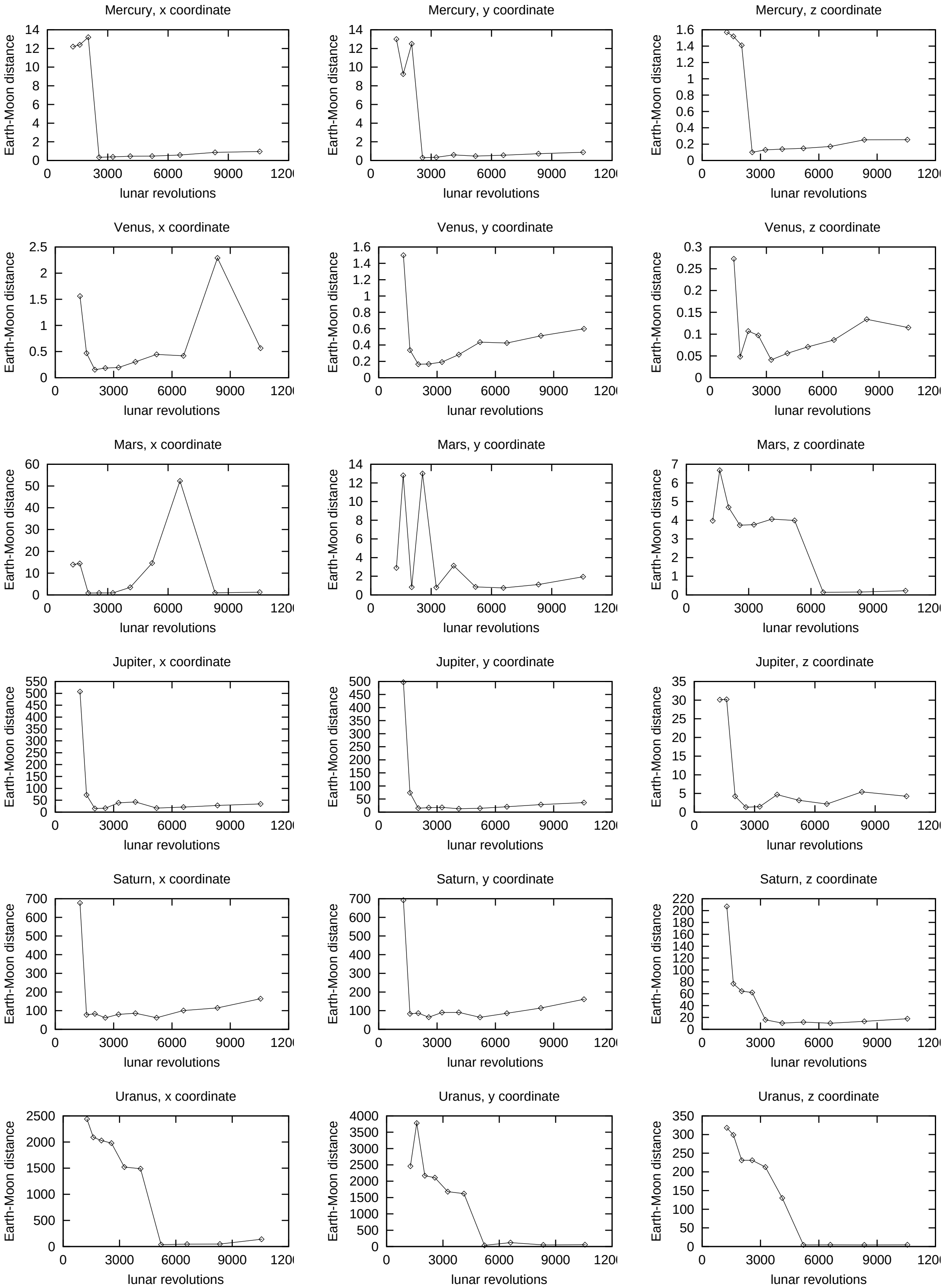

Figure 5.4: Error results of the Fourier analysis of the coordinates of the Solar System bodies (in adimensional coordinates) for the Earth–Moon case. For each value of T explored, we have represented the minimum value of d_{max} with respect to N. They are continued in Fig. 5.5.

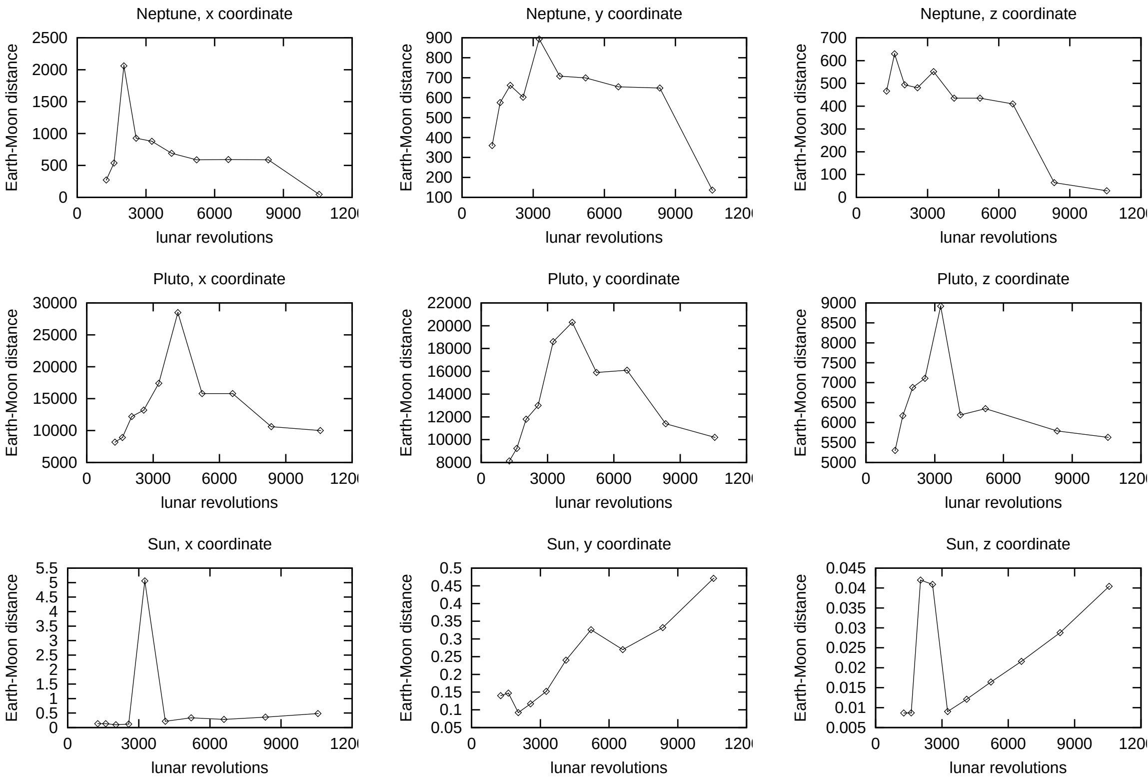

Figure 5.5: Continuation of Fig. 5.4.

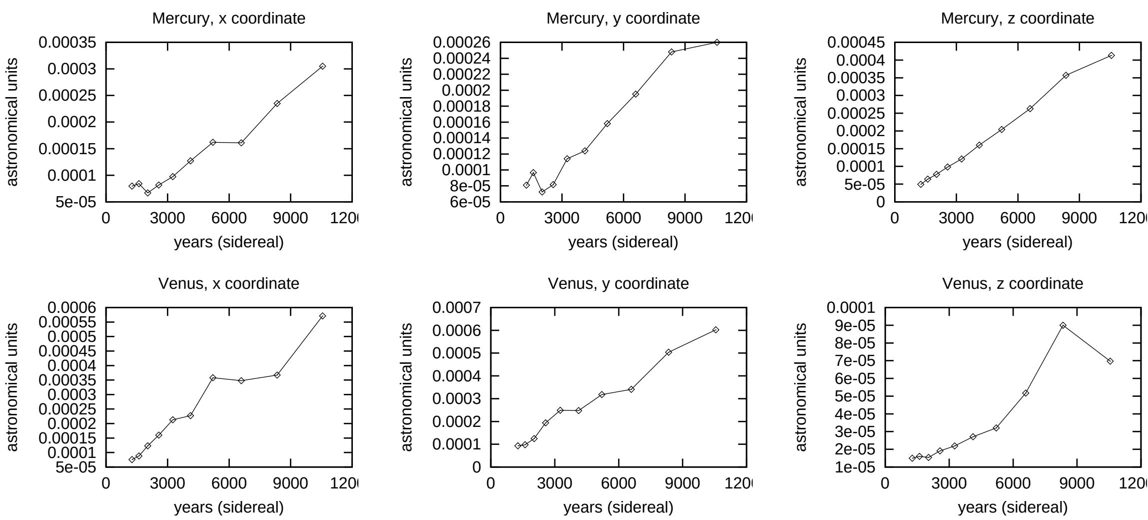

Figure 5.6: Same as Fig. 5.4 but for the Sun–Earth+Moon case (continued in Fig. 5.7).

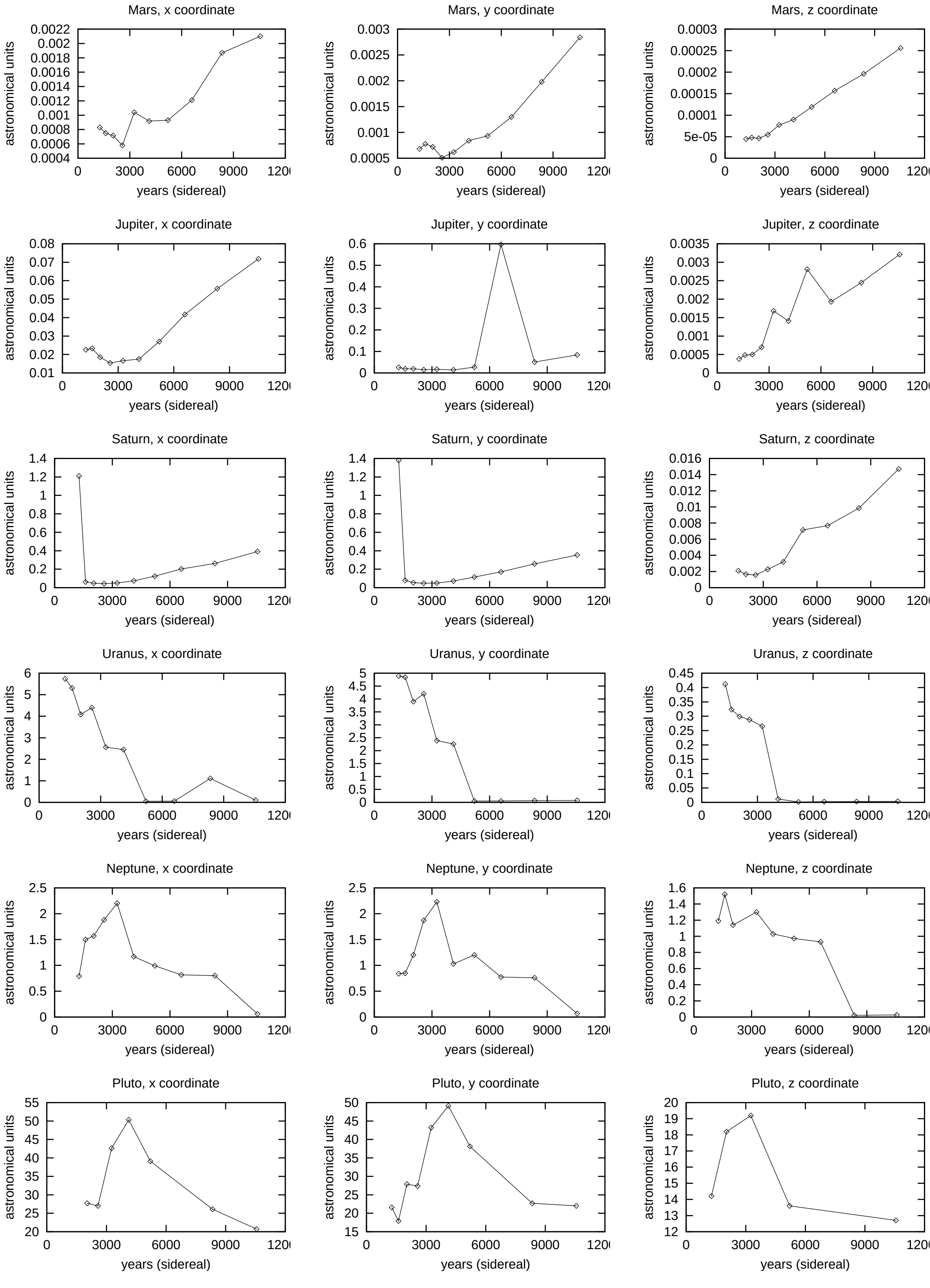

Figure 5.7: Continuation of Fig. 5.6.

body	coord.	T (days)	T (years)	T (J–rev)	N	p_{max}	d_{max}
Mercury	x	70288.7	192.440	2572.64	65536	1.37E–02	3.41E–01
Mercury	y	70288.7	192.440	2572.64	65536	1.08E–02	2.89E–01
Mercury	z	70288.7	192.440	2572.64	32768	3.18E–03	9.99E–02
Venus	x	55551.4	152.091	2033.24	65536	5.13E–03	1.53E–01
Venus	y	55551.4	152.091	2033.24	65536	5.60E–03	1.65E–01
Venus	z	88935.7	243.493	3255.14	65536	1.25E–03	4.10E–02
Mars	x	55551.4	152.091	2033.24	65536	3.61E–02	8.43E–01
Mars	y	180155.5	493.239	6593.89	131072	3.21E–02	7.53E–01
Mars	z	180155.5	493.239	6593.89	131072	3.26E–03	1.38E–01
Jupiter	x	55551.4	152.091	2033.24	32768	1.40E+00	1.53E+01
Jupiter	y	112529.5	308.089	4118.71	65536	5.39E–01	1.31E+01
Jupiter	z	70288.7	192.440	2572.64	32768	1.37E–01	1.31E+00
Saturn	x	70288.7	192.440	2572.64	32768	6.07E+00	6.19E+01
Saturn	y	142382.6	389.822	5211.36	65536	2.53E+00	6.46E+01
Saturn	z	180155.5	493.239	6593.89	65536	3.87E–01	1.04E+01
Uranus	x	142382.6	389.822	5211.36	131072	2.33E+00	3.75E+01
Uranus	y	142382.6	389.822	5211.36	131072	2.33E+00	3.76E+01
Uranus	z	364938.0	999.146	13357.14	131072	2.42E–01	4.14E+00
Neptune	x	288422.1	789.657	10556.57	262144	3.12E+00	4.52E+01
Neptune	y	364938.0	999.146	13357.14	262144	2.37E+00	4.51E+01
Neptune	z	364938.0	999.146	13357.14	131072	1.80E+00	2.72E+01
Pluto	x	364938.0	999.146	13357.14	262144	4.15E+00	1.69E+02
Pluto	y	364938.0	999.146	13357.14	262144	2.08E+01	2.93E+02
Pluto	z	364938.0	999.146	13357.14	131072	2.42E+00	5.16E+01
Sun	x	55551.4	152.091	2033.24	65536	4.41E–03	9.73E–02
Sun	y	55551.4	152.091	2033.24	65536	4.41E–03	9.21E–02
Sun	z	34698.8	95.000	1270.01	16384	8.49E–04	8.65E–03

Table 5.4: Best Fourier analysis parameters for the positions of the Solar System bodies in adimensional coordinates in the Earth–Moon case.

body	coord.	T (days)	T (J–rev)	N	p_{max}	d_{max}
Mercury	x	55551.4	152.089	16384	6.56E–06	6.68E–05
Mercury	y	55551.4	152.089	16384	6.56E–06	7.24E–05
Mercury	z	34698.8	94.998	8192	1.64E–06	4.93E–05
Venus	x	34698.8	94.998	4096	7.61E–06	7.57E–05
Venus	y	34698.8	94.998	4096	7.61E–06	9.32E–05
Venus	z	34698.8	94.998	4096	1.93E–06	1.50E–05
Mars	x	70288.7	192.436	8192	4.87E–05	5.80E–04
Mars	y	70288.7	192.436	8192	4.87E–05	5.11E–04
Mars	z	34698.8	94.998	4096	3.00E–06	4.48E–05
Jupiter	x	70288.7	192.436	8192	3.56E–03	1.54E–02
Jupiter	y	112529.5	308.083	16384	9.35E–04	1.41E–02
Jupiter	z	34698.8	94.998	4096	7.68E–05	3.82E–04
Saturn	x	70288.7	192.436	8192	1.29E–02	4.29E–02
Saturn	y	70288.7	192.436	8192	1.29E–02	4.82E–02
Saturn	z	70288.7	192.436	8192	5.39E–04	1.57E–03
Uranus	x	142382.6	389.815	16384	5.57E–03	4.82E–02
Uranus	y	142382.6	389.815	16384	5.57E–03	5.10E–02
Uranus	z	142382.6	389.815	16384	2.45E–04	1.25E–03
Neptune	x	288422.1	789.642	32768	5.40E–03	6.15E–02
Neptune	y	288422.1	789.642	32768	5.41E–03	6.71E–02
Neptune	z	227949.2	624.079	32768	4.10E–03	2.10E–02
Pluto	x	364938.0	999.127	65536	1.27E–02	2.92E–01
Pluto	y	364938.0	999.127	65536	1.41E–02	3.72E–01
Pluto	z	364938.0	999.127	32768	6.19E–03	7.64E–02

Table 5.5: Best Fourier analysis parameters for the positions of the Solar System bodies in adimensional coordinates in the Sun–Earth+Moon case.

5.3 Generation of simplified Solar System models

In this section we will develop simplified Solar System models based on the Fourier expansions computed in the previous section. The models obtained will be compared with other models though the computation of residual accelerations along selected orbits.

5.3.1 Adjustment by linear combinations of basic frequencies

In order to turn the output of our Fourier analysis procedures into the usual form of a quasi–periodic function (3.1), we need to adjust frequencies as linear combinations, with integer coefficients, of basic ones. We will distinguish two cases:

- the case in which we do not know the basic frequencies, which need to be extracted from the list of frequencies to be adjusted, and
- the case in which the basic frequencies are known.

A simple approach for the first case would be: choose a maximum order of the linear combinations to be found, and a tolerance for the adjustment of frequencies as linear combination of the basic ones. Then, for each frequency, try out all the linear combinations of the current set of basic frequencies up the chosen maximum order. If one of these linear combinations fulfills the requirements, take it, otherwise add the current frequency to the set of basic frequencies.

This procedure may add extra basic frequencies (and thus end up with a rationally dependent set) in some cases, for instance, if the current frequency is an integer divisor of one of the basic frequencies. In order to avoid this, when the current frequency cannot be adjusted as a linear combination of the current basis, for each frequency in the current basis we can try to substitute it by the non–adjusted one and see if all the pre–processed frequencies adjust to this modified basis. If this is not the case, the new frequency is added to the basic set.

These considerations lead to the following

Algorithm 5.3.1 *Given* $\{f_1, \dots, f_{N_f}\}$ *the set of frequencies to be adjusted as linear combination of basic ones to be selected in the set, a tolerance* tol *for the adjustments and a maximum order* maxor *for the linear combinations to be found, compute the basis* $\{\omega_1, \dots, \omega_{n_b}\}$ *and the linear combinations* $\{(k_1^i, \dots, k_{n_b}^i)\}_{i=1\div N_f}$ *as*

$\omega_1 \leftarrow f_1$, $k_1^1 \leftarrow 1$, $n_b \leftarrow 1$
for $i = 2 \div N_f$
  if $f_i \in \mathrm{lc}(\{\omega_l\}_l, \mathrm{tol}, \mathrm{maxor})$
    $(k_1^i, \dots, k_{n_b}^i) = \mathrm{adjust}(f_i, \{\omega_l\}_l, \mathrm{tol}, \mathrm{maxor})$
  else
    if $\exists j \in \{1, \dots, n_b\} : f_1, \dots, f_i \in \mathrm{lc}(\{\omega_1, \dots, \overset{(j}{f_i}, \dots, \omega_{N_f}\}, \mathrm{tol}, \mathrm{maxor})$
      $\omega_j \leftarrow f_i$
      for $l = 1 \div i$
        $(k_1^l, \dots, k_{n_b}^l) = \mathrm{adjust}(f_i, \{\omega_m\}_m, \mathrm{tol}, \mathrm{maxor})$

else
$n_b \leftarrow n_b + 1$
$(k_1^i, \dots k_{n_b}^i) = (0, \dots, 0, 1)$
for $l = 1 \div i - 1$
$k_{n_b}^l = 0$

In this formulation, we have introduced two functions lc *and* adjust*, defined as follows:*

- $\mathrm{lc}(\{\omega_i\}_{i=1\div n_b}, \mathrm{tol}, \mathrm{maxor})$ *is defined as the set of real numers* f *such that there exists* $(k_1, \dots, k_{n_b})$ *with* k_i *integer,* $|k_1| + \dots + |k_{n_b}| \le \mathrm{maxor}$ *and* $|f - k_1\omega_1 - \dots - k_{n_b}\omega_{n_b}| \le \mathrm{tol}$*,*

- *for* f *real,* $\mathrm{adjust}(f, \{\omega_i\}_{i=1\div n_b}, \mathrm{tol}, \mathrm{maxor})$ *returns the first* $(k_1, \dots, k_{n_b})$*, in increasing order and increasing lexicographical order within each order, with order* $\le \mathrm{maxor}$*, such that* $|f - k_1\omega_1 - \dots - k_{n_b}\omega_{n_b}| \le \mathrm{tol}$*. In the case that there is no* $(k_1, \dots, k_{n_b})$ *of order less than* maxor *with* $|f - k_1\omega_1 - \dots - k_{n_b}\omega_{n_b}| \le \mathrm{tol}$*, the one with minimum* $|f - k_1\omega_1 - \dots - k_{n_b}\omega_{n_b}|$ *is returned.*

Of course, in an actual implementation the role of these functions is accomplished by the same code.

In the second case, in which the basic frequencies $\{\omega_1, \dots, \omega_{n_b}\}$ are know, we can just take the best linear combination for each frequency. This can be stated as

Algorithm 5.3.2 *Given* $\{f_1, \dots, f_{N_f}\}$ *the set of frequencies to be adjusted as linear combination of the frequency basis* $\{\omega_1, \dots, \omega_{n_b}\}$*, a tolerance* tol *for the adjustments and a maximum order* maxor *for the linear combinations to be found, compute the linear combinations* $\{(k_1^i, \dots, k_{n_b}^i)\}_{i=1\div N_f}$ *as*

for $i = 1 \div N_f$
$(k_1^i, \dots, k_{n_b}^i) = \mathrm{adjust}(f_i, \{\omega_l\}_l, \mathrm{tol}, \mathrm{maxor})$

5.3.2 Simplified models for the Earth–Moon case

In a rather accurate theory for the lunar motion, as the simplified Brown theory given in [8], the fundamental parameters can be expressed in terms of five basic frequencies:

- The mean longitude of the Moon, which is equal to 1.0.

- The mean elongation of the Moon from the Sun, 0.925195997455093. This is the frequency of the time-dependent part in the Bicircular Problem (BCP) and the Quasi–Bicircular Problem, (QBCP, see Appendix A).

- The mean longitude of the lunar perigee, which is equal to $8.45477852931292 \times 10^{-3}$.

- The longitude of the mean ascending node of the lunar orbit on the ecliptic, $4.01883841204748 \times 10^{-3}$.

- the Sun's mean longitude of perigee, $3.57408131981537 \times 10^{-6}$.

The units used for these frequencies are cycles per lunar revolution. In what follows, these frequencies will be denoted $\{\omega_1, \dots, \omega_5\}$.

The value of the last frequency in the above set is close to the lower amplitudes of our Fourier expansions, which is close to the precision we can expect in the determination of frequencies, since all Fourier analysis have stopped due to the detection of too close frequencies. In order to avoid the difficulties due this fact, and in order to have a set of basic frequencies with astronomical meaning, we have adopted these frequencies as the basic set, instead of the ones provided by Algorithm 5.3.1.

For the simplified models to be developed in this section, we will only take into account the coordinates of the Sun in (5.4). This avoids the introduction of additional basic frequencies, and is also enough for our purposes, as it will become clear later. In this way, we will only use the Fourier expansions of $c_1, \dots, c_{13}$ and x_S, y_S, z_S.

Starting from the frequency basis $\{\omega_i\}_{i=1\div 5}$, we will look for a new basis $\{\nu_i\}_{i=1\div 5}$. In terms of this new basis, we will generate 5 models SSSM$_i$, $i = 1 \div 5$, in such a way that the equations of motion of SSSM$_i$ are

$$\left\{ \begin{array}{rcl} \ddot{x} & = & c_1^i + c_4\dot{x} + c_5^i\dot{y} + c_7^i x + c_8^i y + c_9^i z + c_{13}^i \dfrac{\partial \Omega^i}{\partial x} \\ \ddot{y} & = & c_2^i - c_5^i\dot{x} + c_4^i\dot{y} + c_6^i\dot{z} - c_8^i x + c_{10}^i y + c_{11}^i z + c_{13} \dfrac{\partial \Omega^i}{\partial y} \\ \ddot{z} & = & c_3^i - c_6\dot{y} + c_4^i\dot{z} + c_9^i x - c_{11}^i y + c_{12}^i z + c_{13}^i \dfrac{\partial \Omega^i}{\partial z} \end{array} \right.$$

being

$$\begin{aligned} \Omega \;=\; & \frac{1-\mu_{E,M}}{\sqrt{(x-\mu_{E,M})^2+y^2+z^2}} + \frac{\mu_{E,M}}{\sqrt{(x-\mu_{E,M}+1)^2+y^2+z^2}} \\ & + \frac{\mu_{E,M,S}}{\sqrt{(x-x_S^i)^2+(y-y_S^i)^2+(z-z_S^i)^2}}. \end{aligned}$$

Here c_j^i, $j = 1 \div 13$ and x_S^i, y_S^i, z_S^i stand for their Fourier expansions, computed in the previous section, but keeping only the frequencies that are expressed as linear combinations (with integer coefficients) of the frequencies $\nu_1, \dots, \nu_i$.

We have used Algorithm 5.3.2 of the previous section with $tol = 10^{-6}$ and $maxor = 20$ to adjust the frequencies found in the analysis of table 5.2 as linear combinations of the $\{\omega_i\}_{i=1\div 5}$. The results for the first 15 frequencies detected in each c_i and x_S, y_S, z_S are shown in tables 5.6 to 5.16. The full expansions are given in Appendix C.

We will take $\nu_1 = \omega_2$ as the first frequency of our new basis. The reason for that is that it is the main frequency of c_1, c_2, x_S and y_S, and in this way it can be considered the main "planar frequency". This is coherent with the fact that ω_2 is also the frequency of the BCP and QBCP models (see Appendix A).

We observe that, except for c_3, c_6, c_9, c_{11} and z_S, the main frequencies of the remaining functions can be expressed as linear combinations of ω_2 and $\omega_1 - \omega_3$. Thus, we will take $\nu_2 = \omega_1 - \omega_3$. Note that, in this way, c_i for $i = 3, 6, 9, 11$ and z_S will be poorly approximated in SSSM$_2$, but this will not give a poor global approximation because c_i for $i = 3, 6, 9, 11$ are smaller than the remaining c_i, and z_S is also smaller than x_S, y_S.

freq	ampl	err	k_1	k_2	k_3	k_4	k_5	order
0.00000000000	3.49728E–04	0.00000E+00	0	0	0	0	0	0
0.92519578630	2.16240E+00	–2.11120E–07	0	1	0	0	0	1
1.91674083000	1.77450E–01	–3.88880E–07	1	1	–1	0	0	3
0.85039537680	7.53250E–02	–1.92240E–07	–1	2	0	0	1	4
0.06634926290	7.39730E–02	3.88600E–08	1	–1	–1	0	0	3
1.78404231460	3.41170E–02	–4.56330E–07	–1	3	1	0	0	5
2.77558735940	2.39690E–02	–6.33010E–07	0	3	0	0	0	3
2.90828587990	1.36950E–02	–5.60520E–07	2	1	–2	0	0	5
1.84194060340	7.31080E–03	–1.87100E–07	0	2	–1	0	1	4
1.08284144950	3.91270E–03	–2.29900E–07	2	–1	0	2	0	5

Table 5.6: First 10 frequencies of the Fourier analysis of c_1. The frequencies have been adjusted as linear combinations of $\{\omega_i\}_{i=1\div5}$. From left to right the columns are: frequency, in cycles per lunar revolution, amplitude, error ($\mathrm{freq} - k_1\omega_1 - \ldots - k_5\omega_5$), coefficients of the linear combination that approximates freq, and order of the linear combination ($|k_1| + \ldots |k_5|$).

freq.	ampl.	err.	k_1	k_2	k_3	k_4	k_5	order
0.00000000000	–6.70000E–09	0.00000E+00	0	0	0	0	0	0
0.92519578630	2.16960E+00	–2.11120E–07	0	1	0	0	0	1
1.91674083000	1.77820E–01	–3.88890E–07	1	1	–1	0	0	3
0.85039537680	7.58320E–02	–1.92220E–07	–1	2	0	0	1	4
0.06634926260	4.64680E–02	3.85950E–08	1	–1	–1	0	0	3
1.78404231460	3.41920E–02	–4.56320E–07	–1	3	1	0	0	5
2.77558735930	2.39940E–02	–6.33040E–07	0	3	0	0	0	3
2.90828587990	1.37170E–02	–5.60520E–07	2	1	–2	0	0	5
1.84194060340	7.33860E–03	–1.87100E–07	0	2	–1	0	1	4
1.08284144950	3.95090E–03	–2.29860E–07	2	–1	0	2	0	5

Table 5.7: Same as table 5.6 but for the c_2 function.

freq.	ampl.	err.	k_1	k_2	k_3	k_4	k_5	order
0.00000000000	–1.41400E–07	0.00000E+00	0	0	0	0	0	0
0.07882283210	1.90520E–01	–8.87040E–09	1	–1	0	1	0	3
0.15362345870	6.56920E–03	1.89270E–07	2	–2	0	1	–1	6
0.91272221270	5.20890E–03	–1.67780E–07	0	1	–1	–1	0	3
1.07036787670	5.21170E–03	–1.85760E–07	2	–1	–1	1	0	5
0.78002369690	1.09620E–03	–2.35620E–07	–2	3	1	–1	0	7
0.93766935940	1.08610E–03	–2.54980E–07	0	1	1	1	0	3
1.92921440450	3.96610E–04	–4.31370E–07	1	1	0	1	0	3
1.77156873960	3.60950E–04	–4.14380E–07	–1	3	0	–1	0	5
0.00402218340	3.31660E–04	–2.29130E–07	0	0	0	1	1	2

Table 5.8: Same as table 5.6 but for the c_3 function.

freq.	ampl.	err.	k_1	k_2	k_3	k_4	k_5	order
0.00000000000	0.00000E+00	0.00000E+00	0	0	0	0	0	0
0.99154505160	1.07920E–01	–1.69890E–07	1	0	–1	0	0	2
1.85039157300	2.94710E–02	–4.21940E–07	0	2	0	0	0	2
0.85884652970	1.68610E–02	–2.43690E–07	–1	2	1	0	0	4
1.98309009370	8.82140E–03	–3.49210E–07	2	0	–2	0	0	4
2.84193661720	3.80000E–03	–5.99130E–07	1	2	–1	0	0	4
1.77559111020	1.93150E–03	–4.56240E–07	–1	3	0	0	1	5
2.97463513490	6.78820E–04	–5.29470E–07	3	0	–3	0	0	6
2.70923810000	7.14080E–04	–6.68310E–07	–1	4	1	0	0	6
0.78404586970	6.38340E–04	–4.75270E–07	–2	3	1	0	1	7

Table 5.9: Same as table 5.6 but for the c_4 function.

freq.	ampl.	err.	k_1	k_2	k_3	k_4	k_5	order
0.00000000000	2.00003E+00	0.00000E+00	0	0	0	0	0	0
0.99154503470	2.17650E–01	–1.86770E–07	1	0	–1	0	0	2
1.85039156830	4.29420E–02	–4.26650E–07	0	2	0	0	0	2
0.85884653190	3.81670E–02	–2.41550E–07	–1	2	1	0	0	4
1.98309007300	1.48070E–02	–3.69960E–07	2	0	–2	0	0	4
2.84193660360	5.36300E–03	–6.12800E–07	1	2	–1	0	0	4
1.77559105180	2.84910E–03	–5.14630E–07	–1	3	0	0	1	5
0.78404613980	1.55830E–03	–2.05220E–07	–2	3	1	0	1	7
0.91674466300	1.30720E–03	–1.30020E–07	0	1	–1	0	1	3
0.92519587730	1.12100E–03	–1.20200E–07	0	1	0	0	0	1

Table 5.10: Same as table 5.6 but for the c_5 function.

freq.	ampl.	err.	k_1	k_2	k_3	k_4	k_5	order
0.00000000000	0.00000E+00	0.00000E+00	0	0	0	0	0	0
0.84637295300	1.44550E–03	–2.03520E–07	–1	2	0	–1	0	4
1.00401861550	1.44530E–03	–2.22890E–07	1	0	0	1	0	2
0.01247357960	1.89340E–04	–3.72940E–08	0	0	1	1	0	2
0.14517208260	1.88980E–04	1.76520E–08	2	–2	–1	1	0	6
0.77157269570	8.78480E–05	–3.23250E–08	–2	3	0	–1	1	7
0.92921810820	3.54680E–05	–3.01790E–07	0	1	0	1	1	3
1.07881913160	3.51310E–05	–1.35230E–07	2	–1	0	1	–1	5
0.92117316420	1.72620E–05	–4.20780E–07	0	1	0	–1	–1	3
0.21997272480	1.09360E–05	2.31350E–07	3	–3	–1	1	–1	9

Table 5.11: Same as table 5.6 but for the c_6 function.

freq.	ampl.	err.	k_1	k_2	k_3	k_4	k_5	order
0.00000000000	1.00478E+00	0.00000E+00	0	0	0	0	0	0
0.99154504270	1.65040E–01	–1.78730E–07	1	0	–1	0	0	2
0.85884652970	3.24780E–02	–2.43700E–07	–1	2	1	0	0	4
1.85039157280	1.84070E–02	–4.22070E–07	0	2	0	0	0	2
1.98309009370	1.35090E–02	–3.49200E–07	2	0	–2	0	0	4
2.84193661730	3.29470E–03	–5.99110E–07	1	2	–1	0	0	4
0.13269851610	1.45030E–03	6.80760E–08	2	–2	–2	0	0	6
0.78404586980	1.39870E–03	–4.75200E–07	–2	3	1	0	1	7
1.77559111010	1.25920E–03	–4.56320E–07	–1	3	0	0	1	5
2.97463513460	1.08280E–03	–5.29830E–07	3	0	–3	0	0	6

Table 5.12: Same as table 5.6 but for the c_7 function.

freq.	ampl.	err.	k_1	k_2	k_3	k_4	k_5	order
0.00000000000	–7.00000E–10	0.00000E+00	0	0	0	0	0	0
1.85039159880	8.24730E–03	–3.96070E–07	0	2	0	0	0	2
2.84193667480	9.04550E–04	–5.41620E–07	1	2	–1	0	0	4
0.85884652020	9.17510E–04	–2.53210E–07	–1	2	1	0	0	4
1.77559103310	5.07100E–04	–5.33340E–07	–1	3	0	0	1	5
0.99154507800	1.95970E–04	–1.43510E–07	1	0	–1	0	0	2
2.70923811510	1.73420E–04	–6.53300E–07	–1	4	1	0	0	6
3.70078319630	1.14930E–04	–7.93520E–07	0	4	0	0	0	4
1.92519194710	9.57130E–05	–4.76300E–07	1	1	0	0	–1	3
3.83348174850	8.00900E–05	–6.89320E–07	2	2	–2	0	0	6

Table 5.13: Same as table 5.6 but for the c_8 function.

freq.	ampl.	err.	k_1	k_2	k_3	k_4	k_5	order
0.00000000000	–0.00000E+00	0.00000E+00	0	0	0	0	0	0
0.84637295300	7.24530E–04	–2.03520E–07	–1	2	0	–1	0	4
1.00401861550	7.24450E–04	–2.22890E–07	1	0	0	1	0	2
0.01247357980	4.82170E–05	–3.71330E–08	0	0	1	1	0	2
0.14517208260	4.80940E–05	1.76380E–08	2	–2	–1	1	0	6
0.77157269560	4.41510E–05	–3.24260E–08	–2	3	0	–1	1	7
1.99556365120	4.00140E–05	–4.08710E–07	2	0	–1	1	0	4
1.83791798820	3.99960E–05	–3.89770E–07	0	2	–1	–1	0	4
0.92921810800	1.78950E–05	–3.01960E–07	0	1	0	1	1	3
1.07881913140	1.76710E–05	–1.35470E–07	2	–1	0	1	–1	5

Table 5.14: Same as table 5.6 but for the c_9 function.

freq.	ampl.	err.	k_1	k_2	k_3	k_4	k_5	order
0.00000000000	1.00478E+00	0.00000E+00	0	0	0	0	0	0
0.99154504270	1.65030E–01	–1.78730E–07	1	0	–1	0	0	2
0.85884652970	3.24780E–02	–2.43700E–07	–1	2	1	0	0	4
1.85039157280	1.84070E–02	–4.22070E–07	0	2	0	0	0	2
1.98309009370	1.35090E–02	–3.49200E–07	2	0	–2	0	0	4
2.84193661730	3.29470E–03	–5.99110E–07	1	2	–1	0	0	4
0.13269851610	1.45030E–03	6.80760E–08	2	–2	–2	0	0	6
0.78404586980	1.39870E–03	–4.75200E–07	–2	3	1	0	1	7
1.77559111010	1.25920E–03	–4.56320E–07	–1	3	0	0	1	5
2.97463513460	1.08280E–03	–5.29830E–07	3	0	–3	0	0	6

Table 5.15: Same as table 5.6 but for the c_{10} function.

freq.	ampl.	err.	k_1	k_2	k_3	k_4	k_5	order
0.00000000000	–0.00000E+00	0.00000E+00	0	0	0	0	0	0
1.00401861560	7.20820E–04	–2.22850E–07	1	0	0	1	0	2
0.84637295300	6.06950E–04	–2.03500E–07	–1	2	0	–1	0	4
0.14517208280	4.66020E–05	1.78760E–08	2	–2	–1	1	0	6
1.99556364910	3.64300E–05	–4.10800E–07	2	0	–1	1	0	4
1.83791798780	3.65390E–05	–3.90160E–07	0	2	–1	–1	0	4
0.77157269620	3.33090E–05	–3.18310E–08	–2	3	0	–1	1	7
0.01247358100	3.15620E–05	–3.59500E–08	0	0	1	1	0	2
2.85441018260	2.40050E–05	–6.50710E–07	1	2	0	1	0	4
2.69676451900	2.36110E–05	–6.32380E–07	–1	4	0	–1	0	6

Table 5.16: Same as table 5.6 but for the c_{11} function.

freq.	ampl.	err.	k_1	k_2	k_3	k_4	k_5	order
0.00000000000	–1.61183E–03	0.00000E+00	0	0	0	0	0	0
0.99154502640	5.38970E–02	–1.95110E–07	1	0	–1	0	0	2
1.85039157030	2.69200E–02	–4.24600E–07	0	2	0	0	0	2
0.85884654110	8.04870E–03	–2.32340E–07	–1	2	1	0	0	4
1.98309004860	7.32970E–03	–3.94350E–07	2	0	–2	0	0	4
2.84193659510	4.58070E–03	–6.21280E–07	1	2	–1	0	0	4
1.77559129770	1.70370E–03	–2.68790E–07	–1	3	0	0	1	5
2.70923811570	8.46260E–04	–6.52680E–07	–1	4	1	0	0	6
2.97463506060	7.75820E–04	–6.03790E–07	3	0	–3	0	0	6
3.70078314150	5.70720E–04	–8.48320E–07	0	4	0	0	0	4

Table 5.17: Same as table 5.6 but for the c_{12} function.

freq.	ampl.	err.	k_1	k_2	k_3	k_4	k_5	order
0.00000000000	1.00747E+00	0.00000E+00	0	0	0	0	0	0
0.99154504270	1.64840E–01	–1.78730E–07	1	0	–1	0	0	2
0.85884652970	3.15620E–02	–2.43700E–07	–1	2	1	0	0	4
1.85039157290	2.66550E–02	–4.22010E–07	0	2	0	0	0	2
1.98309009370	1.34800E–02	–3.49210E–07	2	0	–2	0	0	4
2.84193661730	4.19930E–03	–5.99110E–07	1	2	–1	0	0	4
1.77559111020	1.76690E–03	–4.56280E–07	–1	3	0	0	1	5
0.13269851610	1.47040E–03	6.80410E–08	2	–2	–2	0	0	6
0.78404586980	1.34660E–03	–4.75200E–07	–2	3	1	0	1	7
2.97463513490	1.07950E–03	–5.29490E–07	3	0	–3	0	0	6

Table 5.18: Same as table 5.6 but for the c_{13} function.

freq.	ampl.	err.	k_1	k_2	k_3	k_4	k_5	order
0.00000000000	–6.27023E–02	0.00000E+00	0	0	0	0	0	0
0.92519578630	3.86480E+02	–2.11130E–07	0	1	0	0	0	1
1.91674083000	3.17140E+01	–3.88890E–07	1	1	–1	0	0	3
0.06634926280	1.32180E+01	3.87440E–08	1	–1	–1	0	0	3
0.99999608230	1.03360E+01	–3.43580E–07	1	0	0	0	–1	2
1.78404231420	6.09200E+00	–4.56710E–07	–1	3	1	0	0	5
2.77558735980	4.27790E+00	–6.32540E–07	0	3	0	0	0	3
0.85039537680	3.79560E+00	–1.92230E–07	–1	2	0	0	1	4
2.90828587090	2.44750E+00	–5.69500E–07	2	1	–2	0	0	5
1.99154129500	1.00420E+00	–3.52350E–07	2	0	–1	0	–1	4

Table 5.19: Same as table 5.6 but for the x_S function.

freq.	ampl.	err.	k_1	k_2	k_3	k_4	k_5	order
0.00000000000	1.60785E–05	0.00000E+00	0	0	0	0	0	0
0.92519578630	3.87760E+02	–2.11130E–07	0	1	0	0	0	1
1.91674083000	3.17800E+01	–3.88890E–07	1	1	–1	0	0	3
0.99999608230	1.03360E+01	–3.43590E–07	1	0	0	0	–1	2
0.06634926280	8.30700E+00	3.87360E–08	1	–1	–1	0	0	3
1.78404231280	6.10530E+00	–4.58110E–07	–1	3	1	0	0	5
2.77558735590	4.28220E+00	–6.36440E–07	0	3	0	0	0	3
0.85039537680	3.85420E+00	–1.92230E–07	–1	2	0	0	1	4
2.90828587990	2.45150E+00	–5.60490E–07	2	1	–2	0	0	5
1.99154129500	1.00460E+00	–3.52360E–07	2	0	–1	0	–1	4

Table 5.20: Same as table 5.6 but for the y_S function.

freq.	ampl.	err.	k_1	k_2	k_3	k_4	k_5	order
0.00000000000	4.24394E–04	0.00000E+00	0	0	0	0	0	0
0.07882283000	3.40520E+01	–1.09480E–08	1	–1	0	1	0	3
0.91272219540	9.30940E–01	–1.85070E–07	0	1	–1	–1	0	3
0.00402231670	9.11850E–01	–9.57650E–08	0	0	0	1	1	2
1.07036785680	9.31450E–01	–2.05600E–07	2	–1	–1	1	0	5
0.15362321080	3.22470E–01	–5.86630E–08	2	–2	0	1	–1	6
0.93766936950	1.93940E–01	–2.44860E–07	0	1	1	1	0	3
0.78002371740	1.95730E–01	–2.15110E–07	–2	3	1	–1	0	7
1.92921439960	7.07670E–02	–4.36290E–07	1	1	0	1	0	3
1.77156873300	6.44060E–02	–4.20950E–07	–1	3	0	–1	0	5

Table 5.21: Same as table 5.6 but for the z_S function.

The remaining ν_i have been taken in order to make the sequence of models SSSM$_3$, SSSM$_4$, SSSM$_5$ decreasing in error in the residual accelerations test that will be discussed bellow. After some trials, we have set

- $\nu_3 = \omega_1 - \omega_2 + \omega_4$, which is the main frequency of c_3,
- $\nu_4 = \omega_1 - \omega_5$, which is the first frequency of x_S which cannot be expressed in terms of ν_1, ν_2, and
- $\nu_5 = \omega_5 - \omega_2$, which is the first frequency of c_3 that cannot be expressed in terms of $\nu_1, \nu_2, \nu_3, \nu_4$.

In this way, we have

$$\begin{pmatrix} \nu_1 \\ \nu_2 \\ \nu_3 \\ \nu_4 \\ \nu_5 \end{pmatrix} = \begin{pmatrix} 0 & 1 & 0 & 0 & 0 \\ 1 & 0 & -1 & 0 & 0 \\ 1 & -1 & 0 & 1 & 0 \\ 1 & 0 & 0 & 0 & -1 \\ 0 & -1 & 0 & 0 & 1 \end{pmatrix} \begin{pmatrix} \omega_1 \\ \omega_2 \\ \omega_3 \\ \omega_4 \\ \omega_5 \end{pmatrix}.$$

Since the above matrix is unimodular, $\{\nu_i\}_{i=1\div 5}$ is a valid basic set of frequencies.

Using residual accelerations, the SSSM$_i$ models, as well as the RTBP, the Bicircular Problem (BCP) and the Quasi–Bicircular problem (QBCP, see Appendix A) have been compared with the real Solar System, as given by (5.3) and (5.4) with the c_i and x_i, y_i, z_i functions evaluated from the JPL DE406 ephemeris files. We have proceed as follows. Given two models to be compared, with differential equations $\ddot{\mathbf{r}} = f(\mathbf{r}, t)$ and $\ddot{\mathbf{r}} = g(r, t)$, respectively, and given a trajectory (positions and velocities) $\gamma : \mathbb{R} \to \mathbb{R}^6$, which does not need to be a trajectory of any of the models, we compute the "mean relative residual acceleration over γ" as

$$\frac{1}{L}\int_0^T \frac{\|f(\gamma(s), t) - g(\gamma(s), t)\|}{\|g(\gamma(s), t)\|} \|\gamma'(s)\| ds, \tag{5.6}$$

where t is a fixed epoch (in adimensional units) and

$$L = \int_0^T \|\gamma'(s)\| ds$$

is the length of the trajectory.

It must be noted that, the BCP and the QBCP as stated in appendix A assume that, for $t = 0$, the vector from the Earth to the Moon and the one from the Earth–Moon barycenter to the Sun form an angle of 180 degrees. Therefore, we must set the origin of adimensional time, both in the SSSM_i models and the real Solar System, such that Earth, Moon and Sun are in a configuration close to the one of the BCP and the QBCP for $t = 0$. For the test of Table 5.22, we have chosen as $t = 0$ the first epoch after Jan 1st, 2001 in which the projection of the vector from the Earth–Moon barycenter to the Sun over the Earth–Moon instantaneous plane of motion forms an angle of 180 degrees with the vector from the Earth to the Moon. This is the Julian day 2451919.3489 (Jan 9th, 2001).

The results of the residual accelerations test are given in Table 5.22. From this table, it becomes clear that the best one–frequency models that we can use, using the residual acceleration criterium, are the BCP and the QBCP. But, when we allow two or more frequencies, the models we get fit the JPL one much better. As it has been said, only the Sun has been taken into account in all the intermediate models. By adding additional Solar System bodies, the residual accelerations are of the same order of magnitude than the ones obtained just using the Sun.

5.3.3 Simplified models for the Sun–Earth+Moon case

In this case, we will extract the basic frequencies from the Fourier analysis of Section 5.2 using Algorithm 5.3.1 for its determination.

From the numerical data obtained (see Appendix C), we first observe that the maximum modulus of the highest Fourier coefficient of c_1, c_2, c_3, c_6, c_8, c_9, c_{11} is 3.521E–05, whereas the minimum modulus of the highest Fourier coefficient of the remaining c_i is 1.669E–02. Therefore, in order to detect basic frequencies, we will only take into consideration the c_4, c_5, c_7, c_{10}, c_{12} and c_{13} functions. In addition to this simplification, we will not consider any Solar System body in (5.4), since, just using the c_i, we are already taking the Sun into account.

Applying Algorithm 5.3.1 to the c_{13} function, setting tol = 1E–5, $maxor = 20$, we get the following 4 basic frequencies:

$$\nu_1 = 0.9999926164, \ \nu_2 = 0.6255242728, \ \nu_3 = 0.9147445983, \ \nu_4 = 1.8313395538.$$

These 4 basic frequencies allow to adjust the frequencies of the best analysis of the c_4, c_5, c_7, c_{10} and c_{12} functions. For that, we have applied the second algorithm of section 5.3.1 with tol = 1E–5 amd $maxor = 20$. The results are given in tables 5.23 to 5.27. With these frequencies, we construct the $\mathrm{SSSM}_1, \ldots, \mathrm{SSSM}_4$ as we did in the Earth–Moon case.

In Table 5.29, we compare the models RTBP, SSSM_1 and SSSM_4 with the real Solar System using the same residual acceleration test that we used in the Earth–Moon case. We

z-a.	RTBP	BCP	QBCP	SSSM_1	SSSM_2	SSSM_3	SSSM_4	SSSM_5
0.020	0.140126	0.146459	0.138580	0.365299	0.095769	0.010674	0.001374	0.000727
0.022	0.138397	0.144693	0.136908	0.359442	0.094562	0.010534	0.001360	0.000724
0.025	0.136603	0.142856	0.135174	0.353302	0.093293	0.010388	0.001346	0.000720
0.028	0.134760	0.140962	0.133392	0.346913	0.091967	0.010235	0.001331	0.000716
0.031	0.132882	0.139025	0.131578	0.340305	0.090590	0.010076	0.001315	0.000711
0.034	0.130985	0.137059	0.129747	0.333509	0.089166	0.009913	0.001299	0.000707
0.038	0.129087	0.135080	0.127914	0.326550	0.087699	0.009744	0.001282	0.000702
0.043	0.127204	0.133103	0.126097	0.319452	0.086191	0.009570	0.001265	0.000696
0.048	0.125352	0.131141	0.124312	0.312235	0.084643	0.009393	0.001247	0.000691
0.053	0.123549	0.129209	0.122576	0.304915	0.083056	0.009211	0.001229	0.000685
0.059	0.121813	0.127324	0.120905	0.297505	0.081429	0.009024	0.001210	0.000678
0.066	0.120162	0.125502	0.119319	0.290018	0.079760	0.008833	0.001191	0.000671
0.073	0.118614	0.123757	0.117835	0.282462	0.078045	0.008637	0.001171	0.000664
0.082	0.117189	0.122108	0.116473	0.274845	0.076280	0.008436	0.001150	0.000655
0.091	0.115905	0.120571	0.115249	0.267173	0.074461	0.008229	0.001128	0.000646
0.102	0.114778	0.119161	0.114181	0.259453	0.072581	0.008016	0.001105	0.000636
0.113	0.113823	0.117895	0.113283	0.251690	0.070634	0.007796	0.001081	0.000625
0.126	0.113052	0.116784	0.112566	0.243889	0.068612	0.007568	0.001056	0.000612
0.141	0.112471	0.115836	0.112037	0.236056	0.066510	0.007331	0.001030	0.000598
0.157	0.112080	0.115057	0.111695	0.228199	0.064322	0.007085	0.001002	0.000583
0.175	0.111872	0.114443	0.111533	0.220325	0.062042	0.006831	0.000973	0.000566
0.195	0.111829	0.113984	0.111535	0.212440	0.059667	0.006566	0.000942	0.000547
0.217	0.111928	0.113663	0.111672	0.204551	0.057196	0.006292	0.000910	0.000526
0.242	0.112133	0.113450	0.111909	0.196665	0.054632	0.006008	0.000875	0.000504
0.269	0.112400	0.113311	0.112201	0.188782	0.051978	0.005716	0.000840	0.000481
0.300	0.112678	0.113200	0.112492	0.180899	0.049240	0.005417	0.000802	0.000456

Table 5.22: Mean residual accelerations between several models and the real Solar System over selected halo orbits of the RTBP around L_2 in the Earth–Moon case. The first column displays the z–amplitude of the halo orbit used as test orbit. The remaining columns show the mean residual acceleration between the corresponding model and the real Solar System over the test orbit.

note that the $SSSM_4$ model gives worse results than $SSSM_1$. This is not a contradiction. Examining table 5.23 to 5.27 we can see that the maximum amplitude of the frequencies of c_4, c_5, c_7, c_{10} and c_{12} that are not multiple of ν_1 is 6.695E–05. Because of that, adding frequencies does not improve significantly the approximation of the c_i functions, and in this way the structure of the equations 5.3 "takes over" the fact that the c_i terms of $SSSM_4$ are closer to the ones of the real Solar System than the corresponding terms of $SSSM_1$.

Therefore, for the Sun–Earth+Moon case, we will give $SSSM_1$ as simplified Solar System model. Note that this is a model with very few frequencies that significantly improves the RTBP.

freq.	ampl.	err.	k_1	k_2	k_3	k_4	order
0.00000000000	1.30000E–09	0.00000E+00	0	0	0	0	0
0.99999261980	3.33720E–02	3.38800E–09	1	0	0	0	1
1.99998564390	8.35280E–04	4.11070E–07	2	0	0	0	2
1.25103997640	3.93800E–05	–8.56920E–06	0	2	0	0	2
1.83134352170	3.40050E–05	3.96790E–06	0	0	0	1	1
0.91473091670	2.84920E–05	–1.36820E–05	0	0	1	0	1
2.99997409570	1.97160E–05	–3.75350E–06	3	0	0	0	3
1.87659754110	9.29780E–06	2.47230E–05	0	3	0	0	3

Table 5.23: Frequencies of the best analysis of c_4 adjusted as linear combinations of $\{\nu_i\}_{i=1\div 4}$. From left to right the columns are: frequency, in cycles per lunar revolution, amplitude, error (freq. $- k_1\nu_1 - \ldots k_4\nu_4$), coefficients of the linear combination that approximates freq., and order of the linear combination ($|k_1| + \ldots + |k_4|$).

freq.	ampl.	err.	k_1	k_2	k_3	k_4	order
0.00000000000	2.00000E+00	0.00000E+00	0	0	0	0	0
0.99999261700	6.67490E–02	5.51530E–10	1	0	0	0	1
1.99998563790	1.39230E–03	4.05090E–07	2	0	0	0	2
1.25103998380	6.69550E–05	–8.56180E–06	0	2	0	0	2
0.91475203530	6.12480E–05	7.43700E–06	0	0	1	0	1
1.83134663800	4.85690E–05	7.08420E–06	0	0	0	1	1
2.99997541480	3.01690E–05	–2.43440E–06	3	0	0	0	3
0.62552353770	2.92970E–05	–7.35060E–07	0	1	0	0	1

Table 5.24: Same as Table 5.23 but for the c_5 function.

freq.	ampl.	err.	k_1	k_2	k_3	k_4	order
0.00000000000	1.00042E+00	0.00000E+00	0	0	0	0	0
0.99999261500	5.00800E–02	–1.41660E–09	1	0	0	0	1
1.99998562010	1.25350E–03	3.87270E–07	2	0	0	0	2
0.91475953220	4.82370E–05	1.49340E–05	0	0	1	0	1
1.25103999430	4.22440E–05	–8.55130E–06	0	2	0	0	2
2.99998010500	3.08040E–05	2.25580E–06	3	0	0	0	3
0.62552269280	2.71900E–05	–1.58000E–06	0	1	0	0	1
1.83133006690	1.76890E–05	–9.48690E–06	0	0	0	1	1

Table 5.25: Same as Table 5.23 but for the c_7 function.

freq.	ampl.	err.	k_1	k_2	k_3	k_4	order
0.00000000000	1.00042E+00	0.00000E+00	0	0	0	0	0
0.99999261500	5.00800E–02	–1.41650E–09	1	0	0	0	1
1.99998562010	1.25350E–03	3.87270E–07	2	0	0	0	2
0.91475953220	4.82370E–05	1.49340E–05	0	0	1	0	1
1.25103999430	4.22440E–05	–8.55130E–06	0	2	0	0	2
2.99998010500	3.08040E–05	2.25580E–06	3	0	0	0	3
0.62552269280	2.71900E–05	–1.58000E–06	0	1	0	0	1
1.83133006690	1.76890E–05	–9.48690E–06	0	0	0	1	1

Table 5.26: Same as Table 5.23 but for the c_{10} function.

freq.	ampl.	err.	k_1	k_2	k_3	k_4	order
0.00000000000	–1.39300E–04	0.00000E+00	0	0	0	0	0
0.99999262330	1.66930E–02	6.87550E–09	1	0	0	0	1
1.99998564990	6.96230E–04	4.17110E–07	2	0	0	0	2
1.83134558880	3.11050E–05	6.03500E–06	0	0	0	1	1
1.25103987210	2.46550E–05	–8.67350E–06	0	2	0	0	2
2.99997235010	2.26070E–05	–5.49910E–06	3	0	0	0	3
0.91470513360	1.30450E–05	–3.94650E–05	0	0	1	0	1
1.87659675410	8.75900E–06	2.39360E–05	0	3	0	0	3
2.50211836990	5.41250E–06	2.12790E–05	0	4	0	0	4

Table 5.27: Same as Table 5.23 but for the c_{12} function.

freq.	ampl.	err.	k_1	k_2	k_3	k_4	order
0.00000000000	1.00042E+00	0.00000E+00	0	0	0	0	0
0.99999261640	5.00800E–02	5.35290E–12	1	0	0	0	1
1.99998562580	1.25340E–03	3.93030E–07	2	0	0	0	2
1.25104010020	4.71180E–05	–8.44540E–06	0	2	0	0	2
0.91474459830	4.67440E–05	–4.82540E–11	0	0	1	0	1
2.99997729050	3.07760E–05	–5.58700E–07	3	0	0	0	3
1.83133955380	2.81230E–05	–9.85990E–12	0	0	0	1	1
0.62552427280	1.62760E–05	1.35640E–11	0	1	0	0	1

Table 5.28: Same as Table 5.23 but for the c_{13} function.

z-a.	RTBP	SSSM$_1$	SSSM$_4$
0.020000	3.446497E–02	9.901526E–05	8.905454E–04
0.022288	3.429997E–02	9.844882E–05	8.842048E–04
0.024838	3.411184E–02	9.779360E–05	8.768670E–04
0.027680	3.390024E–02	9.701858E–05	8.684772E–04
0.030846	3.366579E–02	9.616913E–05	8.589500E–04
0.034375	3.341007E–02	9.521763E–05	8.482675E–04
0.038308	3.313580E–02	9.416327E–05	8.364166E–04
0.042691	3.284681E–02	9.300703E–05	8.234040E–04
0.047575	3.254789E–02	9.175134E–05	8.092527E–04
0.053018	3.224472E–02	9.039967E–05	7.939978E–04
0.059084	3.194355E–02	8.895610E–05	7.776813E–04
0.065843	3.165101E–02	8.742482E–05	7.603471E–04
0.073376	3.137381E–02	8.582841E–05	7.420444E–04
0.081771	3.111844E–02	8.413352E–05	7.227963E–04
0.091126	3.089082E–02	8.236183E–05	7.026421E–04
0.101551	3.069597E–02	8.051628E–05	6.816096E–04
0.113169	3.053770E–02	7.859979E–05	6.597243E–04
0.126117	3.041819E–02	7.661569E–05	6.370130E–04
0.140545	3.033772E–02	7.450252E–05	6.135638E–04
0.156624	3.029470E–02	7.240496E–05	5.893022E–04
0.174543	3.028516E–02	7.020714E–05	5.643885E–04
0.194512	3.030323E–02	6.801648E–05	5.388121E–04
0.216766	3.034115E–02	6.579492E–05	5.127031E–04
0.241565	3.038961E–02	6.350846E–05	4.862056E–04
0.269202	3.043825E–02	6.123496E–05	4.593820E–04
0.300000	3.047577E–02	5.898080E–05	4.323859E–04

Table 5.29: Mean relative residual accelerations between several models and the real Solar System over selected halo orbits of the RTBP around L_2 in the Sun–Earth+Moon case.

Part II

The neighborhood of the collinear equilibrium points in the RTBP

This part is devoted to the study of the vicinity of the collinear equilibrium points of the RTBP for the Earth–Moon mass parameter. The study is based in the continuation of the families of periodic orbits and invariant 2–dimensional tori of the central manifold of the equilibrium points. The methodology used is described in Chapter 6. The results are presented in Chapter 7, and consist in the continuation of Lyapunov and halo–type families of periodic orbits, including some of its bifurcations, as well as the invariant tori around the previous families of periodic orbits with elliptic normal part. At the end of Chapter 7, the results are summarized by displaying Poincaré $\{z = 0\}$ sections of all the computed objects for some energy levels.

Chapter 6

Methodology for the computation of families of periodic orbits and 2D invariant tori

This chapter is devoted to the development of the methodology used for the continuation of families of periodic orbits and invariant 2D tori of the central manifold of the collinear equilibrium points of the RTBP. After the description of the methodology, we discuss some computational aspects of the continuation of invariant tori, including its practical implementation in a parallel computer.

6.1 Refinement and continuation of periodic orbits

The following guidelines have been taken into account to design the methodology for the numerical refinement and continuation of periodic orbits in this section:

- As, in principle, we are not looking for periodic orbits with any kind of symmetry, the integrations will be carried out for the full period of each orbit.
- We will use multiple shooting ([28]), in order to avoid the difficulties due to the integration of very unstable orbits over large periods.
- We want to be able to continue the families of periodic orbits (p.o.) with respect to different parameters using the same routines.

6.1.1 The system of equations

Consider the Hamiltonian of the RTBP, $H(\mathbf{x})$, with vector-field $X_H(\mathbf{x})$ and flow $\phi_t(\mathbf{x})$ for $\mathbf{x} \in \mathbb{R}^6$ so that $\frac{d}{dt}\phi_t(\mathbf{x}) = X_H(\phi_t(\mathbf{x}))$ and $\phi_0(\mathbf{x}) = \mathbf{x}$. Let $\{g(\mathbf{x}) = 0\}$ be a surface of section and $T(\mathbf{x})$ the time necessary to intersect transversally $\{g(\mathbf{x}) = 0\}$, in the direction of $\nabla g(\mathbf{x})$, starting at $\mathbf{x}$. Then, the system of equations used to refine m initial conditions

$\mathbf{x}_0, \ldots, \mathbf{x}_{m-1} \in \mathbb{R}^6$ to a periodic orbit can be written as

$$\begin{cases} H(\mathbf{x}_0) - h & = \ 0, \\ T(\mathbf{x}_{m-1}) - \frac{\tau}{m} & = \ 0, \\ \phi_{\frac{\tau}{m}}(\mathbf{x}_i) - \mathbf{x}_{i+1} & = \ 0, \qquad i = 0 \div m-2, \\ \phi_{T(\mathbf{x}_{m-1})}(\mathbf{x}_{m-1}) - \mathbf{x}_0 & = \ 0, \end{cases} \tag{6.1}$$

where the multiple shooting equations $\phi_{\frac{\tau}{m}}(\mathbf{x}_i) - \mathbf{x}_{i+1} = 0$ are assumed not to exist if $m = 1$. This is a system of $6m + 2$ equations and $6m + 2$ unknowns: $h, \tau \in \mathbb{R}$ and $\mathbf{x}_0, \ldots, \mathbf{x}_{m-1} \in \mathbb{R}^6$. Note that, due to the definition of $T(\mathbf{x})$, the last equation implicitly forces $g(\mathbf{x}_0) = 0$.

In order to implement Newton's method, the derivatives of all the above equations are needed. They can be calculated directly in terms of $X_H(\mathbf{x})$, $D\phi_t(\mathbf{x})$ and $DT(\mathbf{x})$. $D\phi_t(\mathbf{x})$ can be obtained from the first variational equations, and $DT(\mathbf{x})$ can be obtained by differentiating $g(\phi_{T(\mathbf{x})}(\mathbf{x})) \equiv 0$, which gives

$$DT(\mathbf{x}) = -\frac{Dg(\phi_{T(\mathbf{x})}(\mathbf{x}))D\phi_{T(\mathbf{x})}(\mathbf{x})}{Dg(\phi_{T(\mathbf{x})}(\mathbf{x}))X_H(\phi_{T(\mathbf{x})}(\mathbf{x}))}.$$

In all our computations the surface of section $\{g(\mathbf{x}) = 0\}$ is an hyperplane, so $Dg(\phi_{T(\mathbf{x})}(\mathbf{x}))$ is a constant row vector.

System (6.1) does not need to be compatible. In fact the two first equations are not independent, because a level of energy determines uniquely a periodic orbit (locally) within a family, as well as a prescribed value of the period does. Our strategy consists in eliminating certain equations and keeping constant certain unknowns of (6.1) in order to perform continuations with respect to different parameters, as will be explained bellow. From now on, by "eliminating an unknown" we will mean keeping this unknown constant.

6.1.2 Refinement of a periodic orbit

To refine a p.o. we eliminate equations and unknowns of system (6.1) in order to get a new system of equations which has the periodic orbit as its unique solution (except in the case of bifurcation orbits). Several possibilities are:

- Refinement of a p.o. of a given energy level: we eliminate the second equation and unknowns h, τ.
- Refinement of a p.o. of a given period: we eliminate the first equation and the unknowns h, τ.
- Refinement of a p.o. of a given energy level and with a prescribed value of a coordinate: we eliminate the second equation and the unknowns h and the prescribed coordinate.

After elimination of equations and unknowns, we apply standard Newton's method to the system obtained. Let us denote it by $F(X) = 0$, then given a first approximation $X^{(0)}$ we proceed iteratively as

$$\begin{aligned} DF(X^{(k)})Y^{(k)} &= F(X^{(k)}) \\ X^{(k+1)} &= X^{(k)} - Y^{(k)}, \end{aligned} \tag{6.2}$$

stopping at the first k such that $\|F(X^{(k)})\|$ or $\|X^{(k)}-X^{(k-1)}\|$ are under a given tolerance.

We remark that, in the three possibilities above defined, (6.2) is a full–rank non–square linear system. A square system could be obtained by eliminating a further equation, for instance the equation corresponding to a coordinate that is determined by the surface of section. This approach would have the drawback of being section–dependent. An alternative is to use a method for solving linear systems that does not depend on the linear system being square, for instance a QR factorization or singular value decomposition (SVD [9]). We have used SVD because it is also well suited for the continuation of periodic orbits. The loss of efficiency, in terms of computing effort, with respect to other methods is not important in this case, since we are dealing with small dimensions.

6.1.3 Continuation of a family of p.o.

As in any Hamiltonian system, periodic orbits are not isolated in the RTBP but embedded in families. Once we have computed a single periodic orbit, we want to continue the corresponding family. The general ideas used are those of [24].

Our strategy for the continuation consists in eliminating equations and unknowns of system (6.1) in order to get a new system of equations which has the family of p.o. as a solution. Several possibilities are:

- Continuation w.r.t. energy: we eliminate the 2nd equation and τ.
- Continuation w.r.t. period: we eliminate the 1st equation and h.

Let $F(X) = 0$ be the system of equations obtained after elimination. Given a p.o., in order to predict a new p.o. of the family in which it is embedded, we consider the family as a manifold and move along its tangent space. Since this manifold is expressed by $F(X) = 0$, its tangent space, at a given orbit X, is given by $\operatorname{Ker} DF(X)$. Therefore, we proceed in the following manner: given $X^{(k)}$,

- We compute
$$Y^{(k)} = X^{(k)} + \delta V^{(k)} \tag{6.3}$$
being $\delta \in \mathbb{R}$, $V^{(k)} \in \operatorname{Ker} DF(X^{(k)})$ and $\|V^{(k)}\|_2 = 1$.
- We refine $Y^{(k)} =: Y^{(k,0)}$ using Newton's method:
$$\begin{aligned} DF(Y^{(k,j)})Z^{(j)} &= F(Y^{(k,j)}) \\ Y^{(k,j+1)} &= Y^{(k,j)} - Z^{(j)}, \end{aligned} \tag{6.4}$$
- We take as new member of the family, $X^{(k+1)}$, the first $Y^{(k,j)}$ such that $\|F(Y^{(k,j)})\|$ or $\|Y^{(k,j)} - Y^{(k,j-1)}\|$ is under a given tolerance.

The continuation step, δ, is corrected during the process in order to keep constant the number of iterates necessary for refinement.

Note that, because $F(X) = 0$ has the family of p.o. as solution, the linear system (6.4) has not unique solution but a 1–dimensional kernel. When solving (6.4) we choose the minimum Euclidean norm solution, in order to find the "closest" p.o. of the family. In the computations we have used SVD, because it directly gives both the kernel of $DF(X^{(k)})$ for computing $V^{(k)}$ and the minimum-norm solution of (6.4).

An additional comment is needed for the continuation w.r.t. energy using multiple shooting ($m > 1$). The unknown τ, which is kept fixed, does not need to be the period of the p.o., but it should be close, in order to get the conditions $\mathbf{x}_0, \dots, \mathbf{x}_{m-1}$ well spaced along the orbit. Thus it is advisable to set τ equal to the period of the p.o. after each continuation step. This implies to correct $\mathbf{x}_1, \dots, \mathbf{x}_{m-1}$ in order to satisfy $F(X) = 0$ again.

6.2 Refinement and continuation of invariant tori

The procedure used here for the refinement and continuation of invariant tori is based on looking for the Fourier series of the parametrization of an invariant curve on a torus, asking numerically for quasi-periodic motion. This kind of procedures have been introduced in [7].

Concretely, let $H(\mathbf{x})$, $X_H(\mathbf{x})$ and $\phi_t(\mathbf{x})$ be as above. We can look for a parametrization of a 2-dimensional torus $\psi : \mathbb{T}^2 = \mathbb{R}^2/2\pi\mathbb{Z} \to \mathbb{R}^n$ ($n = 6$ for the RTBP), satisfying

$$\psi(\theta + \omega t) = \phi_t(\psi(\theta)), \qquad \forall \theta \in \mathbb{T}^2, \ \forall t \in \mathbb{R}, \tag{6.5}$$

where $\omega = (\omega_1, \omega_2) \in \mathbb{R}^2$ is the vector of frequencies of the torus. Let us denote by T_i the period corresponding to the ω_i frequency, that is $T_i = 2\pi/\omega_i$, and $\theta = (\xi, \eta)$.

In order to reduce the dimension of the problem, instead of looking for the parametrization of the whole torus, we can look for the parametrization of a curve $\{\eta = \eta_0\}$ (or $\{\xi = \xi_0\}$) on the torus, which is invariant under ϕ_{T_2}, namely

$$\phi_{T_2}(\psi(\xi, \eta_0)) = \psi(\xi + \omega_1 T_2, \eta_0), \qquad \forall \xi \in \mathbb{T}^1. \tag{6.6}$$

Then, we look for a parametrization $\varphi : \mathbb{T}^1 \to \mathbb{R}^n$ satisfying

$$\varphi(\xi + \rho) = \phi_\delta(\varphi(\xi)), \qquad \forall \xi \in \mathbb{T}^1, \tag{6.7}$$

where $\delta = T_2$ and $\rho = \delta\omega_1$. Note that ρ is the rotation number of the curve we are looking for.

The original two–dimensional parametrization of the whole torus can be recovered from a parametrization of the invariant curve $\{\eta = \eta_0\}$. This is because (6.5) allows to reach any point of the torus integrating from a suitable point of the invariant curve, namely

$$\psi(\xi, \eta) = \phi_{\frac{\eta-\eta_0}{2\pi}\delta}\Big(\varphi(\xi - \frac{\eta - \eta_0}{2\pi}\rho)\Big). \tag{6.8}$$

In fact, given a parametrization φ of an invariant curve satisfying (6.7), then equation (6.8) defines a 2D parametrization of a 2D torus containing the invariant curve $\{\varphi(\xi)\}_{\xi \in \mathbb{T}^1}$ and satisfying (6.5), as shown in the following

Proposition 6.2.1 *The function ψ defined as in (6.8), where φ is assumed to satisfy (6.7), is 2π–periodic in each component and satisfies*

$$\phi_t(\psi(\xi, \eta)) = \psi\Big((\xi, \eta) + t(\frac{\rho}{\delta}, \frac{2\pi}{\delta})\Big). \tag{6.9}$$

Proof: The 2π–periodicity in ξ comes from the 2π–periodicity of φ. With respect to the 2π–periodicity in η, we have

$$\begin{aligned}\psi(\xi, \eta + 2\pi) &= \phi_{\frac{\eta-\eta_0}{2\pi}\delta+\delta}\Big(\varphi(\xi - \frac{\eta-\eta_0}{2\pi}\rho - \rho)\Big) = \phi_{\frac{\eta-\eta_0}{2\pi}\delta}\Big(\phi_\delta\Big(\varphi(\xi - \frac{\eta-\eta_0}{2\pi}\rho - \rho)\Big)\Big) \\ &\overset{(6.7)}{=} \phi_{\frac{\eta-\eta_0}{2\pi}\delta}\Big(\varphi(\xi - \frac{\eta-\eta_0}{2\pi}\rho)\Big) = \psi(\xi, \eta).\end{aligned}$$

Finally,

$$\begin{aligned}\phi_t(\psi(\xi,\eta)) &= \phi_{\frac{\eta-\eta_0}{2\pi}\delta+t}\Big(\varphi(\xi - \frac{\eta-\eta_0}{2\pi}\rho)\Big) \\ &= \phi_{\frac{\eta+t\frac{2\pi}{\delta}-\eta_0}{2\pi}\delta}\Big(\varphi\Big(\xi - \frac{\eta+t\frac{2\pi}{\delta}-\eta_0}{2\pi}\rho + t\frac{\rho}{\delta}\Big)\Big) \\ &= \psi(\xi + t\frac{\rho}{\delta}, \eta + t\frac{2\pi}{\delta}),\end{aligned}$$

and this ends the proof. □

Note that if equation (6.7) is satisfied for a value of ρ, it is also satisfied if we replace ρ by $\rho + 2\pi j$, $j \in \mathbb{Z}$. From (6.9), this gives a frequency vector $((\rho + 2\pi j)/\delta, 2\pi/\delta)$, which is different from $(\rho/\delta, 2\pi/\delta)$. This is a particular case of the following

Proposition 6.2.2 *Assume that $\psi : \mathbb{T}^d \to \mathbb{R}^n$ is a parametrization of a d–dimensional torus such that there exists a vector $\omega \in \mathbb{R}^d$ of rationally independent frequencies (that is, $k \in \mathbb{Z}^d$, $k \cdot \omega = 0 \Rightarrow k = 0$, where $\cdot$ denotes the Euclidean scalar product) verifying*

$$\phi_t(\psi(\theta)) = \psi(\theta + t\omega), \qquad \forall\theta \in \mathbb{T}^d, \quad \forall t \in \mathbb{R}.$$

Let A be a $d \times d$ unimodular matrix (that is, with integer coefficients and determinant ± 1) and define $\nu = A\omega$. Then there exists a parametrization $\widetilde{\psi} : \mathbb{T}^d \to \mathbb{R}^n$ of the same torus (i.e.$\{\psi(\theta)\}_{\theta\in\mathbb{T}^d} = \{\widetilde{\psi}(\theta)\}_{\theta\in\mathbb{T}^d}$) satisfying

$$\phi_t(\widetilde{\psi}(\theta)) = \widetilde{\psi}(\theta + t\nu), \qquad \forall\theta \in \mathbb{T}^d, \quad \forall t \in \mathbb{R}.$$

Proof: Assume $\psi(\theta) = \sum_{k\in\mathbb{Z}^d} a_k e^{ik\cdot\theta}$. Then,

$$\psi(\omega t) = \sum_{k\in\mathbb{Z}^d} a_{A^\top k} e^{i(A^\top k)^\top \omega t} = \sum_{k\in\mathbb{Z}^d} a_{A^\top k} e^{ik^\top (A\omega) t} = \widetilde{\psi}(\nu t),$$

being

$$\widetilde{\psi}(\theta) = \sum_{k\in\mathbb{Z}^d} a_{A^\top k} e^{ik\cdot\theta}.$$

Then, for any $t \in \mathbb{R}$,

$$\widetilde{\psi}(\nu t) = \psi(\omega t) = \phi_t(\psi(0)) = \phi_t(\widetilde{\psi}(0)) \tag{6.10}$$

Now let $\theta \in [0, 2\pi]^d$ and let $\{s_n\}_{n\in\mathbb{N}} \subset \mathbb{R}$ with $s_n\nu \pmod{2\pi} \overset{n\to\infty}{\longrightarrow} \theta$ (such a sequence exists because of the rational independence of ω), where we denote

$$(\theta_1, \ldots, \theta_d) \pmod{2\pi} = (\theta_1 - 2\pi[\theta_1/(2\pi)], \ldots, \theta_d - 2\pi[\theta_d/(2\pi)])$$

and [ ] denotes integer part. Then, for any $t \in \mathbb{R}$, using the continuity and 2π–periodicity in each argument of $\widetilde{\psi}$, we have

$$\begin{aligned}\widetilde{\psi}(\theta + t\nu) &= \lim_{n\to\infty} \widetilde{\psi}(s_n\nu + t\nu) \overset{(6.10)}{=} \lim_{n\to\infty} \phi_t(\phi_{s_n}(\widetilde{\psi}(0))) \\ &\overset{(6.10)}{=} \lim_{n\to\infty} \phi_t(\widetilde{\psi}(s_n\nu)) = \phi_t(\widetilde{\psi}(\lim_{n\to\infty} s_n\nu\%2\pi)) \\ &= \phi_t(\widetilde{\psi}(\theta)),\end{aligned}$$

which ends the proof. □

6.2.1 Indeterminations of the Fourier representation

We will look for φ as a truncated Fourier series,

$$\varphi(\xi) = A_0 + \sum_{k=1}^{N_f} (A_k \cos(k\xi) + B_k \sin(k\xi)), \tag{6.11}$$

with A_k, $B_k \in \mathbb{R}^n$. This representation of the geometrical torus $\{\psi(\theta)\}_{\theta\in\mathbb{T}^2}$ is non unique for two reasons:

- For each choice of η_0 we have a different φ in (6.11), i.e., a different invariant curve on the torus $\{\psi(\theta)\}_{\theta\in\mathbb{T}^2}$.
- Given the parametrization (6.11), for each $\xi_0 \in \mathbb{T}^1$, $\varphi(\xi - \xi_0)$ is a different one with a different Fourier expansion of the same invariant curve $\{\varphi(\xi)\}_{\xi\in\mathbb{T}^1}$ of the torus $\{\psi(\theta)\}_{\theta\in\mathbb{T}^2}$. Indeed, its Fourier expansion is

  $$\varphi(\xi - \xi_0) = A_0 + \sum_{k=1}^{N_f} (\widetilde{A}_k \cos(k\xi) + \widetilde{B}_k \sin(k\xi)),$$

  being

  $$\begin{aligned}\widetilde{A}_k &= A_k \cos(k\xi_0) - B_k \sin(k\xi_0) \\ \widetilde{B}_k &= A_k \sin(k\xi_0) + B_k \cos(k\xi_0).\end{aligned} \tag{6.12}$$

  We will call this “coefficient modulation”, in analogy with the terminology used in signal processing

Our approach to overcome the first indetermination has been to keep constant (i.e. to eliminate as unknown) one coordinate of A_0. Care must be taken to verify that this condition is valid along the continuation of the tori.

As for the second indetermination, we remark that, for any $k \geq 1$, if $(A_k^j, B_k^j) \neq (0,0)$ (here A_k^j denotes the j-th coordinate of A_k), from (6.12) there exists a ξ_0 that gives $\widetilde{A}_k^j = 0$. Thus by setting $A_k^j = 0$ we will avoid the indetermination, as long as B_k^j remains different from zero. Usually we have taken $k = 1$ and j has been selected in order to maximize $\|(A_1^j, B_1^j)\|_2$. In order to not to depend on B_k^j being different from zero, an alternative strategy is described in section 6.2.5.

6.2.2 Multiple shooting

In order to deal with high instability, we will use a multiple shooting procedure. It consists in looking for several invariant curves on the torus $\{\psi(\theta)\}_{\theta\in\mathbb{T}^2}$ instead of just one, in order to reduce the maximum time of integration to a fraction of δ. Concretely, we will look for m parametrizations $\varphi_0 = \varphi, \varphi_1, \dots, \varphi_{m-1}$ satisfying

$$\left\{ \begin{array}{rcll} \varphi_{j+1}(\xi) & = & \phi_{\frac{\delta}{m}}(\varphi_j(\xi)) & (j = 0 \div m-2) \\ \varphi_0(\xi+\rho) & = & \phi_{\frac{\delta}{m}}(\varphi_{m-1}(\xi)), & \end{array} \right. \tag{6.13}$$

for all $\xi \in \mathbb{T}^1$.

6.2.3 The system of equations

Following [7], we will turn (6.13) into a finite system of equations by discretizing $\mathbb{T}^1$ in $2N_f+1$ values of ξ. We will simply take

$$\xi_i = i\frac{2\pi}{1+2N_f} \qquad (i = 0 \div 2N_f). \tag{6.14}$$

In addition to the Fourier coefficients, we have to consider δ, ρ as unknowns since they are expected to vary along continuations. In order to describe the tori in terms of energy, we will add a new unknown h and a new equation $H(\varphi_0(0)) - h = 0$, which will prescribe an energy level for the torus being computed.

In order to simplify the notation, let us denote the Fourier coefficients as

$$\mathcal{F} = (A_0, A_1, B_1, \dots, A_{N_f}, B_{N_f})$$

and

$$\Psi(\xi, \mathcal{F}) = A_0 + \sum_{k=1}^{N_f} (A_k \cos(k\xi) + B_k \sin(k\xi)).$$

Then, the system of equations to be solved is

$$\begin{array}{rcll} H(\Psi(0,\mathcal{F}_0)) - h & = & 0 & \\ \Psi(\xi_i, \mathcal{F}_{j+1}) - \phi_{\frac{\delta}{m}}(\Psi(\xi_i, \mathcal{F}_j)) & = & 0 & j = 0 \div m-2,\ i = 0 \div 2N_f \\ \Psi(\xi_i+\rho, \mathcal{F}_0) - \phi_{\frac{\delta}{m}}(\Psi(\xi_i, \mathcal{F}_{m-1})) & = & 0 & i = 0 \div 2N_f, \end{array} \tag{6.15}$$

where the unknowns are $h, \delta, \rho, \mathcal{F}_0, \dots, \mathcal{F}_{m-1}$. $\mathcal{F}_i$ stands for the Fourier coefficients of the curve φ_i in the multiple shooting (6.13). As in the case of periodic orbits, the multiple shooting equations $\Psi(\xi_i, \mathcal{F}_{j+1}) - \phi_{\frac{\delta}{m}}(\Psi(\xi_i, \mathcal{F}_j)) = 0$ do not exist if $m = 1$.

6.2.4 Refinement of an invariant torus

In order to refine an invariant torus, we first eliminate two unknowns in system (6.15) in order to set an invariant curve on the torus we want to refine and avoid coefficient modulation. After that we eliminate two more unknowns in order to have the torus we are looking for as unique solution of our system of equations. This is because the tori we will compute are always embedded in two–parametric Cantorian families. A concrete example, with the actual unknowns eliminated, will be given at the beginning of section 7.3.

After elimination of these four unknowns, we use Newton's method to the system obtained as in the case of periodic orbits. Equation (6.2) applies if we denote this system by $F(X) = 0$. As for the numerical method used to solve (6.1), we have used QR decomposition instead of SVD in this case, due to efficiency reasons. Additional details will be given in section 6.4.2.

6.2.5 Continuation of a family of tori

We perform the continuation of families of invariant tori using a predictor–corrector scheme. The idea is the same as in the case of periodic orbits: given a torus, in order to predict a new torus of the family, we consider the family as a manifold of invariant tori and move along its tangent space. Since this manifold is expressed as $F(X) = 0$, its tangent space at a given torus X is given by $\operatorname{Ker} DF(X)$. Note that this is not strictly true, since the manifolds of invariant tori are Cantorian, but it works in practice as long as the "gaps" due to resonances are not too large.

Therefore, we proceed as in the case of p.o.: given a torus of the family $X^{(k)}$, we predict a new one as $Y^{(k)} = X^{(k)} + \delta V^{(k)}$ where $\|V^{(k)}\|_2 = 1$, $V^{(k)} \in \operatorname{Ker} DF(X^{(k)})$, and then we correct it by Newton's method.

Due to the indetermination introduced by coefficient modulation, we will use different systems of equations for prediction and correction. The system we use for prediction is obtained from (6.15) by eliminating two unknowns, one in order to set an invariant curve on the torus and another in order to fix an one–parametric family (our families of tori are two–parametric). Let us denote this system as $F_p(X) = 0$. Then $\operatorname{Ker} DF_p(X)$ is two–dimensional and includes coefficient modulation. We choose $V^{(k)} \in \operatorname{Ker} DF_p(X)$ orthogonal to the direction corresponding to coefficient modulation, which can be obtained by derivating (6.12) with respect to ξ_0.

In order to perform the correction, we will remove from $F_p(X) = 0$ an additional unknown, which will be chosen according to the following criteria:

- We will eliminate A_1^J or B_1^J, where J chosen in order to have $\|(A_1^J, B_1^J)\|_2 = \max_{i=1\div n} \|(A_1^i, B_1^i)\|_2$. The reason for this choice is heuristic and tries to prevent asking conditions on harmonics of low amplitude.

- Between A_1^J and B_1^J, we select the coordinate for which $\min(|A_1^J|, |B_1^J|)$ is achieved. This avoids situations like the following: assume that, before the correction, $A_1^J = 0$ and $|B_1^J| = \alpha$. If we eliminate B_1^J, we are forcing $\|(A_1^J, B_1^J)\|_2 > \alpha$ and therefore we will not be able to continue if $\|(A_1^J, B_1^J)\|_2$ decreases along the family. If $|A_1^J|$ is different from zero but small, we will be able to continue but the continuation step δ will be artificially reduced.

We prefer this strategy for coefficient modulation instead of the one pointed out in 6.2.1 in order to not to depend on a Fourier coefficient being different from zero.

As in the case of periodic orbits, the linear system solved during correction is rank–deficient. We solve it using QR with column pivoting instead of SVD for efficiency reasons. Additional details will be given in sections 6.4.2 and 6.4.3.

6.2.6 Error estimation

In order to have some control over the error due to the discretization of $\mathbb{T}^1$, we proceed as in [7]: we evaluate (6.15) over a finer discretization than (6.14) and increase the number of harmonics until the maximum norm is under a given tolerance. That is, we increase N_f until

$$\max_{\substack{i=0\div 2N_f,\ j=0\div m-2 \\ k=0\div M(1+2N_f)-1}} \left\| \begin{array}{c} \Psi(\widetilde{\theta}_k, \mathcal{F}_{j+1}) - \phi_{\frac{\delta}{m}}(\Psi(\widetilde{\theta}_k, \mathcal{F}_j)) \\ \Psi(\widetilde{\theta}_k + \rho, \mathcal{F}_0) - \phi_{\frac{\delta}{m}}(\Psi(\widetilde{\theta}_k, \mathcal{F}_{m-1})) \end{array} \right\|_\infty < tol, \qquad (6.16)$$

being $\widetilde{\theta}_k = k\frac{2\pi}{M(1+2N_f)}$. We have typically used $tol = 10^{-10}$ and $M = 50$.

6.3 Starting the continuation of tori from the central part of a periodic orbit

Let $\phi_t(\mathbf{x})$ be the flow associated to the Hamiltonian $H(\mathbf{x})$ of the RTBP. The normal behavior of a T–periodic orbit through $\mathbf{x}_0$ is studied in terms of the time–T flow around $\mathbf{x}_0$, whose linear approximation is given by the monodromy matrix $M = D\phi_T(\mathbf{x}_0)$ of the periodic orbit:

$$\phi_T(\mathbf{x}) = \mathbf{x}_0 + M(\mathbf{x} - \mathbf{x}_0) + O(\|\mathbf{x} - \mathbf{x}_0\|^2).$$

As the monodromy matrix M is symplectic,

$$\operatorname{Spec} M = \{1, 1, \lambda_1, \lambda_1^{-1}, \lambda_2, \lambda_2^{-1}\}.$$

The stability parameters of the periodic orbit, that are defined as $s_j = \lambda_j + \lambda_j^{-1}$ for $j = 1, 2$, can be of one of the following kinds:

- *Hyperbolic*: $s_j \in \mathbb{R}$, $|s_j| > 2$. It is equivalent to $\lambda_j \in \mathbb{R}\backslash\{-1, 1\}$.
- *Elliptic*: $s_j \in \mathbb{R}$, $|s_j| < 2$. It is equivalent to $\lambda_j = e^{i\rho}$ with $\rho \in \mathbb{R}$ (if $|s_j| = 2$, then it is said to be *parabolic*).
- *Complex unstable*: $s_j \in \mathbb{C}\backslash\mathbb{R}$. It is equivalent to $\lambda_j \in \mathbb{C}\backslash\mathbb{R}$, $|\lambda_j| \neq 1$.

If s_j is complex unstable, then s_{3-j} is also complex unstable and, in fact, $s_{3-j} = \overline{s_j}$. If s_j is hyperbolic, then the periodic orbit has stable and unstable manifolds, whose sections at $\mathbf{x}_0$ through the $\{\lambda_j, \lambda_j^{-1}\}$–eigenplane of M are tangent to the $\{\lambda_j, \lambda_j^{-1}\}$–eigenvectors at $\mathbf{x}_0$. If s_j is elliptic, the $\{\lambda_j, \lambda_j^{-1}\}$–eigenplane of M through $\mathbf{x}_0$ is foliated (in the linear approximation) by invariant curves of the restriction of the linearization of ϕ_T (that is, the map $\mathbf{x} \to \mathbf{x}_0 + M(\mathbf{x} - \mathbf{x}_0)$), which have rotation number ρ. For the full system, some of these invariant curves subsist and give rise to 2D tori.

In what follows, we will say that a periodic orbit has central part if one of the stability parameters s_1, s_2 is elliptic. If $|s_i| < 2$ for $i = 1, 2$, the periodic orbit is linearly stable.

Given a periodic orbit with central part, we use the linear approximation of the flow in order to get an initial seed to start the computation of an invariant torus around this orbit. Let $\mathbf{x}_0$ be an initial condition of a periodic orbit of period T so that $\phi_T(\mathbf{x}_0) = \mathbf{x}_0$. We denote the linearized time t flow around $\mathbf{y}$ by

$$L^{\mathbf{y}}_{\phi_t}(\mathbf{x}) = \phi_t(\mathbf{y}) + D\phi_t(\mathbf{y})(\mathbf{x} - \mathbf{y}).$$

Let $\cos\nu + i\sin\nu$ be an eigenvalue of the monodromy matrix of the periodic orbit, $M = D\phi_T(\mathbf{x}_0)$, and let $\mathbf{v}_1 + i\mathbf{v}_2$ be an associated eigenvector. Define L_φ as

$$\begin{aligned} L_\varphi(\xi) &= \mathbf{x}_0 + \gamma(\mathbf{v}_1\cos\xi_0 + \mathbf{v}_2\sin\xi_0)\cos\xi \\ &\quad + \gamma(\mathbf{v}_1\sin\xi_0 - \mathbf{v}_2\cos\xi_0)\sin\xi, \end{aligned} \tag{6.17}$$

where $\gamma \in \mathbb{R}$ is a parameter. Then we have the following

Proposition 6.3.1 *For all $\xi \in [0, 2\pi]$, L_φ verifies*

$$L_\varphi(\xi + \nu) - L^{\mathbf{x}_0}_{\phi_T}(L_\varphi(\xi)) = 0. \tag{6.18}$$

Proof: Since $\mathbf{v}_1 + i\mathbf{v}_2 \in \operatorname{Spec} M$, we have

$$\begin{aligned} M(\mathbf{v}_1 + i\mathbf{v}_2) &= (\cos\nu + i\sin\nu)(\mathbf{v}_1 + i\mathbf{v}_2) \\ &= (\mathbf{v}_1\cos\nu - \mathbf{v}_2\sin\nu) + i(\mathbf{v}_1\sin\nu + \mathbf{v}_2\cos\nu), \end{aligned}$$

which can be rewritten as

$$M[\mathbf{v}_1, \mathbf{v}_2] = [\mathbf{v}_1, \mathbf{v}_2]\begin{pmatrix} \cos\nu & \sin\nu \\ -\sin\nu & \cos\nu \end{pmatrix} = [\mathbf{v}_1, \mathbf{v}_2]R_\nu, \tag{6.19}$$

where $[\mathbf{v}_1, \mathbf{v}_2]$ denotes the 6×2 matrix with columns $\mathbf{v}_1$, $\mathbf{v}_2$ and

$$R_\xi = \begin{pmatrix} \cos\xi & \sin\xi \\ -\sin\xi & \cos\xi \end{pmatrix}$$

is the rotation of the plane of angle ξ. Now,

$$\begin{aligned} L^{\mathbf{x}_0}_{\phi_T}(L_\varphi(\xi)) &= \mathbf{x}_0 + M[\mathbf{v}_1, \mathbf{v}_2]\begin{pmatrix} \cos(\xi - \xi_0) & \sin(\xi - \xi_0) \\ -\sin(\xi - \xi_0) & \cos(\xi - \xi_0) \end{pmatrix}\begin{pmatrix} \gamma \\ 0 \end{pmatrix} \\ &= \mathbf{x}_0 + M[\mathbf{v}_1, \mathbf{v}_2]R_{\xi-\xi_0}\begin{pmatrix} \gamma \\ 0 \end{pmatrix} \overset{(6.19)}{=} \mathbf{x}_0 + [\mathbf{v}_1, \mathbf{v}_2]R_\nu R_{\xi-\xi_0}\begin{pmatrix} \gamma \\ 0 \end{pmatrix} \\ &= \mathbf{x}_0 + M[\mathbf{v}_1, \mathbf{v}_2]R_{\xi+\nu-\xi_0}\begin{pmatrix} \gamma \\ 0 \end{pmatrix} = L_\varphi(\xi + \nu), \end{aligned}$$

as the proposition states. $\square$

Note that equation (6.18) is the linearized version of (6.7). We can therefore use (6.8) to construct the one–parametric family, with parameter γ, of 2D tori invariant by the linear approximation of the flow around the periodic orbit, namely

$$L_\psi(\xi,\eta) = L^{\mathbf{x}_0}_{\phi_{\frac{\eta}{2\pi}T}}(L_\varphi(\xi - \frac{\eta}{2\pi}\nu)). \tag{6.20}$$

Doing similar calculations to the ones of Proposition 6.2.1, it can be verified that

$$L^{\phi_{\frac{\eta}{2\pi}T}(\mathbf{x}_0)}_{\phi_t}(L_\psi(\xi,\eta)) = L_\psi\Big((\xi,\eta) + t(\frac{\nu}{T},\frac{2\pi}{T})\Big).$$

Therefore, we expect to find in a neighborhood of the periodic orbit 2D invariant tori with frequency vector close to $(\nu/T, 2\pi/T)$.

Note that, since $e^{\pm i\nu} \in \operatorname{Spec} M$, ν is determined up to its sign and an integer multiple of 2π. This gives for the frequency vector the following possibilities:

$$\Big(\frac{\pm\nu + 2\pi j}{T}, \frac{2\pi}{T}\Big), \quad j \in \mathbb{Z}, \tag{6.21}$$

which, according to Proposition 6.2.2, are unimodular transformations of the initial frequency vector, namely

$$\begin{pmatrix} \frac{\pm\nu+2\pi j}{T} \\ \frac{2\pi}{T} \end{pmatrix} = \begin{pmatrix} \pm 1 & j \\ 0 & 1 \end{pmatrix} \begin{pmatrix} \frac{\nu}{T} \\ \frac{2\pi}{T} \end{pmatrix}.$$

With this, what we have are invariant tori for the linear flow around the periodic orbit. We will use these tori to get an initial seed for the procedure.

6.3.1 Starting "longitudinally" to the periodic orbit

By this we mean to look for an initial torus integrating "along" the periodic orbit, that is, taking δ in (6.7) close to the period of the periodic orbit. We will therefore look for an invariant curve on this initial torus close to $\{L_\psi(\xi,0)\}_{\xi\in\mathbb{T}^1}$. From equations (6.20), (6.18) and (6.17), we will take as initial seed

$$\begin{array}{rcl@{\qquad}rcl} h &=& H(\mathbf{x}_0), & A_0 &=& \mathbf{x}_0, \\ \delta &=& T, & A_1 &=& \gamma(\mathbf{v}_1\cos\xi_0 + \mathbf{v}_2\sin\xi_0), \\ \rho &=& \nu, & B_1 &=& \gamma(\mathbf{v}_1\sin\xi_0 - \mathbf{v}_2\cos\xi_0), \\ & & & A_j, B_j &=& 0 \qquad (j \geq 2). \end{array} \tag{6.22}$$

If multiple shooting is used, then initial approximations of the Fourier coefficients of the remaining invariant curves can be taken from

$$\begin{aligned} L^{\mathbf{x}_0}_{\phi_{j\frac{T}{m}}}(L_\varphi(\xi)) &= \phi_{j\frac{T}{m}}(\mathbf{x}_0) + \gamma(\mathbf{w}_1^j\cos\xi_0 + \mathbf{w}_2^j\sin\xi_0)\cos\xi \\ &\quad + \gamma(\mathbf{w}_2^j\sin\xi_0 - \mathbf{w}_2^j\cos\xi_0)\sin\xi, \end{aligned}$$

where $\mathbf{w}_i^j = D\phi_{j\frac{T}{m}}(\mathbf{x}_0)\mathbf{v}_i$.

Note that ξ_0 is free. It can be used to set to zero the coordinate we want to eliminate in order to prevent coefficient modulation.

If, during the refinement of the initial seed (6.22), we keep constant one nonzero coordinate of A_1 or B_1, we will avoid "falling back" to the periodic orbit, since it will no longer be a solution of our system of equations. In particular, the unknowns δ and ρ, which were originally set equal to the values of the periodic orbit, will be corrected to the values of the torus being refined. This avoids the need to know a priori the behavior (increasing or decreasing) of ρ when we start the computation of the tori at a given periodic orbit.

6.3.2 Starting "transversally" to the periodic orbit

By this we mean to look for an initial torus integrating "across" the periodic orbit, that is taking δ in (6.7) close to the normal period of the p.o. that gives central part. We will therefore look for an invariant curve on this initial torus close to $\{L_\psi(0,\eta)\}_{\eta\in\mathbb{T}^1}$ (in particular, to the p.o.), so we will use as initial seed for the Fourier coefficients $A_0, A_1, B_1, \ldots$ the Fourier expansion of

$$L_\psi(0,\eta) = L_{\phi_{\frac{\eta}{2\pi}T}}\Big(L_\varphi(-\frac{\eta}{2\pi}\nu)\Big),$$

which can be efficiently computed from the FFT of $\{L_\psi(0,\frac{2\pi j}{N})\}_{j=0}^{N-1}$ for a suitable N. If multiple shooting is used, we take the Fourier coefficients of φ_j from a Fourier expansion of $\phi_{j\frac{\delta}{m}}(L_\psi(0,\eta))$.

The initial value for δ is taken as the period associated to the first frequency in (6.21)

$$\delta = \frac{2\pi}{\pm\nu + 2\pi j}T, \tag{6.23}$$

and, following the deduction of (6.7) from (6.6) (but exchanging the role of the two frequencies), the value for ρ is taken as δ times the second frequency in (6.21), that is

$$\rho = \delta\frac{2\pi}{T} = \frac{(2\pi)^2}{\pm\nu + 2\pi j}. \tag{6.24}$$

6.4 Computational aspects

In this section we will give some details of the actual implementation of the above methodology. We will focus in the continuation of families of invariant tori, since it is the critical part in terms of computing time.

6.4.1 Continuation of a 1–parametric family of tori

The first step in the continuation of a family of invariant tori is to get an initial seed by starting either longitudinally or transversally to a periodic orbit, as was described in section 6.3. A typical value used for the parameter γ has been 10^{-4}. This initial seed, which corresponds to an invariant torus of the linear flow around the periodic orbit, is refined to an invariant curve of a torus of the actual flow following section 6.2.4.

Once we have an initial torus of the family, we choose an small initial continuation step δ and proceed iteratively as follows:

1. We predict a new torus of the family following section 6.2.5.
2. We correct the predicted torus according to section 6.2.5. If the correction fails, we divide by 2 the continuation step and go to step 1.
3. We check the angle formed by the three last tori (to compute this angle we take into account h, δ, ρ and the Fourier coefficients of order zero). If it is greater than a given tolerance (we have typically used 15 degrees), we divide by 2 the continuation step and go to step 1. In some situations, it is necessary to restart the process from the first of the three last tori.
4. We check the error bound condition (6.16) and, if it is not satisfied, we increase N_f, set to zero the new Fourier coefficients and go to step 2.
5. We correct the continuation step δ in order to keep the number of Newton iterations needed in step 2 within a given interval.

The continuation is stopped if one of the following conditions is true:

- The amplitude of the harmonics of order ≥ 1 becomes zero. This means we have fallen longitudinally to a periodic orbit.
- In step 4, N_f reaches the maximum allowable value without satisfying the bound condition (6.16).
- In steps 2, 3 or 5, the continuation step is reduced to a value under a minimum.

Note that we do not take into account possible bifurcations.

6.4.2 On the computing effort

The computing effort necessary for the refinement and continuation of a family of invariant tori is distributed in three main blocks:

- The evaluation of the system of nonlinear equations (6.15) and its differential. This involves the numerical integration of $1 + 2N_f$ initial conditions through the flow of the system of differential equations formed by the RTBP equations (A.2) and its first variational equations.
- The solution of linear systems with the differential of the system of equations (6.15) as coefficient matrix. This applies to the refinement of a single invariant torus (section 6.2.4) and both to prediction and refinement in the continuation of an one–parametric family (section 6.2.5).
- The computation of the error bound (6.16). This involves the numerical integration of $M(1 + 2N_f)$ initial conditions through the flow of the RTBP equations (A.2).

As N_f grows, the dominant part of the computing time is expended in the solution of linear systems.

In the case of refinement of a single torus (sec. 6.2.4), the linear system corresponding to Newton's method is $(1+m(1+2N_f)n)\times(m(1+2N_f)n-1)$ and is full-rank. At it has been said, we use a standard QR algorithm ([9]) for solving it. In the case of continuation (sec. 6.2.5), the linear system corresponding to prediction is $(1+m(1+2N_f)n)\times(1+m(1+2N_f))$, and the one corresponding to Newton's method with minimum–norm correction is $(1+m(1+2N_f)n)\times m(1+2N_f)$. Both systems are rank–deficient. We have used QR with column pivoting [9] in these two cases. SVD can also be used, but QR with column pivoting is much faster. Concretely, for an $M\times N$ system of rank R, SVD requires $14MN^2+8N^3$ operations (following [9], we count one sum plus one product as two operations), whereas QR with column pivoting requires $4MNR-2R^2(M+N)+4R^3/3$. For $M=N=R$, this is a factor 16.5.

As a timing example, if we want to continue a torus using multiple shooting with $m=2$ and $N_f=100$ (which has been upper limit for most of the explorations), the linear system we have to solve at each Newton iteration is 2413×2411. Every Newton iteration for these dimensions takes us 613 seconds on an Intel Pentium III at 500 MHz.

6.4.3 Computation of kernel and minimum–norm corrections using QR with column pivoting

Let $Ax=b$ be an $m\times n$ linear system of equations with $m\geq n$ and $\operatorname{rank} A=r<n$. We are interested in computing $\operatorname{Ker} A$ and the minimum–norm solution of $Ax=b$ which we will denote as x_{LS}.

If we apply QR factorization with column pivoting to A [9], we will obtain

$$Q^\top A\Pi=\begin{pmatrix} R_{11} & R_{12}\\ 0 & 0\end{pmatrix},$$

where Π is an $n\times n$ permutation matrix, R_{11} is an $r\times r$ upper triangular matrix and R_{12} is an $r\times(n-r)$ matrix. Then, if we denote $\Pi^\top x=(y,z)^\top$ and $Q^\top b=(c,d)^\top$, the general least–squares solution of $Ax=b$ is given by (see [9], p. 259)

$$\Pi^\top x=\left\{\begin{pmatrix} y:\; R_{11}y=c-R_{12}z\\ z\end{pmatrix}\right\}_{x\in\mathbb{R}^{n-r}}. \tag{6.25}$$

At this point, a complete orthogonal factorization ([9]) would directly give us x_{LS}, but since we also need $\operatorname{Ker} A$ we have followed a different approach. Let x_B be a particular least–squares solution of $Ax=b$, which can be obtained setting $z=0$ in (6.25), and let $\{v_1,\ldots,v_{n-r}\}$ be a basis of $\operatorname{Ker} A$, which can be obtained setting $c=d=0$ and $z=e_1,\ldots,e_{n-r}$ in (6.25), where $\{e_1,\ldots,e_{n-r}\}$ is the standard basis of $\mathbb{R}^{n-r}$. Then we have

$$\Pi^\top x_{LS}=\Pi^\top x_B-K\lambda,$$

where K is the $n\times(n-r)$ matrix with columns $v_1,\ldots,v_{n-r}$ and $\lambda\in\mathbb{R}^{n-r}$ is the least–squares solution of $K\lambda=\Pi^\top x_B$. Since this last system of equations is over-determined and full–rank, it can be solved by a QR decomposition without pivoting.

6.4.4 Parallel strategies

For the continuation of invariant tori, two parallel strategies have been implemented. In the first one, several families are continued at once, so that at a given moment each processor is working in a different family. In the second one, all the processors work in the same family.

The first strategy is intended for the simultaneous continuation of n_c one–parametric families of invariant tori. The "breaking point" to parallelize has been the continuation step. It has been implemented using a master-slave model. The master program spawns n_e copies of the slave program and distributes the n_c continuations among them. Given a torus of a family, the slave program computes the next by performing one continuation step.

The master program searches for continuation steps to perform cyclically among the families to be continued. In this way, we can carry out simultaneously the continuation of more families than processors ($n_c > n_e$). The slaves are ordered in a list where the master searches for free slaves from the beginning to the end. Then, when more than $n_c - n_e$ continuations finish and some slaves become idle, the load "goes up" to the beginning of the list of slaves. This allows to take advantage of an heterogeneous network by putting the fastest processors in the beginning of this list.

PVM has been used as message–passing library for the communication between the master and slave processes. For the part of the slave code that solves linear systems, we have used the routines for QR decomposition with and without column pivoting of the LAPACK library [2], mainly DGEQPF, DGEQRF, DORMQR and DTRTRS.

Proceeding in this manner, the maximum values of the parameters reachable are given by the speed and amount of memory available in each node of the parallel computer being used. The second strategy overcomes these restrictions, at the expense of working just in one family.

With respect to this second strategy, it consists on parallelizing every item of section 6.4.2 individually, namely:

- For the evaluation of system (6.15) an its differential, an strategy is to distribute the $1 + 2N_f$ numerical integrations to perform among the processors. In our implementation, each process performs just the integrations necessary to generate the piece of matrix it will own during the resolution of linear systems. Depending on the distribution of the matrix, which in our case is given by ScaLAPACK conventions, this can lead to several processes performing the same integrations. An alternative is to distribute the integration in a manner independent of the distribution of the matrix, but this requires extra communication among processes before starting the resolution of linear systems.

- The resolution of linear systems has been parallelized by using parallel versions of the QR algorithms with and without column pivoting. Our implementation uses the ScaLAPACK library [4], mainly the routines PDGEQPF, PDGEQRF, PDORMQR and PDTRTRS.

- The computation of the bound (6.16) can be parallelized just by distributing the $M(1 + 2N_f)$ numerical integrations to perform among the processors.

As a final remark, note that these two strategies could be combined.

Chapter 7

Numerical Results

In this Chapter we give the results of the continuation of families of periodic orbits and 2D invariant tori of the central manifold of the collinear equilibrium points of the RTBP. We start with the Lyapunov families of p.o. that originate at the equilibrium points. Then we follow some of its bifurcated families, including the well–known halo families and some period–doubled and triplicated bifurcations of them. After that, we describe the 2–parametric families of invariant tori around the families of periodic orbits with elliptic normal part. At the end of this Chapter, all the computed objects are represented in the Poincaré section $\{z = 0, p_z > 0\}$ for some energy levels.

7.1 Lyapunov families of periodic orbits around the libration points

According to Lyapunov's center theorem, there are two families of periodic orbits emanating from each equilibrium point. We will denote these families as the vertical Lyapunov family and the planar Lyapunov family. The starting energy levels for them are those of the corresponding equilibrium points, which are given, for the Earth–Moon mass ratio, in table 7.1.

L_1	L_2	L_3
-1.59417	-1.58608	-1.50607

Table 7.1: Energy values of the three collinear equilibrium points for $\mu = 0.012150585$

For all three points, the vertical family starts as an infinitesimal oscillation in the z direction. All three families end at bifurcating planar orbits. For the L_1 case, the termination orbit surrounds the massive primary m_1 and the equilibrium points L_1 and L_3. This is an orbit of the (g) family, following Stromgren's terminology. For the L_2 point this planar orbits surrounds both primaries and L_1 ((l) family), and for L_3 it surrounds both primaries and the three equilibrium points ((l) family). In Fig. 7.1, we give the characteristic curves (energy vs period) of the three families, as well as their stability curves. When the range of the stability parameters is very large (usually for the L_1 and

L_2 families), we have plotted $2\,\mathrm{asinh}(\text{stab.par.})/\,\mathrm{asinh}\,2$. In Fig. 7.2 we show the planar termination orbits of the three families.

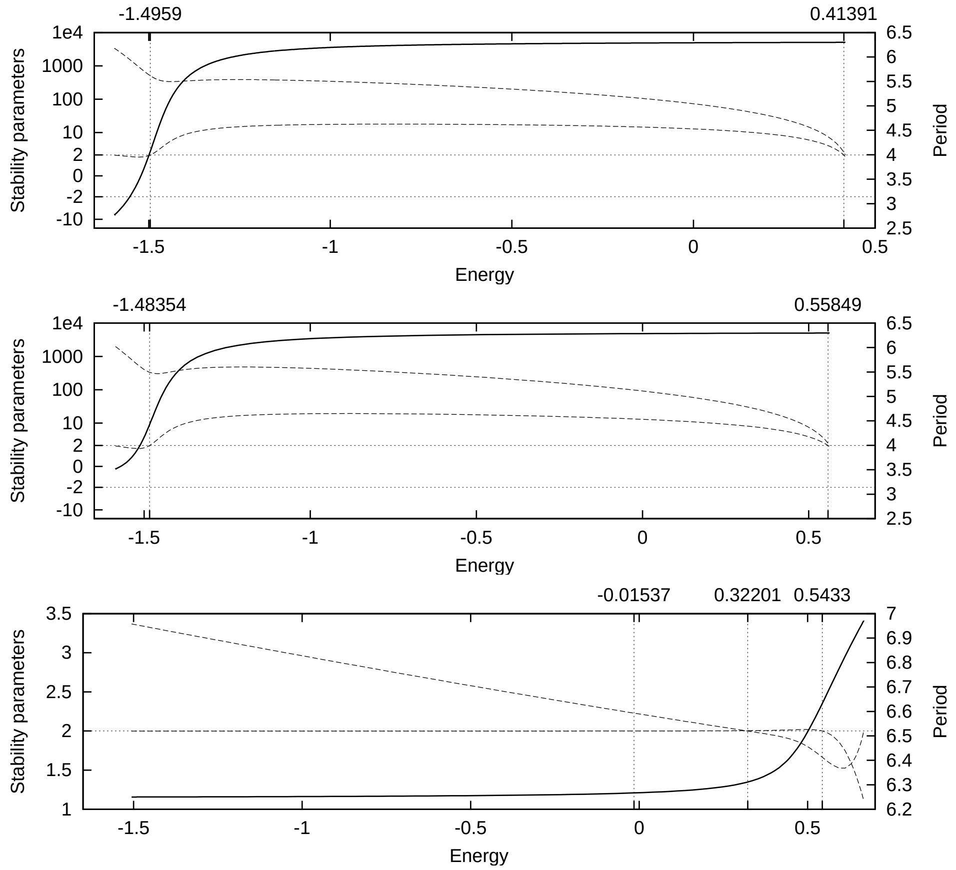

Figure 7.1: Characteristic curves (solid line) and stability parameters (dashed lines) of the vertical Lyapunov families of periodic orbits for L_1, L_2 and L_3 (from top to bottom). The vertical lines correspond to the energy levels of the bifurcation orbits (see table 7.2).

Aside from the termination orbit, there appear along the families additional bifurcation orbits. Their energy values are given in table 7.2. We will come back to these orbits later on.

For the planar Lyapunov families around L_1, L_2 and L_3, which correspond to families (c), (a) and (b) in Stromgren's classification, we have stopped the continuation when a collision orbit with one of the primaries appears. This is due to the fact that we are only interested in the dynamics in a neighborhood of the libration points, and the collision orbits are already large (see Fig.7.4). For L_1 and L_3 the collision takes place with the largest primary, whereas for the L_2 case it happens with the small one. In Fig. 7.3 we give the characteristic and stability curves for these families.

According to Hénon ([15]), the vertical stability character of a planar periodic orbit indicates whether or not this orbit is at the same time a member of a family of 3D periodic orbits. Only what Hénon calls *vertical critical orbits* ($|a_v| = 1$) can be embedded in 3D families of periodic orbits. Considering small out–of–plane perturbations of the periodic

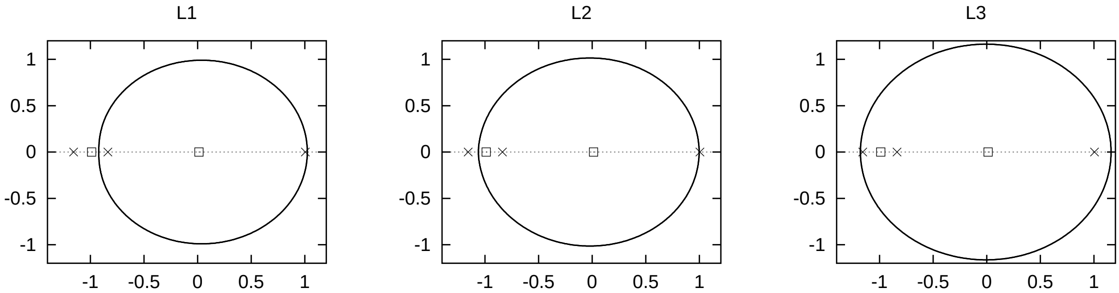

Figure 7.2: Termination planar orbits of the vertical Lyapunov families of periodic orbits around L_1, L_2 and L_3. On the x axis we have displayed the position of both primaries ($\square$) and the equilibrium points ($\times$). The three orbits are traveled clockwise.

#	L_1	L_2	L_3
1	-1.49590	-1.48354	-0.01537
2	0.41391	0.55849	0.32201
3			0.54330

Table 7.2: Energy levels of the bifurcation orbits of the Lyapunov vertical families of periodic orbits. For each L_i, the last bifurcation orbit corresponds to the termination of the family.

orbit after one revolution, and using

$$\begin{pmatrix} \Delta z \\ \Delta \dot{z} \end{pmatrix}_{\text{final}} = \begin{pmatrix} a_v & b_v \\ c_v & d_v \end{pmatrix} \begin{pmatrix} \Delta z \\ \Delta \dot{z} \end{pmatrix}_{\text{initial}},$$

three different kinds of bifurcated solutions can be considered (see [15]):

- Type A: Symmetrical periodic orbits with respect to the xy–plane and generated from planar orbits with $a_v = 1$, $c_v = 0$.
- Type B: Symmetrical periodic orbits with respect to the x–axis, generated from planar ones with $a_v = 1$, $b_v = 0$.
- Type C: Symmetrical periodic orbits with respect to both the xy–plane and the x–axis, generated from planar periodic orbits with $a_v = -1$ and $c_v = 0$ or $a_v = -1$ and $b_v = 0$.

In table 7.3 we give the bifurcations of the three families before the appearance of a collision orbit. Further bifurcations can be found in [15] for the value of the mass ratio $\mu = 0.5$. The bifurcated families will be described in the following sections. In all three cases, the first bifurcated family is formed by the so–called halo type orbits. These are 3D periodic orbits symmetric with respect to the $\{y = 0\}$ plane.

For the three equilibrium points, the two Lyapunov families are connected by two-lane bridges of periodic orbits going from bifurcation orbit #1 of the vertical family to

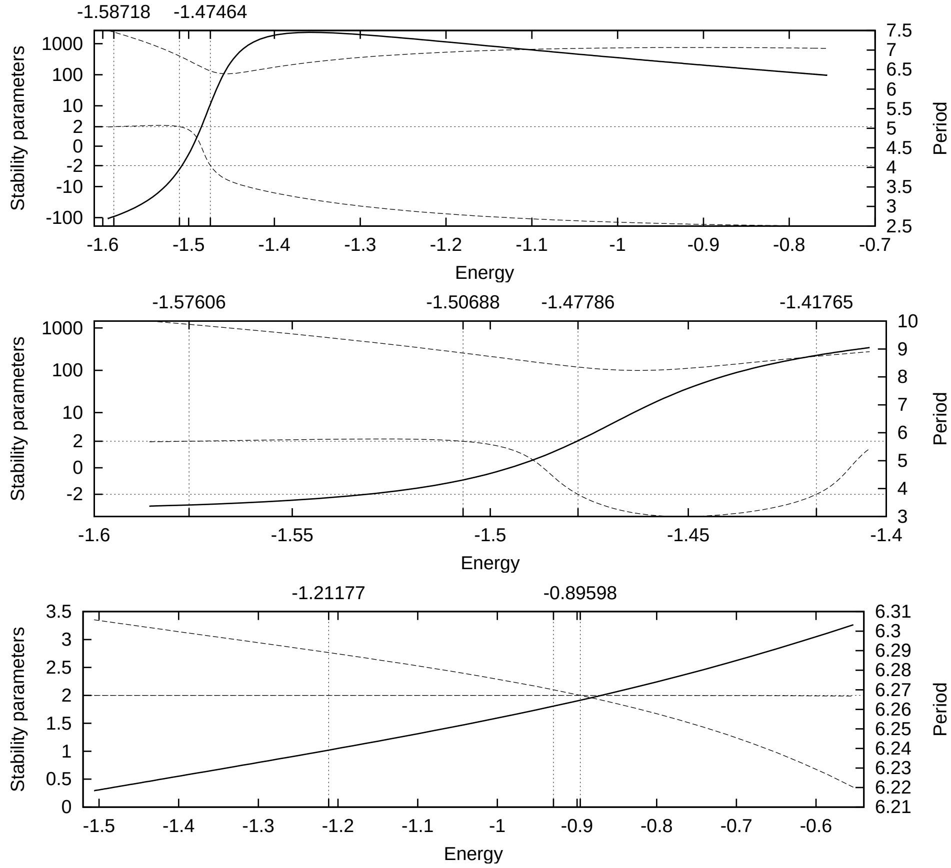

Figure 7.3: Characteristic curves (solid line) and stability parameters (dashed lines) of the planar Lyapunov families of periodic orbits for L_1, L_2 and L_3 (from top to bottom). The vertical lines correspond to the energy levels of the bifurcation orbits (see table 7.3).

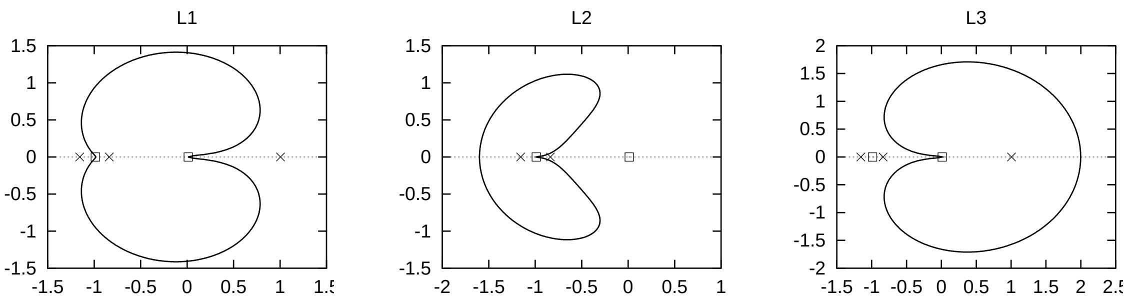

Figure 7.4: First collision orbits of the Lyapunov families of periodic planar orbits around L_1, L_2 and L_3. On the x axis we have displayed the position of both primaries ($\square$) and the equilibrium points ($\times$). The three orbits are traveled clockwise.

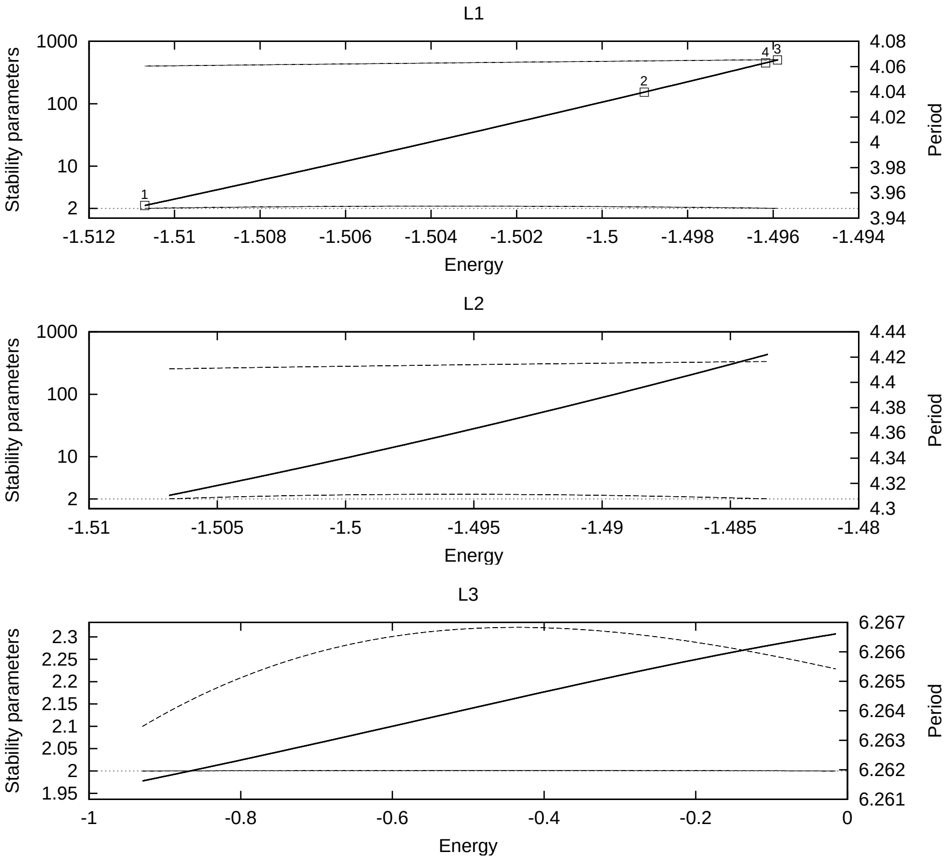

Figure 7.5: Characteristic curves (solid line) and stability parameters (dashed lines) of the bridges between the planar Lyapunov families and the vertical ones for L_1, L_2 and L_3.

	L_1		L_2		L_3	
#	Energy	Type	Energy	Type	Energy	Type
1	-1.58718	A	-1.57606	A	-1.21177	A
2	-1.51070	B	-1.50688	B	-0.92954	B
3	-1.47464	C	-1.47786	C	-0.89598	B
4			-1.41765	C		

Table 7.3: Energy levels and type of the vertical critical orbits of the Lyapunov planar families of periodic orbits.

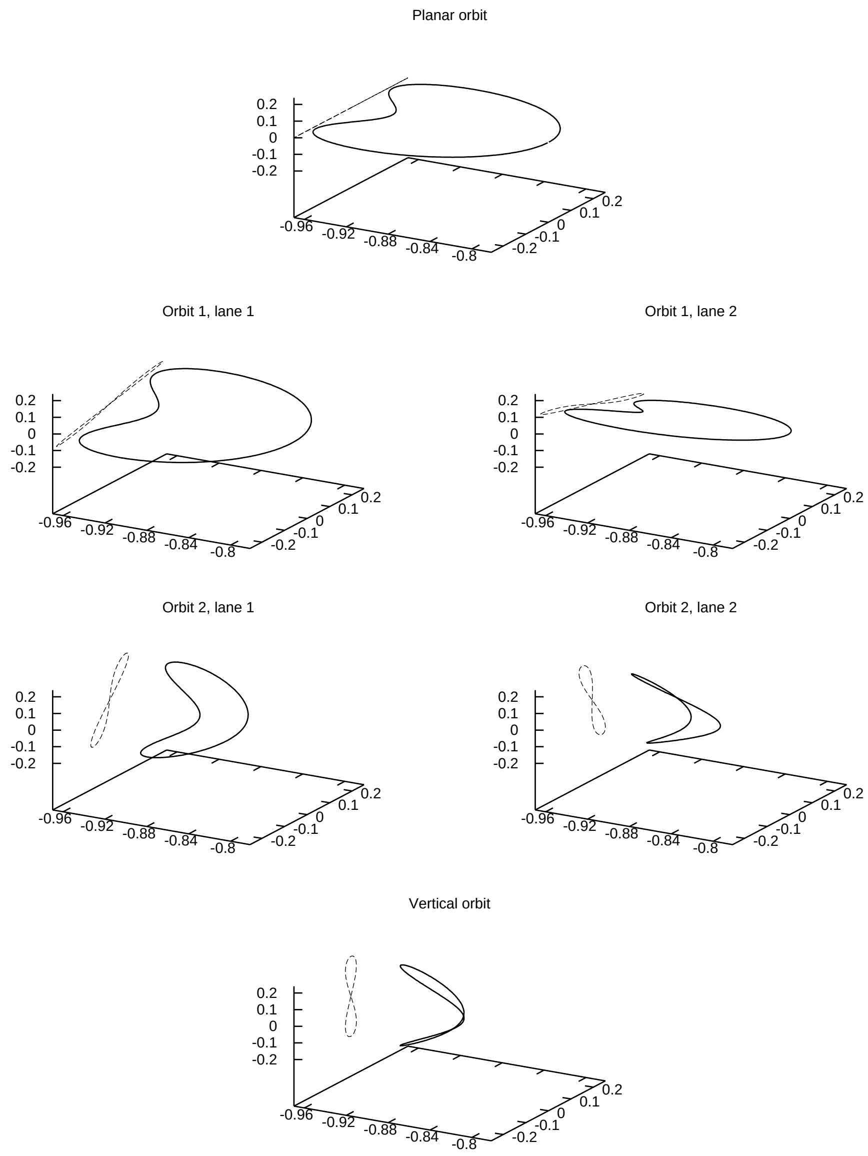

Figure 7.6: 3D projections (solid lines) and yz projections (dashed lines) of some periodic orbits of the bridge connecting the two Lyapunov families in the L_1 case. The orbit in the top is the planar bifurcation orbit, and the one in the bottom is the vertical bifurcation one. The orbits at both sides are on the two lanes of the bridge connecting the two previous orbits.

bifurcation orbit #2 (B type) of the planar one. Each orbit in one lane has a symmetrical orbit, with respect to the $\{z = 0\}$ plane, in the other lane. In Fig. 7.5 the characteristic and stability curves for these families are displayed. Just for illustrating purposes, we show some orbits of the bridge in the L_1 case in Fig. 7.6.

7.2 Halo–type orbits

As it has already been said, from the three planar Lyapunov families bifurcate families of 3D periodic orbits which are symmetrical with respect to the $\{y = 0\}$ plane. These orbits are known as halo orbits. There are other orbits with the same symmetry (and a similar shape) which bifurcate from the families of halo orbits by duplication, triplication, etc., of the period. This section is devoted to these kind of families.

At each planar bifurcation orbit number 1 (table 7.3) start two symmetrical families of periodic orbits with respect to the $\{z = 0\}$ plane. They are known as north and south class halo families, according to the maximum value of $|z|$ along the orbit. The bifurcation orbits at which they are born correspond to a 1:1 resonance between the (planar) proper and one of the (vertical) normal frequencies. These orbits are well-known in the literature ([32]).

Their characteristic and stability curves are displayed in Fig. 7.7. The north and south class families around L_1 end simultaneously at a plane orbit around both primaries and L_1, L_2, which is of family (l) in Stromgren's classification. For the other two equilibrium points, we have not followed the families up to their natural termination and the computations have been stopped when a collision orbit has been detected.

A comment is necessary about the representation of the stability parameters. In the L_1 case there appears a bifurcation to complex instability. This means that two pairs of elliptic eigenvalues moving in the unit circle "collide", and after the collision leave the unit circle. In this way, the stability parameters become complex conjugate (they are real in both the hyperbolic and the elliptic case). This happens at energies -1.47034 and 0.47747. In this situation we have represented the real and imaginary parts of one of the stability parameters, as can be better appreciated in Fig. 7.8, which is a magnification of the L_1 case in Fig. 7.7.

As in the Lyapunov families, we have computed some bifurcation orbits, whose energy values are displayed in table 7.4. The first two bifurcations are period doubling, since they correspond to a value of the small stability parameter equal to $2\cos(2\pi/2) = -2$. At the first bifurcation the bifurcated family has one elliptic stability parameter, while the second bifurcation has both stability parameters hyperbolic. These two bifurcations are represented qualitatively in figure 7.9. As for the third bifurcation orbit, the small stability parameter equals to $2\cos(2\pi/3)$, so it gives rise to two period triplicated families. One of the bifurcated families has an elliptic stability parameter, whereas the other has both stability parameters hyperbolic. We must remark that, for the range of the halo family around L_3 explored, there are no bifurcations due to low-order resonances. In a next section we will show the role played by these bifurcations in the geometry of the phase space.

The characteristic curves for these families are given in figures 7.10 and 7.11. A

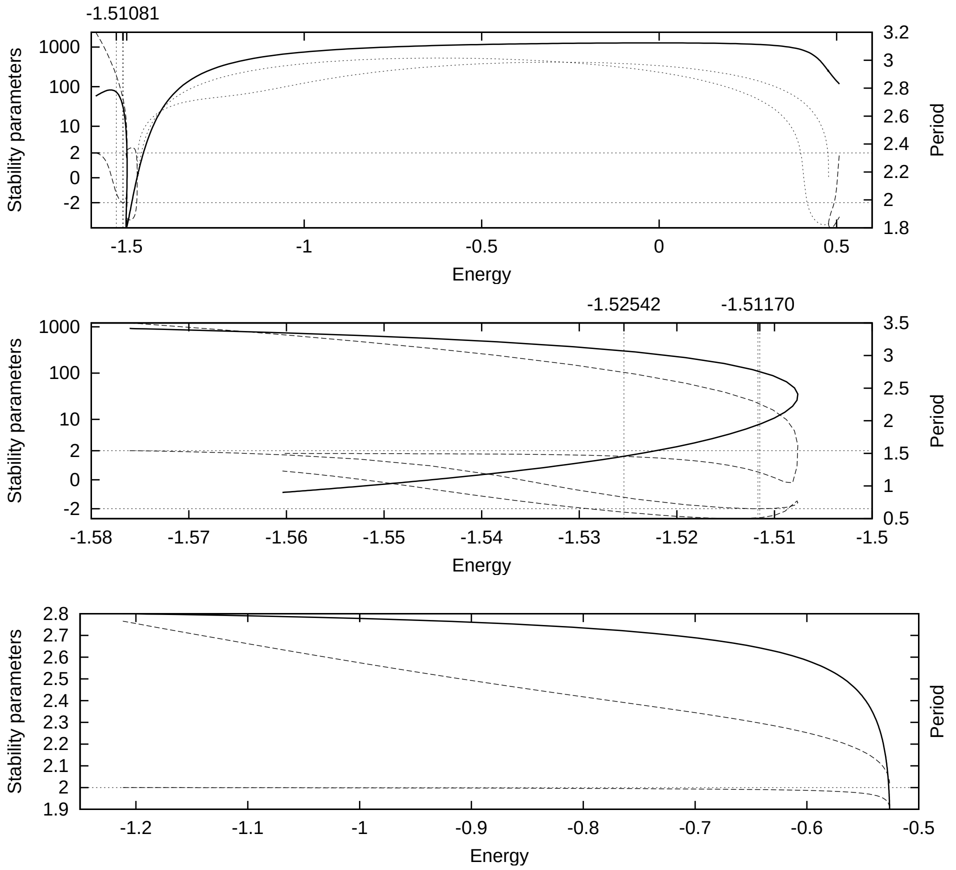

Figure 7.7: Characteristic curves (solid line) and stability parameters (non-solid lines) of the halo families around L_1, L_2 and L_3 (from top to bottom). For the L_1 case, we have represented with dashed lines the stability parameters when they are real, and with dotted lines the real and imaginary parts of one of them in the complex case. The vertical lines correspond to the energy levels of the bifurcation orbits (see table 7.2).

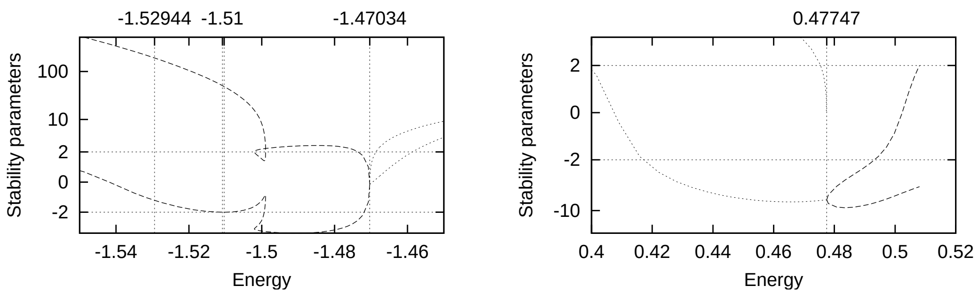

Figure 7.8: Magnification of the L_1 stability curves near the bifurcations to complex instability. The vertical lines correspond to the energy levels of the bifurcation orbits of table 7.2 and the complex instability bifurcations (see explanations in the text).

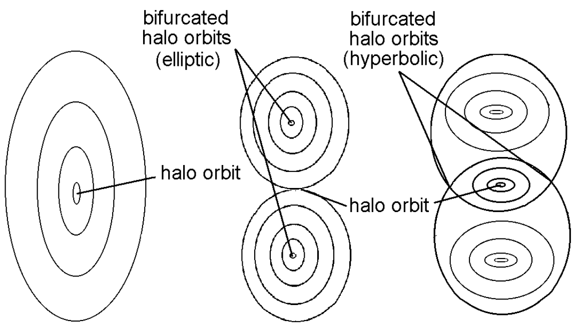

Figure 7.9: Qualitative representation of the two period–doubling bifurcations of the L_1 halo family.

#	L_1	L_2
1	–1.51081	–1.51170
2	–1.51033	–1.51150
3	–1.52944	–1.52542

Table 7.4: Energy values at the period doubling and triplication bifurcation orbits of the halo families (see the details in the text).

comment must be made on the criteria used to stop the continuation of these families. In some cases we have reached a natural termination at a bifurcation orbit. When this has not been possible, we have used as stopping criteria either

- the detection of a collision orbit inside the family, or
- reaching high periods (over 40 RTBP time units).

Table 7.5 gives the contingency that produced the stopping of each continuation.

	L_1		L_2	
	hyperbolic	elliptic	hyperbolic	elliptic
period duplication	natural term.	m_1 collision	m_2 collision	high period
period triplication	high period	m_1 collision	m_2 collision	high period

Table 7.5: Ending conditions of the continuations of the families bifurcated by period duplication and triplication from the halo families of L_1 and L_2.

In order to illustrate how orbits in these families "unfold" from a halo orbit, we give in figures 7.12 and 7.13 some orbits of the elliptic bifurcation by period duplication and of the hyperbolic bifurcation by period triplication, respectively. Both families correspond to the L_1 point.

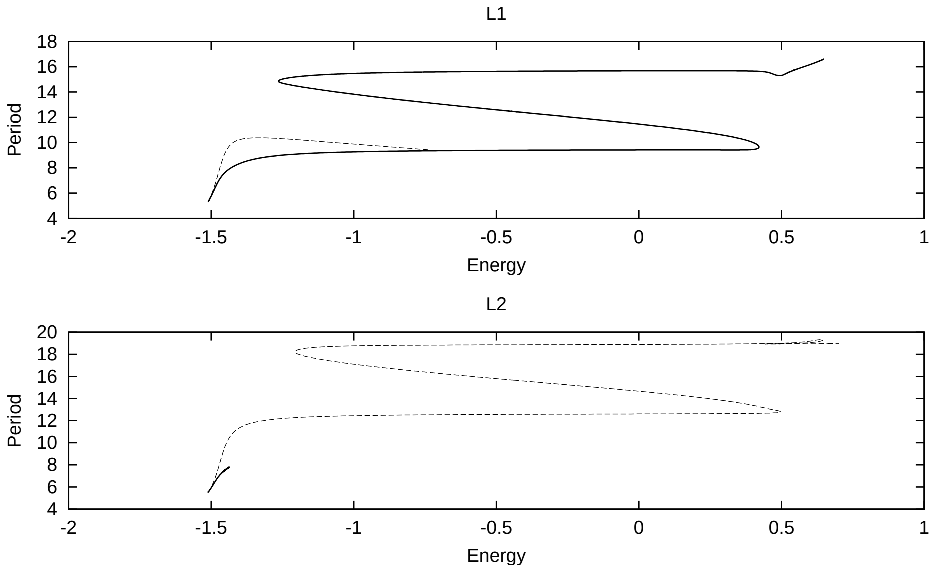

Figure 7.10: Characteristic curves of the families that bifurcate by period duplication from the halo families of L_1 and L_2. The solid lines represent the hyperbolic families, and the dashed ones the elliptic.

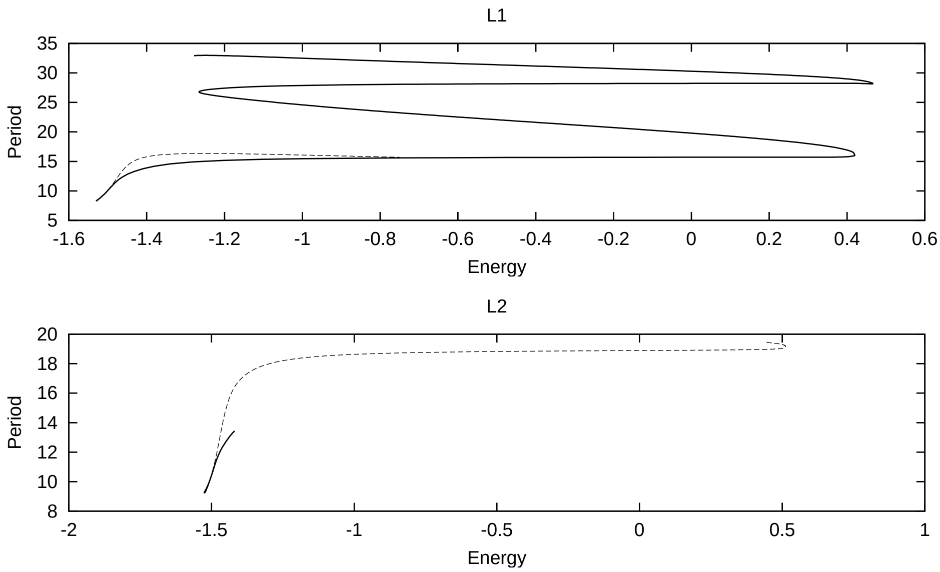

Figure 7.11: Characteristic curves of the families that bifurcate by period triplication from the halo families of L_1 and L_2. The solid lines represent the hyperbolic families, and the dashed ones the elliptic.

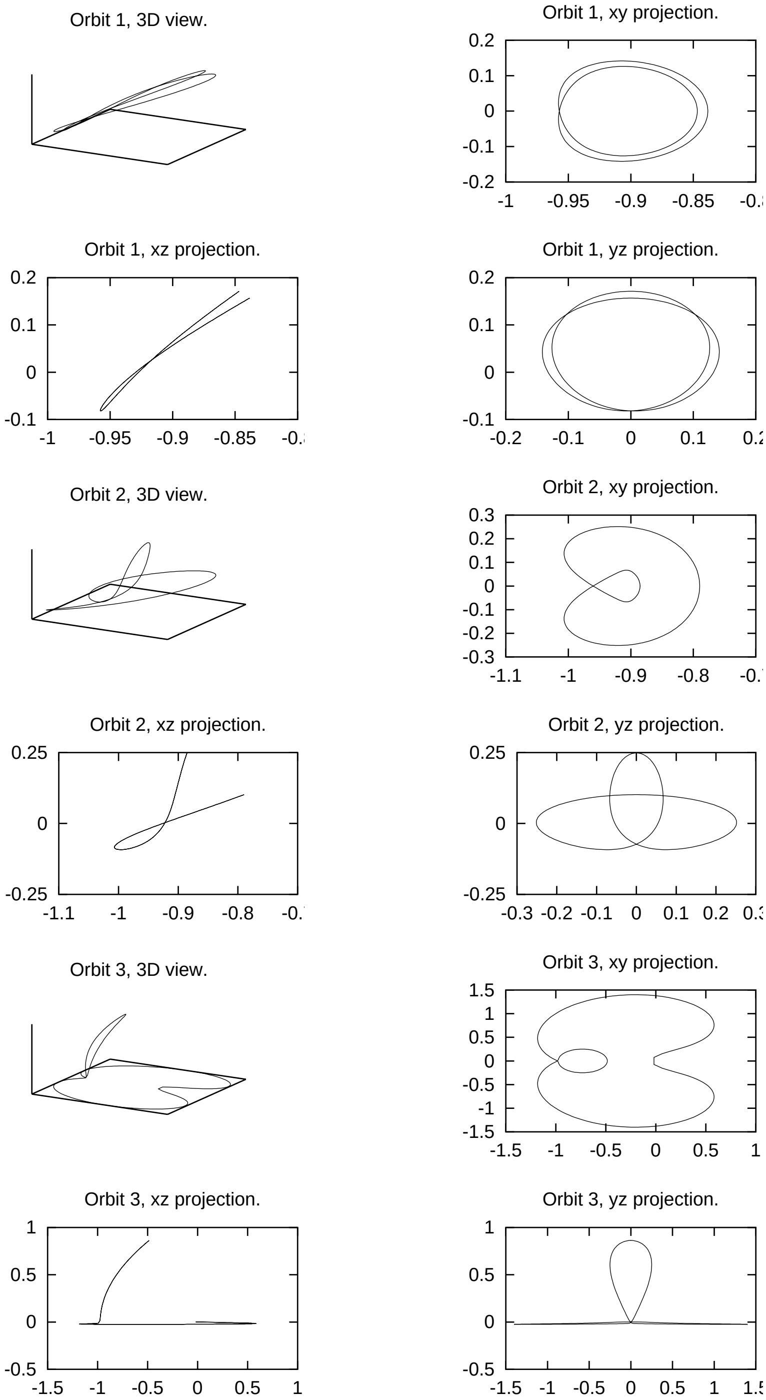

Figure 7.12: Some orbits of the elliptic bifurcation by period duplication of the L_1 halo family. Orbit 1: energy=–1.51061, period=5.34666. Orbit 2: energy=–1.49158, period=6.35119. Orbit 3: energy=–0.99683, period=9.87531.

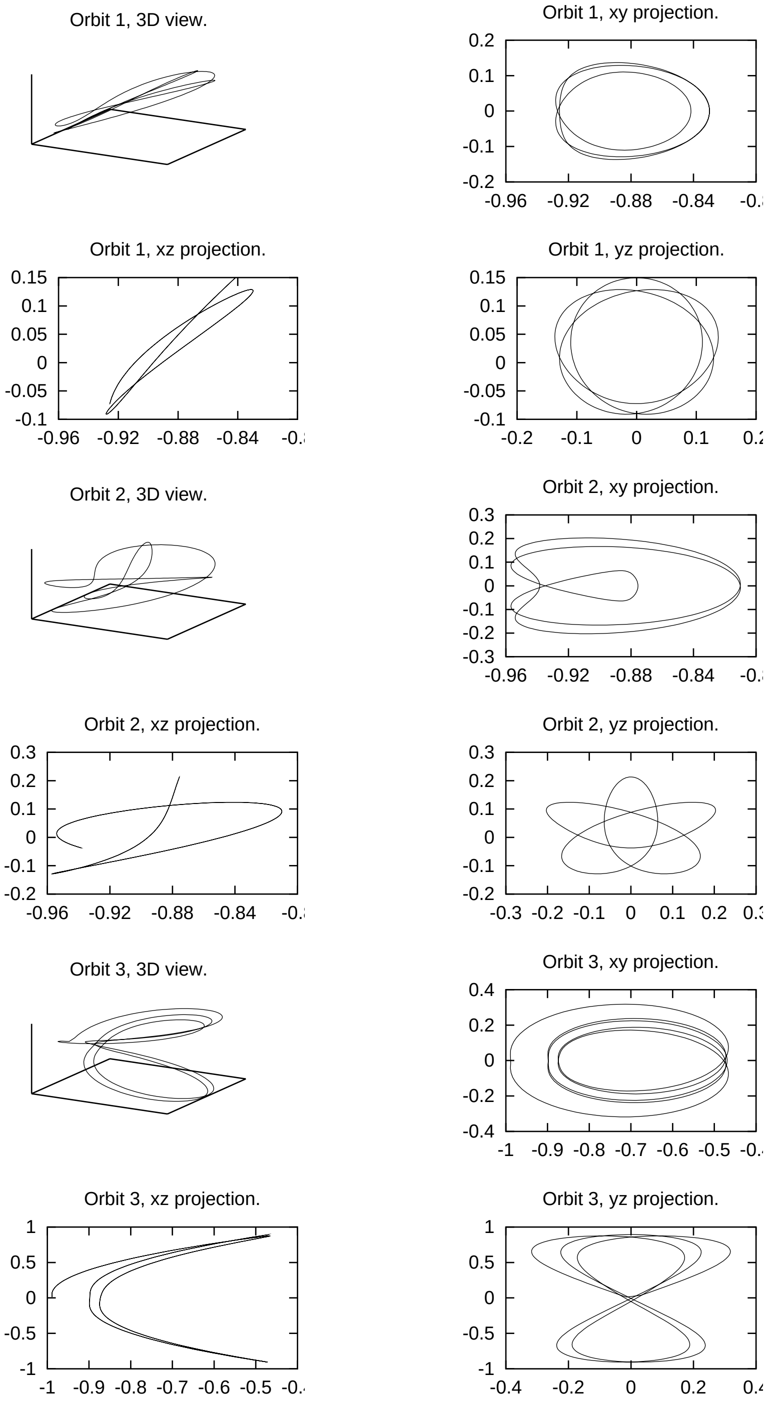

Figure 7.13: Some orbits of the hyperbolic bifurcation by period triplication of the L_1 halo family. Orbit 1: energy=–1.52853, period=8.36012. Orbit 2: energy=–1.51026, period=9.36247. Orbit 3: energy=–0.99208, period=15.46609.

7.3 Families of invariant tori

As a first example of the methodology described for the computation of families of tori, we will show the results related to the computation of a family of tori that starts at a vertical Lyapunov orbit around L_1 at the energy level -1.59. We will follow this family keeping fixed the value of the energy. For this value of the energy, the family ends at a planar Lyapunov orbit.

To start the computation of the family, an initial torus was estimated starting longitudinally to the vertical orbit. In a first step, this torus was refined keeping constant h, A_0^z (to fix the first invariant curve on the torus), A_1^x (to avoid falling back to the p.o.) and A_1^y (to avoid coefficient modulation). In the next steps of the predictor–corrector scheme, we have keep fixed h and A_0^z for the predictor (in order to have a 2D kernel to choose a direction orthogonal to coefficient modulation, as has been already described), and for the corrector we have added a new coordinate chosen according to the procedure described in section 6.2.1. We have used a multiple shooting strategy with two invariant curves ($m = 2$). All the Fourier coefficients just mentioned correspond to the first one.

At the beginning, δ is taken as the period of the vertical orbit and the rotation number ρ is related to a normal frequency of the starting vertical orbit. More concretely, $2\cos\rho$ is the smallest stability parameter of the vertical orbit. At the end of the continuation, we get two new values of the parameters ρ and δ. Now ρ is related to the frequency of the ending planar orbit through

$$\rho = \delta\frac{2\pi}{T} - 2\pi,$$

where T is the period of the ending planar orbit. The final value of the parameter δ is checked to be

$$\delta = \frac{2\pi}{2\pi - \nu}T,$$

where $2\cos\nu$ is the smallest stability parameter of the planar orbit. This determines the sign of ν and the value of j in equations (6.23) and (6.24). These values will be used in the next section when performing the constant rotation number continuations starting from the planar orbits.

Some tori of this continuation are shown in Fig. 7.14.

The next step is to extend the above computations to energy values covering the full range of vertical Lyapunov periodic orbits with central part.

7.3.1 Invariant tori starting around vertical orbits

In Fig. 7.15 we have displayed, for the three equilibrium points, the regions, in the energy–rotation number plane, covered by the 2–parametric family of tori computed starting from the vertical Lyapunov families of periodic orbits. Each region is surrounded by a curve formed by several pieces:

- The lower left piece α (from vertex 1 to 2) is related to the the planar Lyapunov family. The orbits of this family represented in the curve are just the first piece of the family with central part. The horizontal coordinate is the energy level h of the

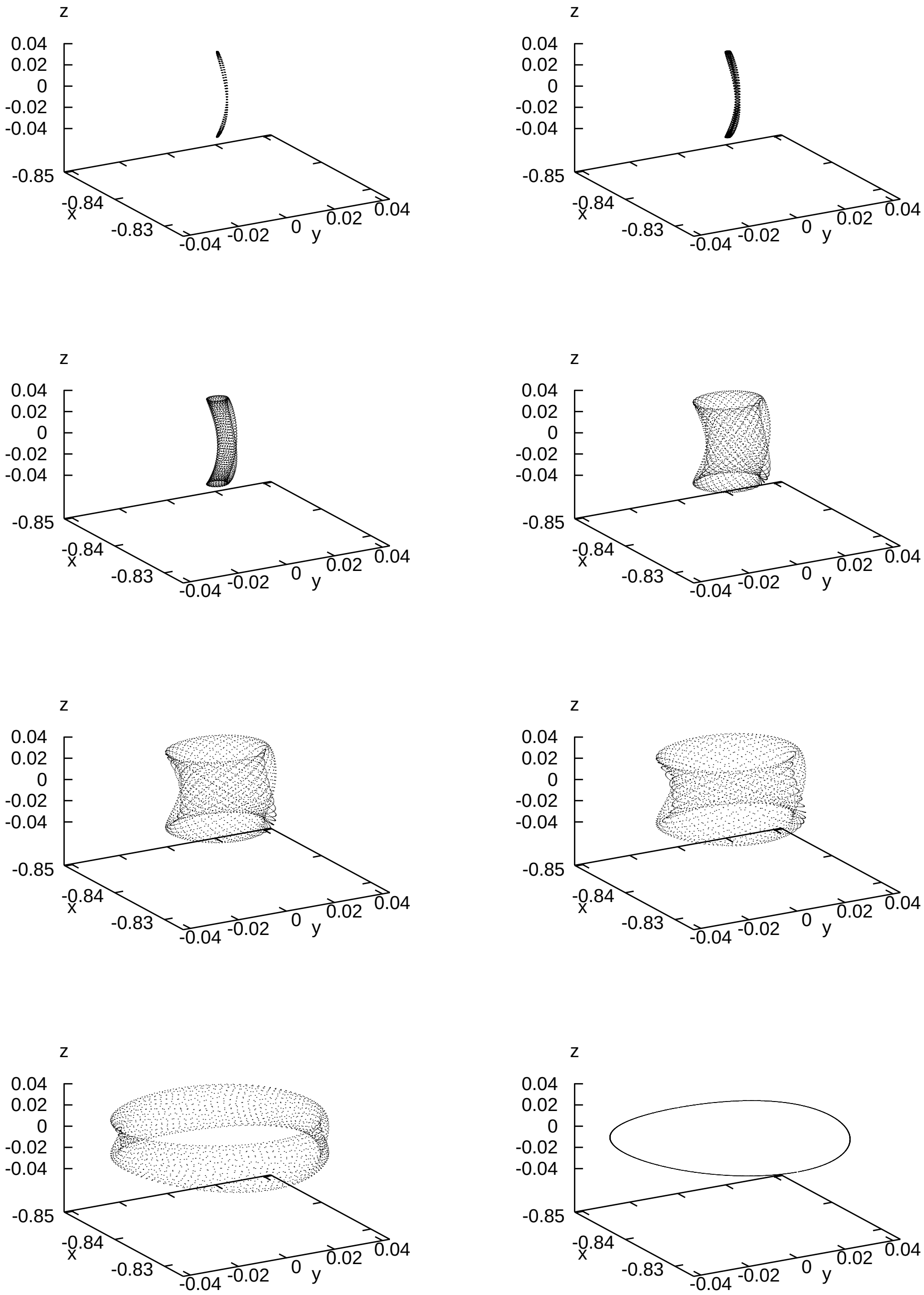

Figure 7.14: Isoenergetic family of 2D tori starting at a vertical Lyapunov orbit and ending at a planar one. Energy level: -1.59, equilibrium point: L_1.

curve and the vertical coordinate is $\rho = \frac{(2\pi)^2}{2\pi-\nu} - 2\pi$, where $2\cos\nu$ is the stability parameter of the orbit.

- The upper piece β (from vertex 2 to 3) is strictly related to the vertical Lyapunov family. The points on this curve are (h, ρ) where h is the energy of the orbit and the rotation number ρ is such that the elliptic stability parameter of this orbit is $2\cos\rho$. Note that this relation between ρ and ν is different from the previous item. This is because, in order to have continuity of ρ along an isoenergetic family of tori, we are forced to begin/end transversally at one family (the planar one, in our case) and end/begin longitudinally at the other (vertical), or vice-versa.

- The bottom boundary γ (from vertex 3 to 1), that corresponds to $\rho = 0$, begins at the value of the energy where the halo families are born. It is related to a separatrix between the tori around the vertical Lyapunov families and the halo ones.

In the three diagrams, there is a narrow range of energies (in the left–hand side of the plots) for which the isoenergetic families of tori start at a vertical p.o. and end at a planar orbit, as was the case in the example of the beginning of this section.

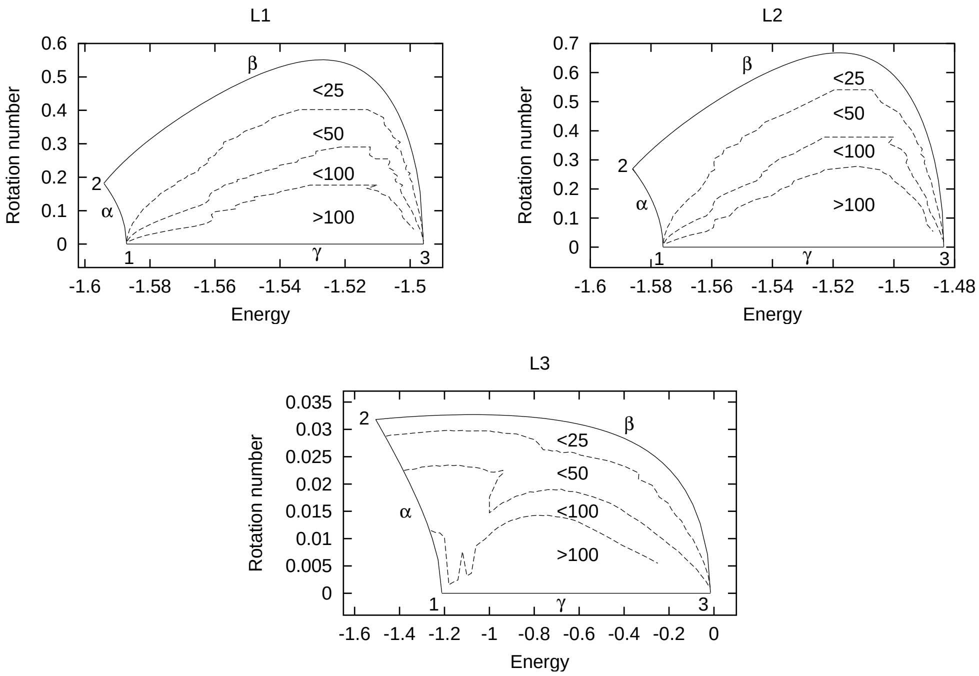

Figure 7.15: Regions in the energy–rotation number plane covered by the two-parametric family of tori computed starting at the vertical Lyapunov families of p.o. for L_1, L_2 and L_3. The number of harmonics used for the computation of the tori (< 25, < 50, < 100 and > 100) is shown in the figures. Vertex 1 is at the value of the energy at which the halo families is born. Vertex 2 is at the value of the energy of the equilibrium point. Vertex 3 is at the value of the energy of the first bifurcation of the vertical Lyapunov family (see tables 7.3, 7.1 and 7.2, respectively).

There are different ways for computing the tori within the region surrounded by the curves mentioned above. We always start from the pieces of boundary formed by periodic orbits. One possibility is then to perform the continuation procedure keeping fixed the value of the energy h. Another one is to allow variation of the energy but keeping fixed the rotation number ρ. In this last case, and in order to be as close as possible of conditions that guarantee the existence of tori for the nonlinear system, it is convenient to set the rotation number "as irrational as possible". To this end, when we have used this second strategy, we have set the values of ρ such that $\frac{2\pi}{\rho}$ is an integer plus the golden number $(\frac{1+\sqrt{5}}{2})$. In both cases, and for all L_1, L_2 and L_3 cases, we have always reached a region where the number of harmonics N_f is larger than the maximum value allowed, which at most has been set equal to 100. Larger values of this parameter make computing time prohibitive. Just to have an idea of the computing effort, the constant rotation number family with $\rho = 0.176$ requires about 3 days of CPU time of an Intel Pentium III at 500MHz, and the complete picture around 100 days (this means around 1.5 days in our Beowulf cluster).

For L_1 and L_2, the continuations have been done keeping constant the rotation number, starting longitudinally from the vertical p.o. (β curve) and transversally from the planar p.o. (α curve). When starting transversally, the sign of ν and the value of j of equations (6.23) and (6.24) have been adjusted as it has been explained at the beginning of this section. The computations for L_3 have been done starting (longitudinally) from vertical orbits only, but keeping constant the value of the energy.

7.3.2 Invariant tori starting around halo and halo–type orbits

In this section we will give a brief summary about the results obtained relative to tori around halo orbits, as well as the bifurcated families obtained by duplication and triplication of the period.

For the exploration corresponding to the L_1 case, we have used the piece of the halo family that starts at the bifurcation from the planar family, at energy -1.58718, and ends at the local maximum of the small stability parameter at energy -1.49899. This is the maximum energy value for which the halo family of p.o. has central part (see Fig. 7.8). For L_2, the initial value of the energy is -1.57606 and the value of the energy at the local maximum is -1.50769 (see Fig. 7.7). The range of energy values explored for L_3 begins at -1.21177 and ends when a close approach to the larger primary appears.

As in the computations in the previous section, we have used both kinds of continuations (keeping fixed either h or ρ) for these explorations. Also as before, all the computations have been stopped when the maximum number of harmonics allowed (100) is reached. In Fig. 7.16 we display the regions in the h, ρ plane where these tori do exist. In the same figures, the number of harmonics needed in order to have a tolerance less than 10^{-10} in (6.16) is given. All the computations have been done using at most $m = 4$ for the multiple shooting procedure.

The bottom border of these regions is shared with the ones displayed in Fig. 7.15. The lower–left vertex of the three plots correspond to vertex number 1 of the plots in Fig. 7.15. This vertex corresponds to the bifurcating planar orbit that gives rise to the two halo families. In all the cases, as $\rho \to 0$, we are approaching to a (transversal)

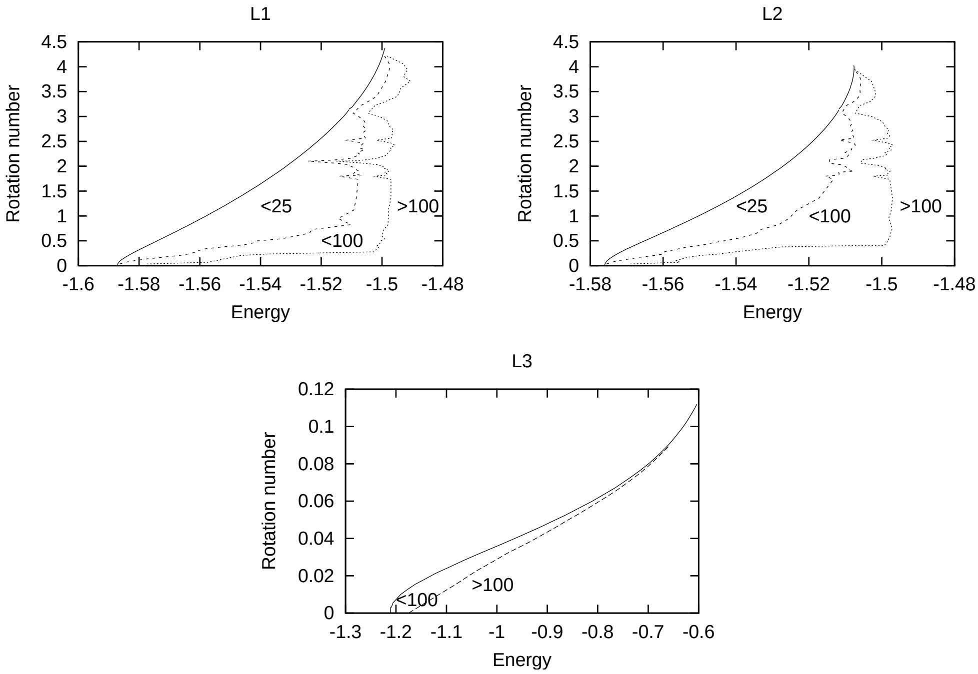

Figure 7.16: Regions in the energy–rotation number plane covered by the two-parametric family of invariant tori around the halo families around L_1, L_2 and L_3. As in the previous figure, we show the number of harmonics used for the computation of the tori.

homoclinic connection [14].

The right–hand side border is in some sense fictitious since it corresponds to reaching the maximum number of harmonics allowed. Anyway, it reflects in a clear way the crossings of the rotation number ρ through low–order resonances, at which the tori collapse to periodic orbits. The four main peaks detected correspond to values of the rotation number equal to $2\pi/2$, $4\pi/5$, $2\pi/3$, $2\pi/4$ (from top to bottom). The first and third peaks correspond to the 1:3 and 1:2 resonances (the 1:1 resonance, $\rho = 0$, is related to the origin of the halo family) related to the bifurcating families of halo–type orbits already mentioned. As it was discussed, some of these families have central part, so we can expect to find invariant tori around them. They have been also computed, and the h–ρ diagrams are given in figures 7.17 and 7.18.

Just for illustrating purposes, in Fig. 7.19 we have displayed some of the tori that appear around the families bifurcated from halo orbits.

7.4 Summary of results

In order to compare the obtained results with the ones computed in previous works using the reduction to the central manifold ([10],[16]), in this section we will show the evolution (with respect to the energy) of the behavior of the Poincaré sections through $z = 0$, $p_z > 0$, of all the different sorts of orbits computed.

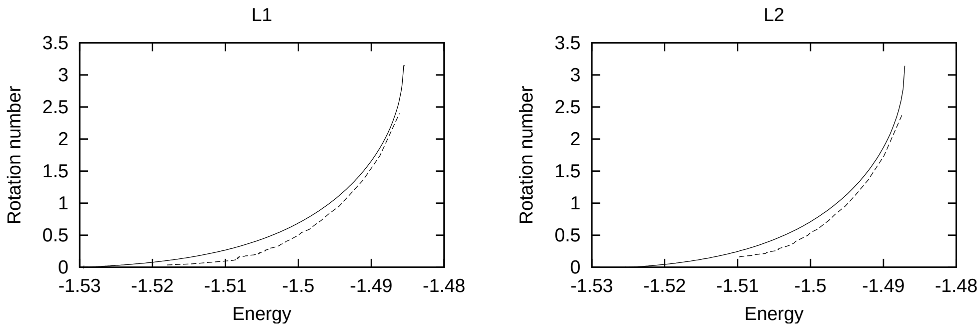

Figure 7.17: Regions in the energy–rotation number plane covered by the two-parametric families of invariant tori around the elliptic families bifurcated from halo orbits by period triplication. Between the solid curve and the dotted one, the number of harmonics required for the computation of tori is less than 100. To the right of the dotted curve more than 100 harmonics are required.

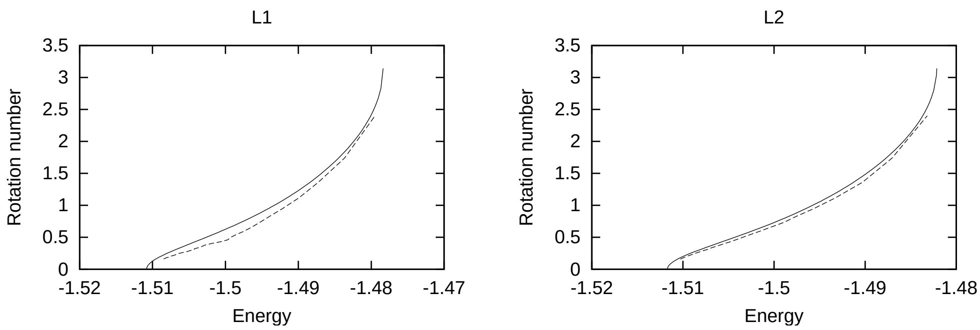

Figure 7.18: Regions in the energy–rotation number plane covered by the two-parametric families of invariant tori around the elliptic families bifurcated from halo orbits by period duplication. The meaning of the dotted line is the same as in figure 7.17.

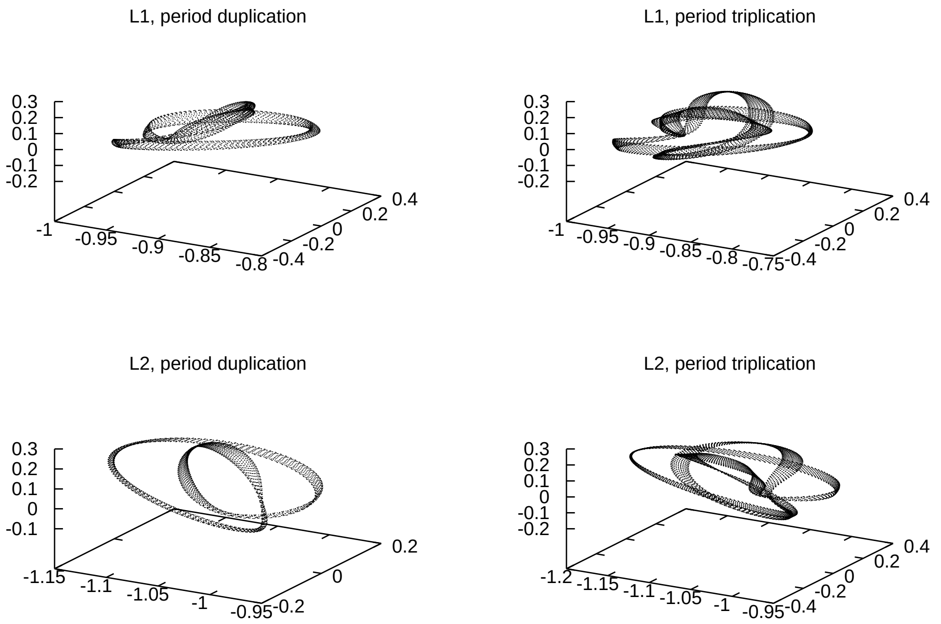

Figure 7.19: Tori around the bifurcated halo-type orbits. The two on the top are in the families around L_1 and have energy $h = -1.501$ and rotation numbers $\rho = 0.54081$ (left) and $\rho = 0.59175$. The two on the bottom are in the families around L_2 and have energy $h = -1.507$ and rotation numbers $\rho = 0.35663$ and $\rho = 0.33748$.

Figures 7.20, 7.21 and 7.22 show the results for L_1, L_2 and L_3, respectively. In all these figures we have represented the x–y coordinates at the intersections with $z = 0$, $p_z > 0$. All the plots have a similar structure. The exterior curve in each plot is the Lyapunov planar orbit of the energy level corresponding to the plot. As this orbit is planar, it is completely included in the surface of section, and is the only orbit for which this happens. The motion inside the region bounded by the Lyapunov planar orbit is quasi-periodic, except at some gaps which cannot be distinguished from the pictures. In all the plots there is a fixed point on the x axis associated to the vertical Lyapunov orbit.

For the three equilibrium points, and for small energy values, the whole picture is formed by invariant curves surrounding the fixed point associated to the vertical orbit. They are associated to the intersections of the Lissajous type trajectories around the vertical periodic orbit, whose evolution from the planar Lyapunov periodic orbits to the vertical one was displayed in figure 7.14. At the energy levels associated to the first bifurcation of the Lyapunov planar family (first bifurcation of table 7.3) there appear the halo orbits. This can be seen clearly in the Poincaré map representations, since there appear two additional fixed points surrounded by invariant curves. Increasing the values of the energy, as it was discussed in previous sections, the L_1 and L_2 families of halo orbits have two relevant bifurcations, by period triplication and duplication. Both bifurcations can be also detected on the Poincaré representations. This additional structure has not been detected for the L_3 case. As it was already said, within the bifurcated families

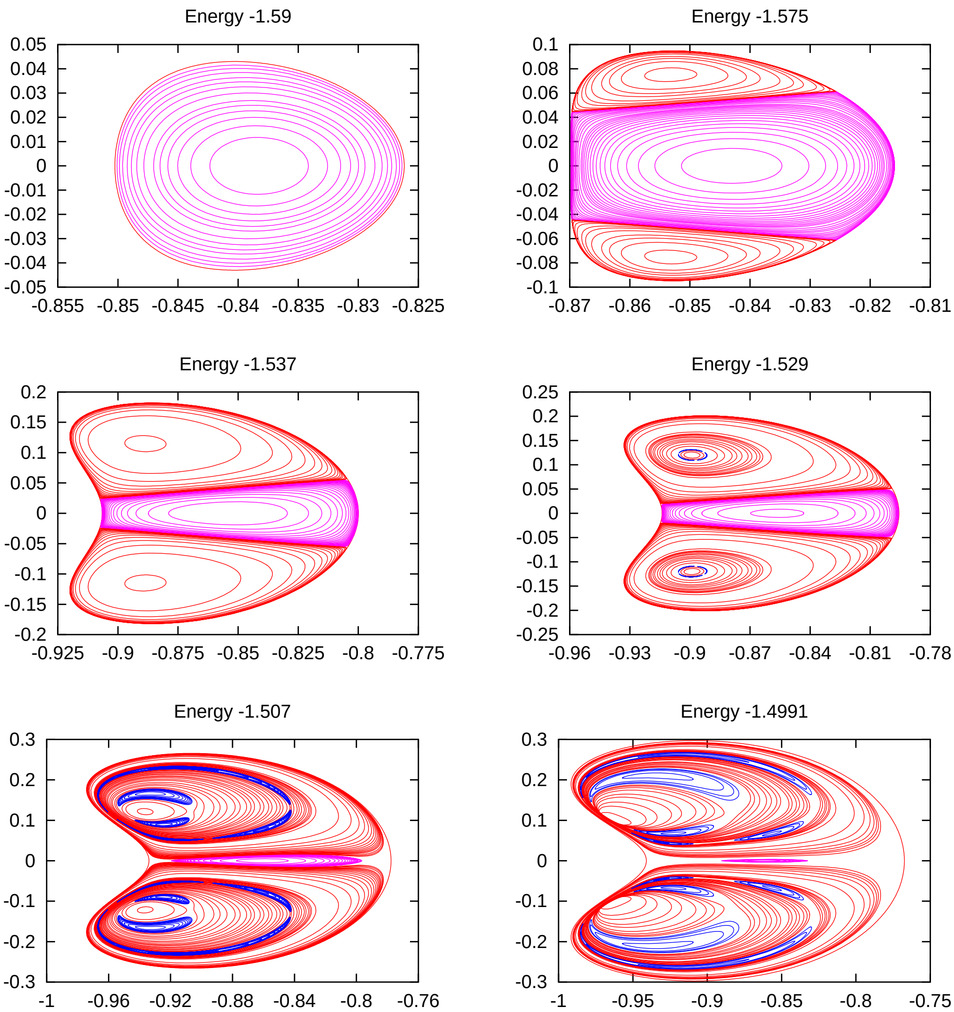

Figure 7.20: Energy slices of the section $z = 0$, $p_z > 0$ of the invariant tori around L_1 computed in the previous section.

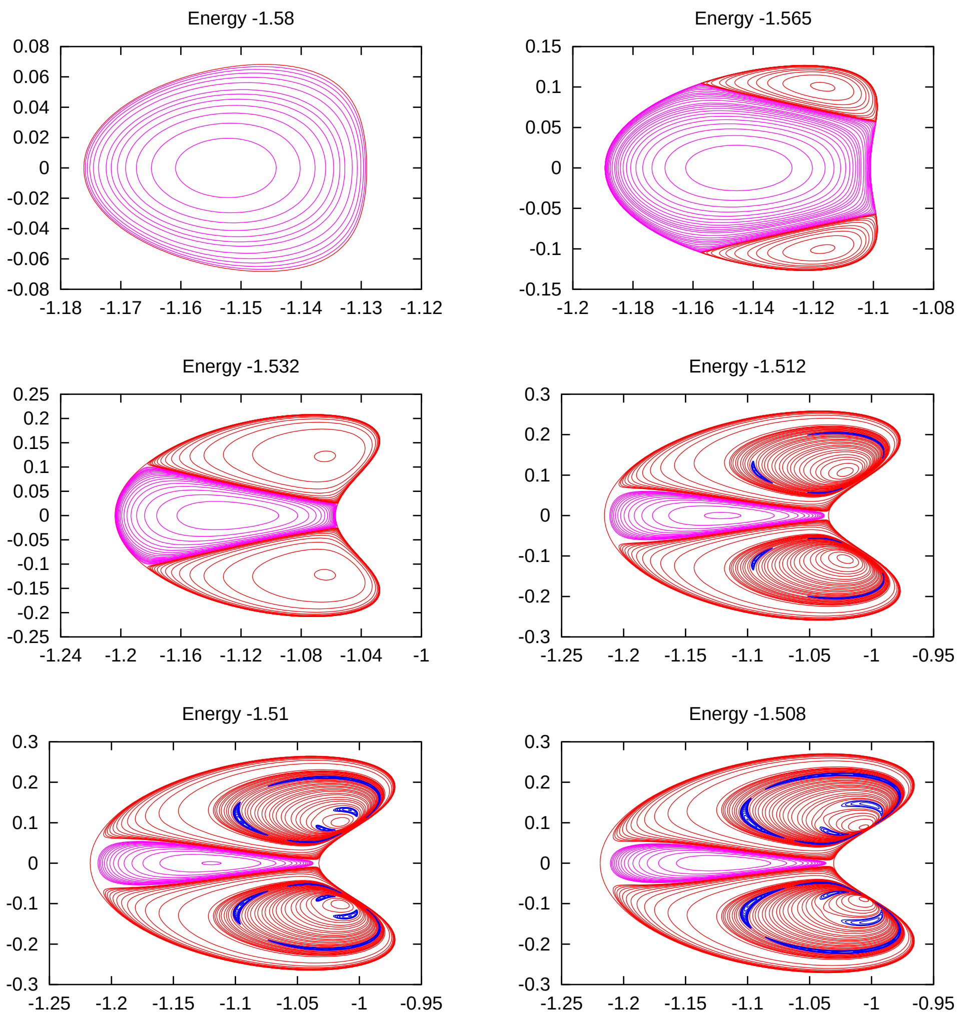

Figure 7.21: Energy slices of the section $z = 0$, $p_z > 0$ of the invariant tori around L_2 computed in the previous section.

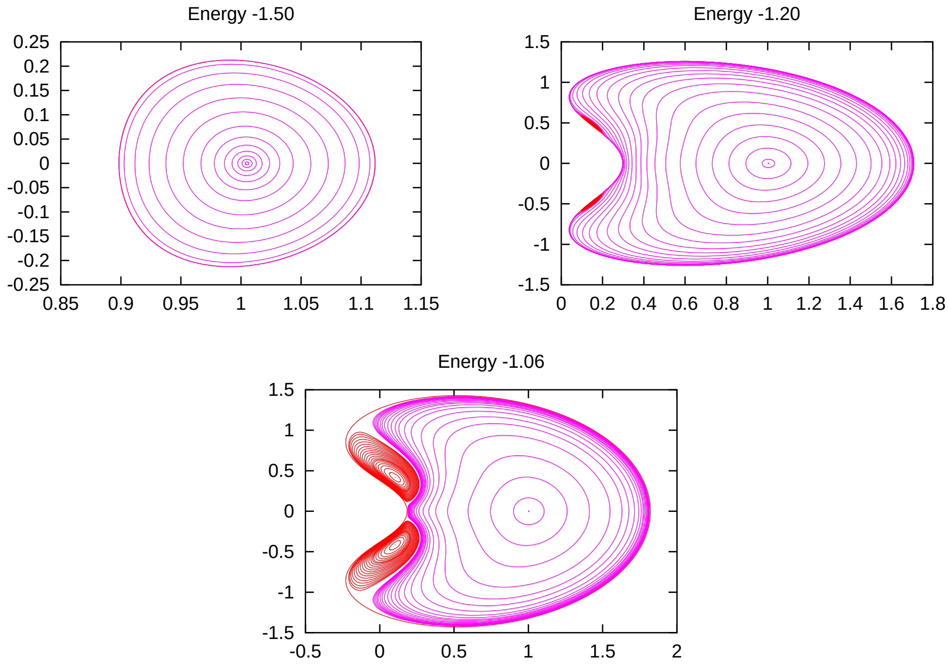

Figure 7.22: Energy slices of the section $z = 0$, $p_z > 0$ of the invariant tori around L_3 computed in the previous section.

there are some with central part, which are surrounded by invariant tori. These tori give rise to the "island chain" structure typical of two–dimensional area–preserving maps. To display more clearly this behavior, in figures 7.23 and 7.24 we display a magnification of the bifurcated periodic orbits and its surrounding invariant tori.

The region between the tori around the vertical Lyapunov orbit and the tori around the halo orbits should be filled with the traces, on the surface of section, of the invariant manifolds of the Lyapunov planar orbit. These manifolds act as separatrices between both kinds of motion. The same thing happens between the islands of the bifurcated halo–type orbits and the tori around the halo orbits. In this case, the region between both kinds of tori is filled with the traces of the invariant manifolds of the bifurcated hyperbolic halo–type orbits. In all these boundary regions, the motion should have a chaotic behavior. With our tools we have not been able to compute these separatrices, which can be found in [14] for values of the energy not too far from the ones of the equilibrium.

The "empty region" inside the planar Lyapunov orbit of the bottom plots of Fig. 7.20 has additional structure. In Fig. 7.25 we display a magnification of the plot of Fig. 7.20 corresponding to energy -1.507. For this level of energy the two–lane bridge between the planar and vertical Lyapunov families of p.o. have already bifurcated, so the planar family has gained central part and therefore has invariant tori around them. The $z = 0$ sections of these tori have been represented, for energy -1.507, in Fig. 7.20, together with the $\{z = 0, p_z > 0\}$ sections of the orbits of the two–lane bridge of energy -1.507, one of each lane. It seems that the invariant manifolds of these p.o. separate the family of invariant tori around the Lyapunov planar orbits from the families of invariant tori

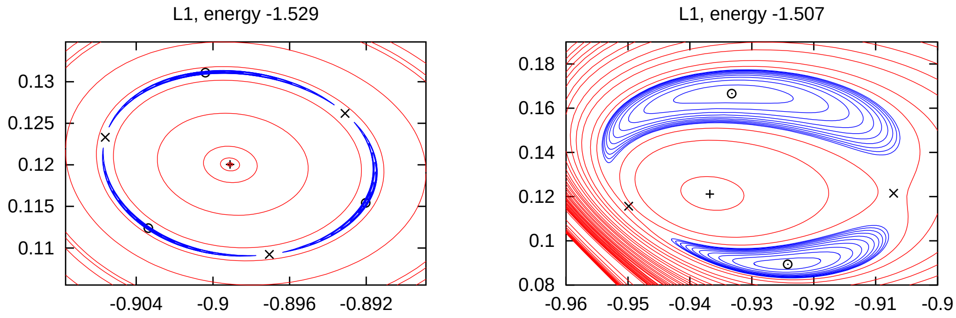

Figure 7.23: Magnification of two intermediate slices of figure 7.20 displaying the bifurcated halo-type orbits and the tori surrounding them in the L_1 case. The points marked with a $+$ represent the $z = 0$, $p_z > 0$ sections of halo orbits, those with $\times$ represent the sections of hyperbolic bifurcations of halo orbits by period duplication or triplication, and the $\odot$ points represent the elliptic ones.

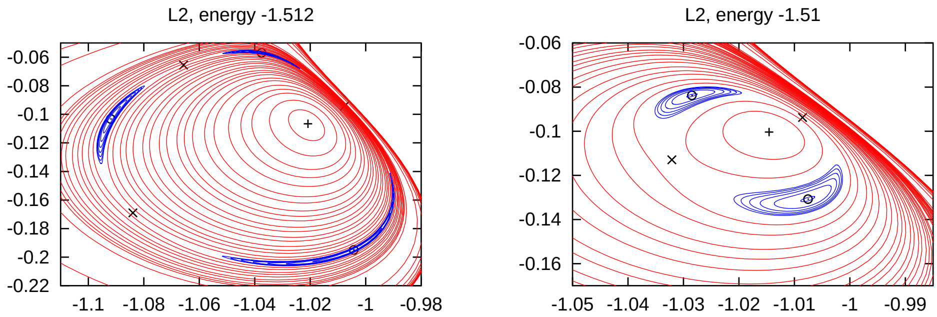

Figure 7.24: Magnification of two intermediate slices of figure 7.21 displaying the bifurcated halo-type orbits and the tori surrounding them in the L_2 case.

around Lyapunov vertical and halo orbits.

7.5 Additional families of invariant tori

Following the evolution of the halo family in Fig. 7.8, at the local maximum of the small stability parameter the halo family has a turning point in the energy, this is for $h = -1.49892$. After that, energy goes backwards up to a second turning point, which occurs at $h = -1.50201$. At any value of the energy between -1.50201 and -1.49892 we have three halo orbits, one corresponding to the branch before the first turning point, another one corresponding to the branch before the second turning point, and a third one on the branch after the second turning point. We label these branches as 1, 2 and 3 (see Fig.7.26). Branch 1 has one two–parametric family of invariant tori around it, corresponding to the small stability parameter. Branch 2 has two two–parametric families of invariant tori around it (one for each stability parameter) up to energy -1.49932, in which the small

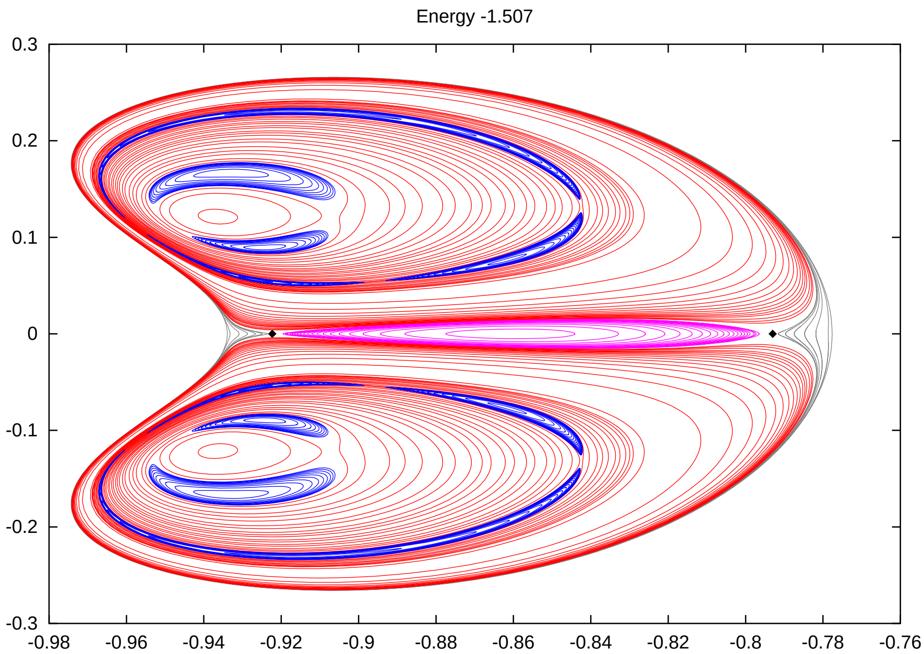

Figure 7.25: Section with $\{z = 0, p_z > 0\}$ of the tori around the planar Lyapunov family of energy -1.507, together with the families of tori displayed in Fig. 7.20 for the same value of energy. The two $\diamond$ points represent the $\{z = 0, p_z > 0\}$ sections of the orbits in the two–lane bridge between the planar and vertical Lyapunov families described in Section 7.1. Each point corresponds to one lane.

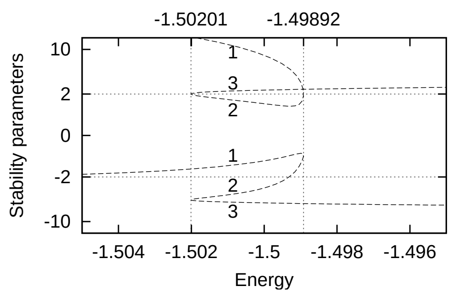

Figure 7.26: Magnification of the stability parameters of the halo family around L_1 in the range of energies between the two turning points. We have labeled, in each of the stability parameters, the branches called 1, 2 and 3 in the text.

stability parameter intersects -2. After that, only the family corresponding to the larger stability parameter subsists. Branch 3 has both stability parameters outside $[-2, 2]$, and therefore has no invariant tori around it.

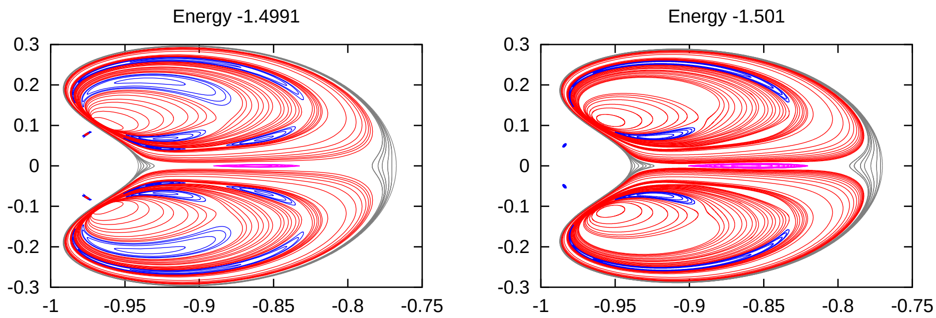

Figure 7.27: Sections with $\{z = 0, p_z > 0\}$ of the families of tori around branches 2 and 3 (defined in the text) of the halo family and around planar Lyapunov orbits, as well as all the families displayed in Fig. 7.20. The sections are done at energy levels -1.4991 and -1.501.

Fig. 7.27 shows the section with $\{z = 0, z > 0\}$ of all the above families at energy levels -1.501 and -1.4991, which show the two situations above explained. For $h = -1.4991$, the sections of the two families of tori around branch 2 overlap. They are given separately and magnified in Fig. 7.28. These two families have been computed at constant energy, and have ended because of reaching the maximum allowed number of harmonics. In Fig. 7.29, we give, for these two values of the energy, a sample torus from each family (excluding the tori around the bifurcated halo families by period duplication and triplication).

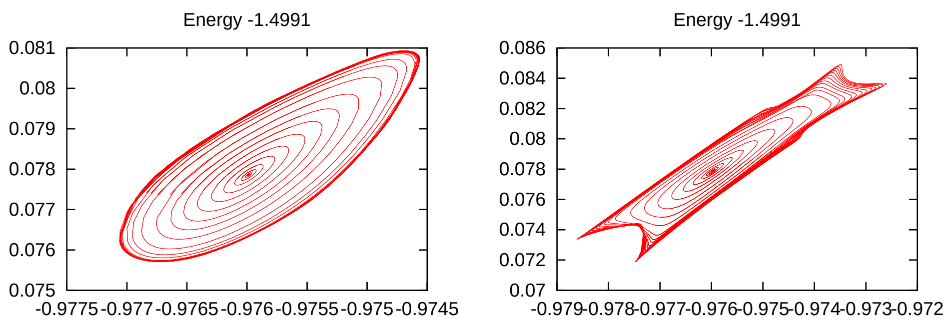

Figure 7.28: Magnification of the families of tori around branch 2 of the halo family of the left plot of Fig. 7.27. The left plot corresponds to the smaller stability parameter of the halo family. The right plot corresponds to the larger stability parameter.

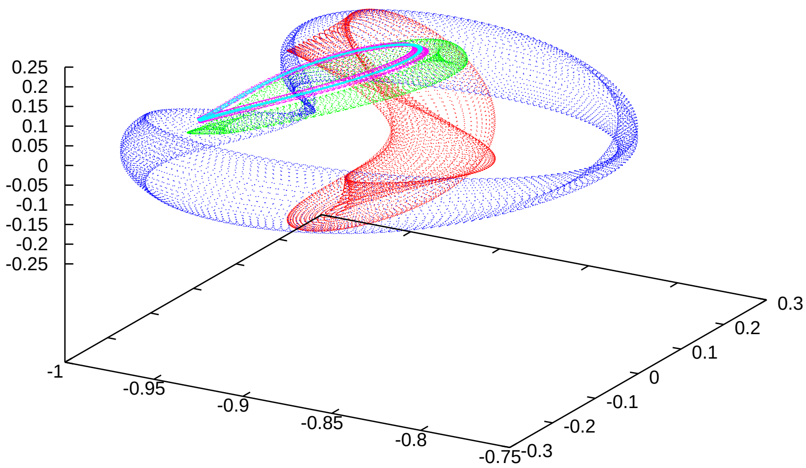

Figure 7.29: A sample torus from each of the following families: tori around Lyapunov planar orbits, tori around Lyapunov vertical orbits, tori around branch 1 of halo orbits (the largest one), tori around branch 2 of halo orbits corresponding to the larger stability parameter (the thickest one of the two above the previous one) and tori around branch 2 of halo orbits corresponding to the smaller stability parameter (the thinest one).

Part III

Appendices

This last part of the work includes additional results, organized in appendices, which have been taken out of the main text in order to improve readability. Appendix A introduces some known models that are used through this work, namely the Restricted Three–Body problem (RTBP), the Bicircular Problem (BCP), the Quasi–Bicircular Problem (QBCP) and the real Solar System, written as a time–dependent perturbation of the RTBP. We understand by "real Solar System" the Moon, the Sun and the planets as given by the JPL DE406 numerical ephemeris. The use of these ephemeris introduces discontinuities in accelerations and over–accelerations of the Solar System bodies, which are quantified in Appendix B. These discontinuities are propagated to the functions whose Fourier analysis the models developed in Chapter 5 are based on. Appendix C gives all the Fourier expansions computed in Chapter 5. Finally, Appendix D completes the results of Chapter 7 by displaying graphically the evolution of the families of periodic orbits computed there.

Appendix A

Known models for the motion in the Solar System

In this Appendix we introduce some known models used for the motion of a particle in the real Solar System. They are the Restricted Three–Body Problem (RTBP, see, e.g., [30]), the Bicircular Problem (BCP, see [25]), the Quasi–Bicircular problem (QBCP, see [3]) and the real Solar System written as a time–dependent perturbation of the RTBP (see [12], [10]). For this last model, we give the details about the deduction of its equations.

A.1 The Restricted Three Body Problem (RTBP)

As it is well known, the RTBP describes the motion of a massless particle under the attraction of two bodies of masses m_1 and m_2, called primaries, which are assumed to move in circular orbits around their center of mass. Taking a coordinate system that rotates with the primaries and suitable units, the primaries can be assumed to have masses $1-\mu$ and μ with $\mu \in [0, 1/2]$, to be fixed at coordinates $(\mu, 0, 0)$ and $(\mu - 1, 0, 0)$, and to complete one inertial revolution in 2π time units. Under these assumptions, the massless particle is governed by the following second-order differential equations (see [30])

$$\begin{aligned} \ddot{x} - 2\dot{y} &= \Omega_x, \\ \ddot{y} + 2\dot{x} &= \Omega_y, \\ \ddot{z} &= \Omega_z, \end{aligned} \tag{A.1}$$

where

$$\Omega = \frac{1}{2}(x^2 + y^2) + \frac{1-\mu}{r_1} + \frac{\mu}{r_2} + \frac{1}{2}\mu(1-\mu),$$

and $r_1 = \sqrt{(x-\mu)^2 + y^2 + z^2}$, $r_2 = \sqrt{(x-\mu+1)^2 + y^2 + z^2}$ are the distances from the particles to the primaries. The above system of differential equations has a first integral, called the Jacobi integral, which is defined as

$$C(x, y, z, p_x, p_y, p_z) = 2\Omega - \dot{x}^2 - \dot{y}^2 - \dot{z}^2.$$

The RTBP has five libration points, two of them, L_4 and L_5, form an equilateral triangle with the primaries and are located at $(-1/2 + \mu, \mp\sqrt{3}/2, 0)$, respectively. The other three are collinear, with $y = z = 0$. If x_{L_j} denotes the value of the x coordinates for $j = 1, 2, 3$, we will assume that the positions of these points and the primaries are such that

$$x_{L_2} < \mu - 1 < x_{L_1} < \mu < x_{L_3}.$$

For small values of μ, both $\mu - 1 - x_{L_2}$ and $\mu - 1 - x_{L_1}$ are $3^{-1/3}\mu^{1/3} + O(\mu^{2/3})$ and $x_{L_3} = 1 + O(\mu)$.

By introducing momenta as $p_x = \dot{x} - y$, $p_y = \dot{y} + x$ and $p_z = \dot{z}$, the RTBP can be written in Hamiltonian form with Hamiltonian function

$$H(x, y, z, p_z, p_y, p_z) = \frac{1}{2}(p_x^2 + p_y^2 + p_z^2) - xp_y + yp_x - \frac{1-\mu}{r_1} - \frac{\mu}{r_2}.$$

The differential equations are then

$$\begin{array}{rclrcl} \dot{x} & = & p_x + y, & \dot{p}_x & = & p_y - \dfrac{1-\mu}{r_1^3}(x-\mu) - \dfrac{\mu}{r_2^3}(x - \mu + 1), \\ \dot{y} & = & p_y - x, & \dot{p}_y & = & -p_x - \dfrac{1-\mu}{r_1^3}y - \dfrac{\mu}{r_2^3}y, \\ \dot{z} & = & p_z, & \dot{p}_z & = & -\dfrac{1-\mu}{r_1^3}z - \dfrac{\mu}{r_2^3}z. \end{array} \tag{A.2}$$

All the computations that follow, have been done using this last set of equations. We will refer to the value of the Hamiltonian as the "energy", and it is related to the Jacobi constant, C, by

$$C = -2H - \mu(1-\mu).$$

The linearized equations around any collinear equilibrium point, are given by the second order terms of the Hamiltonian, which can be written as

$$H_2 = \frac{1}{2}\left(p_x^2 + p_y^2\right) - xp_y + yp_x - c_2(x^2 - \frac{y^2}{2}) + \frac{p_z^2}{2} + c_2\frac{z^2}{2},$$

where c_2 is a positive constant (in fact, $c_2 > 1$) that depends on the equilibrium point and the value of the mass parameter μ. Its values are represented in Fig. A.1 ([23]).

From the above expression for H_2, it is clear that, linearly, the z direction is uncoupled form the planar ones and the motion in the vertical direction is an harmonic oscillator with vertical frequency $\omega_v = \sqrt{c_2}$. The characteristic polynomial associated to the planar motion is

$$p(\lambda) = \lambda^4 + (2 - c_2)\lambda^2 + (1 + c_2 - 2c_2^2).$$

Denoting $\eta = \lambda^2$, we have that the roots of $p(\lambda) = 0$ are given by

$$\eta_{1,2} = \frac{c_2 - 2 \pm \sqrt{9c_2^2 - 8c_2}}{2},$$

so, according to the values of c_2, we have that $\eta_1 > 0$ and $\eta_2 < 0$. This shows that the three equilibrium points are of the type center $\times$ center $\times$ saddle. The constant $\omega_p = \sqrt{-\eta_2}$ is usually called the planar frequency.

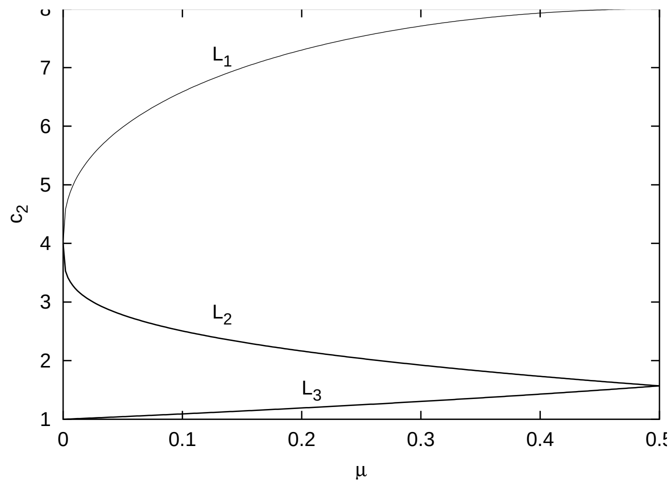

Figure A.1: Values of the $c_2(\mu)$ function, $\mu \in [0, 0.5]$, for $L_{1,2,3}$.

A.2 The Bicircular Problem (BCP)

The bicircular problem is a simplified version of a restricted four body problem. It can be suitable to describe the motion of a massless particle under the gravitational attraction of Earth, Moon and Sun. In this model we suppose that the Earth and the Moon are revolving in circular orbits around the center of masses of the Sun–Earth–Moon system. We remark that, with these assumptions, the motion of these three bodies is not coherent, that is, the assumed motions do not satisfy Newton's equations. However the model is extremely useful as an intermediate model between the RTBP and the "real" problem.

Let μ the mass of the Moon, $1-\mu$ the mass of the Earth and m_S the mass of the Sun. Let the distance from the Earth to the Moon be taken as unity. Then the distance from B to the Sun is a_S. We use synodic coordinates with respect to the Earth–Moon system, so that the positions of Earth and Moon are fixed at $(\mu, 0, 0)$ and $(\mu-1, 0, 0)$, respectively. The mean angular velocity of the Sun in these synodic coordinates is denoted by ω_S.

To keep a Hamiltonian form we use synodic coordinates x, y, z for the position of the massless body, but instead of the velocities we use momenta p_x, p_y, p_z, defined by $p_x = \dot{x} - y$, $p_y = \dot{y} + x$, $p_z = \dot{z}$.

In this way the equations of the bicircular problem are

$$
\begin{aligned}
\dot{x} &= p_x + y, \\
\dot{y} &= p_y - x, \\
\dot{z} &= p_z, \\
\dot{p}_x &= p_y - \frac{1-\mu}{r_{PE}^3}(x-\mu) - \frac{\mu}{r_{PM}^3}(x-\mu+1) - \frac{m_S}{r_{PS}^3}(x-x_S) - \varepsilon_S \cos\theta, \\
\dot{p}_y &= -p_x - \Big(\frac{1-\mu}{r_{PE}^3} + \frac{\mu}{r_{PM}^3}\Big)y - \frac{m_S}{r_{PS}^3}(y-y_S) + \varepsilon_S \sin\theta, \\
\dot{p}_z &= -\Big(\frac{1-\mu}{r_{PE}^3} + \frac{\mu}{r_{PM}^3} + \frac{m_S}{r_{PS}^3}\Big)z,
\end{aligned}
$$

where

$$\begin{aligned} r_{PE}^2 &= (x-\mu)^2 + y^2 + z^2, \\ r_{PM}^2 &= (x-\mu+1)^2 + y^2 + z^2, \\ r_{PS}^2 &= (x-x_S)^2 + (y-y_S)^2 + z^2, \\ x_S &= a_S \cos\theta, \\ y_S &= -a_S \sin\theta, \\ \theta &= \omega_S t + \theta_0, \end{aligned}$$

amb θ_0 is some initial phase of the Sun. For shortness we have used the perturbation parameter of the Sun $\varepsilon_S = \frac{m_S}{a_S}$.

The related Hamiltonian is

$$H = \frac{1}{2}(p_x^2 + p_y^2 + p_z^2) + yp_x - xp_y - \frac{1-\mu}{r_{PE}} - \frac{\mu}{r_{PM}} - \frac{m_S}{r_{PS}} - \frac{m_S}{a_S^2}(y\sin\theta - x\cos\theta)$$

The semimajor axis of the Sun is related to its mean angular motion through Kepler's third law:

$$a_S = \left(\frac{1+m_S}{(1-\omega_S)^2}\right)^{1/3}.$$

A.3 The Quasi–Bicircular problem (QBCP)

It has been recently developed a bicircular–coherent model, called the Quasi–Bicircular problem (QBCP) [3]. It is based on a planar solution of the general three–body problem for the Earth, the Moon and the Sun which is close to bicircular and satisfies Newton's equations. Its main advantage is that, although it is still a time–periodic perturbation of the RTBP with the same frequency as the BCP, it is dynamically closer to the real problem. In some sense is "the best we can do" assuming planar motion for the Sun–Earth–Moon system.

The QBCP can be formulated in Hamiltonian form, with Hamiltonian

$$\begin{aligned} H_{QBCP} &= \frac{1}{2}\alpha_1(p_x^2 + p_y^2 + p_z^2) + \alpha_2(p_x x + p_y y + p_z z) \\ &\quad + \alpha_3(p_x y - p_y x) + \alpha_4 x + \alpha_5 y \\ &\quad - \alpha_6\Big(\frac{1-\mu}{((x-\mu)^2 + y^2 + z^2)^{1/2}} + \frac{\mu}{((x-\mu+1)^2 + y^2 + z^2)^{1/2}} \\ &\qquad + \frac{\mu_S}{((x-\alpha_7)^2 + (y-\alpha_8)^2 + z^2)^{1/2}}, \end{aligned}$$

where S stands for the Sun and $\mu_S = \frac{m_S}{m_E + m_M}$, being m_S, m_E and m_M the masses of Sun, Earth and Moon, respectively. The α_1,…,α_8 are periodic functions with the same basic frequency as the BCP, and thus are evaluated by means of the following Fourier expansions:

$$\alpha_i(t) = \alpha_{i,0} + \sum_{k\geq 1}(\alpha_{i,k,c}\cos(j\omega_S t) + \alpha_{i,k,s}\sin(j\omega_S t)).$$

The actual values of the $\alpha_{i,k,c}$ and $\alpha_{i,k,s}$ coefficients are given in [3].

A.4 The Solar System equations of motion as a perturbation of the RTBP equations

In this Section, we will derive the equations of motion of a spacecraft under the Newtonian attraction of the bodies of the Solar System in the form of a perturbated RTBP ([12], [10]).

As we did in Chapter 5, we will denote the Solar System as $\mathcal{S} = \{P_1, \ldots, P_9, P_{10}, P_{11}\}$, where P_1,...,P_9 are the planets ordered by increasing distance from the Sun, P_{10} is the Moon and P_{11} is the Sun.

In some cases, for instance when studying the Sun–Earth+Moon problem, it is convenient to consider the Earth and the Moon as a single body, located at the Earth–Moon barycenter and with mass the sum of masses of Earth and Moon. In this case, the Solar System will be denoted as $\mathcal{S} = \{P_1, P_2, P_4, \ldots, P_9, P_{11}, P_{12}\}$, being P_{12} the Earth–Moon barycenter.

All the following arguments can be applied to the case in which Earth and Moon are considered different bodies as well as the case in which are considered a single body.

A.4.1 Deduction of the equations

In an inertial reference frame, Newton's equations for the motion of a spacecraft can be written as

$$\mathbf{R}'' = G \sum_{i \in \mathcal{S}} m_i \frac{(\mathbf{R}_i - \mathbf{R})}{\|\mathbf{R} - \mathbf{R}_i\|}. \tag{A.3}$$

Here $\mathbf{R} = (X, Y, Z)^T$ is the position of the spacecraft (in km), $\mathbf{R}_i$ is the position of the body $i \in \mathcal{S}$, G is the gravitational constant, m_i is the mass of the body $i \in \mathcal{S}$, $\|\cdot\|$ is the Euclidean norm, and the primes denote derivative with respect to time (in Julian days), which we will denote as t^*. From now on, $\mathbf{R}$ and t^* will be called *inertial coordinates* and *inertial time*, respectively.

The above system can be written in Lagrangian form as

$$L(\mathbf{R}, \mathbf{R}', t^*) = \frac{1}{2}\mathbf{R}'\mathbf{R}' + \sum_{i \in \mathcal{S}} \frac{Gm_i}{\|\mathbf{R} - \mathbf{R}_i\|}.$$

Here $\mathbf{R}'\mathbf{R}'$ is the dot product between $\mathbf{R}'$ and $\mathbf{R}'$.

In order to write the previous system as a perturbed RTBP, we choose two primaries $I, J \in \mathcal{S}$ with $m_I > m_J$ and perform a change of coordinates in order to leave I and J at the constant positions $(\mu, 0, 0)$ and $(\mu - 1, 0, 0)$ respectively, being $\mu = m_J/(m_I + m_J)$. This is done in several steps:

- A translation through
$$\mathbf{B} = \frac{m_I \mathbf{R}_I + m_J \mathbf{R}_J}{m_I + m_J}$$
which leaves the barycenter of the primaries at the origin,

- a rotation through the orthogonal matrix $C = (\mathbf{e}_1, \mathbf{e}_2, \mathbf{e}_3)$, where
$$\mathbf{e}_1 = \frac{\mathbf{R}_{JI}}{\|\mathbf{R}_{JI}\|}, \quad \mathbf{e}_3 = \frac{\mathbf{R}_{JI} \times \mathbf{R}'_{JI}}{\|\mathbf{R}_{JI} \times \mathbf{R}'_{JI}\|}, \quad \mathbf{e}_2 = \mathbf{e}_3 \times \mathbf{e}_1,$$
being $\mathbf{R}_{ij} = \mathbf{R}_j - \mathbf{R}_i$. This turns the instantaneous plane of motion of the primaries into the xy plane and leaves the primaries on the x axis,
- a scaling through $k = \|\mathbf{R}_{JI}\|$, which makes the distance between the primaries to be constant and equal to 1.

The change of coordinates to be performed is written as
$$\mathbf{R} = \mathbf{B} + kC\mathbf{r}, \tag{A.4}$$
where $\mathbf{r} = (x, y, z)^T$. From now on $\mathbf{r}$ will be called *adimensional coordinates.* It is important to note that the previous change of coordinates is non–autonomous, because $\mathbf{B}$, k and C depend on time.

It can be verified that the change of coordinates (A.4) preserves Lagrangian form and, therefore, the Lagrangian in the new coordinates is
$$\begin{aligned} L(\mathbf{r}, \mathbf{r}', t^*) \quad = \quad & \frac{1}{2}\mathbf{B}'\mathbf{B}' + k'\mathbf{B}\mathbf{s} + k\mathbf{B}'\mathbf{s}' + \frac{1}{2}k'^2\mathbf{r}\mathbf{r} + kk'\mathbf{s}\mathbf{s}' + \frac{1}{2}k^2\mathbf{s}'\mathbf{s}' + \\ & + \frac{Gm_I}{k[(x-\mu)^2 + y^2 + z^2]^{1/2}} + \frac{Gm_J}{k[(x-\mu+1)^2 + y^2 + z^2]^{1/2}} + \\ & + \sum_{i \in \mathcal{S}^*} \frac{Gm_i}{k\|\mathbf{r} - \mathbf{r}_i\|}, \end{aligned}$$
where $\mathbf{s} = C\mathbf{r}$, $\mathbf{r}_i$ is the position of the body i in adimensional coordinates and $\mathcal{S}^*$ represents the Solar System bodies considered without the two primaries I, J. Here we have used that C is an orthogonal matrix and, hence, it preserves the scalar product and the Euclidean norm.

Now we want to use the same time units as the RTBP, where 2π time units correspond to one revolution of the primaries. In order to do so, let a and n be the semi-major axis and the mean motion of J with respect to I, which are chosen to satisfy Kepler's third law: $G(m_I + m_J) = n^2a^3$. Then we perform the change of time
$$t = n(t^* - t_0^*), \tag{A.5}$$
where t_0^* is a fixed epoch, for instance 2451544.5 (1st Jan 2000). From now on, t will be called *adimensional time.* In Table A.1 we give the values of n, a used in the computations of Chapter 5.

It can be verified that the time change (A.5) preserves Lagrangian form too. If we denote by a dot the derivative with respect to t, then the new Lagrangian can be written as
$$\begin{aligned} L(\mathbf{r}, \dot{\mathbf{r}}, t) \quad = \quad & n^2\Big(\frac{1}{2}\dot{\mathbf{B}}\dot{\mathbf{B}} + \dot{k}\dot{\mathbf{B}}\mathbf{s} + k\dot{\mathbf{B}}\dot{\mathbf{s}} + \frac{1}{2}\dot{k}^2\mathbf{r}\mathbf{r} + k\dot{k}\mathbf{s}\dot{\mathbf{s}} + \frac{1}{2}k^2\dot{\mathbf{s}}\dot{\mathbf{s}}\Big) + \\ & + \frac{Gm_I}{k[(x-\mu)^2 + y^2 + z^2]^{1/2}} + \frac{Gm_J}{k[(x-\mu+1)^2 + y^2 + z^2]^{1/2}} + \\ & + \sum_{i \in \mathcal{S}^*} \frac{Gm_i}{k\|\mathbf{r} - \mathbf{r}_i\|}. \end{aligned}$$

Earth–Moon	Sun–Earth+Moon
0.22997154619514	0.01720209883844

Table A.1: Values for the mean motion used in the Earth–Moon and Sun–Earth+Moon cases.

Since the equations of motion are

$$\frac{d}{dt}\frac{\partial L}{\partial \dot{\mathbf{r}}} = \frac{\partial L}{\partial \mathbf{r}}, \tag{A.6}$$

neither adding a term that does not depend on $\mathbf{r}, \dot{\mathbf{r}}$ nor scaling the Lagrangian by a constant affect the equations of motion. We can therefore skip the term $\frac{n^2}{2}\dot{\mathbf{B}}\dot{\mathbf{B}}$ and multiply by $\frac{a}{G(m_I+m_J)} = \frac{1}{n^2a^2}$ to get

$$\begin{aligned} L(\mathbf{r},\dot{\mathbf{r}},t) &= \frac{1}{a^2}\Big(\dot{k}\dot{\mathbf{B}}\mathbf{s} + k\dot{\mathbf{B}}\dot{\mathbf{s}} + \frac{1}{2}\dot{k}^2\mathbf{r}\mathbf{r} + k\dot{k}\mathbf{s}\dot{\mathbf{s}} + \frac{1}{2}k^2\dot{\mathbf{s}}\dot{\mathbf{s}}\Big) + \\ &+\frac{a}{k}\Big(\frac{1-\mu}{[(x-\mu)^2+y^2+z^2]^{1/2}} + \frac{\mu}{[(x-\mu+1)^2+y^2+z^2]^{1/2}} + \\ &\quad + \sum_{i\in\mathcal{S}^*}\frac{\mu_i}{\|\mathbf{r}-\mathbf{r}_i\|}\Big). \end{aligned} \tag{A.7}$$

Here $\mu_i = \frac{m_i}{m_I+m_J}$.

Since $\mathbf{e}_1, \mathbf{e}_2, \mathbf{e}_3$ form an orthogonal basis we have $\mathbf{e}_i\mathbf{e}_j = \delta_{ij}$, $\dot{\mathbf{e}}_i\mathbf{e}_j = -\mathbf{e}_i\dot{\mathbf{e}}_j$ and $\dot{\mathbf{e}}_i\mathbf{e}_i = 0$ for $i,j = 1,2,3$. It can be further shown that $\dot{\mathbf{e}}_1\dot{\mathbf{e}}_2 \equiv 0$, $\dot{\mathbf{e}}_2\dot{\mathbf{e}}_3 \equiv 0$ and $\dot{\mathbf{e}}_1\mathbf{e}_3 \equiv 0$. Writing $\mathbf{s} = C\mathbf{r} = \mathbf{e}_1x + \mathbf{e}_2y + \mathbf{e}_3z$ and using the previous relations, we get

$$\begin{aligned} L(\mathbf{r},\dot{\mathbf{r}},t) &= a_1(\dot{x}^2+\dot{y}^2+\dot{z}^2) + a_2(x\dot{x}+y\dot{y}+z\dot{z}) + a_3(x\dot{y}-\dot{x}y) + \\ &+a_4(y\dot{z}-\dot{y}z) + a_5x^2 + a_6y^2 + a_7z^2 + a_8xz + \\ &+a_9\dot{x} + a_{10}\dot{y} + a_{11}\dot{z} + a_{12}x + a_{13}y + a_{14}z + \\ &+a_{15}\Big(\frac{1-\mu}{[(x-\mu)^2+y^2+z^2]^{1/2}} + \frac{\mu}{[(x-\mu+1)^2+y^2+z^2]^{1/2}} + \\ &\quad + \sum_{i\in\mathcal{S}^*}\frac{\mu_i}{[(x-x_i)^2+(y-y_i)^2+(z-z_i)^2]^{1/2}}\Big), \end{aligned}$$

where

$$\begin{aligned} &a_1 = \frac{k^2}{2a^2}, && a_6 = \frac{1}{2}\Big(\frac{\dot{k}^2}{a^2} + \frac{k^2}{a^2}\dot{\mathbf{e}}_2\dot{\mathbf{e}}_2\Big), && a_{11} = \frac{k}{a^2}(\dot{\mathbf{B}}\mathbf{e}_3), \\ &a_2 = \frac{k\dot{k}}{a^2}, && a_7 = \frac{1}{2}\Big(\frac{\dot{k}^2}{a^2} + \frac{k^2}{a^2}\dot{\mathbf{e}}_3\dot{\mathbf{e}}_3\Big), && a_{12} = \frac{\dot{k}}{a^2}\dot{\mathbf{B}}\mathbf{e}_1 + \frac{k}{a^2}\dot{\mathbf{B}}\dot{\mathbf{e}}_1, \\ &a_3 = \frac{k^2}{a^2}\dot{\mathbf{e}}_1\mathbf{e}_2, && a_8 = \frac{k^2}{a^2}\dot{\mathbf{e}}_1\dot{\mathbf{e}}_3, && a_{13} = \frac{\dot{k}}{a^2}\dot{\mathbf{B}}\mathbf{e}_2 + \frac{k}{a^2}\dot{\mathbf{B}}\dot{\mathbf{e}}_2, \\ &a_4 = \frac{k^2}{a^2}\dot{\mathbf{e}}_2\mathbf{e}_3, && a_9 = \frac{k}{a^2}\dot{\mathbf{B}}\mathbf{e}_1, && a_{14} = \frac{\dot{k}}{a^2}\dot{\mathbf{B}}\mathbf{e}_3 + \frac{k}{a^2}\dot{\mathbf{B}}\dot{\mathbf{e}}_3, \\ &a_5 = \frac{1}{2}\Big(\frac{\dot{k}^2}{a^2} + \frac{k^2}{a^2}\dot{\mathbf{e}}_1\dot{\mathbf{e}}_1\Big), && a_{10} = \frac{k}{a^2}\dot{\mathbf{B}}\mathbf{e}_2, && a_{15} = \frac{a}{k}. \end{aligned}$$

If we we introduce momenta as

$$p_x = \frac{\partial L}{\partial \dot{x}}, \quad p_y = \frac{\partial L}{\partial \dot{y}}, \quad p_z = \frac{\partial L}{\partial \dot{z}}, \tag{A.8}$$

we have

$$\begin{aligned} p_x &= 2a_1\dot{x} + a_2x - a_3y + a_9, \\ p_y &= 2a_1\dot{y} + a_2y + a_3x - a_4z + a_{10}, \\ p_z &= 2a_1\dot{z} + a_2z + a_4y + a_{11}. \end{aligned} \tag{A.9}$$

It is known that, in this case, the Hamiltonian of the model is given in terms of the Lagrangian as $H(\mathbf{r},\mathbf{p},t) = \dot{x}p_x + \dot{y}p_y + \dot{z}p_z - L(\mathbf{r},\dot{\mathbf{r}},t)$, where $\mathbf{p} = (p_x,p_y,p_z)^T$ and $\dot{x}$, $\dot{y}$, $\dot{z}$ can be written in terms of p_x, p_y, p_z from (A.9). After expanding the previous expression of H, skipping terms that do not depend on $\mathbf{r},\mathbf{p}$ and collecting we obtain

$$\begin{aligned} H(\mathbf{r},\mathbf{p},t) = {} & b_1(p_x^2+p_y^2+p_z^2) + b_2(xp_x+yp_y+zp_z) + b_3(yp_x - xp_y) + \\ & + b_4(zp_y - yp_z) + b_5x^2 + b_6y^2 + b_7z^2 + b_8xz + \\ & + b_9p_x + b_{10}p_y + b_{11}p_z + b_{12}x + b_{13}y + b_{14}z + \\ & + b_{15}\Big(\frac{1-\mu}{[(x-\mu)^2+y^2+z^2]^{1/2}} + \frac{\mu}{[(x-\mu+1)^2+y^2+z^2]^{1/2}} + \\ & \qquad + \sum_{i\in\mathcal{S}^*}\frac{\mu_i}{[(x-x_i)^2+(y-y_i)^2+(z-z_i)^2]^{1/2}}\Big), \end{aligned} \tag{A.10}$$

where

$$\begin{aligned} b_1 &= \frac{a^2}{2k^2}, & b_9 &= \frac{-1}{k}\dot{\mathbf{B}}\mathbf{e}_1, \\ b_2 &= \frac{-\dot{k}}{k}, & b_{10} &= \frac{-1}{k}\dot{\mathbf{B}}\mathbf{e}_2, \\ b_3 &= \dot{\mathbf{e}}_1\mathbf{e}_2, & b_{11} &= \frac{-1}{k}\dot{\mathbf{B}}\mathbf{e}_3, \\ b_4 &= \dot{\mathbf{e}}_2\mathbf{e}_3, & b_{12} &= \frac{k}{a^2}\Big((\dot{\mathbf{e}}_1\mathbf{e}_2)(\dot{\mathbf{B}}\mathbf{e}_2) - \dot{\mathbf{B}}\dot{\mathbf{e}}_1\Big), \\ b_5 &= \frac{k^2}{2a^2}\Big((\dot{\mathbf{e}}_1\mathbf{e}_2)^2 - \dot{\mathbf{e}}_1\dot{\mathbf{e}}_1\Big), & b_{13} &= \frac{k}{a^2}\Big((\dot{\mathbf{e}}_2\mathbf{e}_3)(\dot{\mathbf{B}}\mathbf{e}_3) - \\ b_6 &= \frac{k^2}{2a^2}\Big((\dot{\mathbf{e}}_1\mathbf{e}_2)^2 + (\dot{\mathbf{e}}_2\mathbf{e}_3)^2 - \dot{\mathbf{e}}_2\dot{\mathbf{e}}_2\Big) & & \qquad - (\dot{\mathbf{e}}_1\mathbf{e}_2)(\dot{\mathbf{B}}\mathbf{e}_1) - \dot{\mathbf{B}}\dot{\mathbf{e}}_2\Big), \\ b_7 &= \frac{k^2}{2a^2}\Big((\dot{\mathbf{e}}_2\mathbf{e}_3)^2 - \dot{\mathbf{e}}_3\dot{\mathbf{e}}_3\Big), & b_{14} &= \frac{-k}{a^2}\Big((\dot{\mathbf{e}}_2\mathbf{e}_3)(\dot{\mathbf{B}}\mathbf{e}_2) + \dot{\mathbf{B}}\dot{\mathbf{e}}_3\Big), \\ b_8 &= \frac{k^2}{a^2}\Big(-(\dot{\mathbf{e}}_1\mathbf{e}_2)(\dot{\mathbf{e}}_2\mathbf{e}_3) - \dot{\mathbf{e}}_1\dot{\mathbf{e}}_3\Big), & b_{15} &= \frac{-a}{k} \end{aligned}$$

From (A.6) we get the second–order differential equations given in (5.3), where the c_i

are defined as

$$
\begin{aligned}
c_1 &= \frac{-1}{k}(\ddot{\mathbf{B}}\mathbf{e}_1), & c_6 &= 2(\dot{\mathbf{e}}_2\mathbf{e}_3), & c_{11} &= \frac{2\dot{k}}{k}(\dot{\mathbf{e}}_2\mathbf{e}_3) + (\ddot{\mathbf{e}}_2\mathbf{e}_3),\\
c_2 &= \frac{-1}{k}(\ddot{\mathbf{B}}\mathbf{e}_2), & c_7 &= (\dot{\mathbf{e}}_1\dot{\mathbf{e}}_1) - \frac{\ddot{k}}{k}, & c_{12} &= (\dot{\mathbf{e}}_3\dot{\mathbf{e}}_3) - \frac{\ddot{k}}{k},\\
c_3 &= \frac{-1}{k}(\ddot{\mathbf{B}}\dot{\mathbf{e}}_3) & c_8 &= \frac{2\dot{k}}{k}(\dot{\mathbf{e}}_1\mathbf{e}_2) + (\ddot{\mathbf{e}}_1\mathbf{e}_2), & c_{13} &= \frac{a^3}{k^3},\\
c_4 &= \frac{-2\dot{k}}{k} & c_9 &= (\dot{\mathbf{e}}_1\dot{\mathbf{e}}_3), & &\\
c_5 &= 2(\dot{\mathbf{e}}_1\mathbf{e}_2), & c_{10} &= (\dot{\mathbf{e}}_2\dot{\mathbf{e}}_2) - \frac{\ddot{k}}{k}. & &
\end{aligned}
$$

As in the deduction of the Lagrangian, to obtain these expressions for c_i it has been used that $\dot{\mathbf{e}}_1\dot{\mathbf{e}}_2 \equiv 0$ and $\dot{\mathbf{e}}_2\dot{\mathbf{e}}_3 \equiv 0$.

Appendix B

The discontinuities in accelerations and over–accelerations of the JPL ephemeris

In this Appendix we discuss the jump discontinuities introduced in the evaluation of accelerations and over–accelerations of the positions of the Sun, the planets and the Moon due to the use of the JPL numerical ephemeris.

B.1 Structure of JPL's ephemeris files

The JPL ephemeris files ([26],[27]) contain the coefficients of a large set of Chebyshev polynomials, each of which is used to compute the position or velocity of a Solar System body over a determinated time span called *granule*. The length of these granules is chosen in order to obtain a very accurate approximation with the corresponding Chebyshev polynomial.

All the Chebyshev coefficients are adjusted from the output of a numerical integration which takes into account the latest planetary observations. In this adjustment, Chebyshev polynomials corresponding to neighboring granules are asked to be equal when evaluated at the border points. Therefore, there are no discontinuities in positions and velocities.

In order to evaluate the c_i functions in Chapter 5, we need the accelerations and over–accelerations of the Solar System bodies. They are computed by derivating the Chebyshev polynomials corresponding to the velocities. In this way, a jump discontinuity is introduced at each granule change in accelerations and over–accelerations.

B.2 Jump discontinuities corresponding to DE406

For DE406, which is the JPL ephemeris file used for the computations of Chapter 5, we give in Table B.1 the maximum value of these jumps over the 6000–year time–span of this ephemeris.

body	gr. l.	x''	y''	z''	x'''	y'''	z'''
Sun	64	9.98E–03	8.84E–03	4.81E–03	1.25E–02	1.08E–02	5.91E–03
Mercury	16	4.60E–01	4.14E–01	2.25E–01	2.69E+00	2.47E+00	1.34E+00
Venus	64	1.29E–02	1.19E–02	5.60E–03	1.49E–02	1.40E–02	7.47E–03
EMB	32	3.55E–02	3.34E–02	1.67E–02	3.00E–02	2.67E–02	1.28E–02
Mars	64	2.92E–03	2.71E–03	1.21E–03	1.59E–03	1.23E–03	5.72E–04
Jupiter	64	9.93E–05	8.32E–05	3.38E–05	1.67E–04	1.37E–04	5.83E–05
Saturn	64	6.77E–06	6.82E–06	2.58E–06	3.91E–06	4.10E–06	1.49E–06
Uranus	64	3.43E–07	2.96E–07	1.23E–07	6.50E–08	5.54E–08	2.36E–08
Neptune	64	5.96E–08	5.18E–08	2.17E–08	9.15E–09	7.81E–09	3.17E–09
Pluto	64	5.07E–08	5.19E–08	1.94E–08	6.34E–09	7.18E–09	2.96E–09
Moon	8	1.27E–01	1.24E–01	5.84E–02	1.41E+00	1.31E+00	6.66E–01

Table B.1: Jump discontinuities in the JPL DE406 ephemeris file. For each Solar System body, we give the maximum jump in accelerations (in km/JD^2, JD stands for "Julian days") and over–accelerations (in km/JD^3) over the whole time span covered by this ephemeris, which is from JD 625360.5 (Feb. 23, 3000 B.C.) to 2816848.5 (March 3, 3000 A.C.). We also give, in the second column, the granule length (in JD) for each body. In the table, EMB stands for "Earth-Moon barycenter".

Appendix C

Fourier expansions

We give in this appendix all the Fourier expansions referenced in Chapter 5. These include the c_i functions and the positions of the Solar System bodies in adimensional coordinates, both in the Earth–Moon and the Sun–Earth+Moon cases. For the c_i functions of the Earth–Moon case, we also give the coefficients that adjust them as linear combinations of the 5 basic frequencies of Brown's simplified lunar theory given in [8].

C.1 Notation

Each table in this Appendix corresponds to a Fourier expansion of the form

$$A_0^c + \sum_{l=1}^{N_f} \Big(A_l^c \cos(f_l(t - t_0)) + A_l^s \sin(f_l(t - t_0)) \Big),$$

where A_0^c is given in the first entry of the table, f_l, A_l^c, A_l^s are given in the remaining entries and $N_f + 1$ is the total number of entries of the table. The time t above is assumed to be in adimensional units, and therefore the units of f_l are cycles per revolution of the primaries (note that this depends on the primaries chosen). The parameter t_0 corresponds to the starting date of the Fourier analysis, which is the Julian Day 2451910.5 (Jan 1st, 2001), as mentioned in Chapter 5. In the above formula, t_0 must be set according to the origin of time needed. For instance, for the computations of Table 5.22, we set

$$t_0 = (2451919.3489 - 2451910.5)n,$$

being n the mean motion in the Earth–Moon case.

C.2 Expansions of the c_i functions, Earth–Moon case

In tables C.1 to C.13 we give the Fourier expansions computed for the c_i functions in the Earth–Moon case. In addition to the frequencies f_l and Fourier coefficients A_l^c, A_l^s, we display in these tables the amplitudes,

$$A_l = \sqrt{(A_l^c)^2 + (A_l^s)^2},$$

the coefficients of the adjustment of the frequencies as linear combinations of the 5 basic frequencies $\omega = (\omega_1, \ldots, \omega_5)$ from Brown's simplified lunar theory (see Section 5.3.2),

$$k_l = (k_l^1, \ldots, k_l^5) \in \mathbb{Z}^5,$$

the order of these linear combinations,

$$|k_l| = |k_l^1| + \ldots + |k_l^5|,$$

and its error, $f_l - k_l\omega$.

Table C.1: Fourier analysis of the c_1 function in the Earth–Moon case.

f_l	A_l^c	A_l^s	A_l	k_l^1	k_l^2	k_l^3	k_l^4	k_l^5	$\|k_l\|$	$f_l - k_l\omega$
0.00000000000	3.49728352384E−04	0.00000000000E+00	0.00E+00	0	0	0	0	0	0	0.00E+00
0.92519578633	6.11424843788E−01	−2.07418797009E+00	2.16E+00	0	1	0	0	0	1	−2.11E−07
1.91674083005	9.86980050137E−02	1.47470649298E−01	1.77E−01	1	1	−1	0	0	3	−3.89E−07
0.85039537676	1.84739724027E−02	−7.30244372310E−02	7.53E−02	−1	2	0	0	1	4	−1.92E−07
0.06634926288	6.79099306828E−02	2.93309343012E−02	7.40E−02	1	−1	−1	0	0	3	3.89E−08
1.78404231456	3.36502864099E−02	5.62537249256E−03	3.41E−02	−1	3	1	0	0	5	−4.56E−07
2.77558735935	−1.81647617922E−02	1.56389320446E−02	2.40E−02	0	3	0	0	0	3	−6.33E−07
2.90828587988	−1.36201204397E−02	−1.42944852785E−03	1.37E−02	2	1	−2	0	0	5	−5.61E−07
1.84194060336	4.29226286451E−03	5.91815966141E−03	7.31E−03	0	2	−1	0	1	4	−1.87E−07
1.08284144947	1.73778166384E−03	−3.50558609743E−03	3.91E−03	2	−1	0	2	0	5	−2.30E−07
0.99999608580	−1.19150925903E−03	3.53655992224E−03	3.73E−03	1	0	0	0	−1	2	−3.40E−07
1.05789429677	−3.07241003106E−03	1.55611903813E−03	3.44E−03	2	−1	−2	0	0	5	−1.49E−07
3.76713240391	−6.08881828453E−05	−3.69529711823E−03	3.70E−03	1	3	−1	0	0	5	−8.10E−07
1.70924216643	2.64745450493E−03	3.42227127121E−04	2.67E−03	−2	4	1	0	1	8	−1.76E−07
0.14114984241	2.21715980197E−03	1.06470732416E−03	2.46E−03	2	−2	−1	0	−1	6	1.90E−07
2.70078684154	−1.77905198818E−03	1.65814811377E−03	2.43E−03	−1	4	0	0	1	6	−7.22E−07
0.77559511766	4.51845611742E−04	−2.12193487364E−03	2.17E−03	−2	3	0	0	2	7	−2.29E−08
1.99154129499	−6.16552315269E−04	−1.00470510178E−03	1.18E−03	2	0	−1	0	−1	4	−3.52E−07
3.89983092217	7.41953246429E−04	−7.22192495846E−04	1.04E−03	3	1	−3	0	0	7	−7.40E−07
1.85039170167	8.04906243666E−04	5.20157776726E−04	9.58E−04	0	2	0	0	0	2	−2.93E−07
0.00845138932	6.65622320815E−04	−2.56010200523E−04	7.13E−04	0	0	1	0	−1	2	1.85E−07
3.63443388582	−5.34183218572E−04	−4.86728021205E−04	7.23E−04	−1	5	1	0	0	7	−8.80E−07
2.83348530843	−6.46647280720E−04	−4.19030497728E−05	6.48E−04	1	2	−2	0	1	6	−7.03E−07
1.94168801634	−5.70156567948E−04	−2.01298040697E−04	6.05E−04	1	1	1	2	0	5	−4.36E−07
2.64288884133	−2.30111081823E−05	5.15506926653E−04	5.16E−04	−2	5	2	0	0	9	−7.03E−07
4.75867745029	3.31598521437E−04	2.66986910545E−04	4.26E−04	2	3	−2	0	0	7	−9.85E−07
3.69233204989	−2.20450941041E−05	−4.01689512934E−04	4.02E−04	0	4	−1	0	1	6	−7.35E−07
2.04943934140	7.89082727159E−05	−3.43946293640E−04	3.53E−04	3	−1	−3	0	0	7	−3.26E−07
4.62597893259	3.17812781243E−04	−4.39748393952E−05	3.21E−04	0	5	0	0	0	5	−1.05E−06
0.79249727839	1.46147169122E−04	2.50176540225E−04	2.90E−04	−2	3	2	0	0	7	−2.71E−07
2.85038749322	2.29034795813E−04	−1.82906642935E−04	2.93E−04	1	2	0	0	−1	4	−9.28E−07
1.85884282406	−2.68393879459E−04	−5.59346373905E−05	2.74E−04	0	2	1	0	−1	4	−3.75E−07
2.07438649155	1.00104220995E−04	2.26431623377E−04	2.48E−04	3	−1	−1	2	0	7	−4.09E−07
1.76713975394	1.46841353083E−04	1.85677393011E−04	2.37E−04	−1	3	−1	0	2	7	−6.08E−07
0.99154552975	−9.98303822273E−05	1.18636745420E−04	1.55E−04	1	0	−1	0	0	2	3.08E−07
2.98308653320	1.58715139628E−04	2.32065297134E−05	1.60E−04	3	0	−2	0	−1	6	−3.36E−07
2.62598647989	−1.09612744138E−04	1.10344395335E−04	1.56E−04	−2	5	0	0	2	9	−6.56E−07
0.76755012989	1.78020427952E−05	−1.56694202456E−04	1.58E−04	−2	3	0	−2	0	7	−1.86E−07
2.84193687948	−1.40489977606E−04	4.37454238194E−05	1.47E−04	1	2	−1	0	0	4	−3.37E−07
1.92518236638	−1.20781449732E−04	−7.71669622302E−05	1.43E−04	1	1	0	0	−4	6	6.65E−07
1.63444105798	1.36659514559E−04	1.16813694410E−05	1.37E−04	−3	5	1	0	2	11	−8.56E−07
0.09129636592	−1.35682361867E−04	3.23729916781E−05	1.39E−04	1	−1	1	2	0	5	−9.20E−08
1.15764188855	6.25218147810E−05	−1.14606606715E−04	1.31E−04	3	−2	0	2	−1	8	−2.19E−07
1.13269454643	−1.14980469674E−04	5.28598414079E−05	1.27E−04	3	−2	−2	0	−1	8	−3.28E−07
0.98309391503	−1.00601880441E−04	5.59572601745E−05	1.15E−04	1	0	−2	0	1	4	−1.02E−07
3.55963358492	−8.08697481496E−05	−6.81910186892E−05	1.06E−04	−2	6	1	0	1	10	−7.52E−07
0.85667921182	−5.57341314954E−05	5.36860930410E−05	7.74E−05	1	0	−16	−2	−1	20	−3.08E−06
4.89137596488	6.00146407056E−06	7.72048105887E−05	7.74E−05	4	1	−4	0	0	9	−9.18E−07
0.21595025012	6.41383670711E−05	3.39355239073E−05	7.26E−05	3	−3	−1	0	−2	9	1.69E−07
0.99368985120	2.47053910368E−05	6.79242266002E−05	7.23E−05	0	1	10	−4	5	20	3.55E−06
5.61752397365	−3.38221623028E−05	5.43299057021E−05	6.40E−05	1	5	−1	0	0	7	−1.24E−06

Table C.1: (continued)

f_l	A_l^c	A_l^s	A_l	k_l^1	k_l^2	k_l^3	k_l^4	k_l^5	$\|k_l\|$	$f_l - k_l\omega$
0.83161613915	6.12150108682E−05	4.03281949393E−07	6.12E−05	−2	3	9	−5	1	20	2.58E−05
3.84193273653	−1.37471572688E−06	6.32779781570E−05	6.33E−05	2	2	−1	0	−1	6	−9.06E−07
2.56808837322	−3.22503237248E−07	6.29799538494E−05	6.30E−05	−3	6	2	0	1	12	−7.43E−07
0.70079476312	9.84685095663E−06	−5.70172128806E−05	5.79E−05	−3	4	0	0	3	10	5.11E−08
3.82503051749	3.79951259667E−05	−3.99656672370E−05	5.51E−05	2	2	−3	0	1	8	−7.16E−07
4.55117827917	5.23327741201E−05	−9.42146772880E−06	5.32E−05	−1	6	0	0	1	8	−1.28E−06
0.85897289547	3.08660636249E−05	−4.33322044081E−05	5.32E−05	−1	2	1	0	16	20	6.89E−05
0.87840517073	−2.73362433751E−05	−3.62382703721E−05	4.54E−05	1	0	−12	−5	−2	20	−3.61E−05
4.68387732034	3.93920826409E−05	2.93893345115E−05	4.91E−05	1	4	−2	0	1	8	−6.87E−07
0.92106437583	−3.25555627393E−05	2.83209740769E−05	4.32E−05	0	1	0	−1	−18	20	−4.84E−05
2.70924074179	−1.96760960640E−05	3.94475946590E−05	4.41E−05	−1	4	1	0	1	7	−1.60E−06
5.75022249274	−4.22685502911E−05	8.50598750911E−06	4.31E−05	3	3	−3	0	0	9	−1.16E−06
1.77558406592	3.33326712151E−05	1.79239466613E−05	3.78E−05	−1	3	0	0	−1	5	−3.52E−07
0.92931687630	−1.03272351611E−05	−3.64307852312E−05	3.79E−05	0	1	0	1	18	20	3.77E−05
3.04098438397	2.12611214652E−05	2.79126334707E−05	3.51E−05	4	−1	−4	0	0	9	−5.04E−07
0.07479106172	−3.44903527052E−05	1.22146523056E−07	3.45E−05	1	−1	0	0	−4	6	1.36E−06
0.78820512789	3.56765000296E−05	−5.37751229718E−07	3.57E−05	−2	3	1	1	13	20	9.71E−05
1.07479604325	1.19713246690E−05	−3.17125369130E−05	3.39E−05	2	−1	0	0	−2	5	−8.11E−07
0.95013822530	−1.17152065460E−05	−2.95053250873E−05	3.17E−05	1	0	−4	−4	9	18	5.26E−07
1.75909561820	−2.25640187122E−05	−2.37000568921E−05	3.27E−05	−1	3	−1	−2	0	7	8.12E−08
1.98308844057	−5.20568672527E−06	−2.71757521633E−05	2.77E−05	2	0	−2	0	−1	5	1.57E−06

Table C.2: Fourier analysis of the c_2 function in the Earth–Moon case.

f_l	A_l^c	A_l^s	A_l	k_l^1	k_l^2	k_l^3	k_l^4	k_l^5	$\|k_l\|$	$f_l - k_l\omega$
0.00000000000	−6.69060194679E−09	0.00000000000E+00	0.00E+00	0	0	0	0	0	0	0.00E+00
0.92519578633	−2.08103238269E+00	−6.13442419291E−01	2.17E+00	0	1	0	0	0	1	−2.11E−07
1.91674083004	1.47778923754E−01	−9.89043356525E−02	1.78E−01	1	1	−1	0	0	3	−3.89E−07
0.85039537678	−7.35157689775E−02	−1.85982826047E−02	7.58E−02	−1	2	0	0	1	4	−1.92E−07
0.06634926261	−1.84248845643E−02	4.26593425274E−02	4.65E−02	1	−1	−1	0	0	3	3.86E−08
1.78404231457	5.63768935330E−03	−3.37239534583E−02	3.42E−02	−1	3	1	0	0	5	−4.56E−07
2.77558735933	1.56548442710E−02	1.81832380635E−02	2.40E−02	0	3	0	0	0	3	−6.33E−07
2.90828587987	−1.43178677458E−03	1.36424019055E−02	1.37E−02	2	1	−2	0	0	5	−5.61E−07
1.84194060336	5.94066139233E−03	−4.30858282343E−03	7.34E−03	0	2	−1	0	1	4	−1.87E−07
1.08284144951	−3.53987678055E−03	−1.75478096993E−03	3.95E−03	2	−1	0	2	0	5	−2.30E−07
0.99999608598	3.36805943382E−03	1.13474357362E−03	3.55E−03	1	0	0	0	−1	2	−3.40E−07
3.76713240393	−3.69822504600E−03	6.09357266032E−05	3.70E−03	1	3	−1	0	0	5	−8.10E−07
1.70924216643	3.43306609402E−04	−2.65580617619E−03	2.68E−03	−2	4	1	0	1	8	−1.76E−07
2.70078684157	1.66037784063E−03	1.78144503430E−03	2.44E−03	−1	4	0	0	1	6	−7.22E−07
0.77559511787	−2.14710976867E−03	−4.57210066527E−04	2.20E−03	−2	3	0	0	2	7	−2.27E−08
1.05789429444	8.19959186171E−04	1.61887055560E−03	1.81E−03	2	−1	−2	0	0	5	−1.51E−07
0.14114984132	−5.16667985576E−04	1.07593090188E−03	1.19E−03	2	−2	−1	0	−1	6	1.89E−07
1.99154129484	−9.98441492896E−04	6.12712412342E−04	1.17E−03	2	0	−1	0	−1	4	−3.53E−07
3.89983092216	−7.23194051763E−04	−7.42981705411E−04	1.04E−03	3	1	−3	0	0	7	−7.40E−07
1.85039170219	5.19759664007E−04	−8.04287495147E−04	9.58E−04	0	2	0	0	0	2	−2.93E−07
3.63443388590	−4.87125677594E−04	5.34619147885E−04	7.23E−04	−1	5	1	0	0	7	−8.80E−07
2.83348530824	−4.20188745840E−05	6.48447333205E−04	6.50E−04	1	2	−2	0	1	6	−7.04E−07
1.94168801639	−2.01690620802E−04	5.71267646297E−04	6.06E−04	1	1	1	2	0	5	−4.36E−07
2.64288884115	5.16411039850E−04	2.30507636537E−05	5.17E−04	−2	5	2	0	0	9	−7.03E−07
4.75867745004	2.67166148391E−04	−3.31821601079E−04	4.26E−04	2	3	−2	0	0	7	−9.85E−07
3.69233205026	−4.02103527563E−04	2.20667737844E−05	4.03E−04	0	4	−1	0	1	6	−7.35E−07
4.62597893287	−4.39982267533E−05	−3.17985028852E−04	3.21E−04	0	5	0	0	0	5	−1.05E−06
2.04943934059	−2.86195080490E−04	−6.56571998810E−05	2.94E−04	3	−1	−3	0	0	7	−3.26E−07
0.09129639705	−7.16445449641E−05	−3.00381875874E−04	3.09E−04	1	−1	1	2	0	5	−6.08E−08
2.85038749272	−1.82692994943E−04	−2.28764028381E−04	2.93E−04	1	2	0	0	−1	4	−9.28E−07
1.85884282415	−5.56540946513E−05	2.67045551329E−04	2.73E−04	0	2	1	0	−1	4	−3.75E−07
2.07438649178	2.26815124643E−04	−1.00273289385E−04	2.48E−04	3	−1	−1	2	0	7	−4.09E−07
1.76713975228	1.86810707270E−04	−1.47740726023E−04	2.38E−04	−1	3	−1	0	2	7	−6.10E−07
0.79249728138	1.94471368911E−04	−1.13605156901E−04	2.25E−04	−2	3	2	0	0	7	−2.68E−07
0.76755012789	−2.07804780484E−04	−2.36073068497E−05	2.09E−04	−2	3	0	−2	0	7	−1.88E−07
2.98308653436	2.31614097072E−05	−1.58387930928E−04	1.60E−04	3	0	−2	0	−1	6	−3.35E−07
2.62598647994	1.10533921097E−04	1.09801089455E−04	1.56E−04	−2	5	0	0	2	9	−6.56E−07
2.84193688002	4.37500930417E−05	1.40506546876E−04	1.47E−04	1	2	−1	0	0	4	−3.36E−07
0.99154557296	1.04874476457E−04	8.83339112201E−05	1.37E−04	1	0	−1	0	0	2	3.51E−07
1.92518236335	−7.73344192492E−05	1.21048507356E−04	1.44E−04	1	1	0	0	−4	6	6.62E−07

Table C.2: (continued)

f_l	A_l^c	A_l^s	A_l	k_l^1	k_l^2	k_l^3	k_l^4	k_l^5	$\|k_l\|$	$f_l - k_l\omega$
1.63444105775	1.17316169732E−05	−1.37250560288E−04	1.38E−04	−3	5	1	0	2	11	−8.56E−07
1.15764188875	−1.16758589093E−04	−6.36957769010E−05	1.33E−04	3	−2	0	2	−1	8	−2.19E−07
3.55963358475	−6.82591428843E−05	8.09507487588E−05	1.06E−04	−2	6	1	0	1	10	−7.53E−07
0.98309392752	4.72468926974E−05	8.49580577255E−05	9.72E−05	1	0	−2	0	1	4	−8.95E−08
1.13269454580	3.57707565531E−05	7.78080580926E−05	8.56E−05	3	−2	−2	0	−1	8	−3.28E−07
0.00845139102	3.07372495670E−05	7.99153552907E−05	8.56E−05	0	0	1	0	−1	2	1.87E−07
0.85667925660	5.42041228168E−05	5.62886970508E−05	7.81E−05	1	0	−16	−2	−1	20	−3.04E−06
4.89137596570	7.72995796986E−05	−6.00835760277E−06	7.75E−05	4	1	−4	0	0	9	−9.18E−07
0.99368987435	6.80820698338E−05	−2.47538844521E−05	7.24E−05	0	1	10	−4	5	20	3.57E−06
5.61752397501	5.43544558703E−05	3.38377582417E−05	6.40E−05	1	5	−1	0	0	7	−1.23E−06
0.83161614019	4.06781758845E−07	−6.16327472408E−05	6.16E−05	−2	3	9	−5	1	20	2.58E−05
3.84193276517	6.32511818071E−05	1.39328742897E−06	6.33E−05	2	2	−1	0	−1	6	−8.77E−07
0.70079455470	−5.81108814028E−05	−9.95295573976E−06	5.90E−05	−3	4	0	0	3	10	−1.57E−07
2.56808837326	6.31213546372E−05	3.23326162216E−07	6.31E−05	−3	6	2	0	1	12	−7.43E−07
0.85895856940	−5.22584798038E−05	−3.10498111850E−05	6.08E−05	−1	2	1	0	16	20	5.46E−05
3.82503051818	−4.00554803608E−05	−3.80807259644E−05	5.53E−05	2	2	−3	0	1	8	−7.15E−07
4.55117827594	−9.42879903626E−06	−5.23663095418E−05	5.32E−05	−1	6	0	0	1	8	−1.28E−06
0.87840517268	−3.64612185758E−05	2.75036574637E−05	4.57E−05	1	0	−12	−5	−2	20	−3.61E−05
4.68387732037	2.94147120321E−05	−3.94259543654E−05	4.92E−05	1	4	−2	0	1	8	−6.86E−07
0.92106449259	2.83731922032E−05	3.27059258332E−05	4.33E−05	0	1	0	−1	−18	20	−4.83E−05
2.70924074401	3.94712853588E−05	1.96884587744E−05	4.41E−05	−1	4	1	0	1	7	−1.60E−06
5.75022249277	8.51114689521E−06	4.22936129318E−05	4.31E−05	3	3	−3	0	0	9	−1.16E−06
1.77558402408	1.78544957566E−05	−3.32228575311E−05	3.77E−05	−1	3	0	0	−1	5	−3.94E−07
0.22399475718	2.19291001908E−05	−3.34446601846E−05	4.00E−05	3	−3	−1	2	0	9	−1.49E−07
1.07479609830	−3.56801737639E−05	−1.35029307970E−05	3.81E−05	2	−1	0	0	−2	5	−7.56E−07
0.07479371116	3.16273337164E−07	−3.62067080278E−05	3.62E−05	1	−1	0	0	−3	5	4.31E−07
0.92931706129	−3.65481037822E−05	1.02866353914E−05	3.80E−05	0	1	0	1	18	20	3.79E−05
0.78820509888	−5.42823874818E−07	−3.58993863796E−05	3.59E−05	−2	3	1	1	13	20	9.70E−05
3.04098438273	2.57496423087E−05	−1.96141294193E−05	3.24E−05	4	−1	−4	0	0	9	−5.06E−07
1.75909563274	−2.30048302843E−05	2.18984956824E−05	3.18E−05	−1	3	−1	−2	0	7	9.57E−08
0.95013782809	−2.71894147140E−05	1.08560888150E−05	2.93E−05	1	0	−4	−4	9	18	1.29E−07

Table C.3: Fourier analysis of the c_3 function in the Earth–Moon case.

f_l	A_l^c	A_l^s	A_l	k_l^1	k_l^2	k_l^3	k_l^4	k_l^5	$\|k_l\|$	$f_l - k_l\omega$
0.00000000000	−1.41391624431E−07	0.00000000000E+00	0.00E+00	0	0	0	0	0	0	0.00E+00
0.07882283209	1.65129188649E−02	−1.89806776179E−01	1.91E−01	1	−1	0	1	0	3	−8.87E−09
0.15362345869	8.33621582882E−04	−6.51608735752E−03	6.57E−03	2	−2	0	1	−1	6	1.89E−07
0.91272221273	−4.27672165735E−03	−2.97357058176E−03	5.21E−03	0	1	−1	−1	0	3	−1.68E−07
1.07036787667	3.70099062228E−03	3.66945459845E−03	5.21E−03	2	−1	−1	1	0	5	−1.86E−07
0.78002369686	−1.07260772392E−03	2.26147319359E−04	1.10E−03	−2	3	1	−1	0	7	−2.36E−07
0.93766935941	1.08547184161E−03	−3.71888565840E−05	1.09E−03	0	1	1	1	0	3	−2.55E−07
1.92921440450	−2.43197278645E−04	3.13293384083E−04	3.97E−04	1	1	0	1	0	3	−4.31E−07
1.77156873957	1.68764438879E−04	−3.19061397781E−04	3.61E−04	−1	3	0	−1	0	5	−4.14E−07
0.00402218336	−1.54002140911E−05	3.31300055196E−04	3.32E−04	0	0	0	1	1	2	−2.29E−07
1.90426726120	2.73607073938E−04	−7.53915633969E−05	2.84E−04	1	1	−2	−1	0	5	−3.41E−07
2.06191292066	−2.83381722882E−04	2.70997465732E−05	2.85E−04	3	−1	−2	1	0	7	−3.63E−07
0.05387572603	1.85346701099E−04	−2.07607303241E−04	2.78E−04	1	−1	−2	−1	0	5	1.19E−07
0.83792177167	−1.79476696083E−04	−1.14611543575E−04	2.13E−04	−1	2	−1	−1	1	6	−1.80E−07
0.22842390460	3.12697229285E−05	−1.85938023676E−04	1.89E−04	3	−3	0	1	−2	9	2.07E−07
1.14516815726	1.05223966858E−04	1.12633389177E−04	1.54E−04	3	−2	−1	1	−1	8	−3.34E−07
0.07480318375	8.89008076597E−05	−2.76548656160E−06	8.89E−05	1	−1	0	0	0	2	−8.19E−07
0.70522330073	−8.40364542539E−05	2.11601703817E−05	8.67E−05	−3	4	1	−1	1	10	−2.03E−07
2.76311379200	2.24174258219E−05	5.45551681753E−05	5.90E−05	0	3	−1	−1	0	5	−5.83E−07
2.92075944712	−1.30892284939E−05	−5.95464884695E−05	6.10E−05	2	1	−1	1	0	5	−6.10E−07
0.86286898456	4.53619420419E−05	−3.30451500664E−06	4.55E−05	−1	2	1	1	1	6	−2.01E−07
0.21152103150	3.29470715251E−05	−2.61161694662E−05	4.20E−05	3	−3	−2	1	0	9	−2.57E−07
1.69676853402	1.66059660683E−05	−3.44732946823E−05	3.83E−05	−2	4	0	−1	1	8	−1.91E−07
0.98752246425	2.75952346653E−05	2.07779909894E−05	3.45E−05	1	0	−1	−1	−1	4	−3.45E−07
1.01246970438	2.99609444339E−05	1.21118028516E−07	3.00E−05	1	0	1	1	−1	4	−3.38E−07
0.84637310372	−2.72072488623E−05	−5.52059724270E−06	2.78E−05	−1	2	0	−1	0	4	−5.28E−08
1.00401874181	2.58124113020E−05	1.01371658955E−05	2.77E−05	1	0	0	1	0	2	−9.66E−08
1.85441423986	−1.63357434395E−05	2.27380033473E−05	2.80E−05	0	2	0	1	1	4	−1.68E−07
0.99556772201	1.78522824142E−05	1.64330442345E−05	2.43E−05	1	0	−1	1	1	4	8.81E−08
1.09531495627	−1.91740914228E−05	−2.68124551197E−06	1.94E−05	2	−1	1	3	0	7	−3.40E−07

Table C.3: (continued)

f_l	A_l^c	A_l^s	A_l	k_l^1	k_l^2	k_l^3	k_l^4	k_l^5	$\|k_l\|$	$f_l - k_l\omega$
2.89581231904	−7.14840108044E−06	1.57717180188E−05	1.73E−05	2	1	−3	−1	0	7	−5.04E−07
3.05345796678	9.83357156690E−06	−1.44042440703E−05	1.74E−05	4	−1	−3	1	0	9	−5.39E−07
1.82946700626	1.27244562339E−05	−4.03272295341E−06	1.33E−05	0	2	−2	−1	1	6	−1.67E−07
0.01247355131	3.76785612705E−06	1.16454453678E−05	1.22E−05	0	0	1	1	0	2	−6.56E−08
2.78806092755	−9.95195809787E−06	−5.95246344045E−06	1.16E−05	0	3	1	1	0	5	−6.82E−07
1.63887022472	−3.68937570758E−06	−1.08131073000E−05	1.14E−05	−3	5	2	−1	0	11	−4.81E−07
1.79651589740	1.72047264987E−06	1.09949641348E−05	1.11E−05	−1	3	2	1	0	7	−4.90E−07
2.63041526638	1.03274181954E−05	3.95218551934E−06	1.11E−05	−2	5	1	−1	0	9	−6.61E−07
1.04542073532	1.56929729941E−06	1.05332084899E−05	1.06E−05	2	−1	−3	−1	0	7	−9.32E−08
2.00401490831	−6.53150996540E−06	7.76351743764E−06	1.01E−05	2	0	0	1	−1	4	−3.56E−07
0.85482363678	8.66655396082E−06	−1.50567256134E−06	8.80E−06	−1	2	1	−1	−1	6	−7.24E−07
0.12867636242	5.27843669813E−06	−5.43363042093E−06	7.58E−06	2	−2	−2	−1	−1	8	3.27E−07
0.01032838748	−4.31750283561E−06	4.91979830811E−06	6.55E−06	1	−1	−10	5	−3	20	−1.13E−05
2.68831322944	2.71561250282E−06	5.92501264482E−06	6.52E−06	−1	4	−1	−1	1	8	−7.18E−07
0.76312187241	−5.92636702789E−06	−3.49438110641E−06	6.88E−06	−2	3	−1	−1	2	9	3.49E−07
2.13671337285	−6.99079745142E−06	3.91421215994E−07	7.00E−06	4	−2	−2	1	−1	10	−3.40E−07
3.75465883357	−5.91388181368E−06	−1.85819901236E−06	6.20E−06	1	3	−2	−1	0	7	−7.63E−07
3.91230449343	5.62061870306E−06	2.91171617063E−06	6.33E−06	3	1	−2	1	0	7	−7.85E−07
0.14732397123	3.31100613301E−06	5.67102602595E−06	6.57E−06	0	0	16	3	−1	20	−5.43E−06
0.14516151179	2.93966084666E−06	−5.24112782175E−06	6.01E−06	2	−2	−1	1	−3	9	1.69E−07
3.77960597917	5.23287820170E−06	−1.83559797441E−06	5.55E−06	1	3	0	1	0	5	−8.52E−07
3.62196032482	−4.70264389647E−06	2.63584079152E−06	5.39E−06	−1	5	0	−1	0	7	−8.24E−07
0.17240241859	−5.02625528012E−06	−1.93088183641E−06	5.38E−06	2	−2	−3	12	−1	20	−6.37E−05
0.30322396832	1.01239980774E−06	−4.93809351615E−06	5.04E−06	4	−4	0	1	−3	12	−1.58E−07
0.63042306441	−4.30829432810E−06	1.26047389061E−06	4.49E−06	−4	5	1	−1	2	13	−1.11E−08
1.84636921092	−2.13829040280E−06	3.68403897944E−06	4.26E−06	0	2	0	−1	−1	4	−3.72E−07
2.84595897287	−1.14977732228E−06	−4.39455978492E−06	4.54E−06	1	2	−1	1	1	6	−6.56E−07
0.07084658749	−1.32257614976E−06	3.66740083483E−06	3.90E−06	1	−1	0	−1	17	20	6.64E−07
0.92121047321	3.32897838341E−06	1.80097731218E−06	3.78E−06	−1	2	6	5	−1	15	−8.11E−07
0.12559267841	2.97799400653E−06	−2.41342894957E−06	3.83E−06	0	0	12	6	2	20	1.52E−05
1.21996826630	2.62250686885E−06	3.02525726671E−06	4.00E−06	4	−3	−1	1	−2	11	−6.53E−07
0.23646805584	−8.91224052428E−07	3.39432751678E−06	3.51E−06	3	−3	0	3	0	9	−4.67E−07
1.97906770169	−3.22548624714E−06	7.54617691232E−07	3.31E−06	2	0	−2	−1	−1	6	−3.29E−07

Table C.4: Fourier analysis of the c_4 function in the Earth–Moon case.

f_l	A_l^c	A_l^s	A_l	k_l^1	k_l^2	k_l^3	k_l^4	k_l^5	$\|k_l\|$	$f_l - k_l\omega$
0.00000000000	5.69258520818E−12	0.00000000000E+00	0.00E+00	0	0	0	0	0	0	0.00E+00
0.99154505158	8.29312818040E−02	6.90594554837E−02	1.08E−01	1	0	−1	0	0	2	−1.70E−07
1.85039157297	−1.59855561906E−02	2.47583666135E−02	2.95E−02	0	2	0	0	0	2	−4.22E−07
0.85884652974	1.67379008687E−02	−2.03538562041E−03	1.69E−02	−1	2	1	0	0	4	−2.44E−07
1.98309009374	−8.67558194562E−03	1.59743794050E−03	8.82E−03	2	0	−2	0	0	4	−3.49E−07
2.84193661725	−1.13437968478E−03	−3.62678210826E−03	3.80E−03	1	2	−1	0	0	4	−5.99E−07
1.77559111021	−9.83411685349E−04	1.66244731351E−03	1.93E−03	−1	3	0	0	1	5	−4.56E−07
2.97463513494	3.32702813179E−04	−5.91697263186E−04	6.79E−04	3	0	−3	0	0	6	−5.29E−07
2.70923810004	−6.42274853037E−04	−3.12072836643E−04	7.14E−04	−1	4	1	0	0	6	−6.68E−07
0.78404586971	6.30043768779E−04	−1.02605170318E−04	6.38E−04	−2	3	1	0	1	7	−4.75E−07
0.91674491443	4.87250400233E−04	3.75982197195E−04	6.15E−04	0	1	−1	0	1	3	1.21E−07
1.06634556273	−4.33955866827E−04	−3.91494270207E−04	5.84E−04	2	−1	−1	0	−1	5	−8.72E−08
0.92519583107	5.03784551164E−04	1.48616536954E−04	5.25E−04	0	1	0	0	0	1	−1.66E−07
1.01649220427	−4.20014027252E−04	−2.21144199403E−05	4.21E−04	1	0	1	2	0	4	−2.51E−07
3.83348166144	3.65674483436E−04	1.50825201000E−04	3.96E−04	2	2	−2	0	0	6	−7.76E−07
3.70078314515	3.51159321364E−04	−1.58573311046E−04	3.85E−04	0	4	0	0	0	4	−8.45E−07
1.92519179753	1.84773719973E−04	−2.63670140967E−04	3.22E−04	1	1	0	0	−1	3	−6.26E−07
2.76713632148	−9.23378252333E−05	−2.60052648396E−04	2.76E−04	0	3	−1	0	1	5	−4.66E−07
1.71769305450	6.70614923558E−05	2.71624147662E−04	2.80E−04	−2	4	2	0	0	8	−4.92E−07
0.93364709822	−1.19541040936E−04	9.68816359057E−06	1.20E−04	0	1	1	0	−1	3	−1.04E−07
1.90828958176	−1.01569901478E−04	2.28876021128E−05	1.04E−04	1	1	−2	0	1	5	−4.33E−07
0.13269851619	−7.10058903144E−05	6.68741105560E−05	9.75E−05	2	−2	−2	0	0	6	6.82E−08
2.05789024161	9.15159940257E−05	−1.33417420819E−05	9.25E−05	3	−1	−2	0	−1	7	−6.30E−07
1.91674095806	−7.69296156723E−05	5.14261794575E−05	9.25E−05	1	1	−1	0	0	3	−2.61E−07
1.12424356617	−5.48139799797E−06	−8.96405072839E−05	8.98E−05	3	−2	−3	0	0	8	−1.03E−07
1.70079079393	−4.21751108077E−05	7.79545524388E−05	8.86E−05	−2	4	0	0	2	8	−3.44E−07
0.99998863023	−8.35547718548E−05	−2.51035175322E−05	8.72E−05	1	0	0	0	−3	4	−6.48E−07
2.63443786699	−7.13693831406E−05	−3.14223239666E−05	7.80E−05	−2	5	1	0	1	9	−4.73E−07

Table C.4: (continued)

f_l	A_l^c	A_l^s	A_l	k_l^1	k_l^2	k_l^3	k_l^4	k_l^5	$\lvert k_l \rvert$	$f_l - k_l\omega$
4.69232818958	−1.89983786838E−05	6.85986722270E−05	7.12E−05	1	4	−1	0	0	6	−1.02E−06
2.91673702305	1.56984107763E−05	5.80705902926E−05	6.02E−05	2	1	−1	0	−1	5	−6.22E−07
1.14919073360	−3.48979290285E−05	−4.12035019781E−05	5.40E−05	3	−2	−1	2	0	8	−1.70E−07
3.96618017455	1.82356277479E−05	4.78277747740E−05	5.12E−05	4	0	−4	0	0	8	−7.11E−07
3.62598256632	4.50035705721E−05	−2.25433248131E−05	5.03E−05	−1	5	0	0	1	7	−9.95E−07
4.82502670768	−3.32657461013E−05	1.75408926184E−05	3.76E−05	3	2	−3	0	0	8	−9.52E−07
1.78404602877	−6.51927989981E−06	3.43864713625E−05	3.50E−05	−1	3	1	0	1	6	−3.16E−07
3.75868102278	2.94173830466E−05	1.07709699534E−05	3.13E−05	1	3	−2	0	1	7	−9.87E−07
1.64289264852	6.40150293653E−06	2.22012156996E−05	2.31E−05	−3	5	2	0	1	11	−4.70E−07
0.70924540702	1.85960068168E−05	−3.78209782003E−06	1.90E−05	−3	4	1	0	2	10	−5.09E−07
0.83389953731	−1.78052037539E−05	−1.02333734402E−05	2.05E−05	−1	2	−1	−2	0	6	−2.24E−09
0.07480035535	−7.01789009483E−07	1.81812418915E−05	1.82E−05	1	−1	0	0	−1	3	−7.31E−08
1.99153897762	1.23884290431E−05	−7.70680691288E−06	1.46E−05	2	0	−1	0	−2	5	9.04E−07
3.56808462838	4.64454761812E−06	−1.35035965570E−05	1.43E−05	−2	6	2	0	0	10	−9.13E−07
2.86688391328	1.12459120695E−05	8.14339107788E−06	1.39E−05	1	2	1	2	0	6	−5.37E−07
4.55962967174	7.10217278133E−06	1.17099428726E−05	1.37E−05	−1	6	1	0	0	8	−1.09E−06
2.69233642245	−5.03758394471E−06	−1.27356301464E−05	1.37E−05	−1	4	−1	0	2	8	6.30E−08
2.11578861411	1.04948628922E−05	7.70526119749E−06	1.30E−05	4	−2	−4	0	0	10	−2.77E−07
2.89983478885	5.49303841618E−06	−1.07137701306E−05	1.20E−05	2	1	−3	0	1	7	−4.47E−07
1.00844351252	−1.24287524256E−05	8.58260657781E−07	1.25E−05	1	0	1	0	−3	5	−5.44E−07
2.78403856475	1.08549597986E−05	5.80939190056E−06	1.23E−05	0	3	1	0	−1	5	−6.32E−07
1.87533964054	−7.23315183407E−07	−1.14247198873E−05	1.14E−05	0	2	2	2	0	6	4.12E−07
2.77558724978	8.05881460213E−06	9.36814891652E−06	1.24E−05	0	3	0	0	0	3	−7.43E−07
2.90828617867	1.12754209694E−06	−1.06000818559E−05	1.07E−05	2	1	−2	0	0	5	−2.62E−07
3.04943549784	−5.56886022302E−06	9.06384155744E−06	1.06E−05	4	−1	−3	0	−1	9	−5.95E−07
1.05788851103	−4.69455465425E−06	−8.55344449205E−06	9.76E−06	2	−1	−2	0	−2	7	1.21E−06
5.68387323721	−5.52405713382E−06	−7.96698964867E−06	9.69E−06	2	4	−2	0	0	8	−1.20E−06
2.00803713924	−6.34952837799E−06	6.86566203020E−06	9.35E−06	2	0	0	2	0	4	−5.38E−07
0.84194494406	7.53035053307E−06	5.38874653268E−06	9.26E−06	−1	2	−1	0	2	6	5.80E−07
4.61752778262	−2.26852749876E−06	9.64188312665E−06	9.91E−06	0	5	−1	0	1	7	−1.00E−06
0.15764566683	−1.56621823023E−06	8.93245023735E−06	9.07E−06	2	−2	0	2	0	6	−1.51E−08
3.77558379863	−7.69430333804E−06	3.10747393377E−06	8.30E−06	1	3	0	0	−1	5	−6.20E−07
2.14073570044	8.08187751910E−06	−7.10311454171E−08	8.08E−06	4	−2	−2	2	0	10	−4.24E−07
3.90828224509	−7.48795085991E−06	−3.44752191789E−06	8.24E−06	3	1	−2	0	−1	7	−6.21E−07
0.99573453469	4.65850734281E−06	6.12989858827E−06	7.70E−06	0	1	5	7	7	20	1.08E−04
1.14114597284	−4.96572505631E−06	−4.84311487044E−06	6.94E−06	3	−2	−1	0	−2	8	−1.06E−07
0.20749882044	−5.00117260573E−06	4.36223014901E−06	6.64E−06	3	−3	−2	0	−1	9	−5.61E−08
5.55117471845	−5.50687453407E−06	−8.27552411974E−07	5.57E−06	0	6	0	0	0	6	−1.27E−06
2.55963667065	−4.91417155735E−06	−1.91149007145E−06	5.27E−06	−3	6	1	0	2	12	−1.24E−06
1.08284044368	−4.01849139912E−06	−1.95891304252E−06	4.47E−06	2	−1	0	2	0	5	−1.24E−06
2.57653958792	−4.11676976502E−06	1.56388748277E−06	4.40E−06	−3	6	3	0	0	12	−7.32E−07
1.69274572021	−1.51255835578E−06	3.59431392651E−06	3.90E−06	−2	4	0	−2	0	8	−5.93E−07
1.82544916188	3.85062231348E−06	−1.30708775583E−06	4.07E−06	0	2	−2	−2	1	7	8.27E−07
4.95772522920	−3.61226335289E−06	−1.23786067268E−06	3.82E−06	5	0	−5	0	0	10	−8.78E−07
3.55118217058	3.48286485441E−06	−1.91413417641E−06	3.97E−06	−2	6	0	0	2	10	−9.62E−07
0.79250294631	3.28156966126E−06	−1.78893552705E−06	3.74E−06	−2	3	2	0	2	9	−1.75E−06
1.62598688715	−1.46092271866E−06	3.15163604831E−06	3.47E−06	−3	5	0	0	2	10	−2.48E−07
1.19904412046	−7.34810480685E−08	−3.41794990606E−06	3.42E−06	4	−3	−3	0	−1	11	2.25E−08
1.79249330162	−6.87749096117E−07	−3.32041416969E−06	3.39E−06	−1	3	2	0	−1	7	−6.74E−07
5.81657175340	7.04451225438E−07	−3.31964786630E−06	3.39E−06	4	2	−4	0	0	10	−1.13E−06
4.75022625415	−2.78566837152E−06	1.61074466444E−06	3.22E−06	2	3	−3	0	1	9	−9.77E−07
1.85882993466	4.16180661397E−07	−2.89866123031E−06	2.93E−06	1	1	−5	−6	6	19	−5.84E−07
2.85037248271	1.93795831811E−06	2.09952811403E−06	2.86E−06	2	1	−6	−6	5	20	3.16E−07
0.98750599511	9.73950054944E−07	−2.30023048331E−06	2.50E−06	1	0	−1	−1	−6	9	1.06E−06
4.48482931269	1.33200205902E−06	2.01589960261E−06	2.42E−06	−2	7	1	0	1	11	−1.02E−06
1.70920430077	2.39266045306E−07	2.38004459063E−06	2.39E−06	−1	3	−5	−6	1	16	−3.43E−07

Table C.5: Fourier analysis of the c_5 function in the Earth–Moon case.

f_l	A_l^c	A_l^s	A_l	k_l^1	k_l^2	k_l^3	k_l^4	k_l^5	$\lvert k_l \rvert$	$f_l - k_l\omega$
0.00000000000	2.00002531222E+00	0.00000000000E+00	0.00E+00	0	0	0	0	0	0	0.00E+00
0.99154503470	−1.39262526978E−01	1.67268469653E−01	2.18E−01	1	0	−1	0	0	2	−1.87E−07
1.85039156826	−3.60764692902E−02	−2.32919068442E−02	4.29E−02	0	2	0	0	0	2	−4.27E−07
0.85884653189	4.60700119614E−03	3.78883517587E−02	3.82E−02	−1	2	1	0	0	4	−2.42E−07
1.98309007298	−2.68306511802E−03	−1.45621710605E−02	1.48E−02	2	0	−2	0	0	4	−3.70E−07

Table C.5: (continued)

f_l	A_l^c	A_l^s	A_l	k_l^1	k_l^2	k_l^3	k_l^4	k_l^5	$\lvert k_l \rvert$	$f_l - k_l\omega$
2.84193660358	5.11831718890E−03	−1.60131441069E−03	5.36E−03	1	2	−1	0	0	4	−6.13E−07
1.77559105182	−2.45250369261E−03	−1.44994031463E−03	2.85E−03	−1	3	0	0	1	5	−5.15E−07
0.78404613976	2.48070111393E−04	1.53843288507E−03	1.56E−03	−2	3	1	0	1	7	−2.05E−07
0.91674466299	−7.96904617992E−04	1.03615142247E−03	1.31E−03	0	1	−1	0	1	3	−1.30E−07
0.92519587725	−3.17428122603E−04	1.07511143482E−03	1.12E−03	0	1	0	0	0	1	−1.20E−07
2.97463510080	9.11159641497E−04	5.12115111071E−04	1.05E−03	3	0	−3	0	0	6	−5.64E−07
1.06634564227	7.56547334654E−04	−8.38553005289E−04	1.13E−03	2	−1	−1	0	−1	5	−7.66E−09
2.70923810214	4.47023359972E−04	−9.19991167575E−04	1.02E−03	−1	4	1	0	0	6	−6.66E−07
1.01649216639	4.36707007591E−05	−8.32487891521E−04	8.34E−04	1	0	1	2	0	4	−2.89E−07
3.83348163818	−2.07293619318E−04	5.02761410358E−04	5.44E−04	2	2	−2	0	0	6	−8.00E−07
3.70078313673	2.10196157149E−04	4.65419755642E−04	5.11E−04	0	4	0	0	0	4	−8.53E−07
1.71769305309	−4.97258344562E−04	1.22769448777E−04	5.12E−04	−2	4	2	0	0	8	−4.94E−07
0.07480022695	−4.80719057617E−04	−1.83089058972E−05	4.81E−04	1	−1	0	0	−1	3	−2.02E−07
1.92519202224	3.79217664229E−04	2.66359541480E−04	4.63E−04	1	1	0	0	−1	3	−4.01E−07
2.76713592402	3.69924980801E−04	−1.32377207938E−04	3.93E−04	0	3	−1	0	1	5	−8.64E−07
0.13269849998	−1.86639333771E−04	−1.98137830013E−04	2.72E−04	2	−2	−2	0	0	6	5.19E−08
0.93364712167	−2.07358784210E−05	−2.55493044788E−04	2.56E−04	0	1	1	0	−1	3	−8.02E−08
0.99997255631	3.62018627833E−05	−1.73565732903E−04	1.77E−04	2	−1	−6	−6	3	18	−4.67E−07
1.90828957561	−3.92893685937E−05	−1.74568822220E−04	1.79E−04	1	1	−2	0	1	5	−4.39E−07
1.91674112230	−8.73915270715E−05	−1.30986309714E−04	1.57E−04	1	1	−1	0	0	3	−9.66E−08
2.05789060404	2.16574958687E−05	1.50727691953E−04	1.52E−04	3	−1	−2	0	−1	7	−2.67E−07
1.12424353662	1.43818624168E−04	−8.81906866549E−06	1.44E−04	3	−2	−3	0	0	8	−1.33E−07
1.70079090059	−1.16866785487E−04	−6.32838032291E−05	1.33E−04	−2	4	0	0	2	8	−2.37E−07
0.15764565046	−1.22741918961E−04	−2.15106467326E−05	1.25E−04	2	−2	0	2	0	6	−3.15E−08
2.63443738603	4.51151605299E−05	−1.03242858325E−04	1.13E−04	−2	5	1	0	1	9	−9.54E−07
1.14919069284	7.76571422819E−05	−6.58014246897E−05	1.02E−04	3	−2	−1	2	0	8	−2.11E−07
4.69232817345	−8.92862215261E−05	−2.47193231990E−05	9.26E−05	1	4	−1	0	0	6	−1.04E−06
2.91673693109	−8.13369600914E−05	2.20463130634E−05	8.43E−05	2	1	−1	0	−1	5	−7.14E−07
3.96618013709	−6.98398107877E−05	2.66434972479E−05	7.47E−05	4	0	−4	0	0	8	−7.49E−07
3.62598283878	2.98836653007E−05	5.99130602130E−05	6.70E−05	−1	5	0	0	1	7	−7.23E−07
1.78404761389	−5.49100697124E−05	−1.06493909055E−05	5.59E−05	−1	3	1	0	1	6	1.27E−06
0.83389964937	2.59627649456E−05	−4.51088304892E−05	5.20E−05	−1	2	−1	−2	0	6	1.10E−07
0.70924618727	9.86496824234E−06	4.95213601315E−05	5.05E−05	−3	4	1	0	2	10	2.71E−07
4.82502667103	−2.36091997739E−05	−4.47526042520E−05	5.06E−05	3	2	−3	0	0	8	−9.88E−07
1.64289243393	−4.17059205157E−05	1.20836093933E−05	4.34E−05	−3	5	2	0	1	11	−6.84E−07
3.75868136860	−1.49826084235E−05	4.06860797808E−05	4.34E−05	1	3	−2	0	1	7	−6.41E−07
1.99153221996	1.38593274784E−05	2.03905584791E−05	2.47E−05	2	0	−1	0	−4	7	1.29E−06
1.00844456204	−1.58874971007E−06	−2.48120469178E−05	2.49E−05	1	0	1	0	−3	5	5.06E−07
0.84194317573	−1.20486585799E−05	1.71286182619E−05	2.09E−05	−1	2	−1	0	2	6	−1.19E−06
2.86688385130	−1.16357686982E−05	1.60821728759E−05	1.99E−05	1	2	1	2	0	6	−5.99E−07
2.11578859826	−1.15507773200E−05	1.57348901050E−05	1.95E−05	4	−2	−4	0	0	10	−2.93E−07
3.56808463779	1.89933721693E−05	6.53378648668E−06	2.01E−05	−2	6	2	0	0	10	−9.04E−07
2.89983443878	1.67772355217E−05	8.56013873620E−06	1.88E−05	2	1	−3	0	1	7	−7.97E−07
1.87533945757	2.00365232698E−05	−1.29131346626E−06	2.01E−05	0	2	2	2	0	6	2.29E−07
2.69233581561	1.82939360549E−05	−7.31246581406E−06	1.97E−05	−1	4	−1	0	2	8	−5.44E−07
1.05788561422	1.57554375108E−05	−8.86725735594E−06	1.81E−05	2	−1	−2	0	−2	7	−1.68E−06
4.55962965915	−1.53441102618E−05	9.30764351708E−06	1.79E−05	−1	6	1	0	0	8	−1.10E−06
2.78403841529	−8.24662321955E−06	1.54350661046E−05	1.75E−05	0	3	1	0	−1	5	−7.82E−07
0.20749868831	−1.13616718790E−05	−1.30189670718E−05	1.73E−05	3	−3	−2	0	−1	9	−1.88E−07
3.04943547176	−1.37822498103E−05	−8.46626551572E−06	1.62E−05	4	−1	−3	0	−1	9	−6.21E−07
2.90828631382	1.64450569322E−05	1.76184438265E−06	1.65E−05	2	1	−2	0	0	5	−1.27E−07
0.99572699638	−1.08962727848E−05	8.59153863250E−06	1.39E−05	0	1	5	7	7	20	1.00E−04
2.14073567493	1.17373541400E−07	1.31985586204E−05	1.32E−05	4	−2	−2	2	0	10	−4.50E−07
4.61752774410	−1.25941041399E−05	−2.96334027463E−06	1.29E−05	0	5	−1	0	1	7	−1.04E−06
1.14114153793	8.75438674701E−06	−9.39712467292E−06	1.28E−05	3	−2	−1	0	−3	9	−9.66E−07
5.68387320622	1.02361774955E−05	−7.09996538934E−06	1.25E−05	2	4	−2	0	0	8	−1.23E−06
0.06634574152	−1.10740336878E−05	−4.55690794850E−06	1.20E−05	1	−1	−1	0	−1	4	9.16E−08
3.77558328540	−4.12957973347E−06	−1.01462055348E−05	1.10E−05	1	3	0	0	−1	5	−1.13E−06
3.90828180523	4.68738057722E−06	−1.02498756656E−05	1.13E−05	3	1	−2	0	−1	7	−1.06E−06
0.14960108151	−1.07041108372E−05	−8.48459047204E−07	1.07E−05	2	−2	0	0	−2	6	2.25E−07
2.77558306766	−7.55143475528E−06	6.78503355623E−06	1.02E−05	0	3	0	0	−1	4	−1.35E−06
0.79250938126	4.33957433490E−06	8.53439178453E−06	9.57E−06	−2	3	2	0	3	10	1.11E−06
1.08284144849	3.73788081691E−06	−7.57474250383E−06	8.45E−06	2	−1	0	2	0	5	−2.31E−07
0.72614808243	6.71645410170E−06	4.94710710237E−06	8.34E−06	−3	4	3	0	0	10	−2.43E−07
2.55963716572	2.81307414135E−06	−7.16708806083E−06	7.70E−06	−3	6	1	0	2	12	−7.46E−07
2.00803761750	5.62254374942E−06	5.22884178639E−06	7.68E−06	2	0	0	2	0	4	−5.93E−08

Table C.5: (continued)

f_l	A_l^c	A_l^s	A_l	k_l^1	k_l^2	k_l^3	k_l^4	k_l^5	$\|k_l\|$	$f_l - k_l\omega$
1.82544761410	2.47668855633E−06	7.04678852264E−06	7.47E−06	0	2	−2	−2	1	7	−7.21E−07
2.57653956312	−2.59609917296E−06	−6.83150602842E−06	7.31E−06	−3	6	3	0	0	12	−7.57E−07
0.23244459161	−7.46048645668E−06	−1.55038850071E−06	7.62E−06	3	−3	0	2	−1	9	−1.52E−06
5.55117470356	1.04822131913E−06	−6.97909614485E−06	7.06E−06	0	6	0	0	0	6	−1.28E−06
1.79249372596	6.06715372452E−06	−1.24064340363E−06	6.19E−06	−1	3	2	0	−1	7	−2.49E−07
1.19904405268	5.56215852980E−06	−1.23207392920E−07	5.56E−06	4	−3	−3	0	−1	11	−4.53E−08
1.62598632562	−4.82524193301E−06	−2.21518833222E−06	5.31E−06	−3	5	0	0	2	10	−8.10E−07
4.95772516437	1.74065590601E−06	−5.08530016770E−06	5.37E−06	5	0	−5	0	0	10	−9.43E−07
1.69274581115	−4.79961263068E−06	−2.02343750944E−06	5.21E−06	−2	4	0	−2	0	8	−5.02E−07
1.85880317192	4.93935966320E−06	3.99010651585E−08	4.94E−06	0	2	1	0	−12	15	−7.13E−07

Table C.6: Fourier analysis of the c_6 function in the Earth–Moon case.

f_l	A_l^c	A_l^s	A_l	k_l^1	k_l^2	k_l^3	k_l^4	k_l^5	$\|k_l\|$	$f_l - k_l\omega$
0.00000000000	4.35184546580E−11	0.00000000000E+00	0.00E+00	0	0	0	0	0	0	0.00E+00
0.84637295298	1.41671041967E−03	2.86993453344E−04	1.45E−03	−1	2	0	−1	0	4	−2.04E−07
1.00401861552	−1.34572932338E−03	−5.27264980036E−04	1.45E−03	1	0	0	1	0	2	−2.23E−07
0.01247357965	−5.97175993899E−05	−1.79680583333E−04	1.89E−04	0	0	1	1	0	2	−3.73E−08
0.14517208262	8.96762308339E−05	−1.66351495182E−04	1.89E−04	2	−2	−1	1	0	6	1.77E−08
0.77157269571	8.67028940271E−05	1.41402700717E−05	8.78E−05	−2	3	0	−1	1	7	−3.23E−08
0.92921810815	−3.35065025771E−05	−1.16303694795E−05	3.55E−05	0	1	0	1	1	3	−3.02E−07
1.07881913165	−3.21811101671E−05	−1.40909922482E−05	3.51E−05	2	−1	0	1	−1	5	−1.35E−07
0.92117316418	−1.67752610064E−05	−4.06864341536E−06	1.73E−05	0	1	0	−1	−1	3	−4.21E−07
0.21997272479	5.57287416324E−06	−9.40958574481E−06	1.09E−05	3	−3	−1	1	−1	9	2.31E−07
2.85441018360	−5.42761603524E−06	−7.53745595885E−06	9.29E−06	1	2	0	1	0	4	−6.50E−07
2.69676451863	6.83522174704E−06	6.66986908255E−06	9.55E−06	−1	4	0	−1	0	6	−6.33E−07
0.07882273770	6.06084362799E−07	−7.00417513713E−06	7.03E−06	1	−1	0	1	0	3	−1.03E−07
0.08727424077	−1.81385049433E−06	−6.29369941854E−06	6.55E−06	1	−1	1	1	−1	5	1.95E−07
1.70521951753	−4.29148280168E−07	5.41649834747E−06	5.43E−06	−2	4	1	−1	0	8	−4.12E−07
1.86286514653	1.30475372865E−06	−5.05880335167E−06	5.22E−06	0	2	1	1	0	4	−4.65E−07
1.92921439924	−2.69639610010E−06	3.47378094963E−06	4.40E−06	1	1	0	1	0	3	−4.37E−07
1.77156874649	2.05713416681E−06	−3.88855402282E−06	4.40E−06	−1	3	0	−1	0	5	−4.07E−07
0.06232679689	−1.44433280255E−06	3.84107296568E−06	4.10E−06	1	−1	−1	−1	−1	5	−1.46E−08
0.69677182156	3.62334128723E−06	4.37694769096E−07	3.65E−06	−3	4	0	−1	2	10	−4.78E−07
1.13671718122	−1.19014503947E−06	−2.96394468688E−06	3.19E−06	3	−2	−2	1	0	8	−1.05E−07
1.16166429024	−2.23107418092E−06	−1.35868592266E−06	2.61E−06	3	−2	0	3	0	8	−2.30E−07
1.99556366734	1.94941135485E−06	−1.07259380867E−06	2.23E−06	2	0	−1	1	0	4	−3.93E−07
1.83791799116	−1.76212479965E−06	1.41514193352E−06	2.26E−06	0	2	−1	−1	0	4	−3.87E−07
0.71367452075	1.26655023253E−06	−8.94653064437E−07	1.55E−06	−3	4	2	−1	0	10	−1.88E−07
2.62196399961	8.92865661026E−07	8.05169376943E−07	1.20E−06	−2	5	0	−1	1	9	−7.23E−07
0.78002483392	1.06244810252E−06	−2.31916627526E−07	1.09E−06	−2	3	1	−1	0	7	9.01E−07

Table C.7: Fourier analysis of the c_7 function in the Earth–Moon case.

f_l	A_l^c	A_l^s	A_l	k_l^1	k_l^2	k_l^3	k_l^4	k_l^5	$\|k_l\|$	$f_l - k_l\omega$
0.00000000000	1.00478056978E+00	0.00000000000E+00	0.00E+00	0	0	0	0	0	0	0.00E+00
0.99154504274	−1.05600650110E−01	1.26826992087E−01	1.65E−01	1	0	−1	0	0	2	−1.79E−07
0.85884652974	3.92058551530E−03	3.22407546273E−02	3.25E−02	−1	2	1	0	0	4	−2.44E−07
1.85039157284	−1.54636618183E−02	−9.98429642886E−03	1.84E−02	0	2	0	0	0	2	−4.22E−07
1.98309009374	−2.44632884858E−03	−1.32858575697E−02	1.35E−02	2	0	−2	0	0	4	−3.49E−07
2.84193661727	3.14452154764E−03	−9.83537953676E−04	3.29E−03	1	2	−1	0	0	4	−5.99E−07
0.13269851611	9.94318811401E−04	1.05575138924E−03	1.45E−03	2	−2	−2	0	0	6	6.81E−08
0.78404586978	2.24821535313E−04	1.38051798711E−03	1.40E−03	−2	3	1	0	1	7	−4.75E−07
1.77559111013	−1.08376329529E−03	−6.41094169882E−04	1.26E−03	−1	3	0	0	1	5	−4.56E−07
2.97463513459	9.43812864541E−04	5.30689337498E−04	1.08E−03	3	0	−3	0	0	6	−5.30E−07
0.91674491440	−6.24266810578E−04	8.09012155764E−04	1.02E−03	0	1	−1	0	1	3	1.21E−07
0.92519583006	−2.52368102371E−04	8.55498941663E−04	8.92E−04	0	1	0	0	0	1	−1.67E−07
1.06634556274	5.60048250594E−04	−6.20791407218E−04	8.36E−04	2	−1	−1	0	−1	5	−8.72E−08
1.01649220452	3.27278898515E−05	−6.21575632570E−04	6.22E−04	1	0	1	2	0	4	−2.51E−07
2.70923810041	2.80592159028E−04	−5.77482493788E−04	6.42E−04	−1	4	1	0	0	6	−6.68E−07
1.71769305471	−5.09936623145E−04	1.25898469358E−04	5.25E−04	−2	4	2	0	0	8	−4.92E−07
0.07480035406	−4.46737125036E−04	−1.72431561415E−05	4.47E−04	1	−1	0	0	−1	3	−7.44E−08
3.83348166121	−1.59647770116E−04	3.87066302230E−04	4.19E−04	2	2	−2	0	0	6	−7.77E−07

Table C.7: (continued)

f_l	A_l^c	A_l^s	A_l	k_l^1	k_l^2	k_l^3	k_l^4	k_l^5	$\|k_l\|$	$f_l - k_l\omega$
3.70078314470	1.16912147500E−04	2.58898640125E−04	2.84E−04	0	4	0	0	0	4	−8.45E−07
2.76713632199	2.32834961805E−04	−8.26728736626E−05	2.47E−04	0	3	−1	0	1	5	−4.66E−07
0.93364709839	−1.70906358851E−05	−2.10876303159E−04	2.12E−04	0	1	1	0	−1	3	−1.04E−07
1.92519179279	1.56051754448E−04	1.09352748960E−04	1.91E−04	1	1	0	0	−1	3	−6.31E−07
1.90828958191	−3.69781664716E−05	−1.64101588399E−04	1.68E−04	1	1	−2	0	1	5	−4.33E−07
1.91674094402	−8.06227857015E−05	−1.20612265635E−04	1.45E−04	1	1	−1	0	0	3	−2.75E−07
2.05789024063	1.95622380176E−05	1.34179365013E−04	1.36E−04	3	−1	−2	0	−1	7	−6.31E−07
0.99998863487	3.81238384159E−05	−1.26885121225E−04	1.32E−04	1	0	0	0	−3	4	−6.43E−07
0.15764565868	−1.34558102659E−04	−2.35876974526E−05	1.37E−04	2	−2	0	2	0	6	−2.32E−08
3.96618016962	−7.98172593525E−05	3.04353766124E−05	8.54E−05	4	0	−4	0	0	8	−7.16E−07
2.00803725224	5.62378665351E−05	5.20725840742E−05	7.66E−05	2	0	0	2	0	4	−4.25E−07
1.14919073107	5.98915529397E−05	−5.07276572169E−05	7.85E−05	3	−2	−1	2	0	8	−1.72E−07
2.63443786601	2.90003095725E−05	−6.58691654322E−05	7.20E−05	−2	5	1	0	1	9	−4.74E−07
1.70079080375	−5.43275440727E−05	−2.93969125488E−05	6.18E−05	−2	4	0	0	2	8	−3.34E−07
4.69232818955	−5.98069468024E−05	−1.65634989241E−05	6.21E−05	1	4	−1	0	0	6	−1.02E−06
0.83389949603	2.81093914971E−05	−4.89334732998E−05	5.64E−05	−1	2	−1	−2	0	6	−4.35E−08
0.20749881825	3.16551944440E−05	3.62913558210E−05	4.82E−05	3	−3	−2	0	−1	9	−5.82E−08
0.70924541539	9.50838122469E−06	4.67640677134E−05	4.77E−05	−3	4	1	0	2	10	−5.01E−07
2.91673702561	−4.90131286651E−05	1.32493580622E−05	5.08E−05	2	1	−1	0	−1	5	−6.19E−07
0.06634897910	4.09690700931E−05	1.75778748849E−05	4.46E−05	1	−1	−1	0	0	3	−2.45E−07
1.64289264250	−4.38668294916E−05	1.26505763702E−05	4.57E−05	−3	5	2	0	1	11	−4.76E−07
4.82502670586	−2.12911304788E−05	−4.03768530073E−05	4.56E−05	3	2	−3	0	0	8	−9.53E−07
1.78404454094	−3.73048438182E−05	−6.73471944607E−06	3.79E−05	−1	3	1	0	0	5	1.77E−06
3.62598256600	1.67398216286E−05	3.34178274884E−05	3.74E−05	−1	5	0	0	1	7	−9.95E−07
0.02494718598	−2.75031621538E−05	2.05459387543E−05	3.43E−05	0	0	2	2	0	4	−4.79E−08
3.75868102259	−1.16819519001E−05	3.19053919515E−05	3.40E−05	1	3	−2	0	1	7	−9.87E−07
2.77558740703	2.17374372405E−05	−1.87198193057E−05	2.87E−05	0	3	0	0	0	3	−5.85E−07
0.72614799035	2.20561143139E−05	1.62268218870E−05	2.74E−05	−3	4	3	0	0	10	−3.35E−07
1.99153780609	1.18796352082E−05	1.89816102368E−05	2.24E−05	2	0	−1	0	−2	5	−2.67E−07
2.89983478751	1.78783848204E−05	9.16620621715E−06	2.01E−05	2	1	−3	0	1	7	−4.48E−07
1.87533906868	1.97567154577E−05	−1.31532362272E−06	1.98E−05	0	2	2	2	0	6	−1.60E−07
1.00844344524	−1.29865312683E−06	−1.86874959543E−05	1.87E−05	1	0	1	0	−3	5	−6.11E−07
0.84194476574	−9.90783890811E−06	1.38815086948E−05	1.71E−05	−1	2	−1	0	2	6	4.01E−07
2.90828602715	1.71433080883E−05	1.81030346034E−06	1.72E−05	2	1	−2	0	0	5	−4.13E−07
3.04943549875	−1.39435526316E−05	−8.56716534202E−06	1.64E−05	4	−1	−3	0	−1	9	−5.94E−07
3.56808462848	1.51663983305E−05	5.21648327947E−06	1.60E−05	−2	6	2	0	0	10	−9.13E−07
2.86688390210	−7.95992888686E−06	1.09939834674E−05	1.36E−05	1	2	1	2	0	6	−5.48E−07
2.69233626629	1.18896095970E−05	−4.71817742483E−06	1.28E−05	−1	4	−1	0	2	8	−9.32E−08
4.55962967194	−1.03587659249E−05	6.28266012816E−06	1.21E−05	−1	6	1	0	0	8	−1.09E−06
2.14073577037	1.01491982934E−07	1.20572498841E−05	1.21E−05	4	−2	−2	2	0	10	−3.54E−07
0.99573421889	−9.34872231326E−06	7.14004460212E−06	1.18E−05	0	1	5	7	7	20	1.07E−04
2.78403855131	−5.09208899377E−06	9.51653037782E−06	1.08E−05	0	3	1	0	−1	5	−6.46E−07
0.14960040892	−9.79067809937E−06	−7.35057827463E−07	9.82E−06	2	−2	0	0	−2	6	−4.48E−07
2.11578859531	−5.74048440534E−06	7.82101779007E−06	9.70E−06	4	−2	−4	0	0	10	−2.96E−07
5.68387323698	8.06630538970E−06	−5.59291867334E−06	9.82E−06	2	4	−2	0	0	8	−1.20E−06
0.79250188242	4.78680542875E−06	8.66556650077E−06	9.90E−06	−2	3	2	0	1	8	7.59E−07
1.05788564137	8.12254192125E−06	−4.63256714072E−06	9.35E−06	2	−1	−2	0	−2	7	−1.66E−06
1.14114595160	6.31513010095E−06	−6.47703061026E−06	9.05E−06	3	−2	−1	0	−2	8	−1.27E−07
2.57653958492	−3.01732707991E−06	−7.94253995489E−06	8.50E−06	−3	6	3	0	0	12	−7.35E−07
4.61752778242	−8.49898064235E−06	−1.99961489619E−06	8.73E−06	0	5	−1	0	1	7	−1.00E−06
3.90828224740	3.58161507307E−06	−7.77905574185E−06	8.56E−06	3	1	−2	0	−1	7	−6.19E−07
1.82544587273	2.84705189682E−06	7.87302832242E−06	8.37E−06	0	2	−2	−2	0	6	1.11E−06
0.23244610300	−7.90625473216E−06	−1.70707784901E−06	8.09E−06	3	−3	0	2	−1	9	−7.37E−09
2.99958232250	−7.50116247535E−06	9.75582145208E−07	7.56E−06	3	0	−1	2	0	6	−5.76E−07
0.00845113073	−6.49225604174E−06	2.40814249377E−06	6.92E−06	0	0	1	0	−1	2	−7.37E−08
4.95772521212	2.15761743915E−06	−6.29848595379E−06	6.66E−06	5	0	−5	0	0	10	−8.95E−07
1.79249332447	6.41739840729E−06	−1.32872031490E−06	6.55E−06	−1	3	2	0	−1	7	−6.51E−07
1.08284063444	2.68307835796E−06	−5.48682790003E−06	6.11E−06	2	−1	0	2	0	5	−1.04E−06
3.77558379710	−2.25045074160E−06	−5.57186316158E−06	6.01E−06	1	3	0	0	−1	5	−6.21E−07
2.55963667121	1.81988599822E−06	−4.67859295536E−06	5.02E−06	−3	6	1	0	2	12	−1.24E−06
5.55117471847	7.02302684922E−07	−4.67336998863E−06	4.73E−06	0	6	0	0	0	6	−1.27E−06
3.76713270158	7.43713912880E−08	4.93363984609E−06	4.93E−06	1	3	−1	0	0	5	−5.12E−07
1.85883679620	4.47165311845E−06	8.42122400091E−07	4.55E−06	0	2	1	0	−3	6	7.45E−07
5.81657175093	4.46431125381E−06	9.47288016402E−07	4.56E−06	4	2	−4	0	0	10	−1.13E−06
4.75022625182	−1.99397919827E−06	−3.44830884877E−06	3.98E−06	2	3	−3	0	1	9	−9.79E−07

Table C.7: (continued)

f_l	A_l^c	A_l^s	A_l	k_l^1	k_l^2	k_l^3	k_l^4	k_l^5	$\lvert k_l \rvert$	$f_l - k_l\omega$
0.98750650924	3.47508385557E−06	1.51060872270E−06	3.79E−06	1	0	−1	−1	−6	9	1.57E−06

Table C.8: Fourier analysis of the c_8 function in the Earth–Moon case.

f_l	A_l^c	A_l^s	A_l	k_l^1	k_l^2	k_l^3	k_l^4	k_l^5	$\lvert k_l \rvert$	$f_l - k_l\omega$
0.00000000000	−7.00705929731E−10	0.00000000000E+00	0.00E+00	0	0	0	0	0	0	0.00E+00
1.85039159884	−4.47493105278E−03	6.92765214672E−03	8.25E−03	0	2	0	0	0	2	−3.96E−07
2.84193667476	−2.69643391730E−04	−8.63422974426E−04	9.05E−04	1	2	−1	0	0	4	−5.42E−07
0.85884652023	−9.10789980883E−04	1.10814616798E−04	9.18E−04	−1	2	1	0	0	4	−2.53E−07
1.77559103310	−2.57643412420E−04	4.36771127059E−04	5.07E−04	−1	3	0	0	1	5	−5.33E−07
0.99154507796	−1.50568191113E−04	−1.25437901608E−04	1.96E−04	1	0	−1	0	0	2	−1.44E−07
2.70923811505	−1.55972094319E−04	−7.58095953300E−05	1.73E−04	−1	4	1	0	0	6	−6.53E−07
3.70078319630	1.04768101402E−04	−4.72555847568E−05	1.15E−04	0	4	0	0	0	4	−7.94E−07
1.92519194707	5.49538098115E−05	−7.83654950169E−05	9.57E−05	1	1	0	0	−1	3	−4.76E−07
3.83348174853	7.40181830184E−05	3.05885138588E−05	8.01E−05	2	2	−2	0	0	6	−6.89E−07
2.76713621096	−2.05637558776E−05	−5.78121531006E−05	6.14E−05	0	3	−1	0	1	5	−5.77E−07
0.78404581899	−5.14255880457E−05	8.44348666926E−06	5.21E−05	−2	3	1	0	1	7	−5.26E−07
1.98309015831	2.90779368434E−05	−5.33905161017E−06	2.96E−05	2	0	−2	0	0	4	−2.85E−07
2.00803725475	−2.05946747599E−05	2.22394081329E−05	3.03E−05	2	0	0	2	0	4	−4.22E−07
1.70079041093	−1.00749220240E−05	1.87692860977E−05	2.13E−05	−2	4	0	0	2	8	−7.27E−07
2.77558740720	1.33684435175E−05	1.55389206885E−05	2.05E−05	0	3	0	0	0	3	−5.85E−07
4.69232828283	−5.34611548544E−06	1.92493676848E−05	2.00E−05	1	4	−1	0	0	6	−9.28E−07
0.13269851410	−1.32181244126E−05	1.24513029616E−05	1.82E−05	2	−2	−2	0	0	6	6.61E−08
2.63443783949	−1.66662661529E−05	−7.34938531063E−06	1.82E−05	−2	5	1	0	1	9	−5.00E−07
3.62598249513	1.30908156659E−05	−6.57544949819E−06	1.46E−05	−1	5	0	0	1	7	−1.07E−06
2.91673711995	3.89096456937E−06	1.44397716162E−05	1.50E−05	2	1	−1	0	−1	5	−5.25E−07
1.71769304977	−2.78386551236E−06	−1.12748925691E−05	1.16E−05	−2	4	2	0	0	8	−4.97E−07
0.91674470879	−8.62088533371E−06	−6.64001979415E−06	1.09E−05	0	1	−1	0	1	3	−8.42E−08
0.92519579258	−9.53021970051E−06	−2.80992555411E−06	9.94E−06	0	1	0	0	0	1	−2.05E−07
1.06634562519	−4.98627536013E−06	−4.50626085908E−06	6.72E−06	2	−1	−1	0	−1	5	−2.47E−08
4.82502678865	−5.81426918931E−06	3.06593645634E−06	6.57E−06	3	2	−3	0	0	8	−8.71E−07
3.75868136201	5.55497614194E−06	2.04872183310E−06	5.92E−06	1	3	−2	0	1	7	−6.47E−07
1.78403932539	−6.77284678504E−07	4.98004778276E−06	5.03E−06	−1	3	1	0	−1	6	1.29E−07
0.93364676144	4.49437002626E−06	−3.77454163873E−07	4.51E−06	0	1	1	0	−1	3	−4.40E−07
4.55962965282	2.02825079055E−06	3.34233656935E−06	3.91E−06	−1	6	1	0	0	8	−1.11E−06
2.97463519857	−1.63097418314E−06	2.89891228594E−06	3.33E−06	3	0	−3	0	0	6	−4.66E−07
0.83389936110	2.92854211526E−06	1.67836070770E−06	3.38E−06	−1	2	−1	−2	0	6	−1.78E−07
1.01649218329	−3.03157552117E−06	−1.59313564777E−07	3.04E−06	1	0	1	2	0	4	−2.72E−07
2.99958233581	−3.79697464557E−07	−2.92389665436E−06	2.95E−06	3	0	−1	2	0	6	−5.62E−07
2.78403872627	2.73452977885E−06	1.47110913250E−06	3.11E−06	0	3	1	0	−1	5	−4.71E−07
3.56808456483	9.67582421661E−07	−2.81529727153E−06	2.98E−06	−2	6	2	0	0	10	−9.77E−07
2.69233584944	−1.03894316241E−06	−2.58938919515E−06	2.79E−06	−1	4	−1	0	2	8	−5.10E−07
2.86688368690	2.21921396158E−06	1.60128041271E−06	2.74E−06	1	2	1	2	0	6	−7.63E−07
4.61752767999	−6.16168623475E−07	2.63227239025E−06	2.70E−06	0	5	−1	0	1	7	−1.10E−06
3.77558343367	−2.35417647549E−06	9.58400131956E−07	2.54E−06	1	3	0	0	−1	5	−9.85E−07
5.68387370958	−1.41945554543E−06	−2.06345151471E−06	2.50E−06	2	4	−2	0	0	8	−7.23E−07
3.76713248719	−2.64001615450E−06	4.19093721789E−08	2.64E−06	1	3	−1	0	0	5	−7.27E−07
0.70924619656	−2.02440652632E−06	3.97840344722E−07	2.06E−06	−3	4	1	0	2	10	2.80E−07
1.90828997021	1.88089807577E−06	−4.17159855282E−07	1.93E−06	1	1	−2	0	1	5	−4.43E−08
2.70078675746	1.30245497592E−06	1.39387601381E−06	1.91E−06	−1	4	0	0	1	6	−8.06E−07
3.90828220017	−1.57394965446E−06	−7.23905934696E−07	1.73E−06	3	1	−2	0	−1	7	−6.66E−07
1.69274590345	−6.69401762197E−07	1.58551005809E−06	1.72E−06	−2	4	0	−2	0	8	−4.10E−07
5.55117478027	−1.69133959045E−06	−2.54779662574E−07	1.71E−06	0	6	0	0	0	6	−1.20E−06
2.55963754255	−1.09234772947E−06	−4.32820478154E−07	1.17E−06	−3	6	1	0	2	12	−3.69E−07
1.64289263646	−3.24000258975E−07	−1.12293779241E−06	1.17E−06	−3	5	2	0	1	11	−4.82E−07
3.55118290180	9.85884242732E−07	−5.34366185100E−07	1.12E−06	−2	6	0	0	2	10	−2.31E−07

Table C.9: Fourier analysis of the c_9 function in the Earth–Moon case.

f_l	A_l^c	A_l^s	A_l	k_l^1	k_l^2	k_l^3	k_l^4	k_l^5	$\lvert k_l \rvert$	$f_l - k_l\omega$
0.00000000000	−7.81507984935E−12	0.00000000000E+00	0.00E+00	0	0	0	0	0	0	0.00E+00
0.84637295298	−7.10110645400E−04	−1.43852321929E−04	7.25E−04	−1	2	0	−1	0	4	−2.04E−07
1.00401861552	6.74520153392E−04	2.64281111393E−04	7.24E−04	1	0	0	1	0	2	−2.23E−07

Table C.9: (continued)

f_l	A_l^c	A_l^s	A_l	k_l^1	k_l^2	k_l^3	k_l^4	k_l^5	$\|k_l\|$	$f_l - k_l\omega$
0.01247357981	1.52072890278E−05	4.57563924719E−05	4.82E−05	0	0	1	1	0	2	−3.71E−08
0.14517208261	−2.28213271180E−05	4.23340872668E−05	4.81E−05	2	−2	−1	1	0	6	1.76E−08
0.77157269561	−4.35749424620E−05	−7.10656156646E−06	4.42E−05	−2	3	0	−1	1	7	−3.24E−08
1.99556365117	−3.50563880350E−05	1.92919302229E−05	4.00E−05	2	0	−1	1	0	4	−4.09E−07
1.83791798820	3.11844099441E−05	−2.50445230538E−05	4.00E−05	0	2	−1	−1	0	4	−3.90E−07
0.92921810798	1.69052805474E−05	5.86793238619E−06	1.79E−05	0	1	0	1	1	3	−3.02E−07
1.07881913140	1.61874627893E−05	7.08790846099E−06	1.77E−05	2	−1	0	1	−1	5	−1.35E−07
1.70521949521	6.74060930318E−07	−8.52185039572E−06	8.55E−06	−2	4	1	−1	0	8	−4.35E−07
0.92117316404	8.34743331304E−06	2.02456789414E−06	8.59E−06	0	1	0	−1	−1	3	−4.21E−07
1.86286515009	−2.13459749749E−06	8.27561715696E−06	8.55E−06	0	2	1	1	0	4	−4.62E−07
2.85441018463	−1.87194327768E−06	−2.59963866843E−06	3.20E−06	1	2	0	1	0	4	−6.49E−07
0.07882277963	−2.69253775656E−07	3.10406177567E−06	3.12E−06	1	−1	0	1	0	3	−6.13E−08
2.69676452295	2.18947891228E−06	2.13661510480E−06	3.06E−06	−1	4	0	−1	0	6	−6.28E−07
1.76311759891	2.04343567765E−06	−1.77557307947E−06	2.71E−06	−1	3	−1	−1	1	7	−3.51E−07
0.21997272376	−1.43137028520E−06	2.41684298328E−06	2.81E−06	3	−3	−1	1	−1	9	2.30E−07
2.98710868548	4.67525721214E−07	−2.41533211754E−06	2.46E−06	3	0	−2	1	0	6	−5.96E−07
2.82946302607	−4.33278704283E−08	2.45206426837E−06	2.45E−06	1	2	−2	−1	0	6	−5.73E−07
0.97907143133	1.11927729455E−06	1.80215133906E−06	2.12E−06	1	0	−2	−1	0	4	−1.73E−07
1.92921432439	1.23598338386E−06	−1.59359447623E−06	2.02E−06	1	1	0	1	0	3	−5.11E−07
1.77156872576	−9.43363804323E−07	1.78275831314E−06	2.02E−06	−1	3	0	−1	0	5	−4.28E−07
0.69677182605	−1.82816610115E−06	−2.20897031991E−07	1.84E−06	−3	4	0	−1	2	10	−4.74E−07
0.08727423872	4.67844537917E−07	1.62326619728E−06	1.69E−06	1	−1	1	1	−1	5	1.93E−07
1.16166428714	1.12275064325E−06	6.83711634756E−07	1.31E−06	3	−2	0	3	0	8	−2.33E−07
1.92076307468	−1.07646614833E−06	6.49460927570E−07	1.26E−06	1	1	−1	1	1	5	−5.57E−07
0.87131994111	−1.04810135219E−06	4.97053684222E−07	1.16E−06	−1	2	2	1	0	6	−4.49E−07
0.06232678652	3.77539650035E−07	−1.00417771242E−06	1.07E−06	1	−1	−1	−1	−1	5	−2.50E−08

Table C.10: Fourier analysis of the c_{10} function in the Earth–Moon case.

f_l	A_l^c	A_l^s	A_l	k_l^1	k_l^2	k_l^3	k_l^4	k_l^5	$\|k_l\|$	$f_l - k_l\omega$
0.00000000000	1.00478110242E+00	0.00000000000E+00	0.00E+00	0	0	0	0	0	0	0.00E+00
0.99154504274	−1.05600563324E−01	1.26826887856E−01	1.65E−01	1	0	−1	0	0	2	−1.79E−07
0.85884652974	3.92056944749E−03	3.22406224965E−02	3.25E−02	−1	2	1	0	0	4	−2.44E−07
1.85039157284	−1.54640947885E−02	−9.98457598191E−03	1.84E−02	0	2	0	0	0	2	−4.22E−07
1.98309009374	−2.44632900752E−03	−1.32858584333E−02	1.35E−02	2	0	−2	0	0	4	−3.49E−07
2.84193661727	3.14452363555E−03	−9.83538606697E−04	3.29E−03	1	2	−1	0	0	4	−5.99E−07
0.13269851611	9.94326126838E−04	1.05575915520E−03	1.45E−03	2	−2	−2	0	0	6	6.81E−08
0.78404586978	2.24819793124E−04	1.38050728856E−03	1.40E−03	−2	3	1	0	1	7	−4.75E−07
1.77559111013	−1.08380091276E−03	−6.41116423496E−04	1.26E−03	−1	3	0	0	1	5	−4.56E−07
2.97463513459	9.43812919630E−04	5.30689368441E−04	1.08E−03	3	0	−3	0	0	6	−5.30E−07
0.91674491440	−6.24261950615E−04	8.09005858916E−04	1.02E−03	0	1	−1	0	1	3	1.21E−07
0.92519583006	−2.52365727320E−04	8.55490881876E−04	8.92E−04	0	1	0	0	0	1	−1.67E−07
1.06634556274	5.60052394795E−04	−6.20796001170E−04	8.36E−04	2	−1	−1	0	−1	5	−8.72E−08
1.01649220452	3.27243933606E−05	−6.21509131672E−04	6.22E−04	1	0	1	2	0	4	−2.51E−07
2.70923810041	2.80594189483E−04	−5.77486671282E−04	6.42E−04	−1	4	1	0	0	6	−6.68E−07
1.71769305471	−5.09936384039E−04	1.25898409588E−04	5.25E−04	−2	4	2	0	0	8	−4.92E−07
0.07480035406	−4.46685055851E−04	−1.72411495031E−05	4.47E−04	1	−1	0	0	−1	3	−7.44E−08
3.83348166121	−1.59647649292E−04	3.87066009309E−04	4.19E−04	2	2	−2	0	0	6	−7.77E−07
3.70078314470	1.16909372133E−04	2.58892494094E−04	2.84E−04	0	4	0	0	0	4	−8.45E−07
2.76713632199	2.32835224471E−04	−8.26729682270E−05	2.47E−04	0	3	−1	0	1	5	−4.66E−07
0.93364709838	−1.70908794849E−05	−2.10879227873E−04	2.12E−04	0	1	1	0	−1	3	−1.04E−07
1.92519179279	1.56046688217E−04	1.09349202009E−04	1.91E−04	1	1	0	0	−1	3	−6.31E−07
1.90828958191	−3.69781758748E−05	−1.64101632818E−04	1.68E−04	1	1	−2	0	1	5	−4.33E−07
1.91674094402	−8.06231829629E−05	−1.20612861734E−04	1.45E−04	1	1	−1	0	0	3	−2.75E−07
2.05789024063	1.95622337954E−05	1.34179335883E−04	1.36E−04	3	−1	−2	0	−1	7	−6.31E−07
0.99998863481	3.81238583071E−05	−1.26885379609E−04	1.32E−04	1	0	0	0	−3	4	−6.43E−07
0.15764565869	−1.35081086420E−04	−2.36793842284E−05	1.37E−04	2	−2	0	2	0	6	−2.32E−08
3.96618016962	−7.98172627890E−05	3.04353779191E−05	8.54E−05	4	0	−4	0	0	8	−7.16E−07
2.00803725218	5.64263007310E−05	5.22470282375E−05	7.69E−05	2	0	0	2	0	4	−4.25E−07
1.14919073108	5.98399637598E−05	−5.06839484809E−05	7.84E−05	3	−2	−1	2	0	8	−1.72E−07
2.63443786601	2.90005883636E−05	−6.58697983387E−05	7.20E−05	−2	5	1	0	1	9	−4.74E−07
1.70079080362	−5.43296237967E−05	−2.93979817907E−05	6.18E−05	−2	4	0	0	2	8	−3.34E−07
4.69232818955	−5.98065718269E−05	−1.65633950745E−05	6.21E−05	1	4	−1	0	0	6	−1.02E−06
0.83389949616	2.80756374439E−05	−4.88746291147E−05	5.64E−05	−1	2	−1	−2	0	6	−4.34E−08
0.20749881825	3.16557502830E−05	3.62919933052E−05	4.82E−05	3	−3	−2	0	−1	9	−5.82E−08

Table C.10: (continued)

f_l	A_l^c	A_l^s	A_l	k_l^1	k_l^2	k_l^3	k_l^4	k_l^5	$\|k_l\|$	$f_l - k_l\omega$
0.70924541540	9.50826404179E−06	4.67635139851E−05	4.77E−05	−3	4	1	0	2	10	−5.01E−07
2.91673702561	−4.90130556817E−05	1.32493383251E−05	5.08E−05	2	1	−1	0	−1	5	−6.19E−07
0.06634897917	4.09707078639E−05	1.75786031143E−05	4.46E−05	1	−1	−1	0	0	3	−2.45E−07
1.64289264251	−4.38667909127E−05	1.26505651740E−05	4.57E−05	−3	5	2	0	1	11	−4.76E−07
4.82502670586	−2.12911183457E−05	−4.03768299911E−05	4.56E−05	3	2	−3	0	0	8	−9.53E−07
1.78404454083	−3.73059201514E−05	−6.73488576434E−06	3.79E−05	−1	3	1	0	0	5	1.77E−06
3.62598256600	1.67393689402E−05	3.34169236904E−05	3.74E−05	−1	5	0	0	1	7	−9.95E−07
0.02494718597	−2.75067682058E−05	2.05486334960E−05	3.43E−05	0	0	2	2	0	4	−4.79E−08
3.75868102259	−1.16819421433E−05	3.19053655570E−05	3.40E−05	1	3	−2	0	1	7	−9.87E−07
2.77558740703	2.17350847511E−05	−1.87177947043E−05	2.87E−05	0	3	0	0	0	3	−5.85E−07
0.72614799035	2.20561162308E−05	1.62268233527E−05	2.74E−05	−3	4	3	0	0	10	−3.35E−07
1.99153780609	1.18796276374E−05	1.89815882443E−05	2.24E−05	2	0	−1	0	−2	5	−2.67E−07
2.89983478751	1.78783889064E−05	9.16620844045E−06	2.01E−05	2	1	−3	0	1	7	−4.48E−07
1.87533906869	1.97561819328E−05	−1.31528665719E−06	1.98E−05	0	2	2	2	0	6	−1.60E−07
1.00844344337	−1.29889681669E−06	−1.86876388755E−05	1.87E−05	1	0	1	0	−3	5	−6.13E−07
0.84194476640	−9.90772912443E−06	1.38812279382E−05	1.71E−05	−1	2	−1	0	2	6	4.02E−07
2.90828602715	1.71433233158E−05	1.81030514264E−06	1.72E−05	2	1	−2	0	0	5	−4.13E−07
3.04943549875	−1.39435507301E−05	−8.56716396989E−06	1.64E−05	4	−1	−3	0	−1	9	−5.94E−07
3.56808462848	1.51664222544E−05	5.21649154548E−06	1.60E−05	−2	6	2	0	0	10	−9.13E−07
2.86688390208	−7.96125818194E−06	1.09958228369E−05	1.36E−05	1	2	1	2	0	6	−5.48E−07
2.69233626781	1.18897146035E−05	−4.71808272291E−06	1.28E−05	−1	4	−1	0	2	8	−9.16E−08
4.55962967194	−1.03586583322E−05	6.28259492196E−06	1.21E−05	−1	6	1	0	0	8	−1.09E−06
2.14073577037	1.01499745479E−07	1.20581197346E−05	1.21E−05	4	−2	−2	2	0	10	−3.54E−07
0.99573422023	−9.34875038714E−06	7.13989772175E−06	1.18E−05	0	1	5	7	7	20	1.07E−04
2.78403855112	−5.09205991997E−06	9.51650410498E−06	1.08E−05	0	3	1	0	−1	5	−6.46E−07
0.14960040882	−9.78876920191E−06	−7.34907030514E−07	9.82E−06	2	−2	0	0	−2	6	−4.48E−07
2.11578859529	−5.74048538255E−06	7.82102259516E−06	9.70E−06	4	−2	−4	0	0	10	−2.96E−07
5.68387323698	8.06628895763E−06	−5.59290727994E−06	9.82E−06	2	4	−2	0	0	8	−1.20E−06
0.79250188257	4.78672903389E−06	8.66544698913E−06	9.90E−06	−2	3	2	0	1	8	7.59E−07
1.05788564142	8.12262742049E−06	−4.63261257024E−06	9.35E−06	2	−1	−2	0	−2	7	−1.66E−06
1.14114595156	6.31528312990E−06	−6.47719160553E−06	9.05E−06	3	−2	−1	0	−2	8	−1.27E−07
2.57653958492	−3.01732840540E−06	−7.94254336518E−06	8.50E−06	−3	6	3	0	0	12	−7.35E−07
4.61752778242	−8.49892042178E−06	−1.99960074994E−06	8.73E−06	0	5	−1	0	1	7	−1.00E−06
3.90828224740	3.58161452104E−06	−7.77905453610E−06	8.56E−06	3	1	−2	0	−1	7	−6.19E−07
1.82544587275	2.84705773979E−06	7.87304612325E−06	8.37E−06	0	2	−2	−2	0	6	1.11E−06
0.23244610265	−7.95044335450E−06	−1.71659115598E−06	8.13E−06	3	−3	0	2	−1	9	−7.73E−09
2.99958232249	−7.50223200186E−06	9.75721518453E−07	7.57E−06	3	0	−1	2	0	6	−5.76E−07
0.00845113758	−6.49218601861E−06	2.40777742852E−06	6.92E−06	0	0	1	0	−1	2	−6.69E−08
4.95772521212	2.15761750489E−06	−6.29848615946E−06	6.66E−06	5	0	−5	0	0	10	−8.95E−07
1.79249332454	6.41737937741E−06	−1.32871311994E−06	6.55E−06	−1	3	2	0	−1	7	−6.51E−07
1.08284063382	2.68121792023E−06	−5.48308048585E−06	6.10E−06	2	−1	0	2	0	5	−1.05E−06
3.77558379708	−2.25045438179E−06	−5.57187040690E−06	6.01E−06	1	3	0	0	−1	5	−6.21E−07
2.55963667120	1.81990735549E−06	−4.67864884704E−06	5.02E−06	−3	6	1	0	2	12	−1.24E−06
5.55117471847	7.02305432908E−07	−4.67338830479E−06	4.73E−06	0	6	0	0	0	6	−1.27E−06
3.76713270159	7.43696320049E−08	4.93353401245E−06	4.93E−06	1	3	−1	0	0	5	−5.12E−07
1.85883682855	4.47111046524E−06	8.43025472707E−07	4.55E−06	0	2	1	0	−3	6	7.77E−07
5.81657175093	4.46430963129E−06	9.47287671576E−07	4.56E−06	4	2	−4	0	0	10	−1.13E−06
4.75022625182	−1.99397789639E−06	−3.44830658587E−06	3.98E−06	2	3	−3	0	1	9	−9.79E−07
0.98750650959	3.47513622749E−06	1.51064324783E−06	3.79E−06	1	0	−1	−1	−6	9	1.57E−06

Table C.11: Fourier analysis of the c_{11} function in the Earth–Moon case.

f_l	A_l^c	A_l^s	A_l	k_l^1	k_l^2	k_l^3	k_l^4	k_l^5	$\|k_l\|$	$f_l - k_l\omega$
0.00000000000	−2.31615183927E−11	0.00000000000E+00	0.00E+00	0	0	0	0	0	0	0.00E+00
1.00401861556	−2.62957098385E−04	6.71140420025E−04	7.21E−04	1	0	0	1	0	2	−2.23E−07
0.84637295300	1.20507162114E−04	−5.94869555210E−04	6.07E−04	−1	2	0	−1	0	4	−2.03E−07
0.14517208285	−4.10209114635E−05	−2.21134827821E−05	4.66E−05	2	−2	−1	1	0	6	1.79E−08
1.99556364909	1.75641442393E−05	3.19160691213E−05	3.64E−05	2	0	−1	1	0	4	−4.11E−07
1.83791798781	−2.28796048820E−05	−2.84886387963E−05	3.65E−05	0	2	−1	−1	0	4	−3.90E−07
0.77157269620	5.36161980094E−06	−3.28746162413E−05	3.33E−05	−2	3	0	−1	1	7	−3.18E−08
0.01247358099	2.99514729452E−05	−9.95427267783E−06	3.16E−05	0	0	1	1	0	2	−3.60E−08
2.85441018262	−1.94803015231E−05	1.40275675185E−05	2.40E−05	1	2	0	1	0	4	−6.51E−07
2.69676451902	1.64899961426E−05	−1.68987306465E−05	2.36E−05	−1	4	0	−1	0	6	−6.32E−07
1.07881913200	−7.46570517510E−06	1.70502141866E−05	1.86E−05	2	−1	0	1	−1	5	−1.35E−07
0.92921810674	−5.26934826526E−06	1.51805672385E−05	1.61E−05	0	1	0	1	1	3	−3.03E−07

Table C.11: (continued)

f_l	A_l^c	A_l^s	A_l	k_l^1	k_l^2	k_l^3	k_l^4	k_l^5	$\|k_l\|$	$f_l - k_l\omega$
0.92117316269	−1.91265178494E−06	7.88658670838E−06	8.12E−06	0	1	0	−1	−1	3	−4.22E−07
1.92921443371	3.47773802547E−06	2.70046322288E−06	4.40E−06	1	1	0	1	0	3	−4.02E−07
1.77156875738	−3.58774716302E−06	−1.89779299304E−06	4.06E−06	−1	3	0	−1	0	5	−3.97E−07
2.98710869353	−3.85229440340E−06	−7.45895268232E−07	3.92E−06	3	0	−2	1	0	6	−5.88E−07
2.82946302583	3.84298193601E−06	6.79044660770E−08	3.84E−06	1	2	−2	−1	0	6	−5.74E−07
1.13671714249	−3.47700073510E−06	1.39682147389E−06	3.75E−06	3	−2	−2	1	0	8	−1.44E−07
2.62196399452	1.96684971020E−06	−2.18123296664E−06	2.94E−06	−2	5	0	−1	1	9	−7.28E−07
0.21997272938	−2.56761035662E−06	−1.52077037405E−06	2.98E−06	3	−3	−1	1	−1	9	2.36E−07
1.76311763637	−1.54296606636E−06	−1.77621956297E−06	2.35E−06	−1	3	−1	−1	1	7	−3.13E−07
0.97907147130	1.98997634696E−06	−1.23530939175E−06	2.34E−06	1	0	−2	−1	0	4	−1.33E−07
3.84595522023	1.50401940535E−07	−2.13761072293E−06	2.14E−06	2	2	−1	1	0	6	−8.35E−07
3.68830955463	2.17068151106E−07	2.09284465235E−06	2.10E−06	0	4	−1	−1	0	6	−8.18E−07
2.77960989333	−1.67110181453E−06	1.30369939250E−06	2.12E−06	0	3	0	1	1	5	−5.12E−07
1.16166428056	−7.71993709850E−07	1.26785508055E−06	1.48E−06	3	−2	0	3	0	8	−2.40E−07
0.71367448891	−7.60568053073E−07	−1.07629116865E−06	1.32E−06	−3	4	2	−1	0	10	−2.20E−07
0.69677178696	1.47578344545E−07	−1.22335890241E−06	1.23E−06	−3	4	0	−1	2	10	−5.13E−07

Table C.12: Fourier analysis of the c_{12} function in the Earth–Moon case.

f_l	A_l^c	A_l^s	A_l	k_l^1	k_l^2	k_l^3	k_l^4	k_l^5	$\|k_l\|$	$f_l - k_l\omega$
0.00000000000	−1.61182681516E−03	0.00000000000E+00	0.00E+00	0	0	0	0	0	0	0.00E+00
0.99154502636	3.44840901270E−02	−4.14218970457E−02	5.39E−02	1	0	−1	0	0	2	−1.95E−07
1.85039157031	2.26157606345E−02	1.46015999173E−02	2.69E−02	0	2	0	0	0	2	−4.25E−07
0.85884654110	−9.71198607479E−04	−7.98989552588E−03	8.05E−03	−1	2	1	0	0	4	−2.32E−07
1.98309004859	1.32888312972E−03	7.20825864013E−03	7.33E−03	2	0	−2	0	0	4	−3.94E−07
2.84193659510	−4.37171699192E−03	1.36790743151E−03	4.58E−03	1	2	−1	0	0	4	−6.21E−07
1.77559129766	1.46568606326E−03	8.68466636104E−04	1.70E−03	−1	3	0	0	1	5	−2.69E−07
2.70923811567	−3.69890070497E−04	7.61142109904E−04	8.46E−04	−1	4	1	0	0	6	−6.53E−07
2.97463506062	−6.76377116344E−04	−3.80012279443E−04	7.76E−04	3	0	−3	0	0	6	−6.04E−07
3.70078314150	−2.34898724225E−04	−5.20142694589E−04	5.71E−04	0	4	0	0	0	4	−8.48E−07
3.83348161711	2.24595070666E−04	−5.44856755035E−04	5.89E−04	2	2	−2	0	0	6	−8.21E−07
0.13269847955	−3.52885845179E−04	−3.74564589632E−04	5.15E−04	2	−2	−2	0	0	6	3.15E−08
2.76713625845	−3.05820363210E−04	1.08804453251E−04	3.25E−04	0	3	−1	0	1	5	−5.29E−07
1.92519217681	−2.49617385101E−04	−1.75598010162E−04	3.05E−04	1	1	0	0	−1	3	−2.47E−07
1.06634540593	−2.05889281666E−04	2.28630911956E−04	3.08E−04	2	−1	−1	0	−1	5	−2.44E−07
0.78404633230	−4.74253763794E−05	−2.95406680955E−04	2.99E−04	−2	3	1	0	1	7	−1.27E−08
0.91674453608	1.78149309873E−04	−2.31892689111E−04	2.92E−04	0	1	−1	0	1	3	−2.57E−07
0.92519571383	7.05063889416E−05	−2.39340278611E−04	2.50E−04	0	1	0	0	0	1	−2.84E−07
1.01649223640	−1.12631124775E−05	2.13560466115E−04	2.14E−04	1	0	1	2	0	4	−2.19E−07
1.71769317104	2.17707306264E−04	−5.36374832485E−05	2.24E−04	−2	4	2	0	0	8	−3.76E−07
4.69232816742	1.21126081872E−04	3.35306581369E−05	1.26E−04	1	4	−1	0	0	6	−1.04E−06
2.63443755440	−3.63397424148E−05	8.29868816024E−05	9.06E−05	−2	5	1	0	1	9	−7.85E−07
1.90828952604	1.85511175495E−05	8.22494796765E−05	8.43E−05	1	1	−2	0	1	5	−4.88E−07
1.70079098649	6.61076440900E−05	3.58064044050E−05	7.52E−05	−2	4	0	0	2	8	−1.51E−07
3.96618011230	6.90982422492E−05	−2.63692452805E−05	7.40E−05	4	0	−4	0	0	8	−7.74E−07
3.62598251873	−3.28054425335E−05	−6.55580975669E−05	7.33E−05	−1	5	0	0	1	7	−1.04E−06
1.91673999259	4.20734300411E−05	6.24530913005E−05	7.53E−05	1	1	−1	0	0	3	−1.23E−06
2.05789039058	−1.13270913607E−05	−7.82455248498E−05	7.91E−05	3	−1	−2	0	−1	7	−4.81E−07
2.91673712405	7.16592442237E−05	−1.93514428660E−05	7.42E−05	2	1	−1	0	−1	5	−5.21E−07
4.82502662357	3.11026185220E−05	5.89289825448E−05	6.66E−05	3	2	−3	0	0	8	−1.04E−06
0.93364721094	4.83867994093E−06	5.96091016180E−05	5.98E−05	0	1	1	0	−1	3	9.04E−09
0.99997149800	−9.20610541922E−06	4.35155537612E−05	4.45E−05	1	0	0	0	−8	9	9.07E−08
3.75868122874	1.58025527203E−05	−4.30247393262E−05	4.58E−05	1	3	−2	0	1	7	−7.81E−07
1.14919068318	−2.37061934773E−05	2.00889333355E−05	3.11E−05	3	−2	−1	2	0	8	−2.20E−07
1.78403331861	2.85700581056E−05	3.87375590019E−06	2.88E−05	−1	3	1	0	−3	8	1.27E−06
4.55962968445	2.03910191254E−05	−1.23659340436E−05	2.38E−05	−1	6	1	0	0	8	−1.08E−06
2.77558742868	1.68401493375E−05	−1.45294363420E−05	2.22E−05	0	3	0	0	0	3	−5.64E−07
2.00803722621	1.55691726935E−05	1.44069771002E−05	2.12E−05	2	0	0	2	0	4	−4.51E−07
3.56808471230	−1.95421062432E−05	−6.72838789342E−06	2.07E−05	−2	6	2	0	0	10	−8.29E−07
5.68387317954	−1.62941249837E−05	1.13044850609E−05	1.98E−05	2	4	−2	0	0	8	−1.25E−06
0.06634940452	−1.58269111470E−05	−6.84511671206E−06	1.72E−05	1	−1	−1	0	0	3	1.81E−07
1.64289301363	1.76092844014E−05	−5.05148338491E−06	1.83E−05	−3	5	2	0	1	11	−1.05E−07
4.61752744504	1.67964505037E−05	3.93214874272E−06	1.73E−05	0	5	−1	0	1	7	−1.34E−06
2.86688383099	9.71333752942E−06	−1.34279637276E−05	1.66E−05	1	2	1	2	0	6	−6.19E−07
0.20749921329	−1.16841068197E−05	−1.34432051241E−05	1.78E−05	3	−3	−2	0	−1	9	3.37E−07

Table C.12: (continued)

f_l	A_l^c	A_l^s	A_l	k_l^1	k_l^2	k_l^3	k_l^4	k_l^5	$\|k_l\|$	$f_l - k_l\omega$
2.69233591613	−1.45687185951E−05	5.82008672823E−06	1.57E−05	−1	4	−1	0	2	8	−4.43E−07
2.78403842512	7.03660998470E−06	−1.31633788551E−05	1.49E−05	0	3	1	0	−1	5	−7.72E−07
0.07480052418	−1.44366842420E−05	−5.69729844622E−07	1.44E−05	1	−1	0	0	−1	3	9.57E−08
2.89983448616	−1.20457877967E−05	−6.15264190788E−06	1.35E−05	2	1	−3	0	1	7	−7.50E−07
3.77558338795	4.71156633019E−06	1.15988235765E−05	1.25E−05	1	3	0	0	−1	5	−1.03E−06
3.04943527872	1.05702430341E−05	6.48115744346E−06	1.24E−05	4	−1	−3	0	−1	9	−8.14E−07
0.83389962025	−6.07782756818E−06	1.05597819860E−05	1.22E−05	−1	2	−1	−2	0	6	8.07E−08
1.99153470174	−6.77281436457E−06	−1.01576575278E−05	1.22E−05	2	0	−1	0	−3	6	2.03E−07
3.90828211086	−5.20855905602E−06	1.13530062588E−05	1.25E−05	3	1	−2	0	−1	7	−7.55E−07
5.55117473637	−1.67326538526E−06	1.11305574804E−05	1.13E−05	0	6	0	0	0	6	−1.25E−06
2.90828543420	−1.19423346309E−05	−1.23824780475E−06	1.20E−05	2	1	−2	0	0	5	−1.01E−06
0.02494722184	9.23825799128E−06	−6.90096821455E−06	1.15E−05	0	0	2	2	0	4	−1.20E−08
1.87534012780	−9.33529981331E−06	5.71966542496E−07	9.35E−06	0	2	2	2	0	6	8.99E−07
0.70924608646	−1.73614567151E−06	−8.67425051056E−06	8.85E−06	−3	4	1	0	2	10	1.70E−07
0.72614869845	−7.00467132054E−06	−5.18461264812E−06	8.71E−06	−3	4	3	0	0	10	3.73E−07
2.11578827454	4.66223706292E−06	−6.36772547044E−06	7.89E−06	4	−2	−4	0	0	10	−6.16E−07
2.14073563137	−6.55361040452E−08	−7.20832321322E−06	7.21E−06	4	−2	−2	2	0	10	−4.93E−07
5.81657166638	−6.81363789922E−06	−1.44285609140E−06	6.96E−06	4	2	−4	0	0	10	−1.21E−06
4.95772511383	−2.15111366979E−06	6.28857973713E−06	6.65E−06	5	0	−5	0	0	10	−9.94E−07
1.00843802634	5.51708876680E−07	6.28290267791E−06	6.31E−06	2	−1	−5	−6	6	20	−4.98E−07
2.55963695345	−2.18738574939E−06	5.58927334285E−06	6.00E−06	−3	6	1	0	2	12	−9.58E−07
3.55118190409	−2.74580538672E−06	−4.98283311885E−06	5.69E−06	−2	6	0	0	2	10	−1.23E−06
4.75022618487	2.81604212551E−06	4.86454467880E−06	5.62E−06	2	3	−3	0	1	9	−1.05E−06
1.12424282917	−5.57851515540E−06	3.58318692008E−07	5.59E−06	3	−2	−3	0	0	8	−8.40E−07
2.57654021117	1.72009406935E−06	4.56237607856E−06	4.88E−06	−3	6	3	0	0	12	−1.09E−07
4.48482928661	3.46599725220E−06	−2.29115136039E−06	4.15E−06	−2	7	1	0	1	11	−1.05E−06
0.84194578643	2.44724309838E−06	−3.41566674085E−06	4.20E−06	−1	2	−1	0	2	6	1.42E−06
0.15764553499	3.83757575184E−06	6.70321958345E−07	3.90E−06	2	−2	0	2	0	6	−1.47E−07
1.14114668405	−2.66355101838E−06	2.74538474454E−06	3.83E−06	3	−2	−1	0	−2	8	6.06E−07
1.82544805407	−1.17966643276E−06	−3.40592171695E−06	3.60E−06	0	2	−2	−2	1	7	−2.81E−07
1.69274806659	3.13386555542E−06	1.35417663363E−06	3.41E−06	−2	4	0	−2	0	8	1.75E−06
2.85033272297	2.00574419620E−06	−2.61638051583E−06	3.30E−06	1	2	0	0	−17	20	1.49E−06
4.76712835294	−3.20845053511E−06	−1.02147947735E−06	3.37E−06	2	3	−1	0	−1	7	−1.29E−06

Table C.13: Fourier analysis of the c_{13} function in the Earth–Moon case.

f_l	A_l^c	A_l^s	A_l	k_l^1	k_l^2	k_l^3	k_l^4	k_l^5	$\|k_l\|$	$f_l - k_l\omega$
0.00000000000	1.00747058775E+00	0.00000000000E+00	0.00E+00	0	0	0	0	0	0	0.00E+00
0.99154504274	−1.05478165168E−01	1.26679890046E−01	1.65E−01	1	0	−1	0	0	2	−1.79E−07
0.85884652974	3.80993429061E−03	3.13308217171E−02	3.16E−02	−1	2	1	0	0	4	−2.44E−07
1.85039157290	−2.23925988594E−02	−1.44580571711E−02	2.67E−02	0	2	0	0	0	2	−4.22E−07
1.98309009373	−2.44099202138E−03	−1.32568671417E−02	1.35E−02	2	0	−2	0	0	4	−3.49E−07
2.84193661727	4.00784500153E−03	−1.25356698070E−03	4.20E−03	1	2	−1	0	0	4	−5.99E−07
1.77559111016	−1.52072571288E−03	−8.99576805769E−04	1.77E−03	−1	3	0	0	1	5	−4.56E−07
0.13269851607	1.00813514094E−03	1.07042080296E−03	1.47E−03	2	−2	−2	0	0	6	6.80E−08
0.78404586978	2.16450443392E−04	1.32911476814E−03	1.35E−03	−2	3	1	0	1	7	−4.75E−07
2.97463513492	9.40915417669E−04	5.29062878968E−04	1.08E−03	3	0	−3	0	0	6	−5.29E−07
0.91674491440	−6.17806113466E−04	8.00639593058E−04	1.01E−03	0	1	−1	0	1	3	1.21E−07
0.92519583057	−2.46742165691E−04	8.36420527563E−04	8.72E−04	0	1	0	0	0	1	−1.67E−07
1.06634556272	5.64409841694E−04	−6.25625906950E−04	8.43E−04	2	−1	−1	0	−1	5	−8.72E−08
2.70923810021	3.56383883664E−04	−7.33469843531E−04	8.15E−04	−1	4	1	0	0	6	−6.68E−07
1.01649220445	3.28856746277E−05	−6.24576837020E−04	6.25E−04	1	0	1	2	0	4	−2.51E−07
3.83348166152	−1.90187603625E−04	4.61107637655E−04	4.99E−04	2	2	−2	0	0	6	−7.76E−07
1.71769305465	−4.98664772686E−04	1.23115635916E−04	5.14E−04	−2	4	2	0	0	8	−4.92E−07
3.70078314491	1.64213771978E−04	3.63648317576E−04	3.99E−04	0	4	0	0	0	4	−8.45E−07
0.07480035379	−3.17085347466E−04	−1.22383602540E−05	3.17E−04	1	−1	0	0	−1	3	−7.47E−08
2.76713632170	2.90731863168E−04	−1.03230861425E−04	3.09E−04	0	3	−1	0	1	5	−4.66E−07
1.92519179534	2.34500701460E−04	1.64329407982E−04	2.86E−04	1	1	0	0	−1	3	−6.28E−07
0.93364709839	−1.67222487925E−05	−2.06332065354E−04	2.07E−04	0	1	1	0	−1	3	−1.04E−07
1.90828958191	−3.65555460978E−05	−1.62225971339E−04	1.66E−04	1	1	−2	0	1	5	−4.33E−07
1.91674094867	−8.01815786472E−05	−1.19950599402E−04	1.44E−04	1	1	−1	0	0	3	−2.70E−07
2.05789024100	1.96857060689E−05	1.35028455434E−04	1.36E−04	3	−1	−2	0	−1	7	−6.30E−07
0.99998863787	3.81733249640E−05	−1.27044015135E−04	1.33E−04	1	0	0	0	−3	4	−6.40E−07
0.15764565741	−1.03879215427E−04	−1.82090791269E−05	1.05E−04	2	−2	0	2	0	6	−2.45E−08
3.96618017460	−7.95081768071E−05	3.03145975212E−05	8.51E−05	4	0	−4	0	0	8	−7.11E−07

Table C.13: (continued)

f_l	A_l^c	A_l^s	A_l	k_l^1	k_l^2	k_l^3	k_l^4	k_l^5	$\lvert k_l\rvert$	$f_l - k_l\omega$
2.63443786652	3.63484596818E−05	−8.25586702391E−05	9.02E−05	−2	5	1	0	1	9	−4.73E−07
1.70079079873	−7.31153787897E−05	−3.95600602644E−05	8.31E−05	−2	4	0	0	2	8	−3.39E−07
4.69232818958	−7.90615567806E−05	−2.18960615405E−05	8.20E−05	1	4	−1	0	0	6	−1.02E−06
1.14919073097	6.03954529817E−05	−5.11545272352E−05	7.91E−05	3	−2	−1	2	0	8	−1.72E−07
2.91673702380	−6.34652302864E−05	1.71564995702E−05	6.57E−05	2	1	−1	0	−1	5	−6.21E−07
0.20749881852	3.23666822639E−05	3.71071191790E−05	4.92E−05	3	−3	−2	0	−1	9	−5.80E−08
0.83389949974	2.64075105263E−05	−4.59686445526E−05	5.30E−05	−1	2	−1	−2	0	6	−3.98E−08
4.82502670764	−2.43581417458E−05	−4.61944290892E−05	5.22E−05	3	2	−3	0	0	8	−9.52E−07
3.62598256622	2.33096839394E−05	4.65334061013E−05	5.20E−05	−1	5	0	0	1	7	−9.95E−07
0.06634907294	4.24954859712E−05	1.82722890948E−05	4.63E−05	1	−1	−1	0	0	3	−1.51E−07
2.00803726380	3.40951234835E−05	3.15737376179E−05	4.65E−05	2	0	0	2	0	4	−4.13E−07
0.70924541433	9.09784036786E−06	4.47435151148E−05	4.57E−05	−3	4	1	0	2	10	−5.02E−07
1.64289264360	−4.27430042540E−05	1.23261474164E−05	4.45E−05	−3	5	2	0	1	11	−4.75E−07
1.78404508362	−4.22066433719E−05	−7.75889513837E−06	4.29E−05	−1	3	1	0	1	6	−1.26E−06
3.75868102278	−1.37197339613E−05	3.74709032577E−05	3.99E−05	1	3	−2	0	1	7	−9.87E−07
0.02494717440	−2.75551804397E−05	2.05873061605E−05	3.44E−05	0	0	2	2	0	4	−5.95E−08
0.72614799121	2.20724638156E−05	1.62390392410E−05	2.74E−05	−3	4	3	0	0	10	−3.34E−07
1.99153818895	1.18296448291E−05	1.89389120951E−05	2.23E−05	2	0	−1	0	−2	5	1.16E−07
2.89983478781	1.76638865773E−05	9.05627336799E−06	1.99E−05	2	1	−3	0	1	7	−4.48E−07
1.87533922249	1.93750476903E−05	−1.27291838698E−06	1.94E−05	0	2	2	2	0	6	−6.30E−09
3.56808462835	1.79820593854E−05	6.18490696050E−06	1.90E−05	−2	6	2	0	0	10	−9.13E−07
1.00844346032	−1.29759900120E−06	−1.87186284005E−05	1.88E−05	1	0	1	0	−3	5	−5.96E−07
2.90828607752	1.70746099826E−05	1.80742940171E−06	1.72E−05	2	1	−2	0	0	5	−3.63E−07
0.84194475913	−9.72056684474E−06	1.36199668757E−05	1.67E−05	−1	2	−1	0	2	6	3.95E−07
2.86688390665	−9.56653265698E−06	1.32122957784E−05	1.63E−05	1	2	1	2	0	6	−5.44E−07
3.04943549743	−1.40122111743E−05	−8.60915767730E−06	1.64E−05	4	−1	−3	0	−1	9	−5.95E−07
4.55962967205	−1.37019349158E−05	8.31028924353E−06	1.60E−05	−1	6	1	0	0	8	−1.09E−06
2.69233634811	1.44945829610E−05	−5.74207222916E−06	1.56E−05	−1	4	−1	0	2	8	−1.13E−08
2.78403855834	−6.55859248748E−06	1.22558702819E−05	1.39E−05	0	3	1	0	−1	5	−6.38E−07
5.68387323728	1.01265082194E−05	−7.02139089473E−06	1.23E−05	2	4	−2	0	0	8	−1.20E−06
2.14073574692	1.03662073748E−07	1.21357409043E−05	1.21E−05	4	−2	−2	2	0	10	−3.78E−07
0.99573437574	−9.35012140053E−06	7.12183285492E−06	1.18E−05	0	1	5	7	7	20	1.08E−04
4.61752778262	−1.11333769255E−05	−2.61944541468E−06	1.14E−05	0	5	−1	0	1	7	−1.00E−06
2.11578860820	−5.71480986227E−06	7.78448635708E−06	9.66E−06	4	−2	−4	0	0	10	−2.83E−07
3.90828224591	4.30703252883E−06	−9.35468661853E−06	1.03E−05	3	1	−2	0	−1	7	−6.20E−07
1.05788560184	8.14880043052E−06	−4.65012373629E−06	9.38E−06	2	−1	−2	0	−2	7	−1.70E−06
0.79250186217	4.63655989268E−06	8.39153981402E−06	9.59E−06	−2	3	2	0	1	8	7.39E−07
1.14114595054	6.46664288830E−06	−6.63213112926E−06	9.26E−06	3	−2	−1	0	−2	8	−1.28E−07
3.77558379837	−3.20297747852E−06	−7.93079034523E−06	8.55E−06	1	3	0	0	−1	5	−6.20E−07
2.57653958556	−2.97423261573E−06	−7.82907527671E−06	8.37E−06	−3	6	3	0	0	12	−7.35E−07
1.82544656941	2.73067375014E−06	7.65110670247E−06	8.12E−06	0	2	−2	−2	1	7	−1.77E−06
2.77558755928	6.18641051420E−06	−5.33289991022E−06	8.17E−06	0	3	0	0	0	3	−4.33E−07
0.00845128957	−6.46898380520E−06	2.39199557924E−06	6.90E−06	0	0	1	0	−1	2	8.51E−08
0.14960035934	−6.70836623181E−06	−5.01506951358E−07	6.73E−06	2	−2	0	0	−2	6	−4.98E−07
4.95772522938	2.14829595792E−06	−6.26901411429E−06	6.63E−06	5	0	−5	0	0	10	−8.78E−07
5.55117471881	9.56541900065E−07	−6.36508403852E−06	6.44E−06	0	6	0	0	0	6	−1.27E−06
1.08284060643	2.76973629802E−06	−5.66645972832E−06	6.31E−06	2	−1	0	2	0	5	−1.07E−06
1.79249331810	6.19572083854E−06	−1.28296359086E−06	6.33E−06	−1	3	2	0	−1	7	−6.57E−07
2.55963667163	2.24671033961E−06	−5.77579194280E−06	6.20E−06	−3	6	1	0	2	12	−1.24E−06
0.23244609223	−6.07994884203E−06	−1.31223444897E−06	6.22E−06	3	−3	0	2	−1	9	−1.81E−08
5.81657175339	4.97327144386E−06	1.05536107985E−06	5.08E−06	4	2	−4	0	0	10	−1.13E−06
2.99958234593	−4.58402656390E−06	5.95524774225E−07	4.62E−06	3	0	−1	2	0	6	−5.52E−07
4.75022625405	−2.25692996805E−06	−3.90320117994E−06	4.51E−06	2	3	−3	0	1	9	−9.77E−07
1.85883478214	4.53546434180E−06	7.94264847850E−07	4.60E−06	1	1	−5	−6	7	20	6.89E−07
3.55118216797	1.98448584830E−06	3.61073381747E−06	4.12E−06	−2	6	0	0	2	10	−9.65E−07
0.98750654992	3.47559188040E−06	1.51119557971E−06	3.79E−06	1	0	−1	−1	−6	9	1.61E−06

C.3 Solar System bodies, Earth–Moon case

In tables C.14 to C.38 we give the results of the Fourier analysis of the positions of the Solar System bodies in adimensional coordinates for the Earth–Moon case. We do not give adjustments of the frequencies as linear combinations of basic ones because they have not been used in any model. In order to save space, every row of these tables correspond to two entries, which are separated by a double vertical line.

Table C.14: Fourier analysis of the x coordinate of Mercury in the Earth–Moon case.

f_l	A_l^c	A_l^s	f_l	A_l^c	A_l^s
0.0000000000	−6.1832149315E−02	0.0000000000E+00	0.9251957920	−1.0928063833E+02	3.7077795940E+02
0.6894159197	−1.0101290726E+02	1.0561872925E+02	0.9999964332	8.9935750877E+00	3.6020438652E+01
1.9167408602	−1.7659403352E+01	−2.6374791052E+01	0.3788352812	1.4827352448E+01	1.1066052719E+00
0.0663492681	−1.2130305561E+01	−5.2384722707E+00	1.6809609788	−1.3546555613E+00	−1.1910673956E+01
1.7840423142	−6.0399777014E+00	−9.9527047380E−01	2.7755873701	3.2559715888E+00	−2.8228398320E+00
0.3021291413	−4.0529961158E+00	2.7871949477E−01	0.8503958335	−8.9715754203E−01	3.6202546311E+00
1.9915416053	−2.6594614903E+00	−1.1930071724E+00	2.9082859151	2.4378933530E+00	2.5466184359E−01
1.5482624416	−1.8459849434E+00	−1.3803073693E+00	0.0682546172	−1.3079039259E+00	−1.8541948747E+00
2.5398075035	1.5744072132E+00	−3.7576993313E−01	1.3105776731	1.1647957735E+00	1.9269805437E−01
1.3703803484	−8.4810264639E−01	8.7638456290E−01	0.0084515388	−6.8875342548E−01	8.6205571595E−01
0.1694306054	−5.8750481350E−01	7.1671478126E−01	2.6725060380	7.7318659396E−01	5.0788338438E−01
1.3145999983	−6.8437848778E−01	−4.1822057377E−01	0.6934375512	−7.8430975009E−01	−1.5759580254E−01
1.0828409511	−3.0837951101E−01	6.2830633916E−01	3.7671324360	1.3394409203E−02	6.6478330470E−01
1.0578943232	5.4875428685E−01	−2.7806944362E−01	1.8588429739	−5.0908602645E−01	2.1726123296E−01
1.8419405879	−3.0101281640E−01	−4.1199245476E−01	0.6127097840	2.4014940529E−01	−3.3638981541E−01
0.1411499465	−3.9065397711E−01	−4.6639560025E−02	0.2423259998	−1.0867856784E−01	−3.9575150204E−01
2.8503881520	9.7745522135E−02	−3.6104108644E−01	2.7007870619	2.3998757823E−01	−2.2410520331E−01
1.7092425747	−3.2194983989E−01	−4.2013329944E−02	1.3186213308	4.7482994309E−03	2.9491136099E−01
1.0040184187	−2.3181467869E−01	−9.0670065100E−02	3.5313525748	−1.1085727920E−01	2.2361596283E−01
0.7642165631	1.7699816669E−01	−1.7058558257E−01	1.2376818051	1.0914471880E−02	2.3424807841E−01
0.6146155310	−1.4940790104E−01	1.6875391707E−01	1.1609756477	−4.2600924181E−02	−2.2178724899E−01
2.9830867697	1.8985184390E−01	−1.0049730028E−01	3.8998309641	−1.3278011973E−01	1.2944204328E−01
0.8221144576	1.7796462583E−01	1.3913681574E−03	1.0597996720	1.8551267715E−01	1.4879769349E−02
2.2292268814	−1.3129337808E−01	−9.9398441683E−02	1.8503915261	−1.4456090544E−01	−9.3170475835E−02
3.6344338978	9.6906806343E−02	8.7287062011E−02	1.9416881358	1.0184946842E−01	3.6082771194E−02
2.4650068784	1.0605039349E−01	−2.9939541501E−02	1.4734619748	−8.5242069708E−02	−5.8634187132E−02
1.6061604186	−1.4412913609E−02	−9.3303018960E−02	0.4800112365	−1.8324279736E−02	−9.2484918266E−02
1.6211586652	−6.5149745816E−02	7.0693725000E−02	2.6428888361	3.7166649527E−03	−9.2857224421E−02
2.3021224401	−7.3155398059E−02	6.3495335775E−02	2.3619253945	−1.0096588177E−02	−9.3571364234E−02
1.6251815556	7.7405335675E−02	−2.6049374845E−02	0.3828565298	3.8689596818E−02	7.1721118194E−02
1.7557614338	5.8691337990E−03	7.9022914704E−02	0.5529065688	7.4476120146E−02	3.3307795060E−02
1.0080405734	−6.3215274509E−02	4.2482705595E−02	4.7586774916	−5.9887443339E−02	−4.7829555358E−02
3.6640510968	−6.6917623289E−02	2.0347063000E−02	2.3061450689	6.2241956510E−02	−2.1153246754E−02
1.6849787899	4.9140122366E−02	−4.2898604679E−02	1.6146116431	−3.2354180335E−02	−5.6296359295E−02
1.1326951054	4.2482400204E−02	−4.6207942620E−02	0.9232903400	1.6212963977E−02	6.0840872071E−02
4.6259789572	−5.7399035784E−02	8.3302542667E−03	1.0747969770	−1.4614189019E−02	−5.6139418011E−02
2.0494393193	−1.4050409243E−02	6.1489461656E−02	3.6923319466	3.2374159898E−03	5.5445349822E−02
3.8419333407	3.3167430567E−02	4.4008839247E−02	1.2936742428	3.1737088199E−02	−4.3884216444E−02
0.7924971878	−2.6334754802E−02	−4.4815390108E−02	2.8334854729	5.4342641919E−02	3.4346588066E−03
3.3986540236	1.6981573791E−02	4.5757401241E−02	0.7755942437	−7.0649932841E−03	4.5755453648E−02
1.7059088377	3.0961204791E−02	3.3277413563E−02	2.0743862883	−1.7969511597E−02	−4.0450408531E−02
0.0946298940	−2.5648462233E−02	3.4051408107E−02	0.9271022792	2.6631219328E−02	−2.3798423447E−02
2.4071089637	1.7351511214E−02	−3.0236426352E−02	0.3190327967	1.6862574051E−02	2.8019655972E−02
0.7492190805	−1.9237687596E−02	−2.7624667721E−02	1.6292019609	−2.3475354539E−02	−1.8692250086E−02
4.5228976253	−1.1624337814E−02	−2.6298706164E−02	0.8470971490	2.6945611061E−02	−1.0084461040E−02
0.9915539268	1.9053523977E−02	−1.9448278101E−02	0.7675516824	−3.4039509959E−03	2.8162048736E−02
2.8419364190	2.5206870621E−02	−7.9584037846E−03	3.2207719214	2.4732330433E−02	−5.7518871402E−03
1.9186467545	9.6610538920E−04	2.5173018699E−02	0.4536357141	−2.4890942532E−02	−2.8202996153E−03
0.0912947399	2.4211495121E−02	−6.0836513495E−03	2.3101660046	−1.8873866049E−02	−1.5070693253E−02
0.5358019336	−2.4438757916E−02	−2.9573044012E−03	0.3040346934	2.2926795776E−02	7.8998708934E−04
1.4715571515	2.0087951764E−02	1.1173212204E−02	1.1569235755	−2.3408389881E−02	−3.5426799357E−03
0.2357799381	−2.0967869825E−02	1.0798679184E−02	1.8136594746	−1.4109227679E−02	1.6678856703E−02
0.9830935351	2.1572434452E−02	−3.5236310526E−03	0.2981077931	−1.0250945760E−02	1.8989399232E−02
0.3230550018	−3.1083663701E−03	−2.1330281331E−02	2.0663422442	1.8362142215E−02	1.0602200500E−02
0.2273290275	−2.1026180985E−02	2.2218084172E−03	4.3901990829	−2.0434931289E−02	−7.2072607671E−03
1.9955630308	1.7704957167E−02	−9.7663879593E−03			

Table C.15: Fourier analysis of the y coordinate of Mercury in the Earth–Moon case.

f_l	A_l^c	A_l^s	f_l	A_l^c	A_l^s
0.0000000000	−4.2139923940E−04	0.0000000000E+00	0.9251957920	3.7199834763E+02	1.0963985868E+02
0.6894159197	1.0561709847E+02	1.0101132663E+02	0.9999966996	3.6031719882E+01	−8.9141845910E+00
1.9167408450	−2.6427468092E+01	1.7699376255E+01	0.3788352807	1.1065347156E+00	−1.4827127804E+01
1.6809609788	−1.1910651631E+01	1.3546536334E+00	0.0663492681	3.2910658964E+00	−7.6246850975E+00
1.7840423140	−9.9744458937E−01	6.0530925614E+00	2.7755873778	−2.8254522752E+00	−3.2594102621E+00
0.3021291413	−2.7867367115E−01	−4.0522109790E+00	0.8503951632	3.7999474957E+00	9.8987267714E−01
1.9915416053	−1.1927084739E+00	2.6592758477E+00	2.9082859151	2.5507556991E−01	−2.4418617882E+00
1.5482624416	−1.3803000910E+00	1.8459749237E+00	0.0682546648	−1.8546231364E+00	1.3071639494E+00
2.5398075035	−3.7577231238E−01	−1.5744169462E+00	1.3105776731	1.9266556559E−01	−1.1647737287E+00
1.3703803278	8.7654236579E−01	8.4797295843E−01	0.0084515400	8.5474108961E−01	6.7033534456E−01
0.1694306047	−7.1581540928E−01	−5.8675772335E−01	2.6725060400	5.0789643344E−01	−7.7317954320E−01
1.3146000050	−4.1991055410E−01	6.8705434126E−01	0.6934377448	−1.5933116280E−01	7.8705371928E−01
1.0828411474	6.3387286272E−01	3.1232035017E−01	3.7671324360	6.6530370356E−01	−1.3403638884E−02
1.8588433151	2.1589548004E−01	5.0964300266E−01	1.8419405823	−4.2242064961E−01	3.0435966912E−01
0.6127097865	3.3632201972E−01	2.4010818475E−01	0.2423260061	3.9574314671E−01	−1.0866271003E−01
2.8503881520	−3.6101460611E−01	−9.7709785468E−02	2.7007870614	−2.2458042173E−01	−2.4082565876E−01
1.7092416559	−4.0611587612E−02	3.2458264733E−01	1.0578943322	−1.4653063037E−01	−2.8926152500E−01
0.1411500580	2.7088147387E−03	2.8721299863E−01	1.3186213286	2.9755790699E−01	−4.7959391462E−03
1.1609756494	2.5216118465E−01	−4.8471140320E−02	1.0040182453	−9.0715049005E−02	2.3288569940E−01
3.5313525460	2.2364335253E−01	1.1080606139E−01	0.7642159294	−1.7151227528E−01	−1.7614494561E−01
1.2376818002	2.3424723533E−01	−1.0923668875E−02	0.6146155286	1.6872524619E−01	1.4933479633E−01
2.9830867698	−1.0050322403E−01	−1.8981133762E−01	3.8998309641	1.2962044044E−01	1.3296304438E−01
0.8221144575	1.3912154788E−03	−1.7795793266E−01	1.0597996728	1.4880611070E−02	−1.8551335868E−01
2.2292268461	−9.9361573476E−02	1.3132252137E−01	1.8503914015	−9.2940556044E−02	1.4452750594E−01
3.6344338977	8.7357487652E−02	−9.6984388192E−02	1.9416879809	3.6023627454E−02	−1.0208491081E−01
2.4650075919	−2.9310685379E−02	−1.0615826855E−01	1.4734619763	−5.8634179724E−02	8.5240707853E−02
1.6061604386	−9.3300482233E−02	1.4398294944E−02	0.4800112528	9.2374702874E−02	−1.8284592571E−02
1.6211587177	7.0677238268E−02	6.5165255816E−02	2.6428888361	−9.3017949906E−02	−3.7235983372E−03
2.3021231766	6.3015804384E−02	7.3479383374E−02	2.3619253941	−9.3571324557E−02	1.0096877149E−02
1.6251815875	−2.6136655648E−02	−7.7720339514E−02	0.3828564706	7.1991084402E−02	−3.8877879715E−02
1.7557614338	7.9023406989E−02	−5.8691618262E−03	0.5529070806	−3.3521368603E−02	7.4330084749E−02
1.0080406214	4.3040433886E−02	6.3883785511E−02	4.7586774977	−4.7864583917E−02	5.9925019615E−02
3.6640510968	2.0347067322E−02	6.6917627051E−02	2.3061450726	−2.1160354041E−02	−6.2270010356E−02
1.6849788521	−4.2891780752E−02	−4.9180693778E−02	1.6146116429	−5.6300279073E−02	3.2356529015E−02
1.1326950264	−4.6221267692E−02	−4.2427164162E−02	0.9232904918	−6.0982271238E−02	1.6487164726E−02
4.6259789572	8.3345170637E−03	5.7429574628E−02	1.0747969794	−5.6188286879E−02	1.4606232629E−02
0.7755954413	5.6526427932E−02	1.4674268836E−02	3.6923319463	5.5563261225E−02	−3.2171260298E−03
1.2936741581	4.5185970823E−02	3.2629564759E−02	3.8419333407	4.4000777855E−02	−3.3167695580E−02
0.0912953599	1.3236281363E−02	5.3695320286E−02	2.8334854701	3.6829445617E−03	−5.4978294687E−02
2.0494393861	5.1176796448E−02	1.1719749988E−02	3.3986540235	4.5757531365E−02	−1.6981636963E−02
1.7059087216	3.3249975763E−02	−3.0992869086E−02	2.0743856365	−4.0440544827E−02	1.8221887363E−02
0.7924972522	−3.4906206936E−02	2.0507699882E−02	0.0946304714	−3.3908136553E−02	−2.5789389757E−02
0.7675512164	3.7335133868E−02	4.4101370804E−03	0.9271021911	−2.3812068728E−02	−2.6612832635E−02
2.4071089635	−3.0236380437E−02	−1.7351439153E−02	0.3190329217	2.8650103860E−02	−1.6217531643E−02
0.7492190793	−2.7624426131E−02	1.9237767099E−02	1.6292019653	−1.8860577391E−02	2.3684984714E−02
0.8470876420	−1.2290629014E−02	−2.6669340573E−02	4.5228976253	−2.6298729590E−02	1.1624349362E−02
1.4715555937	−1.2327972262E−02	2.3021533558E−02	2.8419364184	−7.9596044205E−03	−2.5209166543E−02
3.2207719214	−5.7519037054E−03	−2.4732379302E−02	1.9186469351	2.5175937469E−02	−9.3111342172E−04
0.4536354500	−2.7678282358E−03	2.4902630283E−02	0.9915549967	−1.7004982725E−02	−1.7025967311E−02
2.3101660038	−1.5088206669E−02	1.8895983219E−02	0.3040346553	7.8275093538E−04	−2.2903423676E−02
0.2981099929	−1.9786152631E−02	−1.1091442891E−02	0.3230549791	−2.2358418839E−02	3.2951853448E−03
0.2357799900	−1.0778386886E−02	−2.0949732331E−02	1.8136594809	1.6677889064E−02	1.4109912461E−02
0.3270762646	1.5121073625E−02	1.7569778711E−02	2.0663422428	1.0606788092E−02	−1.8365465518E−02
0.2273286915	−2.2752599119E−03	−2.0996325924E−02	4.3901990829	−7.2072565022E−03	2.0434929663E−02
1.9955628418	−9.7991417888E−03	−1.7700752025E−02	2.1694241402	1.8600360946E−02	7.9521204409E−04
2.6146080299	3.8185586397E−03	1.9374805800E−02	0.5115338110	−1.4067930235E−02	1.1396981710E−02
3.4565522967	1.7170645021E−02	7.7245102427E−03	0.5358055130	−2.8157440907E−03	1.8215737765E−02
1.6230630470	1.1602897632E−02	−1.4280612653E−02	0.5567174241	−1.7383263776E−02	9.0643122314E−04
1.0861755967	1.7363327499E−02	−3.9484785337E−03	1.1569170112	−1.8350445075E−03	1.7478817547E−02
2.6259866761	−1.2066157015E−02	−1.1998271362E−02	0.8634832600	−7.3763598754E−03	−1.5465346478E−02
3.5596335699	1.0132465154E−02	−1.2094069866E−02	3.9746315484	1.5252971284E−02	2.5934140392E−03
1.9251975466	1.4050565463E−02	−3.4628167037E−03	0.7905915164	−6.7661683805E−03	1.2680348655E−02
0.5317702407	1.1617938751E−02	7.7683226264E−03	4.8913760485	−1.3851240676E−02	1.0871129399E−03
2.0513447501	1.0265138950E−02	1.0045839957E−02	2.1525204495	−6.6880512542E−03	1.2203500437E−02
0.2159504039	−9.7138579561E−04	1.4335456150E−02	3.1609696356	−8.8231918387E−03	9.6493437804E−03

Table C.15: (continued)

f_l	A_l^c	A_l^s	f_l	A_l^c	A_l^s
2.5977058433	6.6940351636E−03	−1.1065960110E−02	1.6344445652	−1.4886103020E−03	1.2585379945E−02
0.0722759855	−1.1585262111E−02	−4.7438237694E−03	0.0748027138	2.3883240495E−03	1.3266691230E−02
1.9317388241	−1.2617735994E−02	2.8373775756E−03	1.9357657371	1.1304601826E−02	4.7183145108E−03
0.3769294943	3.3486215662E−04	1.2253395380E−02	2.0164837989	−2.5403598344E−03	−1.1723155743E−02
5.6175240041	−9.8775878829E−03	−6.0525734944E−03	1.5522843141	−1.2548539737E−02	−9.5029083678E−04
2.1734465820	−1.1510266844E−02	−5.2485864497E−03	1.2338710813	4.7254693658E−03	−1.0381595461E−02

Table C.16: Fourier analysis of the y coordinate of Mercury in the Earth–Moon case.

f_l	A_l^c	A_l^s	f_l	A_l^c	A_l^s
0.0000000000	−2.7803236118E+00	0.0000000000E+00	0.0788228302	−2.9527711603E+00	3.3930352582E+01
0.3105814105	−1.7595438940E+01	−3.1169441528E+00	0.3146027030	5.0147928139E+00	1.2212242845E+01
0.0040220919	−1.9422791393E+00	2.7569144763E+00	0.6211620110	1.3851746533E+00	−1.1800326158E+00
0.6251833349	−1.2835462398E+00	−3.9553212854E−01	0.9127222247	7.6524206371E−01	5.3171925448E−01
1.0703678936	−6.6126578396E−01	−6.5548181581E−01	1.3021264872	3.7214960979E−01	−3.1400830057E−01
0.6809636021	2.4144375633E−01	−4.2288693966E−01	1.3061477844	−3.4052093289E−01	−1.0721803432E−01
0.1569573404	1.8357701045E−01	2.9225587969E−01	0.6769423608	1.7036464852E−01	3.2198602608E−01
0.9317427003	4.3833289579E−03	2.7779766462E−01	0.1536244738	−7.6799311782E−02	2.1523935526E−01
0.9357639905	1.7109866616E−01	−1.1286076416E−01	0.7800236418	1.9239920925E−01	−4.1137225828E−02
0.9376693493	−1.9376625797E−01	6.7253077135E−03	0.9915427262	9.4844768241E−02	−1.1828396760E−01
0.3065589342	−1.0440100971E−01	2.2190455646E−02	0.9955677623	−2.7382449418E−02	−9.2070266856E−02
0.9875230510	8.9299835761E−02	4.9510413408E−03	1.1694278630	4.8182237916E−03	−8.9377679917E−02
0.5482651119	−2.6145950068E−02	−8.5618675652E−02	0.5442438061	7.3545344798E−02	2.0233128374E−02
1.5398101236	6.8086192407E−02	2.8590546847E−02	1.9292143911	4.3190763872E−02	−5.5597017196E−02
2.1609728448	5.4156089663E−02	5.0201642691E−02	1.1734492259	−5.7284023123E−02	3.2093895268E−02
1.7715687461	−3.0151371244E−02	5.7546267867E−02	2.1649942901	9.8979857977E−03	−5.3237745639E−02
1.9042672888	−4.8972562911E−02	1.3521218955E−02	1.2423233016	−3.9303051957E−02	−3.1332237657E−02
1.6127071147	5.3459124144E−04	4.9582380546E−02	0.3703829894	−4.8862933733E−02	8.4471248065E−03
2.0619129550	5.0596036713E−02	−4.8515441201E−03	0.0538758883	−3.3082826746E−02	3.7118286976E−02
1.6167284177	3.0436346323E−02	−1.9818805648E−02	1.2463446081	−3.8975014454E−03	3.6866725523E−02
0.4675388433	−3.4391774412E−02	−4.0462592385E−03	0.3663617227	1.4280195138E−02	−3.4200621437E−02
1.5357888989	−2.1515267838E−02	1.4959028819E−02	2.2936715083	1.7812165917E−04	2.6535049503E−02
1.6725087114	9.2774270875E−03	2.4863599747E−02	1.6934345461	−2.4936713429E−02	1.1563060688E−02
0.8588469936	−3.2237874826E−03	−2.7680161640E−02	0.8628686569	−2.2553149609E−02	−7.3506191079E−03
1.8503923040	1.9254920183E−02	1.2563687729E−02	1.8544136843	1.6863638489E−02	−1.0838828909E−02
2.2976928187	1.6425106086E−02	−1.0561913303E−02	1.6684874188	−1.9418621293E−02	−4.0940708707E−03
0.8548244269	1.3265097684E−02	−1.2868075477E−02	0.2896555878	−4.5469216054E−03	1.7632796729E−02
0.2398024460	−7.3987369355E−03	−1.6252711028E−02	0.3894030832	5.7773676599E−03	1.5611216758E−02
0.0748023690	−1.5623863707E−02	2.8653213604E−04	0.0821565786	7.7368308644E−03	1.1242357975E−02
1.1485031086	−1.2619506472E−02	−1.7668783344E−03	2.9207594804	2.3270021335E−03	1.0584480350E−02
0.8379188509	1.0374128215E−02	4.3095641848E−03			

Table C.17: Fourier analysis of the x coordinate of Venus in the Earth–Moon case.

f_l	A_l^c	A_l^s	f_l	A_l^c	A_l^s
0.0000000000	−6.2642839565E−02	0.0000000000E+00	0.9251957863	−1.0927968192E+02	3.7071133481E+02
0.8784059694	−1.6727976517E+02	−2.2427016795E+02	1.9167408301	−1.7639352629E+01	−2.6357601900E+01
1.8699510136	2.2915909188E+01	1.2265613550E+00	0.0663492628	−1.2133818206E+01	−5.2407806300E+00
0.9999957119	1.2161215981E+00	−7.8685997480E+00	0.1131390781	1.8152971635E+00	7.5626398399E+00
1.7840423146	−6.0101531838E+00	−1.0056903515E+00	1.7372524954	3.1925701491E+00	−3.0459186625E+00
2.7755873602	3.2440038185E+00	−2.7915580013E+00	0.8503953778	−9.3197829972E−01	3.6754598218E+00
2.7287975433	2.0910353121E−01	3.0914816967E+00	2.9082858705	2.4343303058E+00	2.5545834861E−01
2.8614960545	−1.2042750353E+00	1.2984462091E+00	0.0195594408	1.5401266546E+00	−8.8150358303E−01
0.7568151567	−8.1015926996E−01	4.8107002580E−01	1.9915410064	5.1345276560E−01	6.2354023452E−01
0.8824266457	−1.0431651749E−01	−7.3673057850E−01	1.1256105586	−5.7501556482E−01	4.7445621660E−01
1.0828414489	−3.1061227002E−01	6.2658562762E−01	1.0578942933	5.4861005448E−01	−2.7785938815E−01
3.7671324045	1.0696507497E−02	6.5979649840E−01	1.1296312066	5.5513082454E−01	−1.0296544012E−01
1.8419399583	−3.0280383812E−01	−4.1409771811E−01	0.9532060021	2.6743972473E−01	3.8718278834E−01
3.7203425812	−3.8696818626E−01	−2.8022914052E−01	0.8036053972	−2.7164735317E−01	−3.3532321251E−01
0.9719855974	−3.8872075375E−01	1.4483597884E−01	1.0111045164	−5.9246282969E−02	3.3548805544E−01
1.7092421686	−3.2166587043E−01	−4.1639927983E−02	2.7007868419	2.3941707385E−01	−2.2306999124E−01
1.1215899802	9.1243184864E−02	−2.2779302746E−01	2.6539968089	2.2828106939E−02	2.0975157964E−01
1.6624521441	1.3800536542E−01	−1.4219405751E−01	1.7951506086	1.8078822837E−01	2.6346610316E−03

Table C.17: (continued)

f_l	A_l^c	A_l^s	f_l	A_l^c	A_l^s
3.8998309205	−1.3262054651E−01	1.2907331935E−01	1.8503916999	−1.4436255009E−01	−9.3273343085E−02
1.9447513124	−1.5110445176E−01	−1.3898887134E−02	1.8588425515	1.6320253602E−01	1.2107757846E−02
0.0084508070	1.1148278332E−01	−8.3359861555E−02	3.8530411098	−1.7171764725E−02	−1.3279052345E−01
0.1411500133	−1.0861867193E−01	−6.1748243747E−02	3.6344338869	9.5279898975E−02	8.6885247056E−02
1.8036019180	1.1665388592E−01	−4.2966476521E−02	2.8503872386	−9.3768209690E−02	9.4172791137E−02
1.9416880330	1.0190835997E−01	3.5993549061E−02	1.1046841152	−9.2963788153E−02	−4.5910918547E−02
2.6428888422	4.1355979272E−03	−9.2011417116E−02	3.5876440683	−9.1770903195E−02	1.7513845610E−02
1.8948981805	−7.2452530610E−02	4.8326034407E−02	0.0943598501	7.2468857435E−02	−3.7843421051E−02
1.7483607061	1.2460610386E−02	−7.6268286095E−02	2.9830856299	−7.4612858219E−02	−1.8992415243E−03
4.7586774505	−5.9193675902E−02	−4.7687822034E−02	2.0494404193	−1.4514324089E−02	6.1311121341E−02
2.5960990296	5.1555781552E−02	4.2370744003E−02	1.8739729383	5.2529459696E−02	3.1449144461E−02
2.1171555677	2.6163984638E−04	−6.1102264350E−02	4.6259789316	−5.6696984634E−02	7.8188095125E−03
1.0360514761	2.6658302614E−02	5.2729326646E−02	2.8334852979	5.4455869179E−02	3.5330842221E−03
3.6923320495	3.0223633853E−03	5.5245460440E−02	4.7118876304	5.3334818325E−02	−1.3599596732E−02
0.7755950721	−1.0735498045E−02	4.9586459130E−02	0.7924973102	−2.6106026837E−02	−4.4731133093E−02
2.1211763726	−2.2650778384E−02	4.0343469150E−02	0.0467907180	2.6918202227E−02	3.6276497783E−02
2.0743864952	−1.7893541495E−02	−4.0480955348E−02	2.0026495641	−2.6999372907E−02	−3.1946144654E−02
0.0383387182	1.0970526166E−02	3.9024998782E−02	4.5791891132	2.0095190635E−02	−3.6285117793E−02
2.8035980446	−1.0533241065E−03	−3.7805935068E−02	3.6455420790	−3.0009438161E−02	−1.9980002293E−02
1.8120527642	−2.6412492844E−02	2.3342690806E−02	0.7457075245	3.3117754723E−02	3.8260795426E−03
0.8971853122	−2.6898815481E−02	1.1779612586E−02	0.9915486447	1.9489784667E−02	−2.0468497276E−02
1.9251844877	2.4442573385E−02	1.5246217549E−02	0.7675501857	−3.2057598954E−03	2.8005880698E−02
0.2347303706	−2.4718773416E−02	8.6728688394E−03	2.8419362600	2.5144481438E−02	−7.9571507884E−03
2.7866958968	−1.6154532240E−02	1.8777973629E−02	0.0912963859	2.4246618069E−02	−5.7890290220E−03
0.1879393019	−4.6184521813E−03	−2.3013742984E−02	0.9679649531	−1.4615824724E−02	1.7092999325E−02
3.8419325579	−1.8039481592E−03	−2.3639982246E−02	0.7247809697	−6.8365222503E−03	−2.1402102692E−02
2.9362965158	1.4654757643E−02	−1.4604588447E−02	0.1091186669	1.3564469620E−02	1.4788807294E−02
2.7951465070	−6.3646856964E−03	1.8013196745E−02	1.9635305928	6.4666102450E−03	−1.8430059301E−02
0.1340654895	−1.9645362086E−02	−3.6702801003E−03	0.9447812537	2.2383164223E−03	1.8363471676E−02
2.1131349751	9.5715200129E−03	1.7702408859E−02	1.8784011296	−1.7920694906E−02	5.4919009209E−03
0.7207600212	−1.4502467862E−02	−1.3632300027E−02	1.0747958353	−4.4143806602E−03	1.8169985741E−02
2.6259864890	1.1922503582E−02	−1.1996342500E−02	1.0187756934	−1.3605985223E−02	−8.8351435862E−03
1.6156607908	−9.1416790623E−03	−1.1743860137E−02	3.5596335866	1.1966568337E−02	1.0095510989E−02
1.0080418678	8.4128168887E−03	−1.1967842436E−02	1.0859060071	−2.9918743621E−03	1.3399741117E−02
2.0275967064	−1.3905440237E−02	−3.2164796985E−03	0.1380864528	−1.0439603603E−02	−8.6922197588E−03
4.8913759607	−1.0717832439E−03	−1.3799703027E−02	1.6344410577	−1.2526838400E−02	−1.0748815782E−03
1.9844067848	−1.0879340298E−02	−5.3769083089E−03	1.0040180653	−1.1641668446E−02	−4.5287310833E−03
5.6175239754	6.0380128768E−03	−9.6882898575E−03	1.7412735557	1.1323287620E−02	−3.0543571113E−03
2.6072064234	1.0460088026E−02	3.9342125884E−04	1.1326949964	1.0001082239E−02	−2.7702064182E−03
2.5791963484	1.4949634627E−03	1.0047858230E−02			

Table C.18: Fourier analysis of the y coordinate of Venus in the Earth–Moon case.

f_l	A_l^c	A_l^s	f_l	A_l^c	A_l^s
0.0000000000	6.8113299129E−05	0.0000000000E+00	0.9251957863	3.7193258140E+02	1.0963971764E+02
0.8784059694	−2.2426664007E+02	1.6727713447E+02	1.9167408301	−2.6412608931E+01	1.7676163469E+01
1.8699510136	1.2265587389E+00	−2.2915863127E+01	0.0663492628	3.2938305799E+00	−7.6258421659E+00
0.9999963579	−7.8655705732E+00	−1.2489546238E+00	0.1131390781	−7.5612286125E+00	1.8149602374E+00
1.7840423129	−1.0078177642E+00	6.0232894094E+00	1.7372524954	−3.0459014220E+00	−3.1925521818E+00
2.7755873570	−2.7944517696E+00	−3.2472327638E+00	0.8503953754	3.7413648812E+00	9.4402318624E−01
2.7287975391	3.0914884044E+00	−2.0918645158E−01	2.9082858792	2.5601194446E−01	−2.4383000096E+00
2.8614960545	1.2984456915E+00	1.2042745389E+00	0.0195594410	−8.7999962200E−01	−1.5375083520E+00
0.7568151569	4.8106096806E−01	8.1014980029E−01	1.9915410065	6.2383475960E−01	−5.1363334705E−01
0.8824266460	−7.3964768194E−01	1.0470921629E−01	1.1256105551	4.7634214627E−01	5.7727721049E−01
1.0828414490	6.3270607303E−01	3.1364557274E−01	3.7671324045	6.6031811646E−01	−1.0705056544E−02
1.1296312075	−1.0388637465E−01	−5.6011189567E−01	1.8419405985	−4.1826634325E−01	3.0351918342E−01
0.9719856104	−1.7771106221E−01	−4.7709099926E−01	0.9532066198	3.8833495270E−01	−2.6597277665E−01
3.7203425865	−2.8024382020E−01	3.8696051329E−01	0.8036053973	−3.3522458354E−01	2.7157420433E−01
1.0111045165	3.3546735075E−01	5.9242940322E−02	1.0578942880	−1.4631511409E−01	−2.8885900510E−01
1.7092415589	−4.0484976942E−02	3.2298070115E−01	2.7007868418	−2.2342368206E−01	−2.3977434531E−01
1.1215898504	−2.2782623242E−01	−9.0989939131E−02	2.6539968089	2.0975318872E−01	−2.2828325087E−02
1.6624521441	−1.4219253905E−01	−1.3800375381E−01	1.7951506086	2.6341690112E−03	−1.8078602749E−01
3.8998309205	1.2925194703E−01	1.3280407851E−01	1.8503917039	−9.3206211143E−02	1.4425034030E−01
0.0084508757	−9.0484224956E−02	−1.3002996374E−01	1.9447513125	−1.3899189965E−02	1.5110398952E−01
1.8588425516	1.2125636924E−02	−1.6328858754E−01	3.8530411098	−1.3279051638E−01	1.7171764954E−02

Table C.18: (continued)

f_l	A_l^c	A_l^s	f_l	A_l^c	A_l^s
3.6344338869	8.6955990074E−02	−9.5357530023E−02	1.8036015903	−4.3209814300E−02	−1.1656224962E−01
2.8503878236	9.3809102194E−02	9.4114070585E−02	1.9416880330	3.6063623131E−02	−1.0210668334E−01
1.1046841274	4.7253732523E−02	−9.5668526652E−02	2.6428888420	−9.2172454143E−02	−4.1426808232E−03
3.5876440683	1.7513887103E−02	9.1771157540E−02	1.8948981777	4.8322475280E−02	7.2449471170E−02
0.0943598710	−3.7680037101E−02	−7.2260628225E−02	1.7483606994	−7.6268898947E−02	−1.2457033421E−02
2.9830856300	−1.9049941006E−03	7.4653360172E−02	4.7586774465	−4.7718453837E−02	5.9234774492E−02
2.5960990239	4.2368566846E−02	−5.1556947088E−02	1.8739729371	3.1463324039E−02	−5.2552533429E−02
2.1171555640	−6.1129420646E−02	−2.6075106084E−04	4.6259789326	7.8226768079E−03	5.6727644060E−02
1.0360517864	5.2880607616E−02	−2.6601459813E−02	2.8334852974	3.5350979465E−03	−5.4703978905E−02
0.7755950636	5.2505072951E−02	1.1031616151E−02	2.0494406114	5.0993340617E−02	1.2137876310E−02
0.0912963282	1.2828071502E−02	5.3690840638E−02	3.6923320495	5.5309476841E−02	−3.0277014880E−03
4.7118876304	−1.3599607630E−02	−5.3334859826E−02	2.1211762752	4.0405434312E−02	2.2652535941E−02
0.0467903617	−3.6197373162E−02	2.6961636504E−02	0.1380862282	2.8365473169E−02	−3.4128591768E−02
2.0743864963	−4.0549351193E−02	1.7923342486E−02	2.0026495642	−3.1945545119E−02	2.6998826126E−02
0.0383384591	−3.8882112366E−02	1.1016789790E−02	4.5791891132	−3.6285107281E−02	−2.0095185442E−02
0.7924973141	−3.4794036775E−02	2.0303925287E−02	0.8971854138	−1.3429977403E−02	−3.3687300679E−02
2.8035980434	−3.7805574973E−02	1.0535833316E−03	0.7675501484	3.7133492021E−02	4.2394167679E−03
3.6455420790	−1.9980041400E−02	3.0009508839E−02	1.8120527476	2.3345396694E−02	2.6409997154E−02
0.7457075211	3.8237682881E−03	−3.3104106990E−02	1.9251844784	1.5273959266E−02	−2.4487616925E−02
1.9635306910	2.6709719258E−02	9.3864230435E−03	0.2347303440	−8.6743930567E−03	−2.4711661206E−02
2.8419362615	−7.9578099225E−03	−2.5147587163E−02	0.9915490858	−1.8003314108E−02	−1.7422211814E−02
2.7866958971	1.8777917888E−02	1.6154486817E−02	0.7207600660	−1.8335458546E−02	1.9493523822E−02
0.1879393041	2.3036969294E−02	−4.6122352615E−03	3.8419325580	−2.3648200180E−02	1.8037763151E−03
0.1091186862	−1.5485681730E−02	1.4198973687E−02	2.9362965159	−1.4604514435E−02	−1.4654716469E−02
0.1340684695	−4.2435749923E−03	2.0530315344E−02	2.7951465063	1.8013508596E−02	6.3647856316E−03
0.9447813072	1.8364881766E−02	−2.2367543993E−03	2.1131349760	1.7699015883E−02	−9.5726156670E−03
1.8784011071	5.4958429171E−03	1.7919266589E−02	1.0747958560	1.8135003718E−02	4.4066766419E−03
0.9679649516	1.2709787328E−02	1.0888083053E−02	2.6259864886	−1.2023890182E−02	−1.1946978737E−02
0.7247809502	−1.5920469043E−02	5.0984260156E−03	1.0187756896	−8.6544931277E−03	1.3520551610E−02
1.6156607891	−1.1743802303E−02	9.1417347608E−03	3.5596335865	1.0106139812E−02	−1.1979742559E−02
1.0859060133	1.3396435128E−02	2.9921735386E−03	1.0080418791	−1.1871132010E−02	−8.3965642462E−03
2.0275966997	−3.2156394044E−03	1.3905414032E−02	0.1411499507	−1.2039748859E−02	5.4403418059E−03
4.8913759607	−1.3816585188E−02	1.0730943561E−03	1.6344410566	−1.0762397707E−03	1.2604981126E−02
1.9844089677	−5.5292207050E−03	1.0805111383E−02	1.0040181961	−4.5577478384E−03	1.1683552886E−02
5.6175239754	−9.6926227336E−03	−6.0407110547E−03	1.7412735552	−3.0573810425E−03	−1.1334890792E−02
2.6072064232	3.9344215460E−04	−1.0460186993E−02	1.1326949971	−2.7581905990E−03	−9.9742889674E−03
2.5791963475	1.0049870751E−02	−1.4931048423E−03			

Table C.19: Fourier analysis of the z coordinate of Venus in the Earth–Moon case.

f_l	A_l^c	A_l^s	f_l	A_l^c	A_l^s
0.0000000000	−1.3748688892E−01	0.0000000000E+00	0.0788228281	−2.9501695186E+00	3.3923948955E+01
0.1256126465	2.1459842766E+01	−1.3350277422E+01	0.1215919634	−8.0753415704E+00	1.4516220733E+01
0.9127222451	7.6424094936E−01	5.3166634552E−01	1.0703679054	−6.6126797809E−01	−6.5593587481E−01
0.0040226946	1.5486307171E−01	−6.7889319757E−01	0.8659324232	−6.6204022595E−01	2.1921660275E−01
0.0320330098	4.9090119755E−01	4.3932815582E−01	1.1171577282	−9.4122409121E−02	6.7691169107E−01
0.8699531046	4.4479829856E−01	8.4141674675E−02	1.1131370301	−1.6312048345E−01	−4.2223853460E−01
0.1536232116	−3.6398497260E−02	3.1392093830E−01	0.7800236919	1.9158533241E−01	−4.0367903117E−02
0.9376693466	−1.9381628243E−01	6.6540356452E−03	0.7332338730	−6.1594080923E−02	1.3240136462E−01
0.9844591695	7.8802693267E−02	9.7935907836E−02	1.9760042481	−1.0364739036E−01	−1.7683835305E−03
0.7372545799	6.7323888879E−02	−4.8916924662E−02	0.2472038581	5.1926907389E−02	6.7067912543E−02
0.9804384380	−7.7090504377E−02	−3.1332692590E−02	1.9292144233	4.3383904238E−02	−5.5876365861E−02
1.9719835002	6.0569900422E−02	−3.2323839598E−02	1.7287996482	−4.5039222655E−03	6.8499555592E−02
1.7715687696	−3.0158255162E−02	5.6947902150E−02	0.2431829498	−5.1289486069E−02	−2.1859110363E−02
2.0619129897	5.0643320997E−02	−4.8139875448E−03	1.8824246068	−1.3898610590E−02	−5.0757295142E−02
1.9042673201	−4.8909627479E−02	1.3451332293E−02	0.0538757120	−3.3128338863E−02	3.7102838285E−02
1.7247789514	−2.1401016708E−02	−4.5373132842E−02	2.1087028014	−2.5153477573E−02	−2.7654263806E−02
1.8574775141	1.3915282710E−02	−3.5353037581E−02	0.1006656292	3.4725114931E−02	2.9879937326E−03
0.0508121489	−2.8269661821E−02	1.9161382954E−02	0.2004130397	2.7640138918E−02	−1.5745366049E−02
0.1068334253	1.8601609402E−02	1.8058792288E−02	2.1046820937	2.3369635054E−02	7.8963422633E−03
0.9595120675	8.6035676696E−04	2.4283033075E−02	1.8614982595	−1.9052173601E−02	1.5674399380E−02
0.1175710013	−2.6557887766E−04	2.2411496311E−02	0.9875225450	−2.0564200500E−02	−1.1326624509E−02
0.8908795254	8.2429131583E−03	−1.1827065619E−02	0.0748044152	−1.5828039717E−02	6.4255896267E−05
0.8379219601	1.2176369824E−02	7.9411249123E−03	0.0427675521	−1.0330605854E−02	8.5456011381E−03
0.9955680137	7.2293246020E−03	1.1148456113E−02	2.9675493252	7.4165587977E−03	−8.5993703533E−03

Table C.19: (continued)

f_l	A_l^c	A_l^s	f_l	A_l^c	A_l^s
1.0235780772	−1.0125468581E−02	1.4917906465E−03	2.7631138475	−3.9956307133E−03	−9.7435892083E−03
0.7052230765	1.0213585557E−02	−2.5751154966E−03	2.9207595036	2.3302678573E−03	1.0624035126E−02
2.7163240260	7.7205070023E−03	2.0029626227E−03	2.7203447149	−5.4322430475E−03	−5.1669267524E−03
2.9635286401	−1.5267976479E−03	7.3400459448E−03	0.9915450956	4.7958670238E−03	−5.7559609517E−03
0.2115218354	−5.9104467720E−03	4.6249547718E−03	1.9012035937	−6.8435883237E−03	1.6772727766E−04
0.6584332676	−2.5764967286E−03	6.1829361961E−03	0.2583112116	5.7583377089E−03	1.5273264561E−03
0.7911321409	−5.1724911677E−03	1.9294602756E−03	1.6967682705	−2.2573502629E−03	4.6659738734E−03
0.9096590174	3.3233726036E−03	3.8374340290E−03	0.8463728342	4.8796713479E−03	9.8276405052E−04
1.0040186149	−4.6250679238E−03	−1.8134759620E−03	0.8548236371	−4.9701531907E−03	1.5784731556E−03
1.6539992176	−1.2370286297E−04	4.6319741502E−03	1.8971833512	4.0053632226E−03	−2.3287057494E−03
0.8628689919	−4.3274248523E−03	9.1532958368E−04	0.9407330896	4.0335178391E−03	−1.1521847241E−03
0.8268135624	3.2817427243E−03	2.8801237427E−03	0.7995833298	−3.1078825279E−03	2.7557111051E−03
1.1451683780	−2.8701788933E−03	−3.0083728570E−03	1.8544134557	1.9904575143E−03	−3.6647436733E−03
0.2284236030	−5.3849845379E−04	4.0545725089E−03	1.6499784563	−1.6928835713E−03	−3.2479413765E−03
1.8183585943	−3.4695173312E−03	5.4707419804E−04	0.9056381872	−3.2709449492E−03	−1.1900929791E−03
2.8739696861	3.1906581719E−03	1.4530074576E−03	0.6624540696	2.7326467216E−03	−2.1554895175E−03
1.0953149748	3.4271756321E−03	4.7892676580E−04	1.0423569785	−3.0369401679E−04	3.1674012318E−03
2.8958124179	1.2802074079E−03	−2.8178531095E−03	1.0508084440	8.5738646223E−04	3.1064690336E−03
3.0534580599	−1.7591084824E−03	2.5725457058E−03	1.0383365335	−1.1045734034E−03	−2.5521273543E−03
1.1919582167	4.7306866682E−04	−2.6320755834E−03	0.7951528504	2.7508517831E−03	4.1630141644E−04
1.1421047993	−1.2414186392E−03	−2.2492011692E−03	0.8036037911	2.3101973593E−03	−5.1960656881E−04
0.7443414527	5.0116093160E−04	2.2872401131E−03	2.8490225830	1.1163489177E−03	2.0371202445E−03
1.1879374631	7.4107977279E−04	2.1671295222E−03	3.1002478914	2.2865939632E−03	−9.9104434328E−05
1.2387492788	−2.2932746034E−03	−9.3357925207E−05	0.9447533371	−2.2336356320E−03	−5.0918205850E−04
1.0467878563	−1.6589324401E−03	−1.6929950907E−03	2.8348507680	−2.2935614753E−04	−2.1970617000E−03
0.0124767147	−5.7074378123E−04	−2.1127840687E−03	0.0895589893	1.6221774024E−03	1.5055101226E−03
0.2792376440	1.2743215838E−03	−1.5701023549E−03	1.6388701248	6.5947529213E−04	1.9292750039E−03
1.7965160339	−3.0398136544E−04	−1.9617416450E−03	0.0360558014	6.2684330446E−04	1.9316253087E−03
1.8463689072	7.5599141871E−04	−1.7887570278E−03	1.0454205826	−2.8331024166E−04	−1.8813429835E−03
2.7880609497	1.7734078280E−03	1.0610794122E−03	0.0707734873	−4.7179553626E−04	−1.9386789543E−03
2.6304152779	−1.8423796497E−03	−7.0607190673E−04	0.8949001832	−1.5150374630E−03	7.4201383175E−04
1.1380840296	1.4325188227E−03	8.9232099064E−04	0.7483623281	4.3870144212E−04	−1.4551651903E−03
1.9790679719	1.4426728675E−03	−5.1869346021E−04	2.8530432419	8.0659636964E−06	−1.5083768123E−03
2.5836254931	1.2687186558E−03	−7.9806803480E−04	1.2347283005	1.3554401901E−03	−6.8711593648E−04
0.0147560520	1.4534604535E−03	3.2398805382E−04	1.8076240155	−4.5116402360E−04	−1.4210016761E−03
2.5876461963	−1.4573668058E−03	8.0175579070E−05	3.0962271683	−1.2854690353E−03	7.8869617505E−04
2.8308301290	8.3612044159E−04	1.1962582531E−03	1.5920807086	−1.4455121518E−03	−4.7711397341E−04
1.8433056846	−9.5413656230E−04	9.7982660270E−04	0.8588465294	−1.6697856242E−04	−1.3703021691E−03
1.9510571338	−1.0389820984E−03	−8.0351843740E−04	0.8847117883	9.3407176456E−05	1.2619615170E−03

Table C.20: Fourier analysis of the x coordinate of Mars in the Earth–Moon case.

f_l	A_l^c	A_l^s	f_l	A_l^c	A_l^s
0.0000000000	−6.3777515384E−02	0.0000000000E+00	0.9602263193	5.7280162792E+02	1.2910915039E+02
0.9251957783	−1.0915700675E+02	3.7066105594E+02	0.9999959171	8.1811931736E+01	−3.5653929512E+01
1.9517713631	−3.8201490333E+01	2.9329264265E+01	1.9167408323	−1.7655078643E+01	−2.6306500364E+01
0.9204565886	−1.9834063177E+01	−1.8876646430E+01	0.0313187261	7.4305777386E+00	−1.4532679174E+01
0.0663492843	−1.2140076013E+01	−5.2408345002E+00	1.8190728461	−9.3063678702E−01	9.2137748189E+00
1.9915410280	−1.9674903702E+00	7.1606676322E+00	2.8106178920	−4.5539849352E+00	−4.6423961956E+00
1.7840423209	−5.9816527057E+00	−9.5307216963E−01	2.7755873355	3.1807367060E+00	−2.8048283095E+00
0.8503953821	−8.4923850732E−01	3.7782804376E+00	0.1013798044	−1.2515660296E+00	3.5067749914E+00
2.9433164076	1.4705161298E−01	−3.7137491641E+00	0.0084509203	2.1380644080E+00	1.1447902444E+00
2.9082858910	2.4303392455E+00	2.4948384329E−01	1.9120016466	2.2306719621E+00	−2.5981218550E−01
0.8806868686	5.1276517406E−01	1.8458206805E+00	1.8588423816	7.5213550055E−01	1.2204692723E+00
1.0478108942	−1.0254471730E+00	−5.9397958196E−01	3.8021629298	9.9943528204E−01	−8.1623702556E−02
2.8503875054	−1.0106520889E+00	−1.3177714459E−01	1.0350269492	−9.5414278558E−01	−2.5553075582E−01
0.8901651494	8.5150985636E−01	3.1178162803E−01	0.8854227169	8.9678457833E−01	1.5421245371E−01
1.0437897773	7.6501168072E−01	−3.7945309718E−01	0.9642360020	3.5845619892E−01	7.7269316586E−01
1.0929247468	−3.6413334629E−01	−6.1536117171E−01	0.0710880828	5.2431319404E−02	7.5994711356E−01
1.0828392504	−3.2069320087E−01	6.1599878692E−01	1.0578942662	5.4796751723E−01	−2.7853093640E−01
3.7671323930	1.9293889726E−02	6.5294972524E−01	2.9830860360	−3.3989817113E−01	−4.7194309063E−01
1.0397640786	4.0274635773E−01	−3.4014666376E−01	1.8419399454	−3.0955133912E−01	−4.1334164747E−01
0.1411495005	3.9367867414E−03	4.6727297381E−01	1.7793032368	2.5806322372E−01	−3.4629963275E−01
2.7358176578	−3.2186079703E−01	−3.0431350838E−01	1.7442725941	−2.6250556139E−02	4.1518121117E−01
1.8769724882	−2.9507339302E−01	2.3985095792E−01	1.7092421702	−3.2151157779E−01	−3.8887541769E−02

Table C.20: (continued)

f_l	A_l^c	A_l^s	f_l	A_l^c	A_l^s
2.7007868268	2.3631803371E−01	−2.2394244972E−01	2.7708481807	7.1153258878E−02	2.9473172711E−01
2.0265716515	2.5983128687E−01	−1.8429454007E−01	3.9348614530	2.0866309654E−01	1.8821425721E−01
1.8854231974	−1.2897541905E−01	2.2666123347E−01	1.0040203310	2.1255860190E−01	8.4698404502E−02
1.0228641519	8.4986611981E−02	2.0011281512E−01	3.6694644231	1.2238346275E−01	−1.5320946368E−01
1.9767179668	4.8959510845E−02	−1.7591084269E−01	3.8998309102	−1.3181381700E−01	1.2918914396E−01
0.0616099706	1.3409592100E−01	−1.1059933968E−01	0.1761801265	−6.3769769211E−02	1.5908710846E−01
1.0080402057	−7.4094887674E−02	−1.6344344299E−01	1.8503918034	−1.4421899646E−01	−9.3227849943E−02
2.9035468905	−9.4881517994E−02	1.4504566671E−01	0.8409172168	4.2128258289E−02	−1.5304766652E−01
1.8722321027	−1.4317799391E−01	−6.4729675590E−02	3.8419325958	1.1542767162E−01	−1.0995802958E−01
1.0747964462	−1.4185517809E−01	5.9511366213E−02	2.6779194134	−1.4002583039E−01	2.8192875248E−03
1.1178720260	−1.1452592221E−01	−4.7946995072E−02	3.6344338780	9.5549331048E−02	8.3675640771E−02
4.7937079773	−6.6449721682E−02	9.4496569357E−02	1.9416905046	1.0171110437E−01	3.7326798411E−02
1.1326944881	−8.1906398429E−02	−5.1075451584E−02	0.0350442147	−2.9193939393E−03	9.5705600119E−02
2.0393558128	9.1138009396E−02	−3.3461334424E−02	4.6610094639	1.7506523455E−02	8.5279097612E−02
2.6428888981	2.6841182189E−03	−9.0971296321E−02	2.0844699017	8.6667165137E−02	1.4046975151E−02
0.0434813120	3.5822499971E−02	7.7103699127E−02	2.8854183593	5.3327732611E−02	5.8797176009E−02
3.7273624742	7.5141679458E−02	−9.1088334089E−03	1.8938737784	1.0520140821E−02	−7.3197798139E−02
4.7586774528	−5.9220853371E−02	−4.6314286187E−02	2.0353356524	−1.6655806172E−02	6.7917443599E−02
0.8153643248	6.3227261129E−02	2.0208420819E−02	0.8275274906	−5.7922198305E−02	3.9251268490E−02
1.9557920377	−6.5847430503E−02	−1.8898420147E−02	2.0494394212	−1.3955295942E−02	6.1334670301E−02
1.9251825083	2.9640249337E−02	5.2927117210E−02	0.7755951152	−4.4550954613E−03	5.6922058959E−02
4.6259788840	−5.5503411497E−02	9.0067544803E−03	2.8334850670	5.4623212728E−02	3.0464976109E−03
1.0875824813	5.5410465104E−02	−8.1281332685E−05	3.6923320366	3.4862603211E−03	5.4897262397E−02
0.1108587987	−3.0247359731E−02	−4.3878850088E−02	0.7924972344	−2.6294643885E−02	−4.4328036018E−02
2.8685172274	4.4615194788E−04	−5.2066079760E−02	0.1061063626	−2.0200920566E−02	4.6054991511E−02
3.7623931348	−4.1960358052E−02	−2.0616712997E−02	2.0663411524	1.5898513093E−02	−4.4830814854E−02
1.8817105823	−3.8578066641E−02	2.2427113741E−02	0.9873858853	−4.4383629684E−02	1.1767771300E−02
2.0313124733	−5.8468356896E−04	4.3105154265E−02	2.0743728011	−1.9738953251E−02	−3.9495446415E−02
3.9746310591	4.4578307226E−02	2.4333280166E−03	0.8025414438	4.1429481542E−02	−8.4647160717E−03
3.0181168267	−3.3956321182E−03	4.3294454399E−02	0.8457095415	−2.2972827339E−02	−3.0913325506E−02
0.9936797842	−1.4883995875E−02	−3.8375443939E−02	2.8769656511	−1.4598258605E−02	−3.7531855965E−02
1.9602213345	2.0509711526E−02	−3.3452096116E−02			

Table C.21: Fourier analysis of the y coordinate of Mars in the Earth–Moon case.

f_l	A_l^c	A_l^s	f_l	A_l^c	A_l^s
0.0000000000	−1.4252243158E−03	0.0000000000E+00	0.9602263257	1.2906615176E+02	−5.7279344584E+02
0.9251957881	3.7189513922E+02	1.0947193076E+02	0.9999959456	−3.5676953869E+01	−8.1887208230E+01
1.9517714462	2.9300187177E+01	3.8222775352E+01	1.9167409081	−2.6372482282E+01	1.7675497335E+01
0.9204567430	−1.8940128053E+01	1.9839739817E+01	0.0313187954	1.4522961102E+01	7.4419412504E+00
1.8190727672	9.2150457444E+00	9.1786524916E−01	0.0663493329	3.2950326543E+00	−7.6283884664E+00
1.9915410524	7.1657642293E+00	1.9700462688E+00	2.8106179094	−4.6417865589E+00	4.5545746358E+00
1.7840422222	−9.4511308115E−01	5.9967998645E+00	2.7755873754	−2.8079910877E+00	−3.1842404535E+00
2.9433165682	−3.7134520296E+00	−1.5294309256E−01	0.8503955303	3.6045393016E+00	1.0464411405E+00
0.1013798707	3.5010521851E+00	1.2531136472E+00	2.9082860293	2.5319232536E−01	−2.4339655851E+00
0.0084508462	1.1369027223E+00	−2.1591665721E+00	1.9120018318	−2.5498257802E−01	−2.2348693795E+00
0.8806872563	1.8546770014E+00	−5.0470779054E−01	1.8588424154	1.2211333060E+00	−7.5308512253E−01
1.0478108781	−5.9877773217E−01	1.0348237040E+00	2.8503875283	−1.3165027768E−01	1.0113227654E+00
3.8021630191	−8.1125673601E−02	−9.9947110670E−01	0.8901652497	−3.5527769012E−01	9.6919836683E−01
1.0350271448	−2.6129955316E−01	9.4848547443E−01	0.8854252808	1.5347733780E−01	−8.8677892646E−01
0.9642467864	7.8911566772E−01	−3.1353037503E−01	1.0437904936	−3.7573687191E−01	−7.6921562358E−01
0.0710885474	−7.6056961729E−01	4.8458746811E−02	1.0828414217	6.3260608892E−01	3.1304024335E−01
1.0929249842	−6.1615125325E−01	3.6273886539E−01	3.7671324827	6.5353924621E−01	−1.9028850378E−02
2.9830861599	−4.7254573322E−01	3.3969032339E−01	1.0397667346	−3.2808067608E−01	−4.2549382980E−01
0.1411496406	5.1698628928E−01	−1.0565457787E−01	1.8419401685	−4.1335522281E−01	2.9778504089E−01
2.7358175305	−3.0260213084E−01	3.2069740121E−01	1.7793030759	−3.4747195726E−01	−2.5767987986E−01
1.7442723327	4.1335496185E−01	2.4578746570E−02	1.8769712998	2.3966831500E−01	2.9170704588E−01
2.0265716825	−1.8399861003E−01	−2.5833590312E−01	2.7007869972	−2.2218190180E−01	−2.3594230249E−01
1.0578944565	−1.4580851511E−01	−2.8844291015E−01	1.7092418011	−3.9571588218E−02	3.1944832041E−01
2.7708483793	2.9539620639E−01	−7.0362441072E−02	3.9348616815	1.8867896856E−01	−2.0823833882E−01
1.8854221102	2.2793760972E−01	1.2693343431E−01	1.0040178004	7.8090094291E−02	−2.1293146814E−01
1.0228638726	−2.0599183788E−01	8.7819143957E−02	3.6694643761	−1.5332861682E−01	−1.2223956634E−01
3.8998311641	1.2902420703E−01	1.3233738861E−01	1.0080412632	−1.6493403495E−01	7.3801997452E−02
1.9767184355	−1.7598086277E−01	−4.9307477034E−02	0.0616102203	−1.1016353653E−01	−1.3403638641E−01
1.8503915750	−9.2883028608E−02	1.4429300836E−01	2.9035469231	1.4512113013E−01	9.5255154029E−02

Table C.21: (continued)

f_l	A_l^c	A_l^s	f_l	A_l^c	A_l^s
0.1761802020	1.5830794360E−01	6.3277420027E−02	0.8409172435	−1.5391635039E−01	−4.2061481491E−02
3.8419326404	−1.1000208867E−01	−1.1550501297E−01	1.0747961204	6.0037684640E−02	1.4095324347E−01
1.8722322918	−6.5378399470E−02	1.4347416340E−01	2.6779192267	3.1778819526E−03	1.4002447141E−01
3.6344338322	8.3656003497E−02	−9.5732391990E−02	1.1178719450	−4.7774359974E−02	1.1475110059E−01
4.7937081424	9.4407158229E−02	6.6576801945E−02	1.9416878753	3.5911685097E−02	−1.0216025529E−01
1.1326944435	−5.0986808452E−02	8.2229514965E−02	0.0350305454	9.4487949904E−02	−6.1378096196E−03
2.0393559806	−3.3461879810E−02	−9.1256942200E−02	0.0562657557	−9.1777621423E−02	1.5815743627E−02
2.6428886850	−9.1154726944E−02	−2.4412936110E−03	2.0844701291	1.4294995669E−02	−8.6611307210E−02
4.6610094580	8.5262507432E−02	−1.7585526938E−02	0.0434817562	7.6722736940E−02	−3.5418417794E−02
2.8854184717	5.8700676881E−02	−5.2939938345E−02	3.7273627347	−8.8171278250E−03	−7.4816216135E−02
4.7586776042	−4.6421731123E−02	5.9212212445E−02	1.8938732761	−7.2932447823E−02	−1.0283092721E−02
2.0353352850	6.8049555038E−02	1.6230105611E−02	1.9557965951	−2.7455620349E−02	6.3707528705E−02
0.8275276574	3.9236845020E−02	5.7888710220E−02	0.8153643035	−2.1124111494E−02	6.7742076761E−02
0.9299350287	−1.1660540714E−02	−5.5441127607E−02	0.8025806923	2.7185781989E−03	−5.6083163453E−02
4.6259789321	9.0390753020E−03	5.5538561057E−02	0.0912963012	1.2816129457E−02	5.3627159017E−02
1.8817103369	−2.8001169463E−02	−4.8337033576E−02	3.6923322005	5.4662015994E−02	−3.2427621665E−03
1.9251916759	5.3684478164E−02	−2.5661852343E−02	0.1108576499	4.3602531785E−02	−3.0763117655E−02
1.0875803033	−1.1147732544E−03	−5.5778087947E−02	2.8334861080	4.4456045707E−03	−5.3958129130E−02
2.0494395674	5.0973104471E−02	1.1700266504E−02	2.8685166193	−5.1714111712E−02	−6.0262790598E−04
0.1061190698	−4.2843836327E−02	−2.3804526436E−02	0.7755947083	4.4297457801E−02	1.7387675575E−02
2.0663413956	−4.4670718525E−02	−1.5867878965E−02	3.7623931682	−2.0557755916E−02	4.2088835187E−02
0.9873856258	1.2783090052E−02	4.4410242097E−02	3.9746313455	2.5764241038E−03	−4.4597227894E−02
2.0313110770	4.4079138006E−02	9.2842780863E−04	2.0743865386	−4.0535021017E−02	1.7985166533E−02
3.0181168886	4.3104646740E−02	3.3782913205E−03	0.8456561839	−2.7795701892E−02	3.1532095735E−02
0.9936908742	−3.9550463738E−02	1.2406010600E−02	1.0835601385	3.3519842922E−02	2.1801859916E−02
0.9244774155	−3.9220990570E−02	−6.5861269838E−03	1.0265753931	−2.3167577988E−02	3.2144815290E−02
0.7924971431	−3.4361347990E−02	2.0514452450E−02	2.8769672305	−3.7407910588E−02	1.4405809285E−02
0.7675501362	3.6950826206E−02	3.9091106374E−03	0.9952641257	2.0031737965E−02	−3.1657413657E−02
0.9830943250	−3.5683068482E−02	−1.2525257348E−02	1.9602217677	−3.3115051402E−02	−1.9503274702E−02

Table C.22: Fourier analysis of the z coordinate of Mars in the Earth–Moon case.

f_l	A_l^c	A_l^s	f_l	A_l^c	A_l^s
0.0000000000	2.5290046642E+00	0.0000000000E+00	0.0437922793	−5.2432135542E+01	−8.0053870711E+00
0.0788228161	−2.9481164072E+00	3.3915382126E+01	0.0397718570	1.2849571607E+01	−1.3995350564E+01
0.0040226052	−5.7203907177E+00	−5.6707455799E+00	0.0835619639	2.2940690345E+00	−9.3543835831E−01
1.0353373975	1.0742842139E+00	−9.5020010044E−01	0.9477528423	7.5707437453E−01	−1.2525434354E+00
0.1138533544	−1.3854171460E+00	−3.0034205572E−02	1.0703679359	−6.6183257584E−01	−6.5598387592E−01
0.9127223000	7.6362944501E−01	5.3055082022E−01	0.0795414810	−1.7825255824E−01	8.6921112753E−01
0.9517732711	−5.1716891292E−01	2.4516743753E−02	1.0313169880	6.8450717328E−02	5.1316768663E−01
0.1536231882	−2.1010401885E−01	4.1433624487E−01	0.8150541775	−8.2790566060E−02	−2.9507039803E−01
0.9026387283	7.7339727480E−03	−2.6369110145E−01	1.8941838322	1.6296047861E−01	1.4412341796E−01
0.9875224870	−2.2577893987E−02	−2.2397611451E−01	0.9955678273	2.1269780750E−01	−2.3976938092E−02
0.9376692660	−1.9386682317E−01	7.1397833141E−03	0.7800236422	1.8999401021E−01	−4.1811290611E−02
0.1233315759	−1.0409835403E−01	1.3891023302E−01	0.9915453043	−8.8755826261E−02	1.0547212121E−01
1.9642449102	9.1494284913E−02	6.1838704429E−02	1.8065992968	9.6067622729E−02	4.3084202856E−02
0.8190745788	−6.1741914525E−02	7.2458041096E−02	0.8986183904	7.7338488555E−02	5.5492308060E−02
1.8106197020	−1.3308073006E−02	−7.7355787310E−02	2.0268825172	2.2784575715E−03	7.8415480172E−02
1.9392979617	2.5987342670E−02	7.5380829811E−02	1.8901634124	−7.5977333003E−02	1.9843530629E−02
1.9292144057	4.3744947504E−02	−5.6174201390E−02	0.0188450146	−5.1324783081E−02	−5.1887750825E−02
0.9079831167	−6.0333026382E−02	3.2132307263E−02	0.1185928151	−6.5306830394E−02	−1.2737294795E−02
1.0751070501	−2.0256276944E−02	6.3859116844E−02	0.0310081590	7.1001415882E−02	−7.9109538993E−03
0.1193110355	−2.0664483822E−02	−5.8640280107E−02	1.7715687669	−2.9065158070E−02	5.6739378524E−02
0.0740836169	5.4286021417E−02	3.3827952522E−02	0.1886538284	−5.4568185593E−02	−3.3639808530E−03
2.0619130695	5.0699191725E−02	−4.8451933149E−03	0.0538758963	−3.3220349862E−02	3.7086873953E−02
0.8776917484	3.1856269173E−02	−3.9953304951E−02	0.0357461456	−2.2749120640E−02	4.2385277705E−02
1.9042674266	−4.8793294034E−02	1.3472501124E−02	0.8548237783	−3.7759777944E−02	−2.8559125428E−02
0.8628690791	1.6792958803E−02	−3.1116639061E−02	0.9726997862	3.0462228768E−03	3.0108396832E−02
1.8544141527	1.1187580710E−02	2.6633605529E−02	1.9433183899	1.7027633016E−02	−2.2500828741E−02
2.0228621203	−2.3861934784E−02	−1.5048339379E−02	0.8588460174	3.2938594363E−03	2.5114386138E−02
0.0390527787	2.6502996317E−02	5.4612101823E−04	2.8857289665	−2.3559004709E−02	3.5902443059E−03
0.9120036141	2.1306638932E−02	1.1430331703E−02	1.0710865608	−1.5088432784E−02	−1.8896635595E−02
1.1053984493	1.4146706510E−02	−1.6250448466E−02	1.8503913593	−1.7595109215E−02	−1.1263281744E−02
0.8379219885	1.9106085428E−02	5.3909398709E−03	2.7981444159	−1.5043599265E−02	7.3426891206E−03
1.8463688818	1.5917513517E−02	−3.8151810342E−03	0.0748044020	−1.5943572288E−02	7.5913952692E−05

Table C.22: (continued)

f_l	A_l^c	A_l^s	f_l	A_l^c	A_l^s
2.0040146642	1.5577130977E−02	8.5505408547E−04	0.7752845664	−3.7708913796E−03	1.3808227706E−02
1.8193832593	1.1120319436E−02	9.0268056962E−03	0.7402540697	−4.2188443491E−03	−1.3369020610E−02
0.1631011317	1.4532654865E−03	−1.4337803201E−02	0.0707905917	1.0748780883E−02	−6.6148667162E−03
0.9424082627	6.0491071950E−03	1.0741436796E−02	0.1764909199	−7.0860215403E−03	−1.0300622483E−02
1.9790675917	1.0409240703E−02	6.8082875197E−03	0.8729524031	5.5842597543E−03	−1.0108207468E−02
1.9871129280	−6.1251951825E−03	9.7380245463E−03	0.7052235305	1.0680099554E−02	−3.7531324609E−03
0.0209225083	−1.6314330387E−03	1.0848393987E−02	2.9207595137	2.3508893370E−03	1.0673930966E−02
0.2284234562	−7.5353172354E−03	7.7807191090E−03	0.8278381263	−1.4588586064E−04	−1.0620845677E−02

Table C.23: Fourier analysis of the x coordinate of Jupiter in the Earth–Moon case.

f_l	A_l^c	A_l^s	f_l	A_l^c	A_l^s
0.0000000000	−6.2620069503E−02	0.0000000000E+00	0.9936910960	−6.7515670842E+02	−1.8950362120E+03
0.9251958044	−1.0912296311E+02	3.7076492692E+02	1.9852362001	1.5485308750E+02	5.6986877606E+01
0.9999971358	1.4014006220E+02	4.1943410592E+01	0.0021459201	2.8401446492E+01	−4.8171751539E+01
0.9873852483	2.4502387544E+01	−4.2019847693E+01	1.8525375875	2.8377663122E+01	−1.4189733321E+01
1.9167409046	−1.7701839661E+01	−2.6318382324E+01	2.8440827024	−5.1087776872E+00	2.1686743306E+01
0.0663492938	−1.2135392548E+01	−5.2365808369E+00	0.1348445930	1.2446445361E+01	−2.7959799147E+00
2.9767812942	−1.1028766582E+01	6.3645888780E+00	1.9915424272	−9.9360881373E+00	6.7329974282E+00
1.7840423211	−6.0294237244E+00	−9.0369472851E−01	2.7755874081	3.1744286625E+00	−2.8759449165E+00
0.0084519408	1.5253675344E+00	3.7671639155E+00	1.0143462214	3.5992930007E+00	−1.8770499177E+00
1.9789300049	1.3774178995E+00	3.7457448657E+00	0.8503954306	−7.0756754152E−01	3.7230640236E+00
3.8356278113	−2.0640595613E+00	−2.7463764647E+00	1.0684916260	1.0054567652E+00	3.2250810182E+00
0.9188909503	−1.1404378728E+00	−2.8784693211E+00	0.8567005037	−2.4605267853E+00	1.8901804907E+00
1.1263896822	−1.1175948269E+00	2.1799544965E+00	2.9082859971	2.4356729266E+00	2.4520206660E−01
1.8588434371	−3.4511200636E−01	2.2832381374E+00	1.0103257668	−1.7271859706E+00	1.0928998336E+00
0.9810799001	1.7381227635E+00	−2.9505980176E−01	2.8503888099	−1.0862855262E+00	−1.2054983563E+00
0.9977548812	4.6790682650E−01	−1.6590836121E+00	2.7692824933	−2.9349224450E−01	1.4855022738E+00
1.0012231471	5.9204430555E−01	1.3527974344E+00	1.7777370679	1.2452765352E+00	−6.8652028755E−01
0.0041596687	1.3348204868E+00	2.2146112628E−01			

Table C.24: Fourier analysis of the y coordinate of Jupiter in the Earth–Moon case.

f_l	A_l^c	A_l^s	f_l	A_l^c	A_l^s
0.0000000000	−1.3465271306E−03	0.0000000000E+00	0.9936911266	−1.8952204249E+03	6.7437770536E+02
0.9251958044	3.7198720968E+02	1.0947929099E+02	1.9852362001	5.6986762439E+01	−1.5485279199E+02
0.9999971358	4.1942515314E+01	−1.4013800227E+02	0.0021460339	−4.8121664794E+01	−2.8468013122E+01
0.9873852483	−4.2019242791E+01	−2.4502032257E+01	1.8525375876	−1.4189602468E+01	−2.8377520698E+01
1.9167408993	−2.6371794306E+01	1.7740554964E+01	2.8440827024	2.1686877135E+01	5.1088014001E+00
0.1348445931	−2.7924296370E+00	−1.2430681365E+01	2.9767813053	6.3631191400E+00	1.1029869447E+01
1.9915418579	6.8117029214E+00	9.8938870267E+00	0.0663492932	3.2809390402E+00	−7.6313379131E+00
1.7840423211	−9.0581603049E−01	6.0425664105E+00	2.7755874081	−2.8788021909E+00	−3.1777012196E+00
1.0143462210	−1.8939111139E+00	−3.6315768487E+00	0.0084519050	3.7580156188E+00	−1.5450515603E+00
1.9789304870	3.7520680625E+00	−1.3532313037E+00	0.8503954176	3.6723487699E+00	1.1912991989E+00
3.8356278113	−2.7463818260E+00	2.0640637725E+00	1.0684916259	3.2257304759E+00	−1.0056642941E+00
0.8567005090	−2.1565034327E+00	−2.8080825290E+00	0.9188903607	−2.8709423805E+00	1.1628611527E+00
1.1263896822	2.1798764036E+00	1.1175546609E+00	2.9082859990	2.4565575422E−01	−2.4396500067E+00
1.8588434370	2.2832481774E+00	3.4502032815E−01	1.0103257661	1.0972389648E+00	1.7340006496E+00
0.9810790243	−3.1491401452E−01	−1.7357094305E+00	2.8503888099	−1.2054778738E+00	1.0863287925E+00
0.9977545523	−1.6663862769E+00	−4.6288453266E−01	2.7692824932	1.4855140411E+00	2.9349256073E−01
1.0012231453	1.3527708267E+00	−5.9206926121E−01	1.7777370664	−6.8652697487E−01	−1.2452350016E+00
0.0041602877	−2.3253674131E−01	1.3312107322E+00	1.9104358470	4.0105950399E−01	−1.2339276495E+00
2.0600365741	−4.1466857581E−01	1.0072049652E+00	3.9683263979	−9.4863489963E−01	−1.6429396592E−01
0.1411502135	8.2473239121E−01	4.1953727314E−01	1.9188869675	−4.8807374904E−02	−8.9257774608E−01
2.9830871189	−9.2441186072E−01	−7.3881252408E−02	0.9894540463	6.2241771201E−01	−5.3224993796E−01
0.9949191960	4.8626143970E−01	6.3399382817E−01	1.8462315590	3.0122283734E−01	−7.0519645665E−01
1.0828414527	6.3288606757E−01	3.1334373423E−01	3.7029292079	−7.3822222882E−02	6.6774044885E−01
3.7671325435	6.6040776105E−01	−2.8796365765E−02	2.0101832298	1.7865673891E−01	6.0005426918E−01
0.9924556118	7.2192515745E−02	5.7887337444E−01			

Table C.25: Fourier analysis of the z coordinate of Jupiter in the Earth–Moon case.

f_l	A_l^c	A_l^s	f_l	A_l^c	A_l^s
0.0000000000	3.3033259990E+00	0.0000000000E+00	0.0103273787	1.1904471018E+02	−1.3730139022E+02
0.0063064257	−2.6650151023E+01	3.7093870877E+01	0.0788228305	−2.9606116217E+00	3.3923832668E+01
0.0040215032	−1.3154524207E+01	−1.0830510215E+00	0.9812176678	−5.0133918651E+00	1.0008898249E−01
0.1473182725	2.4441932234E+00	4.0700076354E+00	1.0018724580	7.9196510071E−01	4.8494847072E+00
0.0166331768	−6.8176758418E−01	−4.3376613865E+00	0.9978512860	−3.1427497499E−01	−1.2044610853E+00
0.9852384759	1.2416062287E+00	8.7559621186E−02	0.8485190829	−7.0401028144E−01	7.7905622805E−01
0.0126115182	2.7497430874E−01	1.0674459762E+00	0.9127222098	7.6593618798E−01	5.2950657989E−01
0.8691739153	7.4932436611E−01	5.0537876300E−01	1.0703678911	−6.6242861398E−01	−6.5473881157E−01
1.8607189668	−7.1567805675E−01	2.0816550195E−01	0.1536233434	−3.8154393908E−01	2.6664309783E−01
1.8400641990	−5.0700317989E−02	−3.5713352905E−01	1.9977097953	1.2094040379E−02	−3.7813749150E−01
0.9955670432	2.4704566283E−01	−2.5764565751E−01	0.9875232927	2.0526806762E−01	−3.0117258878E−01
1.9727627269	1.7059900521E−01	−2.1336585462E−01	1.9934175021	−2.3158227252E−01	−1.3643926130E−01
0.0644729443	−1.5380939080E−01	−1.9163678586E−01	0.0145974433	2.6269897116E−01	1.8426324391E−02
0.0851280785	1.5676499680E−01	−1.6675995725E−01	0.8651528394	−2.0072510025E−01	−1.0984935175E−01
0.8525401935	1.6806064264E−01	−1.5482693134E−01	0.7800236656	1.9094843323E−01	−4.3825900387E−02
0.9376692659	−1.9385291683E−01	7.4259456630E−03	1.8440849905	9.6922044473E−03	1.8845229472E−01
0.9915460840	−1.1634310338E−01	1.3731621213E−01	1.8566977073	1.7557404600E−01	−6.9549974523E−02
0.2221186056	9.0526786216E−02	1.6478038317E−01	0.8442267884	5.7718138595E−02	1.6537441892E−01
0.0229373582	−1.3711117008E−01	−8.0963732094E−02			

Table C.26: Fourier analysis of the x coordinate of Saturn in the Earth–Moon case.

f_l	A_l^c	A_l^s	f_l	A_l^c	A_l^s
0.0000000000	−5.6313503058E−02	0.0000000000E+00	0.9974572831	−1.3520672488E+03	−3.4301936115E+03
0.9251957998	−1.0935675751E+02	3.7117220094E+02	1.9890022576	2.8729378248E+02	9.4362025599E+01
0.9999973154	−4.2310526823E+01	2.9288753500E+02	0.0059120332	4.8965229704E+01	−9.0036007080E+01
0.9949195380	−7.7240809593E+01	−6.5848498748E+01	1.8563036620	5.1064929260E+01	−2.7813269482E+01
2.8478488141	−7.9886919667E+00	4.0045513974E+01	1.9167409088	−1.7758972082E+01	−2.6508504930E+01
1.9915398083	−1.6796565765E+01	−1.7248989562E+01	2.9805474139	−1.9800188004E+01	1.2350814709E+01
0.1386106711	2.2616881165E+01	−5.9185483841E+00	0.0663493049	−1.2102815415E+01	−5.2298772571E+00
0.0084513042	−7.0101665316E+00	4.4174222869E+00	1.9864658629	8.2429373679E+00	−1.2610541812E+00
1.0015050703	−1.3012888866E+00	−6.8569182745E+00	1.0105800111	6.7081543836E+00	−3.2202410586E+00
1.0065582270	−6.8104364618E+00	2.3258088998E+00	1.0722575647	2.0565720605E+00	5.8334394147E+00
1.7840422350	−6.2253475070E+00	−9.9075169256E−01	3.8393938498	−3.9590902212E+00	−4.8953195278E+00
0.8529345024	−4.6392546711E+00	3.3036667180E+00	0.9226568028	−2.2863213991E+00	−5.1902744280E+00
0.9986987265	4.7775867033E+00	−2.3244856363E+00	1.8588422851	−4.6173363745E+00	1.3400789219E−02
1.1301557947	−1.9094476400E+00	4.0633856626E+00	2.7755874823	3.3888494732E+00	−2.9649787109E+00
0.9923803115	−4.0669207645E+00	−7.4847663285E−01	0.8503950447	−7.0842004672E−01	3.2525190551E+00
2.8503878708	2.0720872602E+00	−2.4768951272E+00	0.9962265778	3.1069517569E+00	−2.8461137633E−01
1.0025471230	2.7739452196E+00	−1.4039860786E+00	2.7730479905	−4.1930497079E−01	2.7391776218E+00
0.0033742569	2.9619492329E−02	−2.8203632089E+00	1.7815034401	2.2406931394E+00	−1.3259354032E+00

Table C.27: Fourier analysis of the y coordinate of Saturn in the Earth–Moon case.

f_l	A_l^c	A_l^s	f_l	A_l^c	A_l^s
0.0000000000	−1.0386289903E−03	0.0000000000E+00	0.9974572831	−3.4301407310E+03	1.3520450638E+03
0.9251957998	3.7238587940E+02	1.0971292701E+02	1.9890023479	9.4801376023E+01	−2.8719755479E+02
0.9999943567	2.9336302434E+02	2.7961554215E+01	0.0059120331	−9.0018721215E+01	−4.8955716964E+01
0.9949195380	−6.5847353856E+01	7.7239665854E+01	1.8563036620	−2.7813119832E+01	−5.1064654503E+01
2.8478488141	4.0045760988E+01	7.9887427018E+00	1.9167409087	−2.6562888371E+01	1.7795480271E+01
1.9915398083	−1.7248661943E+01	1.6796346088E+01	2.9805474139	1.2350811243E+01	1.9800182259E+01
0.1386106710	−5.9110692494E+00	−2.2588282006E+01	0.0084513060	4.4095754523E+00	6.9921801386E+00
1.9864658629	−1.2610508308E+00	−8.2429219988E+00	0.0663493038	3.2842653740E+00	−7.6117298974E+00
1.0014665009	−4.7097045143E+00	5.0324656920E+00	1.0105800115	−3.2490956948E+00	−6.7683481695E+00
1.0065582315	2.3344457360E+00	6.8374319486E+00	0.8529345013	−3.7585353451E+00	−5.2781457848E+00
1.0722575647	5.8346179064E+00	−2.0569874549E+00	1.7840423036	−9.9996391537E−01	6.2377265663E+00
3.8393939056	−4.8994732851E+00	3.9550628819E+00	0.9226568033	−5.1888583745E+00	2.2856587664E+00
0.9986858670	−3.3526646682E+00	−4.2899862990E+00	1.8588422851	1.3420753258E−02	4.6172196354E+00
1.1301557947	4.0632340876E+00	1.9093764825E+00	0.8503954061	4.2158034504E+00	1.1725587068E+00
2.7755873262	−2.9772269908E+00	−3.3853952455E+00	0.9923803119	−7.4849113455E−01	4.0668448008E+00
2.8503846354	−2.5694918609E+00	−1.9277975371E+00	0.9962163918	−8.0751917221E−01	−3.0587498443E+00
1.0025177238	−2.6556988988E+00	−1.6699271636E+00	2.7730485218	2.7376027203E+00	4.3346878213E−01
0.0033742329	−2.8198891259E+00	−2.8600101149E−02	1.7815030869	−1.3387455428E+00	−2.2327754109E+00

Table C.28: Fourier analysis of the z coordinate of Saturn in the Earth–Moon case.

f_l	A_l^c	A_l^s	f_l	A_l^c	A_l^s
0.0000000000	4.5915192915E+00	0.0000000000E+00	0.0065617705	2.2823704113E+02	−2.4255521617E+02
0.0025411482	−1.2458762909E+02	1.0023067767E+02	0.0788228251	−2.9572906797E+00	3.3971431999E+01
0.0040231243	−6.8621473570E+00	2.5585184091E+01	0.9849834198	−9.1741527935E+00	5.4162792249E−01
0.9981068128	1.0932218475E+00	8.9391850891E+00	0.1510839188	4.7758932526E+00	7.2729362446E+00
0.0091012788	8.7097596112E+00	−2.7236599425E+00	0.0050747138	−4.0451267929E+00	1.2437967444E+00
0.9940860723	6.5784901941E−02	−4.3555407680E+00	0.9890038804	4.2722237237E+00	−8.6105203884E−01
0.8522848313	−1.2335633762E+00	1.4770639605E+00	0.8654082420	1.3353659632E+00	9.8030084339E−01
1.8569533342	−1.3260080876E+00	3.2839429065E−01	0.9127222682	7.6999030490E−01	5.3461766645E−01
1.0703679197	−6.5984366801E−01	−6.5380900595E−01	0.8563055160	4.2454219174E−01	−6.7929665208E−01
0.8613877029	−5.7380959472E−01	−5.5914734242E−01	0.9875209711	6.6324657614E−01	2.9543387729E−01
0.9955686251	−4.1524312596E−01	−5.9111378027E−01	1.8438300282	−1.1764878832E−01	−6.5068977860E−01
1.8478505277	2.0741302985E−01	6.2743282037E−01	1.8529327698	6.5748094017E−01	−6.8587949846E−02
2.0014755366	−5.0329822371E−03	−6.9336946299E−01	1.9765284878	2.9719215267E−01	−4.0294549788E−01
1.9896519752	−4.1364128009E−01	−2.6745240746E−01	0.0682385204	−2.9579631159E−01	−3.3875706588E−01
0.0183852240	4.5244504135E−01	7.8813280569E−02	0.0014052246	−4.1033157472E−01	1.3202950363E−01
0.0813623108	2.9919277997E−01	−2.9331477072E−01	0.1536201327	−1.0436879414E−01	−3.9270449677E−01
0.0116392640	3.6358377758E−01	7.7572492315E−02	0.2258843358	1.7744029361E−01	2.9479875874E−01

Table C.29: Fourier analysis of the x coordinate of Uranus in the Earth–Moon case.

f_l	A_l^c	A_l^s	f_l	A_l^c	A_l^s
0.0000000000	−5.3174148761E−02	0.0000000000E+00	0.9991063703	−5.9420596800E+03	4.4441447063E+03
1.9906514810	3.2140035606E+01	−6.0777481061E+02	0.9999960602	−5.2606880750E+02	2.8711188357E+01
0.9251957992	−1.1011371199E+02	3.7079392406E+02	0.0075612667	−2.0065502029E+02	−4.7782978276E+01
0.9982161696	6.0581416981E+01	−1.6614763516E+02	1.8579528743	−8.0912829930E+01	−8.4553459312E+01
2.8494979704	8.1987406360E+01	−5.6385172064E+00	0.1402598665	−2.3416800816E+01	−4.0811217003E+01
2.9821965909	3.4436518753E+01	3.1938593969E+01	1.9915414546	2.6209194950E+01	−3.4349366117E+01
1.9167409048	−1.7432897177E+01	−2.6651925887E+01	1.0089308525	2.7130210939E+00	1.4726196261E+01
0.0084528235	−9.7171379913E+00	−1.1020319018E+01	1.9897614729	7.2672633371E+00	1.2558938398E+01
0.0663493244	−1.2098805931E+01	−5.2667309530E+00	3.8410430551	−7.4231068399E+00	1.0270219157E+01
0.9243058272	−8.8519593688E+00	7.2052059942E+00	1.0739065534	1.0223783642E+01	−7.1127242526E+00
0.8512852328	−3.9854267419E+00	−1.0748099206E+01	1.1318049615	8.8994792978E+00	1.5623860810E+00
1.8588436895	−1.2565907880E+00	−8.2081252491E+00	0.9973383342	−3.1014279979E−01	6.9341212400E+00
1.7840422148	−6.0955540681E+00	−1.3595892874E+00	2.7746975553	5.5477582364E+00	−5.9884897034E−01
2.8503869513	5.0594528028E+00	2.8583548772E+00	1.7831525243	−3.7640757723E+00	−3.6440938599E+00
0.0066705656	4.6169460017E+00	−1.6954471836E+00	1.9158508596	5.1982960629E−02	−4.7803400110E+00
1.0049113661	−3.0190485701E+00	−3.3648949740E+00	1.0031266424	−4.4557034089E+00	4.6560512616E−01
2.7755874371	3.6008034628E+00	−2.6078244947E+00	2.0654521734	−3.8406002172E−01	3.9940098272E+00
0.8503949613	−1.5715811535E+00	3.1907365917E+00	3.9737416918	−3.5220320658E+00	4.5420708832E−01
2.9830867983	7.2033579599E−01	3.2495728946E+00	1.9243021249	−1.1492347034E+00	−3.0890579874E+00
0.1411502904	1.1927524935E−01	−3.4078216705E+00	1.8570615044	2.7299317923E+00	5.8306218547E−01
0.9839838351	1.2234205710E+00	−2.4625776900E+00	2.9082860740	2.4463843133E+00	3.0600223930E−01

Table C.30: Fourier analysis of the y coordinate of Uranus in the Earth–Moon case.

f_l	A_l^c	A_l^s	f_l	A_l^c	A_l^s
0.0000000000	1.0781024824E−02	0.0000000000E+00	0.9991063703	4.4440756449E+03	5.9419673329E+03
1.9906514810	−6.0777367014E+02	−3.2139973612E+01	0.9999960602	2.8710429783E+01	5.2606062426E+02
0.9251957993	3.7200582798E+02	1.1048569180E+02	0.0075612367	−4.7673167653E+01	2.0062924934E+02
0.9982161696	−1.6614505111E+02	−6.0580477004E+01	1.8579528541	−8.4522898947E+01	8.0937228327E+01
2.8494979728	−5.6353312617E+00	−8.1987943175E+01	0.1402598672	−4.0760009269E+01	2.3386873242E+01
2.9821965909	3.1938585880E+01	−3.4436508432E+01	1.9915414546	−3.4349006912E+01	−2.6209334135E+01
1.9167409049	−2.6707250537E+01	1.7468414320E+01	1.0089308527	1.4858324358E+01	−2.7372956245E+00
0.0084505745	−1.0652904448E+01	1.0091639319E+01	1.9897614729	1.2558914870E+01	−7.2672494981E+00
3.8410430551	1.0270240191E+01	7.4231219591E+00	0.8512852323	1.2226849299E+01	−4.5337073263E+00
0.9243058273	7.2033095520E+00	8.8497094966E+00	1.0739072178	−6.9931581732E+00	−1.0288869389E+01
1.1318049982	1.5677216808E+00	−8.8985012629E+00	1.8588436892	−8.2080685682E+00	1.2565199914E+00
0.0663493237	3.3451708637E+00	−7.5916034385E+00	0.9973383341	6.9340122044E+00	3.1012608920E−01
1.7840422872	−1.3693542423E+00	6.1074553159E+00	2.7746975556	−5.9882431340E−01	−5.5478120243E+00
2.8503892310	3.0568553688E+00	−4.9681935371E+00	1.7831525244	−3.6440692304E+00	3.7640304224E+00
0.0066705629	−1.6953215371E+00	−4.6160155161E+00	1.9158508596	−4.7803024341E+00	−5.1984735726E−02
1.0049106594	−3.3433340677E+00	3.0702170471E+00	1.0031263519	4.8847687498E−01	4.4730571475E+00
2.7755872992	−2.6192927669E+00	−3.5990804680E+00	0.8503956664	4.2840390935E+00	2.2404430157E−01

Table C.30: (continued)

f_l	A_l^c	A_l^s	f_l	A_l^c	A_l^s
2.0654521734	3.9940346026E+00	3.8406191621E−01	3.9737416918	4.5420698927E−01	3.5220323477E+00
2.9830867983	3.2495662235E+00	−7.2029487965E−01	1.9243021247	−3.0892711130E+00	1.1493251519E+00
0.1411503034	−3.3525608058E+00	−2.2137502334E−01	0.9839838793	2.5332763714E+00	1.2609164037E+00
1.8570615052	5.8308485572E−01	−2.7299102580E+00	2.9082860735	3.0649801547E−01	−2.4503130729E+00

Table C.31: Fourier analysis of the z coordinate of Uranus in the Earth–Moon case.

f_l	A_l^c	A_l^s	f_l	A_l^c	A_l^s
0.0000000000	−7.1298225818E+00	0.0000000000E+00	0.0049122179	3.5355617722E+02	5.6941591499E+02
0.0008922515	−9.0731380939E+01	−4.4548503757E+01	0.0040228146	4.3954190343E+01	2.0176729384E+01
0.0788227982	−2.8963894497E+00	3.3960826181E+01	0.9964574459	−1.7938916177E+01	−2.5793880368E+00
0.1527333983	1.1659871980E+01	−1.3066475627E+01	0.9866330049	5.7630795004E+00	1.7573778825E+01
0.0058015152	1.3493918997E−01	−1.6229952074E+01	0.8539341119	3.5200656448E+00	1.6149510916E+00
0.8637585329	−2.5883367299E+00	2.1008933282E+00	0.9924373476	2.5122536748E+00	−1.1266277524E+00
0.9906529811	6.6058503395E−01	−2.6747808336E+00	1.8553037471	4.4196501849E−02	−2.7488252908E+00
0.0017814658	1.2902439827E+00	2.0804766331E+00	2.0031249124	−1.3445573477E+00	3.7374653185E−01
0.9955679708	−1.1842790201E+00	5.5888027396E−01	1.8454793219	−1.2021347286E+00	5.7029514791E−01
0.9875223460	−3.5375918131E−01	1.2854439272E+00	0.1536225387	1.1904503353E+00	−4.0951814863E−02
1.9880025908	7.3672370447E−01	−6.6331559158E−01	1.9781782027	−9.3563156994E−01	−3.7404996310E−01
1.0703680389	−6.5397357793E−01	−6.6090587793E−01	0.9127224147	7.6053781411E−01	5.4439253225E−01
0.0200344965	−8.8331266761E−02	−9.2025246180E−01	0.0698877248	−4.8734671813E−01	7.5029697529E−01
0.0797127453	4.1005838833E−01	7.2756934511E−01	0.2275338577	4.7768708758E−01	−4.9298068135E−01
0.8388118403	−6.4543857800E−01	1.9148483918E−02	0.0066932619	−3.7034678084E−01	4.2121315785E−01
0.8579540005	−2.7932828285E−01	−4.2240668332E−01	0.8597386708	1.6655313573E−01	−4.7806954793E−01
0.9857436297	−3.4616716648E−01	−2.8406804037E−01	0.9973466594	3.3489749404E−01	2.8359236748E−01
1.8494991800	4.1499471257E−01	4.5833193221E−02	0.1518441252	−7.0185899439E−02	4.1809758082E−01
1.8512838825	2.1403837178E−01	3.5869636147E−01	0.9915453277	2.5155698665E−01	−2.9632179893E−01
1.0115797159	−3.1500515630E−01	−2.1665607843E−01	0.0779332712	−2.2690746010E−01	2.6849611635E−01
2.8468489587	2.2762618018E−01	1.9718514242E−01	0.8548231450	1.4994287436E−01	2.3523151918E−01
1.1442785952	3.9365862030E−02	2.6947447332E−01			

Table C.32: Fourier analysis of the x coordinate of Neptune in the Earth–Moon case.

f_l	A_l^c	A_l^s	f_l	A_l^c	A_l^s
0.0000000000	−6.1007425273E−02	0.0000000000E+00	0.9995430555	−7.9150670631E+03	8.5363223679E+03
1.9910882886	−1.1854102513E+02	−9.4750312082E+02	0.9251957659	−1.0883477941E+02	3.7096863565E+02
0.0079978362	−3.2320764992E+02	−1.6028489149E+01	1.8583893817	−1.4921878210E+02	−1.0697164602E+02
0.9999954057	1.1454828002E+02	1.0557892193E+02	2.8499345933	1.2489110744E+02	−3.2029333198E+01
0.1406967396	−4.7386830663E+01	−5.6601826369E+01	2.9826334775	6.1937532120E+01	3.9912392862E+01
0.9990922746	3.8637832346E+01	3.7296922108E+01	1.9167409786	−1.7668935278E+01	−2.6396571094E+01
1.0084940753	8.4554691971E−02	2.3492122813E+01	3.8414798068	−8.5903658531E+00	1.7929555606E+01
1.0743435838	1.3785729763E+01	−1.3620093371E+01	0.8508484734	−3.1479736509E+00	−1.7706961752E+01
0.9247431037	−1.1817208613E+01	1.3252326777E+01	1.0044736970	7.2648820802E+00	−1.3928357471E+01
1.0035638016	−4.1881982995E+00	1.5320394318E+01	0.0663494533	−1.2105950089E+01	−5.2846940958E+00
1.1322419515	1.4175958259E+01	1.2677797356E−02	1.9915403982	−1.2536253997E+01	1.9244010827E+00
2.7751342298	8.3269760234E+00	−2.4663661261E+00	1.7835889978	−6.8051683156E+00	−4.4926136421E+00
1.9162876600	−1.2704880960E+00	−7.3310251346E+00	2.0658888147	4.9980756887E−01	6.2293646550E+00
1.7840421230	−6.0828424791E+00	−8.9186690018E−01	3.9741786847	−5.3214397279E+00	1.6505333618E+00
1.9247388279	−2.6458003103E+00	−4.4443477692E+00	1.9906371870	−4.3941184912E+00	5.3888120001E−01
0.0084501344	−2.8514814734E−01	4.3669864212E+00	2.7755873473	3.2180445633E+00	−2.9091534690E+00
0.9835473738	2.6046407463E+00	−3.4392271435E+00	3.7087809010	1.4331979063E+00	3.6141976674E+00
0.8503957525	−7.3560280368E−01	3.5643743724E+00	2.0160349775	2.5401610613E+00	2.5839437439E+00
0.2154970255	−2.0660258109E+00	−2.6486908624E+00	1.0004501983	−2.3902581385E+00	1.5999466830E+00
2.7172357025	1.3213802354E+00	−2.4424252941E+00	1.8588430702	−1.5087805537E+00	1.9182280815E+00
1.1571886556	1.9564521336E+00	−1.4900987235E+00			

Table C.33: Fourier analysis of the y coordinate of Neptune in the Earth–Moon case.

f_l	A_l^c	A_l^s	f_l	A_l^c	A_l^s
0.0000000000	−3.1426349714E−03	0.0000000000E+00	0.9995430654	8.5329262062E+03	7.9185190535E+03
1.9910882885	−9.4750090525E+02	1.1854321245E+02	0.9251957659	3.7218937725E+02	1.0918893923E+02

Table C.33: (continued)

f_l	A_l^c	A_l^s	f_l	A_l^c	A_l^s
0.0079978361	−1.6025318057E+01	3.2314485349E+02	1.8583893817	−1.0697107246E+02	1.4921798015E+02
0.9999954064	1.0558095189E+02	−1.1454286680E+02	2.8499345933	−3.2029531284E+01	−1.2489187901E+02
0.1406967396	−5.6530370080E+01	4.7326762419E+01	2.9826334935	3.9956826667E+01	−6.1915395846E+01
0.9990881804	3.0162766646E+01	−4.4477076299E+01	1.9167409787	−2.6451396540E+01	1.7705708976E+01
1.0084940753	2.3702877016E+01	−8.5323258774E−02	0.8508484724	2.0142771348E+01	−3.5813986640E+00
3.8414798068	1.7929592216E+01	8.5903833667E+00	1.0743435838	−1.3622841042E+01	−1.3788524909E+01
0.9247424145	1.3593364636E+01	1.1433229408E+01	1.0044724021	−1.4381984997E+01	−6.5338988462E+00
1.0035638017	1.5380160358E+01	4.2051630425E+00	1.1322419515	1.2677321944E−02	−1.4175428277E+01
1.9915442797	−1.3527025091E−01	1.2839948642E+01	2.7751342298	−2.4663859294E+00	−8.3270442444E+00
0.0663494578	3.3134907657E+00	−7.6127727579E+00	1.7835889978	−4.4925692925E+00	6.8050995400E+00
1.9162876600	−7.3309591507E+00	1.2704791017E+00	2.0658888147	6.2294037386E+00	−4.9981007611E−01
1.7840421230	−8.9392523970E−01	6.0959583836E+00	3.9741787141	1.6437869891E+00	5.3228774574E+00
1.9247388279	−4.4446627636E+00	2.6459890218E+00	1.9906371872	5.3883783091E−01	4.3941123889E+00
0.0084501236	4.3572242671E+00	2.6644527597E−01	2.7755873473	−2.9120059472E+00	−3.2213016468E+00
0.9835473514	3.5411698128E+00	2.6768016058E+00	0.8503949650	3.7929523750E+00	1.1415877756E+00
3.7087809366	3.6159217487E+00	−1.4276279091E+00	2.0160349770	2.5838197898E+00	−2.5401372840E+00
0.2154970256	−2.6457530262E+00	2.0637308181E+00	1.0004501978	1.5977394999E+00	2.3904933367E+00
2.7172356980	−2.4426103984E+00	−1.3208905560E+00	1.8588430700	1.9182268811E+00	1.5086768863E+00
1.1571886556	−1.4932875215E+00	−1.9606390738E+00			

Table C.34: Fourier analysis of the z coordinate of Neptune in the Earth–Moon case.

f_l	A_l^c	A_l^s	f_l	A_l^c	A_l^s
0.0000000000	4.8217094624E+00	0.0000000000E+00	0.0044755045	3.8600983964E+02	9.7817214102E+02
0.0004543249	2.6653120721E+01	−3.4925643181E+02	0.0788227967	−2.9342429558E+00	3.3937953717E+01
0.9960207221	−2.6971847716E+01	−9.0034066205E+00	0.1531700903	1.4311131709E+01	−2.3453524963E+01
0.9870697079	1.3837158961E+01	2.5505752341E+01	0.0040213338	−1.2744157685E+01	6.1026033190E+00
0.9910909263	−7.7433845412E+00	−5.5837433549E+00	0.9919995771	6.8047641686E+00	6.6930300096E+00
0.8543708049	5.8880159198E+00	1.5001908903E+00	0.0049283761	−4.6308587395E+00	1.4562699821E+00
0.8633218298	−4.5857098033E+00	2.5150967689E+00	1.8548670465	8.4168654262E−01	−4.2301508991E+00
2.0035616242	−1.9705541556E+00	9.5429084152E−01	1.8459160239	−1.6950689941E+00	1.2183895588E+00

Table C.35: Fourier analysis of the x coordinate of Pluto in the Earth–Moon case.

f_l	A_l^c	A_l^s	f_l	A_l^c	A_l^s
0.0000000000	−1.2239693573E−01	0.0000000000E+00	0.9996954649	5.7931939639E+03	1.3281386122E+04
0.9999969311	−3.4739361425E+03	−4.2846203740E+03	0.9993940377	2.1517267155E+02	1.7651523981E+03
1.9912406200	−1.1407383549E+03	−3.3310303583E+02	1.9915421501	4.5247988845E+02	7.7376214127E+00
0.0081502171	−1.7888942476E+02	3.6087676601E+02	0.9251957554	−1.1453420362E+02	3.6469141813E+02
0.9990925495	−5.4309203179E+01	3.2315401824E+02	1.0002985883	−2.1926279715E+02	1.4659736558E+02
1.8585417623	−1.9622859378E+02	1.1713742435E+02	1.0043200882	1.8656276179E+02	−6.3249595985E+01
1.0037170513	9.4641064135E+01	1.7290500413E+02	2.8500869778	2.5530660648E+01	−1.5844162977E+02
0.0084516500	2.8692031636E+01	−1.5059765190E+02	1.9909392366	−1.2233051760E+02	−7.9391023140E+01
1.0040185562	−1.2887906268E+02	−5.0152747241E+01	0.1408491197	−8.8136341298E+01	2.5956197001E+01
1.8588432309	6.0145606014E+01	−6.2864056691E+01	2.9827858783	7.6375094414E+01	−5.0791329508E+01
0.9987911493	−3.1551374113E+01	6.4073669327E+01	2.8503884206	6.7348196237E+00	6.0732048395E+01
0.0078488073	−3.3744608926E+01	3.6131710374E+01	1.0006000495	−2.5107501645E+01	2.3434341619E+01
0.1411505717	2.9535112437E+01	−1.8583797015E+01	2.9830873861	−2.2934108284E+01	2.6315908346E+01
1.9167411258	−1.3894976943E+01	−2.6685124746E+01	1.8582403039	−2.7170682777E+01	6.9256411782E+00
1.0083416659	−2.6748226833E+01	1.1792488619E+01	1.9906377598	−1.7451880916E+01	−2.0435255306E+01
3.8416322036	1.6180024284E+01	1.8720969570E+01	1.0046215072	1.9655835289E+01	−1.4022130179E+01
1.0744954706	−9.1469299656E+00	−2.2291934307E+01	1.0034156225	5.0045071516E+00	2.3625322947E+01
0.8506960806	1.8631883044E+01	−1.2397099905E+01	0.9248949625	9.7053865890E+00	1.9876044582E+01
1.9918435586	2.1350316113E+00	−2.1533970294E+01	2.8497855652	8.5629800754E+00	−1.7726992254E+01
0.9984897061	−1.1627349269E+01	1.2558373500E+01	1.1323943897	7.0974400723E+00	−1.6151586932E+01
1.9952623052	−1.5845873845E+01	−3.1699670644E+00	1.9958652597	−5.8456055990E+00	1.5072439556E+01
0.0663494867	−1.2279100918E+01	−5.6792792701E+00	1.9955636100	9.9537050799E+00	−5.5520119241E+00
0.1405479364	−1.1282453693E+01	−1.5557622534E−01	0.8503947325	−9.0005277047E+00	6.2034234582E+00
2.7752867850	1.4000801367E+00	−1.0717851772E+01	2.9824845073	1.0762040172E+01	−3.2729856021E+00
1.0080402912	1.1021051681E+01	−1.5665878168E+00	1.7837415354	−8.5424420702E+00	5.4740598810E+00
3.8419336393	−7.8411512156E+00	−5.2262536366E+00	1.9164401921	−8.9852462388E+00	−2.2487678777E+00
1.0747973487	5.4971465258E+00	7.3594908641E+00	0.0075474853	−7.8838728749E+00	4.5635128627E+00
2.0660416108	7.3196516861E+00	2.6564285581E+00	0.0087531786	−7.0124008642E+00	−1.9708828792E+00

Table C.35: (continued)

f_l	A_l^c	A_l^s	f_l	A_l^c	A_l^s
3.9743312411	−8.1006889362E−01	6.8901407214E+00	1.0009014449	−3.6287049062E+00	5.4563462446E+00
1.9248914031	−6.3910351097E+00	7.5914376694E−01	1.1326957787	−9.2598992419E−01	6.6425292431E+00
0.8460713536	3.7156640512E+00	4.6339029830E+00	0.8466744280	5.2120879089E+00	−2.8559199081E+00
1.9903367091	−2.2880243096E+00	−5.3943173879E+00	0.9833948047	5.2297953111E+00	1.2238019587E+00
1.7840422401	−3.5202165712E+00	−3.9710377500E+00	1.8579389161	−5.1633968863E+00	−2.2046640555E−01
0.0127745727	4.5647670490E+00	2.6935965830E+00	0.0121721126	−1.9835195745E+00	4.9160395926E+00
3.7089334279	4.8376215293E+00	1.8925025700E−01	1.0049226377	2.6811739127E+00	−3.5429854272E+00
0.9981883831	−3.7661744081E+00	2.1960083419E+00	1.0031142445	−3.7614638373E−01	4.4278176442E+00

Table C.36: Fourier analysis of the y coordinate of Pluto in the Earth–Moon case.

f_l	A_l^c	A_l^s	f_l	A_l^c	A_l^s
0.0000000000	1.0121033631E−01	0.0000000000E+00	0.9996954656	1.3281365185E+04	−5.7926464680E+03
0.9999968558	−4.2732465634E+03	3.4871316471E+03	0.9993940381	1.7651271260E+03	−2.1514452016E+02
1.9912406751	−3.3579236253E+02	1.1401430397E+03	1.9915421531	7.7918721777E+00	−4.5247478093E+02
0.0081502383	3.6063803986E+02	1.7917038506E+02	0.9251957556	3.6595138331E+02	1.1504062301E+02
0.9990925496	3.2314857606E+02	5.4310437563E+01	1.0002984428	1.4793482801E+02	2.1829471139E+02
1.8585417625	1.1713472790E+02	1.9622880785E+02	1.0043200877	−6.3503310586E+01	−1.8729799363E+02
1.0037170520	1.7359060549E+02	−9.5009294814E+01	2.8500869778	−1.5844260784E+02	−2.5530811838E+01
0.0084516468	−1.5055844178E+02	−2.8713321912E+01	1.9909392401	−7.9409486218E+01	1.2231827407E+02
1.0040186094	−5.0634053272E+01	1.2926129917E+02	0.1408491197	2.5923297446E+01	8.8025466379E+01
1.8588432308	−6.2864033012E+01	−6.0145104870E+01	2.9827858502	−5.0873907651E+01	−7.6304568183E+01
0.9987911503	6.4071393715E+01	3.1553745298E+01	2.8503884206	6.0732451846E+01	−6.7348382900E+00
0.0078488055	3.6126662364E+01	3.3735319931E+01	1.0005999511	2.3536602312E+01	2.5004539842E+01
0.1411505714	−1.8497744899E+01	−2.9598635724E+01	2.9830872563	2.6458761546E+01	2.2806135110E+01
1.9167409135	−2.6616595612E+01	1.4158103192E+01	1.8582403867	6.8291635797E+00	2.7193588816E+01
1.0083416043	1.1971599766E+01	2.6965162064E+01	1.9906377932	−2.0453411852E+01	1.7421823320E+01
0.8506960816	1.4103118113E+01	2.1204142331E+01	3.8416322036	1.8721007018E+01	−1.6180057760E+01
1.0046214927	−1.4087072281E+01	−1.9723509408E+01	1.0744960897	−2.2553756979E+01	8.5769883265E+00
1.0034157245	2.3737762967E+01	−4.9205382193E+00	0.9248949630	1.9864126743E+01	−9.7002899233E+00
1.9918436865	−2.1531508369E+01	−2.2515915628E+00	2.8497855652	−1.7727101671E+01	−8.5630325655E+00
0.9984898077	1.2508565474E+01	1.1681402177E+01	1.1323945582	−1.6111835133E+01	−7.2069421470E+00
1.9952623052	−3.1713873664E+00	1.5852896790E+01	1.9958652597	1.5079121866E+01	5.8482161442E+00
1.9955636101	−5.5544260877E+00	−9.9581220719E+00	0.1405479363	−1.5536537747E−01	1.1268254895E+01
2.7752867850	−1.0717884814E+01	−1.4000727942E+00	2.9824845087	−3.2723400143E+00	−1.0762295340E+01
1.0080402889	−1.5813857609E+00	−1.1119574843E+01	1.7837415750	5.4682080504E+00	8.5411260311E+00
3.8419336393	−5.2262713186E+00	7.8411672521E+00	1.9164401774	−2.2431601469E+00	8.9859120606E+00
1.0747973698	7.3641552040E+00	−5.4914265213E+00	0.0075474851	4.5626866656E+00	7.8823400942E+00
0.0663495205	3.8914545870E+00	−7.5348610504E+00	0.8503944980	6.2094251077E−01	−8.3253872556E+00

Table C.37: Fourier analysis of the z coordinate of Pluto in the Earth–Moon case.

f_l	A_l^c	A_l^s	f_l	A_l^c	A_l^s
0.0000000000	−1.5398308503E+03	0.0000000000E+00	0.0003015705	3.3658844644E+03	−2.8169622998E+03
0.0043231193	−9.2433100819E+02	9.2669590956E+02	0.0006029692	2.9499712757E+02	−4.4976810097E+02
0.0040216696	4.3344531553E+02	−2.4578877485E+02	0.0046245972	−7.6470340031E+01	1.4127799656E+02
0.9912436888	−1.1779586345E+02	2.0715294233E+01	0.9918467050	2.6697041733E−01	1.1958993194E+02
0.0009043844	2.8191236619E+01	−9.4857881588E+01	0.9915452116	5.3926507220E+01	−6.4296799158E+01
0.9958682938	−3.1922118030E+00	−3.5239253204E+01	0.1533224733	−1.9651471299E+01	−2.7986801226E+01
0.0788227976	−2.5781275807E+00	3.3506479517E+01	0.9872220909	3.5984003861E+01	−3.1119591667E+00
0.0049258229	−5.8099567940E+00	2.9039331228E+01	0.0037200524	1.3568781180E+01	1.9581877327E+01
0.0012057922	−6.2332986833E−02	−2.1592289506E+01	0.8591478395	1.6150934306E+01	1.4918732744E+01
0.8585448006	−1.1920687559E+01	1.8476121082E+01	1.8506930510	−1.7993456785E+01	2.3003825516E+00
1.8500900652	−5.3231766182E+00	−1.7344119371E+01	0.8588463488	−1.9203063409E+00	−1.5306197596E+01
0.9909423140	−1.4549320377E+01	−1.7559120976E+00	0.9921481736	4.2349908869E+00	1.4034380632E+01
0.9955668217	−2.4097839121E+00	1.3235740087E+01	0.1536239620	1.0005977741E+01	8.5708247175E+00
1.8503915149	1.0708939604E+01	6.8814618517E+00	0.9875235503	−1.2888504930E+01	4.7999110654E+00
0.8545231994	4.6411723792E+00	−5.9709679030E+00	0.0052273305	5.7325247670E−01	6.4261584768E+00
1.9827889460	3.2700134473E+00	−5.6373159195E+00	1.9833918880	−5.0076103929E+00	−4.1701317286E+00
0.8631692552	−5.1819972141E+00	−3.9457387054E+00	0.0015071643	−1.5119766460E+00	−4.9540658758E+00
1.8547143548	5.2319944538E+00	−1.2095866116E+00	0.9961698552	−1.5956352543E+00	−4.0466594910E+00
1.9830904308	7.9458424154E−01	4.5036355541E+00	0.1530211118	−1.3169569390E+00	−3.9859868211E+00
0.9869206824	4.3383279667E+00	8.9831958942E−01	0.0034184268	1.3543994906E+00	2.7943732860E+00

Table C.37: (continued)

f_l	A_l^c	A_l^s	f_l	A_l^c	A_l^s
0.8548246148	−1.0920016337E+00	2.6634773049E+00	2.0037140875	1.0059588607E−01	2.7238960268E+00
0.9906408461	−2.4732142848E+00	−1.0732337333E+00	0.8594492814	2.4213321157E+00	1.1818685462E+00
0.9924494699	1.4996174552E+00	2.2408699016E+00	0.8582434573	−2.0563105699E+00	1.7393727616E+00
1.8460685807	5.2878966765E−01	2.5440326168E+00			

Table C.38: Fourier analysis of the x coordinate of the Sun in the Earth–Moon case.

f_l	A_l^c	A_l^s	f_l	A_l^c	A_l^s
0.0000000000	−6.2702298846E−02	0.0000000000E+00	0.9251957863	−1.0927756550E+02	3.7071152326E+02
1.9167408300	−1.7639274483E+01	−2.6355901096E+01	0.0663492628	−1.2134309252E+01	−5.2409110115E+00
0.9999960823	3.2997609728E+00	−9.7947018015E+00	1.7840423142	−6.0086163845E+00	−1.0044529781E+00
2.7755873598	3.2419224811E+00	−2.7911158782E+00	0.8503953768	−9.3088935924E−01	3.6796809468E+00
2.9082858709	2.4341251010E+00	2.5532318120E−01	1.9915412950	5.2525518315E−01	8.5592965380E−01
1.0828414495	−3.1060567852E−01	6.2657819781E−01	1.0578942954	5.4860828546E−01	−2.7786631301E−01
3.7671324039	1.0866755465E−02	6.5947188464E−01	1.8419399637	−3.0298654687E−01	−4.1418523868E−01
1.7092421655	−3.2165100171E−01	−4.1576789123E−02	2.7007868417	2.3932227691E−01	−2.2305757474E−01
0.0084513888	1.8970582511E−01	−7.2961596769E−02	1.8588428256	1.9726931947E−01	4.1106250127E−02
3.8998309221	−1.3259559913E−01	1.2906424508E−01	1.8503916631	−1.4436373779E−01	−9.3275186819E−02
2.8503874966	−1.2471941909E−01	9.9598842084E−02	3.6344338860	9.5245128451E−02	8.6784281475E−02
0.1411498405	−9.8155502398E−02	−4.7134257093E−02	1.9416880465	1.0190766012E−01	3.5997575249E−02
2.6428888417	4.1052420132E−03	−9.1961123868E−02	2.9830865339	−8.8981184774E−02	−1.3011473697E−02
4.7586774496	−5.9175888238E−02	−4.7645233070E−02	2.0494393420	−1.4087275076E−02	6.1402632967E−02
4.6259789311	−5.6644798814E−02	7.8382967226E−03	2.8334853083	5.4465062282E−02	3.5293153200E−03
3.6923320497	3.0311331974E−03	5.5229938189E−02	0.7755951203	−1.0627946547E−02	4.9899625148E−02
0.7924972709	−2.6118430639E−02	−4.4710061957E−02	2.0743865065	−1.7892671009E−02	−4.0483675552E−02
1.9251839192	2.5100577328E−02	1.6301305402E−02	0.9915467636	1.8697889545E−02	−2.0917457108E−02
0.7675501271	−3.1813242947E−03	2.8002004865E−02	3.8419327577	6.0892686650E−04	−2.7838586028E−02
2.8419368412	2.5187974591E−02	−7.8560179516E−03	0.0912963877	2.4246455229E−02	−5.7834454516E−03
1.0747961562	−8.0490549173E−03	2.1265653704E−02	1.0080413430	7.9576864105E−03	−1.7685491312E−02
2.6259864870	1.1918654033E−02	−1.1996903193E−02	3.5596335844	1.1964267442E−02	1.0088460622E−02
4.8913759651	−1.0724400398E−03	−1.3797287070E−02	1.6344410508	−1.2529869533E−02	−1.0706206312E−03
5.6175239744	6.0276435007E−03	−9.6823741726E−03	0.9936994549	3.1503172101E−03	1.0108510474E−02
1.7671405992	−5.9246640154E−03	−7.5755030725E−03	0.0747945153	9.2876301532E−03	1.1614854581E−04
0.8588918809	−1.2840253038E−03	8.7105564891E−03	2.5680883741	4.5750933973E−05	−8.9376072281E−03
1.0187754715	−7.2344733544E−03	−4.6504617893E−03	4.5511782786	−7.9263395863E−03	1.4270219096E−03
0.9210738074	6.0676426862E−03	−4.6142709950E−03	3.9746312268	5.7635756949E−03	−5.1941565362E−03
2.7092401284	3.5020825027E−03	−7.0650942345E−03	1.1326945463	6.5593185387E−03	−3.0155490363E−03
5.7502224914	7.5428171328E−03	−1.5180579481E−03	0.9293279339	1.2957041627E−03	6.7427963109E−03
4.6838773148	−5.5078607946E−03	−4.1089612559E−03	3.0409843848	−3.7952950724E−03	−4.9826991619E−03
0.9719860966	5.9792346163E−03	−2.2061176280E−03	1.1576418504	−2.7953877852E−03	5.1278575240E−03
1.7590955677	4.0284162623E−03	4.2289347879E−03	0.9501329880	2.2023723763E−03	5.1622238723E−03
3.7092342900	−4.0027284968E−03	−3.9417472447E−03	0.9830939719	4.5342478069E−03	−2.5202039457E−03
3.8250305197	−3.6001382485E−03	3.7867719609E−03	1.9830815513	1.0993810246E−03	4.8622074658E−03
2.9167332938	−4.5690264033E−03	1.2955449548E−03			

Table C.39: Fourier analysis of the y coordinate of the Sun in the Earth–Moon case.

f_l	A_l^c	A_l^s	f_l	A_l^c	A_l^s
0.0000000000	1.6078519304E−05	0.0000000000E+00	0.9251957863	3.7193289716E+02	1.0963759943E+02
1.9167408300	−2.6410913630E+01	1.7676092770E+01	0.9999960823	−9.7948122827E+00	−3.2997983410E+00
0.0663492628	3.2937774849E+00	−7.6261019182E+00	1.7840423128	−1.0065940114E+00	6.0217538766E+00
2.7755873559	−2.7940242273E+00	−3.2451369334E+00	0.8503953768	3.7365274672E+00	9.4527069376E−01
2.9082858799	2.5588148482E−01	−2.4380953030E+00	1.9915412950	8.5622374679E−01	−5.2543565599E−01
1.0828414495	6.3269739188E−01	3.1363898961E−01	3.7671324039	6.5999362007E−01	−1.0875352048E−02
1.8419406031	−4.1814359803E−01	3.0326831626E−01	1.0578942917	−1.4630549166E−01	−2.8884221902E−01
1.7092415599	−4.0465757552E−02	3.2287452792E−01	2.7007868417	−2.2338133125E−01	−2.3966964096E−01
0.0084507454	−8.0930825151E−02	−2.0786769619E−01	1.8588428256	4.1124142533E−02	−1.9735504740E−01
3.8998309221	1.2924291825E−01	1.3277916101E−01	1.8503916635	−9.3204969777E−02	1.4425469741E−01
2.8503881018	9.9099371240E−02	1.2508265037E−01	3.6344338860	8.6855037590E−02	−9.5322782680E−02
1.9416880464	3.6067619181E−02	−1.0210601280E−01	2.6428888417	−9.2122181816E−02	−4.1124312300E−03
2.9830859127	−1.2659808599E−02	8.9042519642E−02	4.7586774468	−4.7676239990E−02	5.9216623199E−02
4.6259789311	7.8425448954E−03	5.6675440114E−02	2.8334853083	3.5436755843E−03	−5.4686676786E−02
0.7755951228	5.2181576254E−02	1.1114960902E−02	2.0494393411	5.1082065288E−02	1.1719145039E−02

Table C.39: (continued)

f_l	A_l^c	A_l^s	f_l	A_l^c	A_l^s
0.0912963821	1.2812559567E−02	5.3691306106E−02	3.6923320497	5.5290727481E−02	−3.0344692809E−03
2.0743865064	−4.0551958634E−02	1.7922870953E−02	0.7924972717	−3.4772800665E−02	2.0313257618E−02
0.7675501262	3.7124605760E−02	4.2175543488E−03	1.9251839148	1.6329614943E−02	−2.5145364793E−02
3.8419327577	−2.7846812481E−02	−6.0910640361E−04	2.8419368416	−7.8569193723E−03	−2.5191074878E−02
0.9915470001	−1.8445030558E−02	−1.6641376900E−02	1.0747961706	2.1231103491E−02	8.0418541440E−03
1.0080413377	−1.7640726337E−02	−7.9367637473E−03	2.6259864868	−1.2020374823E−02	−1.1941954663E−02
3.5596335844	1.0098938510E−02	−1.1976693416E−02	4.8913759651	−1.3814172656E−02	1.0737525032E−03
1.6344410509	−1.0764494602E−03	1.2597936417E−02	5.6175239744	−9.6867088191E−03	−6.0303419941E−03
0.9936994524	1.0110699048E−02	−3.1511825661E−03	0.8588864210	1.0110666038E−02	1.1606018848E−03
1.7671405657	−7.6797532286E−03	6.0088615409E−03	0.9830939179	−4.5068761798E−03	−8.1024061433E−03
2.5680883741	−8.9587884111E−03	−4.5859275632E−05	1.0187754705	−4.6556512113E−03	7.2426318691E−03
4.5511782786	1.4279692553E−03	7.9316013795E−03	0.9210739902	−4.6178862612E−03	−6.0961411812E−03
3.9746312268	−5.1967764800E−03	−5.7664825788E−03	2.7092401299	−7.0693810956E−03	−3.5042604593E−03
5.7502224914	−1.5189590081E−03	−7.5472942276E−03	1.1326945447	−3.0034293102E−03	−6.5327706246E−03
0.2239949447	−3.9241425243E−03	5.9705476140E−03	0.0747938701	−6.4927687427E−05	6.4708556709E−03
0.9293281462	6.7641973068E−03	−1.2855414118E−03	4.6838773148	−4.1127195937E−03	5.5128984500E−03
0.9719860981	−2.2052539066E−03	−5.9771253924E−03	1.1576418506	5.3621403455E−03	2.9231081981E−03
3.0409843851	−4.5962290727E−03	3.5009079075E−03	0.1411497872	2.4337475896E−03	−5.0719307017E−03
3.7092342900	−3.9430089313E−03	4.0040102562E−03	1.7590955809	4.1048744669E−03	−3.9096593396E−03
3.8250305197	3.7981766550E−03	3.6109808376E−03	0.9501321237	4.7480610225E−03	−2.0491352182E−03
1.9830812433	4.6921164939E−03	−1.0680914322E−03	2.9167332919	1.2972926309E−03	4.5750811618E−03

Table C.40: Fourier analysis of the z coordinate of the Sun in the Earth–Moon case.

f_l	A_l^c	A_l^s	f_l	A_l^c	A_l^s
0.0000000000	4.2439442250E−04	0.0000000000E+00	0.0788228300	−2.9509730443E+00	3.3923683017E+01
0.9127221954	7.6438340350E−01	5.3137655538E−01	0.0040223167	4.3239896732E−02	−9.1082048260E−01
1.0703678568	−6.6150919031E−01	−6.5574605604E−01	0.1536232108	−4.0411511563E−02	3.1992449774E−01
0.9376693695	−1.9382714589E−01	6.6302812856E−03	0.7800237174	1.9152507923E−01	−4.0362720766E−02
1.9292143996	4.3392479583E−02	−5.5902476647E−02	1.7715687330	−3.0112466621E−02	5.6933509628E−02
2.0619128768	5.0643968672E−02	−4.8535749671E−03	1.9042672216	−4.8895562680E−02	1.3483193430E−02
0.0538751930	−3.3050416832E−02	3.7149639393E−02	0.9875226590	−2.3535118519E−02	−1.7768538741E−02
0.9955668829	1.4017854728E−02	1.2778022357E−02	0.0748075800	−1.5835281332E−02	−6.8352106665E−05
0.8379217864	1.2456172922E−02	7.9589914124E−03	2.7631137630	−4.0018680740E−03	−9.7348495224E−03
2.9207594246	2.3369104733E−03	1.0625832801E−02	0.7052230468	1.0265159016E−02	−2.5971325048E−03
0.2115210359	−5.8877081158E−03	4.6639534744E−03	0.8548239500	−6.3830930631E−03	1.0944292331E−03
1.6967685967	−2.2652329554E−03	4.7058153959E−03	0.8463722907	4.8822588962E−03	9.7752581982E−04
1.0040177884	−4.6356502335E−03	−1.7992392621E−03	0.2284235833	−7.0963691640E−04	4.2773595565E−03
1.1451681951	−2.9043882691E−03	−3.1119395494E−03	1.0953150025	3.4270871490E−03	4.7983221834E−04
0.8628690415	−3.2657630482E−03	2.3831054307E−04	1.8544140499	1.8806136434E−03	−2.6257750586E−03
3.0534578816	−1.7563684845E−03	2.5749067818E−03	2.8958122424	1.2764433001E−03	−2.8191202535E−03
1.8463689339	1.1904061293E−03	−2.0574751610E−03	0.0123969031	−1.3349275904E−03	−1.9350142361E−03
0.0707671856	−9.4876350829E−05	−2.2148866326E−03	2.7880609487	1.7742719657E−03	1.0614939688E−03
1.6388703003	6.5756023986E−04	1.9291362465E−03	2.6304152960	−1.8412160006E−03	−7.0492562798E−04
1.7965159443	−3.0651016333E−04	−1.9615873663E−03	1.0454200663	−2.8520195320E−04	−1.8811954664E−03
1.9790676394	1.8137454088E−03	−4.2461497454E−04	3.9123044457	−1.0031227927E−03	−5.1937315709E−04
1.8294668233	−1.0651051479E−03	3.3860110070E−04	3.7546587883	1.0554106083E−03	3.3136337072E−04
0.1452122811	−6.4531044639E−04	8.7754392398E−04			

C.4 Expansions of the c_i functions, Sun–Earth+Moon case

In tables C.41 to C.53 we give the results of the Fourier analysis of the positions of the c_i functions for the Earth–Moon case. We do not give adjustments of the frequencies as linear combinations of basic ones, because they have been given in Chapter 5 for the functions used in the Sun–Earth+Moon model developed there (tables 5.23 to 5.28). In order to save space, every row of tables C.41 to C.53 consists in to two entries, which are separated by a double vertical line.

Table C.41: Fourier analysis of the c_1 function in the Sun–Earth+Moon case.

f_l	A_l^c	A_l^s	f_l	A_l^c	A_l^s
0.000000000	4.225150901E−10	0.000000000E+00	0.915699384	2.845494144E−05	−2.074365743E−05
0.625524313	2.801784640E−06	3.739727121E−06	0.831393603	3.316734961E−06	7.958528060E−07
0.966048547	2.469412922E−06	−1.932203627E−06	3.152095758	−9.598414660E−07	4.952597435E−07
1.915692038	7.291510422E−07	−4.893071306E−07	7.304188603	9.265802489E−08	−4.297107940E−07
0.932139308	1.387727491E−07	−3.188639342E−07	0.084291268	−2.301767205E−07	−1.811220540E−07
0.747084482	1.275307764E−07	2.475656242E−07	11.456281204	9.378304404E−08	1.183956462E−07
0.468316451	8.984488525E−09	1.380324618E−07	0.988502943	−5.504759840E−08	−1.107963544E−07
0.374472282	7.393616331E−08	−9.015581535E−08	1.831385168	8.165982575E−08	2.384525641E−08
1.966039432	6.334215321E−08	−4.582494230E−08	2.251039912	−4.525712017E−08	4.283826928E−08

Table C.42: Fourier analysis of the c_2 function in the Sun–Earth+Moon case.

f_l	A_l^c	A_l^s	f_l	A_l^c	A_l^s
0.000000000	2.955847148E−11	0.000000000E+00	0.915699383	−2.074376729E−05	−2.845501663E−05
0.625524249	−3.739545312E−06	2.802185883E−06	0.831393555	7.956489284E−07	−3.316800066E−06
0.966048547	−1.932199092E−06	−2.469410696E−06	3.152095724	−4.953124633E−07	−9.598311530E−07
1.915691993	−4.893491386E−07	−7.291338967E−07	7.304188615	4.297116082E−07	9.266253341E−08
0.932139346	−3.189012713E−07	−1.387768461E−07	0.084291306	1.810620381E−07	−2.301526011E−07
0.747084256	2.474881326E−07	−1.275970296E−07	11.456281260	−1.184089670E−07	9.378984855E−08
0.468316438	1.380266847E−07	−8.985791564E−09	0.988505599	−1.109132238E−07	5.460008776E−08
0.374472125	−9.005426163E−08	−7.385703339E−08	1.831386016	2.393241772E−08	−8.163107147E−08
1.966039414	−4.583735076E−08	−6.334197731E−08	2.251039310	−4.287303005E−08	−4.522145937E−08

Table C.43: Fourier analysis of the c_3 function in the Sun–Earth+Moon case.

f_l	A_l^c	A_l^s	f_l	A_l^c	A_l^s
0.000000000	−1.826440976E−10	0.000000000E+00	0.084318306	4.703667682E−07	−6.424641081E−07
1.625539568	1.349085365E−07	−2.420960039E−07	4.152103415	1.299001181E−07	2.307561571E−08
0.033970453	1.058498988E−07	−8.522817395E−08	0.168614689	−1.853842489E−08	−7.476615864E−08
8.304193949	−4.085168143E−08	3.490005769E−08	12.456294040	−1.842794902E−10	−1.847969428E−08
0.067916199	1.480656445E−08	−2.086408227E−09	1.084309513	4.112977314E−09	−5.195641107E−09
0.915690688	3.611673289E−09	5.554954738E−09	0.252923067	−5.617211903E−09	−2.821536897E−09
16.608382332	4.706305151E−09	3.763768220E−09	0.531698420	−3.016309561E−09	3.311637561E−09
3.251065484	3.414938193E−09	1.457247283E−09	2.625526132	1.188094369E−09	−1.973094664E−09
0.625545877	1.040257148E−09	−2.058393358E−09	20.760472072	−1.668481149E−09	3.570273751E−10
0.101574336	1.475049895E−09	4.466101363E−10			

Table C.44: Fourier analysis of the c_4 function in the Sun–Earth+Moon case.

f_l	A_l^c	A_l^s	f_l	A_l^c	A_l^s
0.000000000	1.339875562E−09	0.000000000E+00	0.999992620	1.302693420E−03	−3.334664047E−02
1.999985644	6.530634591E−05	−8.327257692E−04	1.251039976	−3.784040129E−05	−1.090341887E−05
1.831343522	−3.255969095E−05	−9.806791300E−06	0.914730917	2.348110593E−05	1.613777371E−05
2.999974096	2.275490035E−06	−1.958404433E−05	1.876597541	−2.951502515E−06	−8.816919960E−06

Table C.45: Fourier analysis of the c_5 function in the Sun–Earth+Moon case.

f_l	A_l^c	A_l^s	f_l	A_l^c	A_l^s
0.000000000	2.000002943E+00	0.000000000E+00	0.999992617	6.669842066E−02	2.605734175E−03
1.999985638	1.388012106E−03	1.088116882E−04	1.251039984	1.852301504E−05	−6.434171710E−05
0.914752035	−3.506788191E−05	5.021465252E−05	1.831346638	1.401276927E−05	−4.650320862E−05
2.999975415	2.996570588E−05	3.495765898E−06	0.625523538	1.754000008E−05	2.346654862E−05

Table C.46: Fourier analysis of the c_6 function in the Sun–Earth+Moon case.

f_l	A_l^c	A_l^s	f_l	A_l^c	A_l^s
0.000000000	2.234751919E−08	0.000000000E+00	1.000013170	−3.948751317E−07	−1.392103129E−06
2.251061608	8.998109308E−07	−1.234264382E−07	0.374487295	−7.328260664E−07	−1.648906121E−07
2.876583617	5.389756198E−07	5.338649738E−07	0.251026995	−4.604528488E−07	−3.823749627E−07
3.502118950	−9.340989695E−08	5.981365702E−07	4.127634149	−4.197135105E−07	2.265826231E−07
1.625525694	2.256564674E−07	−4.131392892E−07	0.831395704	4.692444650E−07	1.562418898E−07
0.876462372	−8.264525422E−09	−4.866374513E−07	1.502093224	3.069686548E−07	−1.977196682E−07
4.753164660	−3.360047067E−07	−1.562231692E−07	2.127612982	2.617706049E−07	9.581812962E−08
5.378682060	−5.948860936E−08	−2.783296044E−07	4.152107870	−2.357042344E−07	−4.282190795E−08
6.004206995	1.427616081E−07	−1.635095808E−07	2.753104336	6.536357151E−08	2.030244654E−07
6.629732978	1.640732551E−07	1.248570511E−08	3.378671408	−9.655065413E−08	1.270996613E−07
0.747674549	2.741352668E−09	1.366384226E−07	0.084322469	8.453132459E−08	−1.145117517E−07
4.004208676	−1.195135959E−07	−2.182566486E−09	7.255254892	6.675856454E−08	1.045552528E−07
1.746201467	5.679484243E−08	−9.616479327E−08	1.915709936	−7.027875952E−08	−9.556834017E−08
8.304195888	8.134356138E−08	−6.930373217E−08	7.880776260	−3.259813336E−08	8.728985900E−08
4.629722545	−5.260075405E−08	−7.188270197E−08	8.506297857	−6.685836136E−08	1.977158536E−08
5.255260846	2.037551888E−08	−6.285876487E−08	1.876178156	3.147879340E−08	4.035369681E−08
2.502125530	−2.192461090E−08	4.548177706E−08	0.932946898	4.124128115E−08	2.745543650E−08
5.880801726	4.648813547E−08	−1.508625919E−08	1.374315655	−5.139577198E−08	1.488008645E−09
9.131822350	−4.169802219E−08	−3.108789061E−08	3.127634139	−4.866781258E−08	1.110282497E−08
3.753468029	−2.760559704E−08	−3.580811383E−08	1.999874830	−3.202758641E−08	−3.169258619E−08
0.122686826	3.614373799E−08	2.513347169E−08	2.625336194	8.531964019E−09	−4.320325684E−08
4.378679977	1.403870429E−09	−4.178233554E−08	0.502409909	4.085393952E−08	−1.013468731E−08
1.127977741	3.084628030E−08	2.689538183E−08	1.084419427	−3.001751285E−08	−2.376578023E−08
9.757347269	−4.690426971E−11	−3.870968155E−08	12.456288268	5.355065579E−10	3.674289816E−08
1.251114630	3.635328289E−08	1.145311483E−08	6.506310080	2.960587183E−08	2.051748695E−08
5.004200227	2.968601455E−08	−2.124934071E−08	5.629683839	3.014012818E−08	8.274843065E−09
1.662889566	2.236736849E−08	1.824088271E−08	10.382868088	2.293253748E−08	−1.730995797E−08
0.915706975	2.226754060E−08	−1.677009357E−08	0.063398950	1.978950420E−08	2.260652081E−08
0.168604112	−2.152563376E−08	−1.564821408E−08	6.255253986	8.834567956E−09	2.464509504E−08
2.662813477	1.601367587E−08	−2.111050017E−08	2.831425551	−2.501945239E−08	−8.527034861E−09
7.131846884	5.421187883E−10	2.644980677E−08	0.531697177	−1.802721007E−08	1.870509508E−08
0.625666239	2.210603340E−08	−1.074108320E−08	2.379388254	−2.274722862E−08	7.901942442E−09
0.404939283	1.902200920E−08	1.424871824E−08	25.791296487	−1.344794040E−08	1.730710501E−08
1.468336740	1.325049234E−08	−1.844684928E−08	6.880765500	−1.165699336E−08	1.822659085E−08
1.053944068	2.753708065E−09	−2.130406183E−08	11.008393743	2.043980930E−08	5.934105413E−09
3.250814601	1.711798079E−08	−1.272831138E−08	7.757388911	−1.550088324E−08	1.166368464E−08
3.005468484	−9.344056872E−09	−1.669919374E−08	3.876480378	1.423318917E−08	1.073340441E−08

Table C.47: Fourier analysis of the c_7 function in the Sun–Earth+Moon case.

f_l	A_l^c	A_l^s	f_l	A_l^c	A_l^s
0.000000000	1.000420821E+00	0.000000000E+00	0.999992615	5.004157957E−02	1.955082517E−03
1.999985620	1.249649676E−03	9.792092308E−05	0.914759532	−2.774407741E−05	3.945963233E−05
1.251039994	1.165852022E−05	−4.060352316E−05	2.999980105	3.059039865E−05	3.623850013E−06
0.625522693	1.628317525E−05	2.177538916E−05	1.831330067	4.896856255E−06	−1.699758943E−05

Table C.48: Fourier analysis of the c_8 function in the Sun–Earth+Moon case.

f_l	A_l^c	A_l^s	f_l	A_l^c	A_l^s
0.000000000	5.928013255E−10	0.000000000E+00	1.831385878	−9.829368623E−06	−2.927946576E−06
1.251048276	−2.458174278E−06	−7.182931795E−07	2.747073502	−2.298066612E−06	8.554502528E−07
0.625524111	1.902199740E−06	−1.426554293E−06	1.876585360	−7.510223822E−07	−2.220761188E−06
2.502096477	1.074925944E−06	−1.681159207E−06	1.747087424	−5.694877626E−07	−1.701026206E−06
3.127620586	1.625590706E−06	−1.209310356E−07	3.753144663	8.541882659E−07	9.790094754E−07
3.152087032	4.747909113E−07	9.045023645E−07	4.378668834	−2.127926577E−07	9.960117510E−07
5.004192968	−7.162276122E−07	3.305927255E−07	2.662774794	−4.975108726E−07	−3.452968753E−07
5.629717072	−5.326478419E−07	−2.878038727E−07	3.662771478	−3.155260317E−07	4.393152388E−07
0.915693464	−3.062500306E−07	−3.984785296E−07	1.932124771	−4.693430882E−07	−1.389273553E−07
6.255241231	−6.775975535E−08	−4.563499912E−07	7.304186416	−4.248178658E−07	−8.919834551E−08
2.831366462	−2.862856063E−07	−2.150262658E−07	6.880765366	2.459721848E−07	−2.483504375E−07
0.831396886	3.491747648E−07	1.535699610E−08	7.506289444	2.610554464E−07	3.616474159E−08
1.915684978	2.029180245E−07	−1.409356473E−07	1.662764154	1.182438338E−07	−1.769342592E−07
8.131813628	9.574995572E−08	1.732718587E−07	1.502110732	1.301824507E−07	−1.387091398E−07

Table C.48: (continued)

f_l	A_l^c	A_l^s	f_l	A_l^c	A_l^s
2.127632571	1.855332500E−07	1.816687576E−08	0.876636579	−1.015497408E−08	−1.772137961E−07
2.753155107	9.120146673E−08	1.471668431E−07	3.578479518	−1.747200889E−07	−4.311599006E−10
0.936633573	2.206922542E−08	1.679256430E−07	3.378683473	−5.752313925E−08	1.438659589E−07
8.757337757	−6.084723462E−08	1.351121532E−07	11.456281224	1.176772501E−07	−9.320769922E−08
0.251054493	−1.272113568E−07	−6.786778332E−08	4.004205801	−1.299909011E−07	3.594649055E−08
1.404949660	−1.328874097E−07	2.565288375E−08	24.737528377	6.573721686E−08	−1.019183134E−07
4.629727348	−9.158718881E−08	−6.953476598E−08	9.382861853	−1.079260697E−07	2.408335038E−08
4.578465821	−1.595843202E−09	1.150770218E−07	3.747189974	−8.602701793E−08	−4.538252373E−08

Table C.49: Fourier analysis of the c_9 function in the Sun–Earth+Moon case.

f_l	A_l^c	A_l^s	f_l	A_l^c	A_l^s
0.000000000	−7.246560761E−09	0.000000000E+00	1.000013114	1.974426024E−07	6.960620886E−07
2.251061628	−4.502807278E−07	6.177382233E−08	0.374487215	3.666475348E−07	8.224893170E−08
2.876583227	−2.698084219E−07	−2.672660944E−07	0.251032166	2.298590045E−07	1.927473473E−07
3.502118994	4.687165472E−08	−2.994903862E−07	4.127634078	2.102602881E−07	−1.134148119E−07
1.625525733	−1.129969998E−07	2.069849193E−07	0.831395713	−2.344646624E−07	−7.814520945E−08
0.876464233	3.357400752E−09	2.431952397E−07	1.502094056	−1.537242458E−07	9.840156357E−08
4.753165089	1.682748784E−07	7.839533318E−08	2.127613577	−1.306939659E−07	−4.827737193E−08
5.378682232	2.970142320E−08	1.395095487E−07	4.152107752	1.179234309E−07	2.139515339E−08
6.004206857	−7.161630085E−08	8.191749827E−08	2.753128143	−3.031912829E−08	−1.016718145E−07
6.629732961	−8.226430120E−08	−6.329127392E−09	3.378673911	4.855100561E−08	−6.320066305E−08
0.747765044	2.475965612E−09	−7.313612000E−08	0.084322441	−4.214831095E−08	5.724396117E−08
4.004213281	5.964090788E−08	1.531233123E−09	7.255254901	−3.343256678E−08	−5.247364375E−08
1.746086220	−2.476973434E−08	4.944636886E−08	1.915709863	3.493786468E−08	4.788691095E−08
8.304195964	−4.057011836E−08	3.461291014E−08	7.880776059	1.639668740E−08	−4.377829874E−08
4.629726490	2.597921315E−08	3.604494534E−08	8.506297447	3.356120856E−08	−9.893113927E−09
1.999924628	1.886844197E−08	2.798429195E−08	5.255267510	−1.047252016E−08	3.123316718E−08
1.374346399	3.181602541E−08	1.003824960E−09	1.876220438	−2.013193510E−08	−1.943334309E−08
2.502129486	8.945892424E−09	−2.626131111E−08	0.122817145	−1.839232086E−08	−1.787648297E−08
2.625366721	−6.405641859E−09	2.506195365E−08	3.127636730	2.562581462E−08	−8.474747475E−09
0.932908693	−2.077747850E−08	−1.310811103E−08	5.880812837	−2.326309193E−08	7.197635339E−09
3.753464028	1.636826029E−08	1.788555951E−08	9.131821978	2.091576201E−08	1.562619022E−08
0.502381539	−2.291824501E−08	6.924129870E−09	4.378685616	6.466384767E−10	2.218719605E−08
1.127981823	−1.712783184E−08	−1.465486656E−08	1.251119186	−2.218188740E−08	−1.167112182E−09
9.757346630	6.168128352E−12	1.943907386E−08	1.084420877	1.416975503E−08	1.274995527E−08
12.456288583	−2.697285880E−10	−1.835610179E−08	5.004201444	−1.497144216E−08	1.209304481E−08
6.506318560	−1.461972532E−08	−1.039033812E−08	3.250926415	−1.649317961E−08	6.973220969E−09
5.629685703	−1.600675218E−08	−3.541701389E−09	3.876518929	−1.144225160E−08	−1.003229729E−08
1.662875647	−1.135663659E−08	−8.914669460E−09	10.382866693	−1.152314445E−08	8.683713896E−09
0.915705162	−1.113444075E−08	8.169048464E−09	0.063410647	−9.616705812E−09	−1.129720638E−08
6.255255593	−5.187743399E−09	−1.265630746E−08	2.379356990	1.219442932E−08	−5.092389609E−09
2.662810727	−8.169134333E−09	1.043026074E−08	2.831425602	1.240702184E−08	4.330182373E−09
7.131859363	−5.405049159E−11	−1.316139418E−08	0.531697391	8.914843769E−09	−9.254568843E−09
0.168608152	6.791550990E−09	8.955398598E−09	0.404936729	−9.376656939E−09	−7.052508564E−09
25.791295171	6.717802548E−09	−8.654156957E−09	6.880765127	5.669144298E−09	−9.734590852E−09
4.502002944	1.017373291E−09	−1.064318120E−08	0.625711416	−7.155505462E−09	8.129741949E−09
1.468336268	−6.604713906E−09	9.126527056E−09	3.005428666	5.608142487E−09	8.762032464E−09
1.053953578	−1.506514544E−09	1.064150158E−08	11.008392504	−1.026793798E−08	−2.989557633E−09

Table C.50: Fourier analysis of the c_{10} function in the Sun–Earth+Moon case.

f_l	A_l^c	A_l^s	f_l	A_l^c	A_l^s
0.000000000	1.000420821E+00	0.000000000E+00	0.999992615	5.004157957E−02	1.955082517E−03
1.999985620	1.249649675E−03	9.792092346E−05	0.914759532	−2.774407729E−05	3.945963225E−05
1.251039994	1.165851986E−05	−4.060352189E−05	2.999980105	3.059039849E−05	3.623849847E−06
0.625522693	1.628317601E−05	2.177539024E−05	1.831330067	4.896856247E−06	−1.699758964E−05

Table C.51: Fourier analysis of the c_{11} function in the Sun–Earth+Moon case.

f_l	A_l^c	A_l^s	f_l	A_l^c	A_l^s
0.000000000	−1.143013482E−08	0.000000000E+00	3.502121722	1.046804228E−06	1.642646845E−07

Table C.51: (continued)

f_l	A_l^c	A_l^s	f_l	A_l^c	A_l^s
2.251060706	−1.394929757E−07	−1.012526489E−06	2.876560187	7.553604017E−07	−7.812777269E−07
4.127632929	4.681819573E−07	8.653893133E−07	4.753174253	−3.749335811E−07	7.937179428E−07
5.378678580	−7.476598163E−07	1.617083157E−07	1.000012690	−6.968157425E−07	1.982052525E−07
6.004204177	−4.914130142E−07	−4.273152613E−07	6.629733774	4.133842616E−08	−5.432361749E−07
4.152108276	−8.900804050E−08	4.891944213E−07	7.255251372	3.783425842E−07	−2.430436681E−07
8.304195038	−2.883075912E−07	−3.381403570E−07	25.791293164	3.035001074E−07	2.347939988E−07
1.625513029	−3.377843556E−07	−1.814873133E−07	7.880776025	3.435212991E−07	1.281861636E−07
8.506300414	8.334929328E−08	2.840022338E−07	2.753074122	2.772598834E−07	−9.511987838E−08
2.127617657	1.029072417E−07	−2.771493024E−07	1.502079396	−1.498689697E−07	−2.288128367E−07
3.378668146	2.144784105E−07	1.624063941E−07	9.131824332	−1.418812907E−07	1.897006811E−07
12.456292408	2.287998933E−07	−2.760155111E−09	4.004202331	−3.216780951E−09	2.385482003E−07
37.205571373	−1.860730727E−07	1.065532303E−07	0.831396174	6.459664939E−08	−1.955045883E−07
4.629811460	−1.721217522E−07	1.112539817E−07	0.876507200	−2.112214071E−07	−3.253350275E−09
9.757347744	−1.878371002E−07	1.839135044E−10	5.255245879	−1.651819174E−07	−5.201784308E−08
10.382864223	−8.950117114E−08	−1.181219350E−07	0.374486992	−3.109609393E−08	1.378504202E−07
5.880809940	−4.372817089E−08	−1.363710162E−07	31.280100029	−1.404783603E−07	3.793175831E−08
48.619848680	−1.666378310E−08	−1.299423438E−07	6.506314950	6.718906909E−08	−9.568838172E−08
19.865824767	6.897429294E−08	8.978239066E−08	11.008393463	3.240637545E−08	−1.115395090E−07
1.915713051	−9.165362050E−08	6.719228237E−08	14.377177528	4.003183205E−08	−9.998348989E−08
1.747514011	−2.243992990E−08	−1.031924875E−07	42.694384921	1.325374243E−08	−9.935459772E−08
2.962719074	−9.995050936E−08	1.301283358E−08	8.451640697	5.816830574E−08	−8.511930153E−08
5.004200687	−5.449222326E−08	−7.662232021E−08	4.378654929	−9.504540338E−08	−1.766280953E−09
11.633917819	8.466852313E−08	−3.187733883E−08	7.131850052	9.410879730E−08	−1.669711793E−09
3.753344856	−6.482332966E−08	5.992601369E−08	60.034121002	8.449278917E−08	2.257599891E−08
5.629696758	2.458929038E−08	−8.620292133E−08	16.608381794	−5.250474735E−08	6.569542215E−08
3.127632518	1.855450601E−08	8.167432850E−08	6.255241394	7.828167265E−08	−2.881243355E−08
6.880771090	6.352563160E−08	4.106404241E−08	7.757384380	4.545347862E−08	5.964146171E−08
0.251002760	−4.639241439E−08	5.734471175E−08	12.259414637	5.978731722E−08	3.641914084E−08
2.502179154	6.176887620E−08	3.267997874E−08	54.108657785	5.992143267E−08	3.450093737E−08
7.506315634	4.163738490E−09	6.701044100E−08	71.448391763	−3.773906351E−08	4.965478672E−08
8.382939583	−1.843872958E−08	5.831917997E−08	1.876381166	5.147939314E−08	−3.005672830E−08
8.131810164	−4.401881731E−08	3.914766998E−08	2.625237631	−5.089184517E−08	−4.840229678E−09
8.757344175	−4.975042330E−08	−1.032016323E−08	65.522933298	−3.927169746E−08	3.033034206E−08
12.884975591	3.772140181E−09	5.365357575E−08	20.760505683	−8.792865377E−09	−4.644062728E−08
0.747498308	4.607674679E−08	−7.839189629E−09	82.862680370	−2.332721527E−08	−4.050299275E−08
9.008414588	−4.343072097E−08	1.644971575E−08	7.304187567	1.453837970E−08	4.236241374E−08
13.510739492	−3.481817763E−08	2.218411669E−08	9.382858041	−1.870775238E−08	−3.887606697E−08
2.831452883	−1.240415720E−08	3.556935614E−08	10.008365320	1.642244163E−08	−3.254319575E−08
9.633950864	−3.018412744E−08	−1.974645530E−08	94.276954803	3.605374934E−08	−4.763555290E−09
1.251082977	9.022469145E−09	−3.402319330E−08	33.729766063	−1.520286148E−08	3.081265109E−08
1.999588313	−1.365561518E−08	3.155169095E−08	76.937209989	−9.724768144E−09	−3.568708796E−08
26.467597137	2.385225716E−08	−2.493824868E−08	2.662821759	−2.801319960E−08	−2.129222412E−08
39.436935473	−3.217203274E−08	3.658821546E−09	3.631432385	−2.794796334E−08	−1.668634714E−08
14.136004939	−3.109803259E−08	−6.492856884E−09	23.341585779	2.681110755E−09	3.004065751E−08
2.380006436	−2.702183532E−09	2.931975051E−08	10.633899506	3.001200003E−08	−5.182476221E−09
105.691225871	−7.385547605E−09	2.818360400E−08	88.351486774	2.823726011E−08	3.576266355E−09
28.022643818	1.501044771E−08	2.663022679E−08	45.144073713	−1.881033948E−08	−2.223594792E−08
3.005226189	−2.255333357E−08	1.756306607E−08	29.048708226	−2.118985522E−08	1.741458571E−08
3.876216487	1.064953194E−08	−2.503081826E−08	10.259487496	−1.309483511E−09	−2.786129132E−08
1.374031067	7.691762048E−09	2.762316867E−08	3.250678906	−2.164630402E−08	−1.706736787E−08
1.127977042	1.612327908E−08	−1.926085970E−08	30.603988711	−6.483883960E−09	−2.510386970E−08
10.456291023	−1.756012939E−08	−1.788449583E−08	42.018070994	2.486465926E−08	5.442478896E−10
36.311001091	1.597547313E−08	−2.101152839E−08	50.851193379	6.822449234E−09	−2.493644357E−08
11.259416029	1.839015216E−08	1.707669233E−08	14.761473489	−1.189835192E−08	−2.255151838E−08
1.662653965	1.180131196E−08	−2.089728632E−08			

Table C.52: Fourier analysis of the c_{12} function in the Sun–Earth+Moon case.

f_l	A_l^c	A_l^s	f_l	A_l^c	A_l^s
0.000000000	−1.392996292E−04	0.000000000E+00	0.999992623	−1.668016536E−02	−6.515654284E−04
1.999985650	−6.940978784E−04	−5.444162504E−05	1.831345589	−9.009397147E−06	2.977202207E−05
1.251039872	−6.827843485E−06	2.369082184E−05	2.999972350	−2.245748083E−05	−2.594375582E−06
0.914705134	7.291706252E−06	−1.081655543E−05	1.876596754	−8.309243705E−06	2.770513990E−06
2.502118370	−4.533234277E−06	−2.957272167E−06			

Table C.53: Fourier analysis of the c_{13} function in the Sun–Earth+Moon case.

f_l	A_l^c	A_l^s	f_l	A_l^c	A_l^s
0.000000000	1.000420082E+00	0.000000000E+00	0.999992616	5.004134039E−02	1.955026993E−03
1.999985626	1.249606727E−03	9.796646876E−05	1.251040100	1.301854822E−05	−4.528356026E−05
0.914744598	−2.667949264E−05	3.838297436E−05	2.999977291	3.056573501E−05	3.589237519E−06
1.831339554	7.986070341E−06	−2.696503381E−05	0.625524273	9.735437991E−06	1.304398161E−05

C.5 Solar System bodies, Sun–Earth+Moon case

In tables C.54 to C.75 we give the results of the Fourier analysis of the positions of the Solar System bodies in adimensional coordinates for the Sun–Earth+Moon case. We do not give adjustments of the frequencies as linear combinations of basic ones because they have not been used in any model. In order to save space, every row of these tables correspond to two entries, which are separated by a double vertical line.

Table C.54: Fourier analysis of the x coordinate of Mercury in the Sun–Earth+Moon case.

f_l	A_l^c	A_l^s	f_l	A_l^c	A_l^s
0.0000000000	−8.9213994854E−04	0.0000000000E+00	3.1520957062	3.3536270344E−01	−1.7306563999E−01
0.9999971877	1.0933638795E−01	−4.7376269997E−02	7.3041883820	−8.0858953382E−03	3.7532464072E−02
2.1521035278	8.2147521073E−03	−4.6502995741E−03	11.4562813322	−3.6378348284E−03	−4.5928630808E−03
1.9999926055	2.7806868666E−03	−1.0732967451E−03	4.1520864543	−2.8460253810E−03	1.3598794372E−03
5.1520958800	−3.8449355682E−04	−3.0224720241E−03	15.6083737903	1.0595072517E−03	1.9751945381E−05
6.3041923201	−1.6368409767E−04	9.4619871332E−04	8.3041823766	7.7925614509E−05	−3.1093954057E−04
9.3041944975	2.2308657496E−04	1.0870486046E−04	1.1521134279	1.8952309202E−04	−1.1729258560E−04
19.7604670285	−1.3685154465E−04	1.6003022988E−04	10.4562886635	−9.5386530118E−05	−1.1120742820E−04
6.1520850568	−6.6253088533E−06	−7.6001121507E−05	2.9999893860	6.6688904196E−05	−2.3338789447E−05
12.4562716391	2.9087578267E−05	3.9287211344E−05	23.9125592732	−7.7285115551E−06	−4.3743534945E−05
13.4562843045	−2.9124722405E−05	1.6301356095E−05	14.6083845984	2.6489165565E−05	−5.0550317242E−07
5.3041985620	−3.2424443228E−06	2.2640677613E−05	1.9018846483	3.4714843944E−06	9.5589722638E−06
2.2356767644	−9.3746798206E−06	1.6396917826E−06	28.0646528032	8.5053580917E−06	4.8033370560E−06
16.6083673900	−8.8265244377E−06	−4.6790588554E−07	3.3280044049	2.2760102901E−06	6.2565252970E−06

Table C.55: Fourier analysis of the y coordinate of Mercury in the Sun–Earth+Moon case.

f_l	A_l^c	A_l^s	f_l	A_l^c	A_l^s
0.0000000000	4.3242735169E−04	0.0000000000E+00	3.1520957062	1.7306604679E−01	3.3536304778E−01
0.9999971870	−4.7371960260E−02	−1.0934268244E−01	7.3041883820	−3.7532457696E−02	−8.0858790031E−03
2.1521035277	4.6503074193E−03	8.2144267122E−03	11.4562813322	4.5928603367E−03	−3.6378347785E−03
1.9999925864	−1.0734234755E−03	−2.7808723603E−03	4.1520866526	−1.3095097228E−03	−2.8546976764E−03
5.1520958555	−3.0326745083E−03	3.6024138787E−04	15.6083737899	−1.9751780313E−05	1.0595067111E−03
6.3041923199	−9.4625047888E−04	−1.6372048129E−04	8.3041823656	3.0928428427E−04	8.1725825102E−05
9.3041946118	1.1130040188E−04	−2.2231479459E−04	1.1521133280	1.1693599525E−04	1.9003595607E−04
19.7604670282	−1.6003023763E−04	−1.3685138563E−04	10.4562886636	1.1121127116E−04	−9.5387791447E−05
6.1520832553	−7.6063441102E−05	6.4062304645E−06	2.9999817217	−2.2161508027E−05	−6.6594916164E−05
12.4562718656	−3.9582595744E−05	2.8609318234E−05	23.9125592722	4.3743509125E−05	−7.7284916842E−06
13.4562841835	1.5963127479E−05	2.9357568535E−05	14.6083845988	5.0538439942E−07	2.6489626048E−05
5.3041993072	−2.2615682870E−05	−3.1922022133E−06	28.0646528031	−4.8033366846E−06	8.5053493703E−06
2.2354122011	−2.8950335877E−06	−8.7601629794E−06	16.6083674153	5.6077282130E−07	−8.8191281454E−06
3.3280091428	−6.2618522457E−06	2.2513318832E−06			

Table C.56: Fourier analysis of the z coordinate of Mercury in the Sun–Earth+Moon case.

f_l	A_l^c	A_l^s	f_l	A_l^c	A_l^s
0.0000000000	−7.1284256366E−03	0.0000000000E+00	4.1521029390	−4.5375386291E−02	−8.0468375405E−03
8.3041960978	3.5740966125E−03	−3.0407711838E−03	12.4562881950	1.1277255805E−05	7.1633318469E−04
5.1520971896	−3.7566142288E−04	−8.2107074983E−05	3.1521117318	−3.8092396415E−04	−5.2508377223E−05
16.6083815616	−1.0130121359E−04	−8.0850321393E−05	0.9999919737	−1.1884611931E−04	−4.6014269722E−06
7.3042028232	2.8782796883E−05	−2.6519278457E−05	9.3041873191	3.0778827940E−05	−2.4203385977E−05

Table C.56: (continued)

f_l	A_l^c	A_l^s	f_l	A_l^c	A_l^s
20.7604732790	2.5199605453E−05	−5.3338159552E−06	6.1520914874	−6.2026988948E−06	−1.6222237034E−06
2.1521213003	−6.3754123216E−06	−7.4946492867E−07	13.4562833576	−1.4421398642E−07	5.9766072107E−06
11.4562977902	3.2551361432E−07	5.9636578851E−06	24.9125669393	−2.5125034108E−06	4.8189207186E−06
1.9999900793	−2.0135450374E−06	−1.5257516083E−07			

Table C.57: Fourier analysis of the x coordinate of Venus in the Sun–Earth+Moon case.

f_l	A_l^c	A_l^s	f_l	A_l^c	A_l^s
0.0000000000	−7.1483976149E−05	0.0000000000E+00	0.6255241203	−4.3334839804E−01	−5.7810339210E−01
0.3744703524	−1.1414093829E−02	1.4040400539E−02	1.0000080520	6.2713308682E−03	3.7581770797E−03
1.6255151622	3.4328320894E−03	4.9617862643E−03	2.2510466731	1.7856312465E−03	−1.6593752648E−03
2.6255548088	−6.1711310663E−04	−3.8523496561E−05	1.3744645033	−2.8235188900E−04	3.2077327503E−04
2.0000047086	1.5305399373E−04	1.0017991998E−04	1.2510576086	3.3228257866E−05	−1.0026330315E−05
3.2510380752	−1.5433114635E−05	1.3289813160E−05	0.2890331269	−6.3361365254E−06	−1.5863949367E−05
3.6255594735	−1.5475683941E−05	−1.9441600858E−06	3.8765723340	9.2826675027E−06	8.1401333328E−06
1.8766021105	−1.0503273935E−05	3.8460284029E−06	2.3743718798	−6.4527823688E−06	8.1236394810E−06

Table C.58: Fourier analysis of the y coordinate of Venus in the Sun–Earth+Moon case.

f_l	A_l^c	A_l^s	f_l	A_l^c	A_l^s
0.0000000000	−2.9070508697E−05	0.0000000000E+00	0.6255241204	5.7808268818E−01	−4.3333312026E−01
0.3744703181	1.4019981419E−02	1.1403628987E−02	1.0000081878	3.7577817773E−03	−6.2710864401E−03
1.6255151261	−4.9610904114E−03	3.4222710164E−03	2.2510466204	1.6603090450E−03	1.7857928196E−03
2.6255543063	−8.1346667894E−05	6.4348936709E−04	1.3744660648	3.2050176151E−04	2.8286035493E−04
2.0000037182	1.0031511046E−04	−1.5315558858E−04	1.2510513575	5.1178494885E−05	4.5372825711E−05
3.2510390476	−1.3240329464E−05	−1.5430317866E−05	0.2890042772	−1.5977457055E−05	5.5454182179E−06
3.6255379221	−2.2947869424E−06	1.5934808905E−05	0.8765902777	−2.4579339555E−06	−1.2688937723E−05
3.8765721234	−8.0922656122E−06	9.3065116595E−06	2.3743873285	7.4076745540E−06	6.4712804726E−06
0.9154119593	5.1114829446E−06	5.8381711910E−06			

Table C.59: Fourier analysis of the z coordinate of Venus in the Sun–Earth+Moon case.

f_l	A_l^c	A_l^s	f_l	A_l^c	A_l^s
0.0000000000	−3.5576845382E−04	0.0000000000E+00	1.6255398595	−2.0847803029E−02	3.7421166120E−02
2.6255283771	−1.8564463324E−04	3.0537137803E−04	0.6255498595	−1.6191278499E−04	3.1866310282E−04
3.2510561739	−1.3310850369E−04	−5.6399261315E−05	0.9999923837	−5.9073190813E−06	−1.7574281075E−07
3.6255149936	−3.2826093406E−06	4.9768521450E−06	0.3744397546	−1.7131807567E−06	−5.2696346637E−06

Table C.60: Fourier analysis of the x coordinate of Mars in the Sun–Earth+Moon case.

f_l	A_l^c	A_l^s	f_l	A_l^c	A_l^s
0.0000000000	1.0432834709E−03	0.0000000000E+00	0.4683164653	−9.8419453476E−02	−1.5130181004E+00
0.9999897985	−1.2129132000E−01	−1.7573755517E−01	0.0633553980	−3.2366633177E−02	−6.2901250820E−02
1.4683080969	−1.0131285483E−03	−3.7893570973E−02	0.5316792701	1.3912834119E−03	−1.2612143186E−02
1.9999812965	−2.8610797057E−03	−4.5065900499E−03	0.5950241825	4.2319221586E−03	2.6120091976E−03
0.9366316807	−9.0972506390E−04	1.5434789051E−03	1.5316539842	−1.1262390159E−03	−8.1215586074E−04
2.4683017740	1.1876292846E−05	−8.9487512271E−04	1.0633569180	2.4440087925E−04	5.3467134969E−04
1.1267048532	−4.0931867015E−04	−8.1846579845E−06	0.4049892842	1.4995338315E−04	−2.4456797650E−05
0.9157137801	−1.1106346324E−04	7.3542356800E−05	2.9999748108	−6.3244409267E−05	−1.0902138915E−04
0.8314205447	6.1672358352E−05	9.5196184594E−05	1.3631083741	−7.9253937230E−05	−3.2907075338E−05
0.0213169010	−4.1965726522E−05	−3.4247536688E−05			

Table C.61: Fourier analysis of the y coordinate of Mars in the Sun–Earth+Moon case.

f_l	A_l^c	A_l^s	f_l	A_l^c	A_l^s
0.0000000000	1.4292762266E−03	0.0000000000E+00	0.4683164657	−1.5130068292E+00	9.8418744589E−02
0.9999897969	−1.7572645067E−01	1.2130139997E−01	0.0633554292	6.2872270879E−02	−3.2346064066E−02
1.4683081009	−3.7893449022E−02	1.0131849710E−03	0.5316798228	1.2531893722E−02	1.2970464722E−03

Table C.61: (continued)

f_l	A_l^c	A_l^s	f_l	A_l^c	A_l^s
1.9999812947	−4.5064762566E−03	2.8611881473E−03	0.5950300054	−2.6095261748E−03	4.1763867954E−03
0.9366309954	1.5437642022E−03	9.0871057513E−04	1.5316528078	−7.0689944825E−04	1.1407722787E−03
2.4683017882	−8.9488297200E−04	−1.1889675641E−05	1.0633466863	−5.3560386756E−04	2.5087846000E−04
1.1266922215	4.3307908473E−06	−4.1126203068E−04	0.4048979301	−2.8666129744E−05	−1.4631234519E−04
0.9157134137	7.3542450804E−05	1.1106948421E−04	2.9999748034	−1.0901816185E−04	6.3246899648E−05
0.8314204656	9.5863580214E−05	−6.2188214173E−05	1.3631098804	−3.0708871283E−05	7.3706057924E−05
0.0207686857	−1.8125561495E−05	4.9068202470E−05			

Table C.62: Fourier analysis of the z coordinate of Mars in the Sun–Earth+Moon case.

f_l	A_l^c	A_l^s	f_l	A_l^c	A_l^s
0.0000000000	6.5908716055E−03	0.0000000000E+00	0.5317017630	3.3166551046E−02	−3.6075756598E−02
1.0633751187	−4.6229625299E−04	2.2367950125E−03	0.4682755789	2.6602303212E−04	3.0981243756E−04
1.5317008929	2.8860809867E−04	−2.8939178434E−04	1.5950494070	−5.2567666640E−05	−1.5080264115E−04
0.9998500566	1.1087567545E−04	8.3875855024E−08	0.0652148392	−1.2675058142E−05	1.6866761410E−05
2.0633621149	−4.5353108161E−06	1.8493075223E−05	2.1267163382	1.0181067540E−05	8.4650259896E−06
1.4679427670	4.9528494029E−06	4.8612625778E−06	2.5316781855	4.9793443253E−06	−4.6664196119E−06
0.3628083946	5.5322828714E−06	−7.4675270122E−07	0.1698819274	−3.1924640860E−06	−5.5023885850E−07

Table C.63: Fourier analysis of the x coordinate of Jupiter in the Sun–Earth+Moon case.

f_l	A_l^c	A_l^s	f_l	A_l^c	A_l^s
0.0000000000	−1.3489221730E−04	0.0000000000E+00	0.9157023655	−4.2048955297E+00	3.0503417231E+00
1.0000001162	2.6789894761E−02	−3.7625726716E−01	0.8314125174	−1.2167988493E−01	−3.0991196842E−02
1.9156876847	−1.0772243332E−01	7.2627842407E−02	0.0842900964	3.4035470995E−02	2.6784951118E−02
1.9999976726	1.0640656742E−03	−9.3720957783E−03	0.7471143257	−1.9850453042E−03	−4.0987395174E−03

Table C.64: Fourier analysis of the y coordinate of Jupiter in the Sun–Earth+Moon case.

f_l	A_l^c	A_l^s	f_l	A_l^c	A_l^s
0.0000000000	3.1410639256E−03	0.0000000000E+00	0.9156997799	3.0587826296E+00	4.1985514443E+00
1.0000034255	−3.7648770250E−01	−2.7554775131E−02	1.9156947246	7.1953589463E−02	1.0789872456E−01
0.8313969892	−2.9774129832E−02	1.2207236316E−01	0.0842964019	−2.6924585636E−02	3.3832615794E−02
1.9999950972	−9.3666741419E−03	−1.0475177237E−03	0.7470919900	−4.0715229081E−03	2.0504761011E−03
1.0163888977	−2.4718069656E−03	−2.9022800556E−03	1.8313887443	−9.8701065010E−04	2.9815793462E−03
2.9156868586	1.5960678121E−03	2.6079122462E−03	0.9321609421	1.2722064598E−03	−1.6220014031E−03
0.8993110800	1.4351192623E−03	−4.2341908298E−04	0.9824731487	1.4221968934E−03	−2.0852616443E−04
0.9660452736	8.1677279128E−04	1.0354775256E−03	0.8150103647	6.3090198178E−04	9.5330508760E−04
0.1685959595	2.0774159607E−04	1.0242838473E−03			

Table C.65: Fourier analysis of the z coordinate of Jupiter in the Sun–Earth+Moon case.

f_l	A_l^c	A_l^s	f_l	A_l^c	A_l^s
0.0000000000	8.5287815348E−03	0.0000000000E+00	0.0843069506	−6.8912932066E−02	9.5882422759E−02
0.1685652183	7.2426127589E−04	2.7572217996E−03	1.0843031226	−6.0662537266E−04	7.7630014704E−04
0.9156835691	−5.4369773302E−04	−8.2129145241E−04	1.0000175063	1.4213700133E−04	5.6969043619E−06
0.2526782846	9.5604505255E−05	3.9514135112E−05			

Table C.66: Fourier analysis of the x coordinate of Saturn in the Sun–Earth+Moon case.

f_l	A_l^c	A_l^s	f_l	A_l^c	A_l^s
0.0000000000	−6.3735794865E−03	0.0000000000E+00	0.9660402104	−7.4558350142E+00	5.9183490060E+00
1.0000006201	7.6948912665E−01	−1.1680178222E−01	0.9320939210	−9.7492282312E−02	2.3994600655E−01
1.9660322375	−1.9200656910E−01	1.4058755317E−01	0.0339558188	6.0119431815E−02	5.1866620518E−02
1.9999946073	1.9344248570E−02	−2.1228742560E−03			

Table C.67: Fourier analysis of the y coordinate of Saturn in the Sun–Earth+Moon case.

f_l	A_l^c	A_l^s	f_l	A_l^c	A_l^s
0.0000000000	1.2478600389E−03	0.0000000000E+00	0.9660402112	5.9183465052E+00	7.4558394226E+00
1.0000006188	−1.1678967625E−01	−7.6954168249E−01	0.9320602009	2.4142790774E−01	9.2406664369E−02
1.9660322375	1.4058757108E−01	1.9200658951E−01	0.0339479554	−5.1524055129E−02	6.0306419770E−02
1.9999946061	−2.1227225872E−03	−1.9344825846E−02			

Table C.68: Fourier analysis of the z coordinate of Saturn in the Sun–Earth+Moon case.

f_l	A_l^c	A_l^s	f_l	A_l^c	A_l^s
0.0000000000	1.2061024051E−02	0.0000000000E+00	0.0339744571	−3.2223219964E−01	2.5790380704E−01
0.0679376399	−1.1119845401E−02	1.6190635353E−03	1.0339656399	−2.7653555367E−03	2.0446784223E−03
0.9660135484	−2.6049680973E−03	−2.2448117482E−03	0.1019026367	−4.2444718954E−04	−1.6921085225E−04

Table C.69: Fourier analysis of the x coordinate of Uranus in the Sun–Earth+Moon case.

f_l	A_l^c	A_l^s	f_l	A_l^c	A_l^s
0.0000000000	−4.3789406363E−03	0.0000000000E+00	0.9880961770	1.5346810684E+01	1.1471763882E+01
0.9999926571	4.7536670525E−01	1.2868748759E+00	1.9880841995	3.7292784450E−01	2.9874485155E−01
0.9761963025	−4.5562678888E−01	−3.0524961877E−02	0.0118893679	−1.3052656529E−01	9.1552004562E−02
1.9999758623	1.0965989726E−02	3.2456681515E−02	0.9644570843	1.7509633077E−02	−3.8379819671E−03
2.9880793025	8.4836323167E−03	7.3963451122E−03	1.9761802800	−1.1330209707E−02	−1.0401615130E−03

Table C.70: Fourier analysis of the y coordinate of Uranus in the Sun–Earth+Moon case.

f_l	A_l^c	A_l^s	f_l	A_l^c	A_l^s
0.0000000000	−1.0531992744E−02	0.0000000000E+00	0.9880961770	1.1471763698E+01	−1.5346810509E+01
0.9999926538	1.2867864429E+00	−4.7541087424E−01	1.9880921106	3.0233354339E−01	−3.7000442201E−01
0.9761963019	−3.0524713406E−02	4.5562663647E−01	0.0118988159	−9.0019836285E−02	−1.3145532521E−01
1.9999993312	3.2667212524E−02	−1.0004084271E−02	0.9644570856	−3.8379682748E−03	−1.7509656827E−02
2.9880793025	7.3963445072E−03	−8.4836324450E−03	1.9761830841	−1.0818358939E−03	1.1329362292E−02

Table C.71: Fourier analysis of the z coordinate of Uranus in the Sun–Earth+Moon case.

f_l	A_l^c	A_l^s	f_l	A_l^c	A_l^s
0.0000000000	−1.8306444486E−02	0.0000000000E+00	0.0119300232	−2.3212176303E−01	−1.1562501171E−01
0.0238302993	3.1316749382E−03	5.3235814673E−03	0.9880626548	−1.9661792858E−03	8.8376179562E−04
1.0119227781	−1.8908521984E−03	−1.0356960450E−03	0.0350725226	−2.3035297220E−04	−2.2083042756E−04
0.9999844664	−3.0437307899E−04	−9.0819155257E−06			

Table C.72: Fourier analysis of the x coordinate of Neptune in the Sun–Earth+Moon case.

f_l	A_l^c	A_l^s	f_l	A_l^c	A_l^s
0.0000000000	−1.6625727530E−03	0.0000000000E+00	0.9939344130	2.6917903859E+01	1.3379531152E+01
1.9939293374	6.5223771538E−01	3.6278118299E−01	0.9999988293	2.2203859941E−01	−3.4286079580E−01
0.0060591114	−2.2707116839E−01	1.0141673091E−01	0.9878613482	4.5518511371E−02	−1.2832187396E−01
2.9939206357	1.4962152227E−02	9.0304187413E−03	1.9999990210	5.9241124038E−03	−8.2237011351E−03
1.0059643111	6.1863884464E−03	3.7543306470E−03			

Table C.73: Fourier analysis of the y coordinate of Neptune in the Sun–Earth+Moon case.

f_l	A_l^c	A_l^s	f_l	A_l^c	A_l^s
0.0000000000	2.9382489206E−03	0.0000000000E+00	0.9939344557	1.3382327669E+01	−2.6916381687E+01
1.9939200210	3.4661881633E−01	−6.5856104877E−01	0.9999988408	−3.4282884923E−01	−2.2206108662E−01
0.0060590961	−1.0149603236E−01	−2.2696022939E−01	0.9878612263	−1.2833691058E−01	−4.5478613411E−02
2.9939206357	9.0304189333E−03	−1.4962152323E−02	2.0000006551	−8.2004834828E−03	−5.9504708507E−03
1.0059574369	2.4868878673E−03	−7.8863518749E−03			

Table C.74: Fourier analysis of the z coordinate of Neptune in the Sun–Earth+Moon case.

f_l	A_l^c	A_l^s	f_l	A_l^c	A_l^s
0.0000000000	1.2168039874E−02	0.0000000000E+00	0.0060830936	8.7269817888E−02	−9.0880793081E−01
1.0060753832	1.0137412052E−03	−7.5006386729E−03	0.9939262187	1.7330889655E−04	7.5800971227E−03

Table C.75: Fourier analysis of the x coordinate of Pluto in the Sun–Earth+Moon case.

f_l	A_l^c	A_l^s	f_l	A_l^c	A_l^s
0.0000000000	5.9538439765E−02	0.0000000000E+00	0.9959716815	2.8649095189E+01	−2.4064309453E+01
1.0000015382	−8.0264712420E+00	1.1750925327E+01	0.9919432766	4.2228013389E+00	−1.8068741751E+00
1.9959652012	7.3388397429E−01	−5.6447918739E−01	0.9879130511	8.4064425685E−01	−9.7613689298E−02
1.0040347212	5.2228849134E−01	4.3436232933E−01	1.9999936324	−2.0960446259E−01	2.8285839343E−01
0.0040157140	−2.3643386725E−01	−2.0695897804E−01	0.9838817458	1.8180577757E−01	3.1085266123E−02
1.9919363723	1.0626517605E−01	−4.0340480536E−02	1.0080658423	7.6108557712E−02	4.5203538322E−02
0.9798531648	3.9551867832E−02	1.9738575851E−02	0.0080520858	−3.4737325510E−02	−1.6866956226E−02
1.9879041938	2.0864043556E−02	−1.6814838585E−03	2.9959590249	1.7718473760E−02	−1.2406833446E−02
1.0120946070	1.6126509262E−02	5.0114761949E−03	2.0040264890	1.2512596204E−02	1.1231859355E−02

Table C.76: Fourier analysis of the y coordinate of Pluto in the Sun–Earth+Moon case.

f_l	A_l^c	A_l^s	f_l	A_l^c	A_l^s
0.0000000000	−1.0118928671E−01	0.0000000000E+00	0.9959724280	−2.3998584614E+01	−2.8707184132E+01
1.0000015599	1.1749419281E+01	8.0275592194E+00	0.9919434301	−1.8047819648E+00	−4.2236383360E+00
1.9959652087	−5.6446149230E−01	−7.3389381110E−01	0.9879130908	−9.7505501278E−02	−8.4065419991E−01
1.0040346495	4.3615002128E−01	−5.2408065447E−01	1.9999936328	2.8284839548E−01	2.0960926836E−01
0.0040237736	2.0659620900E−01	−2.2186198931E−01	0.9838817611	3.1094478466E−02	−1.8180412361E−01
1.9919312091	−4.2023897853E−02	−1.0551357485E−01	1.0080657555	4.5348456507E−02	−7.6386295656E−02
0.9798531607	1.9738249374E−02	−3.9552160455E−02	0.0080506405	1.6116807987E−02	−3.3490884813E−02
1.9879038140	−1.7069267942E−03	−2.0862328467E−02	2.9959590249	−1.2406830002E−02	−1.7718485137E−02
1.0120945098	5.0216134146E−03	−1.6183682994E−02	2.0040264536	1.1252130431E−02	−1.2531638869E−02

Table C.77: Fourier analysis of the z coordinate of Pluto in the Sun–Earth+Moon case.

f_l	A_l^c	A_l^s	f_l	A_l^c	A_l^s
0.0000000000	−3.9731483008E+00	0.0000000000E+00	0.0040316358	8.6852375323E+00	−7.2669392271E+00
0.0080609792	7.6127679666E−01	−1.1603430570E+00	0.0120905431	7.2770391026E−02	−2.4473235494E−01
0.9959636886	6.8664111620E−02	6.3327914596E−02	1.0040256980	7.4242946377E−02	−5.6705368973E−02
0.9999906313	−6.5488281447E−02	−2.2001058683E−03	0.0161199998	−1.5415753587E−04	−5.5710047055E−02
0.0201488464	−3.9050715713E−03	−1.2779864231E−02	0.9919312985	5.9044779495E−03	9.8023617741E−03
1.0080522527	6.6183849279E−03	−9.3378789463E−03			

Appendix D

Evolution of the families of periodic orbits

In Chapter 7, several families of periodic orbits of the RTBP with the Earth-Moon mass parameter were described. For most of the families only the characteristic and stability curves were given. For each of these families, we give in this Appendix some sample orbits, which have been chosen in order to display its evolution in shape.

D.1 Lyapunov families

In Fig. D.1, we give the characteristic and stability curves of the planar Lyapunov families around L_1, L_2 and L_3. We have plotted and labeled some points on these curves, which correspond to the orbits displayed in Fig. D.2. Orbits 2,3,4,5 are magnified with respect to the remaining ones, this is in order to display the "change in shape" along the family that takes place between orbits 1 and 6.

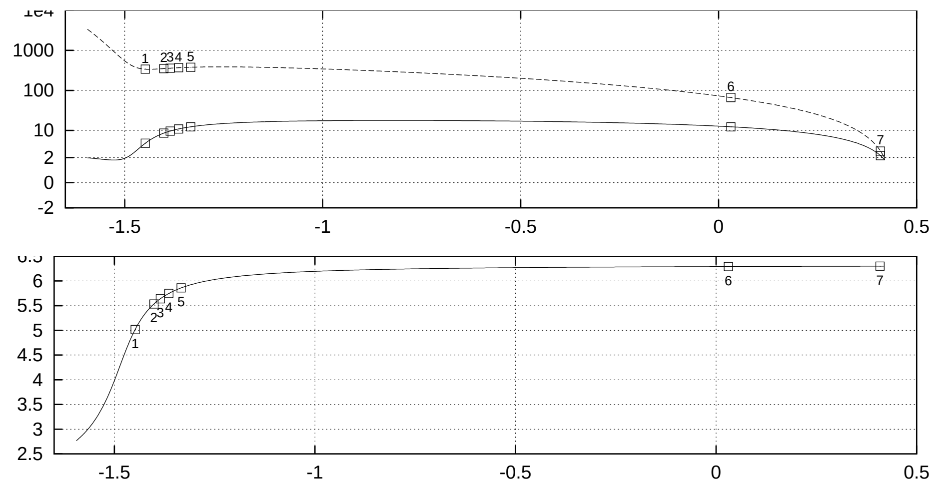

Figure D.1: Top: energy (horizontal axis) vs. stability parameters (vertical axis) of the family of vertical orbits of L_1. Bottom: energy vs. period for the same family. The square points refer to the orbits displayed in figures D.2.

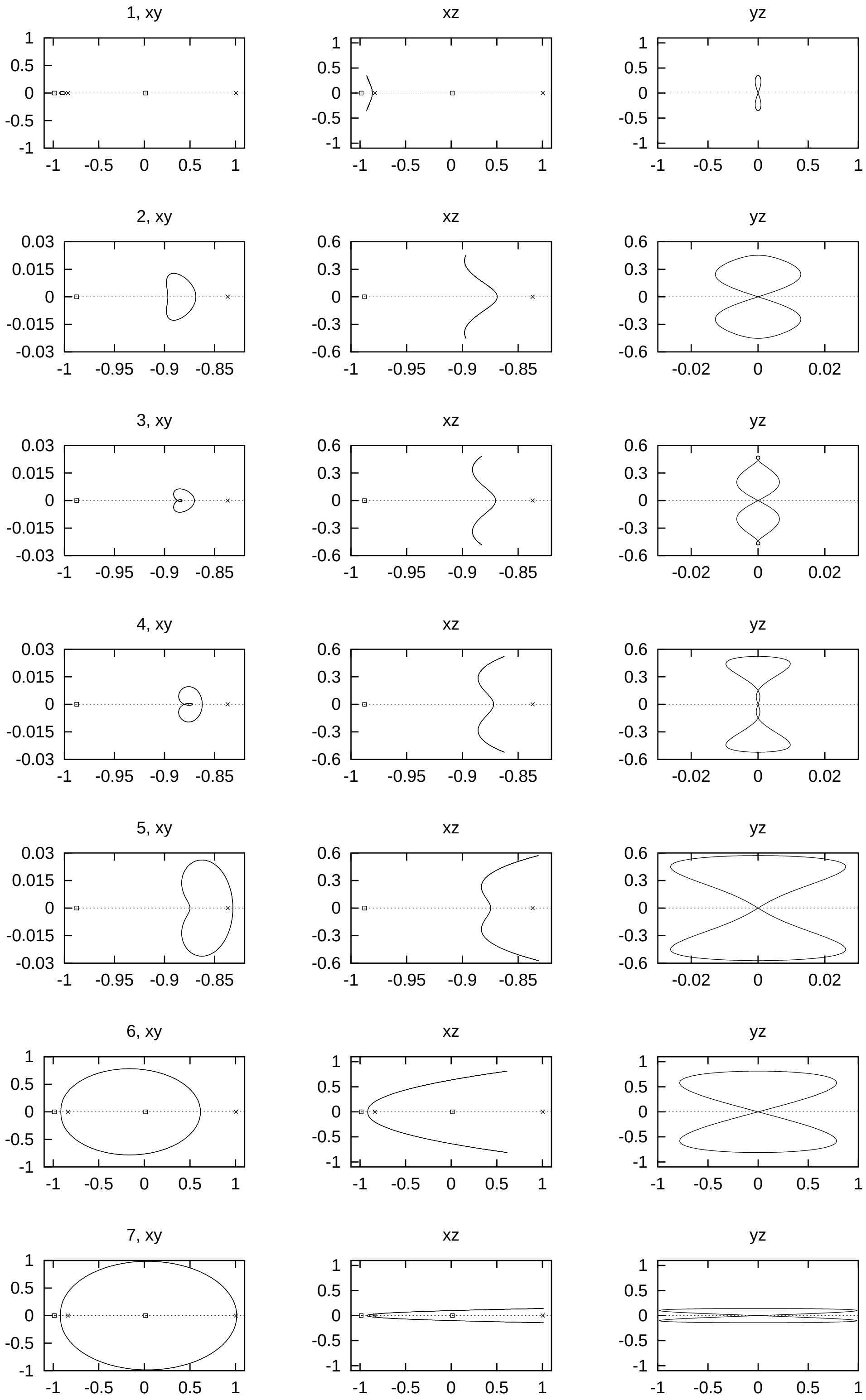

Figure D.2: Projections of orbits 1,. . . ,7 of figure D.1.

In figure D.3 we display stability parameters and the characteristic curve for the vertical Lyapunov family around L_2. In this case there is no change in shape analogous to the L_1 case, and therefore we display less orbits.

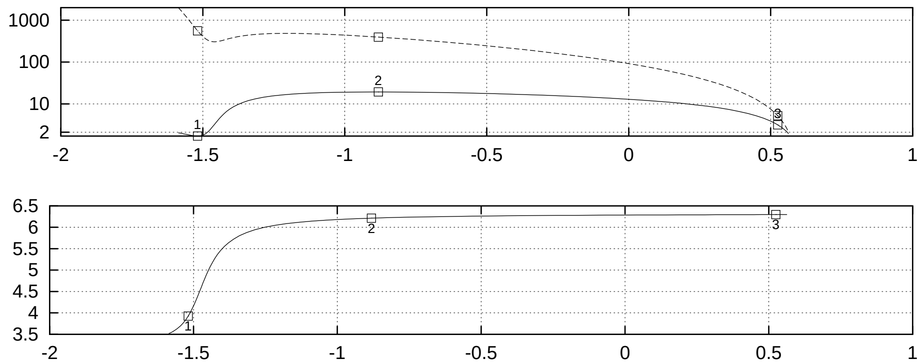

Figure D.3: Top: energy (horizontal axis) vs. stability parameters (vertical axis) of the vertical family of L_2. Bottom: energy vs. period for the same family. The square points refer to the orbits displayed in figure D.4.

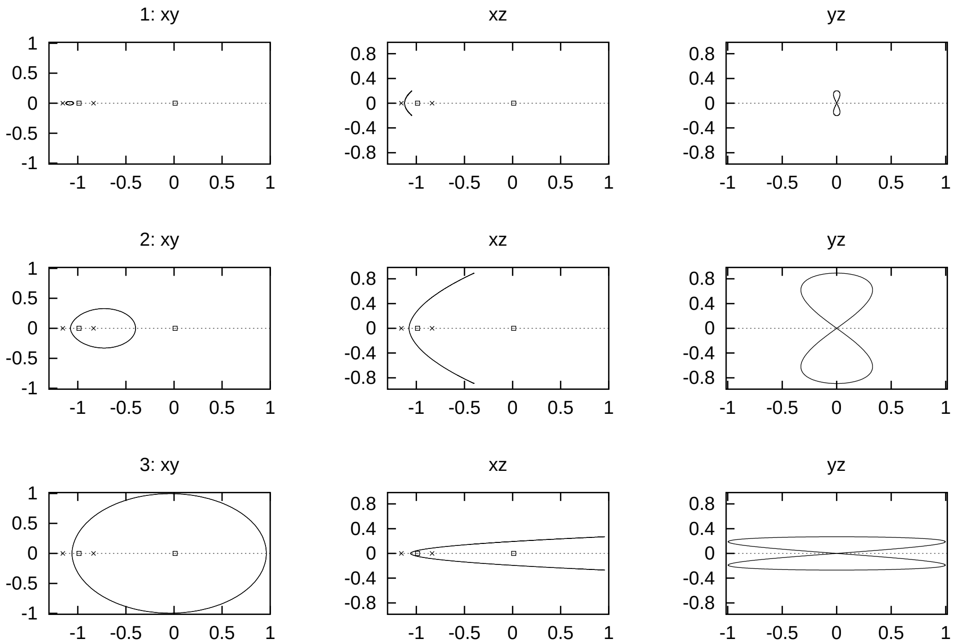

Figure D.4: Projections of the orbits labeled 1,2,3 in figure D.3.

In figures D.5 and D.6 we represent the vertical Lyapunov families around L_3

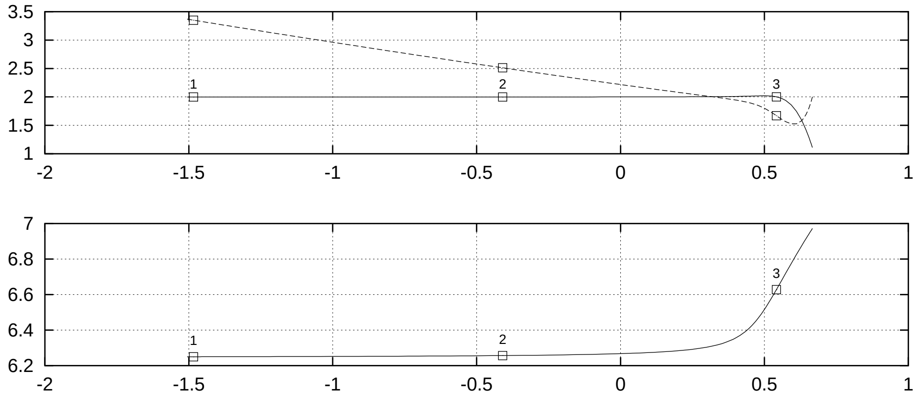

Figure D.5: Top: energy (horizontal axis) vs. stability parameters (vertical axis) of the vertical family of L_3. Bottom: energy vs. period for the same family. The square points refer to the orbits displayed in figure D.6.

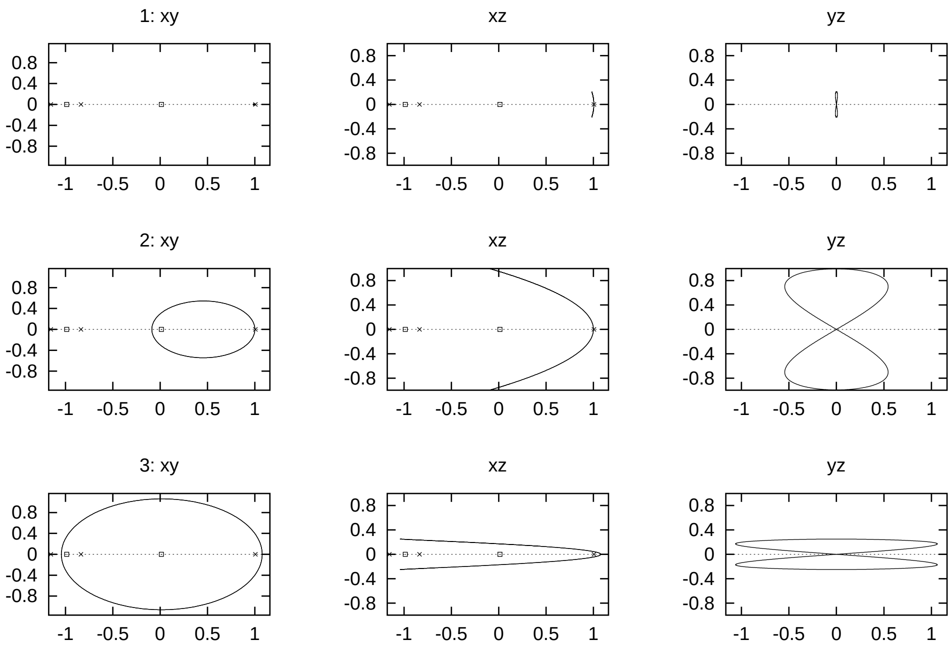

Figure D.6: Projections of the orbits labeled 1,2,3 in figure D.5.

D.1.1 Planar Lyapunov families

As we did for vertical orbits, we display in Fig. D.7 stability parameters and the characteristic curves of the planar Lyapunov family around L_1. Since this family is planar, in Fig. D.8 we display only the xy projections of the orbits labeled in Fig. D.7.

In figures D.9 and D.10 we display stability parameters, the characteristic curve and some sample orbits of the planar Lyapunov family around L_2.

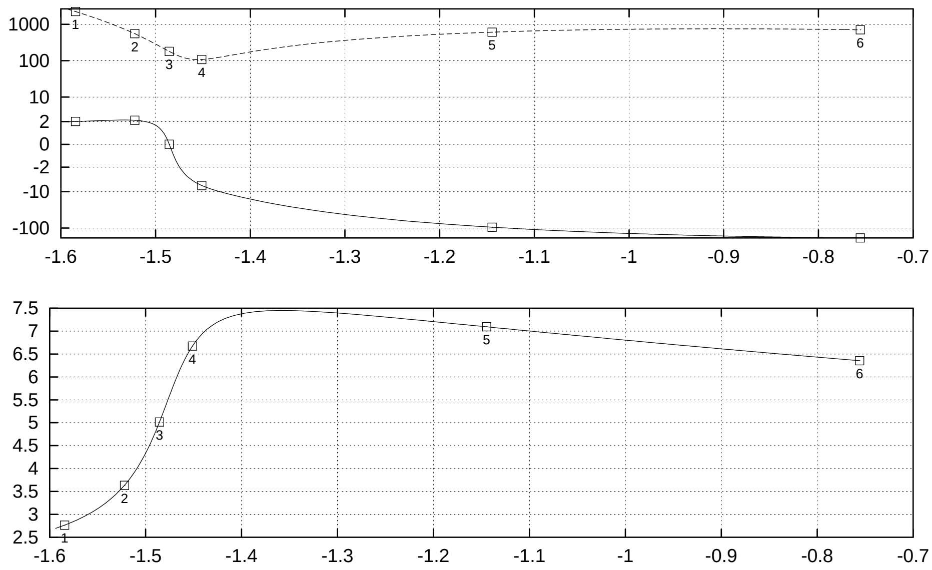

Figure D.7: Top: energy (horizontal axis) vs. stability parameters (vertical axis) of the family of planar orbits of L_1. Bottom: energy vs. period for the same family. The square points refer to the orbits displayed in figure D.8.

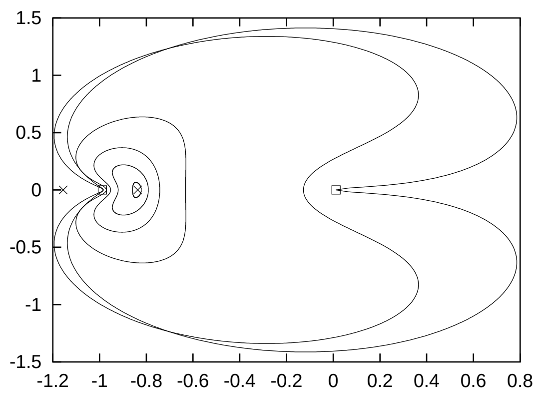

Figure D.8: xy projection of the orbits labeled 1,...,6 (from smaller to larger) in figure D.7.

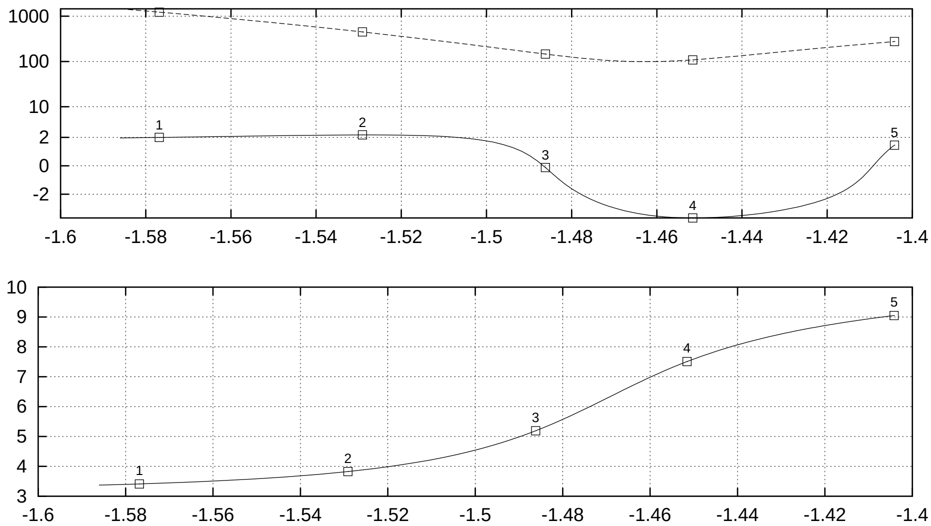

Figure D.9: Top: energy (horizontal axis) vs. stability parameters (vertical axis) of the planar family of L_2. Bottom: energy vs. period for the same family. The square points refer to the orbits displayed in figure D.10.

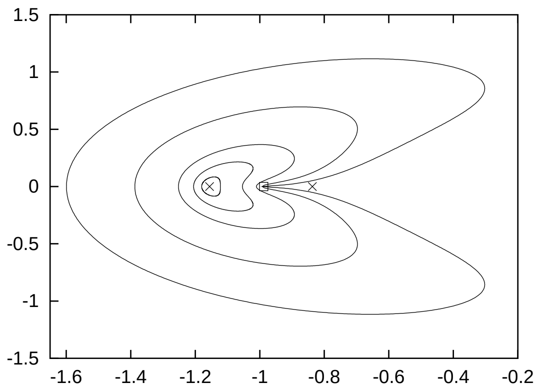

Figure D.10: xy projection of the orbits labeled 1,. . . ,5 (from smaller to larger) in figure D.9.

In figures D.11 and D.12 we do the same for the planar Lyapunov family around L_3.

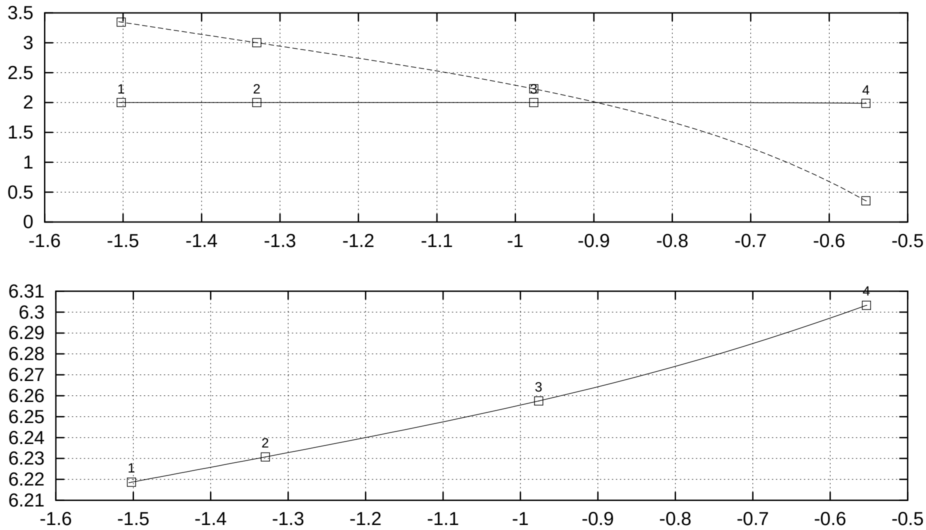

Figure D.11: Top: energy (horizontal axis) vs. stability parameters (vertical axis) of the planar family of L_2. Bottom: energy vs. period for the same family. The square points refer to the orbits displayed in figure D.12.

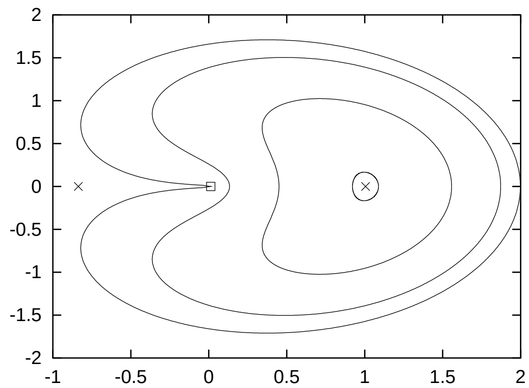

Figure D.12: xy projection of the orbits labeled 1,...,4 (from smaller to larger) in figure D.11.

D.2 Halo and halo–type families

D.2.1 Halo families

As we did in Chapter 7, we magnify in Fig. D.13 a neighborhood of the bifurcations to complex instability of the stability parameters. Also, when the stability parameters are complex conjugate, we display the real and imaginary parts of one of them. We display sample orbits in Fig. D.14.

Figures D.15 and D.16 display stability parameters, the characteristic curve and sample orbits of the halo family for the L_2 case. In figures D.17 and D.18 we do the same for the halo family around L_3.

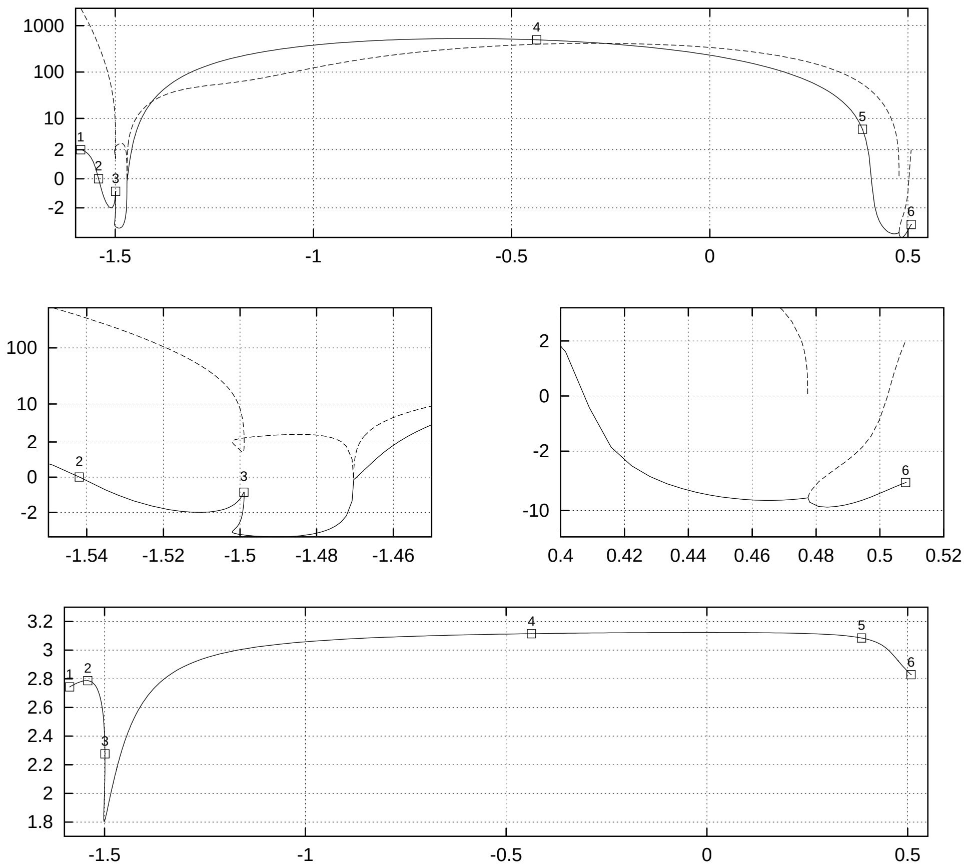

Figure D.13: Top: energy (horizontal axis) vs. stability parameters (vertical axis) of the north-class family of halo orbits of L_1. Middle: two magnifications of the previous plot, in the left one turning points in the energy can be appreciated. Bottom: energy vs. period for the same family. The square points refer to the orbits displayed in figure D.14.

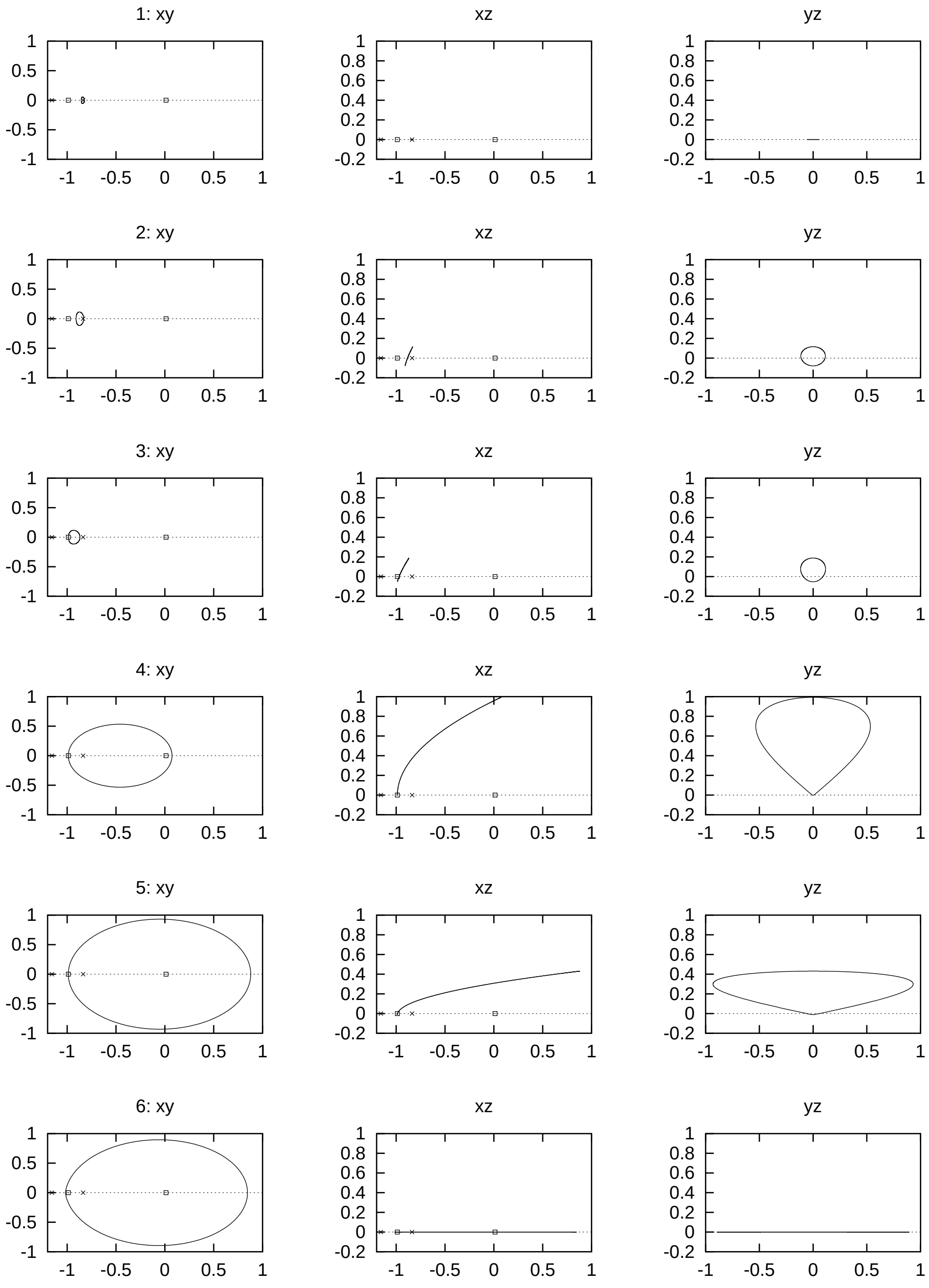

Figure D.14: Halo orbits labeled 1,...,6 in figure D.13.

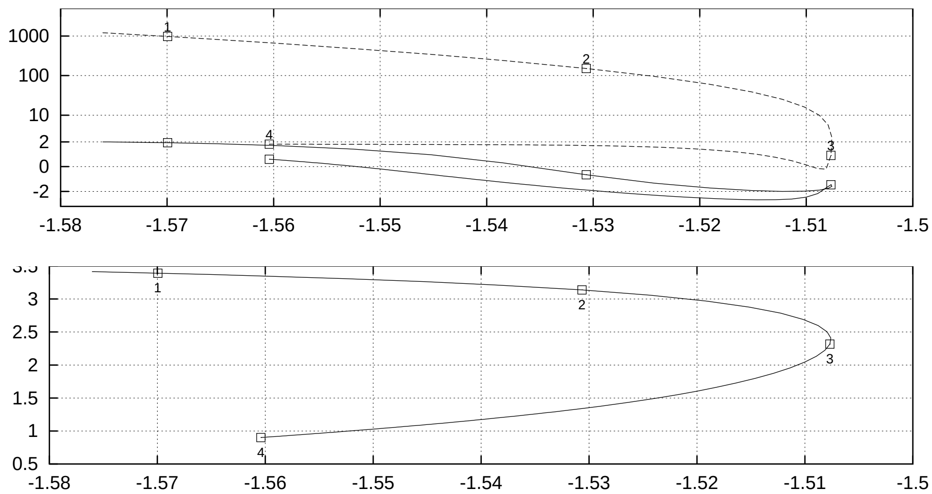

Figure D.15: top: Energy–stability parameters diagram of the halo family of L_2. Bottom: energy–period diagram for the same family. The square points refer to the orbits displayed in figure D.16.

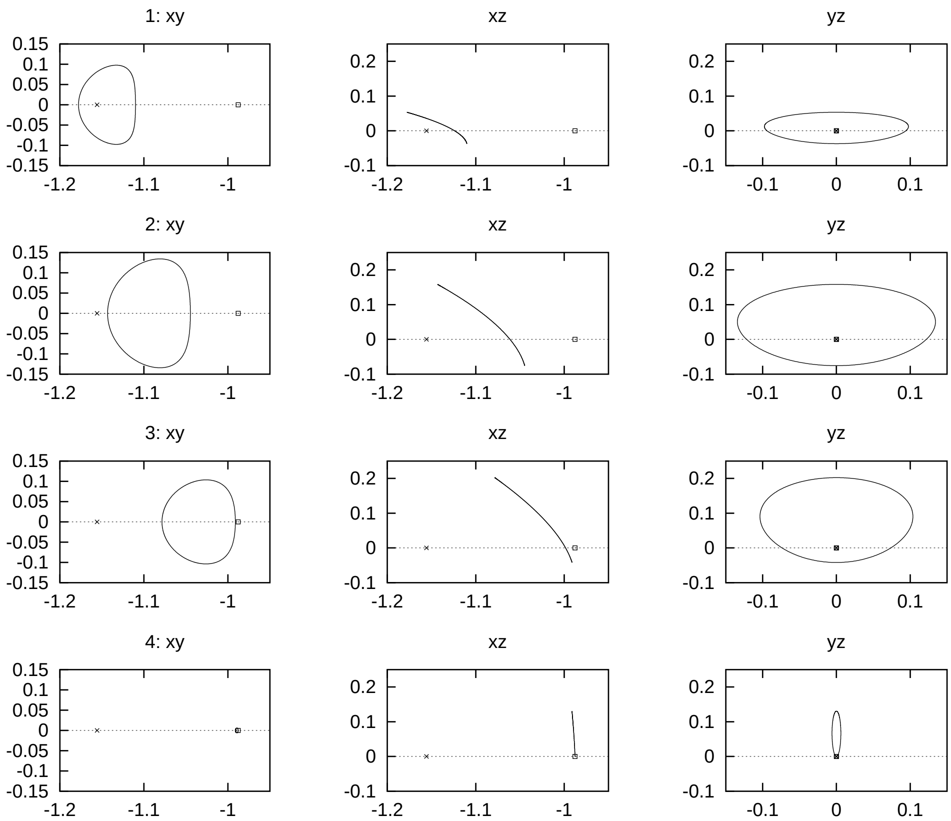

Figure D.16: xyz, xy, xz and yz projections of the halo orbits labeled 1,. . . ,4 in D.15.

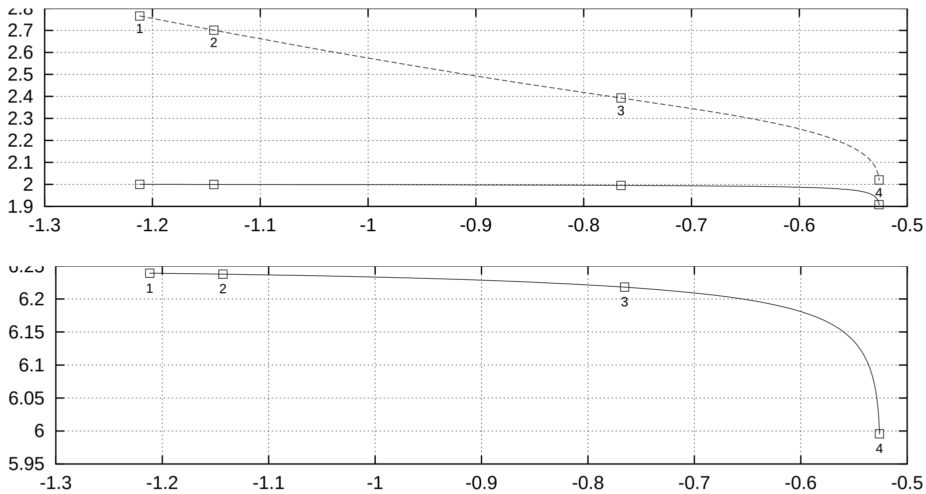

Figure D.17: top: Energy–stability parameters diagram of the halo family of L_3. Bottom: energy–period diagram for the same family. The square points refer to the orbits displayed in figure D.18.

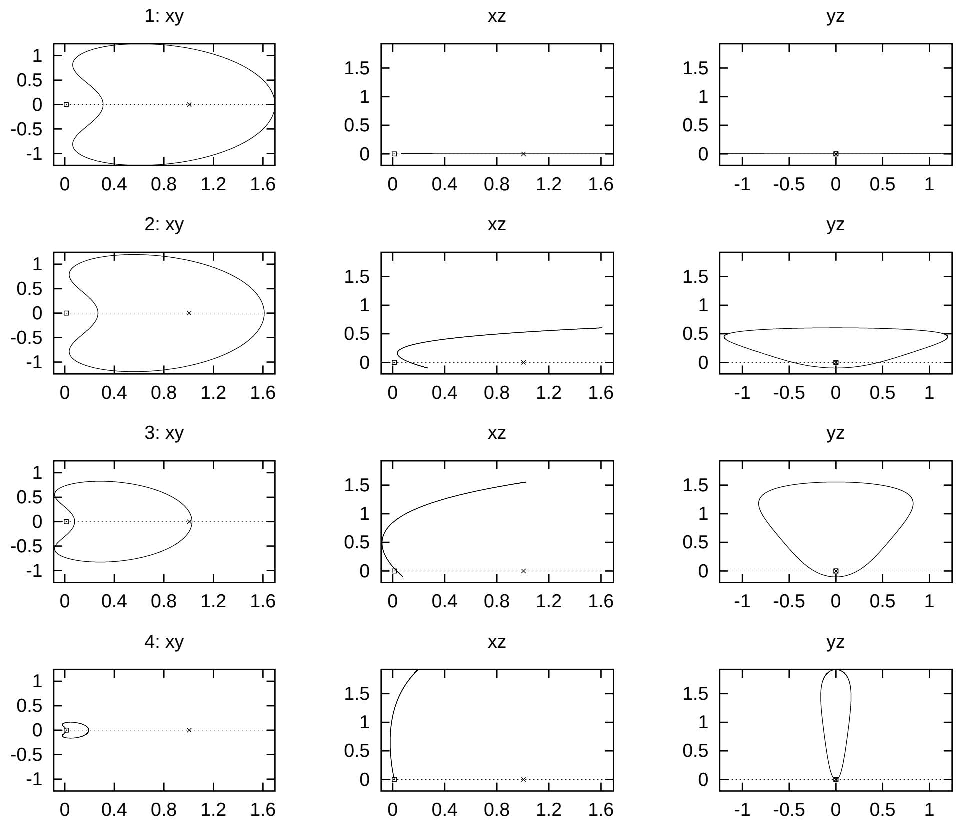

Figure D.18: xyz, xy, xz and yz projections of the halo orbits labeled 1,. . . ,4 in D.17.

D.2.2 Period–duplicated halo families

In Fig. D.19 we display stability parameters and the characteristic curve of the hyperbolic period–duplicated halo family around L_1. In order to simplify the plots, in the complex unstable case only the real part of the stability parameters has been shown. Note that some orbits are highly unstable. In figures D.20 and D.21 we display some sample orbits. This family ends in a plane orbit, as described in Chapter 7.

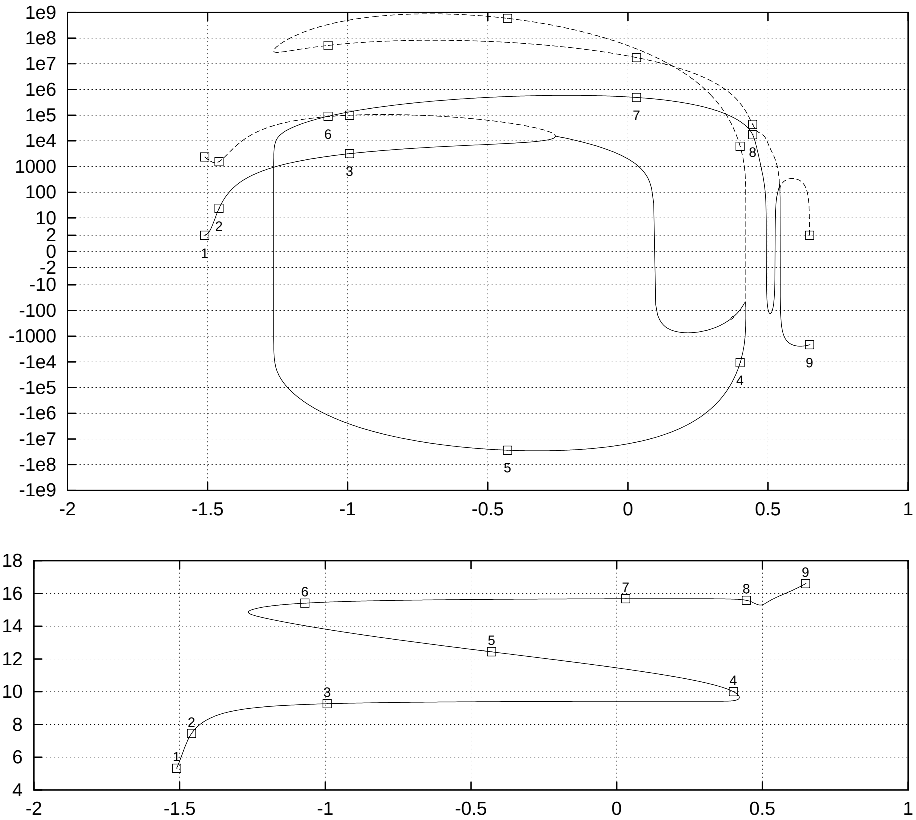

Figure D.19: Top: energy (horizontal axis) vs. stability parameters (vertical axis) of the hyperbolic period doubling bifurcation of the halo family of L_1. Bottom: energy vs. period for the same family. The square points refer to the orbits displayed in figures D.20 and D.21.

We give the stability and characteristic curves of the elliptic bifurcated halo–type orbits by period duplication in Fig. D.22, as well as some sample orbits in Fig. D.23. This family ends in a collision orbit with the massive body.

In Fig. D.24 we give the stability parameters and characteristic curve of the hyperbolic bifurcated halo–type family around L_2. This family ends in a collision orbit with the small body. Some sample orbits are given in Fig. D.25.

As we did before, in the stability parameters curves of the elliptic bifurcated halo–type family around L_2 of Fig. D.26, we have represented just the real part of the stability parameters in the complex unstable case. In this family we have not found a natural termination orbit. We give some sample orbits in figures D.27, D.29 and D.29.

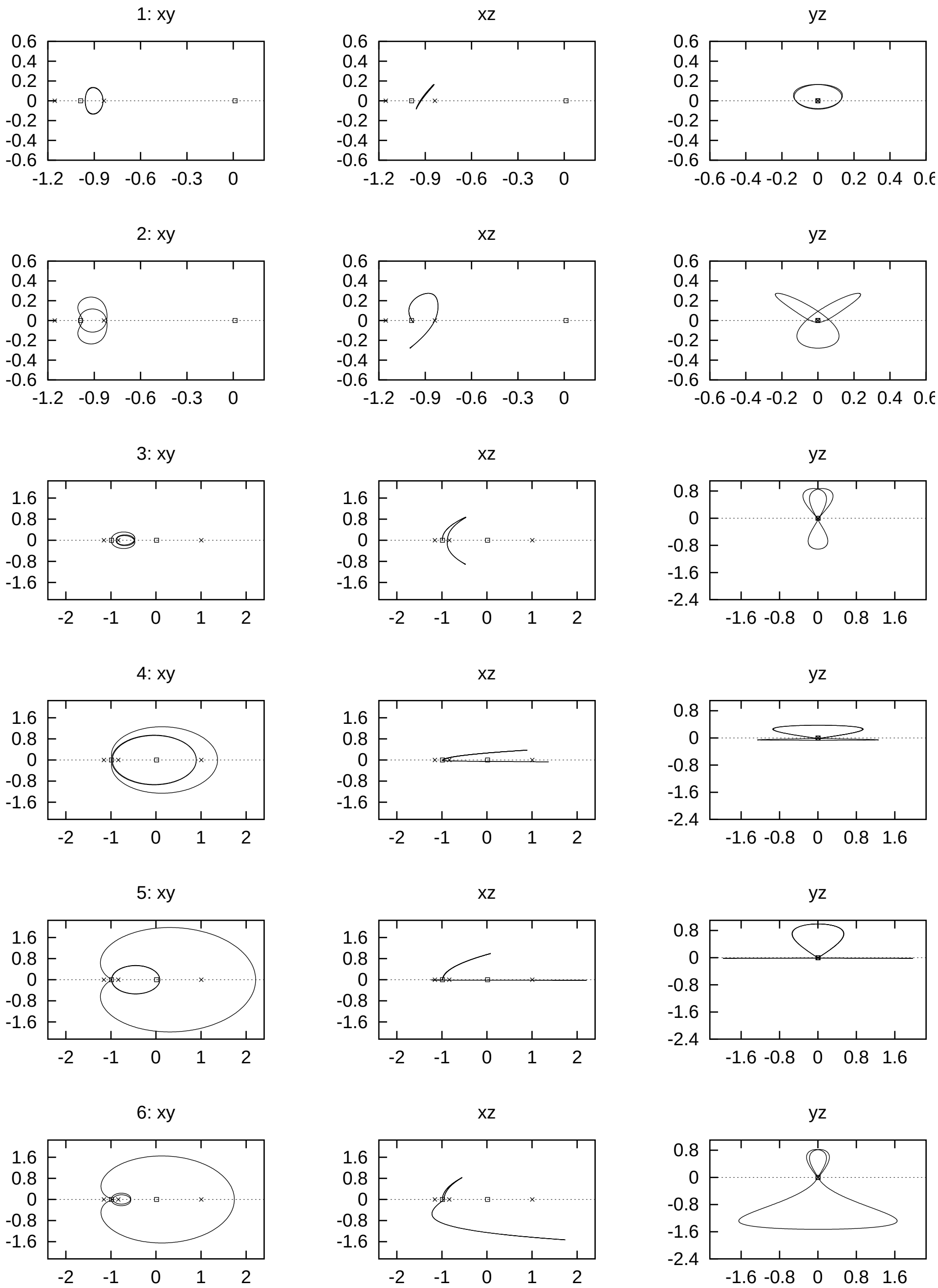

Figure D.20: xyz, xy, xz and yz projections of the orbits labeled 1,. . . ,6 in figure D.19.

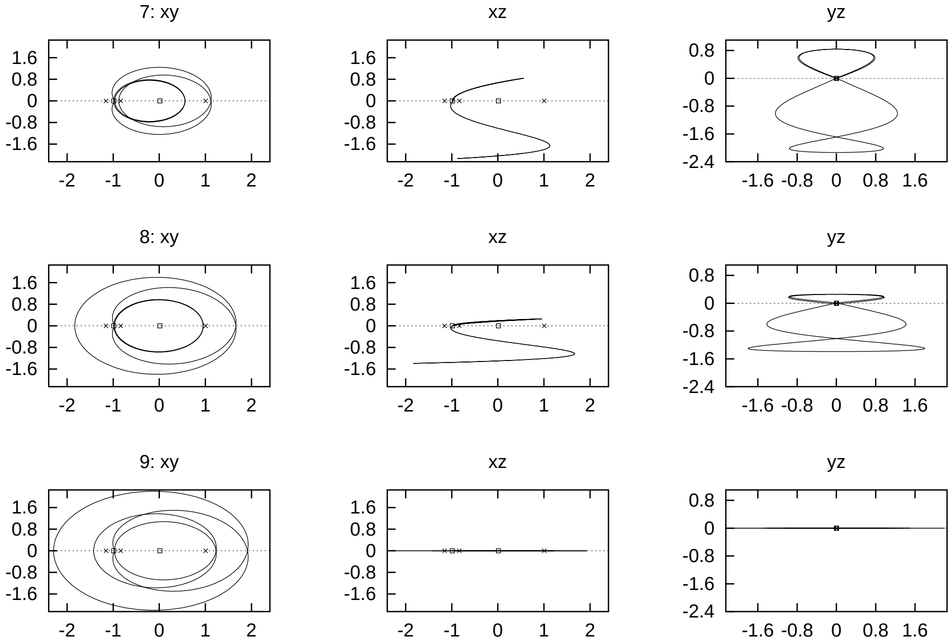

Figure D.21: Projections of the orbit labeled 7,. . . ,9 in figure D.19.

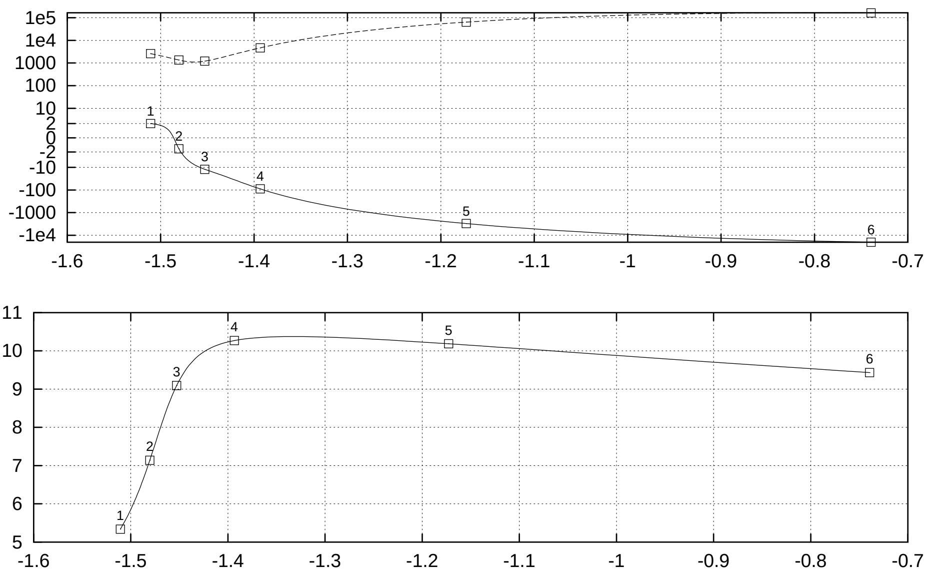

Figure D.22: Top: energy (horizontal axis) vs. stability parameters (vertical axis) of the elliptic period doubling bifurcation of the halo family of L_1. Bottom: energy vs. period for the same family. The square points refer to the orbits displayed in figure D.23.

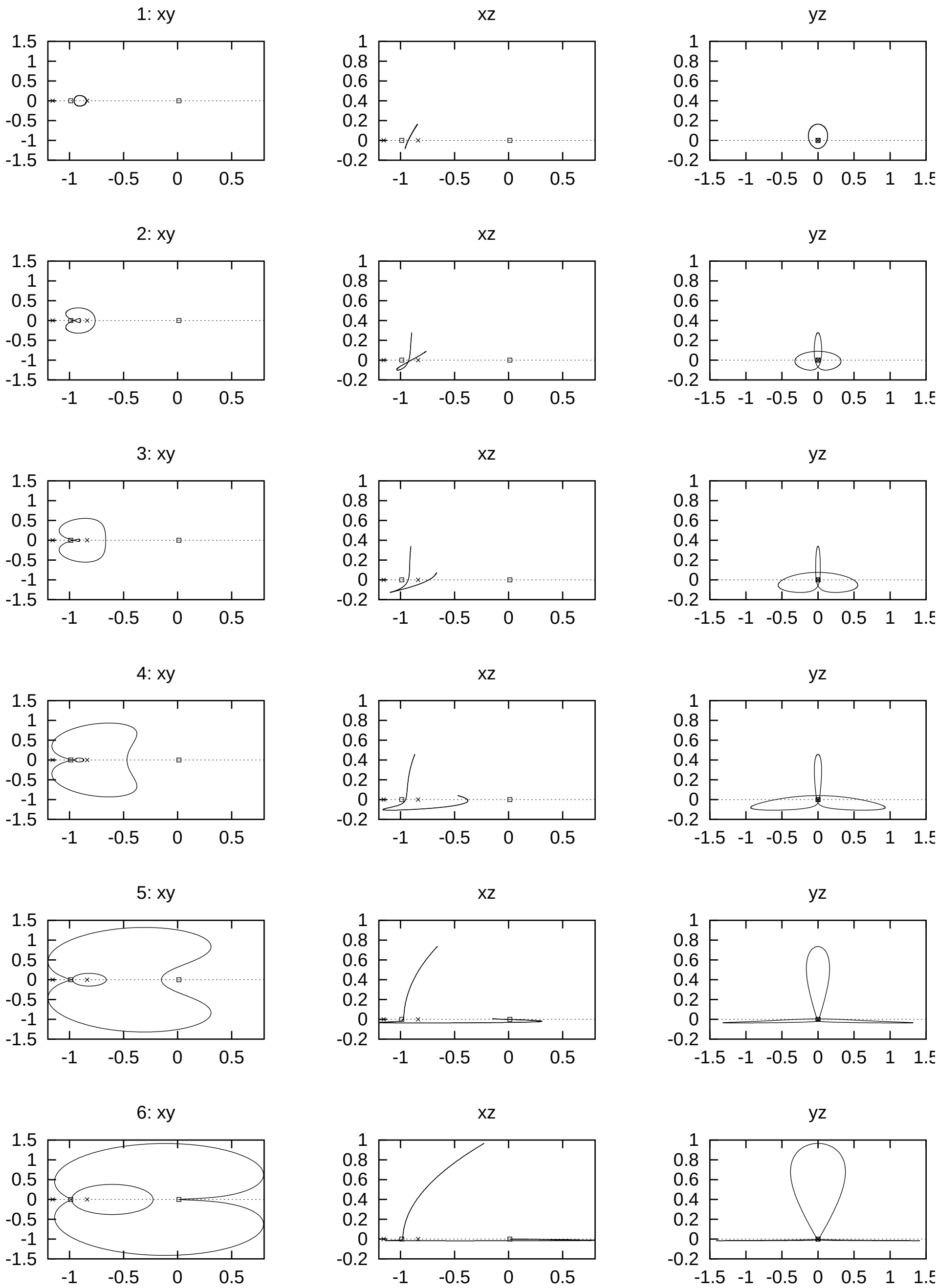

Figure D.23: xyz, xy, xz and yz projections of the orbits labeled 1,. . . ,6 in figure D.22.

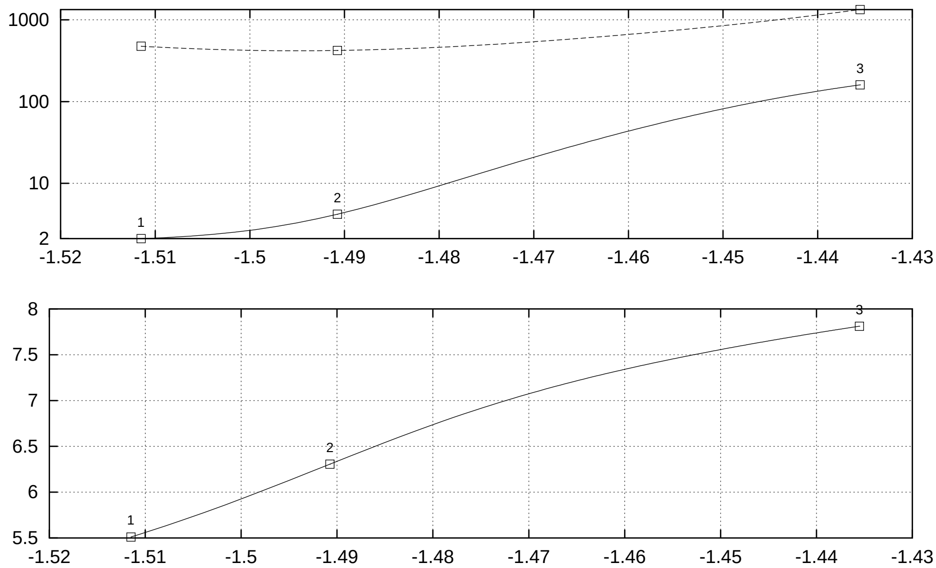

Figure D.24: Top: energy vs. stability parameters of the hyperbolic period doubling bifurcation of the L_2 halo family. Bottom: energy vs. period for the same family. The square points refer to the orbits displayed in figure D.25.

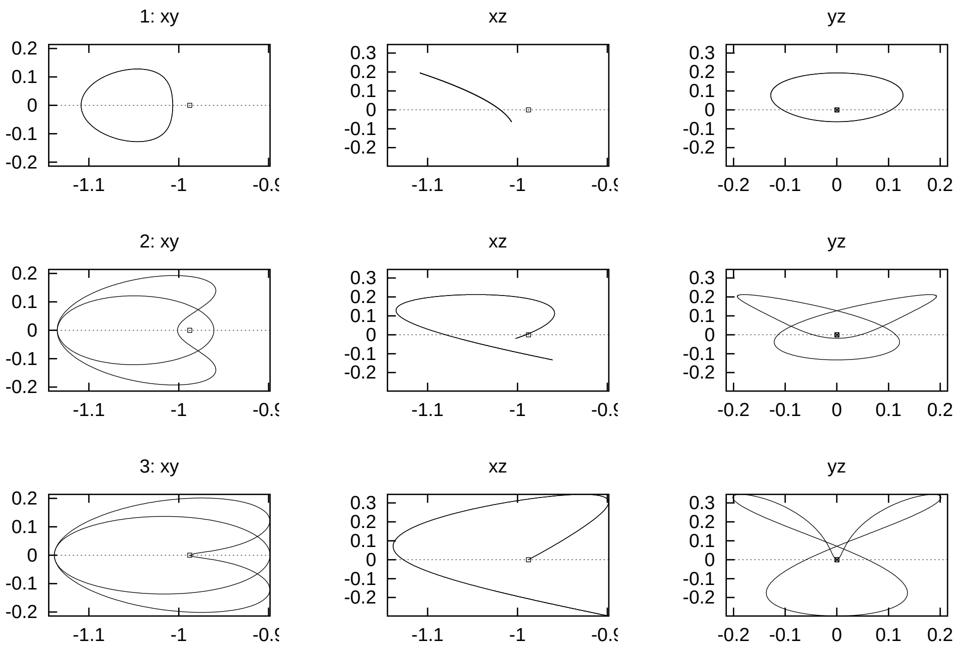

Figure D.25: Projections of the orbits labeled 1,. . . ,3 in figure D.24.

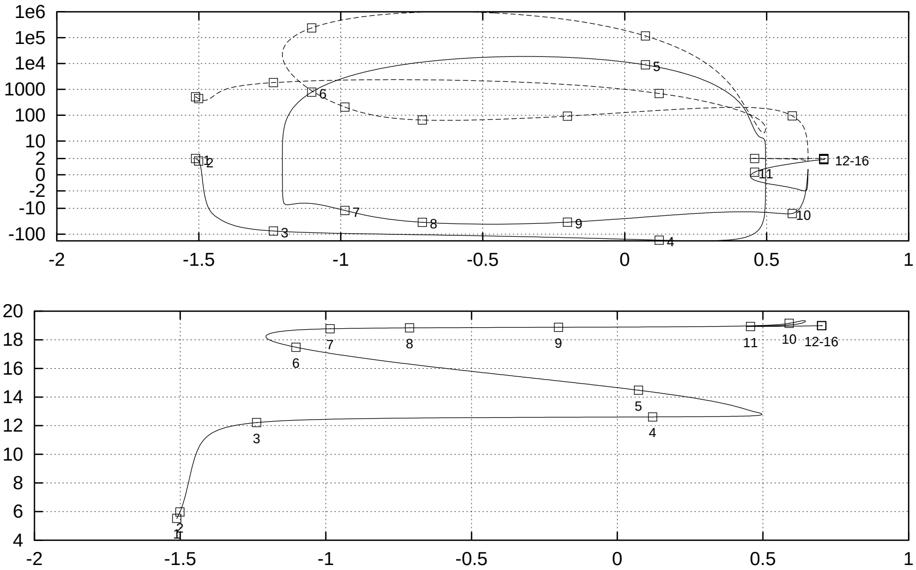

Figure D.26: Top: energy vs. stability parameters of the elliptic period doubling bifurcation of the L_2 halo family. Bottom: energy vs. period for the same family. The square points refer to the orbits displayed in figures D.27, D.28, and D.29.

D.2.3 Period–triplicated halo families

In Fig. D.30 we have represented the stability and characteristic curves of hyperbolic halo–type family bifurcated by period triplication. It has been followed up to periods over 40 because its initial evolution is very similar to the hyperbolic family bifurcated by period duplication, and we expected to find a natural termination orbit like in that case. As before, when the stability parameters are in complex unstable case we have displayed only the real part. Even in this way, the stability diagram is very complicated. We have displayed some sample orbits in figures D.31 through D.35.

In figures D.36 and D.37 we represent the family of elliptic halo–type orbits bifurcated by period triplication around L_1. It ends in a collision orbit with the massive body. Its evolution in shape is similar to the hyperbolic halo–type family bifurcated by period duplication, but with an additional loop.

In figures D.38 and D.39 we represent the hyperbolic halo–type family bifurcated by period triplication around L_2. Its evolution is also similar to the analogous family bifurcated by period duplication, but with an additional loop.

In figures D.40 and D.41 we represent the elliptic halo–type family bifurcated by period triplication around L_2. We have not identified a natural termination orbit for this family. Again, its initial evolution in shape is similar to the analogous family bifurcated by period duplication.

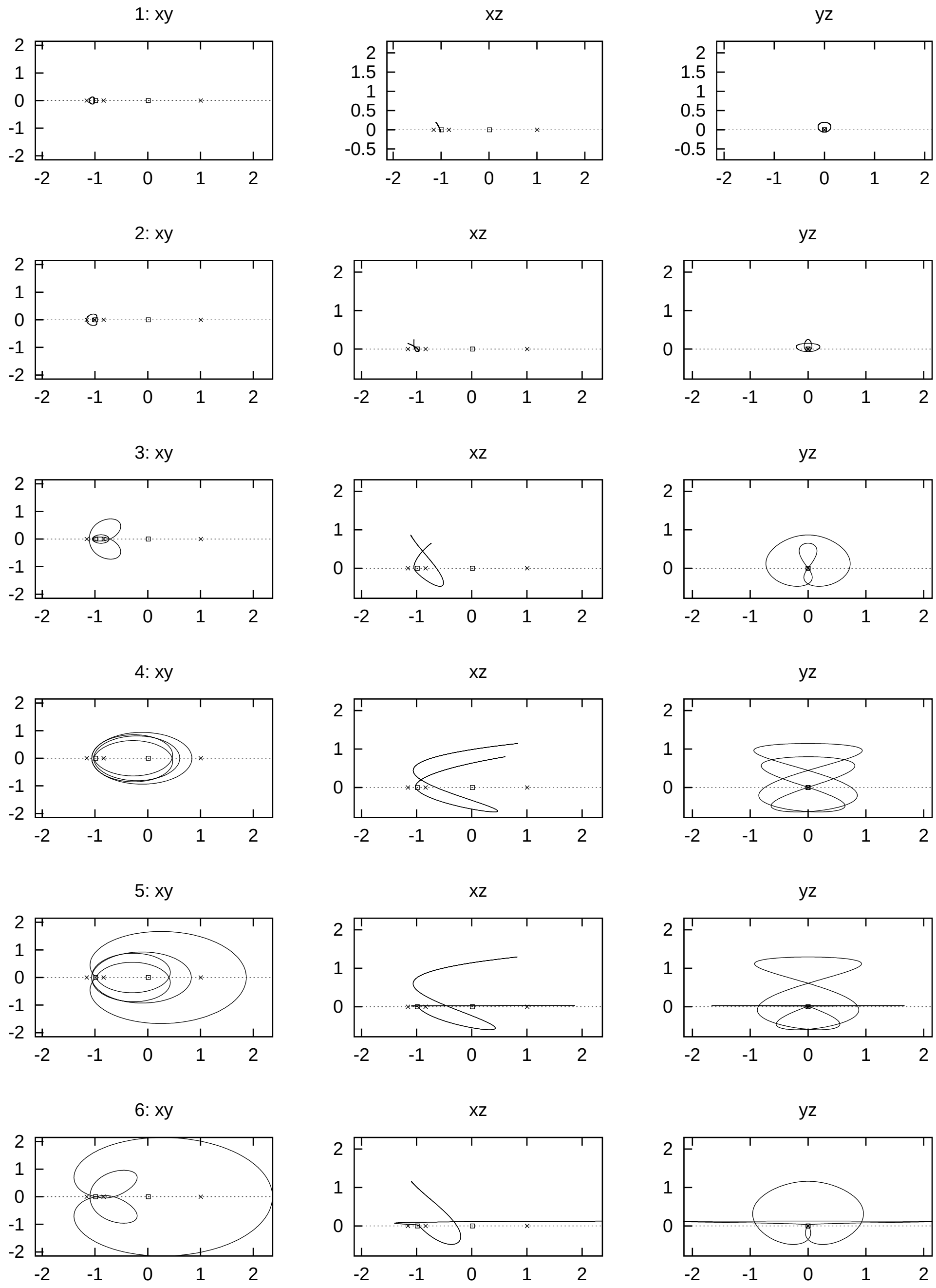

Figure D.27: Projections of the orbits labeled 1,. . . ,6 in figure D.26.

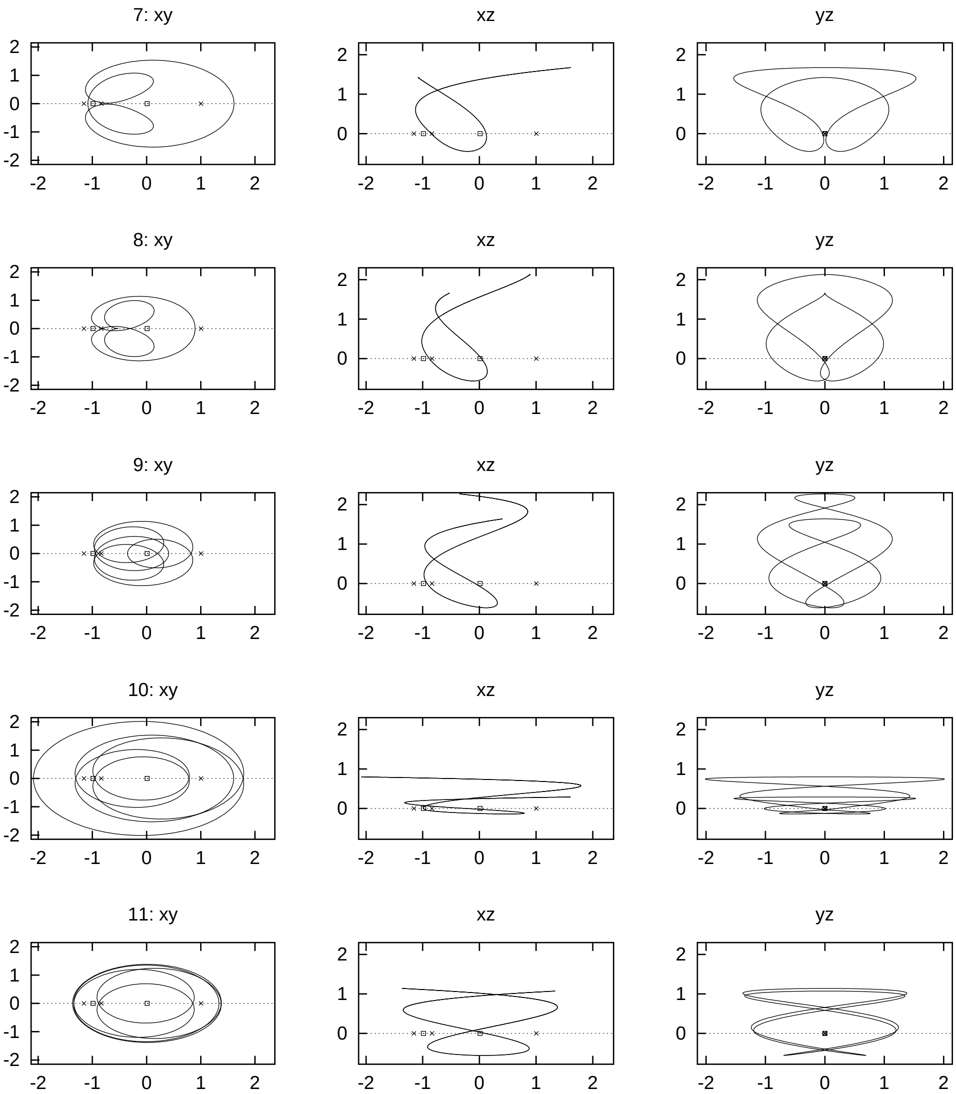

Figure D.28: Projections of the orbits labeled 7,. . . ,11 in figure D.26.

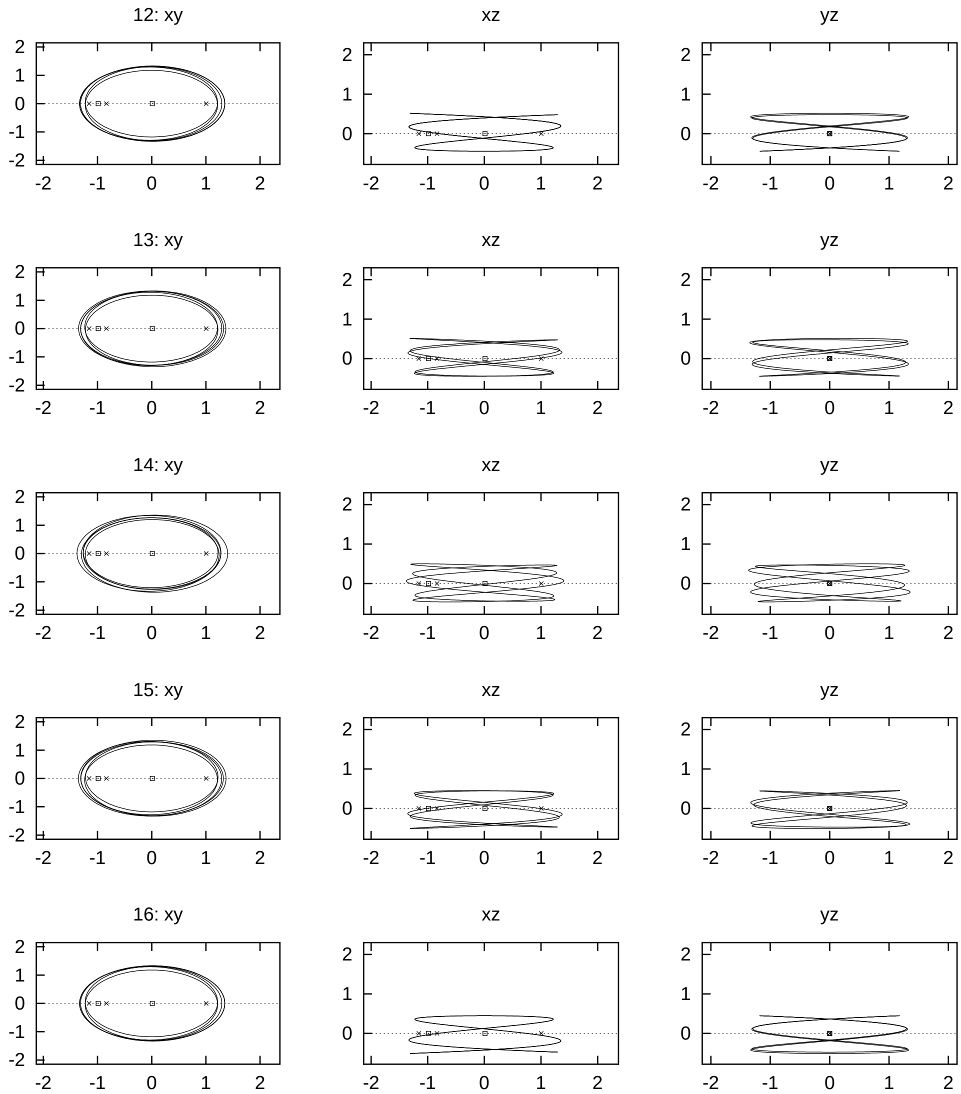

Figure D.29: Projections of the orbits labeled 12,...,16 in figure D.26.

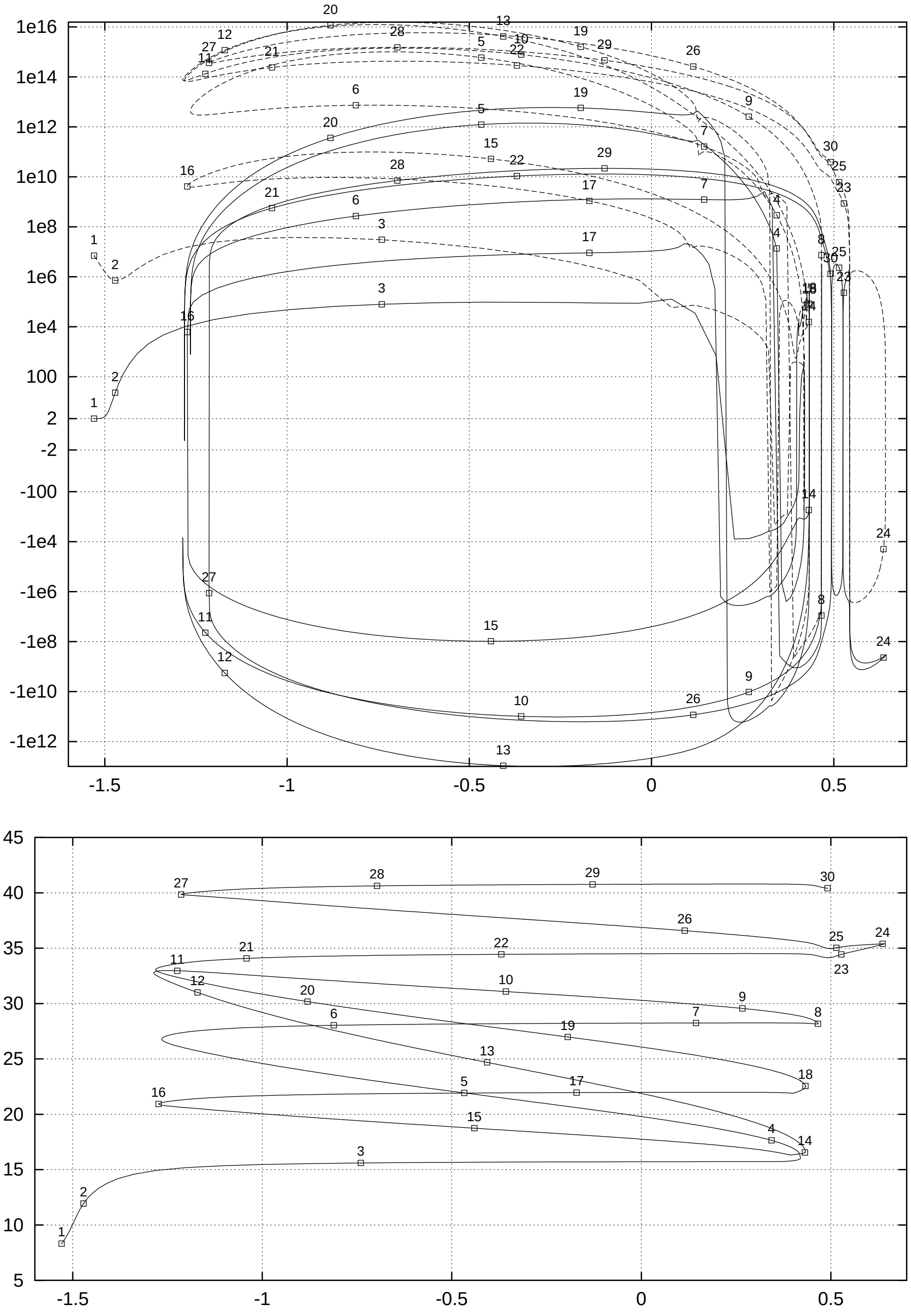

Figure D.30: Top: energy vs. stability parameters of the hyperbolic bifurcation by period triplication of the halo family of L_1. Bottom: energy vs. period for the same family. The square points refer to the orbits displayed in figure D.31 to D.35.

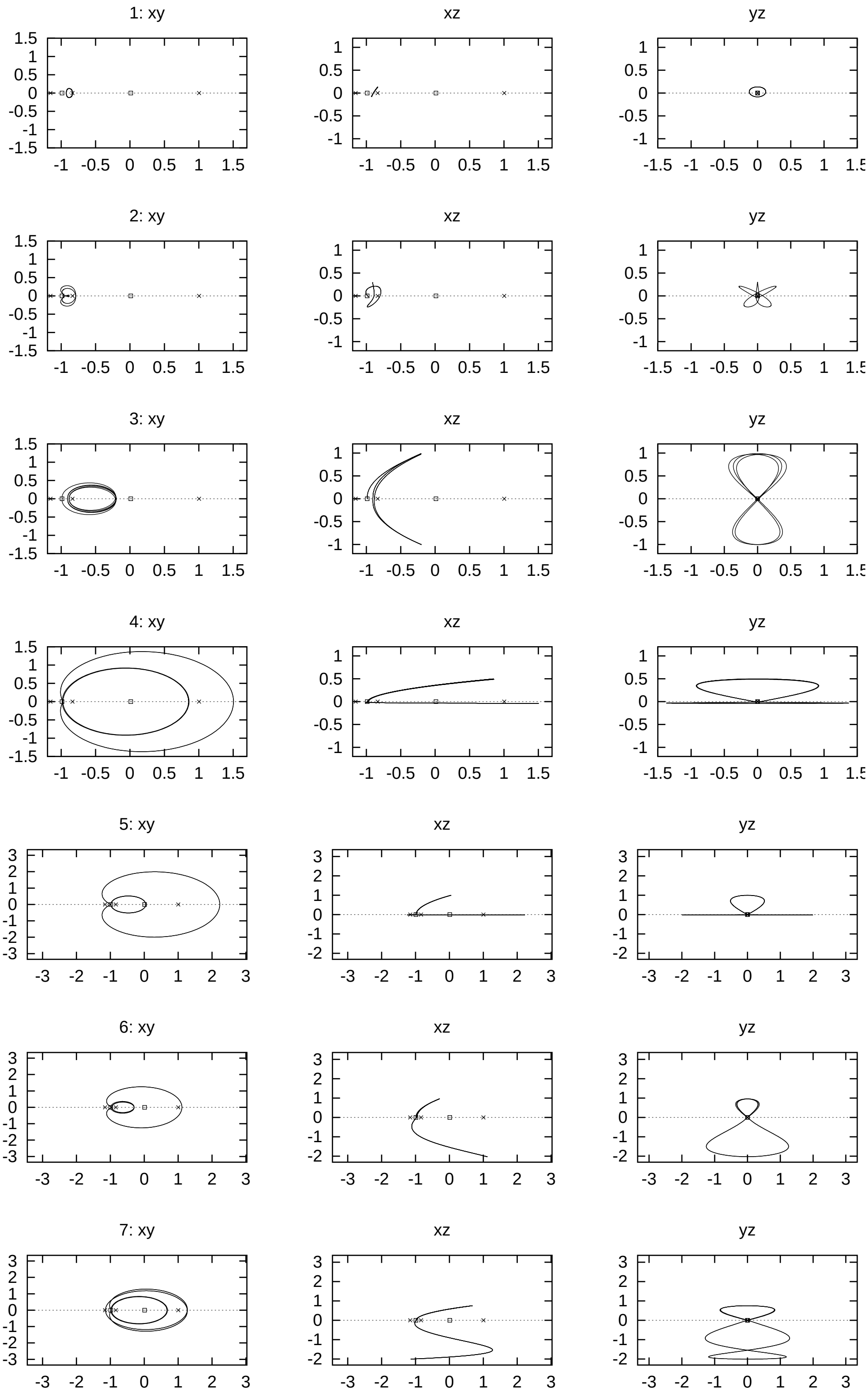

Figure D.31: Orbits labeled 1,. . . ,7 in figure D.30. Each row of graphics shows the xy (left), xz (middle) and yz (right) projections of an orbit.

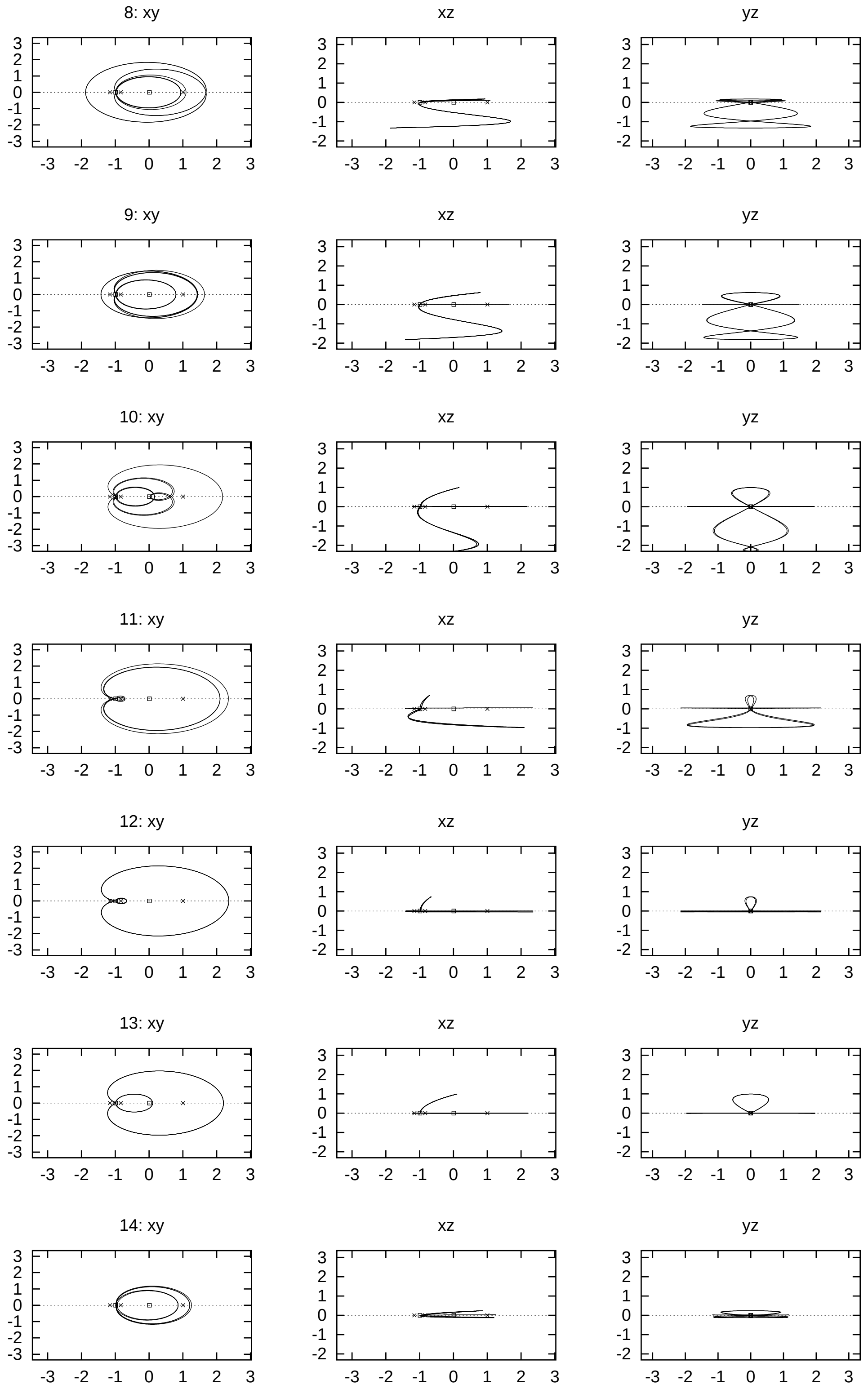

Figure D.32: Orbits labeled 8,...,14 in figure D.30.

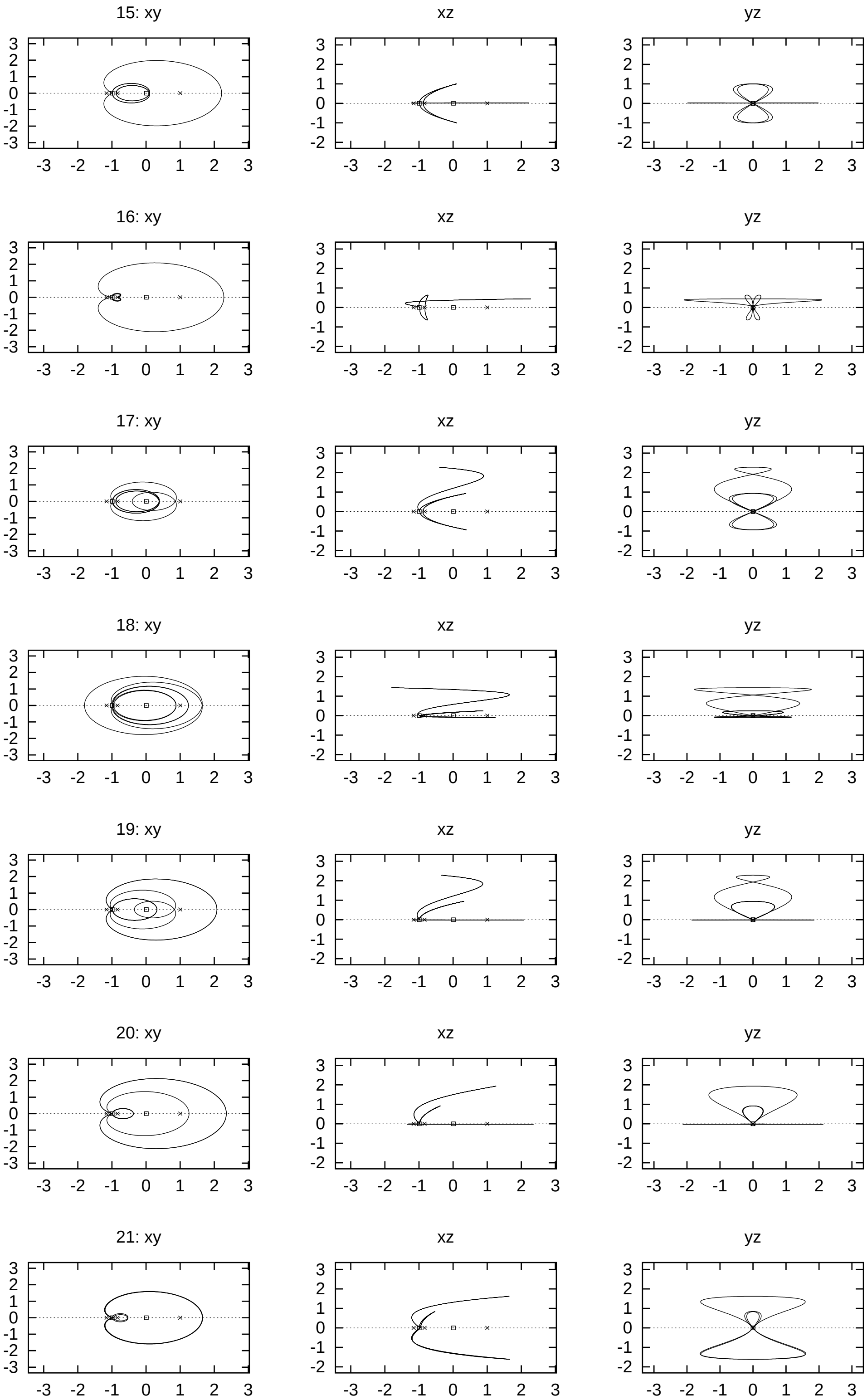

Figure D.33: Orbits labeled 15,...,21 in figure D.30.

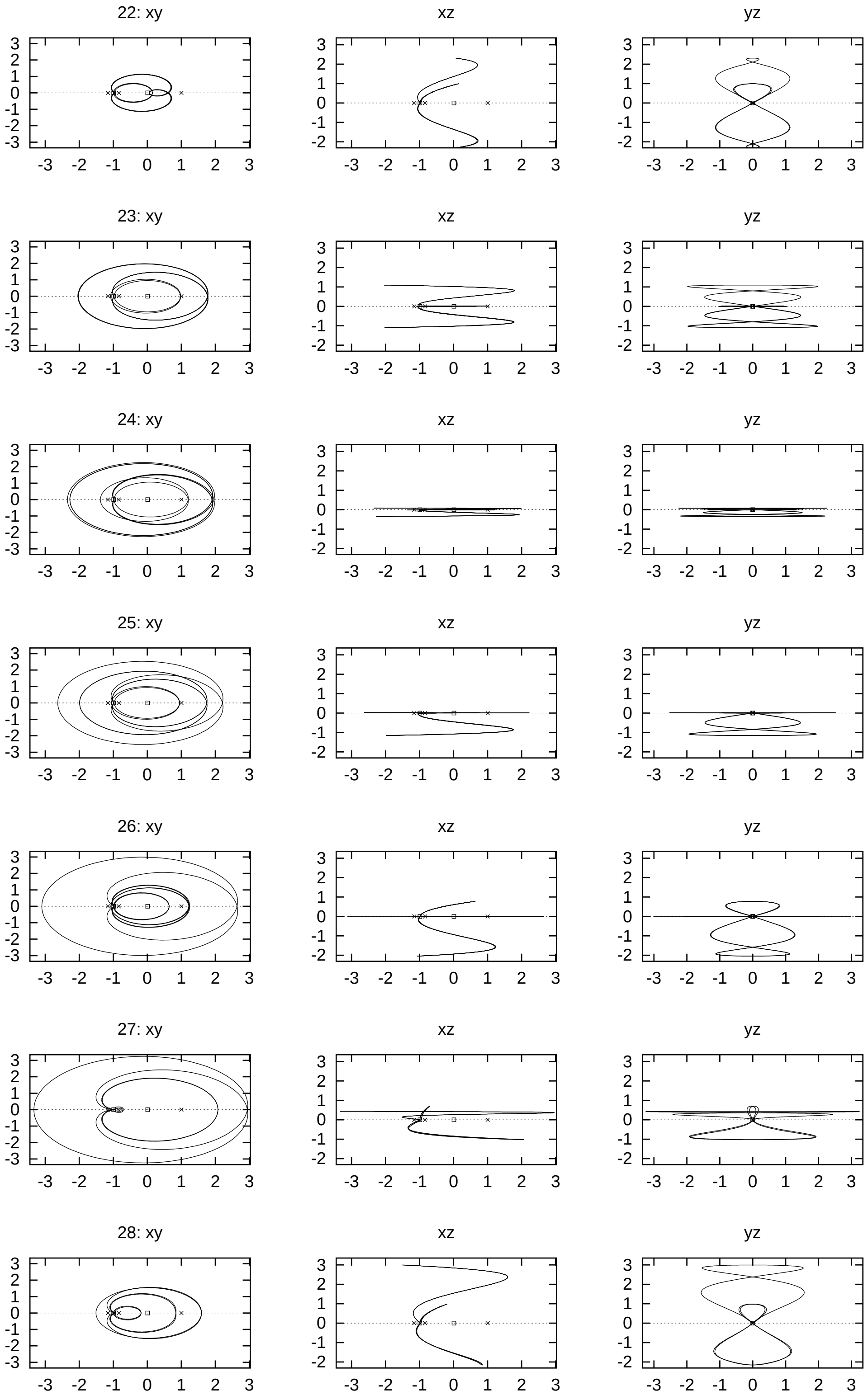

Figure D.34: Orbits labeled 22,. . . ,28 in figure D.30.

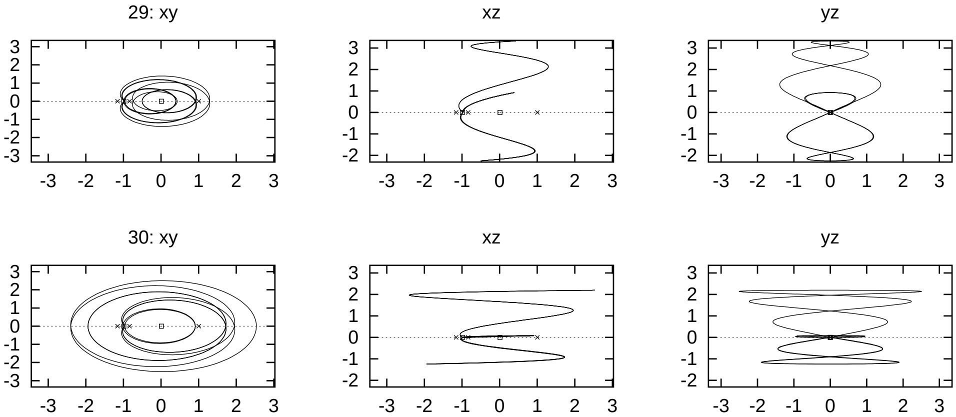

Figure D.35: Orbits labeled 29,30 in figure D.30.

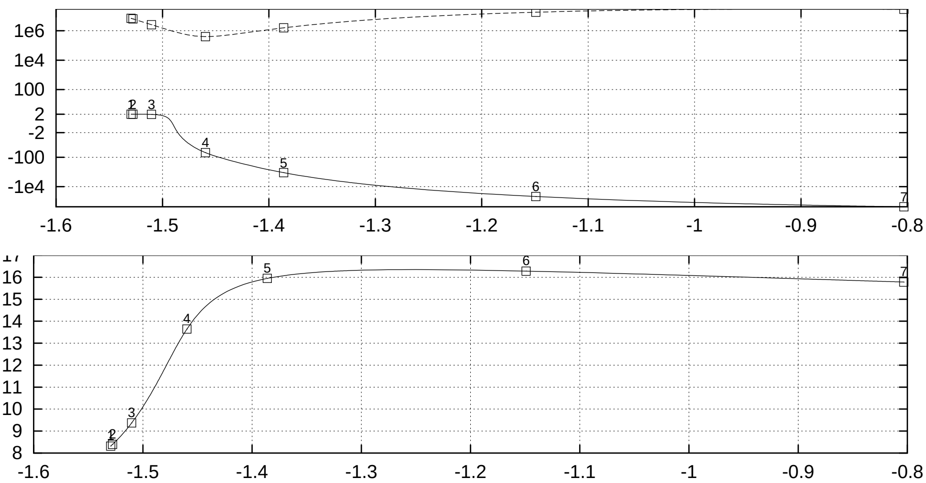

Figure D.36: Top: energy vs. stability parameters of the elliptic bifurcation by period triplication of the halo family of L_1. Bottom: energy vs. period for the same family. The square points refer to the orbits displayed in Fig. D.37.

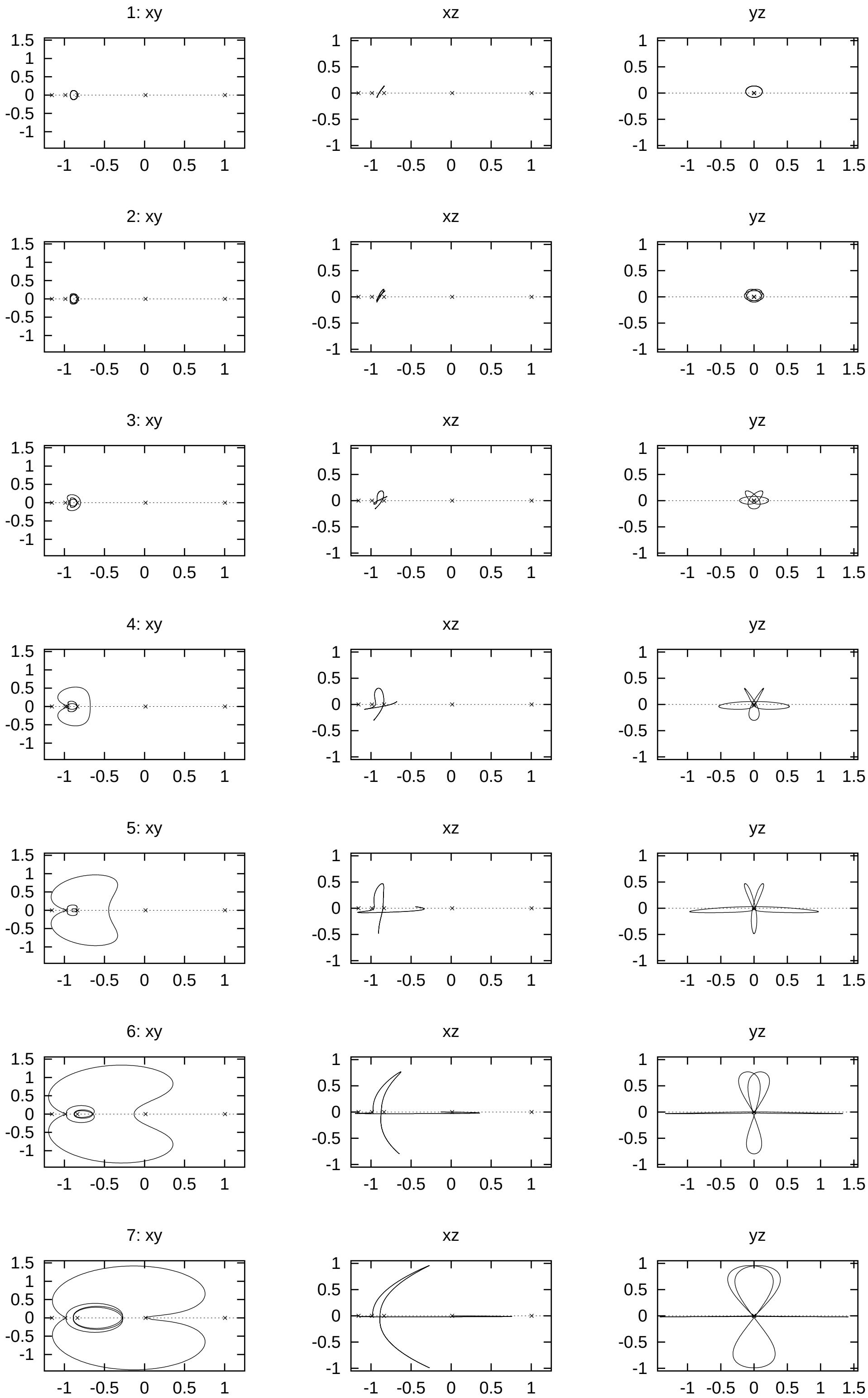

Figure D.37: Projections of the orbits labeled 1,...,7 in figure D.36.

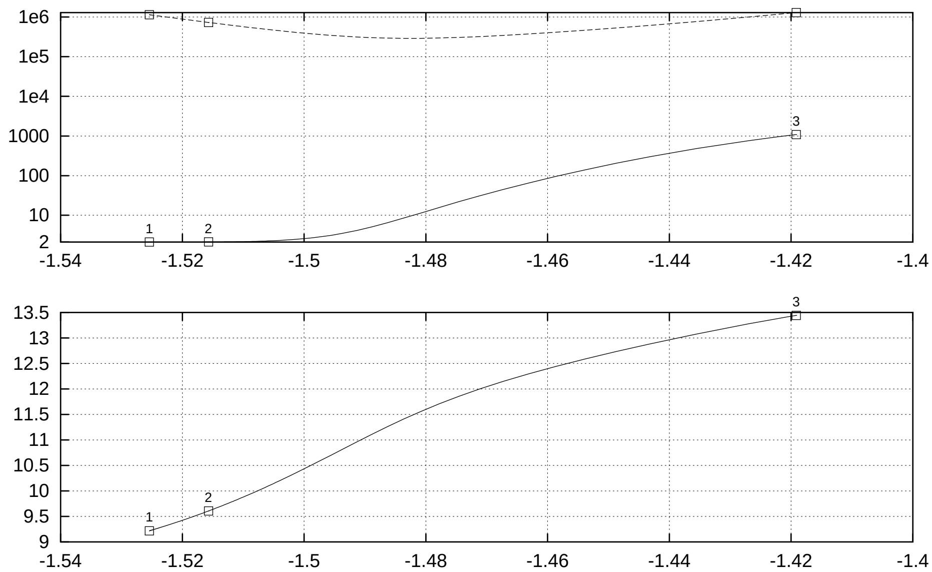

Figure D.38: Top: energy vs. stability parameters of the hyperbolic bifurcation by period triplication of the L_2 halo family. Bottom: energy vs. period for the same family. The square points refer to the orbits displayed in figure D.39.

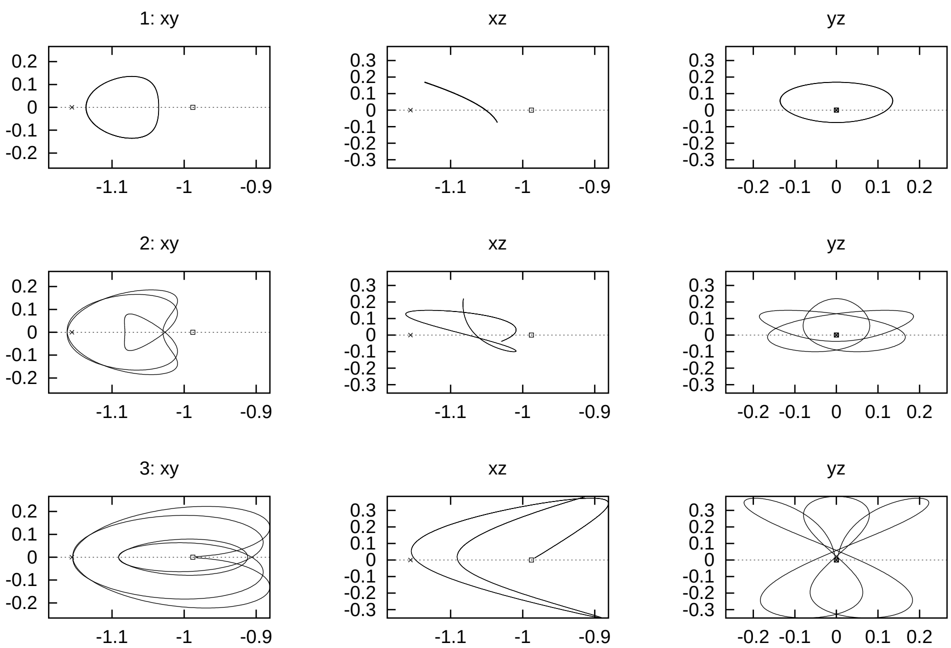

Figure D.39: Projections of the orbits labeled 1,. . . ,3 in figure D.38.

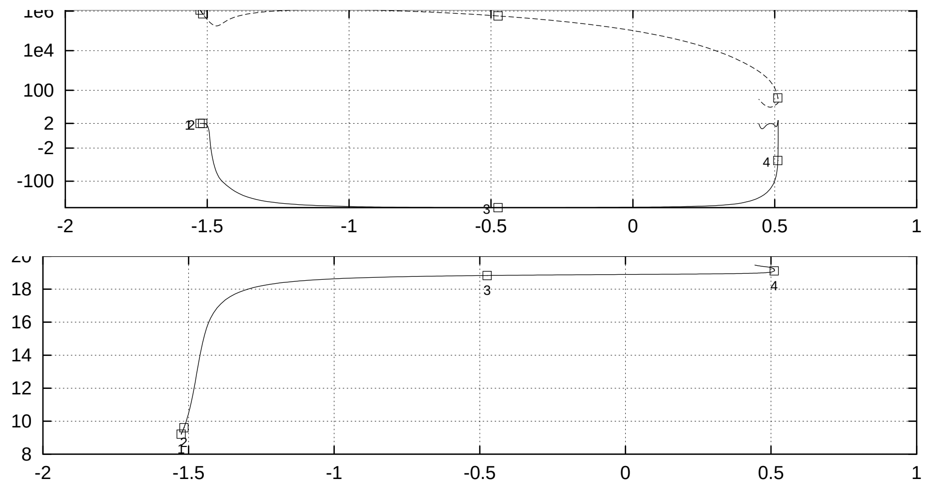

Figure D.40: Top: energy vs. stability parameters of the elliptic bifurcation by period triplication of the L_2 halo family. Bottom: energy vs. period for the same family. The square points refer to the orbits displayed in figure D.41.

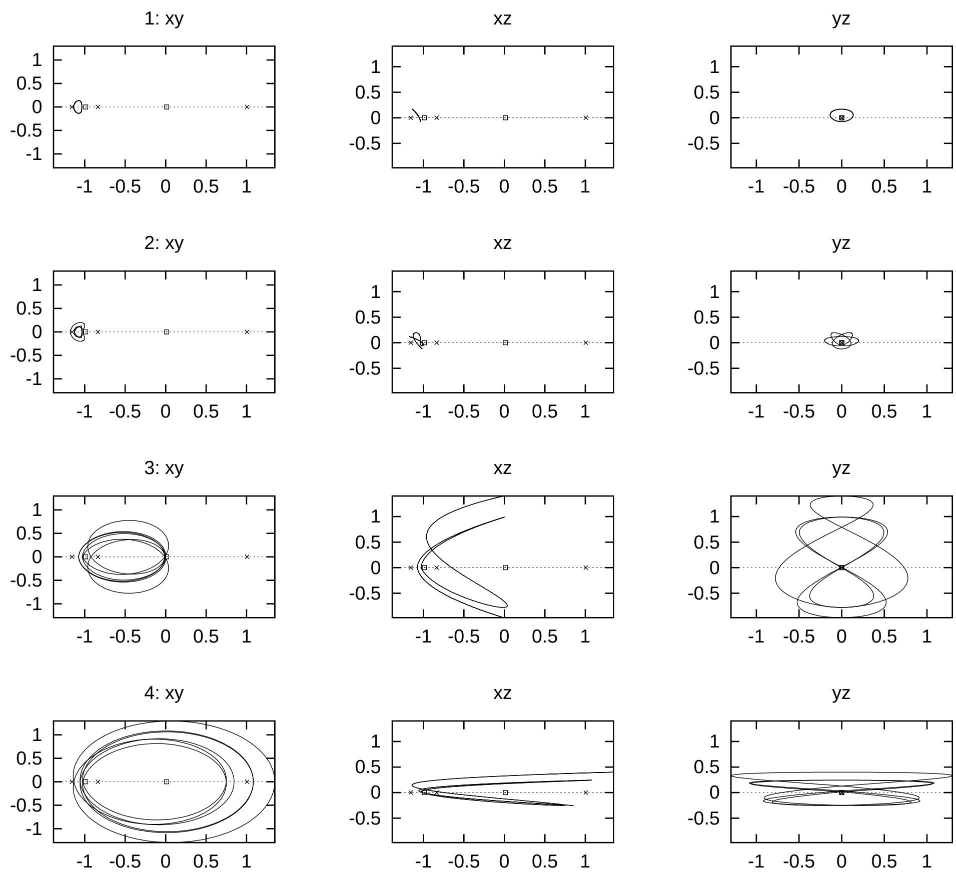

Figure D.41: Projections of the orbits labeled 1,. . . ,4 in figure D.40.

Apèndix E

Resum

La primera part d'aquest treball està dedicada al desenvolupament i estudi d'un procediment per al càlcul acurat de les freqüències d'una funció quasi periòdica, així com dels coeficients de Fourier associats, usant com a única entrada un mostreig equiespaiat de la funció analitzada sobre un interval de temps finit.

La primera tècnica per la determinació acurada de freqüències ha estat introduïda per J. Laskar ([18], [20], [19]). Està basada en la maximització de la fórmula que dóna els coeficients de Fourier d'una funció respecte de l'harmònic, però considerant aquest últim com a quantitat real. Aquest procediment ha estat aplicat a l'estudi de la dinàmica a llarg termini del Sistema Solar ([18]), així com a l'estudi de models químics i d'acceleradors de partícules, a través del càlcul d'*aplicacions de freqüències* ([19]). Metodologia addicional ha estat introduïda en [12],[13],[10],[11]. En aquests treballs, la determinació de freqüències ha estat aplicada al desenvolupament de models semianalítics per al moviment en el Sistema Solar.

El nostre procediment pren la metodologia desenvolupada en [12],[13],[10],[11] com a punt de partida. Està basat en imposar igualtat entre la Transformada Discreta de Fourier (DFT) de la funció analitzada i l'aproximació quasiperiòdica que s'està calculant. Hem obtingut estimacions de l'error que hem il·lustrat amb exemples numèrics. A més, en la línia dels treballs mencionats abans, hem aplicat el nostre procediment al desenvolupament de models simplificats de moviment en el Sistema Solar.

La segona part d'aquest treball està dedicada a l'estudi de la dinàmica en l'entorn dels punts d'equilibri colineals del Problema Restringit de Tres Cossos (RTBP) tridimensional, per al paràmetre de masses Terra–Lluna.

El primer estudi sistemàtic d'aquest veïnatge ha estat realitzat a [10] i [16], usant com a eina la reducció a la varietat central dels punts d'equilibri colineals. Aquest és un procediment semianalític, en el qual la regió que pot ser explorada es veu limitada per la convergència de les expansions obtingudes. La mateixa metodologia ha estat aplicada a l'estudi dels punts d'equlibri colineals d'un model per al sistema Terra–Lluna, anomentat Problema Quasibicircular ([3]). En aquest darrer estudi, les restriccions de convergència encara són més severes.

En aquest treball, continuem les famílies d'òrbites periòdiques i tors invariants bidimensionals de les varietats centrals dels tres punts de libració colineals. D'aquesta manera, podem estendre l'anàlisi de l'espai de fase fet a [10] i [16] a un rang més gran de valors

de l'energia, que ara inclou diverses bifurcacions i el punt d'equilibri L_3. La metodologia usada per al càlcul de tors invariants es basa en [7], amb algunes modificacions per a tenir en compte excitacions variables i paràmetres addicionals necessaris per la nostra exploració. Hem seguit estratègies de computació paral·lela degut als grans requeriments de càlcul. Els càlculs s'han dut a terme a HIDRA, un dels Beowulf clusters del grup de Sistemes Dinàmics de Barcelona.

E.1 Anàlisi de Fourier de funcions quasiperiòdiques

Donats N valors $\{f(t_l)\}_{l=0}^{N-1}$, $t_l = l\frac{T}{N} \in [0,T]$ de certa funció $f(t)$, que suposem quasiperiòdica, volem trobar una aproximació trigonomètrica polinomial amb un nombre de freqüències fixat,

$$Q_f(t) = A_0^c + \sum_{l=1}^{N_f} (A_l^c \cos(\frac{2\pi\nu_l t}{T}) + A_l^s \sin(\frac{2\pi\nu_l t}{T})).$$

En aquesta secció descriurem el nostre procediment d'anàlisi de Fourier per a trobar les freqüències $\{\nu_l\}_{l=1}^{N_f}$ i les amplituds $\{A_l^c\}_{l=0}^{N_f}$, $\{A_l^s\}_{l=1}^{N_f}$. Després d'introduir notació, descriurem les tres etapes en les que es divideix: primera aproximació de freqüències, càlcul de les amplituds corresponents i refinament conjunt de freqüències i amplituds. Finalitzarem la secció amb la descripció de l'algorisme a dur a terme.

E.1.1 Notacions per la DFT

Denotarem els coeficients de la Transformada Discreta de Fourier (DFT) de N punts de f a l'interval $[0,T]$ per

$$\begin{aligned} c_{f,T,N}(j) &= \frac{2}{N}\sum_{l=0}^{N-1} f(t_l)\cos(2\pi\frac{j}{N}l), \quad j = 0, ..., N/2, \\ s_{f,T,N}(j) &= \frac{2}{N}\sum_{l=0}^{N-1} f(t_l)\sin(2\pi\frac{j}{N}l), \quad j = 1, ..., N/2-1. \end{aligned}$$

De vegades treballarem amb la forma complexa de la DFT, que notarem com

$$F_{f,T,N}(j) = \frac{1}{N}\sum_{l=0}^{N-1} f(t_l)e^{-2\pi i \frac{j}{T} t_l}, \quad j = 0, ..., N-1.$$

De cara a reduir *leakage*, treballarem amb les versions filtrades de les anteriors transformades, que denotarem com

$$\begin{aligned} F_{f,T,N}^{n_h}(j) &= F_{H^{n_h}f,T,N}(j), \\ c_{f,T,N}^{n_h}(j) &= c_{H^{n_h}f,T,N}(j), \\ s_{f,T,N}^{n_h}(j) &= s_{H^{n_h}f,T,N}(j). \end{aligned}$$

on $H_T^{n_h}$ són les *funcions de Hanning d'ordre* n_h,

$$H_T^{n_h}(t) = q_{n_h}\left(1 - \cos\left(2\pi\frac{1}{T}t\right)\right)^{n_h},$$

amb

$$q_{n_h} = \left[\frac{1}{T}\int_0^T \left(1 - \cos\left(2\pi\frac{1}{T}t\right)\right)^{n_h} dt\right]^{-1} = \frac{n_h!}{(2n_h-1)!!}.$$

E.1.2 Primera aproximació de freqüències

Consisteix a cercar màxims locals del mòdul de la DFT filtrada, $|F_{f,T,N}^{n_h}(j)|$, de la funció analitzada, suposant que j pren valors reals. La maximització es duu a terme emprant el mètode de Newton. Es prenen els "pics" de la DFT com a aproximacions inicials, és a dir, donat j_0 tal que $|F_{f,T,N}^{n_h}(j_0-1)| < |F_{f,T,N}^{n_h}(j_0)| < |F_{f,T,N}^{n_h}(j_0+1)|$, prenem j_0 com a aproximació inicial.

E.1.3 Càlcul de les amplituds suposant freqüències conegudes

Un cop coneixem les freqüències $\{\nu_l\}_{l=1}^{N_f}$, trobem les amplituds $\{A_l^c\}_{l=0}^{N_f}$, $\{A_l^s\}_{l=1}^{N_f}$ imposant que la DFT de l'aproximació quasiperiòdica actual Q_f coindeixi amb la DFT de les mostres $\{f(t_l)\}_{l=0}^{N-1}$ sobre harmònics adequats. Amb la finalitat d'obtenir un sistema quadrat per a les $1 + 2N_f$ incògnites, seleccionem valors per als harmònics j de manera que obtenim

$$\begin{array}{rcl} A_0^c + \displaystyle\sum_{l=1}^{N_f}\left(A_l^c\overline{c}_{\nu_l,N}^{n_h}(0) + A_l^s\widetilde{c}_{\nu_l,N}^{n_h}(0)\right) &=& c_{f,T,N}^{n_h}(0), \\ A_0^c c_1^{n_h}(j_i) + \displaystyle\sum_{l=1}^{N_f}\left(A_l^c\overline{c}_{\nu_l,N}^{n_h}(j_i) + A_l^s\widetilde{c}_{\nu_l,N}^{n_h}(j_i)\right) &=& c_{f,T,N}^{n_h}(j_i), \\ \displaystyle\sum_{l=1}^{N_f}\left(A_l^c\overline{s}_{\nu_l,N}^{n_h}(j_i) + A_l^s\widetilde{s}_{\nu_l,N}^{n_h}(j_i)\right) &=& s_{f,T,N}^{n_h}(j_i), \end{array}$$

on

$$\begin{array}{rclrcl} c_1^{n_h}(j) &=& c_{1,T,N}^{n_h}(j), && & \\ \overline{c}_{\nu,N}^{n_h}(j) &=& c_{\cos(\frac{2\pi\nu}{T}),T,N}^{n_h}(j), & \overline{s}_{\nu,N}^{n_h}(j) &=& s_{\cos(\frac{2\pi\nu}{T}),T,N}^{n_h}(j), \\ \widetilde{c}_{\nu,N}^{n_h}(j) &=& c_{\sin(\frac{2\pi\nu}{T}),T,N}^{n_h}(j), & \widetilde{s}_{\nu,N}^{n_h}(j) &=& s_{\sin(\frac{2\pi\nu}{T}),T,N}^{n_h}(j), \end{array}$$

i els j_i s'escullen com els enters més propers a ν_i, és a dir, tals que $|j_i - \nu_i| \leq 1/2$ per $i = 1 \div N_f$.

E.1.4 Refinament conjunt de freqüències i amplituds

Donades aproximacions de freqüències i amplituds, les podem refinar simultàniament resolent un sistema d'equacions similar a l'emprat a la secció anterior. Ara necessitem una condició addicional per cada freqüència, donat que les freqüències són desconegudes. Per tant, resolem iterativament el sistema

$$
\begin{array}{rcccccccl}
A_0^c & + & \sum_{l=1}^{N_f} & (& A_l^c \overline{c}_{\nu_l,N}^{n_h}(0) & + & A_l^s \widetilde{c}_{\nu_l,N}^{n_h}(0) &) & = c_{f,T,N}^{n_h}(0), \\
A_0^c c_1^{n_h}(j_i) & + & \sum_{l=1}^{N_f} & (& A_l^c \overline{c}_{\nu_l,N}^{n_h}(j_i) & + & A_l^s \widetilde{c}_{\nu_l,N}^{n_h}(j_i) &) & = c_{f,T,N}^{n_h}(j_i), \\
 & & \sum_{l=1}^{N_f} & (& A_l^c \overline{s}_{\nu_l,N}^{n_h}(j_i) & + & A_l^s \widetilde{s}_{\nu_l,N}^{n_h}(j_i) &) & = s_{f,T,N}^{n_h}(j_i), \\
A_0^c cs_1^{n_h}(j_i^+) & + & \sum_{l=1}^{N_f} & (& A_l^c \overline{cs}_{\nu_l,N}^{n_h}(j_i^+) & + & A_l^s \widetilde{cs}_{\nu_l,N}^{n_h}(j_i^+) &) & = cs_{f,T,N}^{n_h}(j_i^+),
\end{array}
\tag{E.1}
$$

per $\{\nu_l\}_{l=1}^{N_f}$, $\{A_l^c\}_{l=0}^{N_f}$, $\{A_l^s\}_{l=1}^{N_f}$, on j_i i j_i^+ es defineixen com

$$
\begin{array}{ll}
j_i = [\nu_i],\ j_i^+ = [\nu_i] + 1 & \text{si } \nu_i - [\nu_i] \leq 1/2, \\
j_i = [\nu_i] + 1,\ j_i^+ = [\nu_i] & \text{altrament},
\end{array}
$$

per $i = 1 \div N_f$. En la darrera equació de (E.1), cs denota c o s; el criteri per escollir un o l'altre es dóna més endavant.

Si $j_i \geq 1 + n_h$ per $i = 1 \div N_f$, la diferencial de (E.1) respecte de les incògnites

$$
\begin{pmatrix} A_0^c & \nu_1 & A_1^c & A_1^s & \ldots & \nu_{N_f} & A_{N_f}^c & A_{N_f}^s \end{pmatrix},
$$

que es necessita per a poder aplicar el mètode de Newton, es pot escriure com

$$
M = \begin{pmatrix} 2 & v_1 & \ldots & v_{N_f} \\ 0 & B_1^1 & \ldots & B_{N_f}^1 \\ \vdots & \vdots & \ddots & \vdots \\ 0 & B_1^{N_f} & \ldots & B_{N_f}^{N_f} \end{pmatrix},
$$

essent

$$
\begin{array}{rcl}
v_l & = & \begin{pmatrix} A_l^c \partial \overline{c}_{\nu_l,N}^{n_h}(0) + A_l^s \partial \widetilde{c}_{\nu_l,N}^{n_h}(0) & \overline{c}_{\nu_l,N}^{n_h}(0) & \widetilde{c}_{\nu_l,N}^{n_h}(0) \end{pmatrix}, \\
B_{i,l} & = & \begin{pmatrix} A_l^c \partial \overline{c}_{\nu_l,N}^{n_h}(j_i) + A_l^s \partial \widetilde{c}_{\nu_l,N}^{n_h}(j_i) & \overline{c}_{\nu_l,N}^{n_h}(j_i) & \widetilde{c}_{\nu_l,N}^{n_h}(j_i) \\ A_l^c \partial \overline{s}_{\nu_l,N}^{n_h}(j_i) + A_l^s \partial \widetilde{s}_{\nu_l,N}^{n_h}(j_i) & \overline{s}_{\nu_l,N}^{n_h}(j_i) & \widetilde{s}_{\nu_l,N}^{n_h}(j_i) \\ A_l^c \partial \overline{cs}_{\nu_l,N}^{n_h}(j_i^+) + A_l^s \partial \widetilde{cs}_{\nu_l,N}^{n_h}(j_i^+) & \overline{cs}_{\nu_l,N}^{n_h}(j_i^+) & \widetilde{cs}_{\nu_l,N}^{n_h}(j_i^+) \end{pmatrix},
\end{array}
$$

on ∂ denota derivada respecte ν.

Per cada bloc $B_{i,l}$, el criteri emprat per escollir cs entre c i s és prendre el que minimitza $\|B_{i,i}^{-1}\|_\infty$. Això assegura que el sistema (E.1) és no singular i, sota hipòtesis adequades, ben condicionat.

E.1.5 Algorisme

A partir de les mostres $\{f(t_l)\}_{l=0}^{N-1}$ d'una funció de la que es coneix comportament quasiperiòdic, portem a terme la seva anàlisi de Fourier aplicant els tres passos descrits anteriorment. De cara a evitar que algunes freqüències "amaguin" freqüències properes d'amplitud inferior, convé procedir de manera iterativa, de manera que a cada iteració només considerem les freqüències amb amplitud per sobre d'una determinada tolerància. Concretament, l'algorisme que usarem és el següent:

Algorisme E.1.1 *Donada una amplitud mínima b_{min} per a les freqüències per calcular, i un nombre d'iteracions n per al procediment, defineixi's*

$$p_{max} = \max_{j=1\div\frac{N}{2}} p^{n_h}_{f,T,N}(j), \qquad db = (b_{min}/p_{max})^{1/n},$$

i

$$Q_f(t) = 0, \qquad b = p_{max}, \qquad N_f = 0.$$

$Q_f(t)$ serà l'aproximació quasiperiòdica actual, b l'amplitud mínima de les freqüències per detectar en la iteració actual i N_f el nombre de freqüències que es calcularan. Aleshores, mentre $b > b_{min}$,

1. *Assigni's $b \leftarrow b\cdot db$. Siguin $k_{N_f+1},\ldots,\ k_{N_f+m}$ els pics del mòdul de la DFT de $f-Q_f$ amb amplitud mínima b, o sigui, $\{k_{N_f+1},\ldots k_{N_f+m}\} = \{j\in\mathbb{Z} : n_h+2 \le j \le \frac{N}{2}-n_h-2,\ p^{n_h}_{f-Q_f,T,N}(j)\ge b,\ p^{n_h}_{f-Q_f,T,N}(j-1)\le p^{n_h}_{f-Q_f,T,N}(j)\le p^{n_h}_{f-Q_f,T,N}(j+1)\}$. Per cada k_l, apliqui's el procediment de la Secció E.1.2 per obtenir ν_l.*

2. *Resolgui's (E.1.3), d'acord amb la Secció E.1.3, per obtenir $\{A^c_l\}_{l=0}^{N_f+m}$, $\{A^s_l\}_{l=1}^{N_f+m}$ a partir de $\{\nu_l\}_{l=1}^{N_f+m}$.*

3. *Resolgui's (E.1), d'acord amb la Secció E.1.4 per a refinar iterativament $\{\nu_l\}_{l=1}^{N_f+m}$, $\{A^c_l\}_{l=0}^{N_f+m}$, $\{A^s_l\}_{l=1}^{N_f+m}$.*

4. *Actualitzi's el nombre de freqüències i l'aproximació quasiperiòdica actual*

$$N_f \leftarrow N_f + m, \qquad Q_f(t) = A^c_0 + \sum_{l=1}^{N_f}(A^c_l\cos(\frac{2\pi\nu_l t}{T}) + A^s_l\sin(\frac{2\pi\nu_l t}{T}))$$

   i vagi's al pas 1.

Aturem l'algorisme si

- *N_f atansa un nombre màxim de freqüències donat, o si*
- $\max_{l=0\div N-1}|f(t_l)-Q_f(t_l)|$ *és més petit que una tolerància donada, o si*
- $\max_{j=0\div j/2} p^{n_h}_{f-Q_f,T,N}(j)$ *és més petit que una tolerància donada, o si*
- *detectem dues freqüències massa properes. Usualment, considerarem que ν_{l_1}, ν_{l_2} són massa properes si $|\nu_{l_1}-\nu_{l_2}| < 2+n_h$.*

E.1.6 Estudi de l'error

En aquesta secció enunciem un teorema que dóna fites de l'error per als procediments descrites en les seccions E.1.3 i E.1.4. Abans necessitem una definició auxiliar.

Definició E.1.1 *Per $j_1, j_2, \alpha, \delta > 0$ definim les funcions*

$$\begin{aligned} G_f(j_1,j_2,\alpha,\delta) &= \frac{1}{\delta^{\alpha+1}}\chi_{\{j_1\le\frac{\alpha}{\delta}-1\}}\Big(\gamma(\alpha+1,\delta\min([\frac{\alpha}{\delta}]_{j_1},j_2+1))-\gamma(\alpha+1,\delta j_1)\Big)+\\ &\quad \chi_{\{j_1\le\frac{\alpha}{\delta},j_2>\frac{\alpha}{\delta}-1\}}([\frac{\alpha}{\delta}]_{j_1})^\alpha e^{-\delta[\frac{\alpha}{\delta}]_{j_1}}+\\ &\quad \chi_{\{j_1<\frac{\alpha}{\delta}+1,j_2>\frac{\alpha}{\delta}\}}([\frac{\alpha}{\delta}]_{j_1}+1)^\alpha e^{-\delta([\frac{\alpha}{\delta}]_{j_1}+1)}+\\ &\quad \frac{1}{\delta^{\alpha+1}}\chi_{\{j_2>\frac{\alpha}{\delta}+1\}}\Big(\gamma(\alpha+1,\delta j_2)-\gamma(\alpha+1,\max([\frac{\alpha}{\delta}]_{j_1}+1,j_1-1))\Big), \end{aligned}$$

i

$$\begin{aligned} G_\infty(j_1,\alpha,\delta) &= \frac{1}{\delta^{\alpha+1}}\chi_{\{j_1\le\frac{\alpha}{\delta}-1\}}\Big(\gamma(\alpha+1,\delta[\frac{\alpha}{\delta}]_{j_1})-\gamma(\alpha+1,\delta j_1)\Big)+\\ &\quad \chi_{\{j_1\le\frac{\alpha}{\delta}\}}([\frac{\alpha}{\delta}]_{j_1})^\alpha e^{-\delta[\frac{\alpha}{\delta}]_{j_1}}+\\ &\quad \chi_{\{j_1<\frac{\alpha}{\delta}+1\}}([\frac{\alpha}{\delta}]_{j_1}+1)^\alpha e^{-\delta([\frac{\alpha}{\delta}]_{j_1}+1)}+\\ &\quad \frac{1}{\delta^{\alpha+1}}\Gamma(\alpha+1,\delta\max([\frac{\alpha}{\delta}]_{j_1}+1,j_1-1)). \end{aligned}$$

En les fórmules anteriors, $\chi_{\{\text{condició}\}}$ *és igual a* 1 *si* condició *és certa i 0 altrament.*

Teorema E.1.1 *Suposem que duem a terme l'anàlisi de Fourier d'una funció quasi-periòdica analítica,*

$$f(t)=\sum_{k\in\mathbb{Z}^m} a_k e^{i2\pi\omega t},$$

que satisfà les estimacions de Cauchy amb constants $C, \delta > 0$,

$$|a_k| \le Ce^{-\delta|k|}, \tag{E.2}$$

i el vector de freqüències de la qual $\omega = (\omega_1, \ldots, \omega_m)$ satisfà una condició Diofantina de la forma

$$|k\omega| > \frac{D}{|k|^\tau}, \tag{E.3}$$

amb $D, \tau > 0$. Suposem que mostregem f en N punts equiespaiats a l'interval $[0, T]$, i que volem determinar les freqüències $Tk\omega$ amb $1 \le |k| \le r_0 - 1$, $Tk\omega > 0$, i les amplituds corresponents, de les que tenim aproximacions suficientment properes a les reals. Suposem que duem a terme el procediment de la Secció E.1.4 amb $n_h \ge 1$ i que obtenim una aproximació de f de la forma

$$p(t) = A_0^c + \sum_{l=1}^{N_f}\Big(A_l^c\cos(\frac{2\pi\nu_l t}{T}) + A_l^s\sin(\frac{2\pi\nu_l t}{T})\Big).$$

Suposem que N *és tal que* $N-T(2r_0-2)\|\omega\|_\infty > 3+n_h$*, i que* T *és tal que* $\frac{TD}{(2r_0-2)^\tau} > 3+n_h$ *i* $[\nu_{min}] > 2+n_h$*. Aleshores, l'error en freqüències amplituds, que denotem com* Δy*, es pot fitar, en l'aproximació de primer ordre, com*

$$\|\Delta y\| \lesssim \|M^{-1}\|\|\Delta b\|, \tag{E.4}$$

on

$$\|M^{-1}\| \le \frac{\|M_D^{-1}\|}{1-\|M_D^{-1}\|\|M_O\|}$$

i

$$\begin{aligned}
\|M_O\| \;\le\; & \frac{(n_h!)^2}{\pi}\Bigg(\frac{\sqrt{2}(\sum_{l=1}^{N_f} A_l)(\pi+\ln(\frac{TD}{(2r_0-2)^\tau}-1+n_h)-\ln(\frac{TD}{(2r_0-2)^\tau}-2-n_h))+2N_f}{(\frac{TD}{(2r_0-2)^\tau}-1-n_h)^{1+2n_h}} \\
& +\frac{\sqrt{2}(\sum_{l=1}^{N_f} A_l)(\pi+\ln([\nu_{min}]+n_h)-\ln([\nu_{min}]-1-n_h))+2N_f}{([\nu_{min}]-n_h)^{1+2n_h}} \\
& +\frac{4\Big(\sqrt{2}(\sum_{l=1}^{N_f} A_l)(\pi+\ln(N-\Omega_0+n_h)-\ln(N-\Omega_0-1-n_h))+2N_f\Big)(1+\frac{1}{2n_h})}{(N-\Omega_0-n_h)^{1+2n_h}}\Bigg)
\end{aligned}$$

i

$$\|M_D^{-1}\| \le \frac{\|\mathcal{M}_D^{-1}\|}{1-\|\mathcal{M}_D^{-1}\|\varepsilon_1}, \qquad \|\mathcal{M}_D^{-1}\| \le \frac{\|\mathfrak{M}_D^{-1}\|}{1-\|\mathfrak{M}_D^{-1}\|\varepsilon_2}, \qquad \|\mathfrak{M}_D^{-1}\| \le \frac{G_{n_h}}{\min(1,A_{min})},$$

amb G_{n_h} *donades per la taula E.1, essent*

$$\begin{aligned}
\varepsilon_1 &= \frac{4(n_h!)^2\Big(\sqrt{2}A_{max}(\pi+\ln(N-\Omega_0+n_h)-\ln(N-\Omega_0-1-n_h))+2\Big)(1+\frac{1}{2n_h})}{\pi(N-\Omega_0-n_h)^{1+2n_h}}, \\
\varepsilon_2 &= \frac{(n_h!)^2\Big(\sqrt{2}A_{max}(\pi+\ln(2[\nu_{min}]+n_h)-\ln(2[\nu_{min}]-n_h-1))+2\Big)}{\pi(2[\nu_{min}]-n_h)^{1+2n_h}}, \\
\Omega_0 &= T(2r_0-2)\|\omega\|_\infty+1,
\end{aligned}$$

Pel que fa a $\|\Delta b\|$*,*

$$\begin{aligned}
\|\Delta b\| \;\le\; & \frac{2^{m+1}C}{(m-1)!}\Bigg(\\
& \chi_{\{r_*>r_0\}}\frac{(n_h!)^2e^{\delta(r_0-1)}\sum_{l=0}^{m-1}\binom{m-1}{l}(\frac{m}{2}-r_0+1)^{m-1-l}G_f(2r_0-1,r_0+r_*-2,l+\tau(1+2n_h),\delta)}{E_*\pi(TD)^{1+2n_h}} \\
& +\chi_{\{r_*>r_0\}}\frac{2(n_h!)^2e^{\delta\frac{m}{2}}(1+\frac{1}{2n_h})G_f(r_0+\frac{m}{2},r_*-1+\frac{m}{2},m-1,\delta)}{\pi(N-\Omega-n_h)^{1+2n_h}} \\
& +e^{\delta\frac{m}{2}}G_\infty(r_*+\frac{m}{2},m-1,\delta)\Bigg),
\end{aligned} \tag{E.5}$$

on

$$\begin{aligned}
\Omega &= T(r_* + r_0 - 2)\|\omega\|_\infty + 1 \\
r_* &= \max\Big(r_0, \min\Big(\Big[\Big(\frac{TD}{\max((\frac{(n_h!)^2}{\pi})^{\frac{1}{1+2n_h}} + 1 + n_h, 2(1+n_h))}\Big)^{\frac{1}{\tau}} - r_0 + 2\Big], \\
&\qquad \Big[\frac{N-1-n_h}{T\|\omega\|_\infty} - r_0 + 1\Big]\Big)\Big) \qquad \text{(E.6)} \\
E_* &= \frac{(z_* - 1 - n_h)^{1+2n_h}}{z_*^{1+2n_h}}, \\
z_* &= \frac{TD}{(r_* + r_0 - 2)^\tau},
\end{aligned}$$

i les G_f, G_∞ corresponen a la Definició E.1.1.

Si suposem que les freqüències $\{Tk\omega\}_{|k|\le r_0-1}$ són conegudes i volem calcular les amplituds usant el procediment descrit a la Secció E.1.3, la fórmula (E.4) encara és vàl·lida, on les fites per $\|\Delta b\|$ es poden prendre com abans i les fites per $\|M^{-1}\|$ són donades per

$$\|M^{-1}\| \le \frac{\|M_D^{-1}\|}{1 - \|M_D^{-1}\|\|M_O\|}$$

essent

$$\begin{aligned}
\|M_O\| \le \frac{N_f(n_h!)^2}{\pi}\Big(&\frac{\sqrt{2}}{\pi(\frac{TD}{(2r_0-1)^\tau} - \frac{1}{2} - n_h)^{1+2n_h}} + \frac{2}{\pi([\nu_{min}] - n_h)^{1+2n_h}} \\
&+ \frac{8(1+\frac{1}{2n_h})}{\pi(N - T(2r_0-2)\|\omega\|_\infty - \frac{1}{2} - n_h)^{1+2n_h}}\Big)
\end{aligned}$$

i

$$\|M_D^{-1}\| \le \frac{\|\mathcal{M}_D^{-1}\|}{1 - \|\mathcal{M}_D^{-1}\|\varepsilon_1}, \qquad \|\mathcal{M}_D^{-1}\| \le \frac{\|\mathfrak{M}_D^{-1}\|}{1 - \|\mathfrak{M}_D^{-1}\|\varepsilon_2}, \qquad \|\mathfrak{M}_D^{-1}\| \le \frac{5}{3},$$

essent

$$\varepsilon_1 = \frac{8(n_h!)^2(1+\frac{1}{2n_h})}{\pi(N - T(2r_0-2)\|\omega\|_\infty - \frac{1}{2} - n_h)^{1+2n_h}}, \qquad \varepsilon_2 = \frac{2(n_h!)^2}{\pi(2[\nu_{min}] - n_h)^{1+2n_h}}.$$

n_h	0	1	2	3
G_{n_h}	4.84	8.83	13.3	17.7

Taula E.1: Valors de les constants G_{n_h} per $n_h = 0, \dots, 3$.

E.1.7 Un exemple numèric

Amb la finalitat d'il·lustrar els procediments descrits i verificar les fites de l'error obtingudes, hem analitzat una família de funcions quasiperiòdiques per les quals els coeficients de Fourier es poden calcular explícitament. Les funcions són

$$f_\mu(t) = \frac{\sin(2\pi\omega_1 t + \varphi_1)}{1 - \mu\cos(2\pi\omega_1 t)} \cdot \frac{\sin(2\pi\omega_2 t + \varphi_2)}{1 - \mu\cos(2\pi\omega_2 t)}, \qquad \mu \in [0, 1).$$

Verifiquen $f_\mu(t) = \sum_{k\in\mathbb{Z}^2} a_k^{\mu,\varphi} e^{2\pi i(\omega,k)t}$, amb

$$a_k^{\mu,\varphi} = \begin{cases} \frac{-\operatorname{signe}(k_1k_2)}{\mu^2} c_2^{|k|} e^{i(k,\varphi)} & \text{si } k_1, k_2 \neq 0 \\ 0 & \text{si } k_1 = 0 \text{ o } k_2 = 0 \end{cases}$$

essent

$$\omega = (\omega_1, \omega_2), \quad \varphi = (\varphi_1, \varphi_2) \quad \text{i} \quad c = \frac{1 - \sqrt{1-\mu^2}}{\mu}$$

El paràmetre μ està directament relacionat amb el paràmetre δ de les estimacions de Cauchy (E.2), concretament

$$\delta = \operatorname{Im} \arccos \frac{1}{\mu} = -\log c.$$

Hem aplicat l'algorisme descrit a la Secció E.1.5 a les funcions f_μ per $\omega = (1, \sqrt{2})$, $\varphi = (0, 0)$ i diversos valors de μ, T i N. Per al valor escollit de ω, els paràmetres D i τ de la condició Diofantina (E.3) són 0.85355 i 1, respectivament. Hem aturat el procediment quan totes les freqüències d'ordre $|k| \leq 5$ han estat refinades. L'error de l'aproximació de Fourier, així com la fita corresponent, d'acord amb el Teorema E.1.1, es mostren a la Figura E.1.

S'ha de notar que l'error en freqüències i amplituds és molt menor que la diferència entre la funció analitzada f i l'aproximació quasiperiòdica Q_f obtinguda. Per exemple, en el cas de $\mu = 0.9$, de (E.1.7) se segueix que l'amplitud màxima de les freqüències no determinades és ${c_2}^6/\mu^2 = 0.6268$, mentre que el nostre procediment atansa errors tan petits com 10^{-14} per a alguns valors de T i N. Això es deu al fet que els errors de truncament del nostre procediment no provenen de la diferència $f - Q_f$ sinó de la seva DFT.

A la Figura E.1, la fita de l'error es troba diversos odres de magnitud per sobre de l'error real. Això és degut a la condició Diofantina, que dóna només una fita inferior per la diferència entre freqüències. Aquesta diferència atansa la condició Diofantina en molts pos casos, tal com es mostra a la Figura E.2. A la Figura E.3 avaluem la fita del Teorema E.1.1, però substituint el primer terme de la fita de $\|\Delta b\|$ per

$$\max_{i=1\div N_f} \max_{j=j_i,j_i^+} \frac{C(n_h!)^2}{\pi} \sum_{|k|=r_0}^{r_*-1} \frac{e^{-\delta|k|}}{(|Tk\omega - j| - n_h)^{1+2n_h}}. \tag{E.7}$$

Observem que en aquest cas l'error predit i l'error real són molt a prop.

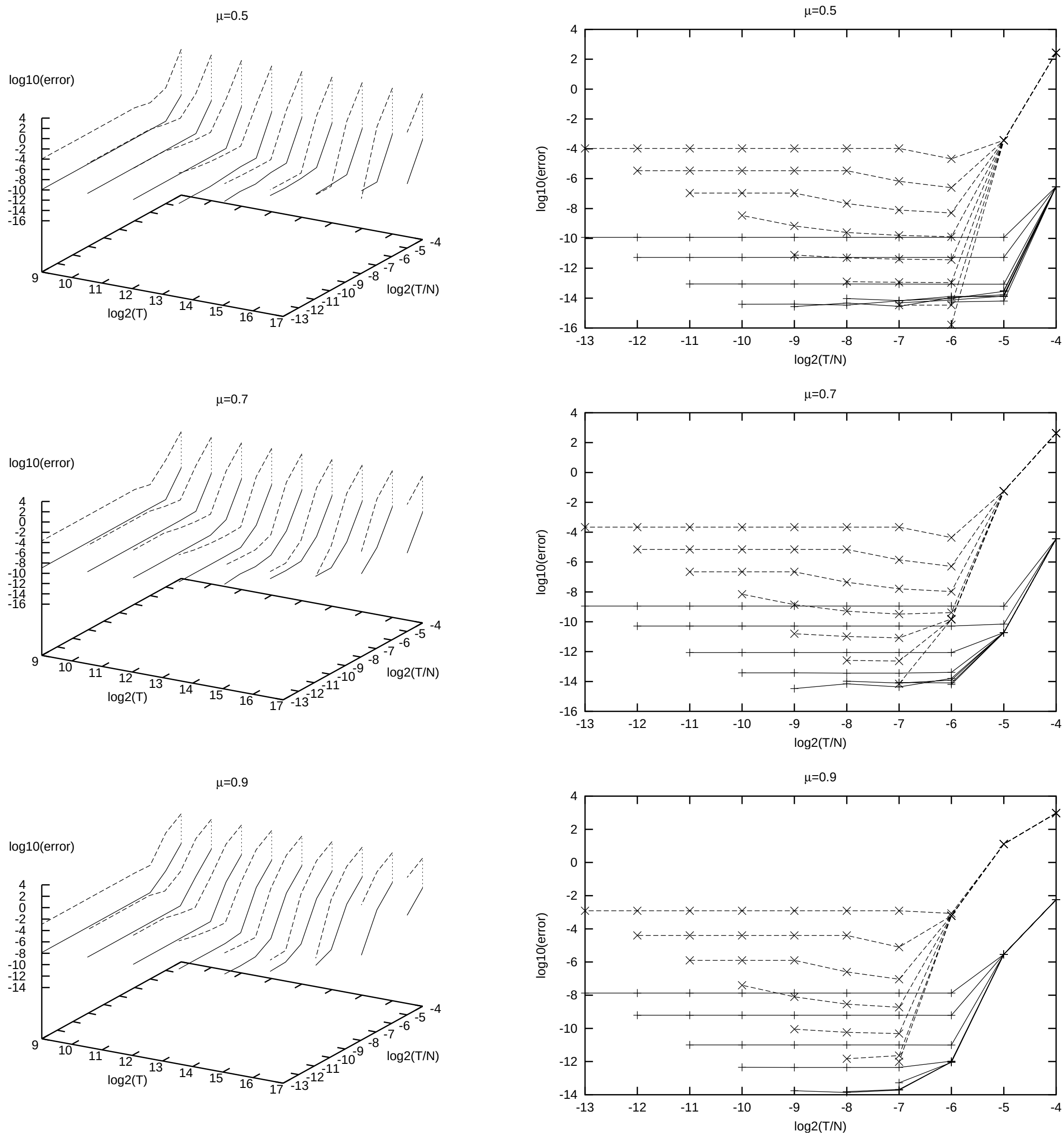

Figura E.1: Anàlisi de Fourier de les funcions f_μ per $\mu = 0.5, 0.7, 0.9$ i diversos valors de T i N. Els punts corresponents a anàlisis amb el mateix valor de T han estat units per línies. Les línies sòlides representen l'error en freqüències i amplituds de les corresponents anàlisis de Fourier. Això significa que hem representat el valor màxim entre l'error en les freqüències i l'error en les amplituds. Els punts units per línies puntejades corresponen a la fita donada pel teorema E.1.1. Les figures de la dreta són la projecció (y, z) de les figures de l'esquerra.

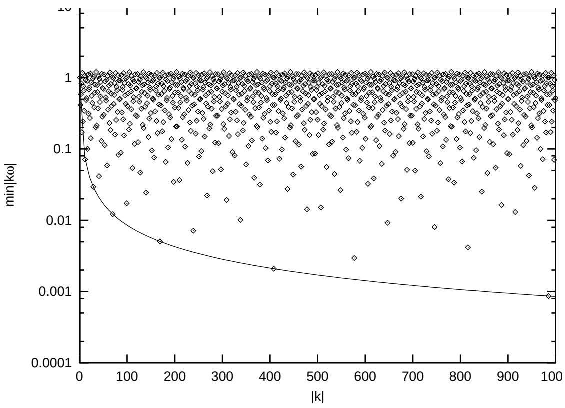

Figura E.2: Il·lustració de la no optimalitat de la condició Diofantina. Els punts representen els valors de $\min_{|k|=\text{const.}} |k\omega|$ per $|k| = 1 \div 1000$. La corba representa els valors de la condició Diofantina $0.85355/|k|$. Els únics punts que es troben aproximadament sobre la corba $0.85355/|k|$ corresponen als valors de $|k|$=1, 2, 5, 12, 29, 70, 169, 408, 985.

E.1.8 Aplicació al desenvolupament de models simplificats de moviment al Sistema Solar

En aquesta secció comentarem els resultats corresponents a l'aplicació del procediment d'anàlisi de Fourier introduit anteriorment al desenvolupament de models simplificats de moviment al Sistema Solar.

Denotarem els cossos del Sistema Solar com

$$\mathcal{S} = \{P_1, \ldots, P_9, P_{10}, P_{11}\} \tag{E.8}$$

on P_1,…,P_{11} denoten Mercuri, Venus, Terra, Mart, Júpiter, Saturn, Urà, Neptú, Plutó, la Lluna i el Sol, respectivament. Denotarem també la Terra, la Lluna i el Sol com E, M i S, respectivament. La massa de $P_I \in \mathcal{S}$ es denotarà com m_{P_I}.

De vegades estarem interessats en considerar la Terra i la Lluna com un únic cos, situat al baricentre Terra–Lluna. Denotarem aquest cos "virtual" com P_{12}. En aquest cas, considerarem un Sistema Solar "modificat",

$$\mathcal{S} = \{P_1, P_2, P_4, \ldots, P_9, P_{11}, P_{12}\}, \tag{E.9}$$

que denotem com abans per a reduir notació.

Considerem dos cossos $I, J \in \mathcal{S}$ (bé el sistema solar "real" o el "modificat") amb $m_I > m_J$, que anomenarem *primaris.* Podem escollir coordenades $(x, y, z)^\top$ i unitats de temps t tals que

- els cossos I, J romanen fixats a les posicions $(\mu_{I,J}, 0, 0)^\top$ i $(\mu_{I,J} - 1, 0, 0)^\top$, respectivament, essent
$$\mu_{I,J} = \frac{m_J}{m_I + m_J},$$
- el cos J completa una revolució al voltant de I en 2π unitats de temps.

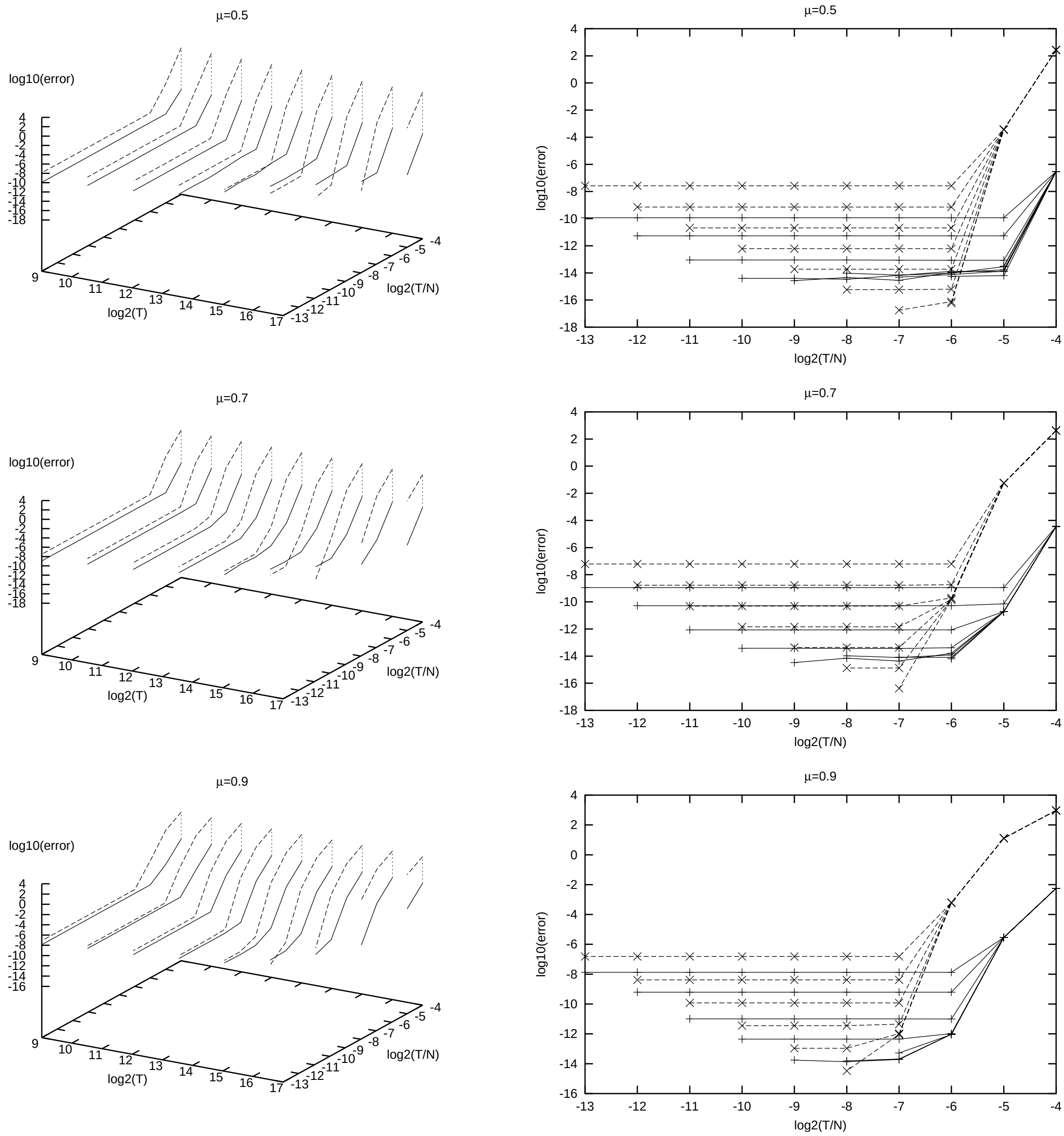

Figura E.3: Aquesta és la mateixa exploració que la de la Figura E.1, llevat que la fita de l'error representada per les línies puntejades s'obté substituint el primer terme de (E.5) per (E.7).

Aquestes coordenades seran anomenades *adimensionals*. En aquestes coordenades, les equacions del moviment d'una partícula sota l'atracció newtoniana dels cossos del Sistema Solar es pot escriure com

$$\left\{ \begin{array}{rcl} \ddot{x} & = & c_1 + c_4\dot{x} + c_5\dot{y} + c_7 x + c_8 y + c_9 z + c_{13}\dfrac{\partial\Omega}{\partial x}, \\ \ddot{y} & = & c_2 - c_5\dot{x} + c_4\dot{y} + c_6\dot{z} - c_8 x + c_{10} y + c_{11} z + c_{13}\dfrac{\partial\Omega}{\partial y}, \\ \ddot{z} & = & c_3 - c_6\dot{y} + c_4\dot{z} + c_9 x - c_{11} y + c_{12} z + c_{13}\dfrac{\partial\Omega}{\partial z}, \end{array} \right. \tag{E.10}$$

essent

$$\begin{aligned} \Omega \;=\; & \frac{1-\mu_{I,J}}{\sqrt{(x-\mu_{I,J})^2+y^2+z^2}} + \frac{\mu_{I,J}}{\sqrt{(x-\mu_{I,J}+1)^2+y^2+z^2}} \\ & + \sum_{\substack{j\in\mathcal{S}\\ j\neq I,J}} \frac{\mu_{I,J,j}}{\sqrt{(x-x_j)^2+(y-y_j)^2+(z-z_j)^2}} \end{aligned} \tag{E.11}$$

on

$$\mu_{I,J,j} = \frac{m_j}{m_I+m_J},$$

i $(x_j, y_j, z_j)^\top$ són les coordenades adimensionals del cos $j \in \mathcal{S}$. Al sistema (E.10), $\{c_i\}_{i=1\div 13}$ són funcions depenent del temps que es poden calcular en termes de les posicions, velocitats, acceleracions i sobreacceleracions dels dos primaris I, J. Si posem $c_5 = 2$, $c_7 = c_{10} = c_{13} = 1$, les restants c_i iguals a zero i eliminem la suma a (E.11), aleshores les equacions (E.10) esdevenen les equacions del Problema Restringit de Tres Cossos (RTBP) amb paràmetre de masses $\mu_{I,J}$. Per tant, podem veure (E.10) com una perturbació de les equacions del RTBP.

De cara a evaluar el sistema d'equacions anterior, necessitem les posicions dels cossos del Sistema Solar, així com les seves derivades respecte del temps fins a ordre tres. Es poden calcular a partir de qualssevol efemèrides planetàries, siguin analítiques o numèriques. En els càlculs hem usat les efemèrides numèriques DE406 del Jet Propulsion Laboratory (JPL), degut a la seva alta precisió al llarg d'un interval de temps de 6000 anys.

Tot seguit desenvoluparem models entre el RTBP i el Sistema Solar "real" (E.10). L'estratègia a seguir és "afegir freqüències bàsiques" al RTBP, tot calculant aquestes freqüències mitjançant l'aplicació de les tècniques d'anàlisi de Fourier descrites anteriorment a les funcions$\{c_i\}_{i=1\div 13}$ i $\{(x_j, y_j, z_j)^\top\}_{j\in\mathcal{S}}$. Els models es desenvoluparan per

- el cas Terra–Lluna, que significa considerar $I = P_3$ i $J = P_{10}$, essent $\mathcal{S}$ tal com a (E.8), i

- el cas Sol–Terra+Lluna, que significa considerar $I = P_{11}$ i $J = P_{12}$, essent $\mathcal{S}$ com a (E.9).

Malgrat que només cobrirem aquests dos casos, la metodologia usada pot ser aplicada a qualsevol parell de primaris.

Models simplificats per al cas Terra–Lluna

En una teoria acurada per al moviment lunar, com la teoria simplificada de Brown donada a [8], els paràmetres fonamentals es poden expressar en termes de cinc freqüències bàsiques:

- La longitud mitjana de la Lluna, que és igual a 1.0.
- L'elongació mitjana de la Lluna respecte del Sol, 0.925195997455093. Aquesta és la freqüència de la part depenent del temps al Problema Bicircular (BCP) i el Problema Quasibicircular (QBCP, veure Apèndix A).
- La longitud mitjana del perigeu lunar, que és igual a $8.45477852931292 \times 10^{-3}$.
- La longitud del node ascendent mitjà de l'òrbita lunar sobre l'eclíptica, $4.01883841204748 \times 10^{-3}$.
- La longitud mitjana del perigeu solar, $3.57408131981537 \times 10^{-6}$.

Les unitats emprades per a aquestes freqüències són cicles per revolució lunar. En el que segueix, aquestes freqüències seran denotades per $\{\omega_1, \ldots, \omega_5\}$.

Per als models simplificats que especificarem a continuació, només tindrem en compte les coordenades del Sol en (E.11). Això estalvia la introducció de freqüències bàsiques addicionals i és suficient per als nostres propòsits, com quedarà clar més endavant. D'aquesta manera, només usarem les expansions de Fourier de $c_1, \ldots, c_{13}$ i x_S, y_S, z_S.

A partir de la base de freqüències $\{\omega_i\}_{i=1\div 5}$, cercarem una nova base $\{\nu_i\}_{i=1\div 5}$. En termes d'aquesta base, generarem cinc models SSSM$_i$, $i = 1 \div 5$, de manera que les equacions del moviment de SSSM$_i$ són

$$\left\{ \begin{array}{rcl} \ddot{x} & = & c_1^i + c_4\dot{x} + c_5^i\dot{y} + c_7^i x + c_8^i y + c_9^i z + c_{13}^i \dfrac{\partial \Omega^i}{\partial x} \\ \ddot{y} & = & c_2^i - c_5^i\dot{x} + c_4^i\dot{y} + c_6^i\dot{z} - c_8^i x - c_{10}^i y + c_{11}^i z + c_{13} \dfrac{\partial \Omega^i}{\partial y} \\ \ddot{z} & = & c_3^i - c_6\dot{y} + c_4^i\dot{z} + c_9^i x - c_{11}^i y + c_{12}^i z + c_{13}^i \dfrac{\partial \Omega^i}{\partial z} \end{array} \right.$$

essent

$$\begin{array}{rcl} \Omega & = & \dfrac{1-\mu_{E,M}}{\sqrt{(x-\mu_{E,M})^2 + y^2 + z^2}} + \dfrac{\mu_{E,M}}{\sqrt{(x-\mu_{E,M}+1)^2 + y^2 + z^2}} \\ & & + \dfrac{\mu_{E,M,S}}{\sqrt{(x-x_S^i)^2 + (y-y_S^i)^2 + (z-z_S^i)^2}}. \end{array}$$

Aquí c_j^i, $j = 1 \div 13$ i x_S^i, y_S^i, z_S^i són les expansions de Fourier de c_j, $j = 1 \div 13$ i x_S, y_S, z_S, respectivament, calculades usant els procediments d'anàlisi de Fourier descrits anteriorment, però mantenint només les freqüències que s'expressen com a combinacions lineals (amb coeficients enters) de les freqüències $\nu_1, \ldots, \nu_i$.

La nova base $\{\nu_i\}_{i=1\div 5}$ ha estat escollida com

- $\nu_1 = \omega_2$, que és la freqüència principal de c_1, c_2, x_S i y_S.

- $\nu_2 = \omega_1 - \omega_3$, que permet ajustar amb combinacions lineals a coeficients enters de ν_1, ν_2 les freqüències més importants de totes les funcions llevat de c_3, c_6, c_9, c_{11} i z_S.
- $\nu_3 = \omega_1 - \omega_2 + \omega_4$, que és la freqüència principal de c_3,
- $\nu_4 = \omega_1 - \omega_5$, que és la primera freqüència de c_3 que no es pot expressar en termes de ν_1, ν_2, i
- $\nu_5 = \omega_5 - \omega_2$, que és la primera freqüència de c_3 que no es pot expressar en termes de $\nu_1, \nu_2, \nu_3, \nu_4$.

D'aquesta manera, tenim

$$\begin{pmatrix} \nu_1 \\ \nu_2 \\ \nu_3 \\ \nu_4 \\ \nu_5 \end{pmatrix} = \begin{pmatrix} 0 & 1 & 0 & 0 & 0 \\ 1 & 0 & -1 & 0 & 0 \\ 1 & -1 & 0 & 1 & 0 \\ 1 & 0 & 0 & 0 & -1 \\ 0 & -1 & 0 & 0 & 1 \end{pmatrix} \begin{pmatrix} \omega_1 \\ \omega_2 \\ \omega_3 \\ \omega_4 \\ \omega_5 \end{pmatrix}.$$

Donat que la matriu anterior és unimodular, $\{\nu_i\}_{i=1\div 5}$ és un conjunt vàl·lid de freqüències bàsiques.

Usant acceleracions residuals, hem comparat els models SSSM$_i$, així com el RTBP, el Problema Bicircular (BCP) i el problema Quasibicircular (QBCP) amb el Sistema Solar real, donat per (E.10) i (E.11) amb les funcions c_i i x_i, y_i, z_i evaluades a partir del fitxer d'efemèrides DE406 del JPL. Hem procedit com segueix. Donats dos models per ser comparats, amb equacions diferencials $\ddot{\mathbf{r}} = f(\mathbf{r}, t)$ i $\ddot{\mathbf{r}} = g(r, t)$, respectivament, i donada una trajectòria (en posicions i velocitats) $\gamma : \mathbb{R} \to \mathbb{R}^6$, que no té perquè ser de cap dels dos models, calculem les "acceleracions mitjes residuals relatives sobre γ" com

$$\frac{1}{L} \int_0^T \frac{\|f(\gamma(s), t) - g(\gamma(s), t)\|}{\|g(\gamma(s), t)\|} \|\gamma'(s)\| ds, \tag{E.12}$$

on t és una època determinada (en unitats adimensionals), i

$$L = \int_0^T \|\gamma'(s)\| ds$$

és la longitud de la trajectòria.

Els resultats del test d'acceleracions residuals es donen a la Taula E.2. D'aquesta taula es conclou que els millors models d'una freqüència que podem usar, d'acord amb el criteri d'acceleracions residuals, són el BCP i el QBCP. Quan permetem dues o més freqüències, els models que obtenim s'ajusten molt millor al model JPL. Com s'ha dit anteriorment, només el Sol ha estat tingut en compte en tots els models intermedis. Afegint cossos addicionals, les acceleracions residuals són del mateix ordre de magnitud que les obtingudes usant només el Sol.

z–a.	RTBP	BCP	QBCP	SSSM_1	SSSM_2	SSSM_3	SSSM_4	SSSM_5
0.020	0.140126	0.146459	0.138580	0.365299	0.095769	0.010674	0.001374	0.000727
0.022	0.138397	0.144693	0.136908	0.359442	0.094562	0.010534	0.001360	0.000724
0.025	0.136603	0.142856	0.135174	0.353302	0.093293	0.010388	0.001346	0.000720
0.028	0.134760	0.140962	0.133392	0.346913	0.091967	0.010235	0.001331	0.000716
0.031	0.132882	0.139025	0.131578	0.340305	0.090590	0.010076	0.001315	0.000711
0.034	0.130985	0.137059	0.129747	0.333509	0.089166	0.009913	0.001299	0.000707
0.038	0.129087	0.135080	0.127914	0.326550	0.087699	0.009744	0.001282	0.000702
0.043	0.127204	0.133103	0.126097	0.319452	0.086191	0.009570	0.001265	0.000696
0.048	0.125352	0.131141	0.124312	0.312235	0.084643	0.009393	0.001247	0.000691
0.053	0.123549	0.129209	0.122576	0.304915	0.083056	0.009211	0.001229	0.000685
0.059	0.121813	0.127324	0.120905	0.297505	0.081429	0.009024	0.001210	0.000678
0.066	0.120162	0.125502	0.119319	0.290018	0.079760	0.008833	0.001191	0.000671
0.073	0.118614	0.123757	0.117835	0.282462	0.078045	0.008637	0.001171	0.000664
0.082	0.117189	0.122108	0.116473	0.274845	0.076280	0.008436	0.001150	0.000655
0.091	0.115905	0.120571	0.115249	0.267173	0.074461	0.008229	0.001128	0.000646
0.102	0.114778	0.119161	0.114181	0.259453	0.072581	0.008016	0.001105	0.000636
0.113	0.113823	0.117895	0.113283	0.251690	0.070634	0.007796	0.001081	0.000625
0.126	0.113052	0.116784	0.112566	0.243889	0.068612	0.007568	0.001056	0.000612
0.141	0.112471	0.115836	0.112037	0.236056	0.066510	0.007331	0.001030	0.000598
0.157	0.112080	0.115057	0.111695	0.228199	0.064322	0.007085	0.001002	0.000583
0.175	0.111872	0.114443	0.111533	0.220325	0.062042	0.006831	0.000973	0.000566
0.195	0.111829	0.113984	0.111535	0.212440	0.059667	0.006566	0.000942	0.000547
0.217	0.111928	0.113663	0.111672	0.204551	0.057196	0.006292	0.000910	0.000526
0.242	0.112133	0.113450	0.111909	0.196665	0.054632	0.006008	0.000875	0.000504
0.269	0.112400	0.113311	0.112201	0.188782	0.051978	0.005716	0.000840	0.000481
0.300	0.112678	0.113200	0.112492	0.180899	0.049240	0.005417	0.000802	0.000456

Taula E.2: Acceleracions residuals mitjes relatives entre diversos models i el Sistema Solar real sobre diverses òrbites halo del RTBP al voltant de L_2 per al cas Terra–Lluna. La primera columna mostra l'amplitud z de la òrbita halo de prova. Les columnes restants mostren l'acceleració residual mitja relativa entre el model corresponent i el Sistema Solar real sobre l'òrbita de prova.

Models simplificats per al cas Sol–Terra+Lluna

Per als models simplificats del casl Sol–Terra+Lluna, només tenim en compte les funcions c_4, c_5, c_7, c_{10}, c_{12} i c_{13}, degut a que les altres es troben, en valor absolut, diversos ordres de magnitud per sota d'aquestes. De les freqüències donades per l'anàlisi de Fourier d'aquestes funcions n'extraiem quatre de bàsiques:

$$\nu_1 = 0.9999926164,\ \nu_2 = 0.6255242728,\ \nu_3 = 0.9147445983,\ \nu_4 = 1.8313395538.$$

Amb aquestes freqüències, construim els models SSSM_1, …, SSSM_4 com vam fer en el cas Terra–Lluna.

z-a.	RTBP	SSSM_1	SSSM_4
0.020000	3.446497E–02	9.901526E–05	8.905454E–04
0.022288	3.429997E–02	9.844882E–05	8.842048E–04
0.024838	3.411184E–02	9.779360E–05	8.768670E–04
0.027680	3.390024E–02	9.701858E–05	8.684772E–04
0.030846	3.366579E–02	9.616913E–05	8.589500E–04
0.034375	3.341007E–02	9.521763E–05	8.482675E–04
0.038308	3.313580E–02	9.416327E–05	8.364166E–04
0.042691	3.284681E–02	9.300703E–05	8.234040E–04
0.047575	3.254789E–02	9.175134E–05	8.092527E–04
0.053018	3.224472E–02	9.039967E–05	7.939978E–04
0.059084	3.194355E–02	8.895610E–05	7.776813E–04
0.065843	3.165101E–02	8.742482E–05	7.603471E–04
0.073376	3.137381E–02	8.582841E–05	7.420444E–04
0.081771	3.111844E–02	8.413352E–05	7.227963E–04
0.091126	3.089082E–02	8.236183E–05	7.026421E–04
0.101551	3.069597E–02	8.051628E–05	6.816096E–04
0.113169	3.053770E–02	7.859979E–05	6.597243E–04
0.126117	3.041819E–02	7.661569E–05	6.370130E–04
0.140545	3.033772E–02	7.450252E–05	6.135638E–04
0.156624	3.029470E–02	7.240496E–05	5.893022E–04
0.174543	3.028516E–02	7.020714E–05	5.643885E–04
0.194512	3.030323E–02	6.801648E–05	5.388121E–04
0.216766	3.034115E–02	6.579492E–05	5.127031E–04
0.241565	3.038961E–02	6.350846E–05	4.862056E–04
0.269202	3.043825E–02	6.123496E–05	4.593820E–04
0.300000	3.047577E–02	5.898080E–05	4.323859E–04

Taula E.3: Acceleracions residuals mitjes relatives entre diversos models i el Sistema Solar real sobre diverses òrbites halo del RTBP al voltant de L_2 en el cas Sol–Terra+Lluna.

A la taula E.3, comparem els models RTBP, SSSM_1 i SSSM_4 amb el Sistema Solar real usant el mateix test d'acceleracions residuals que ha estat usat al cas Terra–Lluna. Notem que el model SSSM_4 dóna pitjors resultats que SSSM_1. Això no és una contradicció, degut a que l'aproximació de les funcions c_i per les expansions de Fourier calculades no millora significativament en afegir freqüències no múltiples de ν_1. D'aquest manera, l'estructura de les equacions (E.10) “s’imposa” sobre el fet que els termes c_i de SSSM_4 són més propers als del Sistema Solar real que els termes corresponents de SSSM_1.

En conseqüència, donem SSSM_1 com model simplificat de moviment al Sistema Solar per al cas Sol–Terra+Lluna. Notem que aquest és un model amb molt poques freqüències que millora significativament el RTBP.

E.2 L’entorn dels punts de libració colineals

Aquesta secció està dedicada a l’estudi de l’entorn dels punts d’equilibri colineals del RTBP per al paràmetre de masses Terra–Lluna. L’estudi està basat en la continuació de les famílies d’òrbites periòdiques i tors invariants 2–dimensionals de la varietat central dels punts d’equilibri. En les següents seccions, presentem un resum de la metodologia emprada i els resultats numèrics obtinguts.

E.2.1 Metodologia

Ens centrarem en el càlcul de tors invariants, donat que el refinament i continuació d’òrbites periòdiques ha estat estudiat exhaustivament amb anterioritat. El procediment de càlcul de tors invariants 2–dimensionals pren com a punt de partida el procediment desenvolupat en [7].

Concretament, sigui $H(\mathbf{x})$ el Hamiltonià del RTBP, $X_H(\mathbf{x})$ el seu camp vectorial i $\phi_t(\mathbf{x})$ el seu flux temps t. Podem cercar la parametrització d’un tor 2–dimensional $\psi : \mathbb{T}^2 = \mathbb{R}^2/2\pi\mathbb{Z} \to \mathbb{R}^n$ ($n = 6$ per al RTBP), satisfent

$$\psi(\theta + \omega t) = \phi_t(\psi(\theta)), \qquad \forall\theta \in \mathbb{T}^2,\ \forall t \in \mathbb{R}, \tag{E.13}$$

on $\omega = (\omega_1, \omega_2) \in \mathbb{R}^2$ és el vector de freqüències del tor. Denotem per T_i el període corresponent a la freqüència ω_i, és a dir, $T_i = 2\pi/\omega_i$, i denotem $\theta = (\xi, \eta)$.

De cara a reduir la dimensió del problema, en comptes de cercar una parametrització del tor sencer, podem cercar la parametrització d’una corba $\{\eta = \eta_0\}$ (o $\{\xi = \xi_0\}$) sobre el tor, que és invariant sota ϕ_{T_2}, concretament

$$\phi_{T_2}(\psi(\xi, \eta_0)) = \psi(\xi + \omega_1 T_2, \eta_0), \qquad \forall\xi \in \mathbb{T}^1. \tag{E.14}$$

Per tant, cercarem una parametrització $\varphi : \mathbb{T}^1 \to \mathbb{R}^n$ satisfent

$$\varphi(\xi + \rho) = \phi_\delta(\varphi(\xi)), \qquad \forall\xi \in \mathbb{T}^1, \tag{E.15}$$

on $\delta = T_2$ i $\rho = \delta\omega_1$. Notem que ρ és el nombre de rotació de la corba que estem cercant.

Indeterminacions de la representació de Fourier

Cercarem φ sota la forma de sèrie de Fourier truncada,

$$\varphi(\xi) = A_0 + \sum_{k=1}^{N_f} (A_k \cos(k\xi) + B_k \sin(k\xi)), \tag{E.16}$$

amb A_k, $B_k \in \mathbb{R}^n$. Aquesta representació del tor geomètric $\{\psi(\theta)\}_{\theta\in\mathbb{T}^2}$ no és única per dues raons:

- Cada elecció de η_0 correspon a una φ diferent en (E.16), és a dir, a una corba invariant diferent sobre el tor $\{\psi(\theta)\}_{\theta\in\mathbb{T}^2}$.
- Donada la parametrització (E.16), per cada $\xi_0 \in \mathbb{T}^1$, $\varphi(\xi-\xi_0)$ és una parametrització diferent amb una expansió de Fourier diferent de la mateixa corba invariant $\{\varphi(\xi)\}_{\xi\in\mathbb{T}^1}$ del tor $\{\psi(\theta)\}_{\theta\in\mathbb{T}^2}$. De fet, la seva expansió de Fourier és

$$\varphi(\xi-\xi_0) = A_0 + \sum_{k=1}^{N_f}(\widetilde{A}_k\cos(k\xi) + \widetilde{B}_k\sin(k\xi)),$$

essent

$$\begin{array}{rcl} \widetilde{A}_k &=& A_k\cos(k\xi_0) - B_k\sin(k\xi_0) \\ \widetilde{B}_k &=& A_k\sin(k\xi_0) + B_k\cos(k\xi_0). \end{array} \tag{E.17}$$

Anomenarem aquest fenòmen "modulació de coeficients", en analogia amb la terminologia usada en processament de senyal.

Per a evitar la primera indeterminació, mantenim constant una coordenada de A_0. S'ha de verificar que aquesta condició sigui vàl·lida per la família de tors que s'estigui continuant.

Respecte de la segona indeterminació, notem que, per qualsevol $k \geq 1$, si $(A_k^j, B_k^j) \neq (0,0)$ (aquí A_k^j denota la j-èsima coordenada de A_k), de (E.17) se segueix que existeix un ξ_0 que dóna $\widetilde{A}_k^j = 0$. Per tant, prenent $A_k^j = 0$ evitarem la indeterminació, sempre i quan B_k^j romangui diferent de zero. Usualment, hem pres $k = 1$ i j ha estat escollit maximitzant $\|(A_1^j, B_1^j)\|_2$.

Tir múltiple

Per poder tractar amb tors altament inestables, usem un procediment de tir múltiple. Consisteix en cercar diverses corbes invariants sobre el tor $\{\psi(\theta)\}_{\theta\in\mathbb{T}^2}$ en comptes de només una, amb la finalitat de reduir el temps màxim d'integració a una fracció de δ. Concretament, cercarem m parametritzacions $\varphi_0 = \varphi, \varphi_1, \dots, \varphi_{m-1}$ satisfent

$$\left\{\begin{array}{rcll} \varphi_{j+1}(\xi) &=& \phi_{\frac{\delta}{m}}(\varphi_j(\xi)) & (j = 0 \div m-2) \\ \varphi_0(\xi+\rho) &=& \phi_{\frac{\delta}{m}}(\varphi_{m-1}(\xi)), & \end{array}\right. \tag{E.18}$$

per a tot $\xi \in \mathbb{T}^1$.

El sistema d'equacions

D'acord amb [7], convertirem (6.13) en un sistema d'equacions finit discretitzant $\mathbb{T}^1$ en $2N_f+1$ valors de ξ. Prendrem, simplement

$$\xi_i = i\frac{2\pi}{1+2N_f} \qquad (i = 0 \div 2N_f). \tag{E.19}$$

A més dels coeficients de Fourier, hem de considerar δ, ρ com a incògnites, donat que s'espera que varïin al llarg de les continuacions. De cara a descriure els tors en termes de l'energia, afegim una nova incògnita h i una nova equació $H(\varphi_0(0)) - h = 0$, que prescriu un nivell d'energia per al tor que s'està calculant.

De cara a simplificar la notació, denotarem els coeficients de Fourier com

$$\mathcal{F} = (A_0, A_1, B_1, \ldots, A_{N_f}, B_{N_f})$$

i

$$\Psi(\xi, \mathcal{F}) = A_0 + \sum_{k=1}^{N_f} (A_k \cos(k\xi) + B_k \sin(k\xi)).$$

El sistema d'equacions que resoldrem és

$$\begin{array}{rcll} H(\Psi(0, \mathcal{F}_0)) - h & = & 0 & \\ \Psi(\xi_i, \mathcal{F}_{j+1}) - \phi_{\frac{\delta}{m}}(\Psi(\xi_i, \mathcal{F}_j)) & = & 0 & j = 0 \div m-2,\ i = 0 \div 2N_f \\ \Psi(\xi_i + \rho, \mathcal{F}_0) - \phi_{\frac{\delta}{m}}(\Psi(\xi_i, \mathcal{F}_{m-1})) & = & 0 & i = 0 \div 2N_f, \end{array} \tag{E.20}$$

on les incògnites són $h, \delta, \rho, \mathcal{F}_0, \ldots, \mathcal{F}_{m-1}$. $\mathcal{F}_i$ representa els coeficients de Fourier de la corba φ_i en el tir múltiple (E.18). Les equacions de tir múltiple

$$\Psi(\xi_i, \mathcal{F}_{j+1}) - \phi_{\frac{\delta}{m}}(\Psi(\xi_i, \mathcal{F}_j)) = 0$$

se suposen inexistents si $m = 1$.

En el sistema d'equacions anterior les incògnites considerades no són independents. L'estratègia que seguim consisteix a mantenir constants determinades incògnites en termes del que volguem calcular.

Refinament i continuació de famílies de tors invariants

Per refinar un tor invariant, mantindrem constants dues incògnites al sistema (E.20) per tal de fixar una corba inveriant sobre el tor refinat i per evitar modulació de coeficients. A més d'això, fixarem dues incògnites addicionals perquè el tor que volem refinar sigui l'única solució (localment) del sistema d'equacions que resolem. Això és necessari perquè els tors que calcularem estaran sempre immersos en famílies cantorianes biparamètriques. Un cop fixades aquestes quatre incògnites, usem el mètode de Newton per a resoldre el sistema obtingut.

Portem a terme la continuació de famílies de tors invariants usant un esquema predictor–corrector. Donat un tor, per predir un nou tor dins la família, considerem la família com una varietat de tors invariants i ens movem al llarg del seu espai tangent. Donat que aquesta varietat s'expressa com $F(X) = 0$ (per F, X adients), el seu espai tangent a un tor X donat ve donat per $\operatorname{Ker} DF(X)$. Notem que això no és estrictament cert, donat que les famílies de tors invariants són cantorianes, però el procediment funciona a la pràctica sempre i quan els "forats" deguts a resonàncies no siguin excessivament grans.

Control de l'error

Per tal de tenir un cert control sobre l'error degut a la discretització de $\mathbb{T}^1$, procedim com a [7]: avaluem (E.20) sobre una discretització més fina que (E.19) i incrementem el nombre d'harmònics fins que la norma màxima estigui sota una tolerància donada. És a dir, incrementem N_f fins que

$$\max_{\substack{i=0\div 2N_f,\ j=0\div m-2 \\ k=0\div M(1+2N_f)-1}} \left\| \begin{array}{c} \Psi(\widetilde{\theta}_k, \mathcal{F}_{j+1}) - \phi_{\frac{\delta}{m}}(\Psi(\widetilde{\theta}_k, \mathcal{F}_j)) \\ \Psi(\widetilde{\theta}_k + \rho, \mathcal{F}_0) - \phi_{\frac{\delta}{m}}(\Psi(\widetilde{\theta}_k, \mathcal{F}_{m-1})) \end{array} \right\|_\infty < tol, \tag{E.21}$$

essent $\widetilde{\theta}_k = k\frac{2\pi}{M(1+2N_f)}$.

Estratègies de càlcul en paral·lel

La part de càlcul més intensiva ha estat duta a terme seguint una estratègia de càlcul en paral·lel, en la qual es continuen n_c famílies de tors invariants en una execució.

Aquest estratègia ha estat implementada segons el model "master–esclau". El programa master engega n_e còpies del programa esclau i distribueix les n_c famílies entre ells. Donat un tor d'una família, el programa esclau calcula un nou tor sobre la família portant a terme un pas de continuació.

El programa master distribueix passos de continuació de manera cíclica entre les famílies de tors que es continuen. D'aquesta manera podem continuar en una execució més famílies que processadors ($n_c > n_e$). Els esclaus s'ordenen en una llista en la qual el master cerca esclaus de començament a final. D'aquesta manera, quan més de $n_c - n_e$ continuacions han estat finalitzades i alguns esclaus es queden sense feina, la càrrega "puja" cap al començament de la llista. Això permet treure profit d'una xarxa heterogènia, col·locant els processadors més ràpids al començament de la llista.

E.2.2 Resultats numèrics

Han estat continuades diverses famílies d'òrbites periòdiques, concretament:

- Les famílies de Lyapunov planes i verticals originades als tres punts d'equlilibri colineals.
- Les famílies d'òrbites halo, que s'obtenen com a bifurcació de la famílies plana de Lyapunov deguda a una resonància 1 : 1, també per als tres punts d'equlilibri.
- Les famílies d'òrbites tridimensionals que fan de "pont" entre les famílies de Lyapunov planes i verticals, que bifurquen de la família de Lyapunov plana després de la bifurcació de la família halo, per als casos de L_1, L_2 i L_3.
- Famílies que bifurquen de les famílies halo per duplicació i triplicació de període. Cadascuna d'aquestes bifurcacions dóna lloc a dues famílies, una sense direccions estables, que anomenarem hiperbòlica, i una altra amb una direcció estable, que anomenarem el·líptica. Aquestes famílies només han estat detectades en els casos de L_1 i L_2, perquè en el cas de L_3 la família halo arriba a una òrbita de col·lisió abans d'atansar les resonàncies 1:2 i 1:3 que donen lloc a les famílies esmentades.

Per a les famílies anteriors d'òrbites periòdiques, han estat continuades les famílies de tors invariants que s'originen a les seves direccions estables.

Tor al voltant de les famílies verticals de Lyapunov

A la Figura E.4 hem representat, per als tres punts d'equlilibri, les regions, al pla h–ρ, determinades per les famílies biparamètriques de tors calculats començant a les famílies d'òrbites periodòdiques de Lyapunov verticals. Cada regió està envoltada per una corba formada per diverses seccions:

- La secció inferior esquerra α (del vèrtex 1 al 2) correspon la família de Lyapunov plana. Les òrbites d'aquesta família representades en la corba corresponen al primer tram de la família amb direccions estables.

- La secció superior β (del vèrtex 2 al 3) correspon a la família d'òrbites de Lyapunov verticals.

- La secció inferior γ (del vèrtex 3 al 1), que es troba sobre $\rho = 0$, comença al valor de l'energia en què neixen les òrbites planes. Correspon a una separatriu entre els tors al voltant de les òrbites de Lyapunov verticals i els tors al voltant de les òrbites halo.

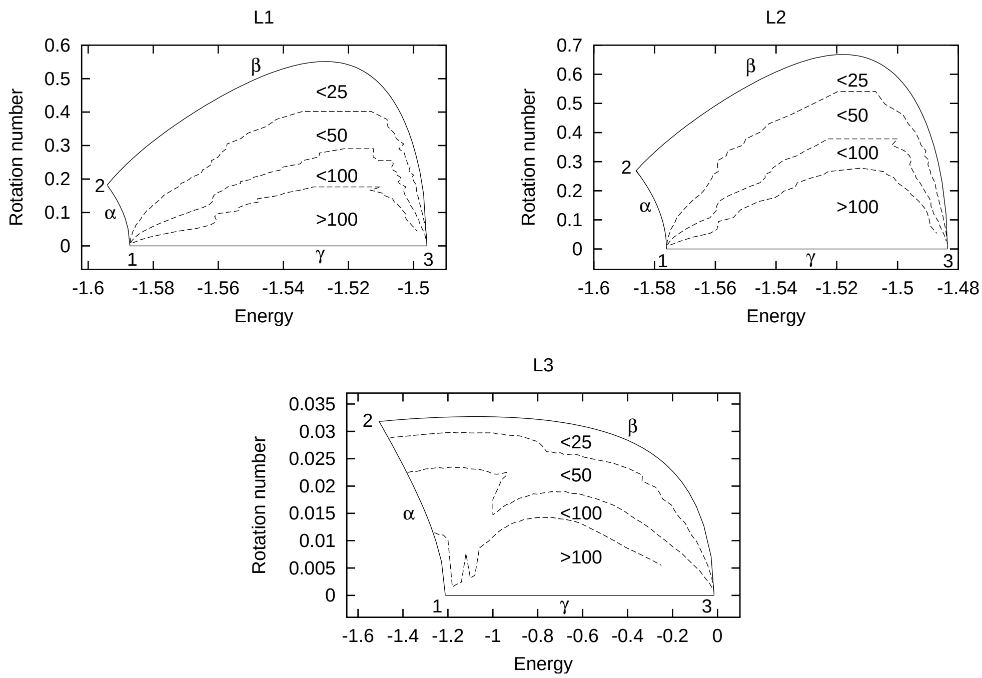

Figura E.4: Regions al pla h–ρ que contenen les famílies 2–paramètriques de tors invariants calculats començant a les famílies verticals de Lyapunov d'òrbites periòdiques per L_1, L_2 i L_3. A les figures es mostra el nombre d'harmònics necessari per al càlcul dels tors (< 25, < 50, < 100 i > 100).

Tors invariants al voltant d'òrbites halo i de tipus halo

A la Figura 7.16 representem les continuacions de les famílies 2–paramètriques de tors invariants al voltant de les òrbites halo.

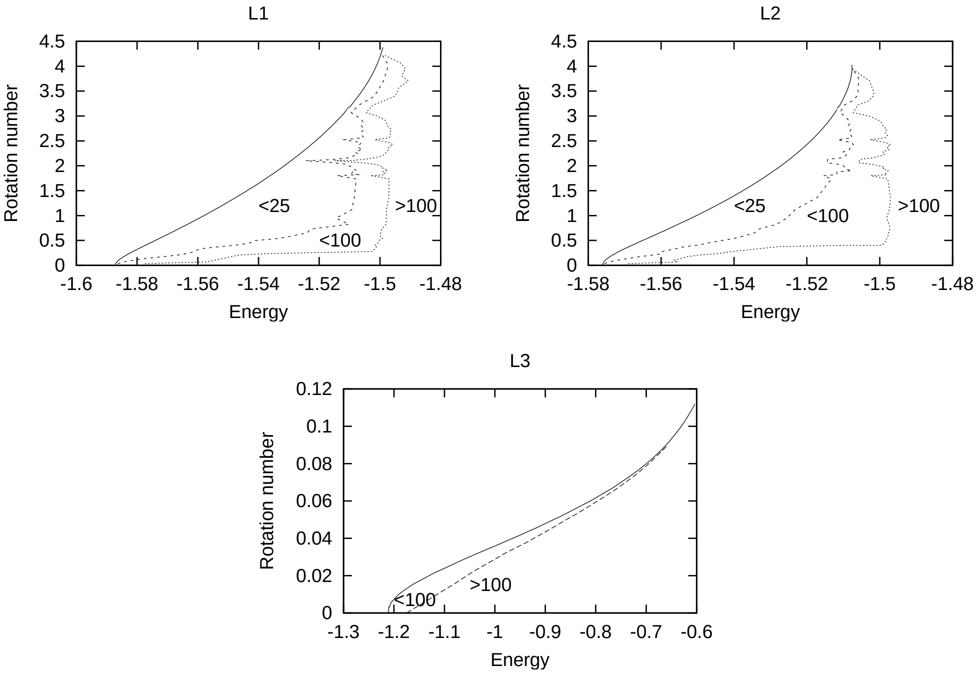

Figura E.5: Regions en el pla h–ρ que contenen les famílies biparamètriques de tors invariants al voltant de les famílies halo de L_1, L_2 i L_3. Com a la figura anterior, mostrem el nombre d'harmònics usat per al càlcul de tors.

Les vores inferiors d'aquestes regions són compartides amb les de les regions mostrades a la Figura E.4. El vèrtex inferior–esquerre dels tres gràfics correspon al vèrtex número 1 dels gràfics de la Figura E.4. Aquest vèrtex correspon a la òrbita plana de bifurcació que origina les famílies halo. En els tres casos, quan $\rho \to 0$ tendim a una connexió homoclínica [14].

La vora dreta és fictícia en cert sentit, donat que correspon a atansar el nombre màxim d'harmònics permès. De totes maneres, reflecteix d'una manera clara quan el nombre de rotació ρ travessa resonàncies d'ordre baix, en els quals els tors col·lapsen a òrbites periòdiques. Els quatre pics principals detectats corresponen a $\rho = 2\pi/2$, $4\pi/5$, $2\pi/3$ i $2\pi/4$ (de dalt a baix). El primer i tercer pics corresponen a les resonàncies 1:3 i 1:2, corresponents a les famílies bifurcades de tipus halo mencionades prèviament. Algunes d'aquestes famílies tenen direccions estables, que donen lloc a famílies de tors invariants al voltant. Aquestes famílies també han estat calculades, per a les quals els diagrames h–ρ es donen a les figures E.6 i E.7.

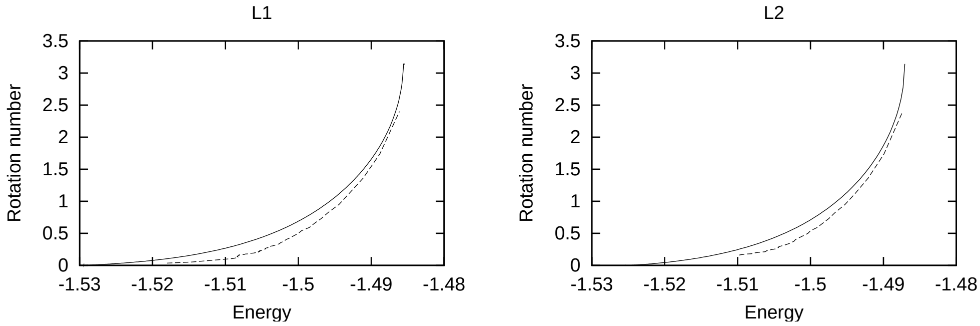

Figura E.6: Regions en el pla h–ρ que contenen les famílies biparamètriques de tors invariants al voltant de les famílies el·líptiques bifurcades de les òrbites halo per triplicació de periode. Entre la corba sòlida i la corba puntejada, el nombre d'harmònics requerit per al càlcul de tors és inferior a 100. A la dreta de la corba puntejada, es requereixen més de 100 harmònics.

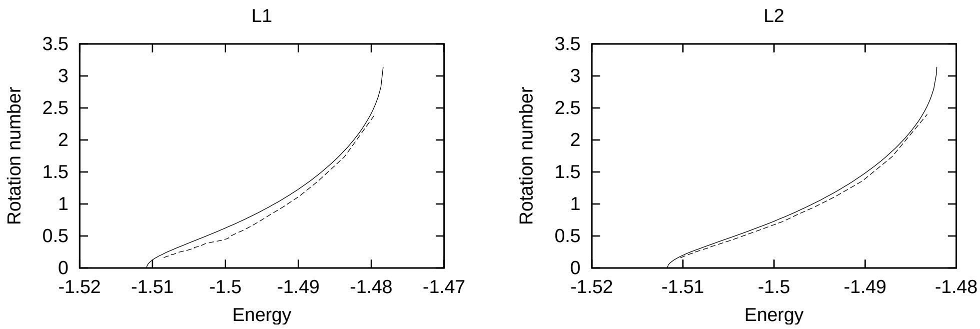

Figura E.7: Regions del pla h–ρ que contenen les famílies biparamètriques de tors invariants al voltant de les famílies el·líptiques bifurcades de les òrbites halo per duplicació de període. El significat de la línia puntejada és el mateix que a la figura E.6.

Seccions de Poincaré amb $\{z = 0\}$

Per tal de comparar els resultats obtinguts amb els resultats de treballs previs usant la reducció a la varietat central ([10],[16]), en aquesta secció mostrarem la evolució respecte de l'energia del comportament de les seccions de Poincaré per $z = 0$, $p_z > 0$ dels diferents tipus d'òrbites calculades.

Les figures E.8, E.9 i E.10 mostren els resultats per L_1, L_2 i L_3, respectivament. En totes aquestes figures, hem representat les coordenades x–y a les interseccions amb $z = 0$, $p_z > 0$. Tots els gràfics tenen una estructura similar. La corba exterior de cada gràfic és l'òrbita plana de Lyapunov del nivell d'energia corresponent al gràfic. Com que aquesta òrbita és plana, està completament inclosa a la superfície de secció, i és l'única òrbita que ho està. El moviment dins la regió fitada per la òrbita plana de Lyapunov és quasiperiòdic, llevat de alguns forats que no poden ser distingits en aquests figures. A tots els gràfics hi ha un punt fix a l'eix x associat amb l'òrbita de Lyapunov vertical.

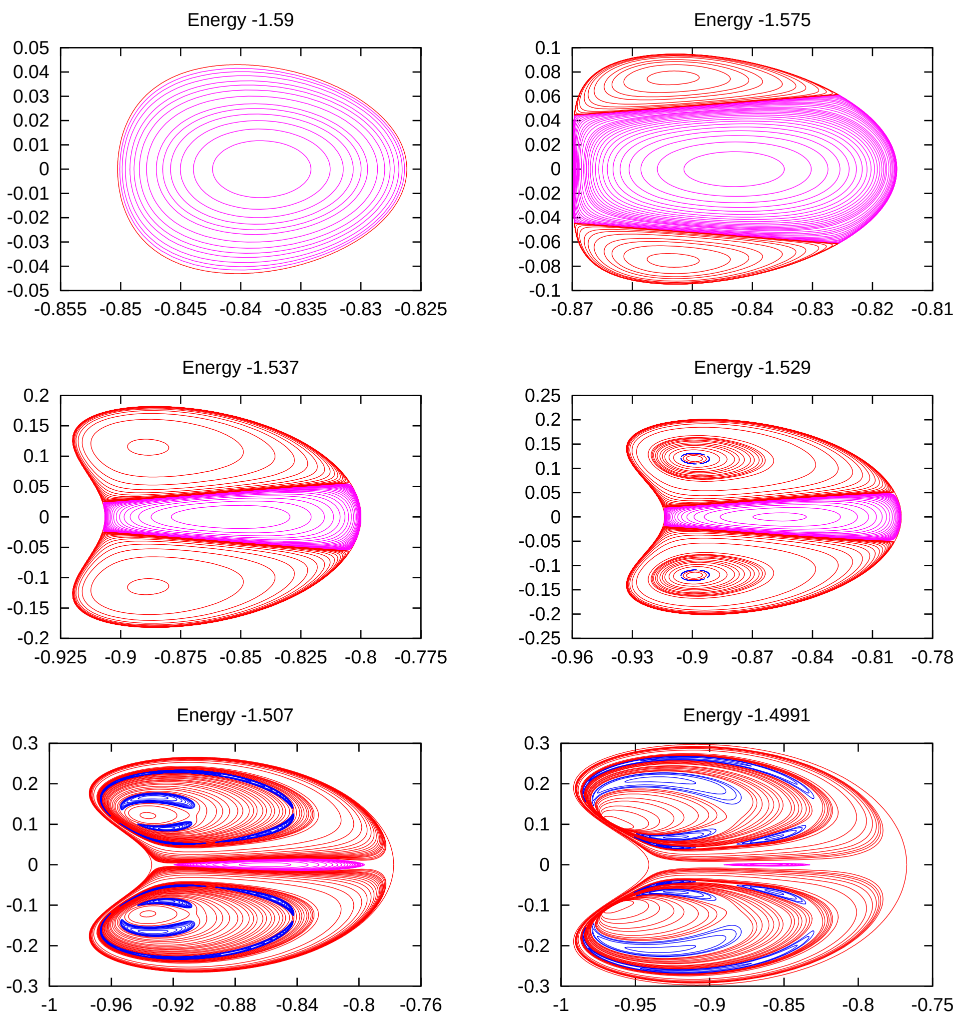

Figura E.8: Llesques a energia constant de la secció $z = 0$, $p_z > 0$ dels tors invariants al voltant de L_1.

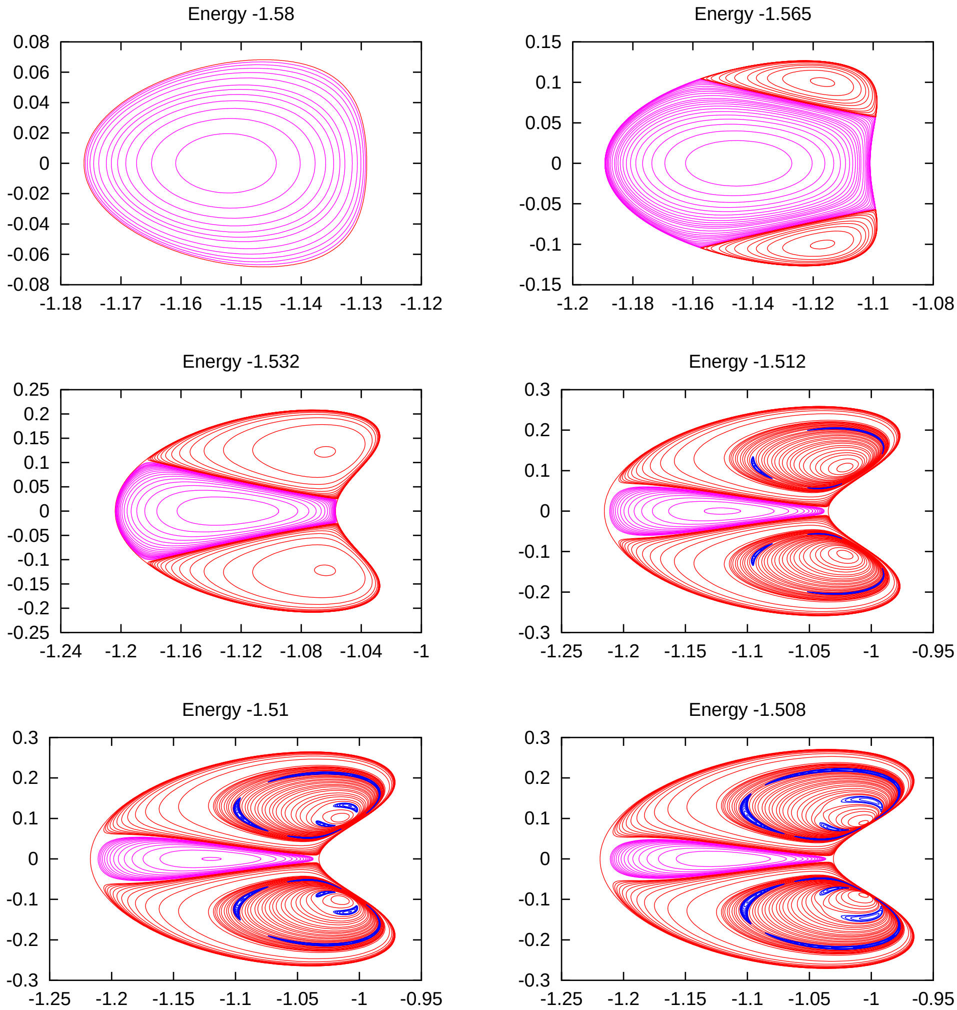

Figura E.9: Llesques a energia constant de la secció $z = 0$, $p_z > 0$ dels tors invariants al voltant de L_2.

Per als tres punts d'equilibri, i per a valors petits de l'energia, tot el gràfic està format per corbes invariants envoltant el punt fix associat a l'òrbita vertical. Aquestes corbes corresponen a les interseccions de les trajectòries de tipus Lissajous al voltant de l'òrbita periòdica vertical. Als nivells d'energia associats a la primera bifurcació de la família plana de Lyapunov, apareixen les òrbites halo. Això es pot veure clarament a les representacions de l'aplicació de Poincaré, donat que apareixen dos punts fixos addicionals envoltats de corbes invariants. En incrementar els valors de l'energia, les famílies d'òrbites halo de L_1 i L_2 tenen dues bifurcacions rellevants, per triplicació i duplicació de període. Les dues bifurcacions són detectades per les representacions de Poincaré. Aquesta estructura addicional no ha estat detectada per al cas de L_3. Tal com s'ha dit, entre les famílies bifurcades n'hi ha amb direccions estables, que estan envoltades per tors invariants. Aquests tors donen lloc a la estructura de "cadena d'illes", típica d'aplicacions 2–dimensionals preservant àrea. Per mostrar aquest comportament amb més claredat, a les figures E.11 i E.12 mostrem una amplició de les òrbites periòdiques

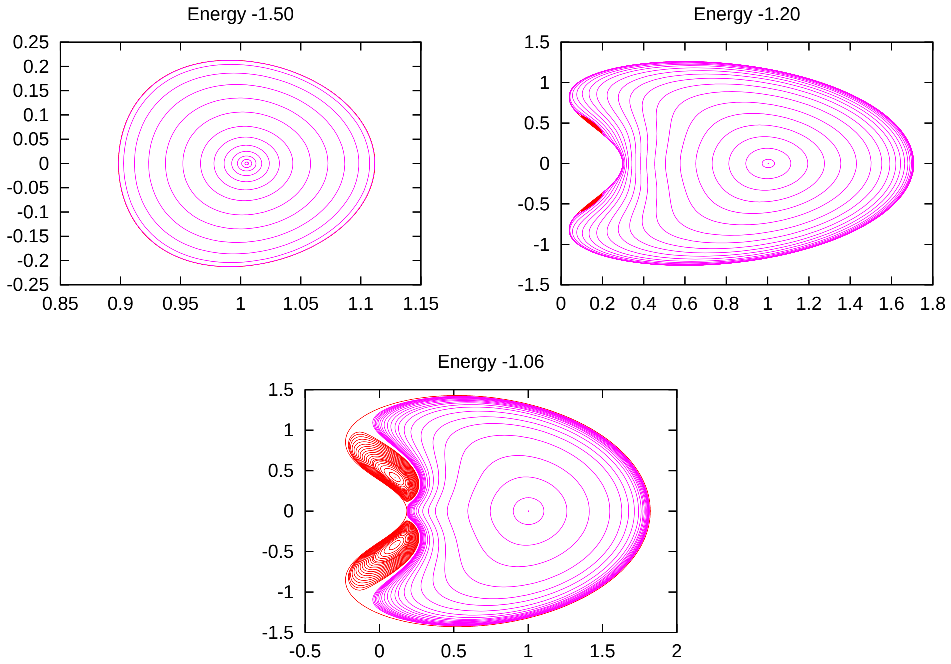

Figura E.10: Llesques a energia constant de la secció $z = 0$, $p_z > 0$ dels tors invariants al voltant de L_3.

bifurcades i els tors invariants que les envolten.

La regió entre els tors envoltant l'òrbita vertical de Lyapunov i els tors al voltant de les òrbites halo és omplerta amb les traces, sobre la superfície de secció, de les varietats invariants de l'òrbita plana de Lyapunov. Aquestes varietats actuen com a separatrius entre els dos tipus de moviment. El mateix succeeix entre les illes de les òrbites bifurcades de tipus halo i els tors que envolten les òrbites halo. En aquest cas, la regió entre els dos tipus de tors és omplerta amb les traces de les varietats invariants de les òrbites bifurcades de tipus halo hiperbòliques. En totes aquestes regions, el moviment és de tipus caòtic. Amb la metodologia desenvolupada en aquest treball no hem pogut calcular aquestes separatrius, que es poden trobar a [14] per valors de l'energia propers als valors dels punts d'equilibri.

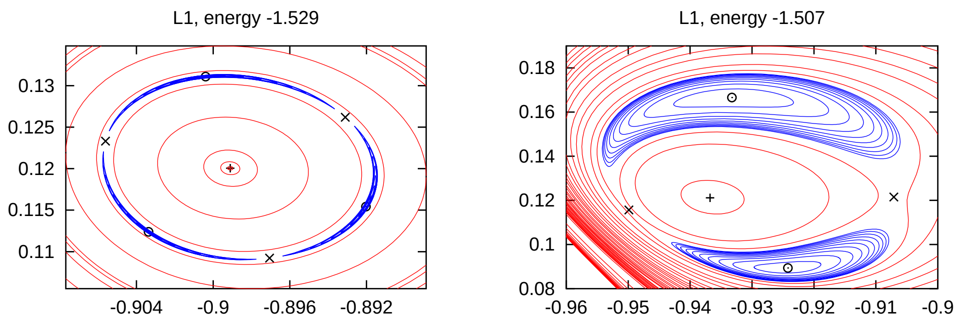

Figura E.11: Ampliació de les dues llesques intermèdies de la figura E.8 mostrant les òrbites bifurcades de tipus halo i els tors invariants que les envolten en el cas de L_1. Els punts marcats amb $+$ representen les seccions amb $z = 0$, $p_z > 0$ de les òrbites halo, els punts marcats amb $\times$ representen les seccions de les bifurcacions hiperbòliques de les òrbites halo per duplicació o triplicació de període, i els punts marcats amb $\odot$ en representen les el·líptiques.

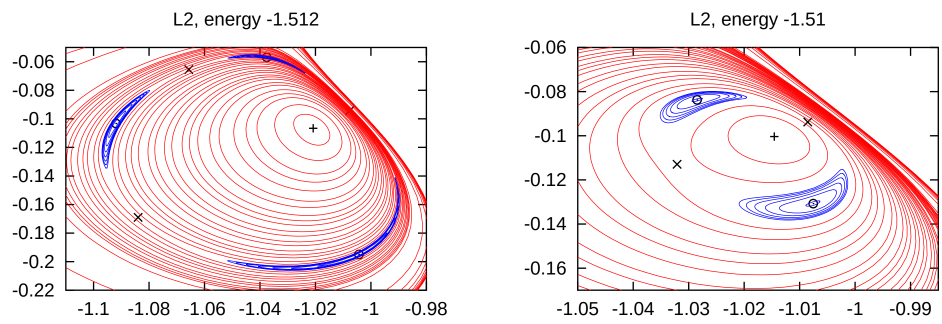

Figura E.12: Ampliació de les dues llesques intermèdies de la figura E.9 mostrant les òrbites bifurcades de tipus halo i els tors invariants que les envolten en el cas de L_2.

Bibliography

[1] M. Abramowitz and I. A. Stegun. *Handbook of Mathematical Functions*. Dover Publications, 1965.

[2] E. Anderson, Z. Bai, C. Bischof, J. Demmel, J. Dongarra, J. D. Croz, A. Greenbaum, S. Hammarling, A. McKenney, S. Ostrouchov, and D. Sorensen. *LAPACK Users' Guide*. SIAM, second edition, 1995.

[3] M. A. Andreu. *The Quasi–Bicircular problem*. PhD thesis, Universitat de Barcelona, 1999.

[4] L. S. Blackford, J. Choi, A. Cleary, E. D'Azevedo, J. Demmel, I. Dhillon, J. Dongarra, S. Hammarling, G. Henry, A. Petitet, K. Stanley, D. Walker, and R. C. Whaley. *ScaLAPACK Users' Guide*. SIAM, 1997.

[5] W. L. Briggs and V. E. Henson. *The DFT: an owner's manual for the Discrete Fourier Transform*. SIAM, 1995.

[6] E. O. Brigham. *The Fast Fourier Transform and its Applications*. Prentice–Hall, 1988.

[7] E. Castellà and A. Jorba. On the vertical families of two–dimensional tori near the triangular points of the bicircular problem. *Celestial Mechanics and Dynamical Astronomy*, 76:35–54, 2000.

[8] P. R. Escobal. *Methods of Astrodynamics*. John Wiley & Sons, 1968.

[9] G. H. Golub and C. R. Van Loan. *Matrix Computations*. The Johns Hopkins University Press, third edition, 1996.

[10] G. Gómez, À. Jorba, J. Masdemont, and C. Simó. *Dynamics and Mission Design Near Libration Point Orbits – Volume 3: Advanced Methods for Collinear Points*. World Scientific, 2000.

[11] G. Gómez, A. Jorba, J. Masdemont, and C. Simó. *Dynamics and Mission Design Near Libration Point Orbits – Volume 4: Advanced Methods for Triangular Points*. World Scientific, 2000.

[12] G. Gómez, J. Llibre, R. Martínez, and C. Simó. *Dynamics and Mission Design Near Libration Point Orbits – Volume 1: Fundamentals: The Case of Collinear Libration Points*. World Scientific, 2000.

[13] G. Gómez, J. Llibre, R. Martínez, and C. Simó. *Dynamics and Mission Design Near Libration Point Orbits – Volume 2: Fundamentals: The Case of Triangular Libration Points*. World Scientific, 2000.

[14] G. Gómez and J. J. Masdemont. Some zero cost transfers between halo orbits. *Advances in the Astronautical Sciences*, 105:1199–1216, 2000.

[15] M. Hénon. Vertical stability of periodic orbits in the restricted problem. *Astronomy & Astrophysics*, 28:415–426, 1973.

[16] A. Jorba and J. J. Masdemont. Dynamics in the center manifold of the restricted three–body problem. *Physica D*, 132:189–213, 1999.

[17] À. Jorba and C. Simó. On the reducibility of linear differential equations with quasiperiodic coefficients. *Journal of Differential Equations*, 98(1):111–124, 1992.

[18] J. Laskar. The chaotic motion of the solar system. a numerical estimate of the size of the chaotic zones. *Icarus*, 88:266–291, 1990.

[19] J. Laskar. Introduction to frequency map analysis. In C. Simó, editor, *Hamiltonian Systems With Three or More Degrees of Freedom*, pages 134–150. Kluwer Academic Pub., 1999.

[20] J. Laskar, C. Froeschlé, and A. Celletti. A measure of chaos by the numerical analysis of the fundamental frequencies. Application to the standard mapping. *Physica D*, 56:253–269, 1992.

[21] W. H. Press, B. P. Flannery, S. A. Teukolsky, and W. T. Vetterling. *Numerical Recipes. The Art of Scientific Computing*. Cambridge University Press, 1987.

[22] A. P. Prudnikov, Y. A. Brychkov, and O. I. Marichev. *Integrals and Series*, volume 1. Gordon and Breach Science Publishers, 1988.

[23] D. Richardson. Analytical construction of periodic orbits about the collinear points. *Celestial Mechanics*, 22(3):241–253, 1980.

[24] C. Simó. On the analytical and numerical approximation of invariant manifolds. In D. Benest and C. Froeshlé, editors, *Modern methods in Celestial Mechanics*, pages 285–330. Editions Frontières, 1990.

[25] C. Simó, G. Gómez, À. Jorba, and J. Masdemont. The bicircular model near the triangular libration points of the RTBP. In A. Roy and B. Steves, editors, *From Newton to Chaos*, pages 343–370. Plenum Press, 1995.

[26] E. M. Standish. User's guide to the jpl lunar and planetary ephemeris export package. Technical report, Jet Propulsion Laboratory, 1985.

[27] E. M. Standish. JPL planetary and lunar ephemerides, DE405/LE405. Technical Report JPL IOM 314.10-127, Jet Propulsion Laboratory, 1998.

[28] J. Stoer and R. Bulirsch. *Introduction to Numerical Analysis*. Springer Verlag, 1983.

[29] J. Stoer and R. Bulirsch. *Introduction to Numerical Analysis*. Springer Verlag, second edition, 1993.

[30] V. Szebehely. *Theory of orbits*. Academic Press, 1967.

[31] E. T. Whittaker and G. N. Watson. *A course of modern analysis*. Cambridge University Press, 1940.

[32] C. Zagouras and P. Kazantzis. Three–dimensional periodic oscillations generating from plane periodic ones around the collinear lagrangian points. *Astrophysics Space Science*, 61(4):389–409, 1979.